

Asymmetric Catalysis with Chiral-at-Metal Complexes: From Non-Photochemical Applications to Photoredox Catalysis

A DISSERTATION

In

Chemistry

Presented to the Faculties of Philipps-Universität Marburg in Partial Fulfillment
of the Requirements for the Degree of Doctor of Science
(Dr. rer. nat.)

Haohua Huo

Guangdong, P. R. China

Marburg/Lahn 2016

Die vorliegende Dissertation entstand in der Zeit von November 2012 bis Juni 2016 am Fachbereich Chemie der Philipps-Universität Marburg unter der Betreuung von Herrn Prof. Dr. Eric Meggers.

Vom Fachbereich Chemie der Philipps-Universität Marburg (Hochschulkennziffer: 1180) als Dissertation am 22.06.2016 angenommen.

Erstgutachter:	Prof. Dr. Eric Meggers
Zweitgutachter:	Prof. Dr. Gerhard Hilt
weitere Mitglieder Prüfungskommission:	Prof. Dr. Ulrich Tallarek

Tag der mündlichen Prüfung: 19.07.2016

Acknowledgements

There are so many people to thank, I owe my sincere gratitude to all of the people who have supervised, inspired, supported, encouraged, advised and accompanied me and made this dissertation possible. The past three and a half years have been an extremely exciting, growing and fruitful period that may very well be some of the best years in my life.

I would first like to thank Prof. Meggers, my advisor, for all the opportunities he has provided me throughout the years. He gave the valuable and quick feedback on my every research report, and taught me how to question thoughts and solve the scientific problems. Followed the high efficient mode of “work-discussion-work”, I really enjoyed the experiments and have few felt frustrated. I am deeply grateful to him for triggering my greatest passion in scientific research and directing me to work hard, think smart and concentrate on both of big picture and the technical details. Under his tailored guidance, I have published a large number of high impact papers. I doubt that there is another group where I can make such a big progress as I did in the Meggers laboratory. My sense of chemistry intuition has been changed dramatically over these years, I hope that one day I would become a competent chemist as good as Prof. Meggers. I also need to thank Prof. Peiqiang Huang, my master advisor, for providing me an opportunity to carry out my first research career on the total synthesis of natural products, and also for introducing me to pursue my Ph.D. study in the Meggers group, and also for his constant encouragement throughout my research in China and abroad.

I would also thank all the members in the Meggers group for keeping excellent academic environment. Dr. Lili Zhang, thanks for getting two key intermediate crystals for the mechanistic study in my Nature paper, you are also one good teacher in my life, and I have learned so much from you. Our secretaries Ina Pinnschmidt, Andrea Tschirch, the technician Katja Kräling, thanks for being so helpful with great patience and kindness. Chen Fu, Xiaodong Shen, Chuanyong Wang, Xiaoqiang Huang, you guys are best, it has been a great pleasure working on projects with you, thanks for helping me publish some work more efficiently! Thomas Cruchter, thanks for nicely translating the abstract of my thesis into German version. Dr. Zhijie Lin, Dr. Yonggang Xiang, Dr. Tom Breiding, Dr. Marianne Kraack, Dr. Manuel Streib, Dr. Peter Göbel, Dr. Kathrin Wähler, Dr. Cornelia Ritter, and thanks for being so patient and for taking the time to teach me what you know, you all have gone off to

do amazing work, and I feel honored to have worked next to you. I must also thank Markus Dörr, Melanie Helms, Jens Henker, Elisabeth Martin, Rajathees Rajaratnam, Wei Zuo, Thomas Mietke, Timo Völker, Nathalie Nett, Jiajia Ma, Yu Zheng, Jie Qin, Dr. Xiao Zhang, Dr. Vladimir Larionov, for your kind cooperation and good friendship, I hope we keep in touch and wish you good luck for the future research or other career.

My gratitude to Prof. Hilt and Prof. Tallarek for agreeing to sit on my thesis committee and being a wealth of knowledge and advice over the past graduate period.

I also need to thank Philipp Röse, a graduate student in Prof. Hilt group, for help with conducting the cyclic voltammetry studies. I must also thank the facilities directors in chemistry department, Dr. Klaus Harms in the X-ray crystallography department, Dr. Xiulan Xie in the NMR department, and Dr. Uwe Linne of MS facility, for help with conducting the single-crystal X-ray diffraction, NMR, and HRMS studies.

I specially thank all my friends and classmates at Xiamen University, Yifeng, Yifei, Jianlong, Liang-An, Kaijiong, Xuekui. Our friendships will surely endure through the years. Our jokes have provided lightness to the dark moments of graduate study. I owe you guys a big party.

Most importantly, I would deeply thank my dear wife, Yuting Ye, for accompanying me throughout my Ph.D. years in Germany. You have been a constant source of love, concern, support and strength all these years. During this period, our lovely daughter, Yining, was born in Marburg. Thanks for giving me all these invaluable happiness. Meanwhile, I would like to express my heartfelt gratitude to my parents, siblings, my wife's parents. Your love and generosity have meant the world to me. Thanks for being patient, caring and supporting.

Finally, I am very grateful to CSC (China Scholarship Council) for the financial support throughout my Ph.D. study in Germany.

Publications and Poster Presentations

Part of this work has been already published:

1. H. Huo, K. Harms, E. Meggers, “Catalytic, Enantioselective Addition of Alkyl Radicals to Alkenes via Visible-Light-Activated Photoredox Catalysis with a Chiral Rhodium Complex”, *J. Am. Chem. Soc.* **2016**, *138*, 6936–6939.
2. H. Huo, E. Meggers, “Cooperative Photoredox and Asymmetric Catalysis”, *Chimia*, **2016**, *70*, 186–191. (review)
3. H. Huo, X. Huang, X. Shen, K. Harms, E. Meggers, “Visible-Light-Activated Enantioselective Perfluoroalkylation with a Chiral Iridium Photoredox Catalyst”, *Synlett*, **2016**, *27*, 749–753.
4. H. Huo, C. Wang, K. Harms, E. Meggers, “Enantioselective, Catalytic Trichloromethylation through Visible-Light-Activated Photoredox Catalysis with a Chiral Iridium Complex”, *J. Am. Chem. Soc.* **2015**, *137*, 9551–9554. (featured in *Synfacts* **2015**, *11*, 1071; *Synform* **2015/12**, A172–A174)
5. H. Huo, X. Shen, C. Wang, L. Zhang, P. Röse, L.-A. Chen, K. Harms, M. Marsch, G. Hilt, E. Meggers, “Asymmetric Photoredox Transition-Metal Catalysis Activated by Visible Light”, *Nature* **2014**, *515*, 100–103. (News & Views Feature by K. Skubi and T. P. Yoon, *Nature* **2014**, *515*, 45–46; *Synfacts* **2015**, *11*, 0153; *Chem. Eng. News* **2014**, Nov. 10, p. 9; *Nachrichten aus der Chemie* **2015**, *2*, 108 and *3*, 283)
6. H. Huo, C. Fu, K. Harms, E. Meggers, “Asymmetric Catalysis with Substitutionally Labile yet Stereochemically Stable Chiral-at-Metal Iridium(III) Complex”, *J. Am. Chem. Soc.* **2014**, *136*, 2990–2993. (“ACS Editors Choice”, featured in *JACS Spotlights* and *Synfacts* **2014**, *10*, 0487)
7. H. Huo, C. Fu, C. Wang, K. Harms, E. Meggers, “Metal-Templated Enantioselective Enamine/H-bonding Dual Activation Catalysis”, *Chem. Commun.* **2014**, *50*, 10409–10411.
8. X. Shen, H. Huo, C. Wang, B. Zhang, K. Harms, E. Meggers, “Octahedral Chiral-at-Metal Iridium Catalysts: Versatile Chiral Lewis Acids for Asymmetric Conjugate Additions”, *Chem. Eur. J.* **2015**, *21*, 9720–9726.
9. C. Wang, L.-A. Chen, H. Huo, X. Shen, K. Harms, L. Gong, E. Meggers, “Asymmetric Lewis Acid Catalysis Directed by Octahedral Rhodium Centrochirality”, *Chem. Sci.* **2015**, *6*, 1094–1100.
10. C. Wang, Y. Zheng, H. Huo, P. Röse, L. Zhang, K. Harms, G. Hilt, E. Meggers, “Merger of Visible Light Induced Oxidation and Enantioselective Alkylation with a Chiral Iridium Catalyst”, *Chem. Eur. J.* **2015**, *21*, 7355–7359.

Poster Presentation:

1. “**ISACS14: Challenges in Organic Chemistry**”, Poster: *Directing Asymmetric Lewis Acid Catalysis with Metal Centrochirality*, 7th–10th August **2014**, Shanghai, China.

Abstract (English)

The discovery of octahedral chiral-at-metal complexes that promote highly enantioselective non-photochemical or photochemical transformations, or both, is a challenging goal. This thesis details the discoveries and applications of two distinct classes of chiral-at-metal iridium(III) complexes for asymmetric catalysis, one is a metal-templated enamine/H-bonding catalyst and the other is a metal-based Lewis-acid catalyst.

The octahedral enamine/H-bonding catalyst (Λ -**Ir4**) promotes the enantioselective α -amination of aldehydes with catalyst loadings down to 0.1 mol%. In this metal-templated design, the iridium serves as a structural center and affords the exclusive source of chirality, whereas the catalysis is mediated through the organic ligand sphere (chapter 3.1).

The chiral-at-metal complex Λ -**IrO** bearing two hemilabile acetonitrile ligands can be used as a chiral Lewis acid catalyst. It efficiently catalyzes the enantioselective Friedel-Crafts addition of indoles to α,β -unsaturated 2-acyl imidazoles with high yields (75-99%) and high enantioselectivities (90-98% *ee*) at low catalyst loadings (0.25-2 mol%). Counterintuitively, this complex maintains its metal-centered configuration despite the rapid acetonitrile ligand exchange which is required for satisfactory catalytic activity. Since this initial discovery, this novel class of reactive chiral-at-metal complexes has been successfully applied to many other asymmetric catalytic reactions in the Meggers group (chapter 3.2).

The Lewis-acid catalyst Λ -**IrO** and its derivative Λ -**IrS** can also be competent photoredox catalyst for challenging asymmetric photoredox catalysis. With a single catalyst Λ -**IrS** (2 mol%), the visible-light-activated enantioselective alkylation of 2-acyl imidazoles with electron-deficient benzyl bromides and phenacyl bromides provided excellent enantioselectivities (90-99% *ee*) and excellent yields (84-100%). In this mono catalysis strategy, the chiral-at-metal complex serves as an *in situ* photosensitizer precursor for photoredox catalysis and at the same time provides very effective asymmetric induction for α -functionalization of ketones (chapter 3.3). Subsequently, this new catalytic strategy has been expanded to realize highly enantioselective α -trichloromethylation (chapter 3.4) and α -perfluoroalkylation (chapter 3.5) through visible-light-activated photoredox catalysis. Previously, most of the successful approaches for asymmetric photoredox catalysis needed two catalysts, one for

the photoredox activation, and the other for stereoinduction. The single catalyst strategy fulfills an unmet need in the photoredox synthetic toolbox and provides new avenues for the efficient and economical synthesis of enantioenriched molecules.

Alternatively, in some cases the synergistic catalysis strategy still has its advantages over the single catalyst system. By merging the chiral Lewis acid Λ -**RhS** with an external photosensitizer, an efficient enantioselective addition of organotrifluoroborates to electron-deficient alkenes was readily realized under photoredox conditions. This practical method provides yields up to 97% with excellent enantioselectivities up to 99% *ee* and can be classified as a redox neutral, electron-transfer-catalyzed reaction. The previously developed dual function photoredox/chiral Lewis acid catalysts Λ -**IrO** or Λ -**IrS** are not applicable for this photoreaction and this has been pinpointed to slow ligand exchange kinetics in the iridium system (chapter 3.6).

Zusammenfassung (Deutsch)

Die Entdeckung oktaedrischer "chiral-at-metal"-Komplexe, die hoch enantioselektive nicht-photochemische- und photochemische Umwandlungen katalysieren oder beide gleichzeitig, ist eine anspruchsvolle Herausforderung. Diese Dissertation beschreibt die Entdeckung und Anwendung zweier unterschiedlicher Klassen von Komplexen mit metallzentrierter Chiralität in der asymmetrischen Katalyse, und zwar einerseits ein Enamin/Wasserstoffbrückenbindungs-Katalysator und zum anderen ein Lewis-Säure-Katalysator.

Der oktaedrische Enamin/Wasserstoffbrückenbindungs-Katalysator (Λ -**Ir4**) katalysiert die enantioselektive α -Aminierung von Aldehyden mit Katalysatorladungen bis hinab zu 0.1 mol%. Bei diesem Metall-basierten Katalysator fungiert das Iridium als strukturelles Zentrum und stellt gleichzeitig das einzige Chiralitätszentrum dar, wohingegen die eigentliche Katalyse durch die Ligandensphäre vermittelt wird (Kapitel 3.1).

Der zwei hemilabile Acetonitril-Liganden enthaltende "chiral-at-metal"-Komplex Λ -**IrO** kann als Lewis-Säure-Katalysator genutzt werden. Dieser katalysiert effizient die enantioselektive Friedel-Crafts-Addition von Indolen an α,β -ungesättigte 2-Acylindole mit hohen Ausbeuten (75-99%) und hohen Enantioselektivitäten (90-98%) bei gleichzeitig niedrigen Katalysatorladungen (0.25-2 mol%). Überraschenderweise behält dieser Komplex seine metallzentrierte Stereoinformation trotz des schnellen Austauschs der Acetonitril-Liganden, welcher für eine zufriedenstellende katalytische Aktivität erforderlich ist. Seit dieser Entdeckung ist diese neue Klasse von Komplexen mit metallzentrierter Chiralität erfolgreich für viele andere asymmetrische Reaktionen im Arbeitskreis Meggers eingesetzt worden (Kapitel 3.2).

Der Lewis-Säure-Katalysator Λ -**IrO** und der davon abgeleitete Katalysator Λ -**IrS** können auch als leistungsfähige Photoredoxkatalysatoren in anspruchsvollen asymmetrischen Photoredoxreaktionen eingesetzt werden. Mit dem Katalysator Λ -**IrS** (2 mol%) ist die durch sichtbares Licht angetriebene Alkylierung von 2-Acylimidazolen mit elektronenarmen Benzyl- und Phenacylbromiden mit exzellenten Enantioselektivitäten (90-99%) und exzellenten Ausbeuten (84-100%) möglich. Bei dieser nur einen Katalysator umfassenden Strategie dient der "chiral-at-metal"-Katalysator als ein *in-situ* Photosensibilisator-Vorläufer für die Photoredoxkatalyse und vermittelt gleichzeitig eine sehr effektive

Stereoiduktion bei der α -Funktionalisierung von Ketonen (Kapitel 3.3). Anschließend wurde diese neue katalytische Strategie ausgedehnt auf die hoch enantioselektive α -Trichloromethylierung (Kapitel 3.4) und α -Perfluoroalkylierung (Kapitel 3.5) durch Licht-aktivierte Photoredoxkatalyse. Zuvor wurden für die meisten erfolgreichen asymmetrischen Photoredoxkatalysen stets zwei Katalysatoren benötigt, einer für die Photoredox-Aktivierung und ein anderer für die Stereoiduktion. Der hier beschriebene Katalysator füllt daher eine Lücke im Werkzeugkasten der Photoredoxsynthese und ermöglicht neuartige und ökonomische Synthesen von enantioangereicherten Molekülen.

Allerdings haben in einigen Fällen synergistische Katalysestrategien ihre Vorteile gegenüber der Verwendung eines einzelnen Katalysators. Durch Hinzufügen eines externen Photosensibilisators zur chiralen Lewis-Säure Λ -**RhS** konnte eine effiziente Addition von Organotrifluoroboraten an elektronenarme Alkene bereitwillig unter Photoredoxbedingungen erzielt werden. Diese praktische Methode liefert Ausbeuten bis zu 97% bei exzellenten Enantioselektivitäten von bis zu 99% *ee* und lässt sich klassifizieren als eine redoxneutrale, Elektronentransfer-katalysierte Reaktion. Die zuvor entwickelten bifunktionalen photoredox-/chirale Lewis-Säure-Katalysatoren Λ -**IrO** und Λ -**IrS** können nicht für diese Reaktion genutzt werden, was nachweislich auf die langsame Ligandenaustauschrate bei den Iridium-Komplexen zurückzuführen ist (Kapitel 3.6).

Table of Contents

Acknowledgements	I
Publications and Poster Presentations	III
Abstract (English)	V
Zusammenfassung (Deutsch)	VII
Table of Contents.....	IX
Chapter 1: Theoretical Part.....	1
1.1 Introduction	1
1.2 Asymmetric Catalysis with Octahedral Chiral-at-Metal Complexes.....	3
1.2.1 Representative Chiral Only-at-Metal Ru(II) and Co(III) Complexes for Asymmetric Catalysis	3
1.2.2 Chiral-at-Metal Ir(III) Complexes for Asymmetric Catalysis Developed in the Meggers Group	4
1.3 Asymmetric Photoredox Catalysis Activated by Visible Light	8
1.3.1 Dual Catalysis Strategies in Asymmetric Photoredox Catalysis.....	8
1.3.2 Single Catalyst Induced Asymmetric Photoredox Catalysis.....	17
1.4 Conclusions	21
Chapter 2: Aim of the Work.....	25
Chapter 3: Results and Discussion	28
Part I: Non-Photochemical Asymmetric Catalysis with a Metal-Templated “Organocatalyst”	28
3.1 Metal-Templated Asymmetric Enamine/H-Bonding Dual Catalysis	29
3.1.1 Catalyst Design and Synthesis.....	29
3.1.2 Reaction Development	32
3.1.3 Proposed Mechanism	36
3.1.4 Conclusions	37
Part II: Non-Photochemical Asymmetric Catalysis with a Chiral Lewis Acid Catalyst	39

3.2 Enantioselective Friedel-Crafts Conjugate Addition with a Chiral-at-Metal Lewis Acid	
Catalyst	40
3.2.1 Catalyst Design	40
3.2.2 Initial Experiments	41
3.2.3 Development of Catalyst Λ -IrO and Δ -IrO	43
3.2.4 Reaction Optimization and Substrate Scope	47
3.2.5 Proposed Mechanistic Model	51
3.2.6 Conclusions	52

Part III: Asymmetric Photoredox Catalysis with Chiral-at-Metal Iridium

Complexes: α-Functionalization of Carbonyl Compounds	55
---	-----------

3.3 Visible-Light-Activated Enantioselective Alkylation with a Chiral Iridium Complex	56
3.3.1 Reaction Design	56
3.3.2 Reaction Optimization.....	59
3.3.3 Substrate Scope	62
3.3.4 Plausible Mechanism.....	66
3.3.5 Mechanistic Investigations	67
3.3.6 Conclusions	76

3.4 Visible-Light-Activated Enantioselective Trichloromethylation with a Chiral Iridium Complex	78
3.4.1 Reaction Design	78
3.4.2 Reaction Optimization and Substrate Scope	79
3.4.3 Efforts to Transformations of 2-Acyl Imidazole Products.....	85
3.4.4 Plausible Mechanism.....	86
3.4.5 Mechanistic Investigations	87
3.4.6 Conclusions	95

3.5 Visible-Light-Activated Enantioselective Perfluoroalkylation with a Chiral Iridium Complex	97
3.5.1 Reaction Design Plan	97
3.5.2 Discovery and Optimization of Visible-Light-Activated Perfluoroalkylation.....	98
3.5.3 Substrate Scope of Perfluoroalkylation	105
3.5.4 Proposed Mechanism	106
3.5.5 Conclusions	108

Part IV: Asymmetric Photoredox Catalysis with a Chiral-at-Metal Rhodium

Complex	110
3.6 Visible-Light-Activated Enantioselective Conjugate Addition	110
3.6.1 Reaction Design	110
3.6.2 Reaction Optimization and Substrate Scope	112
3.6.3 Synthetic Transformations.....	118
3.6.4 Plausible Mechanism.....	119

3.6.5	Mechanistic Investigations	120
3.6.6	Conclusions	130
Chapter 4: Summary and Outlook		133
Chapter 5: Experimental Part		145
5.1	Materials and Methods	145
5.2	Enantioselective α-Amination of Aldehydes with a Chiral-at-Metal Iridium(III) Complex.....	148
5.2.1	Synthesis of the Iridium Catalysts Λ - Ir1-5 and Δ - Ir4	148
5.2.2	Iridium-Catalyzed Reactions	165
5.2.3	Single Crystal X-Ray Diffraction of Iridium Catalyst <i>rac</i> - Ir4	174
5.3	Metal-Centered Chirality Directs Friedel-Crafts Addition.....	175
5.3.1	Synthesis of Iridium Catalysts Λ - IrO and Δ - IrO	175
5.3.2	Synthesis of Substrates	179
5.3.3	Iridium-Catalyzed Reactions	187
5.3.4	Investigation of the Proposed Substrate-Coordinated Catalyst	199
5.3.5	Investigation of the Stability of Iridium Catalyst Λ - IrO	201
5.3.6	Single Crystal X-Ray Diffraction of Iridium Catalyst Δ - IrO	203
5.4	Visible-Light-Activated Asymmetric Alkylation of 2-Acyl Imidazoles	204
5.4.1	Synthesis of Substrates	204
5.4.2	Iridium-Catalyzed Photoredox Reactions.....	213
5.4.3	Assignment of Absolute Configurations for Asymmetric Catalysis Products	224
5.4.4	Mechanistic Experiments	227
5.4.5	Cyclic Voltammetry.....	231
5.4.6	Single-Crystal X-Ray Diffraction Studies	231
5.5	Visible-Light-Activated Enantioselective Trichloromethylation	232
5.5.1	Synthesis of Substrates	232
5.5.2	Iridium-Catalyzed Photoredox Reactions.....	240
5.5.3	Mechanistic Experiments	254
5.5.4	Efforts towards Removal of Imidazole Moieties	261
5.5.5	Single-Crystal X-Ray Diffraction Studies	262
5.6	Visible-Light-Activated Enantioselective Perfluoroalkylation	263
5.6.1	Synthesis of Catalysts.....	263
5.6.2	Synthesis of Substrates	268
5.6.3	Iridium-Catalyzed Photoredox Reactions.....	273
5.6.4	Single-Crystal X-Ray Diffraction Studies	285
5.7	Visible-Light-Activated Enantioselective Addition of Alkyl Radicals to Alkenes with a Chiral Rhodium Complex	286
5.7.1	Synthesis of Substrates	286
5.7.2	Rhodium-Catalyzed Photoredox Reactions.....	292

5.7.3	Synthetic Transformations	316
5.7.4	Mechanistic Experiments	318
5.7.5	Single-Crystal X-Ray Diffraction Studies	328
Chapter 6. Appendices.....		331
6.1	List of Abbreviations	331
6.2	List of Figures	334
6.3	List of Schemes	340
6.4	List of Tables	341
6.5	List of Synthesized Compounds	342
6.5.1	List of Organic Compounds	342
6.5.2	List of Iridium/Rhodium Complexes.....	350
6.6	List of Spectra of Iridium/Rhodium Complexes	352
6.6.1	NMR Spectra of Iridium/Rhodium Complexes	352
6.6.2	CD Spectra of Enantiopure Iridium Complexes	375
6.6.3	HPLC Spectra of Enantiopure Iridium Complexes	383
6.7	List of Crystal Structure Data	385
Statement.....		401
Curriculum Vitae.....		402

Chapter 1: Theoretical Part

1.1 Introduction

Asymmetric catalysis is seen as one of the most efficient strategies to satisfy the growing demand for enantiomerically pure compounds in the fine chemical and pharmaceutical industry¹. Visible light has been recognized as an environmentally friendly and sustainable form of energy for triggering chemical transformations and catalytic chemical processes.² The interaction between light and matter constitutes one of the most active areas of scientific research.³ In 2014, the Nobel prizes for physics and chemistry were awarded for the development of efficient light emitting devices and for the use of fluorescence in ultrahigh-resolution microscopy, respectively. For these reasons, visible-light-driven catalytic asymmetric chemistry is a subject of enormous current interest (Figure 1).²

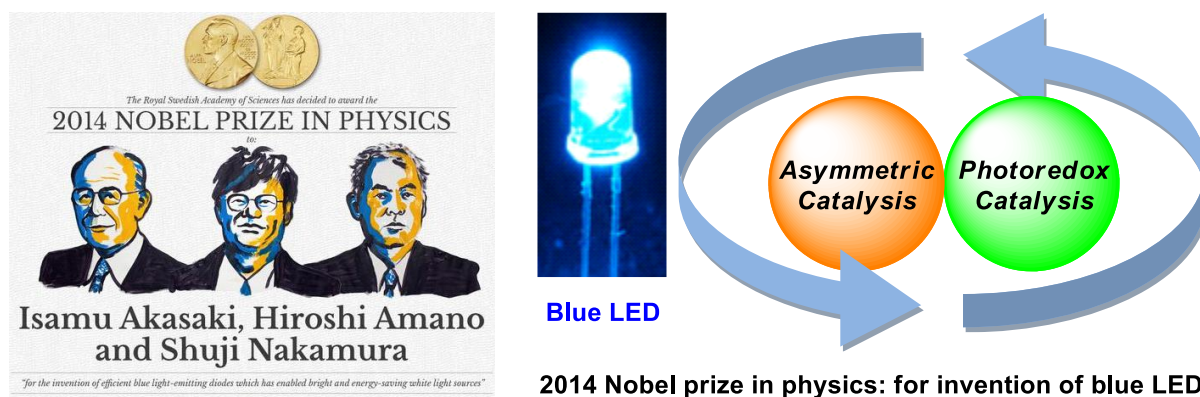
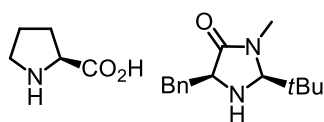


Figure 1 The interaction between light and matter constitutes one of the most active areas of scientific research (Image with respect to Nobel Prize winners was taken from the official web site of the Nobel Prize with permission).

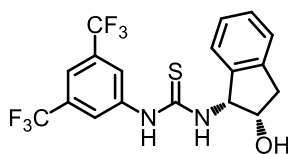
Over the past decade, organocatalysis and metal-based catalysis have emerged as two main branches of asymmetric catalysis.⁴ A wide range of asymmetric organocatalysts have been developed for controlling the stereochemistry of organic reactions (Figure 2a), such as amine catalysis,⁵ H-bonding catalysis,⁶ Brønsted acid catalysis,⁷ carbene catalysis,⁸ counterion catalysis,⁹ and phase transfer catalysis.¹⁰ Asymmetric metal-based catalysis (Figure 2b), in particular asymmetric hydrogenation,¹¹ has been applied to the synthesis of non-racemic compounds extensively. The asymmetric inductions of these catalysts are typically provided by one or more tetrahedral stereogenic centers, axial chirality and planar chirality. In contrast, there have been only few instances of chiral catalysts that transfer

their chirality exclusively from an octahedral stereocenter.¹²

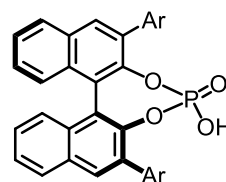
a) asymmetric organocatalysts:



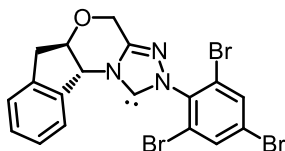
amine catalysts



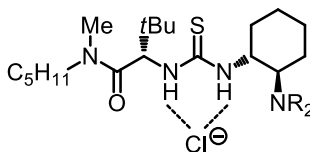
H-bonding catalyst



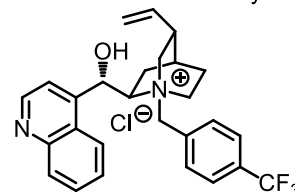
Brønsted acid catalyst



carbene catalyst

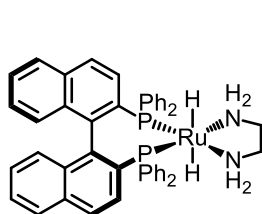


counterion catalyst

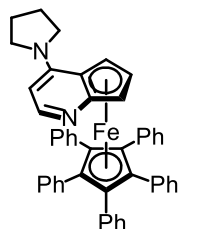


phase transfer catalyst

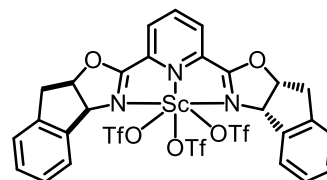
b) asymmetric metal-based catalysts:



hydrogenation catalyst



nucleophilic catalyst



Lewis acid catalyst

Figure 2 Typical chiral organocatalysts and metal-based catalysts for asymmetric catalysis.

Photoredox catalysis provides the opportunity to generate highly reactive radical ion intermediates with often unusual or previously unconventional reactivities under mild reaction conditions.¹³ In such systems, photoactivated sensitizers initiate a single electron transfer from (or to) a closed-shell organic molecule to produce radical cations or radical anions whose reactivities are then exploited for interesting or unusual chemical transformations. However, the high reactive intermediates involved in photoreactions often have very short lifetimes and can be difficult to controlled with external chiral catalysts. Thus, the design of catalysts that promote highly enantioselective photochemical processes has proven to be a formidable challenge.¹⁴

This chapter will summarize and discuss recent progress on: 1) non-photochemical asymmetric catalysis with octahedral chiral only-at-metal complexes, with an emphasis on the applications of chiral iridium(III) complexes developed by Meggers; 2) visible-light-induced enantioselective photoredox catalysis with dual catalysis strategy and mono catalysis strategy (single catalyst).

1.2 Asymmetric Catalysis with Octahedral Chiral-at-Metal Complexes

Despite the enormous numbers of chiral catalysts that have been developed for the generation of enantiopure compounds, no universal catalyst or chiral ligand exists for solving all the problems in asymmetric transformations. For instance, achieving very high turnover numbers (<1 mol% loadings) in organocatalysis remains a significant challenge with few general solutions. On the other hand, most metal-based asymmetric catalysts profoundly rely on chiral organic ligands. These chiral ligands are often more synthetically challenging to approach compared to the achiral analog, which might cause the multiple functional groups cannot be readily installed around the metal center.

The chemistry of using chiral only-at-metal complexes for asymmetric catalysis had been largely ignored over the past decades indicated by the limited number of publications.¹² To develop an efficient chiral-at-metal catalyst, the interdisciplinary research that combines organic, inorganic, organometallic, even biomimetic chemistry, is often required. This great barrier stands between different directions of chemistry, and only few research groups have successfully carried out research in this field.

1.2.1 Representative Chiral Only-at-Metal Ru(II) and Co(III) Complexes for Asymmetric Catalysis

In 2003, Fontecave and co-workers reported a chiral only-at-metal Λ -ruthenium(II) complex which was a competent asymmetric catalyst (Figure 3).¹⁵ Albeit only 18% *ee* was provided by asymmetric oxidation of sulfide to sulfoxide. The authors proposed a Ru(VI)-oxo intermediate as the true oxidant. This example demonstrated, for the first time, that chiral-only-at-metal complexes can be used as true asymmetric catalysts.¹⁶

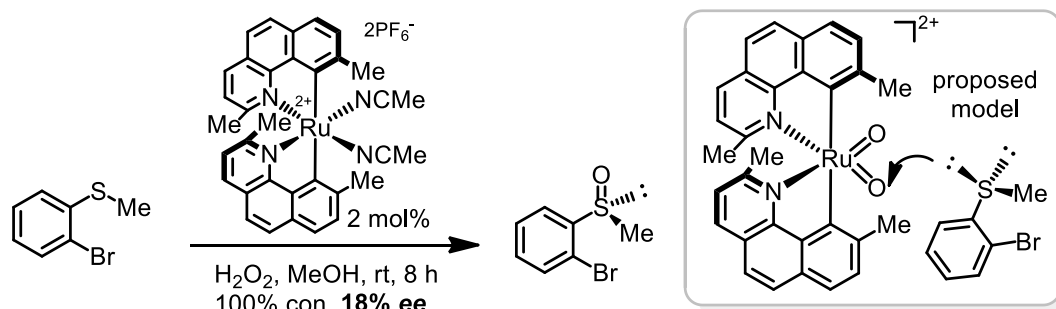


Figure 3 Fontecave's asymmetric oxidation with chiral-at-metal Ru(II) complex.

The Gladysz group recently introduced simple chiral-at-metal Werner complexes which can serve as hydrogen bond catalysts (Figure 4).¹⁷ The Michael addition of dimethyl malonate to cyclopentenone proceeded with only 78% yield and 33% *ee*. The solubility of enantiopure Δ -Werner complex in CH_2Cl_2 was enhanced by the bulky BArF_{24}^- (tetrakis[(3,5-di-trifluoromethyl)phenyl]borate) counterion. Since the catalyst is substitutionally inert, the authors suggested that the asymmetric induction takes place through the N-H bonds as H-bonding donors around the metal center.

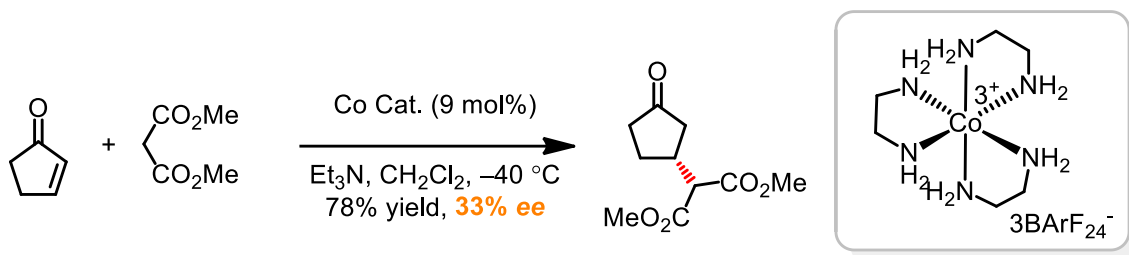


Figure 4 Gladysz's asymmetric Michael addition with chiral-at-metal Co(III) Werner complex.

1.2.2 Chiral-at-Metal Ir(III) Complexes for Asymmetric Catalysis Developed in the Meggers Group

For the past several years, the Meggers group has conducted interdisciplinary research ranging from biochemistry, inorganic chemistry to organic chemistry. Our group has mastered the design and synthesis of chiral-at-metal ruthenium and iridium complexes for enzyme inhibition and asymmetric catalysis.¹⁸

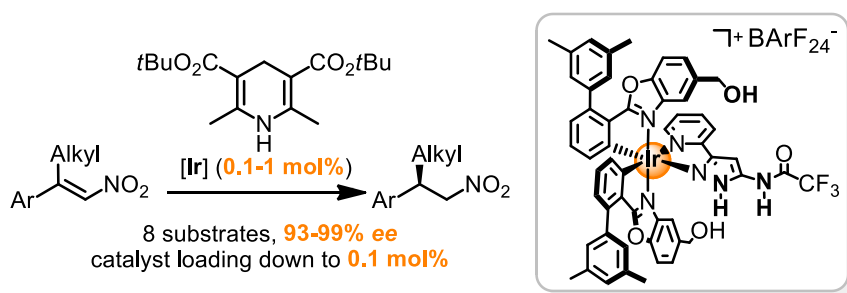


Figure 5 Chiral-at-metal iridium(III) complex catalyzed asymmetric transfer hydrogenation.

In 2013, the Meggers group reported an inert chiral-at-metal iridium(III) complex for highly efficient catalytic asymmetric transfer hydrogenation of β,β -disubstituted nitroalkenes (Figure 5).¹⁹ This metal-templated catalyst mediated chirality transfer relying on exclusive chirality at the metal center. The reactions did not involve any direct metal coordination but operated exclusively through hydrogen bond interactions with functional groups arranged in the ligand sphere of the iridium

complex. Although this iridium complex only relies on the formation of three hydrogen bonds, it surpasses the reactivities of most organocatalysts with respect to the combination of enantiomeric excess (93-99% *ee*) and catalyst loading (down to 0.1 mol%). Remarkably, this seminal work represented the first example of highly enantioselective catalytic reactions being performed with a chiral only-at-metal catalyst.

The proposed mechanistic model for asymmetric transfer hydrogenation is outlined in Figure 6. Accordingly, the nitroalkene is activated by the double hydrogen bonding donor arranged in the amidopyrazole moiety. The steric clash is curious for stabilizing two formed hydrogen bonds between the nitro group and the amidopyrazole. This steric hindrance might facilitate the proper binding mode of the nitroalkene substrate and restricts dynamic motion. Meanwhile, one of the two OH groups, which are placed in the cyclometalated phenylbenzoxazole ligands, serves as a hydrogen bond acceptor to activate the hydride nucleophile through formation of a hydrogen bond between the NH group of Hantzsch ester and a lone pair of the OH group. The three hydrogen bonds formed at the proper position turn the nitroalkene into a stronger electrophile, and the Hantzsch ester into a better hydride donor. Thus, the transfer hydrogenation catalyzed by the bifunctional chiral-at-metal iridium complex smoothly proceeds to afford the chiral nitroalkanes with excellent enantioselectivities and yields. Interestingly, the absolute configuration of the central metal remains unchanged during the overall catalytic process, which can be attributed to the stabilizing bis-cyclometalated chelate effect.

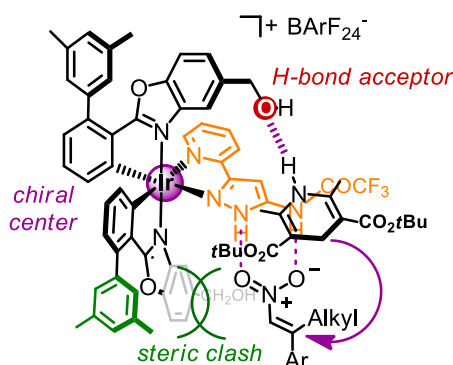


Figure 6 The proposed mechanistic model for asymmetric transfer hydrogenation with a chiral-at-metal iridium(III) complex.

The unique nature of this metal-templated chiral-at-metal catalyst was later expanded to more challenging transformations, such as the asymmetric conjugate addition of indoles to β,β -disubstituted nitroalkenes for the construction of all-carbon quaternary stereocenters with high yields and high enantioselectivities (Figure 7). The reactivity of this catalyst was dramatically improved by replacing the hydroxyl group with *N,N*-diethylcarboxamide, a stronger H-bonding acceptor, as well as switching

the 3,5-dimethylphenyl to a carbazolyl moiety. Interestingly, this catalyst can be recycled multiple times without significant loss of catalytic activity.

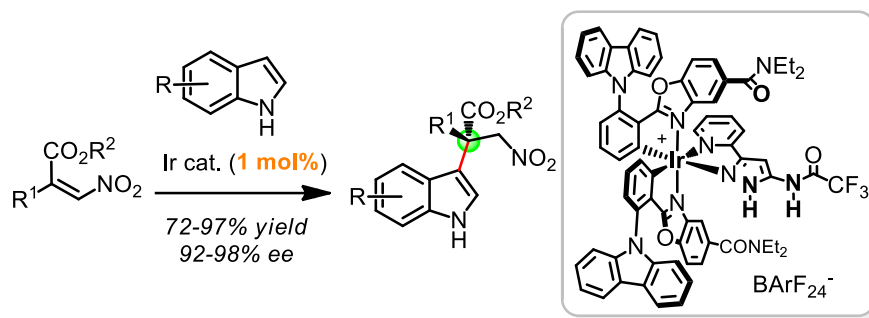


Figure 7 Chiral-at-metal iridium(III) complex catalyzed asymmetric Friedel-Crafts alkylation.

Besides these two applications, subsequent work demonstrated that such inert Ir(III) metal templates can be applied as asymmetric Brønsted base catalysts (Figure 8).²⁰ The treatment of the acidic N-H bond in the aminopyrazolato ligand with base gave rise to a neutral chiral Brønsted base catalyst. Remarkably, the highly effective asymmetric sulfa-Michael addition and aza-Henry reactions can permit catalyst loadings down to 0.02 and 0.25 mol%, respectively. Mechanistically, due to the pKa of the protonated catalyst of about 16, which higher than that of the thiophenol substrate (pKa of about 10), the thiol can be effectively activated through deprotonation. Subsequently, an ion pair between thiolate and cationic Ir(III) complex forms through double H-bonding. Meanwhile, the Michael acceptor is activated *via* a three-center hydrogen bond with one OH group. This dual activation allows the catalytic transformation to proceed with high-rate acceleration and high asymmetric induction.

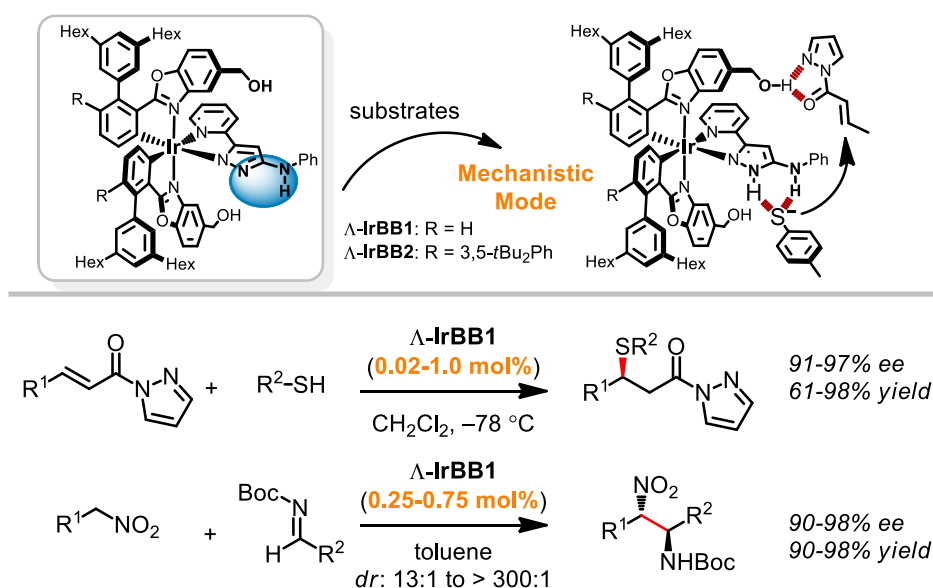


Figure 8 Asymmetric Brønsted base catalysis with chiral-at-metal Ir(III) complexes.

In above enantioselective applications, the octahedral chiral-at-metal iridium(III) complexes developed by Meggers have served as the most efficient chiral-at-metal asymmetric catalysts, which rely on three defined hydrogen bonds between substituents on the periphery of the metal complexes and the substrates, and in which the iridium center serves as an unreactive bystander fulfilling a purely structural role. As achiral ligands are used, the ligand scope for chiral-at-metal complexes is massively increased. That means that multiple functional groups can be more readily introduced to the octahedral skeleton. It can be assumed that multifunctional chiral-at-metal complexes as metal templates could be exploited and applied in many different asymmetric catalysis applications as metal-templated “organocatalysts” in which interactions are only executed through the organic ligand sphere.

However, metal coordination is arguably one of the most powerful approaches for activating substrates towards chemical transformations. Consequently, chiral metal complexes are employed extensively in industry and academia for the catalytic synthesis of non-racemic chiral compounds.¹ A guiding principle for the design of such metal-coordination-based asymmetric catalysts is the generation of a chiral environment around the metal, which is typically introduced through the association with chiral mono- or multidentate organic ligands (Figure 9).²¹ In theory, instead of implementing chirality directly at the reactive metal center by exploiting the metal as a source of centrochirality would be highly attractive since the close proximity of the metal to the coordinating substrate promises a highly effective transfer of chirality during the asymmetric induction.²² However, a considerable obstacle for the realization of such reactive chiral-only-at-metal asymmetric catalysts constitutes the retention of the relative and absolute metal-centered configuration during the reaction since the coordination number at the metal varies during each catalytic cycle and thereby provides ample opportunities for the stereochemistry of the metal to scramble.¹

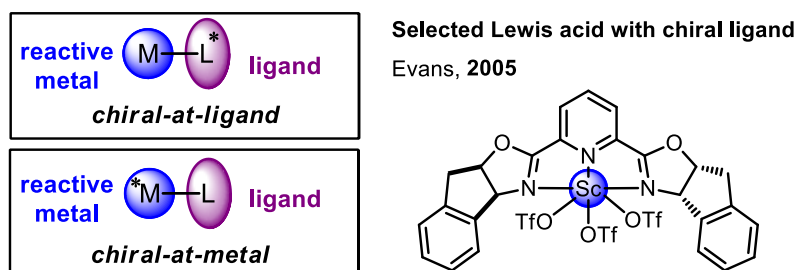


Figure 9 Traditional Lewis acid catalyst and the prospect of a chiral-only-at-metal complex.

1.3 Asymmetric Photoredox Catalysis Activated by Visible Light

Although photoredox chemistry has experienced a renaissance over the last several years, the control of absolute stereochemistry in photoredox reactions is still in its infancy.²³ Two established strategies for visible-light-induced asymmetric catalysis, namely dual catalysis (two catalysts) and mono catalysis (single catalyst), are briefly reviewed in the following sections.

1.3.1 Dual Catalysis Strategies in Asymmetric Photoredox Catalysis

In most of the reported examples, the photoinduced asymmetric catalysis is shared by two catalysts, a racemic or achiral photoredox sensitizer for triggering visible light induced redox chemistry in combination with an asymmetric catalyst (organocatalysts or metal-based complexes) to provide the required stereocontrol and the activation of one substrate.²⁴

1) Enamine catalysis

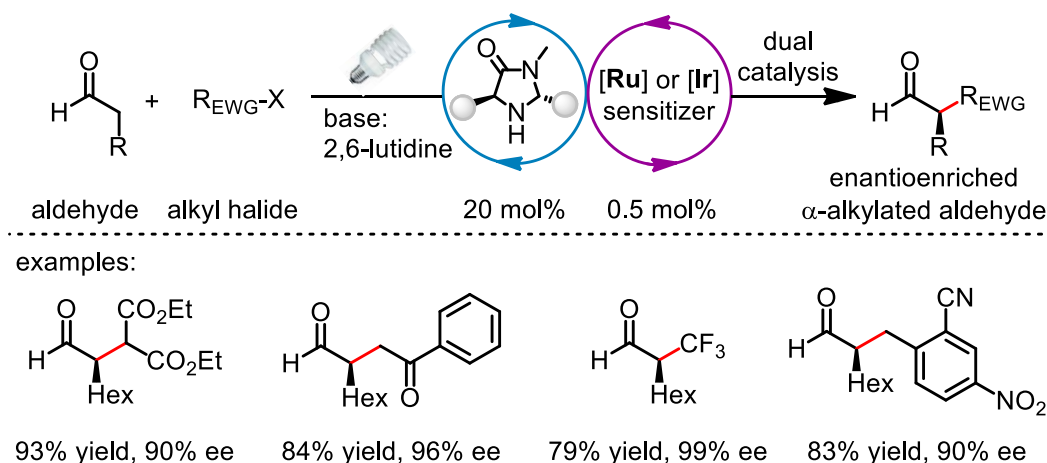


Figure 10 MacMillan's dual catalysis strategies for visible-light-induced asymmetric catalysis.

MacMillan and coworkers reported the first visible light induced asymmetric photoredox catalysis in 2008.²⁵ The direct asymmetric alkylation of aldehydes was accomplished through merging photoredox catalysis with organocatalysis. As shown in Figure 10, in the presence of photosensitizer $\text{Ru}(\text{bpy})_3\text{Cl}_2$ and a 15 W fluorescent light bulb (CFL), the coupling of aldehydes with electron deficient diethyl bromomalonate or phenacyl bromides provided the α -alkylated aldehydes with good yields and enantioselectivities. Subsequently, switching the sensitizer to iridium complex $\text{Ir}(\text{ppy})_2(\text{dtbbpy})\text{PF}_6$ or *fac*- $\text{Ir}(\text{ppy})_3$, MacMillan's group extended this strategy to asymmetric trifluoromethylations and benzylations still with outstanding asymmetric induction.

Mechanistically, the catalytic cycle is initiated by reduction of photoexcited **PS*** with a sacrificial amount of formed enamine (not shown in Figure 11) to produce the reductive **PS⁻**, which transfers a single electron to alkyl halides, such as electron deficient diethyl bromomalonate, phenacyl bromides, perfluoroalkyl iodides or benzyl bromides, followed by release of a halide leaving group with the formation of an electrophilic radical. This radical rapidly reacts with the electron-rich double bond of the stereodefined enamine, which was formed by the condensation of chiral imidazolidinone catalyst with aldehyde substrate. The generated α -aminoalkyl radical is very prone to oxidation and upon removal of an electron, the formed iminium ion hydrolyzes and releases the chiral amine catalyst for a new catalytic cycle. Quantum yields determined by Yoon and coworkers for a representative model reaction reveal that this intermediate α -aminoalkyl radical can directly transfer an electron to another electrophile substrate, thereby rendering this reaction a chain process (not shown in Figure 11).²⁶

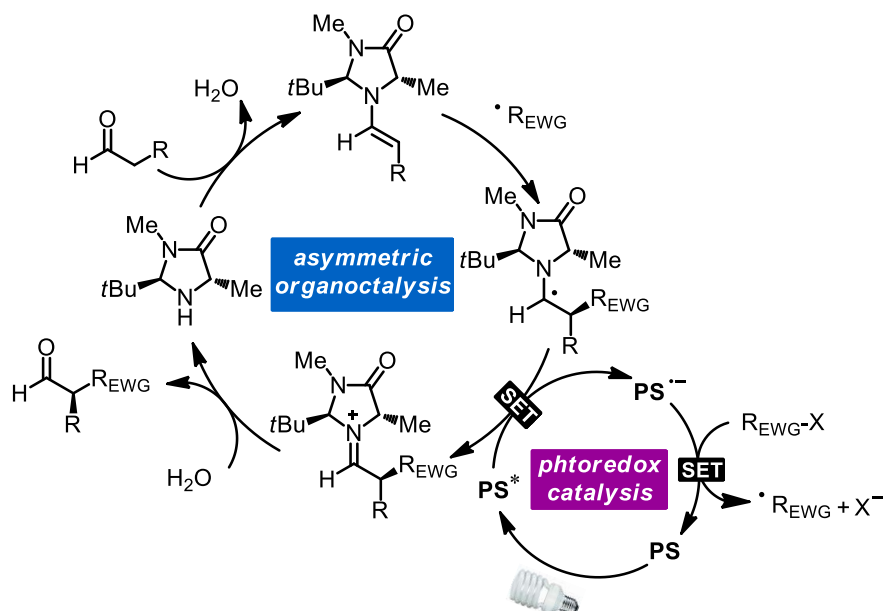


Figure 11 Proposed mechanism for merging photoredox catalysis with asymmetric organocatalysis. PS, photosensitizer; SET, single electron transfer; EWG, electron withdrawing group. The chain mechanism is not shown here for simplification.

Stimulated by this pioneering work, Zeiter, König, and Pericàs later revealed that organic dyes and inorganic semiconductors are also suitable photosensitizers in this and related systems.²⁷ Recently, Luo's group extended this strategy to build all-carbon quaternary stereocenters with high efficacy and enantioselectivities by merging photoredox catalysis and primary amine catalysis (Figure 12).²⁸ This open-shell photoradical approach enables α -alkylations that are challenging under thermal conditions.

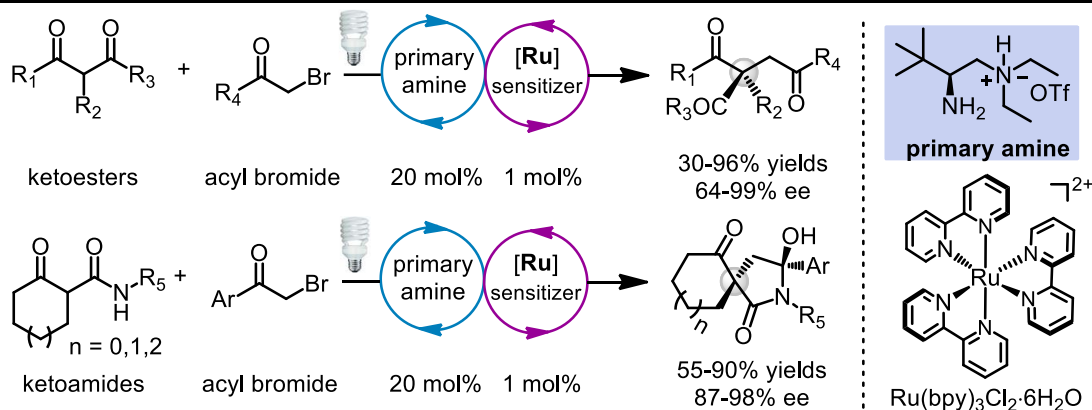


Figure 12 Luo's asymmetric α -photoalkylation of β -ketocarboxylates by primary amine catalysis.

2) Lewis acid catalysis

In 2014, Yoon's group described a strategy for asymmetric [2+2] photocycloadditions of α,β -unsaturated ketones to cyclobutanes by using a dual catalyst system consisting of photoredox catalyst $\text{Ru}(\text{bpy})_3\text{Cl}_2$ and 10 mol% Lewis acid $\text{Eu}(\text{OTf})_3$ in combination with 20-30 mol% chiral ligand (Figure 13).²⁹ A series of cyclobutanes were produced with 34-80% yields and 84-97% *ee*. Notably, switching the chiral Schiff base ligand to the corresponding reduced secondary amine led to a reverse diastereoselectivity from 1,2-*trans* to 1,2-*cis* cyclobutanes, that means both the relative and absolute stereochemistry of the [2+2]-photocycloaddition products can be obtained through the chiral ligand modification.

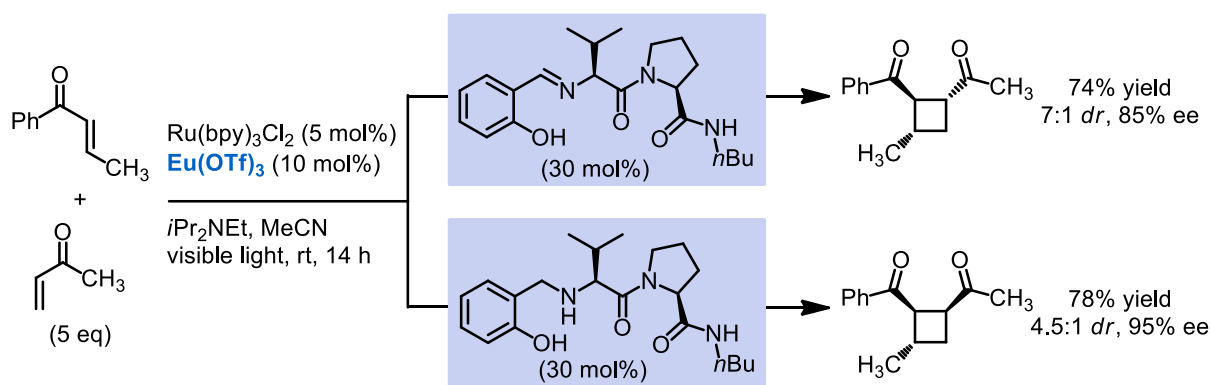


Figure 13 Yoon's asymmetric Lewis acid catalyzed [2+2]-cycloaddition of α,β -unsaturated ketones via photoredox catalysis.

Mechanistically (Figure 14), photoactivated $[\text{Ru}^*(\text{bpy})_3]^{2+}$ accepts an electron from $i\text{Pr}_2\text{NEt}$ to produce the reduced complex $[\text{Ru}(\text{bpy})_3]^+$ which serves as the reducing agent and transfers a single electron to a Lewis acid coordinated aryl enone. The hereby generated intermediate radical anion can subsequently participate in efficient [2+2]-cycloaddition reaction with another Michael acceptor. The formed cyclobutane containing ketyl radical loses an electron and thereby closes the electron catalysis

cycle. Apparently, all reactive intermediates remain coordinated to the chiral europium Lewis acid throughout the catalytic cycle so that high enantio- and diastereoselectivities can be reached. The authors point out that the high enantioselectivities profit from the fact that no background reaction occurs in the absence of the Lewis acid.

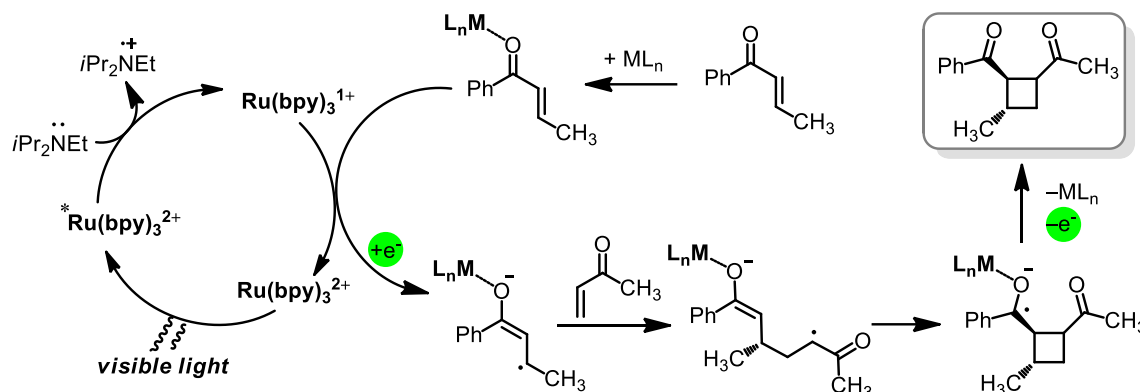


Figure 14 Yoon's proposed mechanism for asymmetric Lewis acid catalyzed [2+2]-cycloaddition via photoredox catalysis.

Yoon and coworkers later reported a catalytic enantioselective addition of α -aminoalkyl radicals to α,β -unsaturated carbonyl compounds using a similar dual catalysis strategy (Figure 15).³⁰ The addition products were obtained with 33-96% yields and 85-96% *ee* under visible light irradiation. They used scandium(III) triflate together with a pybox ligand as a chiral Lewis acid to control the stereochemistry of photoinitiated α -aminoalkyl radical Michael additions. The authors concluded that the rate acceleration afforded by the Lewis acid catalyst must be large enough to overcome a significant racemic background addition in the absence of Lewis acid catalyst. However, catalyst loadings of the employed chiral scandium complex are fairly high, and the system is limited to silanes with amines in α -position.

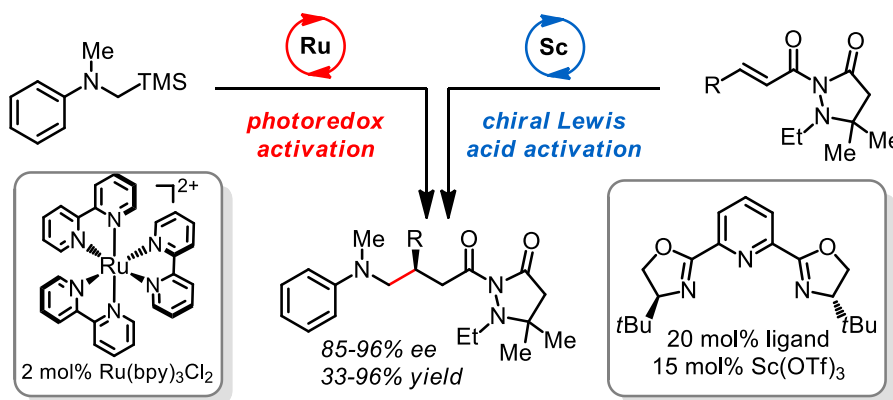


Figure 15 Yoon's dual Lewis acid/photoredox catalysis system for the enantioselective aminoalkylation of α,β -unsaturated carbonyl compounds.

One proposed mechanism is shown in Figure 16, the reaction is initiated by oxidative desilylation to generate nucleophilic α -aminoalkyl radicals, which in turn add to the coordinated alkene acceptor to yield a secondary radical intermediate. It can be expected that the scandium(III) Lewis acid activates the Michael acceptor by bidentate coordination, thereby increasing its reactivity towards the stereocontrolled addition of the nucleophilic α -aminoalkyl radical. A subsequent single electron reduction of the formed α -carbonyl radical followed by protonation provides the product and after decomplexation allows another catalytic cycle. Furthermore, it is likely that chain propagation need to be considered, since the α -silylamines not only can be oxidized by photoexcited ruthenium sensitizer, but also possible by the α -carbonyl radical intermediate.

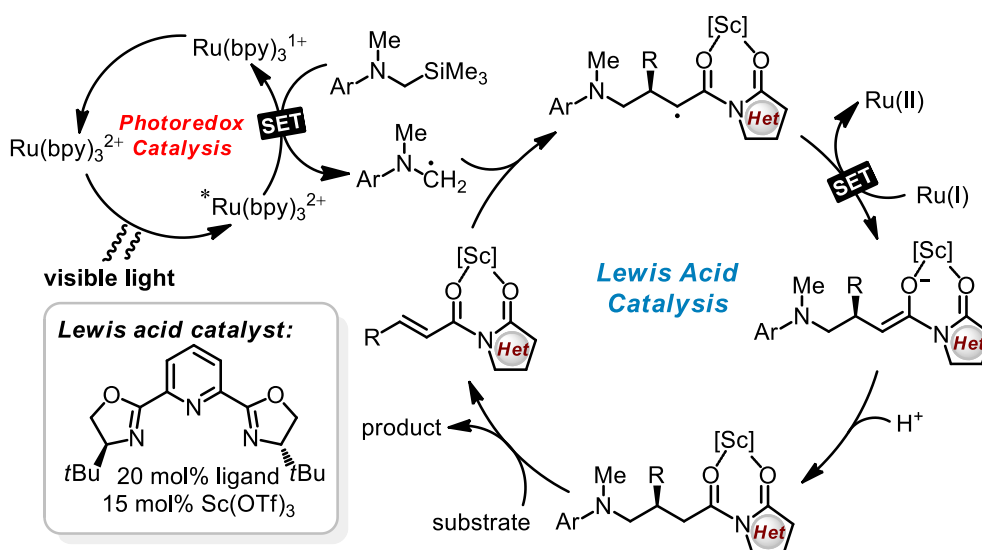


Figure 16 The proposed mechanism for Yoon's enantioselective addition of photogenerated α -amino radicals to Michael acceptors.

3) Brønsted acid catalysis

In 2013, the Knowles group reported a catalytic protocol for enantioselective aza-pinacol cyclizations (Figure 17).³¹ Accordingly, these reactions proceed through a ketyl radical intermediate, which was produced *via* a concerted proton-coupled electron transfer (PCET) event jointly induced by a chiral phosphoric acid catalyst (10 mol%) and the photosensitizer $\text{Ir(ppy)}_2(\text{dtbbpy})\text{PF}_6$ (2 mol%). The authors propose that H-bonding exists between the neutral ketyl radical and the conjugate base of the Brønsted acid. The subsequent C-C bond forming step proceeds under stereocontrol to produce *syn* 1,2-amino alcohol derivatives with 77-95% *ee*. What makes the PCET concept so attractive is the fact that proton-coupling facilitates the single electron reduction of functional groups with very negative reductive potential, and provides an opportunity to achieve asymmetric induction by using chiral

Brønsted acids.

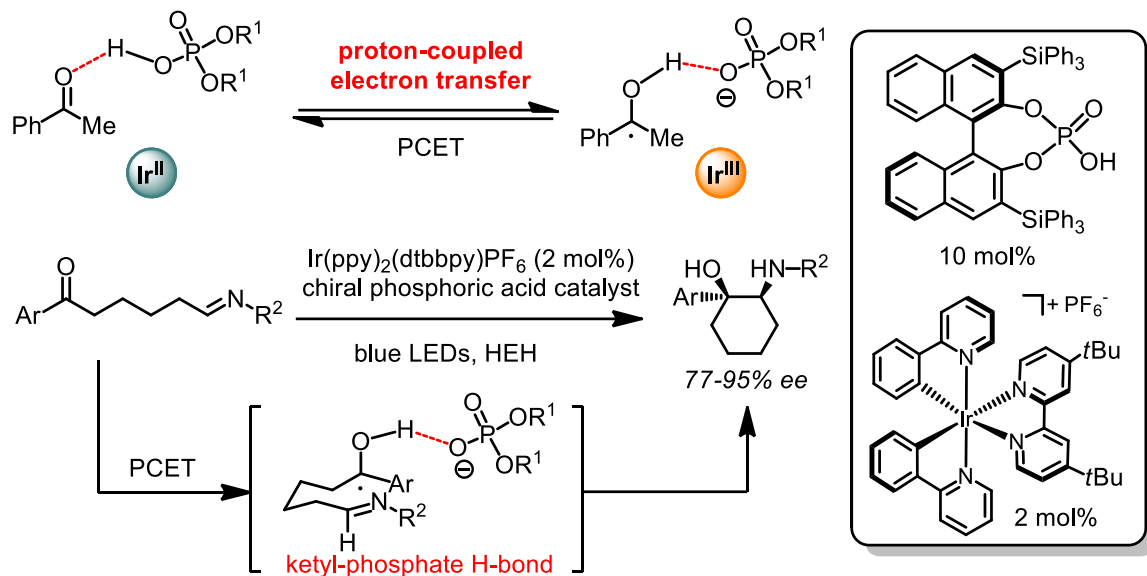


Figure 17 Knowles' asymmetric aza-pinacol cyclization by merged photoredox catalysis and chiral brønsted acid catalysis.

4) Hydrogen bonding/counterion catalysis

Stephenson and Jacobsen recently developed an approach for the oxidative, enantioselective C–H functionalization of tetrahydroisoquinoline derivatives through sequential two steps reactions (Figure 18).³² As shown, in the first step, the photoinduced oxidation with co-oxidant CCl_4 afforded the α -chloramines; In a second step in absence of light, switching the solvent to less polar MTBE at -60°C , and the addition of chiral thiourea ligand (20 mol%) resulted in the formation of counterion pair between H-bonded chloride anion and the iminium cation. The counterion catalytic addition of silyl enol ether to iminium cation provided the products with 14-72% yields and 42-99% ee.

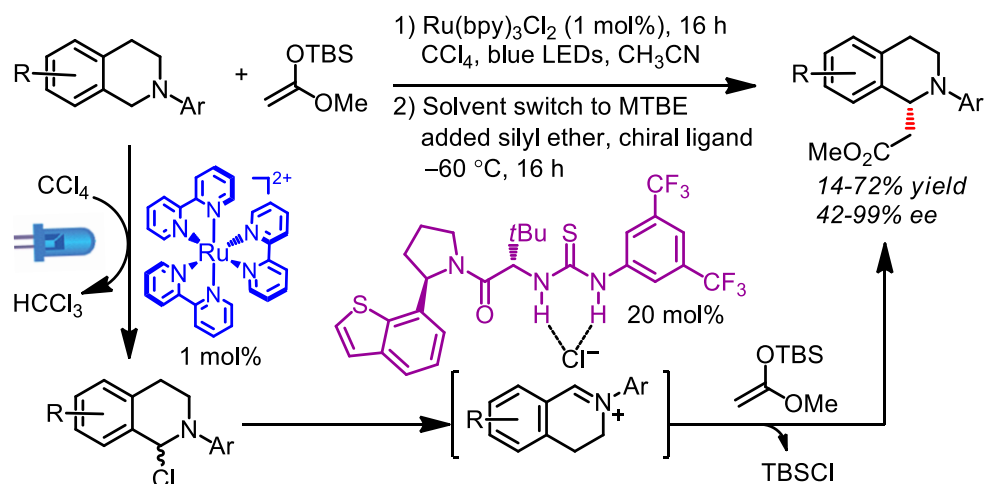


Figure 18 Asymmetric iminium nucleophilic addition *via* sequential catalysis through photoinduced oxidation followed by asymmetric counterion binding catalysis with a chiral thiourea.

5) N-Heterocyclic carbene catalysis

The Rovis group reported a catalytic asymmetric α -acylation of *N*-aryltetrahydroisoquinolines with aldehydes facilitated by the combination of chiral N-heterocyclic carbene catalysis and photoredox catalysis (Figure 19).³³ Under the irradiation by 15 W blue LEDs, the α -acylation products were produced with 51-94% yields and 61-92% *ee*.

Mechanistically, the reaction is initiated by the condensation of an N-heterocyclic carbene catalyst with aldehyde providing a nucleophilic chiral Breslow intermediate, which was trapped by the photo-oxidatively generated iminium ion. That results in an enantioselective α -acylation of *N*-aryltetrahydroisoquinolines. In the photoredox cycle, the stoichiometric *m*-dinitrobenzene (*m*-DNB) serves as an oxidative quencher of the photoexcited $\text{Ru}(\text{bpy})_3^{2+}$ and provides the sensitizer intermediate $\text{Ru}(\text{bpy})_3^{3+}$, which oxidizes the *N*-aryltetrahydroisoquinolines to the corresponding amine radical cations, followed by the hydrogen atom abstraction to afford the iminium ion. Notably, the trace oxygen existing in the reaction mixture likely acts as a terminal oxidant in the photoredox cycle.

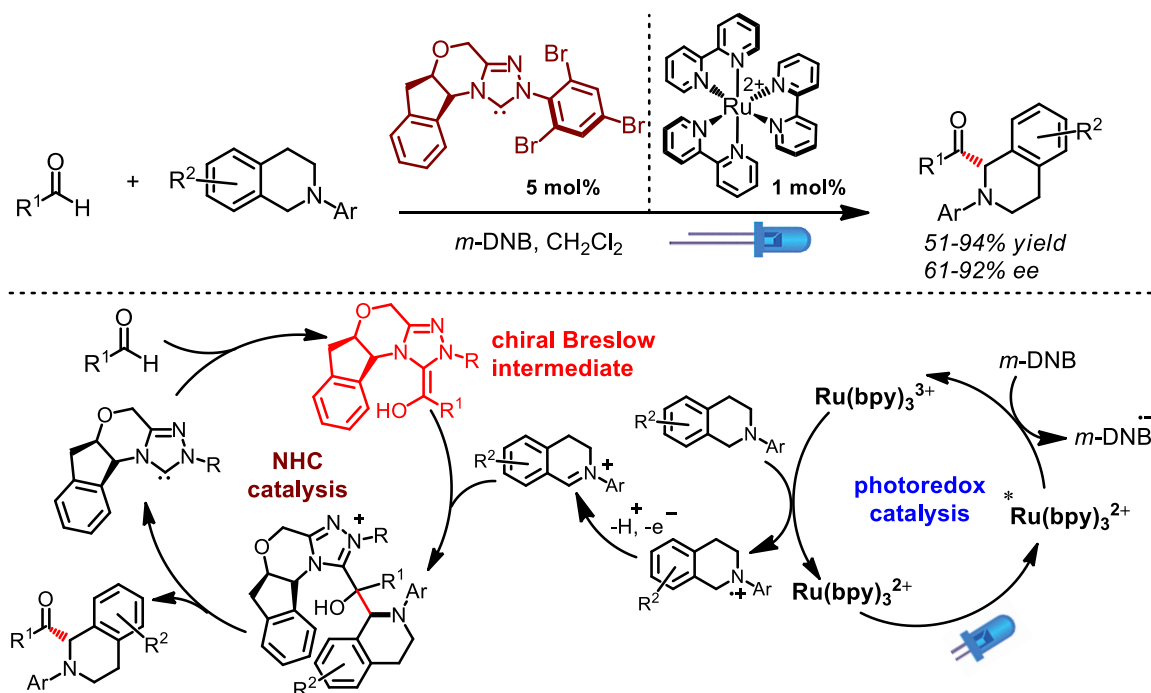


Figure 19 Rovis' asymmetric α -acylation of *N*-aryltetrahydroisoquinolines via N-heterocyclic carbene/photoredox combination.

6) Nickel catalysis

In 2014, Molander³⁴ and MacMillan³⁵ reported an impressive merger of photoredox catalysis and nickel-catalyzed cross-coupling. In the case of the Molander system, alkoxyalkyl- and benzyl trifluoroborates were capable of cross-coupling with aryl bromides under mild photoredox conditions using $\text{Ni}(\text{COD})_2$ /photosensitizer combination (Figure 20).³⁶ Interestingly, Molander and Kozlowski later demonstrated that by employing a chiral bisoxazoline ligand, this protocol can be rendered enantioselective, albeit with only modest enantioselectivities (three examples, 57-65% *ee*).³⁷ Mechanistically, the single electron oxidation of the trifluoroborate induces a fragmentation into BF_3 and an alkylradical, which is supposed to add to a chiral nickel(0) complex and leads to the formation of an alkylnickel(I) intermediate, which in turn undergoes an oxidative addition with the aryl bromide to forge a pentacoordinate chiral nickel(III) intermediate. The intermediate nickel(III) complex undergoes a rapid enantioselective reductive elimination under release of the cross-coupling product and a nickel(I) species which then takes up an electron to close the catalytic cycle.

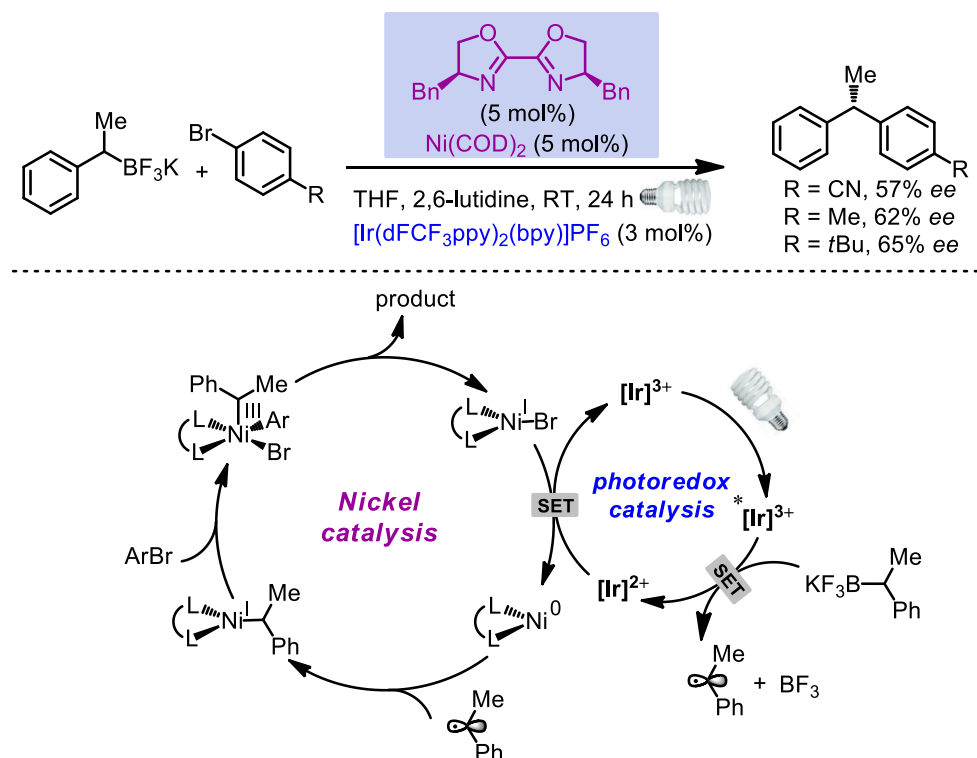


Figure 20 Molander's asymmetric cross-coupling by photoredox/nickel dual catalysis.

MacMillan and Fu later developed an asymmetric decarboxylative $\text{C}_{\text{sp}^3}\text{-C}_{\text{sp}^2}$ cross-coupling *via* the synergistic merger of photoredox and nickel catalysis (Figure 21).³⁸ Compared to Molander's system (Figure 20), the use of α -amino acids as carbon-centered radical precursors, a semicorrin-like chiral

ligand as chirality source, provided the benzylic amines with higher enantioselectivities (82-93% *ee*) under mild photoredox conditions. It is worth noting that the highlighted chiral ligand is commercially available and air stable. This enantioconvergent approach provides ready access to synthesize enantioenriched benzylic amines with low-cost α -amino acids as starting materials.

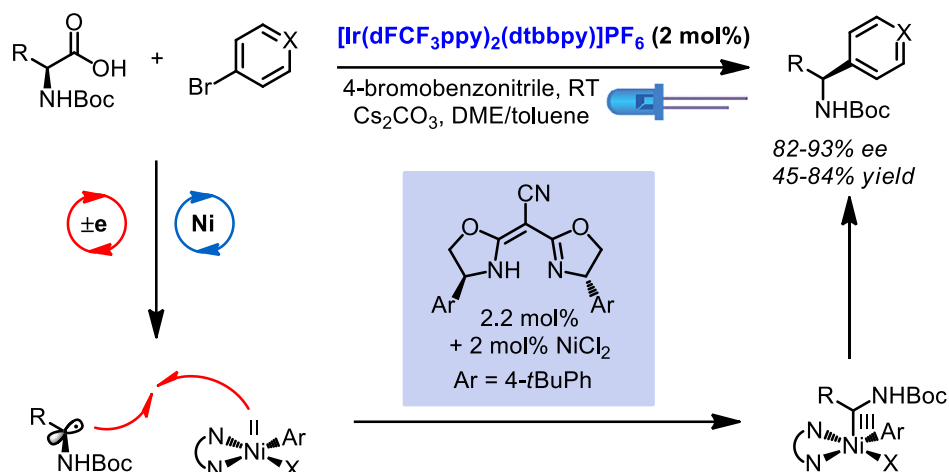


Figure 21 MacMillan and Fu's asymmetric decarboxylative cross-coupling *via* photoredox/nickel dual catalysis.

In preliminary summary, strategies recently have been developed in which efficient catalytic photochemical processes that work under stereochemical control and provide chiral molecules in an asymmetric fashion can be carried out by two catalysts that work in tandem for a single chemical transformation.⁸ In such dual-catalyzed reactions, visible light redox sensitizers are combined with asymmetric co-catalysts, such as chiral secondary amines, chiral Lewis acids, chiral Brønsted acids, chiral thiourea, chiral N-heterocyclic carbenes, or chiral nickel complexes.

The octahedral Ru^{II} and Ir^{III} complexes have proven to be well-suited as photoredox catalysts for these dual catalytic applications. Notably, the octahedral complexes themselves, though chiral, have exclusively been used in racemic form. In above instances, the metal-centered chirality has not been investigated to influence enantioselectivity of visible-light-activated reactions.³⁹

1.3.2 Single Catalyst Induced Asymmetric Photoredox Catalysis

With respect to single catalyst, apart from applications of UV light in combination with hydrogen bonding or Lewis acid interaction has been used previously in pioneering work to trigger enantioselective catalysis,⁴⁰ there have been only few instances shown as below for visible-light-induced asymmetric photoreactions in one-catalyst systems.

1) Hydrogen bonding catalysis

Recently, Bach group reported a chiral thioxanthone H-bonding organocatalyst for enantioselective [2+2] photocycloaddition reactions induced by visible light (Figure 22).⁴¹ In the presence 10 mol% of this catalyst, the [2+2] photocycloadditions of 4-(pent-4-enyl)quinolones and their heteroatom analogues proceeded with good enantioselectivities (87-94% *ee*) and high yields (79-95%). Compared to the previously established UV-light xanthone sensitizers in Bach group,⁴² thioxanthenes have a long wavelength absorption ($\lambda = 387$ nm). Accordingly, the authors proposed an H-bonding complex as the mechanistic model for the asymmetric induction and sensitization. The thioxanthone not only can serve as light-harvesting antenna and transfer the energy of the absorbed photon to the quinolones, but also provides enantioface differentiation by the planar thioxanthone moiety so that attack at the quinolone double bond occurs with good selectivity. The authors mention that the catalyst could be recovered in high yield (85±10%) after the photocatalytic experiments. However, it should be pointed out that the practical synthesis of chiral thioxanthone catalyst is limited to the separation of two enantiomers with semipreparative HPLC. This work acts as one of the few examples in which a single catalyst is capable to forge enantioenriched compounds *via* visible light activation.

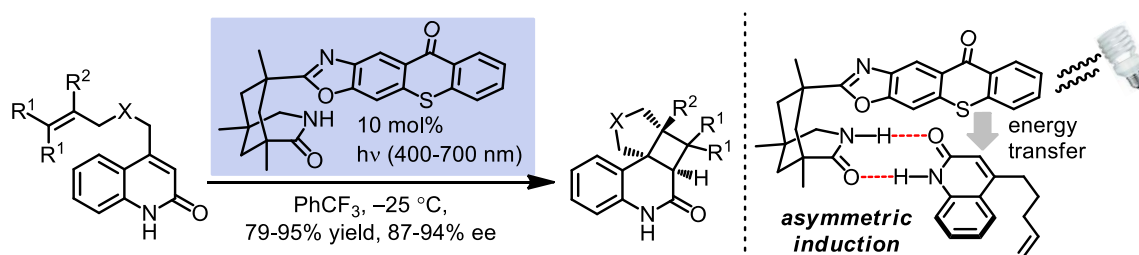


Figure 22 Bach's photoinduced asymmetric [2+2] intramolecular cycloaddition *via* energy transfer.

2) Enamine catalysis

In 2013, Melchiorre and coworkers reported that a chiral amine organocatalyst (20 mol%) can even execute the photocatalytic asymmetric α -alkylation of aldehydes with electron deficient benzyl bromides and phenacyl bromides in the absence of any external photoredox sensitizer (Figure 23).⁴³ Extensive mechanistic work demonstrated that the reactions proceed through a colored transient electron donor-acceptor (EDA) complex **III**, which is capable to absorb visible light and triggers a single electron transfer from the enamine to the organobromine (chiral radical ion pair **IV**). The proposed colored EDA complex consists of an *in situ* formed colorless electron-rich enamine (donor) and a colorless electron-deficient organobromine (acceptor). Thus, EDA formation allows SET-triggered redox neutral transformations to be performed without any external photosensitizers.

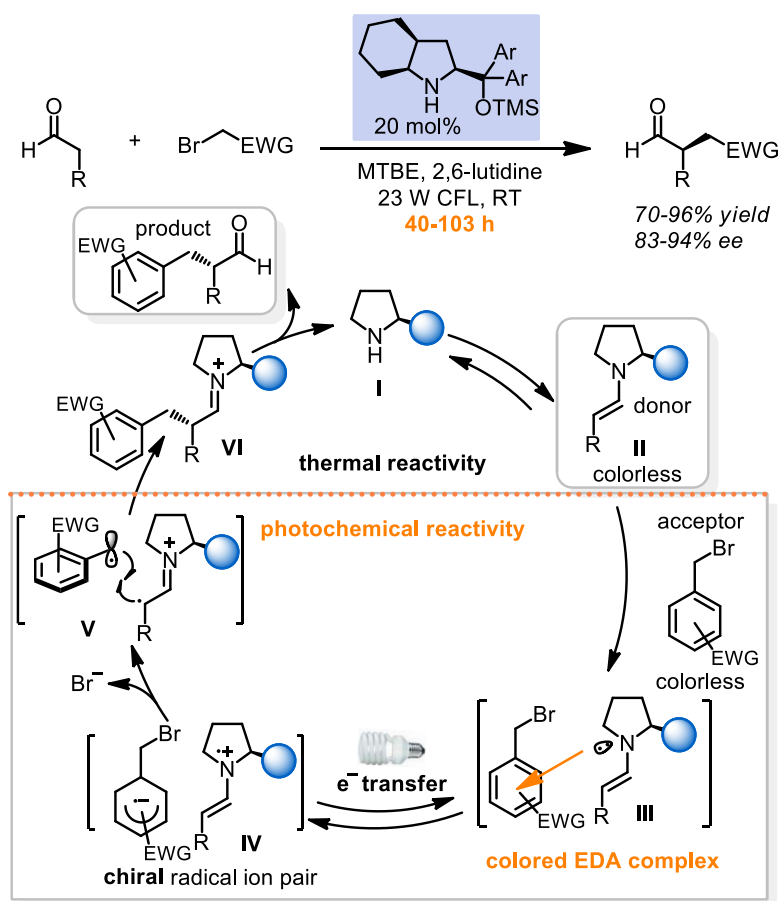


Figure 23 Melchiorre's stereoselective catalytic α -alkylation of aldehydes driven by photoactive electron donor-acceptor complex.

Notably, the proposed EDA complex formation relied on nonpolar solvent, which is unfavorable for the enamine generation, so that high amine catalyst loading is required to hold the effective concentration of *in situ* formed enamine. Compared to the enamine/photosensitizer dual catalysis

strategy (Figure 10), the enantioselectivities are slightly lower which is likely caused by the product racemization under the elongated reaction time (40-103 h). Later, the Melchiorre group extended this strategy to enantioselective α -alkylation of cyclic ketones using a quinidine-derived primary amine catalyst (Figure 24).⁴⁴ After the irradiation (3×23 W CFL) for a long time at 0 °C, the enantioenriched cyclic ketones were provided with 62-95% *ee* and 38-94% yield.

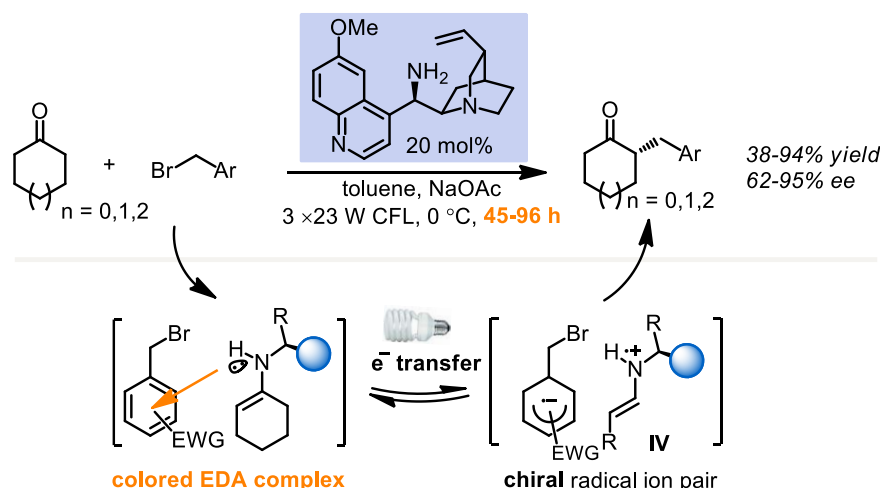


Figure 24 Melchiorre's enantioselective α -alkylation of cyclic ketones by means of photo-organocatalysis.

In a related transformation without any external photosensitizer to generate radicals through reductive fragmentation and combination with enamine catalysis, MacMillan's group reported a photoinduced asymmetric α -amination of aldehydes with 30 mol% chiral secondary amine as catalyst (Figure 25).⁴⁵ Mechanistically, the reaction is likely initiated by reduction of photoexcited 2,4-dinitrophenylsulfonyloxy-*N*-functionalized carbamates with a sacrificial amount of formed enamine to release of 2,4-dinitrophenylsulfonate anion and an (electron-deficient) *N*-centered radical. The *N*-centered radical subsequently undergoes a radical addition to the electron-rich double bond of the formed enamine intermediate. In analogy to the described mechanism in Figure 11, it is likely that the intermediate α -amino radical directly reduces another substrate dinitrophenylsulfonyloxy-*N*-functionalized carbamate, thereby triggering a chain process. Notably, the enamine intermediate and a possible EDA complex are also likely capable of absorbing sufficient visible light to induce single electron transfer.⁴⁶ These two alternative mechanistic pathways were not discussed in this work. Furthermore, it should be noted that the generation of this new developed chiral secondary amine catalyst requires the separation of two enantiomers with preparative SFC which reduces the practical value of this catalyst.

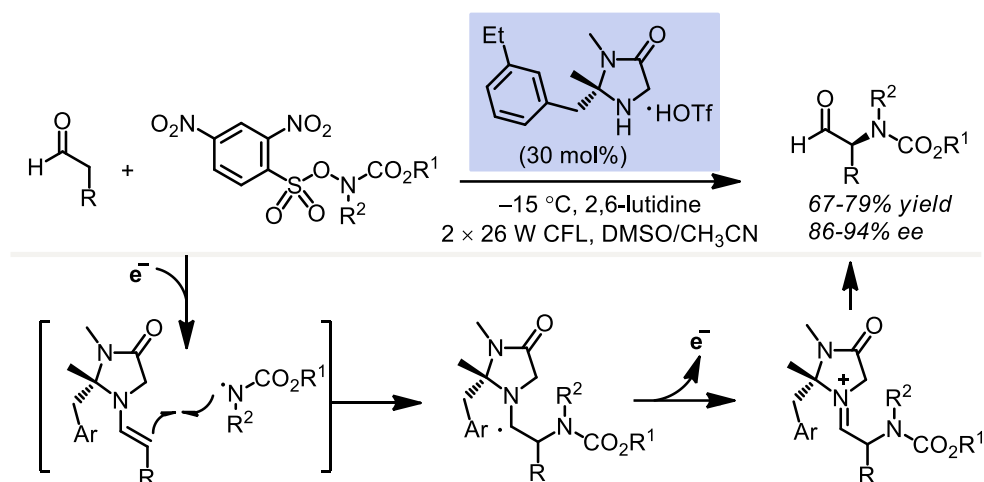


Figure 25 MacMillan's enantioselective α -amination of aldehydes *via* a photoredox mechanism.

To sum up, in single catalyst system, an enantioselective cycloaddition induced by visible light has been introduced, although not including photoinduced electron transfer but instead relying on photoinduced energy transfer. Furthermore, some special case of enamine photocatalysis has been disclosed in which transient electron donor-acceptor (EDA) complexes are capable of absorbing visible light and triggering a charge transfer. However, the photoactive EDA complex system reduces the reaction rate, requires nonpolar solvents and high catalyst loadings. Therefore, general solutions for interfacing visible light induced photoredox chemistry and asymmetric catalysis with single catalysts are highly desirable and will potentially provide new opportunities for reaction design by having a closer control over the entire reaction path including the crucial stereodiscrimination step.

1.4 Conclusions

The Meggers group developed a novel class of octahedral chiral-at-metal asymmetric catalysts. These inert, rigid metal-templated catalysts transfer chirality relying on exclusive chirality at the metal center. A key feature of these synthetic applications is the low catalyst loadings are applicable for all described asymmetric reactions, thereby surpassing the performance of most asymmetric organocatalysts. Besides hydrogen-bonding catalysts, new inert metal-templated “organocatalysts” are highly desirable to be developed through installing other achiral functional ligands around the metal center, such as amines (enamine catalysis), nucleophiles (nucleophilic catalysis), acid functional groups (Brønsted acid catalysis) or imidazolium ions (NHC carbene catalysis).

In the described instances of chiral-at-metal iridium(III) complexes promoted asymmetric reactions, the catalysis was only mediated through the ligand sphere and did not involve any direct metal coordination. In other words, these inert octahedral iridium(III) complexes have limited the nature of metal center serving as Lewis acid. Since there are not substitutionally labile ligands installed around the metal center, substrates cannot be directly activated by the metal center upon ligand exchange.

In above examples of asymmetric photoredox catalysis, the octahedral Ru^{II} and Ir^{III} complexes have been used as photoredox catalysts for photoinduced electron transfer. These racemic octahedral transition-metal complexes have promoted the dual catalytic applications in which the photosensitizer is combined with a second, stereocontrolling catalyst. The few successes in single catalyst induced asymmetric photoreactions profoundly relied on amine catalysts and were restricted to high catalyst loadings (20-30 mol%). These significant efforts have proven the design of catalysts that promote highly enantioselective photoreactions is still a challenging goal.

Considering that the prototypical Ru^{II} and Ir^{III} photoredox catalysts are chiral octahedral complexes, but typically used only as racemates, it is rational to assume that Meggers' chiral-at-metal iridium(III) complexes can also be competent visible-light photoredox catalysts. The development of chiral-at-metal iridium(III) complexes would provide new opportunities to realize highly efficient asymmetric photoredox catalysis with single chiral-at-metal complexes.

References

- 1 P. J. Walsh, M. C. Kozlowski, *Fundamentals of Asymmetric Catalysis*, University Science Books: Sausalito, CA, 2009.
- 2 (a) K. Zeitler, *Angew. Chem. Int. Ed.* **2009**, *48*, 9785–9789. (b) J. M. R. Narayanam, C. R. J. Stephenson, *Chem. Soc. Rev.* **2011**, *40*, 102–113. (c) C. K. Prier, D. A. Rankic, D. W. C. MacMillan, *Chem. Rev.* **2013**, *113*, 5322–5363. (d) D. M. Schultz, T. P. Yoon, *Science* **2014**, *343*, 1239176.
- 3 K. L. Skubi, T. P. Yoon, *Nature* **2014**, *515*, 45–46.
- 4 L. Gong, L.-A. Chen, E. Meggers, *Angew. Chem. Int. Ed.* **2014**, *53*, 10868–10874.
- 5 S. Mukherjee, J. W. Yang, S. Hoffmann, B. List, *Chem. Rev.* **2007**, *107*, 5471–5569.
- 6 M. S. Taylor, E. N. Jacobsen, *Angew. Chem. Int. Ed.* **2006**, *45*, 1520–1543.
- 7 T. Akiyama, J. Itoh, K. Fuchibe, *Adv. Synth. Catal.* **2006**, *348*, 999–1010.
- 8 D. Enders, O. Niemeier, A. Henseler, *Chem. Rev.* **2007**, *107*, 5606–5655.
- 9 I. T. Raheem, P. S. Thiara, E. A. Peterson, E. N. Jacobsen, *J. Am. Chem. Soc.* **2007**, *129*, 13404–13405.
- 10 S. Shirakawa, K. Maruoka, *Angew. Chem. Int. Ed.* **2013**, *52*, 4312–4348.
- 11 (a) R. Noyori, *Angew. Chem. Int. Ed.* **2002**, *41*, 2008–2022. (b) W. S. Knowles, *Angew. Chem. Int. Ed.* **2002**, *41*, 1998–2007.
- 12 For reviews on chiral-at-metal complexes in catalysis, see: (a) H. Brunner, *Angew. Chem. Int. Ed.* **1999**, *38*, 1194–1208. (b) M. Fontecave, O. Hamelin, S. Ménage, *Top. Organomet. Chem.* **2005**, *15*, 271–288. (c) E. B. Bauer, *Chem. Soc. Rev.* **2012**, *41*, 3135–3167. (d) Z.-Y. Cao, W. D. G. Brittain, J. S. Fossey, F. Zhou, *Catal. Sci. Technol.* **2015**, *5*, 3441–3451.
- 13 M. Schmittle, A. Burghart, *Angew. Chem. Int. Ed. Engl.* **1997**, *36*, 2550–2589.
- 14 D. P. Curran, N. A. Porter, B. Giese, *Stereochemistry of Radical Reactions: Concepts, Guidelines and Synthetic Applications*, VCH, 1996.
- 15 M. Chavarot, S. Ménage, O. Hamelin, F. Charnay, J. Pécaut, M. Fontecave, *Inorg. Chem.* **2003**, *42*, 4810–4816.
- 16 For octahedral chiral-at-metal complexes as inducers of asymmetric autocatalysis, see: (a) I. Sato, K. Kadowaki, Y. Ohgo, K. Soai, H. Ogino, *Chem. Commun.* **2001**, 1022–1023. (b) T. Kawasaki, T.

- Omine, M. Sato, Y. Morishita, K. Soai, *Chem. Lett.* **2007**, 36, 30–31.
- 17 C. Ganzmann, J. A. Gladysz, *Chem. Eur. J.* **2008**, 14, 5397–5400.
- 18 (a) E. Meggers, *Chem. Eur. J.* **2010**, 16, 752–758. (b) L. Gong, M. Wenzel, E. Meggers, *Acc. Chem. Res.* **2013**, 46, 2635–2644.
- 19 (a) L.-A. Chen, W. Xu, B. Huang, J. Ma, L. Wang, J. Xi, K. Harms, L. Gong, E. Meggers, *J. Am. Chem. Soc.* **2013**, 135, 10598–10601. (b) L.-A. Chen, X. Tang, J. Xi, W. Xu, L. Gong, E. Meggers, *Angew. Chem. Int. Ed.* **2013**, 52, 14021–14025.
- 20 J.-J. Ma, X.-B. Ding, Y. Hu, Y. Huang, L. Gong, E. Meggers, *Nat. Commun.* **2014**, 5, 5531.
- 21 D. A. Evans, K. R. Fandrick, H.-J. Song, *J. Am. Chem. Soc.* **2005**, 127, 8942–8943.
- 22 It is noteworthy that chiral coordinating ligands may induce metal-centered chirality within asymmetric catalysts. See, for example: (a) T. Ohta, H. Takaya, R. Noyori, *Inorg. Chem.* **1988**, 27, 566–569. (b) M. T. Ashby, M. A. Khan, J. Halpern, *Organometallics* **1991**, 10, 2011–2015.
- 23 E. Meggers, *Chem. Commun.* **2015**, 51, 3290–3301.
- 24 For recent reviews on dual photoredox catalysis, see: (a) M. N. Hopkinson, B. Sahoo, J.-L. Li, F. Glorius, *Chem. Eur. J.* **2014**, 20, 3874. (b) K. L. Skubi, T. R. Blum, T. P. Yoon, *Chem. Rev.* **2016**, DOI: 10.1021/acs.chemrev.6b00018.
- 25 D. A. Nicewicz, D. W. C. MacMillan, *Science* **2008**, 322, 77–80.
- 26 M. A. Cismesia, T. P. Yoon, *Chem. Sci.* **2015**, 6, 5426–5434.
- 27 (a) M. Neumann, S. Földner, B. König, K. Zeitler, *Angew. Chem. Int. Ed.* **2011**, 50, 951–954. (b) M. Cherevatskaya, M. Neumann, S. Földner, C. Harlander, S. Kümmel, S. Dankesreiter, A. Pfizner, K. Zeitler, B. König, *Angew. Chem. Int. Ed.* **2012**, 51, 4062–4066. (c) P. Riente, A. Matas Adams, J. Albero, E. Palomares, M. A. Pericàs, *Angew. Chem. Int. Ed.* **2014**, 53, 9613–9616.
- 28 Y. Zhu, L. Zhang, S. Luo, *J. Am. Chem. Soc.* **2014**, 136, 14642–14645.
- 29 J. Du, K. L. Skubi, D. M. Schultz, T. P. Yoon, *Science* **2014**, 344, 392–396.
- 30 L. R. Espelt, I. S. McPherson, E. M. Wiensch, T. P. Yoon, *J. Am. Chem. Soc.* **2015**, 137, 2452–2455.
- 31 (a) L. J. Rono, H. G. Yayla, D. Y. Wang, M. F. Armstrong and R. R. Knowles, *J. Am. Chem. Soc.* **2013**, 135, 17735–17738. (b) H. G. Yayla, R. R. Knowles, *Synlett* **2014**, 25, 2819–2826.
- 32 G. Bergonzini, C. S. Schindler, C.-J. Wallentin, E. N. Jacobsen, C. R. J. Stephenson, *Chem. Sci.* **2013**, 5, 112–116.

- 33 D. A. DiRocco, T. Rovis, *J. Am. Chem. Soc.* **2012**, *134*, 8094–8097.
- 34 J. C. Tellis, D. N. Primer, G. A. Molander, *Science* **2014**, *345*, 433–436.
- 35 Z. Zuo, D. T. Ahneman, L. Chu, J. A. Terrett, A. G. Doyle, D. W. C. MacMillan, *Science* **2014**, *345*, 437–440.
- 36 (a) D. N. Primer, I. Karakaya, J. C. Tellis, G. A. Molander, *J. Am. Chem. Soc.* **2015**, *137*, 2195–2198. (b) I. Karakaya, D. N. Primer, G. A. Molander, *Org. Lett.* **2015**, *17*, 3294–3297.
- 37 O. Gutierrez, J. C. Tellis, D. N. Primer, G. A. Molander, M. C. Kozlowski, *J. Am. Chem. Soc.* **2015**, *137*, 4896–4899.
- 38 Z. Zuo, H. Cong, W. Li, J. Choi, G. C. Fu, D. W. C. MacMillan, *J. Am. Chem. Soc.* **2016**, *138*, 1832–1835.
- 39 For a rare example, see: T. Hamada, H. Ishida, S. Usui, Y. Watanabe, K. Tsumura, K. Ohkubo, *J. Chem. Soc. Chem. Commun.* **1993**, 909–911.
- 40 (a) A. Bauer, F. Westkämper, S. Grimme, T. Bach, *Nature* **2005**, *436*, 1139–1140. (b) C. Müller, A. Bauer, T. Bach, *Angew. Chem. Int. Ed.* **2009**, *48*, 6640–6642. (c) R. Brimioulle, T. Bach, *Science* **2013**, *342*, 840–843.
- 41 R. Alonso, T. Bach, *Angew. Chem. Int. Ed.* **2014**, *53*, 4368–4371.
- 42 (a) C. Müller, A. Bauer, T. Bach, *Angew. Chem. Int. Ed.* **2009**, *48*, 6640–6642. (b) H. Guo, E. Herdtweck, T. Bach, *Angew. Chem. Int. Ed.* **2010**, *49*, 7782–7785. (c) C. Müller, A. Bauer, M. M. Maturi, M. C. Cuquerella, M. A. Miranda, T. Bach, *J. Am. Chem. Soc.* **2011**, *133*, 16689–16697. (d) S. C. Coote, T. Bach, *J. Am. Chem. Soc.* **2013**, *135*, 14948–14951. (e) R. Brimioulle, T. Bach, *Science* **2013**, *342*, 840–843.
- 43 E. Arceo, I. D. Jurberg, A. Álvarez-Fernández, P. Melchiorre, *Nature Chem.* **2013**, *5*, 750–756.
- 44 E. Arceo, A. Bahamonde, G. Bergonzini, P. Melchiorre, *Chem. Sci.* **2014**, *5*, 2438–2442.
- 45 G. Cecere, C. M. König, J. L. Alleva, D. W. C. MacMillan, *J. Am. Chem. Soc.* **2013**, *135*, 11521–11524.
- 46 M. Silvi, E. Arceo, I. D. Jurberg, C. Cassani, P. Melchiorre, *J. Am. Chem. Soc.* **2015**, *137*, 6120–6123.

Chapter 2: Aim of the Work

The overall aim of this work is to develop new type of chiral-at-metal octahedral asymmetric catalysts and investigate their thermal and photochemical reactivities. The aim of this work contains the following three parts.

2.1 Development and non-photochemical application of metal-templated chiral-at-metal enamine/H-bonding dual catalyst

Recently, our group has reported octahedral chiral-at-metal iridium(III) complexes as low-loading asymmetric hydrogen bonding catalysts.¹ We wish to expand the metal-templated chiral-at-metal technology from H-bonding catalysis to other modes of organocatalysis. The dual activation by multifunctional catalysts has emerged as a powerful concept for the design of high performance asymmetric metal-based catalysts and asymmetric organocatalysts.² A typical bifunctional catalyst interacts with both the nucleophile and electrophile (dual activation) through at least overall two functional groups (bi- or multifunctional catalysis). However, although appealing as a concept, the design of high performance multifunctional catalysts remains challenging since it relies on a distinct positioning of carefully chosen functional groups within the chiral catalyst template in order to gain a maximum advantage from functional group cooperativity. Hence, one can assume that most multifunctional, dual activation catalysts do not reach the theoretically possible rate acceleration and asymmetric induction.

We hypothesize that inert octahedral metal complexes are general, powerful templates for the efficient design of multifunctional catalysts since octahedral stereocenters allow the straightforward construction of molecular entities with high shape and stereochemical complexity. Herein, we try to develop a chiral-at-metal octahedral iridium(III) complex which can serve as a scaffold for the straightforward rational design of asymmetric enamine/H-bonding dual activation catalyst.

2.2 Development and non-photochemical application of chiral-at-metal

Lewis acid catalyst

Metal-based asymmetric synthesis profoundly relies on organic ligands with point or axial chirality, or both.³ The Meggers group has demonstrated that chiral-only-at-metal iridium(III) complexes are capable to mediate the asymmetric induction effectively with exclusive metal-centered chirality. However, in these examples, catalysis was exclusively mediated through the ligand sphere without any direct interaction between the metal center and a substrate. On the other hand, direct metal coordination poses a highly attractive mode of activation. One goal was therefore to expand chiral-at-metal catalysis from merely metal-templated catalysis to catalysis involving reactive metal complexes.

We here wish to develop a substitutionally labile (reactive) yet configurational stable chiral-at-metal iridium(III) Lewis acid catalyst. In the design, the chiral metal center serves the dual function of activating a substrate by metal coordination and at the same time provides the required asymmetric induction. The chirality of the Lewis acid entirely relies on achiral ligands in the coordination sphere. A considerable challenge with respect to these highly desirable features is the potential racemization of the metal complexes. Therefore, the synthesis and stability of such chiral-at-metal Lewis acids will be carefully investigated. Finally, a suitable model reaction will be performed in presence of the newly developed catalyst to verify the viability of this approach.

2.3 Development of catalytic enantioselective photoredox catalysis with chiral-at-metal complexes

The widespread use of octahedral Ir(III) and Ru(II) complexes as photosensitizers can be directly attributed to their ability of visible light absorption going along with an electronic excitation. Such complexes are typically used in racemic form and do not influence the enantioselectivities of the photoreactions.⁴ We here intend to realize the visible-light-activated asymmetric catalysis with newly developed chiral-at-metal complexes. In such a theme, the chiral complex serves both as a photosensitizer to induce redox chemistry in the presence of light and at the same time as an

asymmetric catalyst. An array of well established asymmetric photoreactions based on dual catalysis strategies will be chosen as model reactions to confirm the viability, such as the alkylation of ketones with various electron-deficient electrophiles, namely the visible-light-driven benzylation, trichloromethylation, perfluoroalkylation; and the Michael addition of stabilized alkyl radicals to electron-deficient alkenes.

Several considerable challenges need to be addressed for this strategy. First, the stability of chiral-at-metal complexes under visible light irradiation needs to be investigated, in particular, the possible racemization of the catalyst needs to be excluded. Second, the structural optimization of the catalyst will impact both enantioselectivity and photophysical properties at the same time. Third, the complicated mechanisms of redox chemistry require detailed mechanistic studies to provide insights for reaction optimization. Furthermore, non-photochemical (closed-shell) alternative reactions need to be considered and model reactions should be selected where redox catalysis is highly advantageous or even required.

References:

- 1 (a) L.-A. Chen, W. Xu, B. Huang, J. Ma, L. Wang, J. Xi, K. Harms, L. Gong, E. Meggers, *J. Am. Chem. Soc.* **2013**, *135*, 10598–10601. (b) L.-A. Chen, X. Tang, J. Xi, W. Xu, L. Gong, E. Meggers, *Angew. Chem. Int. Ed.* **2013**, *52*, 14021–14025.
- 2 P. J. Walsh, M. C. Kozlowski, *Fundamentals of Asymmetric Catalysis*, University Science Books: Sausalito, CA, 2009.
- 3 X. Su, *J. Am. Chem. Soc.* **2014**, *136*, 3321–3321.
- 4 (a) C. K. Prier, D. A. Rankic, D. W. C. MacMillan, *Chem. Rev.* **2013**, *113*, 5322–5363. (b) M. N. Hopkinson, B. Sahoo, J.-L. Li, F. Glorius, *Chem. Eur. J.* **2014**, *20*, 3874. (c) K. L. Skubi, T. R. Blum, T. P. Yoon, *Chem. Rev.* **2016**, DOI: 10.1021/acs.chemrev.6b00018.

Chapter 3: Results and Discussion

Part I: Non-Photochemical Asymmetric Catalysis with a Metal-Templated “Organocatalyst”

3.1 Metal-Templated Asymmetric Enamine/H-Bonding Dual Catalysis

3.1 Metal-Templated Asymmetric Enamine/H-Bonding Dual Catalysis

3.1.1 Catalyst Design and Synthesis

Recently, the Meggers group has established that octahedral chiral-at-metal iridium(III) complexes are exceptionally effective asymmetric catalysts for hydrogen bonding catalysis.¹⁻² Herein, a class of chiral-at-metal octahedral iridium(III) complex was rationally designed to serve as a scaffold for asymmetric enamine/H-bonding dual catalysis (Figure. 26). Traditional enamine/H-bonding organocatalysts have been widely developed for enantioselective α -functionalizations of aldehydes, in which the H-bond donor directs the *Re* face approach of electrophile ($A=B$) and at the same time serving as sterically directing group facilitates the formations of (*E*)-anti enamine.³ In this metal-templated setup, an achiral ligand containing a secondary amine is installed around the chiral metal center, which is anticipated to result in the formation of a configurationally inert bis-cyclometalated octahedral complex. There are several factors that seem of particular importance in developing such a metal-templated bifunctional catalyst. First, the coordinated amine ligand must be capable of forming enamine with aldehydes. Second, only one configuration of enamine is favorable to be produced through the steric control of ligand sphere. Third, one of H-bonding donors (XH) needs to be an appropriate distance from the secondary amine moiety to allow for a proper positioning of the approaching electrophile in relation to the enamine intermediate. Finally, the H-bonding directing group must be capable of efficient activation of different electrophiles.

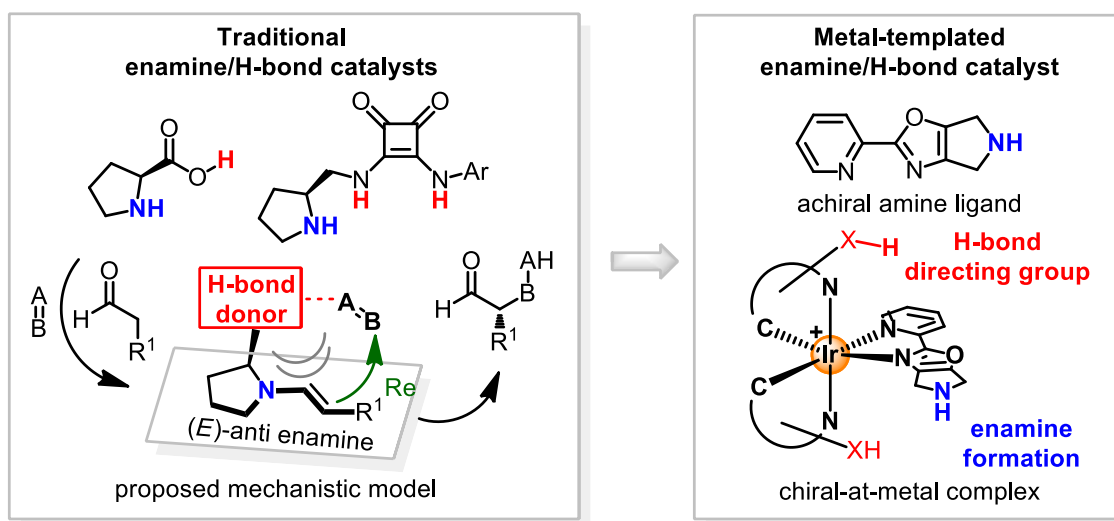


Figure 26 Organic versus metal-templated (this study) bifunctional asymmetric enamine catalysts for enantioselective α -functionalizations of aldehydes.

To confirm the viability of this metal-templated strategy, five bis-cyclometalated octahedral iridium(III) complexes Λ -**Ir1-5** have been devised for the reaction development (Figure 27).⁴ In these designs, a coordinated 2-pyridyl-5,6-dihydro-4*H*-pyrrolo[3,4-*d*][1,3]oxazole ligand contains a secondary amine for performing enamine catalysis (nucleophile activation). In order to use the ready methods for the synthesis of cyclometalating ligands,⁵ a simple hydroxyl (Λ -**Ir1**) or hydroxymethyl substituent (Λ -**Ir2-4**) at the 5-position of the benzoxazole ligands is selected to serve as a potential hydrogen bonding donor for the activation and positioning of an electrophile (electrophile activation). By comparison of Λ -**Ir1** (hydroxyl as H-bond donor) and Λ -**Ir2** (hydroxymethyl as H-bond donor), the effects of the positioning of H-bonding donors can be evaluated. Λ -**Ir5** would verify whether the hydrogen bonding activation exists in the catalytic cycle. While the sterically directing group **R** at the 5-position of metalated phenyl group is envisioned to direct the enamine conformation. Whether this steric hindrance is required or not, which can be figured out by comparison of Λ -**Ir2** and Λ -**Ir3**. If it is essential for the satisfactory asymmetric induction, the catalysts Λ -**Ir3** and Λ -**Ir4** would provide significant insights for intuitional optimization.

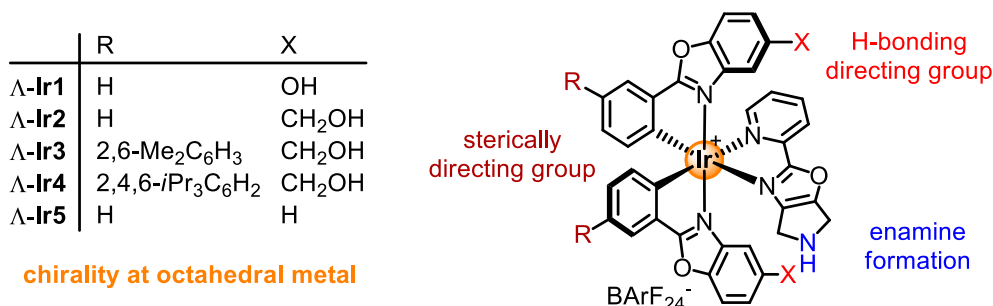
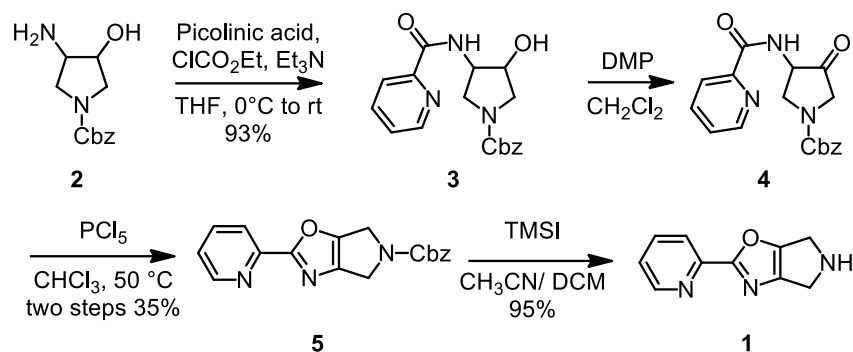


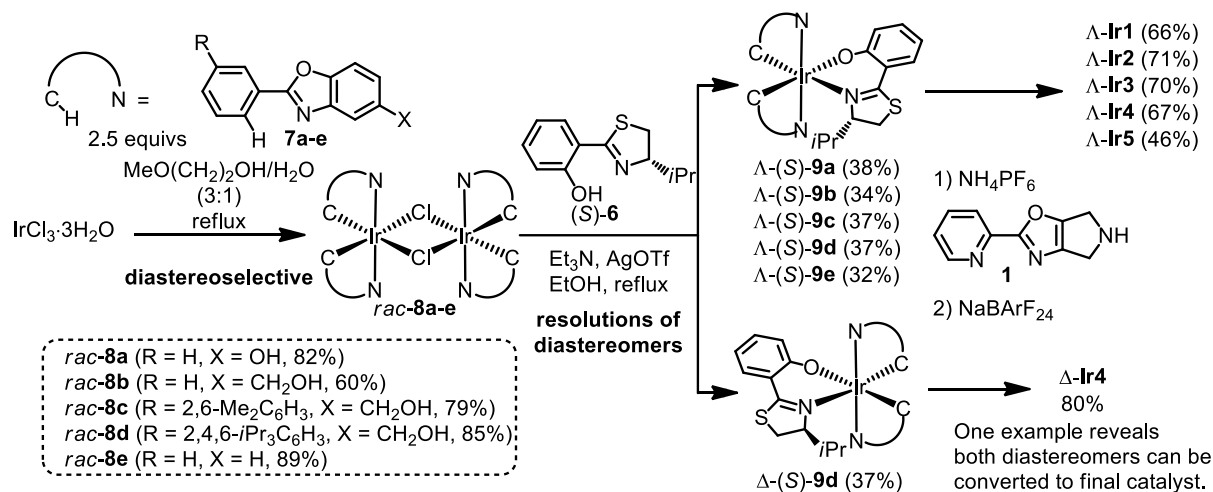
Figure 27 Metal-templated chiral-at-metal enamine/H-bonding catalysts.

With the design of metal-templated enamine/H-bonding catalyst completed, the synthesis of Λ -**Ir1-5** is initiated. The secondary amine ligand **1** was synthesized according to a reported method (Scheme 1).⁶ Cbz-protected amino alcohol **2** was coupled with picolinic acid to afford amide-alcohol **3** in 93% yield. Oxidation with Dess-Martin oxidant provided the ketone **4**, which was unstable on silica gel column. After simple workup by washing with NaOH aqueous solution, the crude product **4** was cyclized using phosphorus pentachloride to afford oxazolopyrrolidine **5**. Deprotection of the Cbz group to yield the secondary amine ligand **1** was achieved using the strong Lewis acid trimethylsilyl iodide. Notably, the typical palladium catalytic hydrogenation for the removal of Cbz is not applicable for this system, since palladium catalyst poisoning can be caused by *N,N*-bidentate coordination.



Scheme 1 Synthesis of secondary amine ligand (**1**).

With the secondary amine ligand **1** in hand, the synthesis of chiral-at-metal dual activation iridium(III) catalysts was investigated. The Meggers group previously developed a synthetic strategy¹ for the generation of enantiomerically pure iridium(III) complexes which relies on the use of (*S*)-4-isopropyl-2-(2'-hydroxyphenyl)-2-thiazoline **6** as a chiral auxiliary. As described in Scheme 2, racemic iridium(III) precursor complexes *rac*-**8a-e** were converted to diastereomeric iridium complexes, then resolved into single diastereomers by flash silica gel column chromatography, and followed by an acid-induced substitution of the auxiliary under complete retention of configuration to afford the enantiomerically pure iridium complexes.⁷



Scheme 2 Outline of the synthesis of the enantiomerically pure catalysts Δ -**Ir1-5** and Δ -**Ir4**. NaBARF_{24} = sodium tetrakis[(3,5-di-trifluoromethyl)phenyl]borate.

Cyclometalated iridium(III) μ -chloro-bridged dimers *rac*-**8a-e** and its derivatives were synthesized according to published procedure,⁸ which involves refluxing $\text{IrCl}_3 \cdot n\text{H}_2\text{O}$ with 2.0–2.5 equivs of cyclometalating ligand in a 3:1 mixture of 2-methoxyethanol and water. Accordingly, the corresponding substituted benzoxazole ligand was added to iridium chloride in a mixture of methoxyethanol/water (3:1). The reaction mixture was heated at reflux (120°C) for 24 h. The resulting

precipitate was collected by centrifugation, washed with diethyl ether and dried to yield the iridium dimer complexes *rac*-**8a-e** as a yellow powder (60-89% crude yield), which were used without further purification. The subsequent reaction of chiral thiazoline auxiliary (*S*)-**6** with dimer complexes afforded iridium(III) complexes Λ -(*S*)-**9a-e** (32-38% yield) and Δ -(*S*)-**9d** (37% yield) as a mixture of diastereomers, which can be resolved and isolated by silica gel chromatography on 500 mg scale.

The separated diastereomers Λ -(*S*)-**9a-e** or Δ -(*S*)-**9d** reacted with secondary amine **1** in the presence of the weak acid NH_4PF_6 to afford the enantiopure iridium catalysts Λ -**Ir1-5** (46-71% yield) or Δ -**Ir4** (80% yield) after counterion exchange. The bulky BArF_{24} anion was used to improve the solubility of the iridium catalysts in nonpolar solvents which are favorable for hydrogen bonding catalysis. The counterion exchange experiments were performed in Et_2O in the presence of 1.0 equivalent NaBArF_{24} (sodium tetrakis[(3,5-di-trifluoromethyl)phenyl]borate) providing the BArF_{24} salt in quantitative yield. Whereas the similar procedures in other solvents (DCM, toluene, CH_3CN) afforded a mixture complexes of $\text{BArF}_{24}/\text{PF}_6$ salts. The absolute configurations of the obtained Λ -configured iridium(III) complexes were verified by CD spectroscopy in analogy to reported complexes.¹ The enantiomeric purities of Λ -**Ir4** and Δ -**Ir4** have been verified by chiral HPLC analysis (> 99% *ee*).

3.1.2 Reaction Development

The reaction development was initiated by screening the reactions which have been well established for α -functionalizations of aldehydes with the typical enamine/H-bonding organocatalysts (Figure 28).³ Disappointingly, in the presence of 4 mol% newly developed Λ -**Ir1**, reacting the aldehyde **1a** with different electrophiles, the desired conjugate addition product (β -Nitrostyrene **11a** as electrophile), hydroxyamination product (nitrosobenzene **11b** as electrophile) and the Mannich reaction product (N-PMP imine **11c** as electrophile) were not afforded by the corresponding reactions. For the hydroxyamination reaction, the electrophile nitrosobenzene **11b** was consumed rapidly (1.5 h) and some unidentified compounds were formed. Switching the temperature to 0 °C or -20 °C, did not provide any improved results. Encouragingly, when the azodicarboxylate was chosen as the electrophile, the configurationally stable amination product *N*-(benzyloxycarbonylamino)oxazolidinone (*S*)-**12a** was obtained after in situ reduction with NaBH_4 and NaOH-induced cyclization in 91% yield and with encouraging 22% *ee*. Notably, to avoid partial

racemisation of the initially formed sensitive α -hydrazino aldehydes, enantioselectivities were determined after aldehyde reduction and subsequent base induced cyclization. Therefore, the direct catalytic α -amination of aldehydes was chosen as a model reaction with azodicarboxylates as the electrophile.⁹

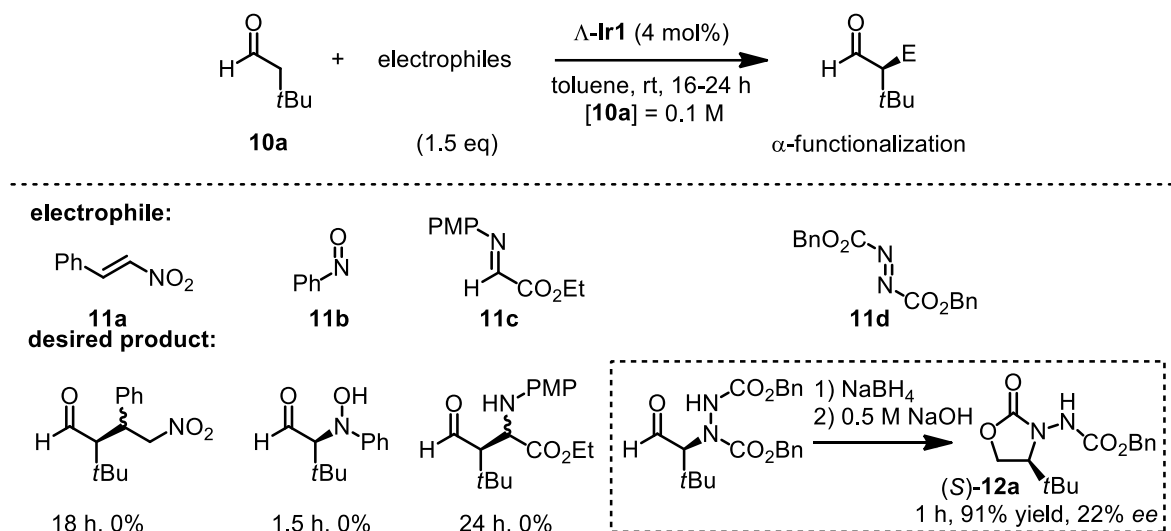


Figure 28 Attempts toward the α -functionalizations of aldehydes with the newly developed metal-templated catalyst $\Lambda\text{-Ir1}$.

The further optimizations toward the α -amination of aldehydes are detailed in Table 1. Accordingly, when aldehyde **10a** reacted with dibenzyl azodicarboxylate **11d** in toluene at 0 °C in the presence of 4 mol% of $\Lambda\text{-Ir1}$, (S)-**12a** was produced with an improved enantioselectivity of 31% *ee* (Table 1, entry 1). A repositioning of the hydrogen-bond donor by replacing the phenolic OH by a hydroxymethyl group slightly improved the *ee* value to 39% ($\Lambda\text{-Ir2}$; Table 1, entry 2). Considering that the low enantiodifferentiation might be the result of a missing discrimination between the two possible enamine conformations upon reaction of the secondary amine of $\Lambda\text{-Ir2}$ with aldehyde **12a**, so that the introduction of steric hindrance at the 5-position of the metalated phenyl group would provide the necessary bias towards a single enamine conformation. Indeed, $\Lambda\text{-Ir3}$, containing a 2,6-Me₂Ph substituent at the 5-position of the metalated phenyl group provided oxazolidinone (S)-**12a** with a significantly improved *ee* value of 65% (Table 1, entry 3). Increasing this steric hindrance with the more bulky 2,4,6-*i*Pr₃Ph substituent ($\Lambda\text{-Ir4}$) further improved the enantioselectivity to 97% *ee* at a yield of 96% with 4 mol% of $\Lambda\text{-Ir4}$ (Table, entry 4). Even with a reduced catalyst loading of 1 mol% $\Lambda\text{-Ir4}$, the oxazolidinone (S)-**12a** was obtained with 91% *ee* at room temperature (Table 1, entry 5). Finally, upon optimization of the reaction conditions by increasing the concentrations of aldehyde **10a**

(1.5 M) and azodicarboxylate **11d** (1.0 M), the reaction time was significantly decreased while improving the enantiodifferentiation to 97% *ee* with 1 mol% Λ -**Ir4** (entry 6). Gladly, under these conditions, the catalyst loading could be decreased further down to 0.2 mol% (entry 7) and even 0.1 mol% (entry 8) while retaining satisfactory enantioselectivities of 94% and 91% *ee*, respectively.

Table 1 Development of a chiral-at-metal iridium(III) catalyst for the enantioselective α -amination of aldehydes with azodicarboxylates^a

Reaction scheme: Aldehyde **10a** (4-oxopentanal) reacts with azodicarboxylate **11d** (di-*n*-butyl azodicarboxylate) under the following conditions: 1.) Λ -**Ir1-5** (cat), toluene; 2.) NaBH₄, MeOH, 0 °C; 3.) 0.5 M NaOH. The product is (S)-**12a**, a 2-*n*-butyloxazolidinone derivative.

Entry	Cat	Loading	Cond	<i>t</i> (h)	yield (%) ^b	<i>ee</i> (%) ^c
1	Λ - Ir1	4 mol%	11d (0.1 M), 0 °C	1.5	87	31
2	Λ - Ir2	4 mol%	11d (0.1 M), 0 °C	2.5	93	39
3	Λ - Ir3	4 mol%	11d (0.1 M), 0 °C	2.5	93	65
4	Λ - Ir4	4 mol%	11d (0.1 M), 0 °C	2.5	96	97
5	Λ - Ir4	1 mol%	11d (0.1 M), RT	36	92	91
6	Λ - Ir4	1 mol%	11d (1.0 M), RT	12	96	97
7	Λ - Ir4	0.2 mol%	11d (1.0 M), RT	30	91	94
8	Λ - Ir4	0.1 mol%	11d (1.0 M), RT	36	89	91
9	Λ - Ir5	4 mol%	11d (0.1 M), 0 °C	6	88	0
10	Λ - Ir4	1 mol%	11d (1.0 M), RT, DMF	8	78	28
11	Λ - Ir4	1 mol%	11d (1.0 M), RT, MeOH	15	13	9

^a Reaction conditions: To a mixture of **11d** (0.20 mmol) and iridium catalyst Λ -**Ir1-5** (0.1-4 mol%) in anhydrous toluene (2.0 mL for entries 1-5 and 9, 0.2 mL for entries 6-8), DMF (0.2 mL) or MeOH (0.2 mL) at 0 °C was added the aldehyde **10a** (0.30 mmol). After being stirred at 0 °C or room temperature for 1.5-36 h under reduced light, MeOH (2.0 mL) was added, followed by the careful addition of NaBH₄ (0.26 mmol) at 0 °C. The products were isolated after basic workup and chromatography. ^b Isolated yields. ^c Enantiomeric excess determined by chiral HPLC analysis.

Under the assumption that the minor enantiomer is formed from the uncatalyzed background reaction, for 0.1 mol% catalyst loading one can calculate an impressive turnover number of almost 10³ with a rate acceleration of 1.0 × 10⁴. Table 2 reveals the substrate scope of Λ -**Ir4**, providing the corresponding β -hydroxyhydrazines (after in situ reduction of the aldehyde) or oxazolidinones (after

NaOH-induced cyclization of the β -hydroxyhydrazines) with satisfactory yields (73-96%) and high enantioselectivities (89-97% *ee*). Thus, rational design with just a few rounds of optimization afforded the highly active chiral-only-at-metal iridium catalyst Λ -**Ir4** for the enantioselective α -amination of aldehydes.

It's worth noting that the catalyst can be recycled several times without any significant loss of enantioselectivity as determined for the conversion **10a+11d**→(*S*)-**12a** catalyzed by Λ -**Ir4** (1 mol%): Cycle 1 (1.0 mmol scale) = 76% yield, 97% *ee*, 81% catalyst recovery; cycle 2 (0.81 mmol scale) = 71% yield, 95% *ee*, 78% catalyst recovery; cycle 3 (0.63 mmol scale) = 67% yield, 96% *ee*, 76% catalyst recovery.

Table 2 Substrate scope of the enantioselective α -amination of aldehydes with iridium catalyst Λ -**Ir4**^a

Entry	R ¹	R ²	Product	<i>t</i> (h)	yield (%) ^b	<i>ee</i> (%) ^c
1	<i>t</i> Bu (10a)	Bn (11d)	(<i>S</i>)- 12a	12	96	97
2	<i>n</i> Bu (10b)	Bn (11d)	(<i>S</i>)- 12b	15	81	94
3	<i>i</i> Pr (10c)	Bn (11d)	(<i>S</i>)- 12c	14	89	95
4	<i>n</i> Pr(10d)	Bn (11d)	(<i>S</i>)- 12d	15	78	96
5	Et (10e)	Bn (11d)	(<i>S</i>)- 12e	15	73	93
6	Allyl (10f)	Bn (11d)	(<i>S</i>)- 12f	14	87	92
7	<i>n</i> Hex (10g)	Bn (11d)	(<i>S</i>)- 12g	15	75	95
8	C ₆ H ₁₁ (10h)	Bn (11d)	(<i>S</i>)- 12h	15	77	95
9	BnOCH ₂ (10i)	Bn (11d)	(<i>S</i>)- 12i	15	75	91
10	Bn (10j)	Bn (11d)	(<i>S</i>)- 12j	15	91	89
11	Bn (10j)	<i>t</i> Bu (11e)	(<i>S</i>)- 13k ^d	15	91	96
12	Bn (10j)	Et (11f)	(<i>S</i>)- 13l ^d	15	88	95

^a Reaction conditions: To a mixture of azodicarboxylate **11d-f** (0.2 mmol) and Λ -**Ir4** (1.0 mol%) in anhydrous toluene (0.2 mL, 1.0 M) at 0 °C was added the aldehyde **10a-j** (0.30 mmol, 1.5 M). After being stirred at RT for 12-15 h, MeOH (0.2 mL) was added followed by the careful addition of NaBH₄ (10 mg, 0.26 mmol) at 0 °C. The products were isolated after basic workup and chromatography. ^b Isolated yields. ^c Enantiomeric excess determined by chiral HPLC analysis. ^d No suitable chiral HPLC conditions to resolve the two enantiomers were found for the corresponding cyclization products.

3.1.3 Proposed Mechanism

The mode of action of iridium complex Λ -**Ir4** can be rationalized by a bifunctional, dual activation catalysis which converts the aldehyde into a nucleophilic enamine, while at the same time activating the azodicarboxylate electrophile through hydrogen bonding with one OH-group (Figure 29). The asymmetric induction is then achieved by sterically enforcing the (*E*)-*syn* enamine conformation through sterically preventing the unfavored (*E*)-*anti* conformation induced by a bulky 2,4,6-*i*Pr₃Ph substituent, in combination with a preference for the *Si* face approach of the electrophile favored by a hydrogen bond between a hydroxymethyl group of the benzoxazole moiety and a nitrogen or carbonyl oxygen atom of the azodicarboxylate. The importance of this hydrogen bond for catalysis rate and enantioselectivity is demonstrated by the result with iridium complex Λ -**Ir5**, devoid of the hydroxyl methyl substituent on the benzoxazole moiety, resulting in the completely racemic formation of oxazolidinone **12a** (Table 1, entry 9). The importance of this key hydrogen bond for catalysis also explains why the aprotic, nonpolar solvent toluene provides superior results to polar (28% *ee* in DMF, entry 10 in Table 1) or protic (9% *ee* and low yield in MeOH, entry 11 in Table 1) solvents in which competing hydrogen bonds disfavor the proposed hydrogen bonded binary complex shown in Figure 29. A structure of the iridium complex cation of the catalyst Λ -**Ir4** (obtained by a former graduate student Dr. Chen Fu in Meggers group), derived from a crystal structure of racemic Λ/Δ -**Ir4**, is shown in Figure 30 and illustrates the local environment around the secondary amine with the steric interference of one closeby isopropyl group and a neighboring hydroxyl group for hydrogen bond interactions, thereby supporting the proposed rationale for the observed efficient asymmetric induction.

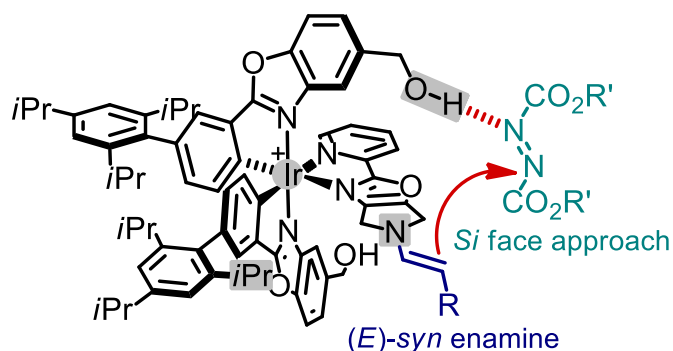


Figure 29 Proposed enamine/H-bonding mechanism of the α -amination of aldehydes (blue) with azodicarboxylates (green) catalyzed by iridium complex Λ -**Ir4**.

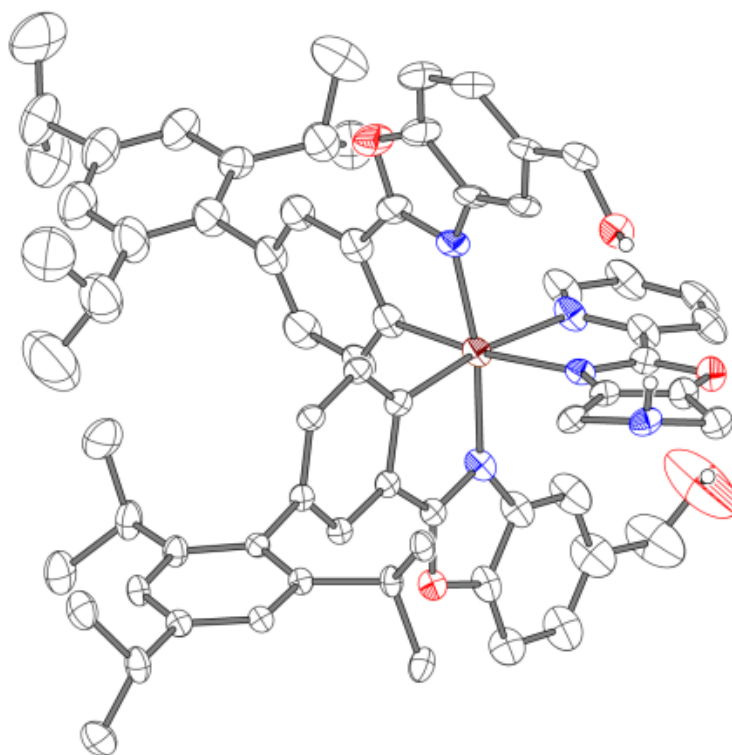


Figure 30 Structure of Δ -**Ir4** (ORTEP drawing with 30% probability thermal ellipsoids). The iridium complex was crystallized as an iodide salt in its racemic form. The iodide counterions and the Δ -isomer are omitted from the unit cell for clarity.

3.1.4 Conclusions

In conclusion, the first example of an asymmetric enamine catalyst build from an octahedral chiral-at-metal complex was presented.¹⁰ With respect to catalyst loading in asymmetric organocatalysis,¹¹ iridium complex Δ -**Ir4** constitutes one of the most efficient catalysts for the enantioselective α -amination of aldehydes to date. The high performance and straightforward design of the developed enamine/H-bonding dual activation catalyst through just a few cycles of ligand optimization indicates the power for a metal-templated design of “organocatalysts”, in which the octahedral stereocenter orchestrates the tailored arrangement of functional groups in the three-dimensional space, whereas the limited flexibility of the metal scaffold provides entropic benefits and promotes the rational catalyst design.

References

- 1 (a) L.-A. Chen, W. Xu, B. Huang, J. Ma, L. Wang, J. Xi, K. Harms, L. Gong, E. Meggers, *J. Am. Chem. Soc.* **2013**, *135*, 10598–10601; (b) L.-A. Chen, X. Tang, J. Xi, W. Xu, L. Gong, E. Meggers, *Angew. Chem. Int. Ed.* **2013**, *52*, 14021–14025.
- 2 For inert octahedral catalysts with chirality-at-metal, see for example: (a) Y. N. Belokon, A. G. Bulychiev, V. I. Maleev, M. North, I. L. Malfanov, N. S. Ikonnikov, *Mendeleev Commun.* **2004**, *14*, 249–250. (b) C. Ganzmann, J. A. Gladysz, *Chem. Eur. J.* **2008**, *14*, 5397–5400. (c) N. Kurono, K. Arai, M. Uemura, T. Ohkuma, *Angew. Chem. Int. Ed.* **2008**, *47*, 6643–6646.
- 3 For recent reviews on H-bonding in aminocatalysis, see: (a) M. Tsakos, C. G. Kokotos, *Tetrahedron* **2013**, *69*, 10199–10222. (b) Ł. Albrecht, H. Jiang, K. A. Jørgensen, *Chem. Eur. J.* **2014**, *20*, 358–368.
- 4 M. Helms, Z. Lin, L. Gong, K. Harms, E. Meggers, *Eur. J. Inorg. Chem.* **2013**, 4164–4172.
- 5 Y. X. Chen, L. F. Qian, W. Zhang, B. Han, *Angew. Chem. Int. Ed.* **2008**, *47*, 9330–9333.
- 6 D. F. Burdi, R. Hunt, L. Fan, T. Hu, J. Wang, Z. Guo, Z. Huang, C. Wu, L. Hardy, M. Detheux, M. A. Orsini, M. S. Quinton, R. Lew, K. Spear, *J. Med. Chem.* **2010**, *53*, 7107–7118.
- 7 L. Gong, M. Wenzel, E. Meggers, *Acc. Chem. Res.* **2013**, *46*, 2635–2644.
- 8 G. Nonoyama, *Bull. Chem. Soc. Jpn.* **1974**, *47*, 767–768.
- 9 (a) A. Bøgevig, K. Juhl, N. Kumaragurubaran, W. Zhuang, K. A. Jørgensen, *Angew. Chem. Int. Ed.* **2002**, *41*, 1790–1793. (b) B. List, *J. Am. Chem. Soc.* **2002**, *124*, 5656–5657. (c) T. Baumann, M. Bächle, C. Hartmann, S. Bräse, *Eur. J. Org. Chem.* **2008**, 2207–2212. (d) A. Quintard, S. Belot, E. Marchal, A. Alexakis, *Eur. J. Org. Chem.* **2010**, 927–936. (e) P.-M. Liu, D. R. Magar, K. Chen, *Eur. J. Org. Chem.* **2010**, 5705–5713. (f) B. S. Kumar, V. Venkataramasubramanian, A. Sudalai, *Org. Lett.* **2012**, *14*, 2468–2471. (g) X. Fan, S. Sayalero, M. A. Pericàs, *Adv. Synth. Catal.* **2012**, *354*, 2971–2976. (h) A. Theodorou, G. N. Papadopoulos, C. G. Kokotos, *Tetrahedron* **2013**, *69*, 5438–5443.
- 10 H. Huo, C. Fu, C. Wang, K. Harms, E. Meggers, *Chem. Commun.* **2014**, *50*, 10409–10411.
- 11 Low loading asymmetric organocatalysis: F. Giacalone, M. Gruttadauria, P. Agrigento, R. Noto, *Chem. Soc. Rev.* **2012**, *41*, 2406–2447.

Chapter 3: Results and Discussion

Part II: Non-Photochemical Asymmetric Catalysis with a Chiral Lewis Acid Catalyst

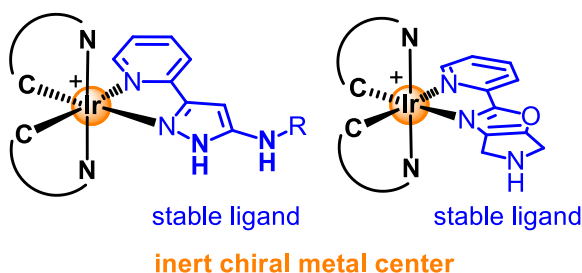
3.2 Enantioselective Friedel-Crafts Conjugate Addition with a Chiral-at-Metal Lewis Acid Catalyst

3.2 Enantioselective Friedel-Crafts Conjugate Addition with a Chiral-at-Metal Lewis Acid Catalyst

3.2.1 Catalyst Design

The recently developed metal-templated chiral-at-metal complexes in Meggers group, which provide asymmetric induction only through the coordinated ligand sphere (Figure 31).¹ These inert chiral-at-metal iridium (III) complexes have limited its potential as Lewis acid catalysts. Herein, a class of chiral-at-metal iridium(III) complex bearing two labile ligands (acetonitrile) was designed to serve as a chiral Lewis acid catalyst. These labile ligands would provide access to iridium center for efficient ligand exchange. The direct interactions between substrate and metal center should be accessible. In this theme, it is envisioned that the reactive metal center can be highly configurational inertness and retains the metal-centered absolute configuration during the asymmetric induction. The bis-cyclometalated ligand plays as a very important role in this design. Since it needs to stabilize the metal-centered configuration during each catalytic cycle and at the same time it needs to be capable of directing one substrate approach to influence the enantioselectivity. Thus, the development of chiral-at-metal Lewis acid catalyst should be initiated by designing the bis-cyclometalated ligand.

Previous work:



This design:

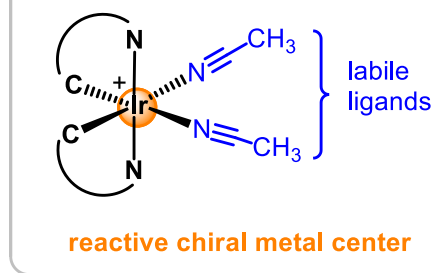


Figure 31 Catalyst design for the substitutionally labile yet configurationally stable chiral-at-metal iridium complex.

3.2.2 Initial Experiments

Considering the H-bonding activation has been well studied in our group, the initial design plan for Lewis acid catalyst was based on Lewis acid/H-bonding dual activation strategy. As shown in Figure 32, the complex Λ -**Ir6** was designed to serve as the first generation chiral Lewis acid catalyst. The Friedel-Crafts addition of indole to α,β -unsaturated 2-acyl pyrazoles was chosen as the model reaction to examine the viability. With respect to the proposed mechanistic model, the 2-acyl pyrazole was supposed to undergo fast ligand exchange with labile acetonitrile ligands to afford a transitional iridium intermediate complex. Meanwhile, the indole was activated and positioned by a formed hydrogen bond between NH group of indole and the lone pair of triazole moiety. The indole attacks the activated double bond of acceptor from *Re* face, which would provide the enantioenriched compounds.

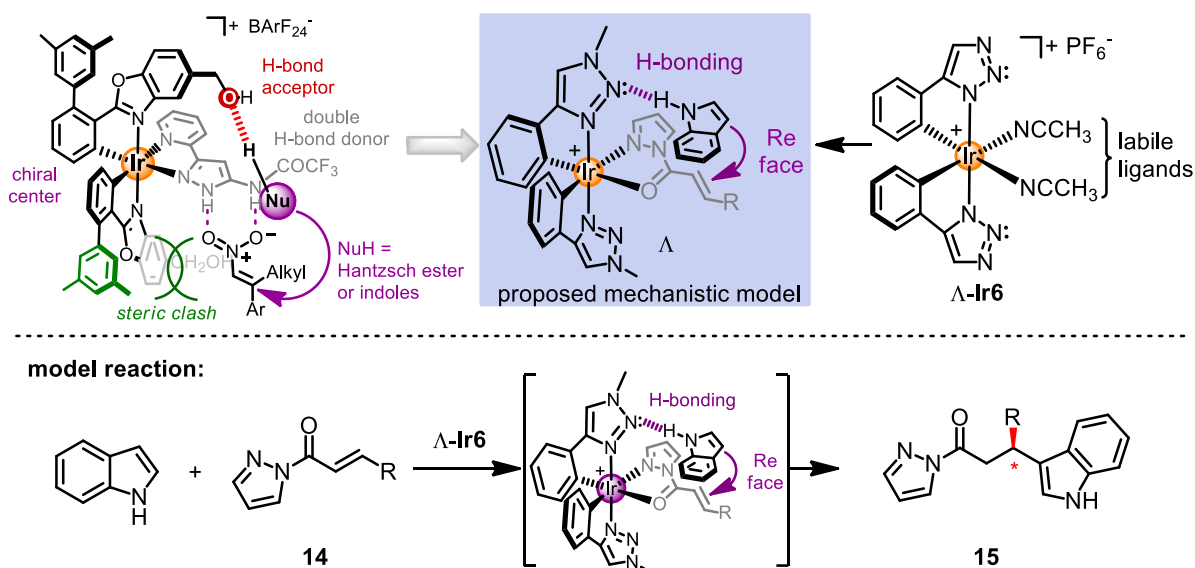


Figure 32 Initial design plan for directing asymmetric catalysis with metal-centered chirality.

Encouragingly, the viability of metal coordination strategy was rapidly confirmed with *rac*-**Ir6** as the Lewis acid catalyst. The reaction of **14c** ($R = H$) with indole (1.5 equiv) in the presence of 10 mol% *rac*-**Ir6** afforded the Friedel-Crafts addition product **15c** in 92% yield (Figure 33). It's confirmed that the C-C bond formation did not occur in absence of *rac*-**Ir6**. When more steric substrate **15a** or **15b** was applied to this protocol, only a negligible amount of addition product was observed, respectively. This transformation did not proceed efficiently either in the presence of higher catalyst loading (20 mol%) or at higher temperature (40 °C). The depressed conversion can be rationalized that the metal center of **Ir6** severed as a Lewis acid is not electron deficient enough due to

the extended π -system of triazole moiety. So next increasing the reactivity of Lewis acid metal center might improve the reaction efficiency.

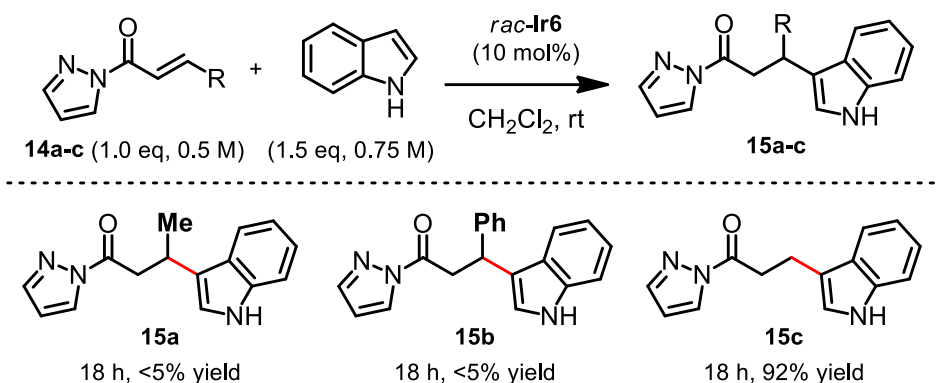
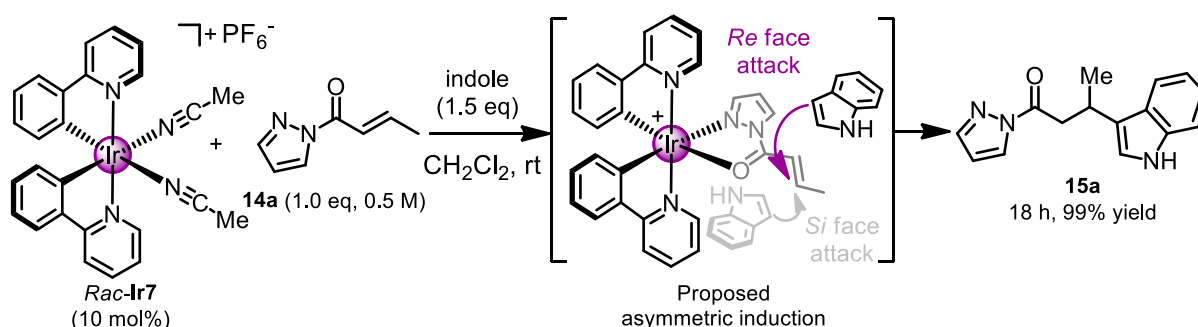


Figure 33 *Rac*-Ir6 catalyzed Friedel-Crafts additions of indole to α,β -unsaturated 2-acyl pyrazoles.

Comparing to that no detectable addition product **15a** was formed with catalyst *rac*-Ir6, a dramatic improvement was observed when a more electron deficient Lewis acid catalyst *rac*-Ir7 was employed (Scheme 3). The 99% yield of **15a** was achieved from the reaction of **14a** with indole in the presence of 10 mol% *rac*-Ir7, which demonstrated that the nature of the metal center is crucial for substrate activation. Whereas the hydrogen bond activation of indole is not required for the Friedel-Crafts Michael addition. Considering the expected asymmetric induction, the nucleophile not only can approach from *Re* face of the coordinated acceptor, but also can attack the coordinated acceptor from *Si* face, both of the sides are not sterically shielded differently. Therefore, the chiral Ir7 was not be synthesized for the further investigation.



Scheme 3 Evaluation of Friedel-Crafts addition with *rac*-Ir7.

3.2.3 Development of Catalyst Λ -IrO and Δ -IrO

Base on the above evaluations, Λ -IrO and Δ -IrO were designed for investigating the scope of asymmetric catalysis with reactive but configurationally stable chiral-only-at-metal complexes (Figure 34). The C_2 -symmetrical complex IrO contains two cyclometalating 5-*tert*-butyl-2-phenylbenzoxazoles and two labile acetonitrile ligands. The *t*Bu group arranged in one of cyclometalating ligand blocks one face of the coordinated electrophile, leaving the other face open for approach of nucleophile. Despite all ligands being achiral, metal-centered chirality leads to a Λ - (left-handed propeller) and Δ -enantiomer (right-handed propeller). In this design, the metal center serves the dual function of activating a substrate by metal coordination and at the same time comprises the configurationally stable sole element of chirality, thus entirely relying on achiral ligands in the coordination sphere.

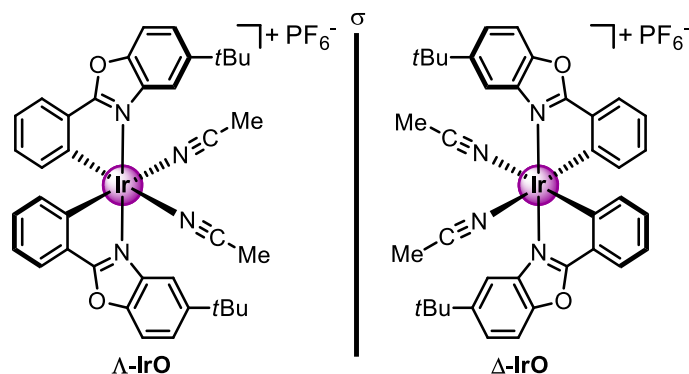
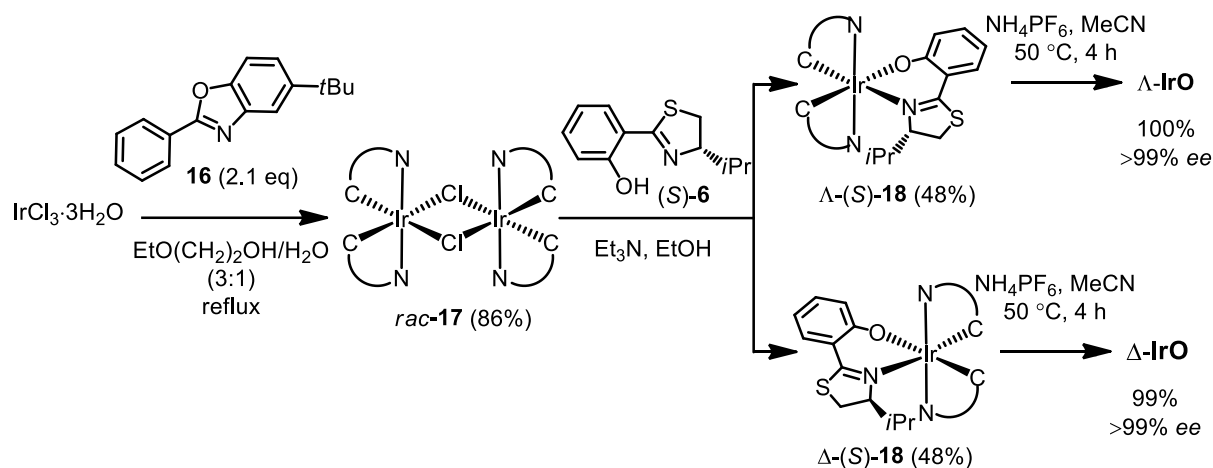


Figure 34 Enantiomers of a substitutionally labile yet configurationally stable chiral-at-metal iridium(III) complex.

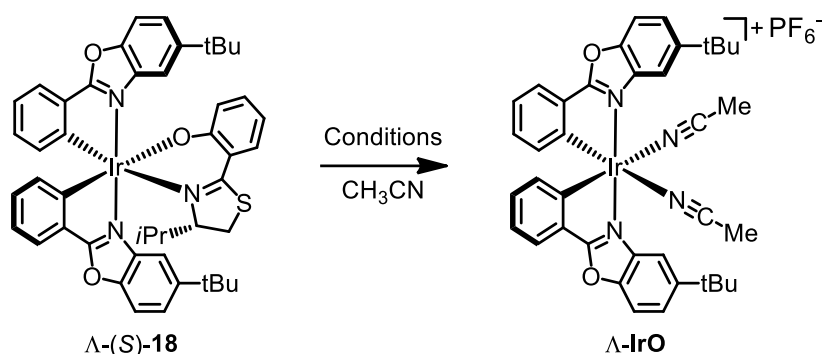
The synthesis of the complexes Λ -IrO and Δ -IrO is straightforward and draws from methodology recently developed in Meggers laboratory.^{2,3} Accordingly, the reaction of $\text{IrCl}_3 \cdot 3\text{H}_2\text{O}$ with benzoxazole **16** affords the cyclometalated racemic iridium(III) dimer *rac*-**17** in a diastereoselective fashion (Scheme 4). The subsequent reaction of *rac*-**17** with the chiral auxiliary ligand (*S*)-4-isopropyl-2-(2'-hydroxyphenyl)-2-thiazoline **6** provides the two diastereomeric complexes Λ -(*S*)-**18** and Δ -(*S*)-**18** which can be resolved by standard silica gel chromatography, followed by the conversion to virtually enantiopure Λ -IrO and Δ -IrO (each >99% *ee*), respectively, through the stereospecific substitution of the chiral auxiliary ligand (upon protonation by NH_4PF_6) by two acetonitrile ligands.



Scheme 4 Synthesis of the enantiomerically pure complexes Δ -IrO and Δ -IrO.

The auxiliary removal of Δ -(S)-**18** has been examined under different conditions (Table 3). According to the reported procedure of related process in Meggers group,² adding 5 equivalents of trifluoroacetic acid to the reaction mixture in acetonitrile, the chiral auxiliary was removed completely in 5 minutes as monitored by TLC (entry 1). When the crude material was subjected to the silica gel column utilizing $\text{CH}_3\text{CN} / \text{KNO}_3 (\text{sat. aq}) / \text{H}_2\text{O} (200:3:1)$ as mobile phase, after the counterion exchange only moderate yield of 41% was obtained. It is worth to point out that counterion anion exchange was processed due to the compatible solubility of PF_6 ion complex in most of organic solvent. The crude acetonitrile complex was found partial decomposed on the reversed phase silica gel column. When hydrochloric acid was used, the same problem caused the lower formation of Δ -IrO in entry 2. When the reaction was performed in the presence of weak acid NH_4PF_6 at 50 °C, Δ -IrO can be directly isolated in quant yield as a PF_6 complex. Combined solvent system in the presence of CH_3CN is curious for stabilization of Lewis acid catalysts on the silica gel column.

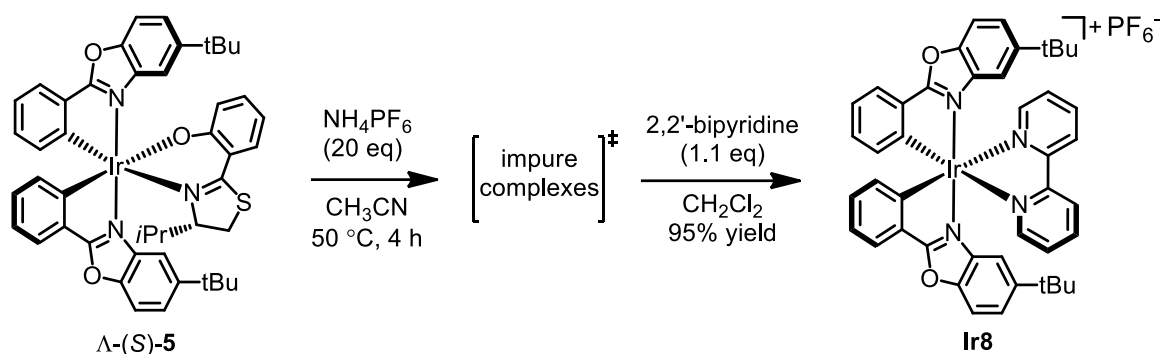
Table 3 The optimization toward the synthesis of enantiopure catalyst Λ -**IrO**.



entry	conditions	yield
1	TFA (5 eq), rt, 5 min, FC purified by CH ₃ CN/KNO ₃ (sat.aq)/H ₂ O (200:3:1) finally precipitated by excess NH ₄ PF ₆ (20 eq)	41%
2	HCl (5 eq), rt, 5 min, FC purified by CH ₃ CN/KNO ₃ (sat.aq)/H ₂ O (200:3:1) finally precipitated by excess NH ₄ PF ₆ (20 eq)	35%
3	NH ₄ PF ₆ (20 eq), 50 °C, 4 h, FC purified by CH ₃ CN/DCM (10:1)	100%
4	TFA (5 eq), rt, 5 min, counterion exchange with excess NH ₄ PF ₆ (20 eq) finally FC purified by CH ₃ CN/DCM (10:1)	87%

Reaction conditions: Diastereomeric complexe Λ -(S)-**18** (0.05 mmol), proton source (5 eq or 20 eq) in CH₃CN (1.0 mL) were stirred at the indicated time under nitrogen. FC = flash chromatography

It's worth noting that the protocol using NH₄PF₆ as proton source (entry 3) sometimes could not be reproduced well due to the unstable commercial quality of NH₄PF₆. After purification by silica gel chromatography, the related products were often obtained as a mixture of iridium complexes. The ¹H-NMR revealed that this mixture did not contain any chiral auxiliary ligand moiety, which seems reasonable considering that these complexes were consistent of non-acetonitrile, mono-acetonitrile and diacetonitrile complexes. When the impure complexes were subjected to follow-up chemistry in the presence of bipyridine (Scheme 5), the desired complex **Ir8** was isolated in 95% yield, which also supported this assumption. So an alternative protocol was developed for the synthesis of Λ -**IrO** (table 1, entry 4). In this case, the counterion exchange is firstly carried out before silica gel chromatography. The reverse mobile phase used in Entry 1-2 is not required for this protocol. Instead, using the combined solvent CH₂Cl₂/CH₃CN as the mobile phase for the chromatography, the pure Λ -**IrO** can be obtained in 87% yield. Despite the yield is slightly worse, this protocol is practical and very easy to be reproduced.



Scheme 5 The transformation of impure complexes derived from the auxiliary complex Δ -(S)-5.

A crystal structure of Δ -**IrO** confirms the assigned absolute metal-centered configurations (Figure 35, obtained by a former graduate student Dr. Chen Fu in Meggers group). HPLC traces using a chiral stationary phase are shown in Figure 36 and reveal the high enantiopurity of the synthesized complexes Δ -**IrO** and Δ -**IrO**. Interestingly, these substitutionally labile chiral-only-at-metal complexes are configurationally stable as Δ -**IrO** did not show any significant sign of configurational lability or decomposition upon standing in CH_2Cl_2 on the benchtop for 8 days, as verified by ^1H -NMR and chiral HPLC analysis (see Experimental Part).

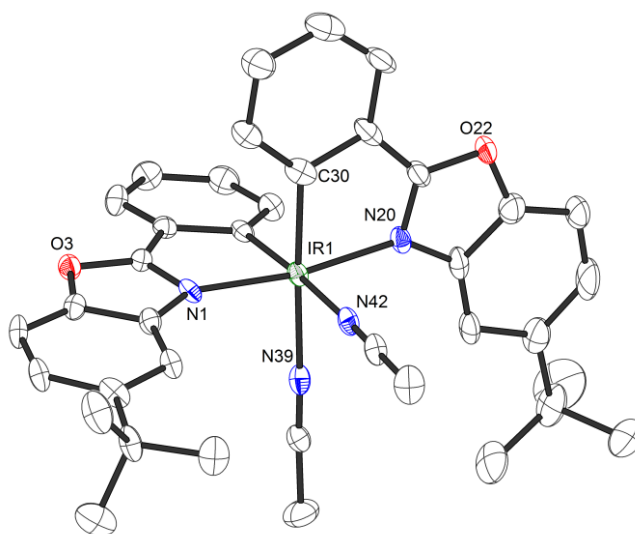


Figure 35 Crystal structure of Δ -**IrO**. The hexafluorophosphate counteranion is omitted for clarity. ORTEP drawing with 50% probability thermal ellipsoids.

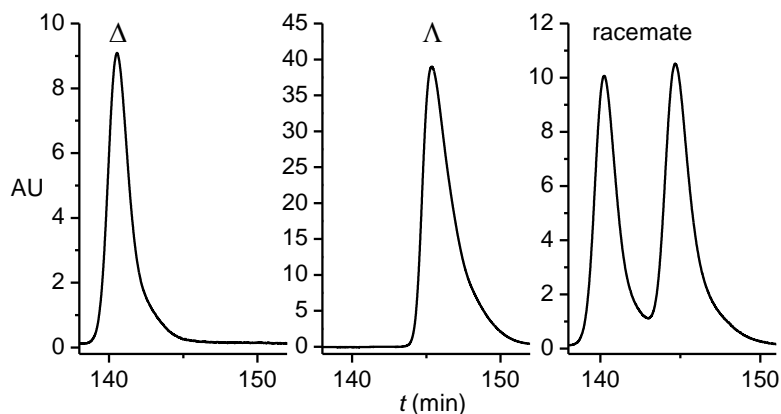


Figure 36 Chiral HPLC traces demonstrating the enantiopurity of synthesized Δ -IrO and Δ -IrO. HPLC conditions: Daicel Chiralcel IB, 250 \times 4.6 mm, flow rate = 0.5 ml/min, 0.1% aq. TFA with MeCN as eluent (20-43% in 60 min).

3.2.4 Reaction Optimization and Substrate Scope

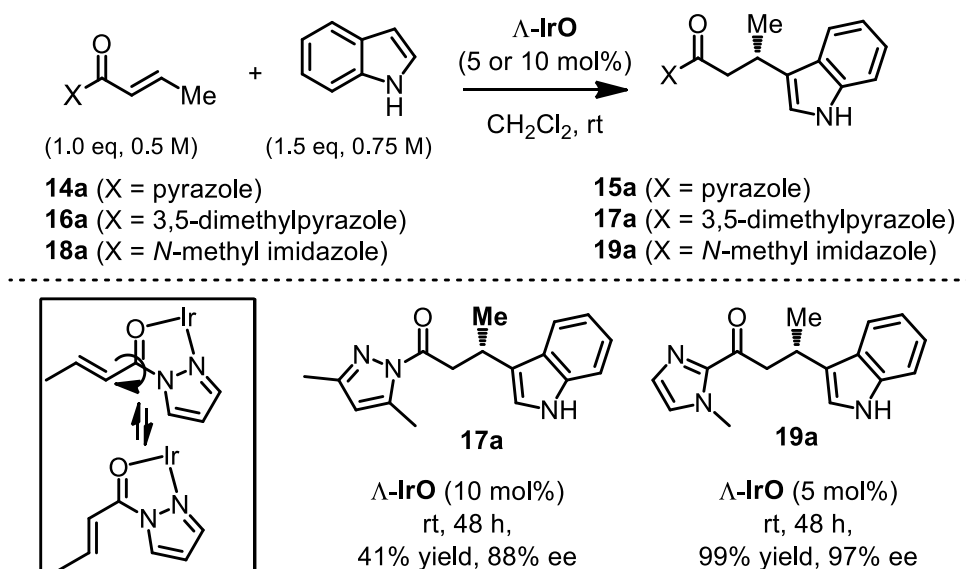
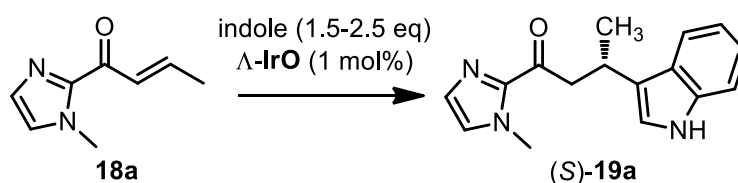


Figure 37 Substrate design results in improved reaction efficiency.

With the enantiopure Δ -IrO in hand, the asymmetric catalytic reactions were performed with substrates bearing the different auxiliaries (Figure 37). Considering the isomerisation of double bond of alkene **14a** will decrease the enantioselectivity, the substrate **14a** was replaced by **16a** bearing the 3,5-dimethyl substitution in the pyrazole moiety to prevent isomerisation. The α,β -unsaturated 2-acyl pyrazole **16a** provided the product **17a** in 41% yield and with encourage 88% *ee*. Using the α,β -unsaturated 2-acyl imidazole **18a**, the yield and enantioselectivity could be improved to 99% and 97% *ee*, respectively.

Based on the above observation, the further optimization was focused on the Friedel-Crafts conjugate addition of indole to α,β -unsaturated 2-acyl imidazole **18a** (Table 4).⁴ Revealingly, the reaction of **18a** with indole (1.5 eq) in the presence of 1 mol% Λ -**IrO** afforded the Friedel-Crafts alkylation product (*S*)-**19a** with high enantioselectivity (95% *ee*) albeit with only a slow conversion of just 35% after 20 h at room temperature in MeCN (Table 4, entry 1). A solvent screening revealed that MeOH, CH₂Cl₂ and THF, among others, provide higher catalysis rates (entries 2-4). Optimization of the reaction conditions with THF as the solvent by increasing the concentration of **18a** and the equivalents of indole (2.5 eq) led to full conversion at room temperature within 20 h and a high *ee* of 96% (entry 5). Interestingly, the reaction is insensitive to air (entry 6) and water (entry 7), and the enantioselectivity can be further improved by reducing the temperature, reaching 97% *ee* at 0 °C (entry 8).

Table 4 Enantioselective Friedel-Crafts addition of indole to α,β -unsaturated 2-acyl imidazole **18a** catalyzed by Λ -**IrO**^a

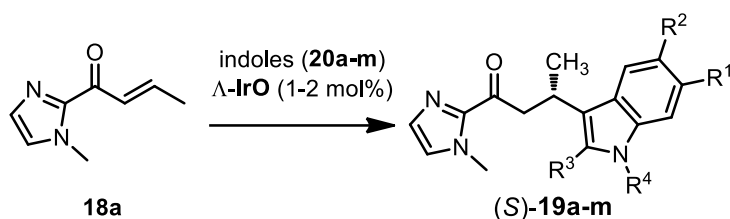


entry	solvent	conditions	conv (%) ^b	<i>ee</i> (%) ^c
1	MeCN	1.5 eq indole (0.75 M), rt, 20 h	35	95
2	MeOH	1.5 eq indole (0.75 M), rt, 20 h	70	95
3	CH ₂ Cl ₂	1.5 eq indole (0.75 M), rt, 20 h	90	94
4	THF	1.5 eq indole (0.75 M), rt, 20 h	85	96
5	THF	2.5 eq indole (2.5 M), rt, 20 h	100	96
6	THF	as entry 5 plus air	100	96
7	THF	as entry 5 plus air and 1% H ₂ O	88	96
8	THF	2.5 eq indole (2.5 M), 0 °C, 36 h	100	97

^a Reaction conditions: Imidazole **18a** (0.30 mmol), indole (0.45 mmol or 0.75 mmol), and Λ -**IrO** (1.0 mol%) in the indicated solvent (0.60 mL or 0.30 mL) were stirred at the indicated temperature under argon or air. ^b Conversion determined by ¹H-NMR. ^c Determined by chiral HPLC analysis.

Next, the substrate scope of catalyst Λ -**IrO** was investigated. Table 5 shows that a selection of thirteen substituted indoles provide the desired Friedel-Crafts alkylation products (*S*)-**19a-m** with high enantioselectivities (90-98% *ee*) in yields of 75-99% in the presence of 1-2 mol% of Λ -**IrO**. Electron acceptor substituted less reactive indoles require a somewhat increased catalyst loading (2.0 mol%) (entries 4 and 5), while the more reactive 2-methyl indole needs a lower reaction temperature to achieve a high *ee* value (entry 12).

Table 5 Enantioselective Friedel-Crafts addition of substituted indoles to α,β -unsaturated 2-acyl imidazole **18a** catalyzed by Λ -**IrO**^a



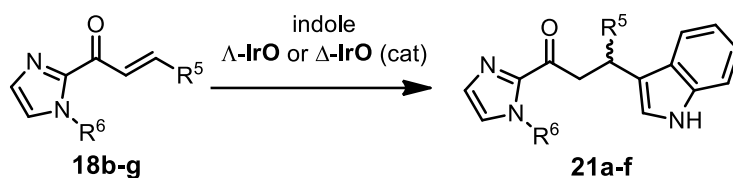
entry	indoles				Λ - IrO (mol%)	T (°C)	t (h)	yield (%) ^b	<i>ee</i> (%) ^c
	R ¹	R ²	R ³	R ⁴					
1	H	H	H	H	1.0	rt	20	97	96
2	H	Me	H	H	1.0	rt	18	98	94
3	H	MeO	H	H	1.0	rt	22	99	94
4	H	Br	H	H	2.0	rt	48	75	92
5	H	Cl	H	H	2.0	rt	48	77	94
6	MeO	H	H	H	1.0	rt	18	91	95
7	H	H	H	Me	1.0	rt	22	99	96
8	H	H	H	Bn	1.0	rt	22	82	95
9	H	Me	H	Bn	1.0	rt	18	92	94
10	H	MeO	H	Bn	1.0	rt	18	91	94
11	MeO	H	H	Bn	1.0	rt	22	90	95
12	H	H	Me	Me	2.0	0	36	93	98
13	H	H	Ph	Me	2.0	rt	40	97	90

^a Data reported as entry, reaction conditions: Indoles **20a-m** (0.75 mmol), imidazole **18a** (0.30 mmol) and Λ -**IrO** (1.0 or 2.0 mol%) in THF (0.30 mL) were stirred at the indicated temperature under argon.

^b Isolated yields. ^c Determined by chiral HPLC analysis.

The substrate scope with respect to different α,β -unsaturated 2-acylimidazoles **18b-g** is shown in Table 6 and demonstrates that upon adjustment of the catalyst loading (1-2 mol% Δ -**1** or Λ -**1**), reaction temperature (0 °C or room temperature), and concentration (1.0 or 2.0 M **18b-g**), very good to excellent enantioselectivities (91-98% *ee*) and yields (78-99%) are achieved for each system (entries 1-6). The α,β -unsaturated 2-acylimidazole **18g**, bearing an *N*-isopropyl substituent at the imidazole instead of a methyl group, even allows to reduce the catalyst loading to 0.25 mol% without affecting the enantioselectivity (97% *ee*) (entries 6-8). This reflects a respectable turnover number of 364, while not affecting the stereochemical integrity of the metal-centered chirality during all the catalytic cycles.

Table 6 Enantioselective Friedel-Crafts addition of indole to α,β -unsaturated 2-acyl imidazoles **18b-g** catalyzed by Λ -**IrO** or Δ -**IrO**^a



entry	imidazoles ^b		cat (mol%)	<i>T</i> (°C)	<i>t</i> (h)	yield (%) ^c	<i>ee</i> (%) ^d
	R^5	R^6					
1	Et	Me	Δ - IrO (2.0)	0	48	89 (21a)	96
2	<i>n</i> Bu	Me	Δ - IrO (2.0)	rt	20	97 (21b)	91
3 ^e	<i>i</i> Pr	Me	Δ - IrO (2.0)	rt	48	78 (21c)	93
4	Ph	Me	Λ - IrO (1.0)	rt	16	98 (21d)	93
5	CO ₂ Et	Me	Δ - IrO (1.0)	rt	24	97 (21e)	98
6	Me	<i>i</i> Pr	Δ - IrO (1.0)	rt	24	99 (21f)	97
7	Me	<i>i</i> Pr	Δ - IrO (0.5)	rt	44	97 (21f)	97
8	Me	<i>i</i> Pr	Δ - IrO (0.25)	rt	60	91 (21f)	97

^a Data reported as entry, reaction conditions: Imidazoles **18b-g** (0.30 mmol), indole (0.75 mmol) and Δ -**IrO** or Λ -**IrO** (0.25-2.0 mol%) in THF (0.30 mL) were stirred at the indicated temperature under argon. ^b **18b-g** consecutively listed from entry 1 to 6. ^c Isolated yields with the individual products indicated in brackets. ^d Determined by chiral HPLC analysis. *R*-configuration: entries 1, 2, and 4-8. *S*-configuration: entry 3. ^e Increased concentration of **18d** (2.0 M) in order to speed up the reaction.

3.2.5 Proposed Mechanistic Model

The C₂-symmetrical iridium complex **IrO** was designed to serve as a chiral Lewis acid by activating α,β -unsaturated 2-acyl imidazoles through bidentate N,O-coordination. A proposed model for the asymmetric induction in the course of the indole addition that is consistent with the experimental results is shown in Figure 38 and demonstrates that one face of the alkene is sterically shielded effectively by one of the *tert*-butyl group, and the other face is leaving open for the approach of nucleophile. An intermediate crystal structure with *N*-*i*Pr 2-acyl imidazole (provided by a former graduate student Dr. Xiaodong Shen in Meggers group), is shown in Figure 39 and reveals the local environment around chiral metal center, thereby supporting the proposed mechanistic mode for observed efficient asymmetric induction.

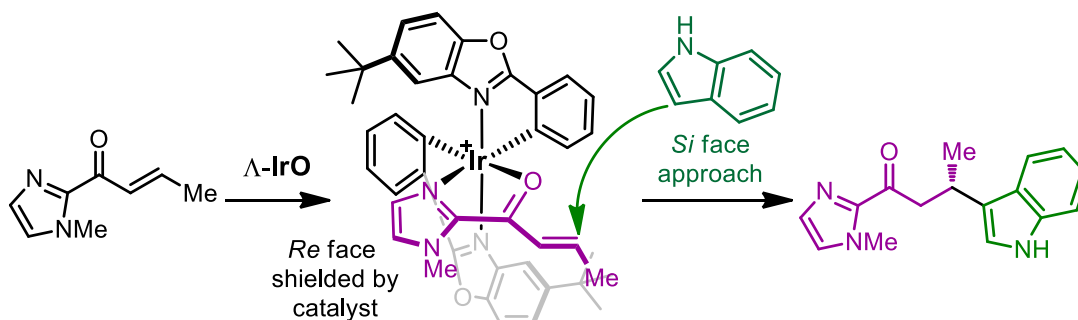


Figure 38 Proposed model for the asymmetric induction in the transition state in which one face of the alkene is shielded by the C₂-symmetrical catalyst.

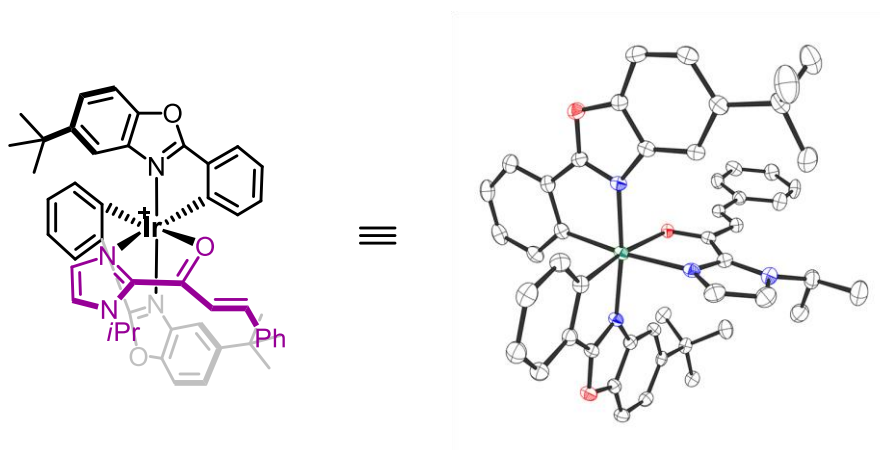


Figure 39 An intermediate crystal structure of α,β -unsaturated 2-acyl imidazole complexes with **IrO**. The hexafluorophosphate counteranion is omitted for clarity. ORTEP drawing with 50% probability thermal ellipsoids.

It is worth noting that the high lability of the coordinated MeCN ligands of catalyst **IrO** is a consequence of the strong *trans*-effect of the Ir-C bonds. ¹H-NMR spectra recorded in CD₂Cl₂ at room temperature after the addition of acyl imidazole **18a** to catalyst **Λ-IrO** support the fast bidentate coordination of **18a** to the catalyst upon release of the two labile acetonitrile ligands (see Experiment Part). Thus, the mechanistic mode of action of catalyst **IrO** relies on the coordinative lability of the MeCN ligands in combination with a high configurational stability of the remaining octahedral coordination sphere in order to retain the metal-centered chirality at all times.

3.2.6 Conclusions

In conclusion, a novel class of asymmetric transition metal catalysts was developed, in which the metal fulfills a dual function by coordinatively activating a substrate and at the same time serving as the sole source of chirality. Whereas typical metal-coordination-based asymmetric catalysts rely on chiral ligands for their asymmetric induction, the here introduced *bis*-cyclometalated iridium(III) complex **IrO** is distinguished by its simplicity as it just contains two achiral cyclometalating phenylbenzoxazoles and two labile acetonitriles. The high configurational stability of the octahedral iridium chiral center is unexpected considering that labile ligands generally reduce the activation barrier for isomerization. Beyond its conceptual appeal, *bis*-cyclometalated octahedral iridium(III) complex **IrO** might be of high practical value as it provides an excellent substrate scope for the highly enantioselective Friedel-Crafts addition of indoles to α,β -unsaturated 2-acyl imidazoles at low catalyst loadings (0.25-2 mol%), while at the same time catalyst **IrO** displays a high solvent tolerance, does not rely on cryogenic temperatures, and can even be used under open flask conditions.⁵ This high performance indicates the value of a direct chirality transfer from the chiral metal to the coordinated substrate.

This novel class of reactive chiral-at-metal complexes has proven to be of high value for a large variety of asymmetric transformation. Since the initial discovery of this chiral-at-metal iridium(III) Lewis catalyst, efforts in this process have proven to be promising. Λ -IrO has been successfully extended to a series of asymmetric transformations (Figure 40). The further optimization and mechanistic insights of listed reactions were investigated by Xiaodong Shen, a graduate student in Meggers group.⁶ Progresses towards these value transformations were detailed in his PhD thesis.

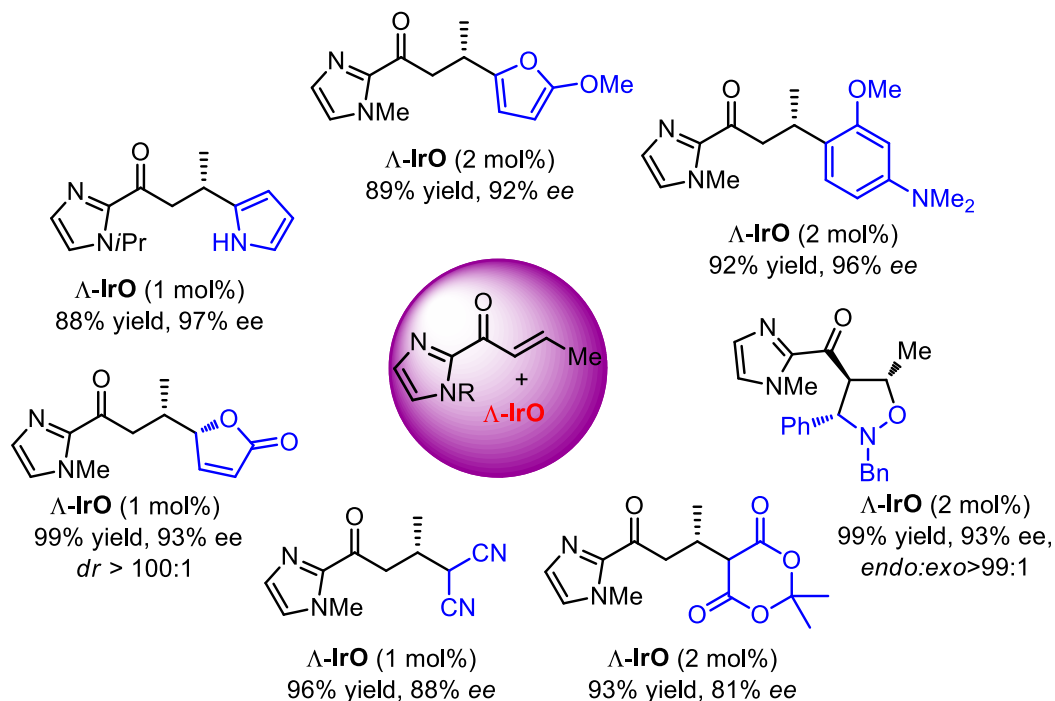


Figure 40 A series of asymmetric reactions were found to be catalyzed by Λ -IrO.

References

- 1 (a) L.-A. Chen, W. Xu, B. Huang, J. Ma, L. Wang, J. Xi, K. Harms, L. Gong, E. Meggers, *J. Am. Chem. Soc.* **2013**, *135*, 10598–10601. (b) L.-A. Chen, X. Tang, J. Xi, W. Xu, L. Gong, E. Meggers, *Angew. Chem. Int. Ed.* **2013**, *52*, 14021–14025. (c) H. Huo, C. Fu, C. Wang, K. Harms, E. Meggers, *Chem. Commun.* **2014**, *50*, 10409–10411.
- 2 M. Helms, Z. Lin, L. Gong, K. Harms, E. Meggers, *Eur. J. Inorg. Chem.* **2013**, 4164–4172.
- 3 L. Gong, M. Wenzel, E. Meggers, *Acc. Chem. Res.* **2013**, *46*, 2635–2644.
- 4 For catalytic enantioselective indole and pyrrole alkylations with α,β -unsaturated 2-acyl imidazoles, see: (a) D. A. Evans, K. R. Fandrick, H.-J. Song, *J. Am. Chem. Soc.* **2005**, *127*, 8942–8943. (b) D. A. Evans, K. R. Fandrick, *Org. Lett.* **2006**, *8*, 2249–2252. (c) D. A. Evans, K. R. Fandrick, H.-J. Song, K. A. Scheidt, R. Xu, *J. Am. Chem. Soc.* **2007**, *129*, 10029–10041. (d) A. J. Boersma, B. L. Feringa, G. Roelfes, *Angew. Chem. Int. Ed.* **2009**, *48*, 3346–3348.
- 5 *N*-Acyl imidazoles can be converted to a wide variety of carbonyl compounds. See ref. 9c and also: (a) S. Ohta, S. Hayakawa, K. Nishimura, M. Okamoto, *Chem. Pharm. Bull.* **1987**, *35*, 1058–1069. (b) A. Miyashita, Y. Suzuki, I. Nagasaki, C. Ishiguro, K.-i. Iwamoto, T. Higashino, *Chem. Pharm. Bull.* **1997**, *45*, 1254–1258.
- 6 X. Shen, H. Huo, C. Wang, B. Zhang, K. Harms, E. Meggers, *Chem. Eur. J.* **2015**, *21*, 9720–9726.

Chapter 3: Results and Discussion

Part III: Asymmetric Photoredox Catalysis with Chiral-at-Metal Iridium Complexes: α -Functionalization of Carbonyl Compounds

3.3 Visible-Light-Activated Enantioselective Alkylation with a Chiral Iridium Complex

3.4 Visible-Light-Activated Enantioselective Trichloromethylation with a Chiral Iridium Complex

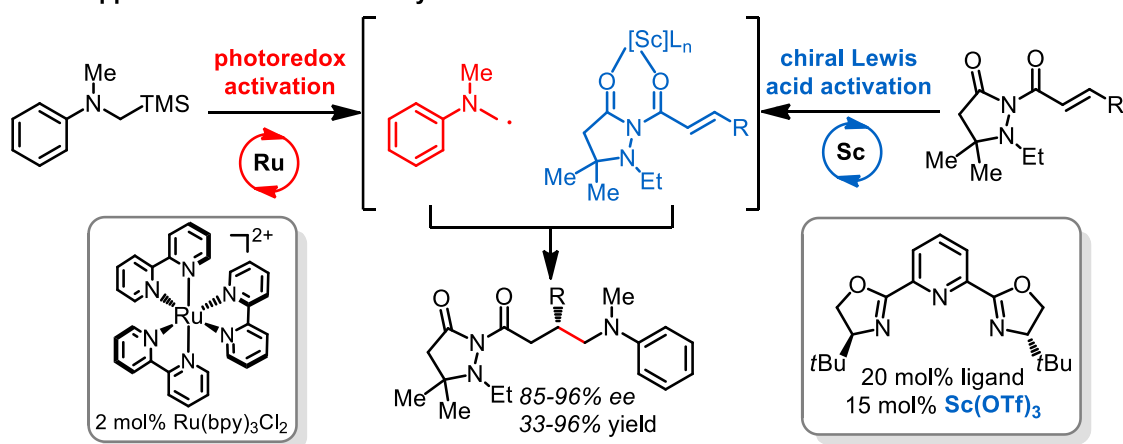
3.5 Visible-Light-Activated Enantioselective Perfluoroalkylation with a Chiral Iridium Complex

3.3 Visible-Light-Activated Enantioselective Alkylation with a Chiral Iridium Complex

3.3.1 Reaction Design

The inherent nature of Λ -**IrO** as a chiral Lewis acid catalyst has been proven by the enantioselective Friedel-Crafts addition of indoles to α,β -unsaturated 2-acyl imidazoles in chapter 3.2,¹ which simulated us to extend the study from non-photochemical applications to asymmetric photoredox catalysis with chiral-at-metal iridium complex.²

Yoon's approach based on two catalysts:



This proposal with single catalyst:

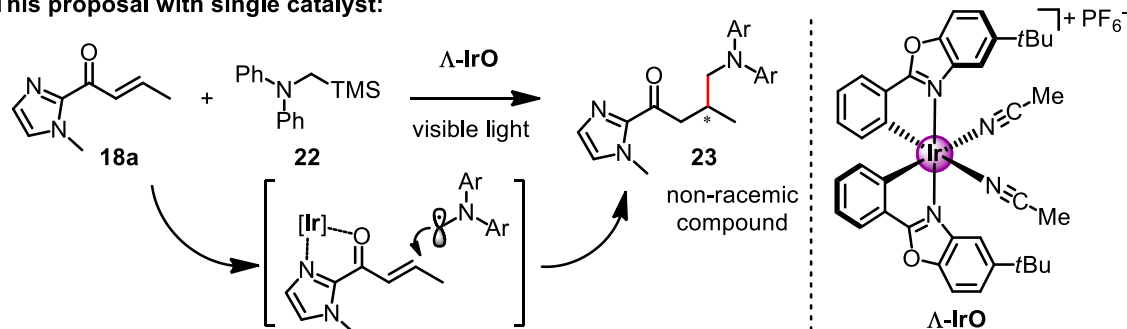


Figure 41 Initial design plan for asymmetric photoredox catalysis with chiral-at-metal Λ -**IrO**.

The Yoon group recently reported enantioselective conjugate addition of α -amino radicals through cooperative catalysis with two catalysts (Figure 41).³ This study was initiated by investigating the similar addition of α -silylamine **22** to α,β -unsaturated 2-acyl imidazole **18a** with single catalyst Λ -**IrO** under photoredox conditions. As shown in Figure 41, the addition of photo-oxidatively generated α -aminoradicals to the coordinating Michael acceptor might produce non-racemic compound. Two possible scenarios were envisioned. First, Λ -**IrO** or the coordinated intermediate complex can sever as

a photosensitizer to mediate the photoredox chemistry. Second, the Λ -**IrO** can strongly accelerate the involved key radical addition step to overcome the racemic background reaction with uncoordinated substrates.

The viability of this initial plan was rapidly confirmed with the newly developed catalyst Λ -**IrO** (Figure 42). In the presence of 20 mol% Λ -**IrO**, the conjugate addition product **23** was provided in 43% yield and with 37% *ee*. The control experiment verified the visible light is essential for the product formation. Disappointingly, with catalytic amount of Λ -**IrO** (10-30 mol%), the further optimization based on the concentration, solvent, temperature, α -amino radical precursors and the ratios of reaction partners did not provide any promising results. That means the prevailing racemic background reaction could not be overcome efficiently in this single catalyst system. Notably, when running the reaction with stoichiometric Λ -**IrO** (100 mol%), the good enantioselectivity (85% *ee*) can be realized, albeit with depressed yield of 16%.

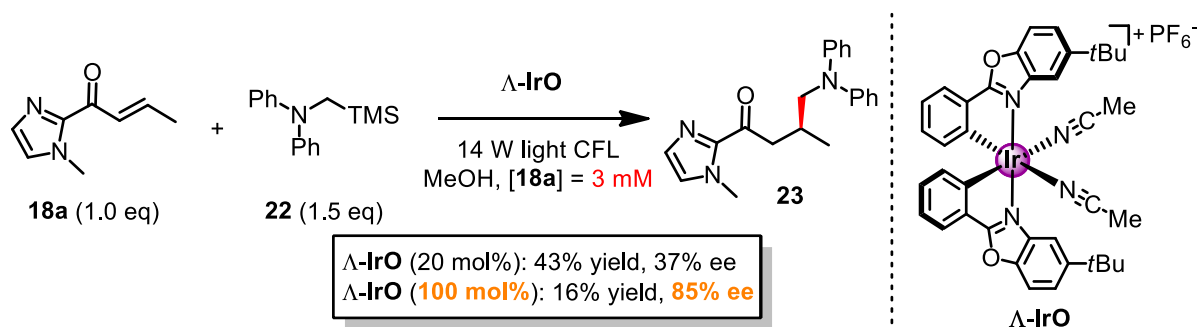
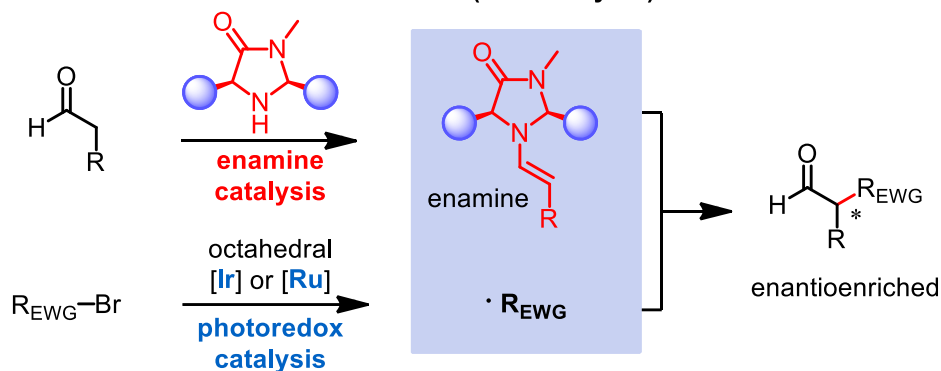


Figure 42 Initial experiments to the photoinduced reaction of α,β -unsaturated 2-acyl imidazole **7** with α -silylamine **22** catalyzed by Λ -**IrO**.

The above observation suggests that the chiral iridium complex **IrO** can serve as a photoredox catalyst and at the same time provide asymmetric induction, while the hindrance caused by uncatalyzed background reactions needs to be addressed with a new strategy. The enamine catalysis has been widely applied in asymmetric photoredox catalysis for the α -alkylation of aldehydes or ketones, in which the electron-rich enamine intermediates enable to couple with various electron-deficient electrophilic radicals under stereocontrol (Figure 43).⁴ Our group recently realized the asymmetric α -amination of 2-acyl imidazoles with Λ -**IrO** through enolate activation mode (non-photochemical application).⁵ Thus, extending the study of asymmetric photoredox catalysis from enamine catalysis to enolate chemistry is highly reasonable. It promises new access to asymmetric photoredox catalysis with a single catalyst. The alkylation of 2-acyl imidazoles with electron-deficient radicals was chosen as the model

reaction. In this system, the formation of enolate species only relies on the coordination activation; the reaction can avoid uncatalyzed background reaction and provide the enantioenriched compounds.

MacMillan's enamine activation mode (two catalysts):



New design based on enolate activation mode (single catalyst):

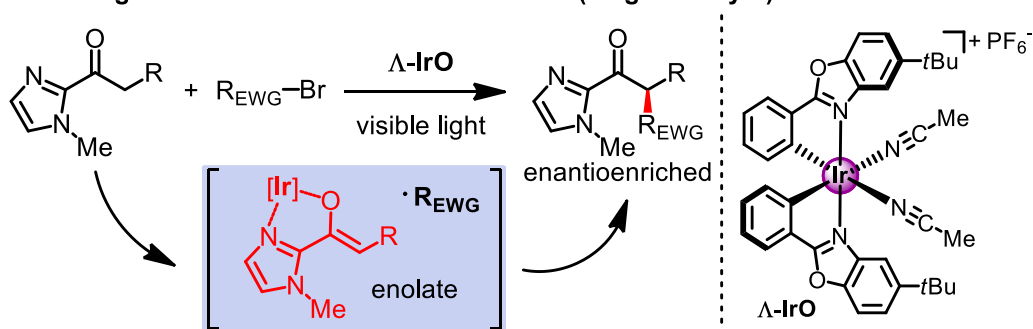


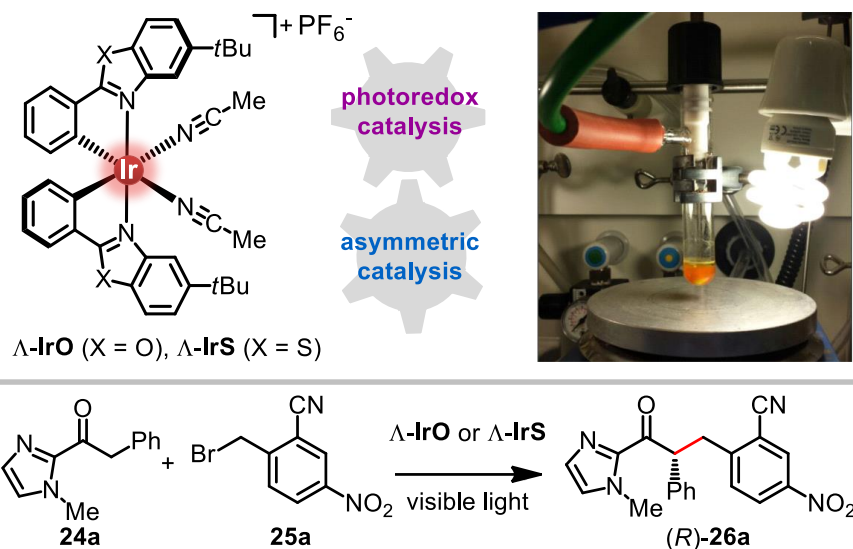
Figure 43 New strategy for photoredox catalysis based on the enolate activation mode.

3.3.2 Reaction Optimization

The reaction of 2-acyl imidazole **24a** with the electron deficient benzyl bromide **25a** was selected as the starting point (Table 7). Encouragingly, in the presence of a 14 W energy saving household lamp, Λ -**IrO** at a loading of 5 mol% was able to catalyze the reaction between **24a** and **25a**, providing the α -alkylation product **26a** in a good yield of 85% and with high enantioselectivity of 95% *ee* after 20 hours photolysis at room temperature (entry 1 of Table 7). Optimization of the reaction conditions by empirically adjusting the solvent, increasing the concentration to speed up the reaction, slightly raising the temperature to promote ligand exchange at the iridium center, and adding the weak base Na_2HPO_4 to facilitate enolate chemistry, provided the product **26a** in an excellent yield of 97% with 95% *ee* already after exposure to visible light for just 3 h in the presence of a reduced catalyst loading of just 2 mol% Λ -**IrO** (entry 4).

The derivative catalyst Λ -**IrS** (firstly synthesized by the Xiaodong Shen, a graduate student in Meggers group) was used for the further optimization.⁶ The catalyst Λ -**IrS** (2 mol%) even provided the α -alkylation product in quantitative yield with a superior enantioselectivity of 99% *ee* and a further reduced reaction time of 1.5 h (entry 5). Remarkably, the loading of the catalyst Λ -**IrS** can be further decreased to merely 0.5 mol% without affecting much the yield (97%) and enantioselectivity (98% *ee*) (entry 6). The reaction was inhibited completely in the presence of air, which is consistent of a radical mechanism. Importantly, neither the catalyst Λ -**IrS** alone in the dark (entry 8) nor visible light in the absence of the catalyst (entry 9) trigger this reaction to a significant degree under these conditions, thus unequivocally demonstrating that it is the combination out of iridium(III) catalyst and visible light that is necessary to catalyze the enantioselective C-C bond formation.

Table 7 Initial evaluation and optimization of the photoinduced enantioselective alkylation of acyl imidazole **24a** with benzyl bromide **25a** catalyzed by Λ -IrO or Λ -IrS.

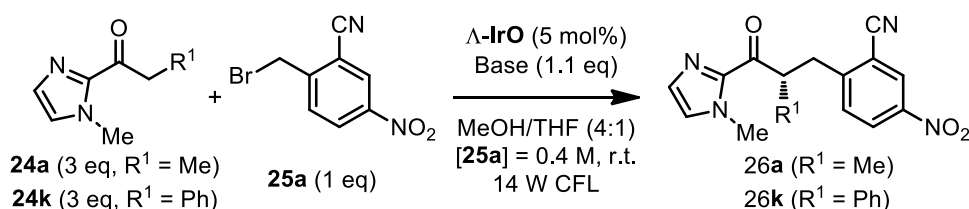


Entry	Catalyst	$h\nu^a$	Reaction conditions ^b	<i>t</i> (h)	yield (%) ^c	<i>ee</i> (%) ^d
1	Λ -IrO (5 mol%)	visible light	24a (0.3 M, 3 eq), MeOH, r.t.	20	85	95
2	Λ -IrO (2 mol%)	visible light	Na ₂ HPO ₄ , 24a (0.6 M, 1.5 eq), MeOH/THF (4:1), r.t.	5	70	89
3	Λ -IrO (2 mol%)	visible light	Na ₂ HPO ₄ , 24a (1.2 M, 3 eq), MeOH/THF (4:1), r.t.	5	97	92
4	Λ -IrO (2 mol%)	visible light	Na ₂ HPO ₄ , 24a (1.2 M, 3 eq), MeOH/THF (4:1), 40 °C	3	97	95
5	Λ -IrS (2 mol%)	visible light	same as entry 4	1.5	100	99
6	Λ -IrS (0.5 mol%)	visible light	same as entry 4	4.5	97	98
7	Λ -IrS (2 mol%)	visible light	same as entry 4, but without degassing	12	0	n.a.
8	Λ -IrS (2 mol%)	dark	same as entry 4	1.5	<5	n.d.
9	none	visible light	same as entry 4	16	0	n.a.

^a Light source: 14 W white light energy saving lamp. ^b All reactions performed under exclusion of air. See Experimental Part for more details. ^c Isolated yields. ^d Enantiomeric excess determined by HPLC analysis on chiral stationary phase. n.d. = not determined, n.a. = not applicable, r.t. = room temperature.

Using **24a** and **24k** as representative substrates, different bases were also evaluated in these alkylation reactions (Table 8). The screening of bases revealed that Na₂HPO₄ was the best choice of base for these reactions and it can significantly accelerate the reaction rate. Although for the acidic substrate **24k**, the base is not essential for the achieving high conversions and excellent enantioselectivities (entry 8), even the base can slightly decrease the enantioselectivity (entry 7). While the base Na₂HPO₄ was still preferred due to the significant rate acceleration. Moreover, the affect of the enantioselectivity caused by the base can be further overcome by raising the reaction temperature to 40 °C to promote the ligand exchange rate (entry 7).

Table 8 Screening of different bases in the photoinduced alkylation reaction.



Entry	R ¹	Base	<i>t</i> (h)	yield (%) ^a	<i>ee</i> (%) ^b
1	Ph	NaHCO ₃	3.5	99	86
2	Ph	Na ₂ CO ₃	5	65	−12
3	Ph	NaOAc	3	73	−21
4	Ph	DTBP ^c	6	85	87
5	Ph	2,6-lutidine	3	99	91
6	Ph	NaH ₂ PO ₄	15	85	76
7	Ph	Na ₂ HPO ₄	2	99	93/97 ^d
8	Ph	none	15	90	97
9	Me	Na ₂ HPO ₄	15	87	91
10	Me	none	15	19	91

^aIsolated yields. ^b Enantiomeric excess determined by HPLC analysis on chiral stationary phase. ^c DTBP = 2,6-Di-*tert*-butylpyridine. ^d The reaction was run at 40 °C.

3.3.3 Substrate Scope

Examples of the photoinduced enantioselective α -alkylation of 2-acyl imidazoles with benzyl bromides catalyzed by Λ -**IrS** are summarized in Figure 44 (next page). A variety of electron acceptor substituted benzyl bromides provide the α -alkylation products in up to quantitative yields (97-100%) and with up to almost perfect enantioselectivities (94-99% *ee*), while requiring only short reaction times of 1.5 to 6 hours (**26a-d**). On the other hand, the 2-phenacyl-*N*-methylimidazole substrates tolerate steric (products **26e** and **26f**), electron donating (product **26g**) and electron accepting (product **26h**) substituents in the phenyl moiety, while the benzene moiety can be replaced by the bicyclic aromatic naphthalene (product **26i**) or heteroaromatic thiophene (product **26j**). Furthermore, the photoredox catalyzed reaction also tolerates less acidic 2-acyl-*N*-methylimidazoles devoid of any aromatic substituent at the methylene group as demonstrated for the products **26k** and **26l**. For these substrates, the addition of a weak base is essential for achieving high conversions and excellent enantioselectivities. A different class of electrophiles were also suitable for this chemistry, namely phenacyl bromides, and found that they readily provide the expected C-C bond formation products with very good yields of 86-91% and high enantioselectivities of 90-91% *ee* (products **26m-p**). In order to reach satisfactory enantioselectivities, the *N*-methyl substituent at the imidazole moiety was replaced against the more bulky isopropyl group (**26m** vs **26m'**, **26n** vs **26n'**). Overall, it can be concluded that Λ -**IrS** highly effectively catalyzes the α -alkylation of acyl imidazoles with acceptor substituted benzyl bromides and phenacyl bromides in the presence of visible light with high to quantitative yields and impressive enantioselectivities, while only using a catalyst loading of 2 mol%.

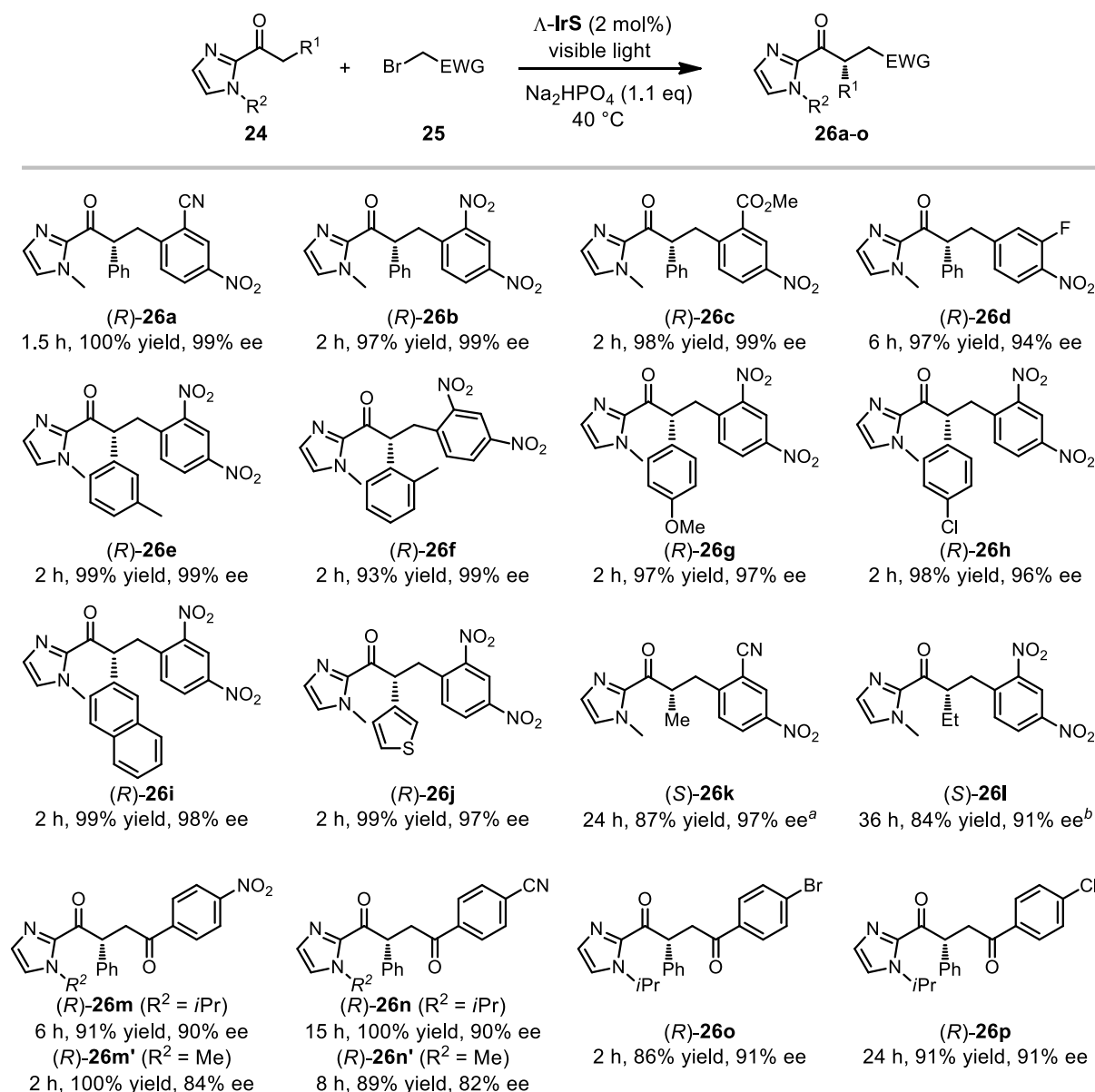


Figure 44 Substrate scope of the photoinduced enantioselective alkylation of 2-acyl imidazoles with acceptor substituted benzyl bromides and phenacyl bromides. Reported yields represent isolated yields after chromatographic purification. Enantiomeric excess was determined by HPLC on a chiral stationary phase. ^aFor comparison, in the absence of base a yield of 18% with 91% ee was obtained after photolysis for 24 h. ^bIrradiated instead with a blue LED light source (3 Watt) in order to improve the yield.

Interestingly, this chemistry is also amenable to α -alkylation of phenacyl bromides without acceptor substituted group (Figure 45), providing general access to the asymmetric synthesis of 1,4-dicarboxylate compounds. The corresponding products were obtained with good enantioselectivities and high yields. Likewise, the adjustment of *N*-substituent group at the imidazole moiety is required for the satisfactory enantioselectivities (**26s** vs **26s'**).

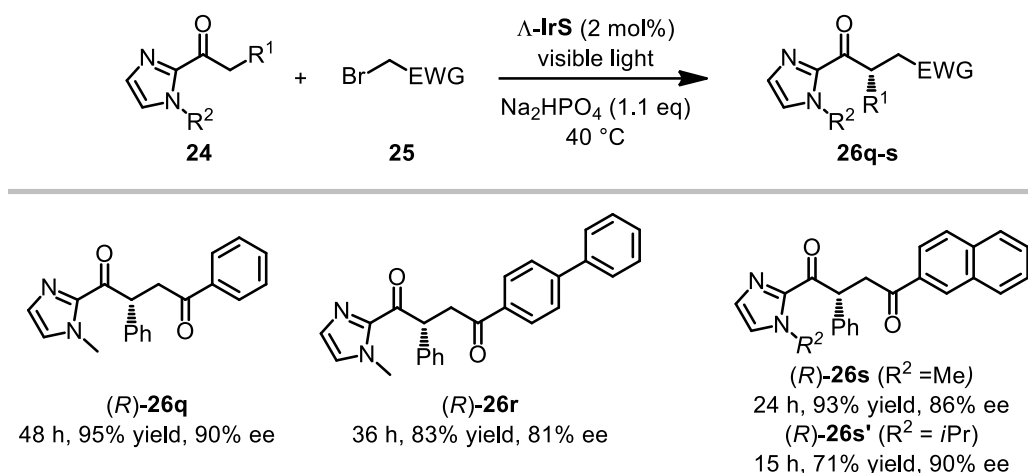


Figure 45 Examples of the photoinduced enantioselective alkylation of 2-acyl imidazoles without acceptor substituted phenacyl bromides.

Before the $\Delta\text{-IrS}$ was applied to this system, a range of different electrophiles had been investigated under the optimal conditions with $\Delta\text{-IrO}$. In order to give a clear comparison of the catalytic efficiency of $\Delta\text{-IrO}$ and $\Delta\text{-IrS}$, the related results were summarized in Figure 46. Apparently, the $\Delta\text{-IrS}$ always provides α -alkylation products with better enantioselectivities. The improved enantioselectivity can be attributed to an increased steric hindrance in $\Delta\text{-IrS}$ compared to $\Delta\text{-IrO}$ created by the long C-S bonds of the benzothiazole moieties which position the two *tert*-butyl groups somewhat closer to the exchange-labile acetonitrile ligands (Figure 47, next page). Therefore, the better steric induction and faster catalytic turnover rate can be achieved by $\Delta\text{-IrS}$.

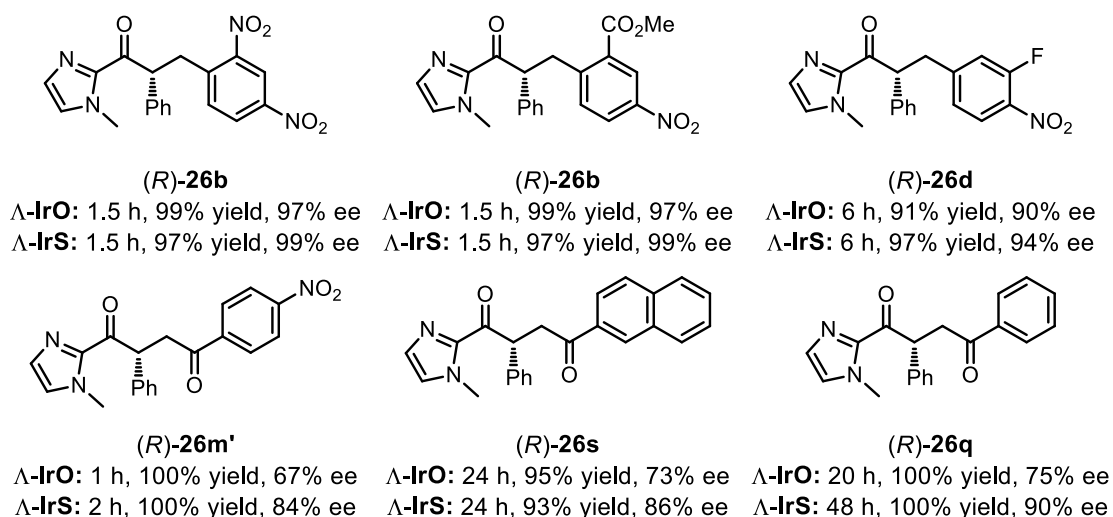


Figure 46 Comparison of the catalytic efficiency of $\Delta\text{-IrO}$ and $\Delta\text{-IrS}$.

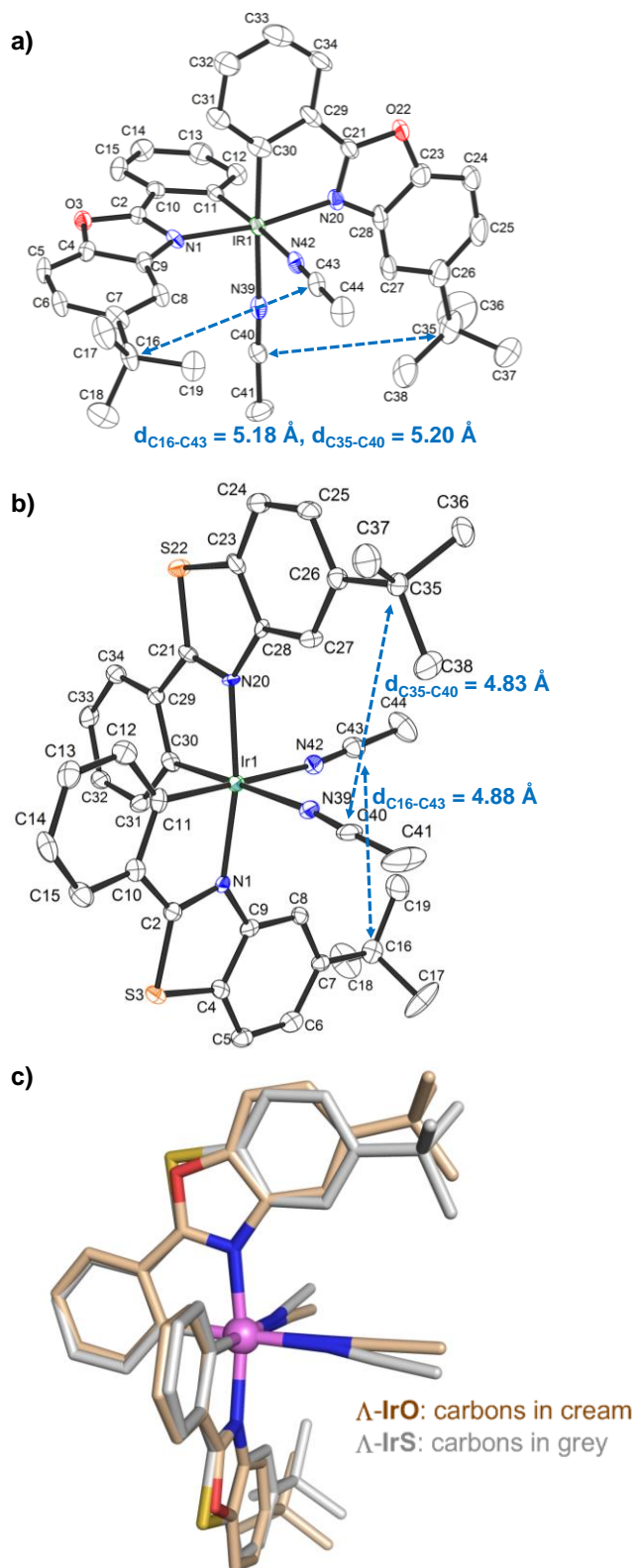


Figure 47 Comparison of the structures of **IrO** and **IrS**. a,b) Distances between the quaternary carbon atoms of the *tert*-butyl groups and the nitrile carbons of the neighboring MeCN ligands in Δ -**IrO** and Δ -**IrS**. c) Superimposed structures of the cationic complexes of Δ -**IrO** and Δ -**IrS**. Δ -**IrO** was obtained by mirror imaging the previous crystal structure of Δ -**IrO**.

3.3.4 Plausible Mechanism

A plausible mechanism in which photoredox catalysis intertwines with asymmetric catalysis is shown in Figure 48. Herein, the catalysis is initiated by the coordination of 2-acyl imidazoles (**24**) to the iridium catalyst in a bidentate fashion (intermediate **I**), followed by the formation of a nucleophilic enolate iridium(III) complex (intermediate **II**) upon deprotonation. The subsequent chirality generating key step constitutes the exergonic addition of a photo-reductively generated electrophilic radical to the electron rich metal-coordinated enolate double bond, thereby affording an iridium-coordinated ketyl radical (intermediate **III**). Oxidation of this ketyl intermediate to a ketone by single electron transfer provides the iridium-coordinated product (complex **IV**), which is released upon exchange against unreacted starting material, followed by a new catalytic cycle. The single electron transfer either regenerates the iridium(III) photosensitizer or leads to the reduction of another arganobromide substrate, thereby initiating a chain reaction. Proposed key intermediate which uniquely connects the asymmetric catalysis with the photoredox cycle is the iridium(III) enolate complex **II**, which not only provides the crucial asymmetric induction in the catalysis cycle and but at the same time serves as the *in situ* generated active chiral photosensitizer.⁷ A series of investigations have been executed to verify the proposed mechanism in the following section.

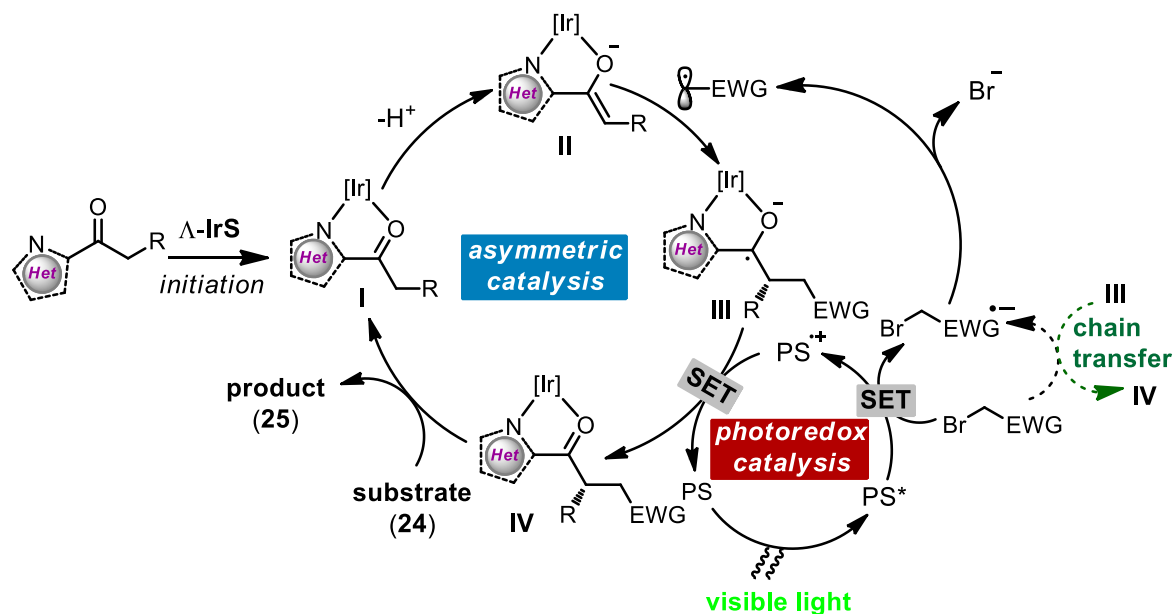


Figure 48 Plausible mechanism for a combined photoredox and asymmetric catalysis. SET = single electron transfer, EWG = electron withdrawing group, PS = photosensitizer in form of enolate complex **II**.

3.3.5 Mechanistic Investigations

1) Crystal structure analysis

To start with, as confirmed by X-ray crystallography (Figure 49), 2-acyl-*N*-methylimidazoles efficiently coordinate to the iridium catalyst Λ -IrS in a bidentate fashion upon release of the two monodentate acetonitrile ligands, thereby providing the proposed intermediate complex **I**. Subsequent deprotonation generated intermediate enolate iridium(III) enolate complex **II**, which was independently isolated and unambiguously characterized by X-ray crystallography (the crystals of intermediate **I** and **II** were obtained by the group member, Dr. Lili Zhang). This structure also illustrates that one face of the prochiral enolate π -bond is blocked by a *tert*-butyl group, thereby rationalizing the observed high asymmetric induction in the course of the proposed diastereoselective addition of the electron-deficient radical to the electron rich double bond (Figure 50).⁸ The determined absolute configurations of the α -alkylation products are consistent with this mechanistic picture. This reaction step relates to recent reports of the photosensitized generation of electron-deficient radicals and their stereoselective addition to electron-rich π systems of chiral enamines.⁹

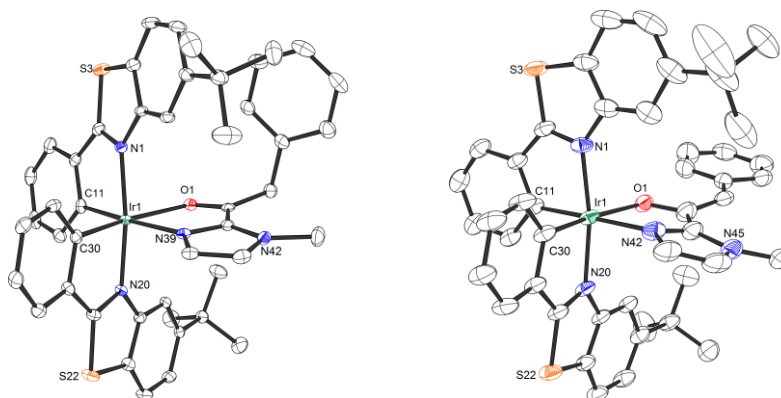


Figure 49 X-Ray crystal structures of the proposed Ir(III) intermediate complex **I** (the left one) and **II** (the right one). These compounds were crystallized as a racemic mixture, and only the Λ -enantiomer is shown here, as an ORTEP drawing with 30% probability ellipsoids.

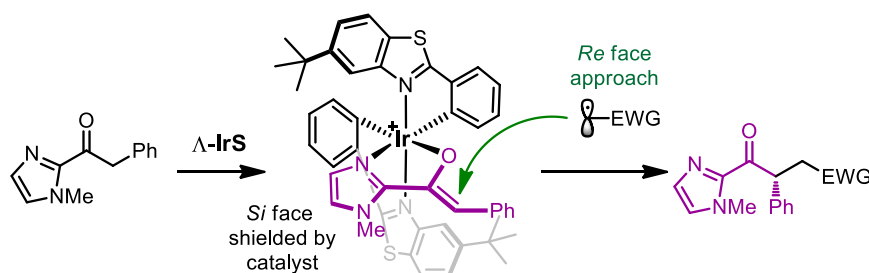
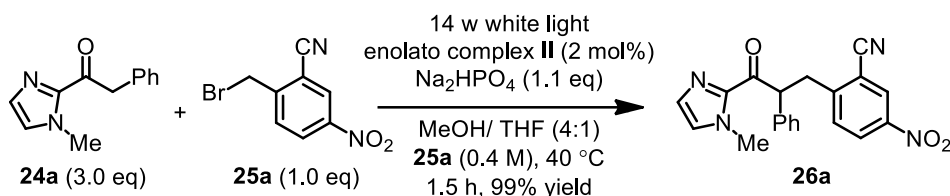


Figure 50 Proposed model for the asymmetric induction of photoredox alkylation reactions.

2) Verification of catalytic activity of enolate complex II

The independently synthesized racemic iridium(III) enolate complex **II** catalyzes the photoredox reaction with an identical efficiency compared to **IrS**, thereby confirming that complex **II** is catalytically competent and supporting the notion that complex **II** has a dual function as a chiral nucleophile in the catalytic cycle and the *in situ* photosensitizer in the photoredox cycle (Scheme 6).

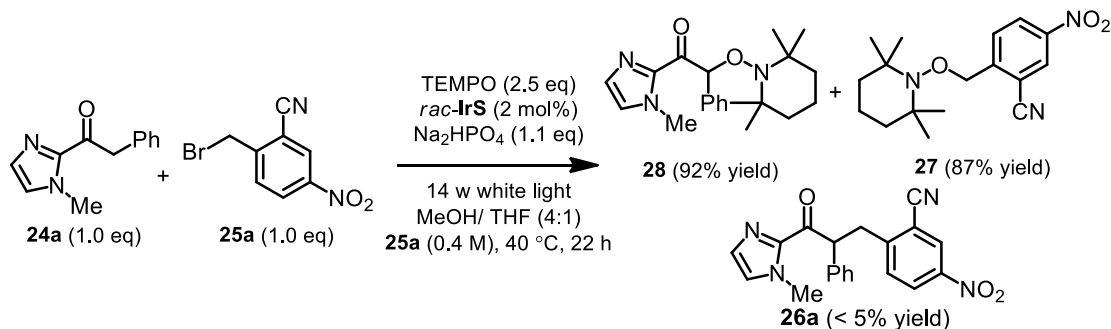


Scheme 6 Evaluation of the catalytic activity of enolate complex **II**.

3) Trapping experiment with TEMPO

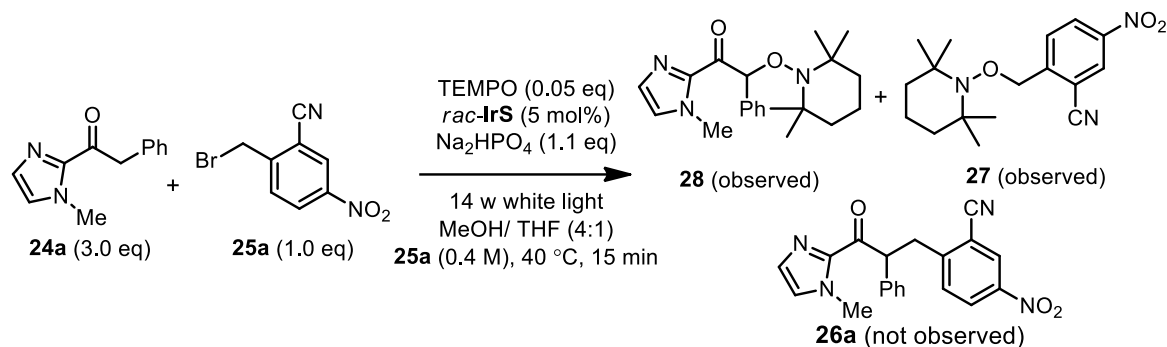
When 2.5 equivalents of 2,2,6,6-tetramethylpiperidine-1-oxyl (TEMPO) were added to the reaction after irradiation for 22 hours, only trace of the benzylation product **26a** was observed. The corresponding alkoxyamine adducts of the 2-acyl imidazole **24a** and of the alkyl fragment of electrophile **25a** were formed in 92% yield and 87% yield, respectively (Scheme 7). The ratio of compound **27** and **28** is nearby 1:1. It was confirmed that this transformation did not occur either under dark conditions or in the absence of the catalyst **IrS**.

The compound **27** can be rationalized as the coupling product between benzyl radical and free TEMPO radical. There are two possible pathways to produce the product **28**. First, it can be generated from the addition of TEMPO radical with electron-rich double bond of iridium(III) enolate complex **II** followed by the single electron oxidation of the corresponding ketyl radical. Second, an alternative formation of **28** was provided by the nucleophilic addition of enolate species to an oxidatively generated *N*-oxoammonium cation. These results support the radical mechanism involved in the photoinduced alkylation of 2-acyl imidazoles.



Scheme 7 Trapping experiment with excess TEMPO.

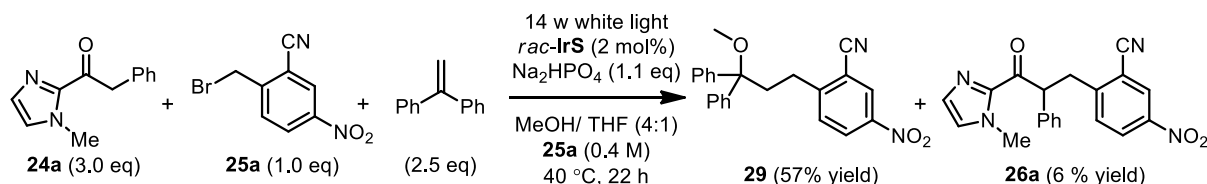
Low concentration of TEMPO (5 mol% with respect to **25a**) was also applied for the trapping experiment (Scheme 8). As a result, TEMPO was consumed within 15 min and products **27** and **28** were observed by ¹H-NMR analysis of the crude reaction mixture. In this case, TEMPO only retarded the commencement of the alkylation process, which then proceeded normally after the TEMPO was consumed completely.



Scheme 8 Trapping experiment with catalytic amount of TEMPO.

4) Trapping experiment with electron rich alkene

Adding 2.5 equivalents of the 1,1-diphenylethylene into the reaction mixture caused a significant inhibition of the formation of **26a**. Instead, the adduct product **29** was obtained in yield of 57% (Scheme 9). Apparently, reductively generated benzyl radicals are trapped effectively by the 1,1-diphenylethylene, which seems reasonable considering that the steady-state concentration of the enolate intermediate complex **II** cannot exceed the catalyst loading (2 mol%) and is therefore much lower compared to 1,1-diphenylethylene. Compound **29** was supposed to be produced through nucleophilic addition of methanol to photo-oxidatively generated diaryl methine carbocation. Whereas the diaryl methine carbocation can be formed from the addition of reductively generated benzyl radical with electron-rich double bond of iridium(III) enolate complex **II** followed by the single electron oxidation of the corresponding diaryl methine radical.



Scheme 9 Trapping experiment with electron rich alkene.

5) Light-dark interval experiment

The direct correlation between photolysis and product formation is demonstrated by a light-dark interval reaction shown in Figure 51. The light-dark interval experiments were performed according to the general catalysis procedure (entry 5 in Table 7) with 0.3 mmol benzyl bromide **25a**. The conversion was determined by ^1H NMR analysis of an aliquot from the reaction mixture. An aliquot was taken out of the reaction system via syringe for every 15 min until complete conversion was achieved. The whole process was performed under argon with Schlenk line. The NMR spectra shown below demonstrate that no significant byproducts are formed in this photoredox reaction (Figure 52).

These results suggested that the light is essential for the present reaction. Although no obvious yield increase of **26a** was observed in the absence of light, which do not definitively exclude the radical chain mechanism due to the short lifetimes of chain propagation process.¹⁰ The asymmetric catalysis and photoredox cycle operate in concert at least to some extent, a contribution of the chain propagation mechanism as a function of the nature of the substrates is feasible, and might even explain the differences in photolysis times for the individual reactions.

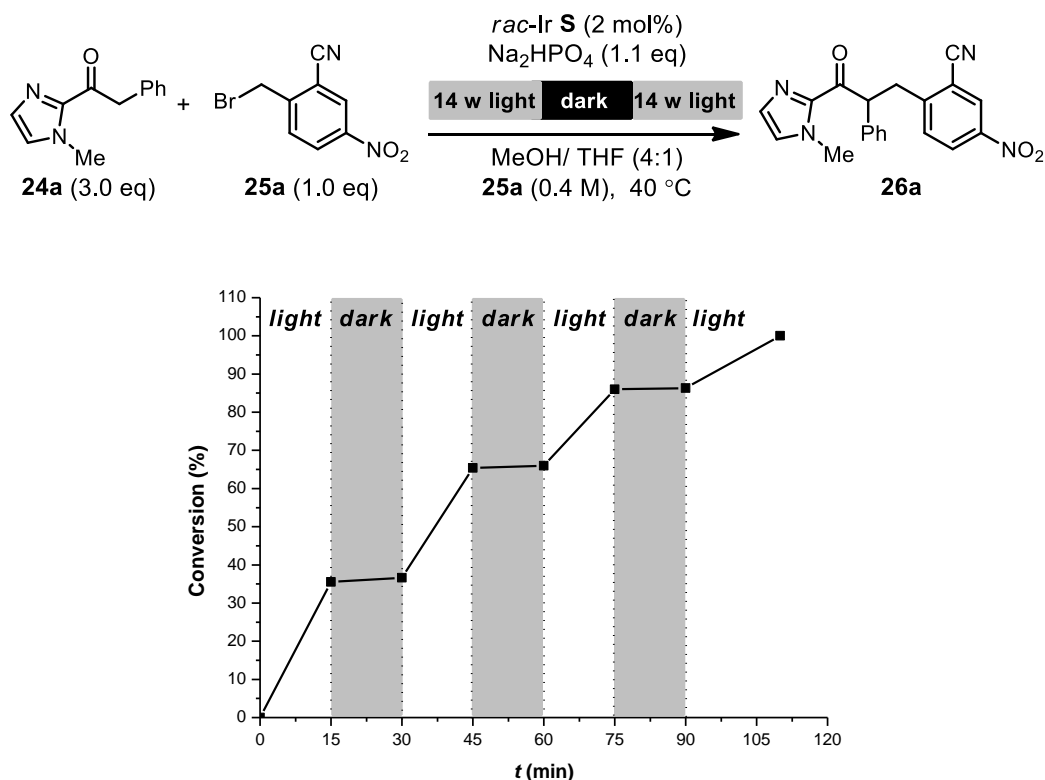


Figure 51 Light-dark interval experiment for the reaction **24a** + **25a** → **26a**.

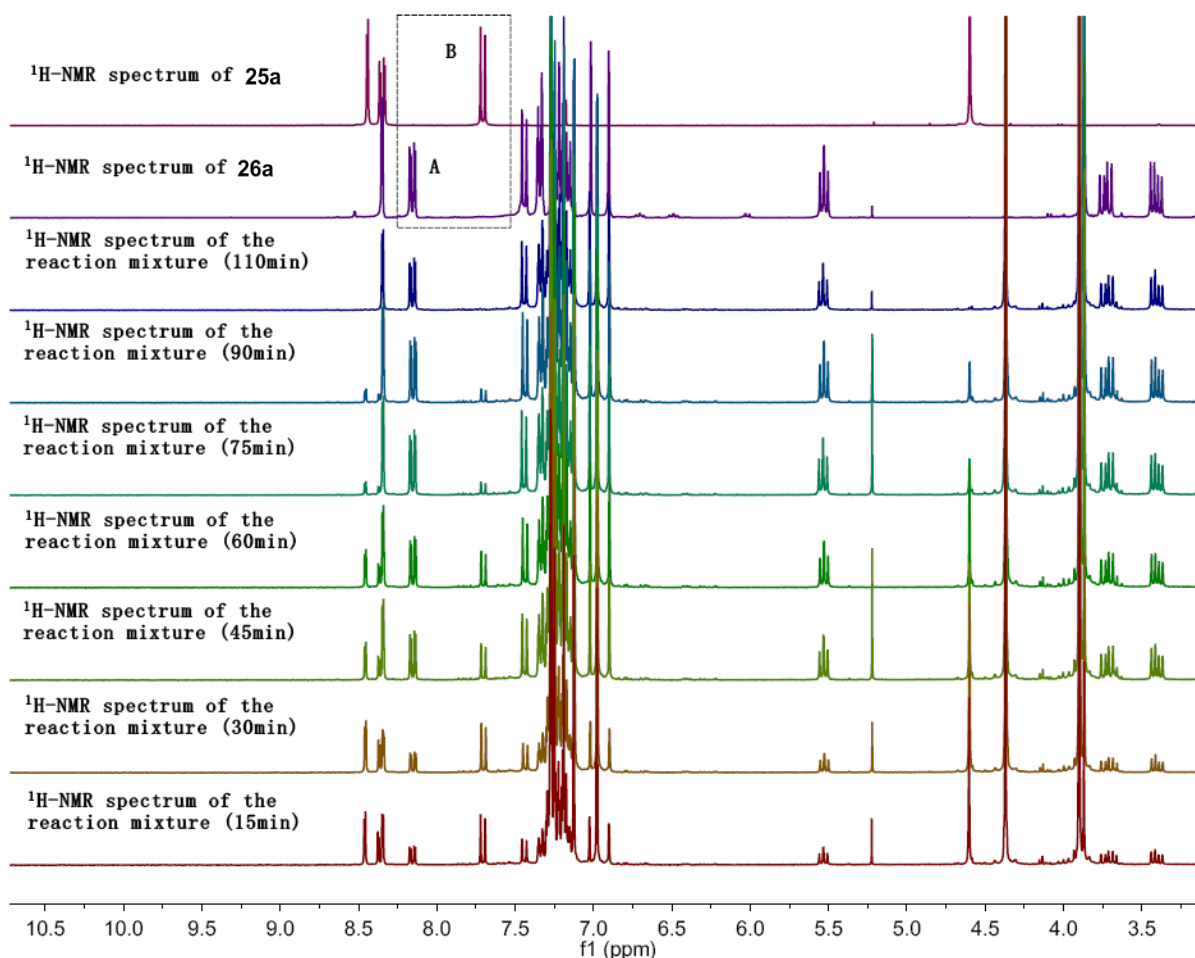


Figure 52 ^1H NMR (300 MHz, in CDCl_3) spectra of **25a**, **26a** (both as reference) and the crude product from the light-dark interval experiment. Conversion was inferred by area integration ratio (signals A and B).

6) Luminescence quenching experiments

In order to verify the potential photosensitizers involving in the photoredox cycle, enolate complex **II** and **IrS** were selected to perform the fluorescence quenching experiments with electrophile **25a**. Accordingly, Stern-Volmer plots (Figure 53) illustrate that the luminescence emission of the enolate complex **II** is quenched by benzyl bromide **25a** much more efficiently compared to **IrS** which can be attributed to a fast electron transfer from the $^3\text{MLCT}/^3\text{LC}$ excited state of enolate iridium complex **II** to the electron deficient benzyl bromide. This result proves that the enolate complex **II** serves as the *in situ* assembled photosensitizer is greatly favored and the Ir(III)/Ir(IV) cycle is operative. It is noteworthy that the possibility of photocatalyst acting *via* energy transfer cannot be excluded by fluorescence quenching experiments. While energy transfer to activate the benzyl substrate or other aromatic system and facilitate the bond homolysis cannot be ruled out. However, no observation of

significant byproducts derived from free radicals, such as dimerization derivatives or hydrogen abstraction, which suggest that energy transfer process is highly unlikely in this catalytic system.

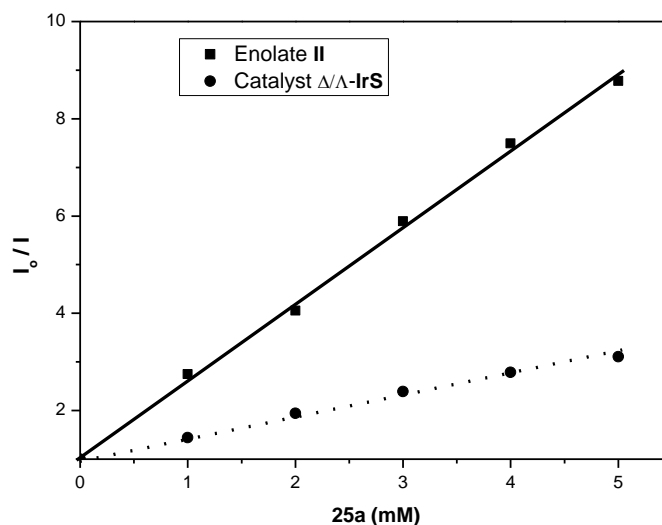


Figure 53 Luminescence quenching experiments. I_0 and I are respectively luminescence intensities in the absence and presence of the indicated concentrations of the electron deficient benzyl bromide **25a**.

7) Cyclic voltammetry measurements

The cyclic voltammetry in collaboration with the Prof. Hilt group (Faculty of Chemistry, University of Marburg), reveals that the enolate complex **II** has a significantly decreased oxidation potential by around 1 V compared to the cationic complex **IrS** and thus comprises a much stronger reducing agent in the ground state and even more so in its photoexcited state (Figure 54). The estimated excited state reduction potential $E_{1/2}(\text{II}^*/\text{II}^+)$ of -1.74 V vs. Ag/AgCl for the enolate complex **II** is comparable to *fac*-[Ir(ppy)₃] (ppy = 2-phenylpyridine),¹¹ an iridium sensitizer that has been used previously for the reductive cleavage of electron deficient benzyl bromides.⁹ These data support the intermediate iridium(III) enolate complex **II** constitutes the active *in situ* assembled photosensitizer in the photoredox cycle. Since iridium(III) complex **II** apparently represents the only neutral iridium(III) complex within the entire reaction mixture, these data is also consistent with observed trends regarding redox and photophysical properties of iridium(III) complexes, namely that neutral *bis*-cyclometalated iridium(III) photosensitizers are significantly stronger photoreducing agents than their cationic counterparts.¹²

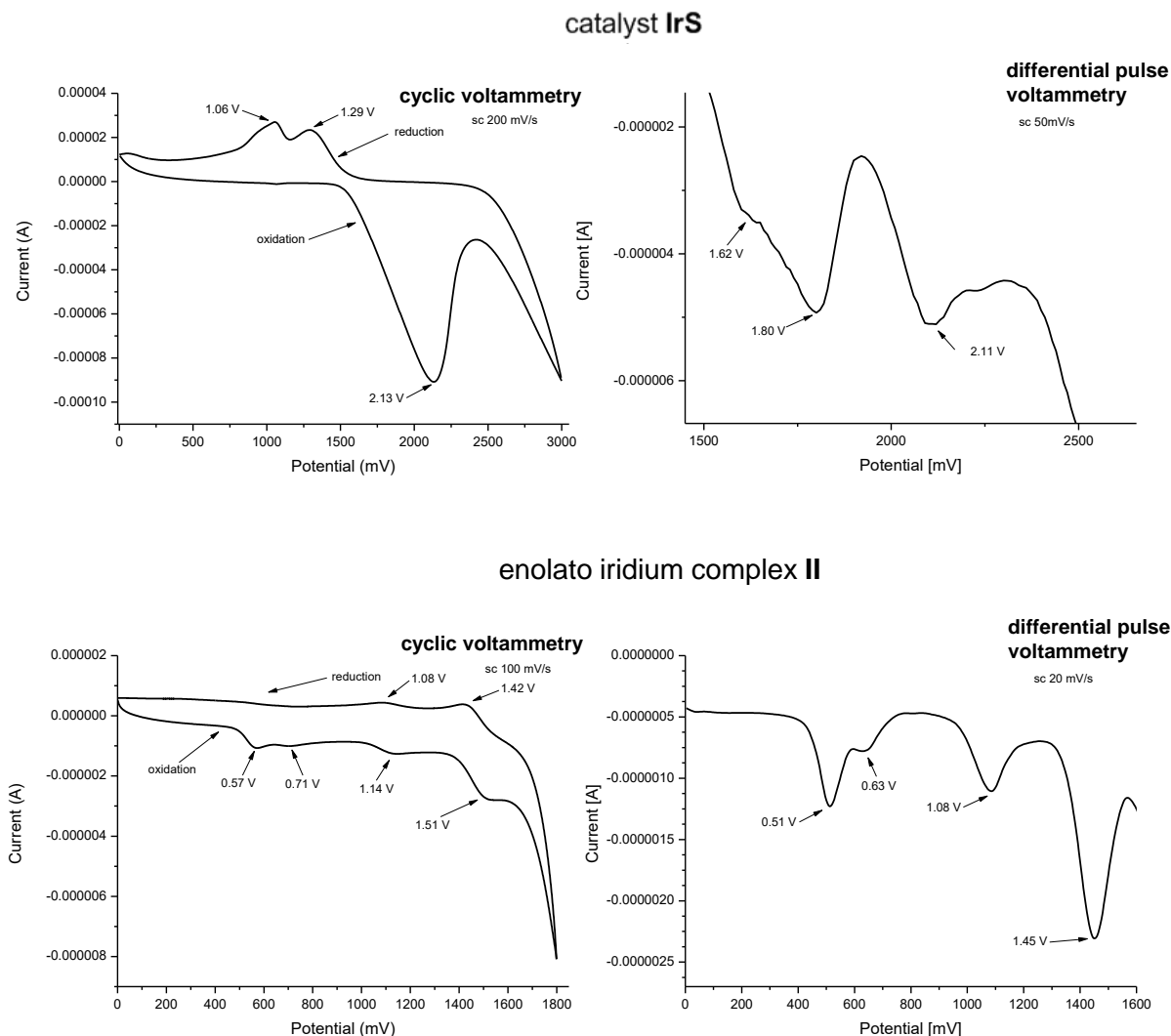


Figure 54 Cyclic voltammetry. Cyclic voltammograms and differential pulse voltammograms of the catalyst **IrS** (0.25 mM) and the enolate iridium complex **II** (0.25 mM) in CH_2Cl_2 containing 0.1 M $n\text{Bu}_4\text{NBF}_4$.

8) UV-visible spectroscopy analysis

As shown in Figure 55, compared to **IrS** and established iridium(III) photosensitizers¹², the enolate complex **II** displays a bathochromically shifted long wavelength absorbance maximum with an additional shoulder at around 500 nm, thus permitting an excitation across half of the visible spectrum ranging from violet to green light. The visible light absorbance of enolate complex **II** is not affected by the presence of organic bromide substrates, thus ruling out that an electron-donor-acceptor complex out of enolate complex **II** and bromide substrate is responsible for the light absorption (Figure 56)¹³.

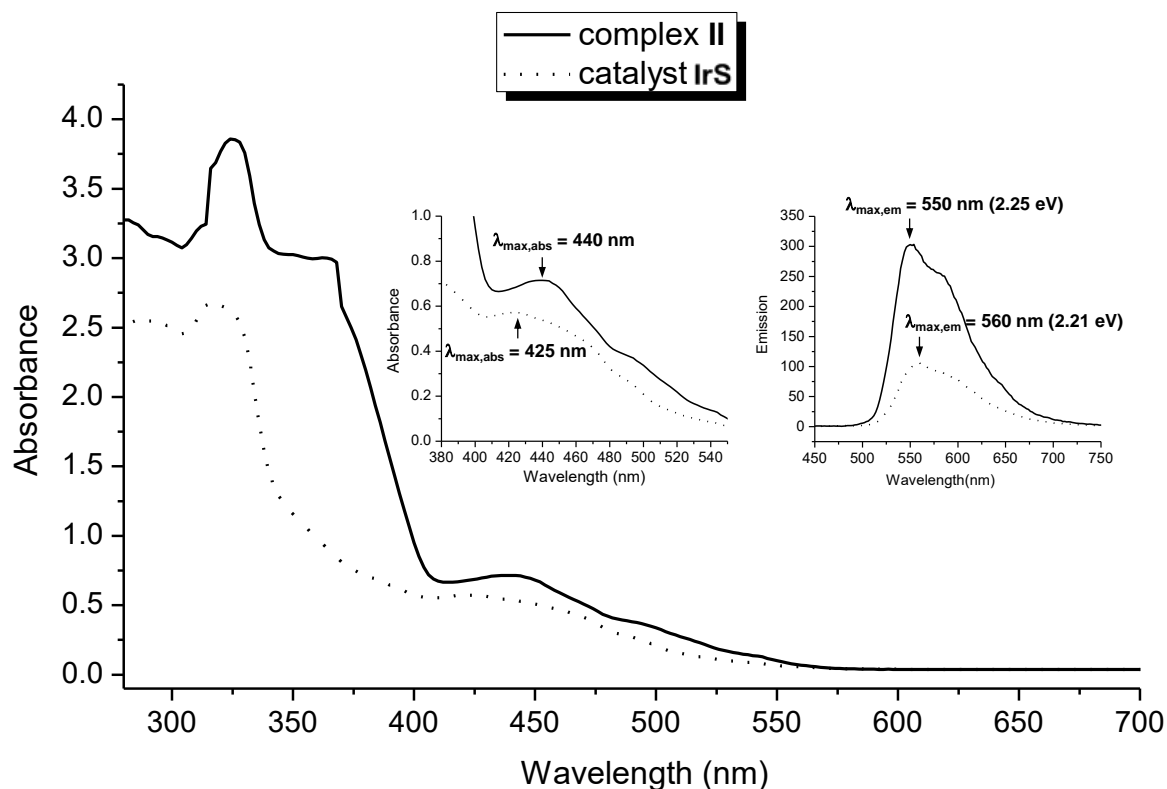


Figure 55 Absorption and emission properties of the catalyst **IrS** and the intermediate iridium enolate complex **II**. The complexes were measured as solutions in solvent MeOH/THF 4:1 (0.1 mM).

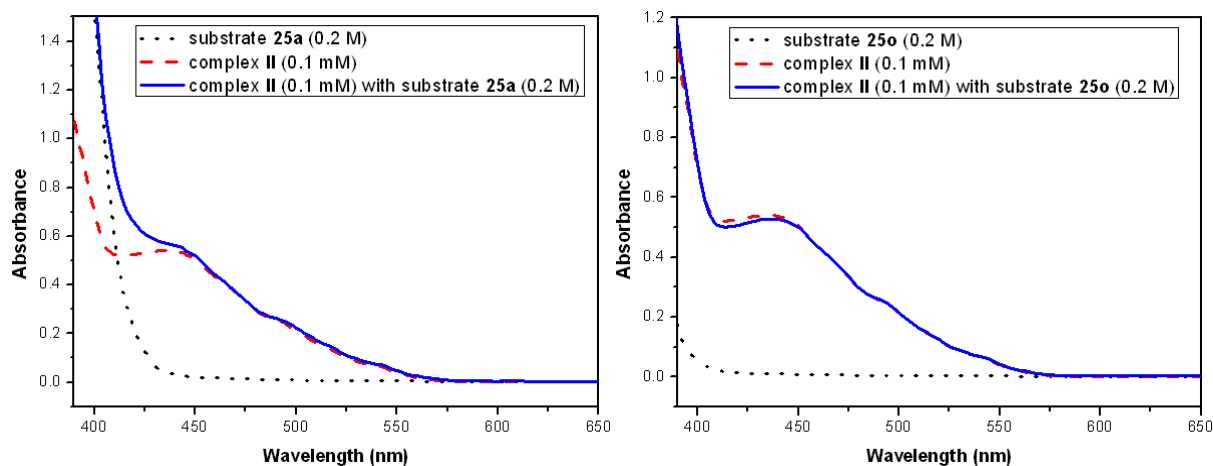


Figure 56 Investigation of the influence of bromide substrates on the optical absorption spectra of enolate complex **II**. Recorded in MeOH/THF 4:1 with enolate complex **II** at a concentration of 0.1 mM and an excess of substrate (0.2 M).

9) An alternative putative mechanism

Finally, one distinct variation of the outlined mechanism needs to be considered (Figure 57). A radical-radical coupling mechanism between the benzyl radical and the oxidized iridium sensitizer is reasonable. However, a major contribution of this recombination process is unlikely since both reactive intermediates will not be generated in close proximity, considering that the fragmentation of the formed radical anion does not occur instantaneously. In this respect, it has been established that the life time of such radical anions significantly increases in protic solvents and with a decreasing energy of the π^* orbitals.¹⁴ This notion is supported by the trapping experiment in which low concentrations of the radical trap TEMPO were still able to capture the intermediate benzyl radical (Scheme 8), thus rendering an efficient radical-radical coupling of the benzyl radical with the oxidized iridium sensitizer unlikely and instead favoring an addition of the intermediate electron-deficient benzyl radical with the electron-rich π -bond of the enolate iridium(III) complex **II** which is present in solution at a much higher steady state concentration.

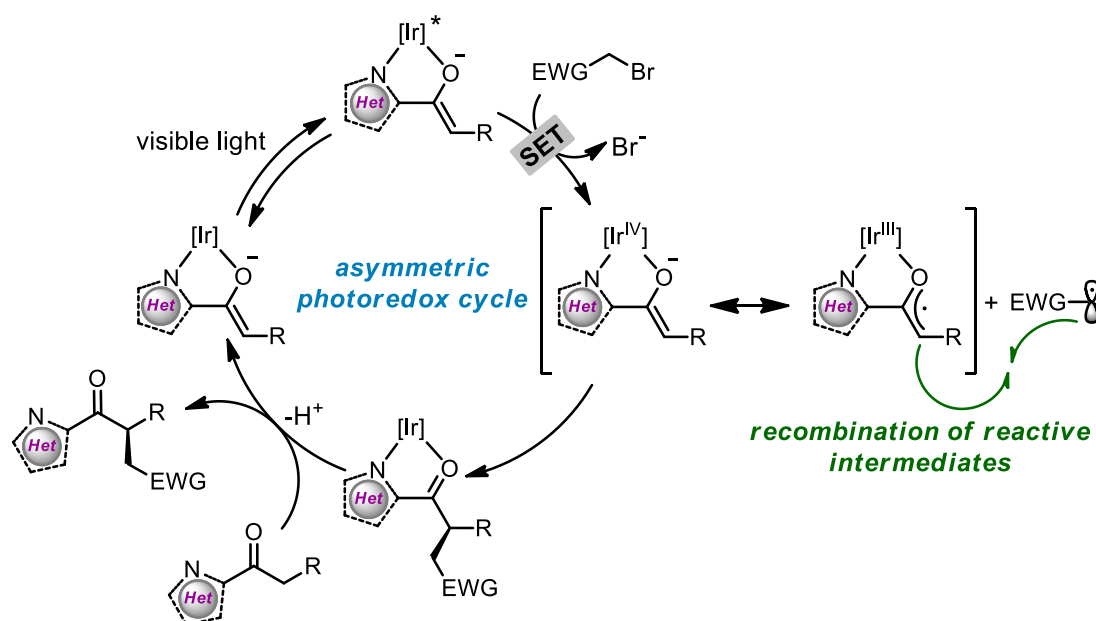


Figure 57 Mechanistical variations based on radical-radical recombination for the combined photoredox and asymmetric catalysis.

3.3.6 Conclusions

In conclusion, a unique case of visible-light-induced asymmetric redox catalysis by a single, structurally simple catalyst has been developed. The two catalytic cycles are connected through an intermediate iridium(III) enolate complex, formed from the initial catalyst and the 2-acyl imidazole substrate, which is not only the key nucleophilic intermediate in the asymmetric catalysis cycle but also constitutes the *in situ* generated active visible light photosensitizer. Despite the structural simplicity of the metal-based catalyst **IrS**, the metal center serves multiple functions at the same time: as a precursor for the photosensitizer, as a chiral Lewis acid for substrate activation, and as the exclusive chiral center for providing a highly effective asymmetric induction in the course of the C-C bond forming reaction.¹⁵ The here introduced reaction scheme may serve as a blueprint for the design of other catalytic asymmetric photoredox reactions, and will most likely provide new avenues for the efficient and green synthesis of non-racemic chiral molecules.

References

- 1 H. Huo, C. Fu, K. Harms, E. Meggers, *J. Am. Chem. Soc.* **2014**, *136*, 2990–2993.
- 2 (a) K. Zeitler, *Angew. Chem. Int. Ed.* **2009**, *48*, 9785–9789. (b) J. M. R. Narayanam, C. R. J. Stephenson, *Chem. Soc. Rev.* **2011**, *40*, 102–113. (c) C. K. Prier, D. A. Rankic, D. W. C. MacMillan, *Chem. Rev.* **2013**, *113*, 5322–5363. (d) D. M. Schultz, T. P. Yoon, *Science* **2014**, *343*, 1239176.
- 3 L. R. Espelt, I. S. McPherson, E. M. Wiensch, T. P. Yoon, *J. Am. Chem. Soc.* **2015**, *137*, 2452–2455. A racemic application, see also: Y. Miyake, Y. Ashida, K. Nakajima, Y. Nishibayashi, *Chem. Commun.* **2012**, *48*, 6966–6968.
- 4 (a) D. A. Nicewicz, D. W. C. MacMillan, *Science* **2008**, *322*, 77–88. (b) H.-W. Shih, M. N. Vander Wal, R. L. Grange, D. W. C. MacMillan, *J. Am. Chem. Soc.* **2010**, *132*, 13600–13603.
- 5 C. Wang, L.-A. Chen, H. Huo, X. Shen, K. Harms, L. Gong, E. Meggers, *Chem. Sci.* **2015**, *6*, 6966–6968.
- 6 X. Shen, H. Huo, C. Wang, B. Zhang, K. Harms, E. Meggers, *Chem. Eur. J.* **2015**, *21*, 9720–9726.
- 7 H. Sato, A. Yamagishi, *J. Photochem. Photobiol. C: Photochem. Rev.* **2007**, *8*, 67–84.
- 8 A. T. Herrmann, L. L. Smith, A. Zakarian, *J. Am. Chem. Soc.* **2012**, *134*, 6976–6979.
- 9 (a) M. N. Hopkinson, B. Sahoo, J.-L. Li, F. Glorius, *Chem. Eur. J.* **2014**, *20*, 3874–3886. (b) D. A. Nicewicz, D. W. C. MacMillan, *Science* **2008**, *322*, 77–80. (c) H.-W. Shih, M. N. Vander Wal, R. L. Grange, D. W. C. MacMillan, *J. Am. Chem. Soc.* **2010**, *132*, 13600–13603. (d) M. Neumann, S. Földner, B. König, K. Zeitler, *Angew. Chem. Int. Ed.* **2011**, *50*, 951–954. (e) M. Cherevatskaya, M. Neumann, S. Földner, C. Harlander, S. Kümmel, S. Dankesreiter, A. Pfitzner, K. Zeitler, B. König, *Angew. Chem. Int. Ed.* **2012**, *51*, 4062–4066.
- 10 M. A. Cismesia, T. P. Yoon, *Chem. Sci.*, **2015**, *6*, 5426–5434.
- 11 C. K. Prier, D. A. Rankic, D. W. C. MacMillan, *Chem. Rev.* **2013**, *113*, 5322–5363.
- 12 J. M. R. Narayanam, C. R. J. Stephenson, *Chem. Soc. Rev.* **2011**, *40*, 102–113.
- 13 E. Arceo, I. D. Jurberg, A. Álvarez-Fernández, P. Melchiorre, *Nat. Chem.* **2013**, *5*, 750–756.
- 14 C. P. Andrieux, A. Le Gorande, J. M. Saveant, *J. Am. Chem. Soc.* **1992**, *114*, 6892–6904.
- 15 E. Meggers, *Chem. Commun.* **2015**, *51*, 3290–3301.

3.4 Visible-Light-Activated Enantioselective Trichloromethylation with a Chiral Iridium Complex

3.4.1 Reaction Design

A simple chiral-at-metal iridium complex (Λ -IrS, Figure 58) as an effective asymmetric photoredox catalyst has been developed for the visible-light-induced enantioselective α -alkylation of 2-acyl imidazoles with electron deficient benzyl bromides and phenacyl bromides (Chapter 3.3).¹ Despite its novelty, one can criticize that α -alkylations of carbonyl compounds with primary organobromides may be well executed under S_N2 conditions without the absolute need for involving redox chemistry.² Going beyond the previous proof-of-principle demonstration, it is therefore highly desirable to seek an application in which redox catalysis is highly advantageous or even required. Electron-deficient bromotrichloromethane is intrinsically amenable electrophile precursor for the redox required chemistry. Addition of electron-deficient trichloromethyl radicals to catalytic enolate should access the direct enantioselective trichloromethylation through the single electron transfer process (SET).

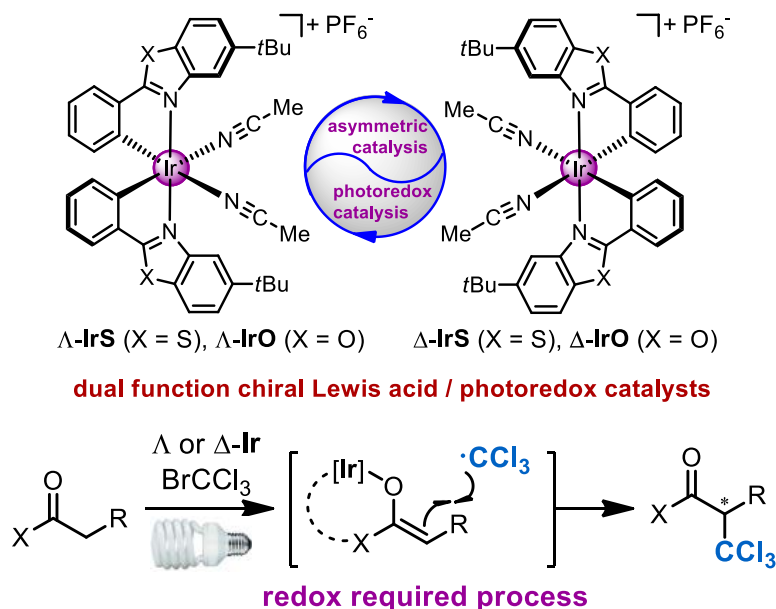
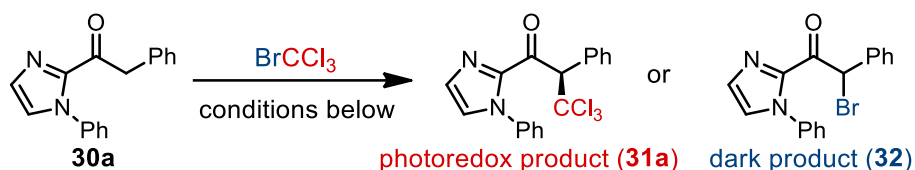


Figure 58 The redox required chemistry induced by visible-light-activated photoredox catalysis with chiral iridium complexes.

3.4.2 Reaction Optimization and Substrate Scope

This study was initiated by investigating the enantioselective α -trichloromethylation of 2-acyl imidazoles. Encouragingly, when 2-acyl imidazole **30a** was reacted with BrCCl₃ in the presence of iridium catalyst Λ -**IrS** and the base Na₂HPO₄ under visible light irradiation, the trichloromethylated product **31a** was obtained in 69% yield and with 94% *ee* (Table 9, entry 1). Using the weaker base NaHCO₃ provided **31a** even in 77% yield and with outstanding 99.7% *ee* (entry 2). In the absence of any base, the yield and enantiomeric excess deteriorated (entry 3). More importantly, in the presence of air no trichloromethylation was observed, but instead a different product was obtained, namely the α -brominated 2-acyl imidazole **32** (entry 4). Compound **32** was also the only observed product in the dark (entry 5), while conversely under visible light irradiation no traces of **32** were generated as confirmed by NMR experiments (entry 2, see the NMR experiments in mechanistic study section). Obviously, in this system, light induces a complete switch in the product formation and the reaction mechanism: Whereas the α -trichloromethylation (**31a**) can be rationalized with photoredox chemistry, the α -bromination (**32**) in the absence of light must rely on closed-shell S_N2 enolate chemistry with BrCCl₃ serving as an electrophilic brominating reagent.³ Apparently, the reductive activation of BrCCl₃ is required for the observed α -trichloromethylation. In this respect it is worth noting that the closely related iridium complex Λ -**IrO** provides inferior results (entry 6), in line with recent observation in Meggers group that this catalyst is more suitable for catalyzing oxidative chemistry.⁴

Table 9 Initial experiments for the catalytic enantioselective α -trichloromethylation activated by visible light^a


entry	catalyst	$h\nu^b$	additive	31a (%) ^c	32 (%) ^c	<i>ee</i> (%) ^d
1	Λ - IrS	yes	Na ₂ HPO ₄	69 ^e	0	94
2	Λ - IrS	yes	NaHCO ₃	77	0	99.7
3	Λ - IrS	yes	none	18	0	87
4	Λ - IrS	yes	NaHCO ₃ , air	0	37	0
5	Λ - IrS	no	NaHCO ₃	0	51	0
6	Λ - IrO	yes	NaHCO ₃	13	0	93

^a Reaction conditions: **30a** with 6 equiv BrCCl₃ with catalyst (2 mol%) in MeOH/THF 4:1 at room temperature, optional with 1.1 equiv NaHCO₃. ^b Light sources 20 W compact fluorescence lamp (CFL). ^c Isolated yields. ^d Enantioselectivities of **31a** determined by HPLC on chiral stationary phase. ^e HCl elimination product was isolated in a yield of 11%.

Having identified the optimal conditions in hand, the scope of the visible light activated enantioselective trichloromethylation was evaluated. Figure 59 shows the Λ -**IrS**-catalyzed α -trichloromethylation of twelve 2-acyl imidazoles, with the products (62-96% yield) featuring different substituents at the stereogenic carbon, such as phenyl groups with electron donating or electron accepting groups (**31a-f**), a naphthyl (**31g**) and thiophenyl (**31h**) moiety, an ether (**31i**), and aliphatic groups (**31j-l**). One of the most remarkable features for this catalytic mode is the excellent enantioselectivities, which is proved by that ten of these products are formed with an enantiomeric excess of 99% or higher. For product **31c**, absolute no traces of the minor enantiomer can be detected ($\geq 99.9\%$ *ee*), demonstrating the high degree of stereocontrol that can be reached in this catalytic reaction.

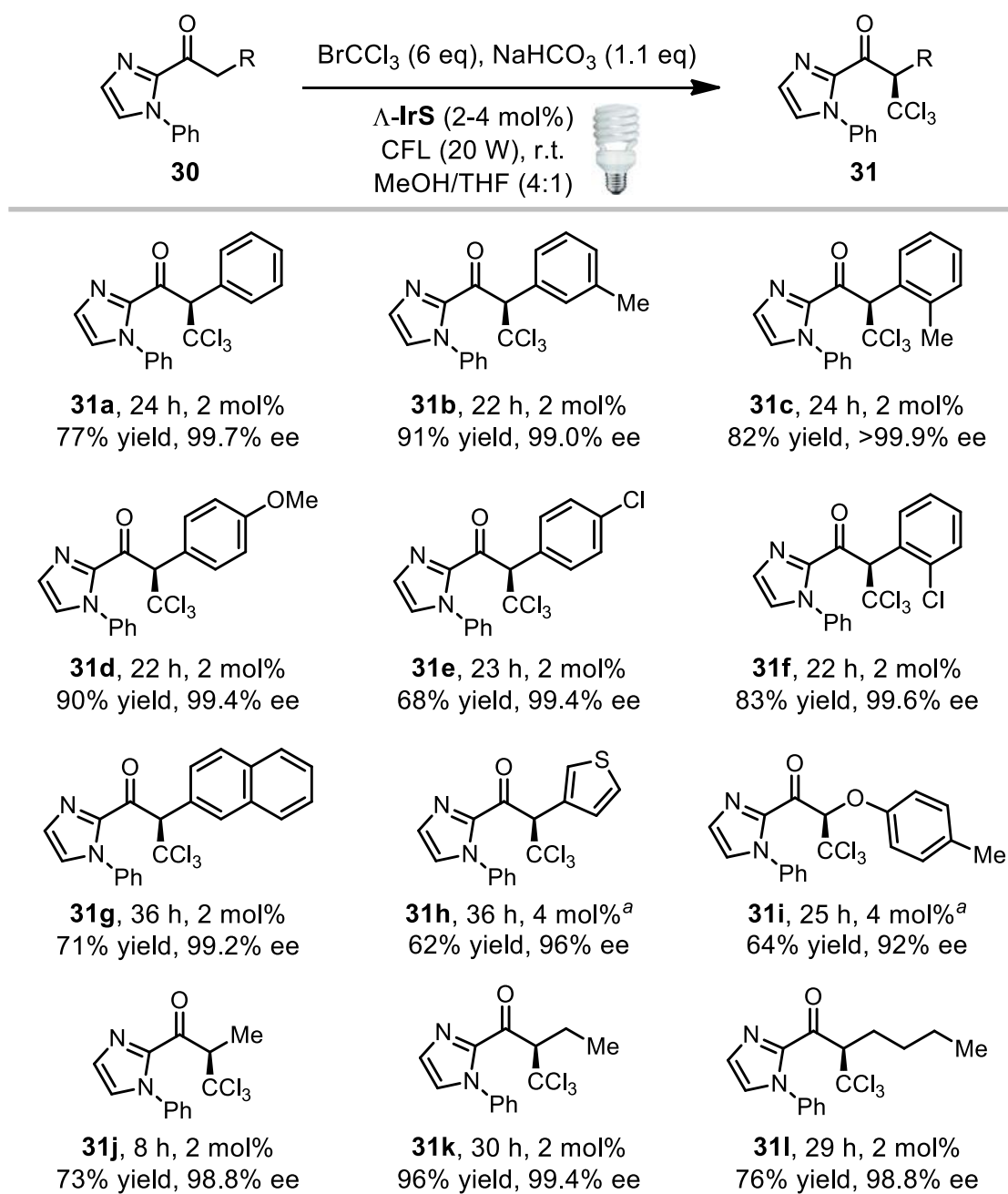


Figure 59 Substrate scope with 2-acyl imidazoles. ^a Higher catalyst loading to increase yield and enantioselectivity.

Unfortunately, there are still some 2-acyl imidazoles were found to be ineffective for α -trichloromethylation (Figure 60). When substituted with steric groups at the stereogenic carbon, only traces of desired products were observed, the starting materials were remained (**31m-p**). Compared to ether moiety (Figure 59, **31i**), the functional group of thiol ether is not similarly tolerant for this protocol (**31q-r**). The substrate decomposition was observed for the formation of **31q** and **31r**, which probably attribute to the oxidation of sulfide unit under the photoredox conditions. The photoexcited iridium complex is not able to compete with sulfide to be oxidized by the bromotrichloromethane, which can reasonable considering that the steady-state concentration of photoexcited iridium complex (2 mol% catalyst loading) is much lower than the amount of reaction free substrate.

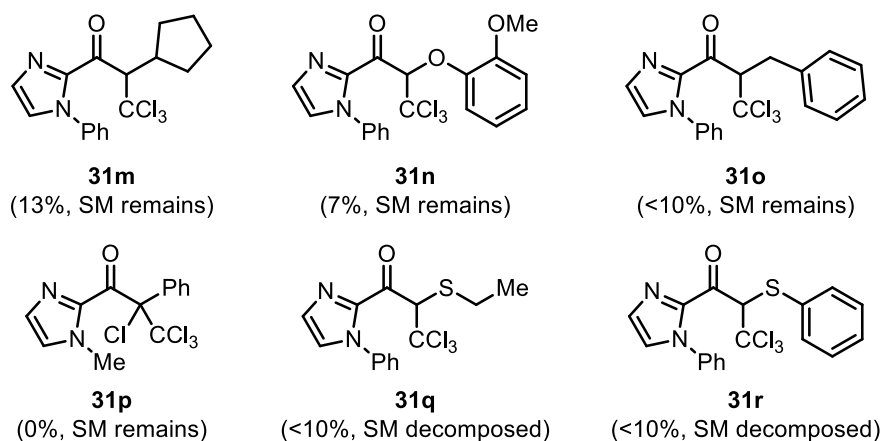


Figure 60 Some limitations of the substrate scope with respect to 2-acyl imidazoles.

Next, the imidazole moiety was thinking to be replaced with another coordinating group and 2-acylpyridines were selected due to the prevalence of pyridines and piperidines in bioactive compounds (Figure 61).⁵ Revealingly, a switch in cosolvent from THF to acetonitrile and at a higher catalyst loading of 4 mol% to compensate for overall slower reaction rates, 2-acyl pyridines **33** were converted to their α -trichloromethylated products **34** in satisfactory to high yields (65-91%) and with high enantioselectivities (90-99.6% *ee*). The 2-acylpyridines substrates readily tolerate aromatic (**34a**, **34i**) and aliphatic (**34b-h**) substituents at the stereogenic carbon. The electron donating (**34c**, **34h**), withdrawing (**34e-g**), aromatic (**34d**) groups are suitable in the pyridine moiety. The pyridine unit can also be replaced by the isoquinoline (**34i**).

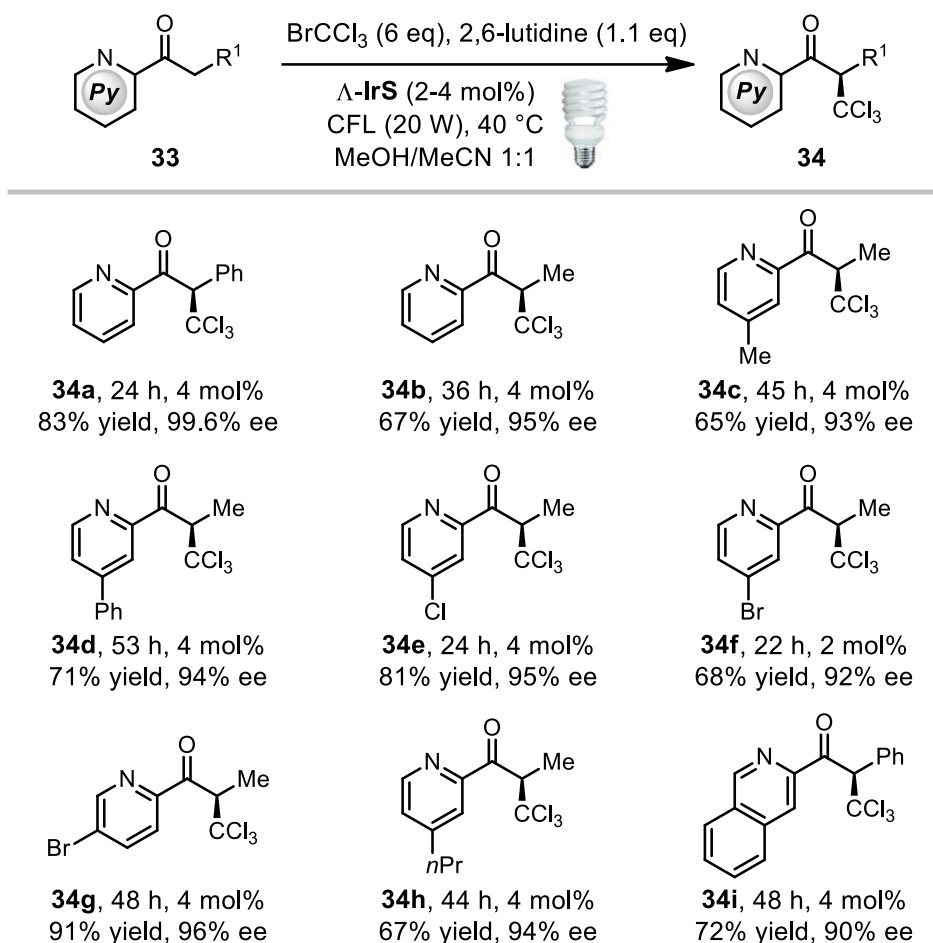


Figure 61 Substrate scope with 2-acyl pyridines.

Similarly, some 2-acylpyridines also have proven to be unreactive or less efficient in this chemistry (Figure 62). The trichloromethylation is inhibited completely by the substitution at the 6-position of pyridine ring (**34j**, **34k**), which can be rationalized that the steric hindrance prevent the efficient bidentate coordination of pyridine moiety to iridium center. An attempt of building the quaternary carbon center was unsuccessful (**34l**). When the methyl group at the stereogenic carbon was replaced by the more steric ethyl or propyl group (**34m**, **34n**), no detectable product formed and the starting material was recovered completely. Although the electron withdrawing group facilitates the deprotonation to provide improving yield, still does not reach the satisfied efficiency (**34o**). The effect of the substitution at 5-position was also investigated. Surprisingly, substitution with electron rich or poor group both resulted in depressed results (**34p**, **34q**). Thinking perhaps the electron rich group reduces the acidity of methylene group which make the deprotonation unfavorable (**34q**), and the electron poor group can cause slight racemization of formed product (**34p**). Overall, these results suggest that only the substitutions at the 4-position of pyridine unit are applicable to achieve

satisfactory yields and enantioselectivities for this photoreaction, the reactivity was highly limited to the steric substitutions.

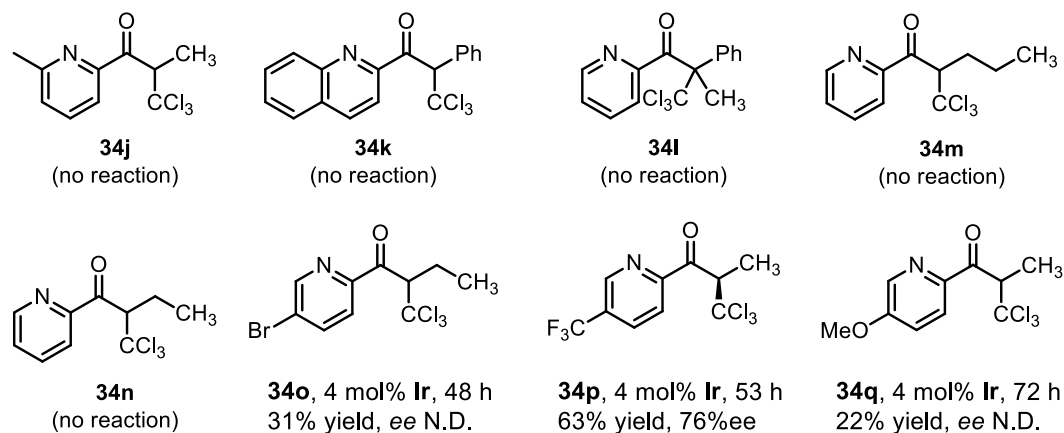


Figure 62 Some limitations of the substrate scope with respect to 2-acylpyridines.

Finally, in order to access the synthetic application for organic synthesis. A variety of auxiliary with bidentate coordination sites have been investigated (Figure 63). Replacing the pyridine moiety with thiazole group, under the same conditions as the reactions in Figure 61, the 2-acyl thiazole substrate provided the trichloromethylation product with 71% yield and 94% *ee* (**35a**). The moderate conversion and enantioselectivity was afforded by the 2-acyl pyrazine substrate (**35b**). Disappointingly, except these two coordinating groups, no more auxiliary was found to be amenable for this transformation. The α -amide ester (**35d**), pyrazole (**35c**) and Shibasaki auxiliary⁶ (**35h**) have been proven to be unreactive for the photocatalytic trichloromethylation. The acidic α -ketoester substrate yield the only product **35e** which can be rationalized as the HCl elimination product of the initial CCl_3 product. Thus, the less acidic substrate (related to **35f**) and tertiary substituted α -ketoester (related to **35g**) were used to address the HCl elimination, but no traces of **35f** and **35g** were detected under different conditions.

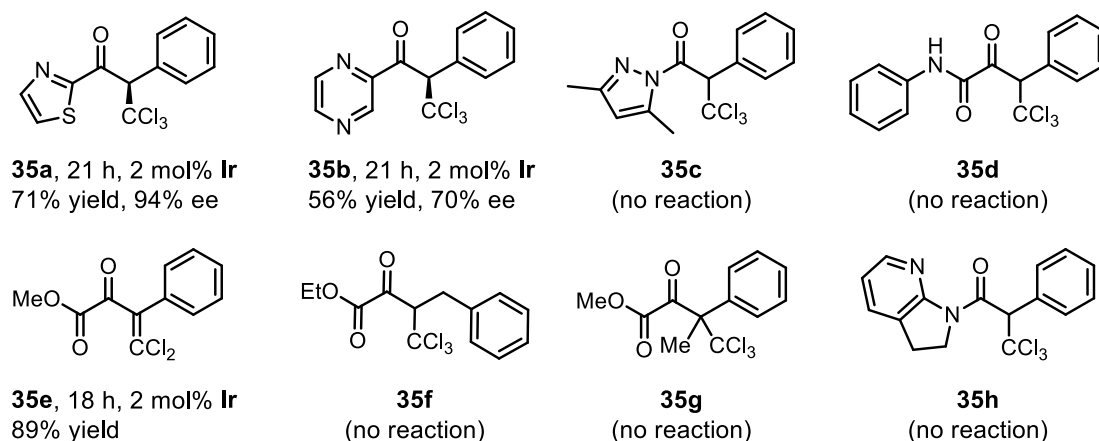
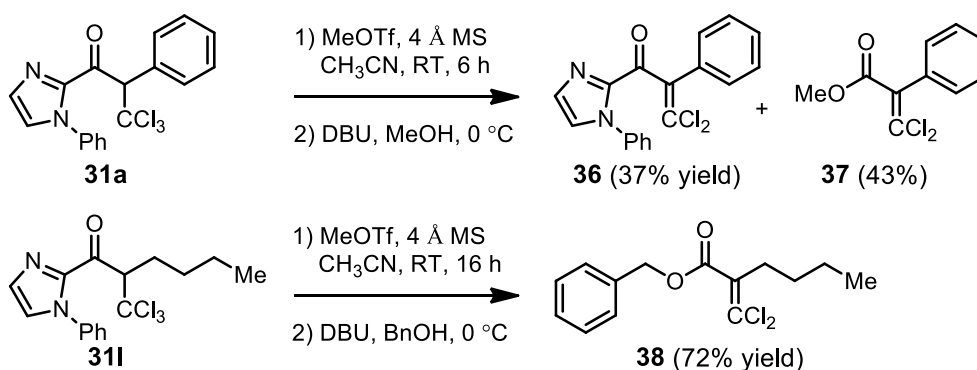


Figure 63 Efforts to extend the coordinating auxiliary scope.

3.4.3 Efforts to Transformations of 2-Acyl Imidazole Products

In order to expand the utility of the catalytic methodology, the cleavage of imidazole group was investigated (Scheme 10). One aromatic (**31a**) and one alkyl substituted (**31l**) products were selected to test the cleavage transformation. Unfortunately, only the HCl elimination derivatives were produced for these two CCl₃ compounds. Although literatures reported 2-acyl imidazoles can be converted to a wide variety of useful organic synthetic blocks,⁷ such as the ketone, alcohol, ester and amide, these methods are not applicable to the trichloromethylation products due to the sensitivity of the CCl₃ group towards HCl elimination under basic conditions. It is also noteworthy that the unsuccessful transformation of imidazoles to other synthetic compounds does not affect the value of this asymmetric catalytic chemistry, since imidazoles themselves are privileged structural motifs in bioactive molecules.⁵



Scheme 10 Efforts towards removal of imidazole auxiliary.

3.4.4 Plausible Mechanism

A plausible mechanism is shown in Figure 64, which can be classified as an electron-transfer-catalyzed nucleophilic substitution *via* $S_{RN}1$.⁸ Accordingly, the catalytic cycle is initiated by bidentate coordinating of the 2-acyl imidazole or 2-acylpyridine substrate to the iridium catalyst (intermediate **I**), followed by base-promoted deprotonation to an electron-rich iridium enolate (intermediate **II**). The subsequent addition of a reductively generated electrophilic trichloromethyl radical to the nucleophilic double bond provides an iridium-coordinated ketyl radical (intermediate **III**), which is oxidized to an iridium-coordinated product (intermediate **IV**) by single electron transfer, followed by product release. The single electron transfer can also leads to the reduction of another bromotrichloromethane, thereby initiating a chain reaction. A series of investigations in the following section have been executed to verify the iridium enolate complex **II** not only provides the crucial asymmetric induction in the catalysis cycle and but at the same time serves as the *in situ* generated active photosensitizer.

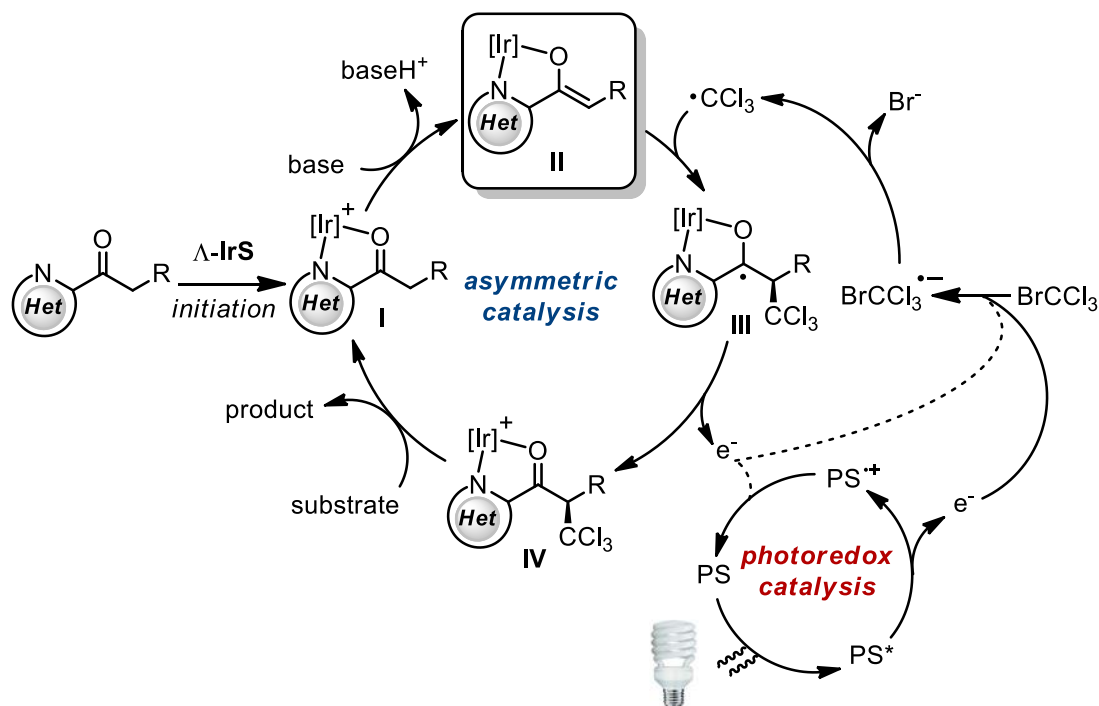


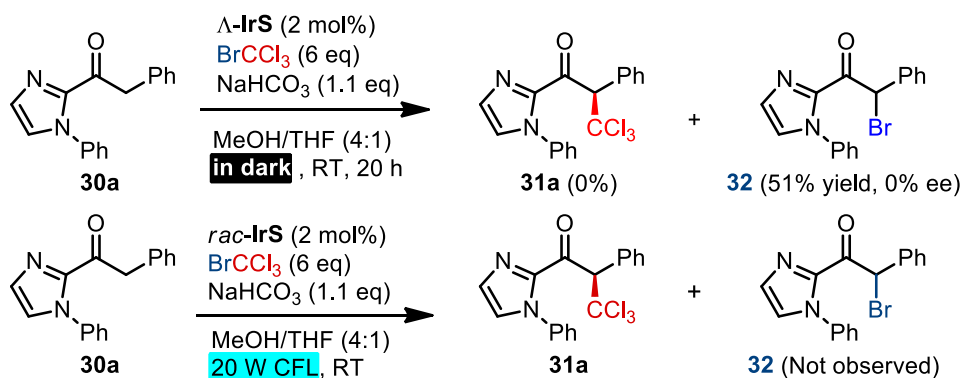
Figure 64 Putative mechanism for the visible light activated asymmetric catalysis. SET = single electron transfer, PS = photosensitizer in form of enolate intermediate **II**.

3.4.5 Mechanistic Investigations

1) Control experiments

1.1) Control experiments in the dark: formation of the brominated product

These control experiments were performed according the general catalysis procedure (see Experimental Part) with 0.2 mmol 2-acyl imidazole **30a**. No trichloromethylated product **31a** was observed in the dark. In contrast, no detectable brominated product **32** was formed in the overall photoredox process, which was demonstrated by the NMR spectra as shown below (Figure 65). The conversion of the photochemical process was determined by ^1H -NMR analysis of aliquots from the reaction mixture taken out of the reaction system via syringe at different times. The light obviously severs as a complete switch in the formation of trichloromethylated and brominated products.



Scheme 11 Control experiments for the comparison of the dark reaction and photoreaction.

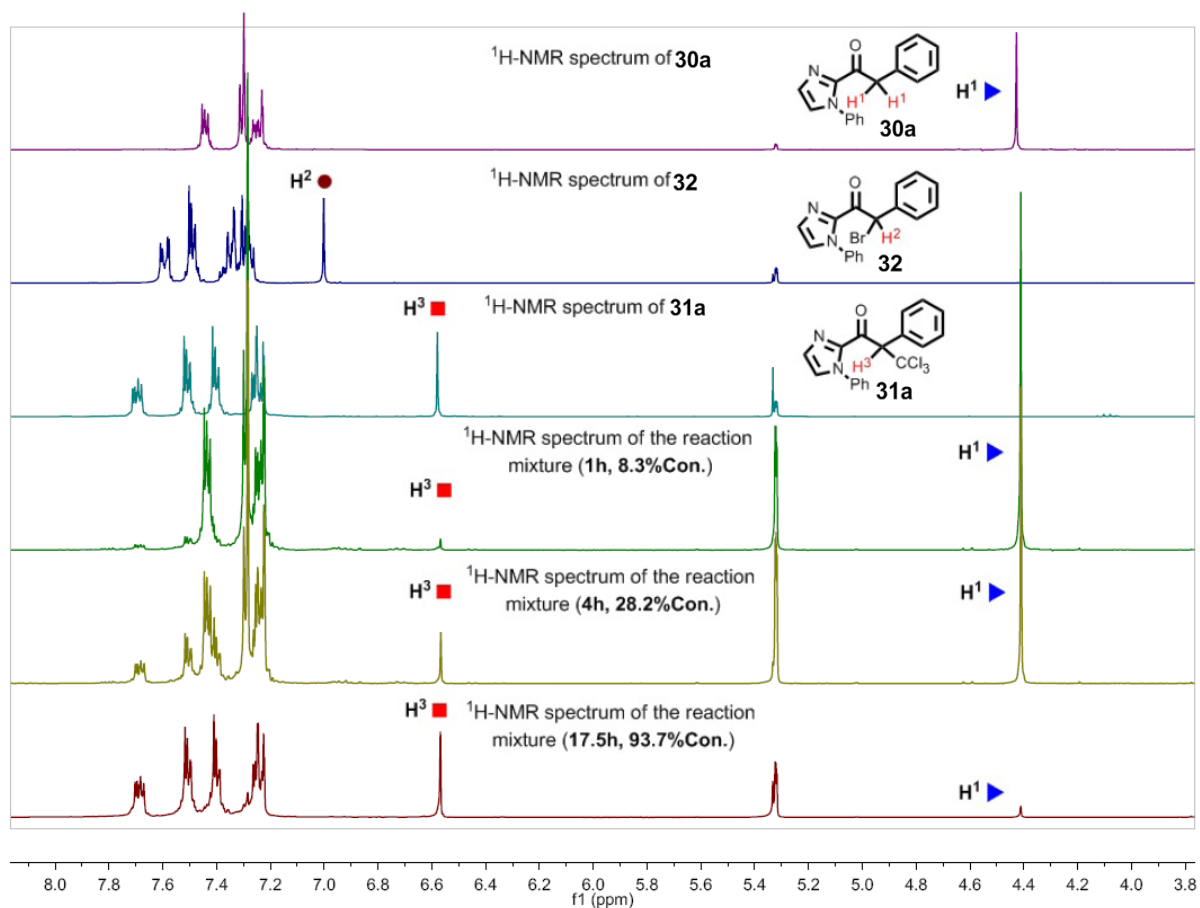
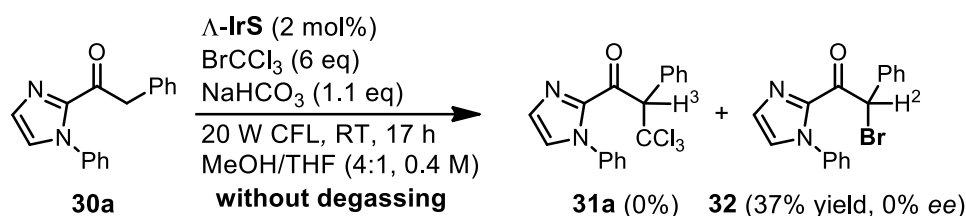


Figure 65 ^1H NMR (300 MHz, in CD_2Cl_2) spectra of **30a**, **31a**, **32** (as references) and the crude product from the photolysis. Conversion was inferred by integration ratio (signals H^1 and H^3).

1.2) Control experiments without degassing: effect of aerobic conditions

As a result shown below, not degassing caused a complete inhibition of the formation of **31a**, which supports the radical mechanism for photoinduced trichloromethylation. Instead, the brominated product **32** was obtained as a racemic compound, which was consistent with the experimental observation in the dark. The inefficient enantioselectivity of **32** was probably caused by the racemization under basic and protic conditions. Compared to CCl_3 , the smaller Br group has a stronger electron withdrawing effect which was verified by the proton NMR shifts of H^2 (6.90 ppm) and H^3 (6.58 ppm). Thus the brominated product **32** was highly sensitive for enolization in the basic reaction system (Scheme 12).



Scheme 12 The effect of aerobic conditions for the photocatalytic trichloromethylation.

1.3) Control experiments toward the base: effect of different Brønsted bases

As shown in Figure 66, the depressed yield was obtained in the absence of base, which was consistent with the enolate activation mode. NaHCO_3 serves as the optimal base to provide **31a** with 77% yield and 99.7% ee, without traces of the HCl elimination product **36**. The stronger bases either provide the product **31a** with partial racemization (Na_2HPO_4), or yield the only elimination product **36** (Na_3PO_4). Thus, the base plays a crucial role for intertwining with product formation and avoiding racemization or HCl elimination.

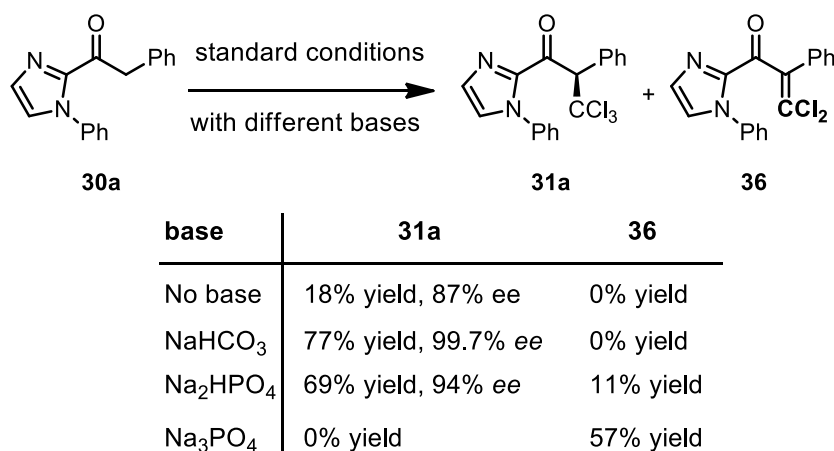
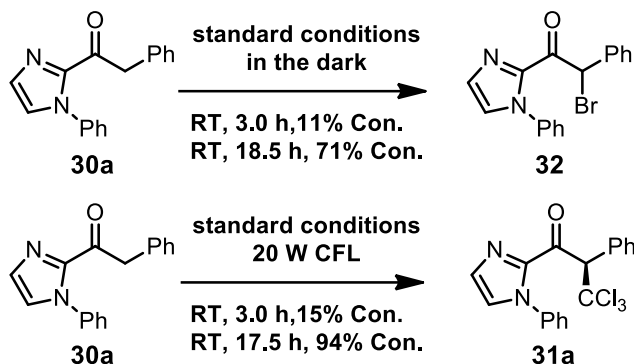


Figure 66 The effect of base for the photocatalytic trichloromethylation.

2) Discussion of competition between bromination and trichloromethylation

As shown in Table 9, the bromination product is the only observed product in the dark, whereas upon photolysis with visible light only the trichloromethylation product is observed. The following control experiments were performed to gain insight into the reason for not observing any brominated product in the presence of light.

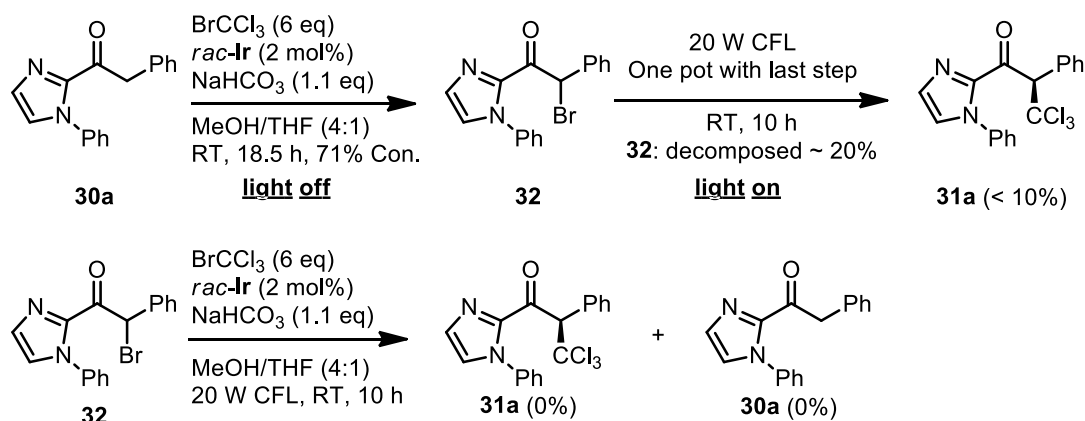
2.1) Comparison of initial rates for the dark reaction and photoreaction:



Scheme 13 The comparison of rates for the formation of **32** and **31a**.

The comparison experiments were performed according to the general catalysis procedure with 0.2 mmol 2-acylimidazole **30a**. The conversion was determined by ¹H-NMR analysis of aliquots from the reaction mixture. Accordingly, the overall rate of the photoreaction is slightly faster compared to the bromination reaction in the dark.

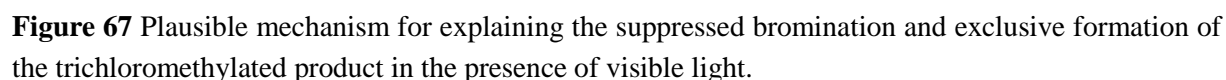
2.2) Considering a possible transformation of the bromination product:



Scheme 14 Evaluating the possible transformation of bromination product **32**.

The reactions were performed with 0.2 mmol 2-acylimidazole **30a**. In a first experiment, the reaction mixture was run in the dark until the brominated product **32** was formed with 71% conversion as monitored by ¹H NMR. Then, the reaction was run for a further 10 hours under 20 W CFL. As a

Based on the above control experiments, the following plausible mechanism is proposed which can explain why the bromination reaction is not able to compete with the trichloromethylation in the presence of light (Figure 67). Accordingly, both catalytic cycles run through the intermediate iridium enolate complex **II**. The bromination product is formed through the reaction of **II** with the electrophile BrCCl_3 , whereas the trichloromethylation product is formed through the reaction of **II** with a reductively formed trichloromethyl radical. Since the radical addition must be a very fast process that is almost diffusion controlled, the bromination reaction with the weak electrophile BrCCl_3 will not be able to compete so that all enolate intermediate **II** only reacts with the trichloromethyl radical. Note that although the enolate reaction steps of the two catalytic cycles differ strongly, this is not the case for the overall reaction cycle which is in large parts dominated by slow ligand exchange processes.



3) Luminescence quenching experiments

The stern-Volmer plot shown in Figure 68 strongly suggest that it is the neutral intermediate iridium enolate complex (**II**) which serves as the active photosensitizer, as its photoexcited state is quenched by BrCCl_3 significantly faster compared to the cationic complexes **I** and *rac*-**IrS**. The oxidative quenching of the photoexcited state of enolate complex **II** indicates the single electron transfer through Ir(III)/Ir(IV) cycle, which is consistent with the experimental observation of photocatalytic α -alkylation in Chapter 3.3 section. While the luminescence quenching experiments cannot exclude the energy transfer to BrCCl_3 and facilitate the bond homolysis. It is need to point out that *N*-Methyl instead of *N*-phenyl imidazole derivatives were used for **I** and **II** due to higher stability of the enolate complex and stronger emission intensities.

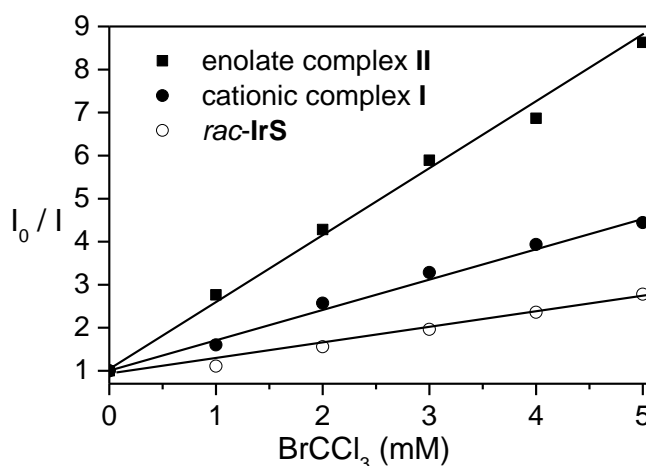
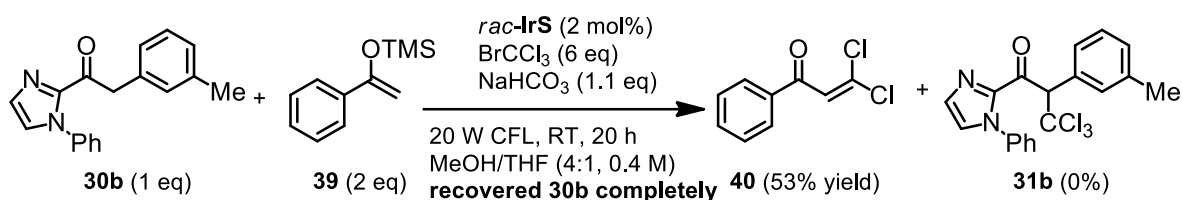


Figure 68 Luminescence quenching experiments. I_0 and I = luminescence intensities in the absence and presence of the indicated concentrations of BrCCl_3 , respectively.

4) Trapping experiments with electron rich alkenes

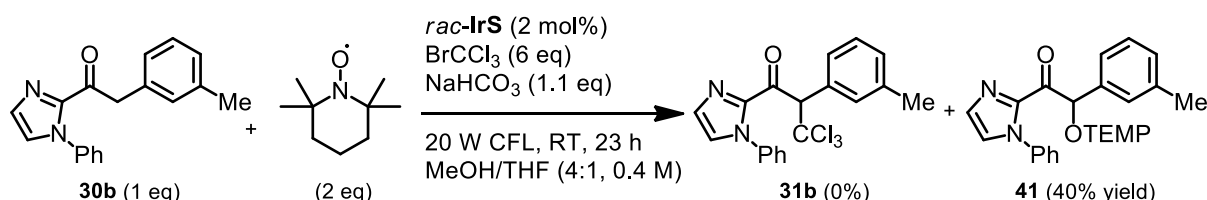
Adding two equivalents of the 1-phenyl-1-(trimethylsilyloxy)ethene (**39**) into the reaction mixture caused a complete inhibition of the formation of **31b** and the 2-acyl imidazole **30b** can be recovered completely (Scheme 15). Instead, the compound **40** was isolated in a yield of 53%. Apparently, reductively generated trichloromethyl radicals are trapped effectively by the enolether **39**, which seems reasonable considering that the steady-state concentration of the enolate intermediate complex **II** cannot exceed the amount of added iridium catalyst (2 mol% catalyst loading) and is therefore much lower compared to **39**. The product **40** can be rationalized as being the HCl elimination product of the initial CCl_3 product which is not stable under the basic conditions.



Scheme 15 Trapping experiments with electron rich silyl enolether **39**.

5) Trapping experiment with TEMPO

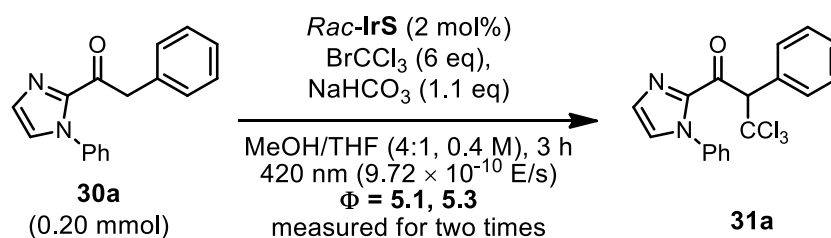
When two equivalents of TEMPO were added to the reaction after irradiation for 23 h, the trichloromethylation product **31b** could not be detected. The corresponding alkoxyamine adduct (**41**) of the 2-acyl imidazole **30b** was formed in 40% yield. It was confirmed that the generation of the oxyaminated product did not occur under dark conditions. The single-electron-oxidized complex **II** can be trapped efficiently, which is consistent of the radical mechanism and supports the enolate complex **II** as a key intermediate in the catalytic cycle.



Scheme 16 Trapping experiment with TEMPO.

6) Quantum yield measurement

The quantum yield was measured by standard ferrioxalate actinometry. A 6 W blue LED lamp (420 nm) was used as the light source. The measured method was designed according to procedures reported by Yoon and coworkers with slight modifications.⁹ The described catalytic cycle (Figure 64) intertwines with a photoredox cycle that generates a trichloromethyl radical upon SET from the photoactivated photosensitizer to BrCCl_3 and subsequent release of bromide. A determined quantum yield of 5 indicates that the trichloromethyl radical is also formed by direct electron transfer from the strongly reducing ketyl radical intermediate **III** to BrCCl_3 , thereby leading to a chain reaction.



Scheme 17 The model reaction for the quantum yield measurement.

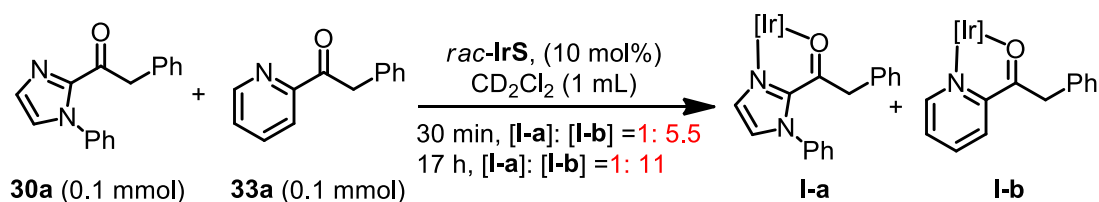
7) Coordination strength comparison of 2-acyl imidazoles and 2-acylpyridines

In order to evaluate the differences in coordinative strength between 2-acylimidazole **30a** and the 2-acylpyridine **33a**, a competition experiment was devised and analyzed by ^1H -NMR (Figure 69). The result demonstrates that the binding constant of the pyridine substrate exceeds the binding constant of the imidazole substrate by around one order of magnitude. In the case of the stronger coordinating 2-acyl pyridines, the replacement of coordinated product with new substrate (**IV**→**I**, Figure 64) is probably mediated by an initial coordination of one or two acetonitriles, thus explaining the requirement for acetonitrile as a cosolvent.

Reaction 1 (serves as a reference): **30a** (0.2 mmol) plus *Rac-IrS* (0.01 mmol, 5 mol%)

Reaction 2 (serves as a reference): **33a** (0.2 mmol) plus *Rac-IrS* (0.01 mmol, 5 mol%)

Reaction 3 (competition reaction): **30a** (0.1 mmol), **33a** (0.1 mmol) plus *Rac-IrS* (0.01 mmol, 10 mol%)



● Signals of *t*Bu in complex **I-a**. ■ Signals of *t*Bu in complex **I-b**. ♥ Signals of released CH_3CN .

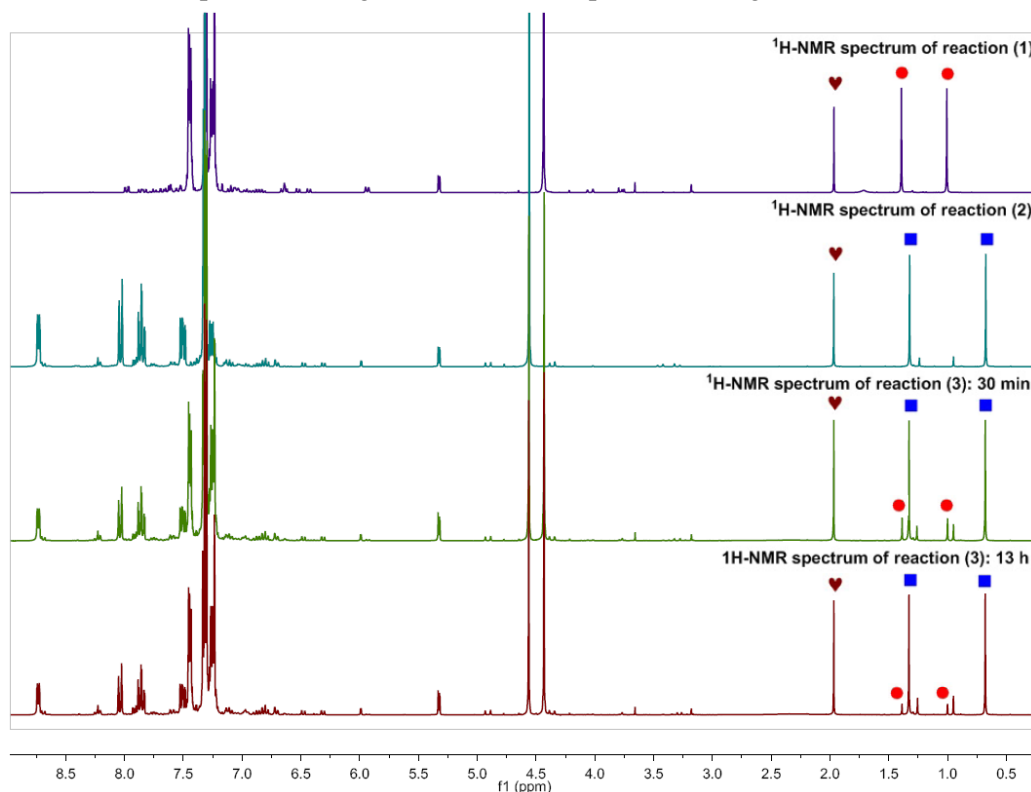


Figure 69 ^1H NMR (300 MHz, in CD_2Cl_2) spectra of reactions 1-3. Conversion was inferred by area integration ratio (signals '●' and '■').

3.4.6 Conclusions

In conclusion, the first example of an enantioselective, catalytic trichloromethylation has been developed and two types of ketone, namely 2-acyl imidazoles and 2-acylpyridines have been applied to this catalytic system with outstanding efficiencies.¹⁰ Excellent enantioselectivities are observed with multiple reactions reaching 99% *ee* and even higher. A range of mechanistic investigations confirmed the chiral iridium complex **IrS** which serves a dual function, as a catalytically active chiral Lewis acid and simultaneously as a precursor for an *in situ* assembled visible-light-triggered photoredox catalyst. The photocatalyst enolate complex **II** has been proven as a common intermediate of both the light and dark reaction cycle, and the observed light-induced switch in product formation can be explained with an out competition of the electrophilic bromination by the fast radical addition step. Unfortunately, attempts at extending the coordination auxiliary from imidazole and pyridine to other functional groups have largely been unsuccessful. Nevertheless, efforts to the cleavage of the imidazole auxiliary in the formed products were not operative, due to the sensitivity of the CCl₃ group towards HCl elimination under basic conditions. Thus, the further research should be considered developing new chelating group which can be removed under mild reaction conditions, or developing new chiral-at-metal complexes which can directly activate the ketone without any prefunctionalizing.

References

- 1 H. Huo, X. Shen, C. Wang, L. Zhang, P. Röse, L.-A. Chen, K. Harms, M. Marsch, G. Hilt, E. Meggers, *Nature* **2014**, *515*, 100–103.
- 2 K. L. Skubi, T. P. Yoon, *Nature* **2014**, *515*, 45–46.
- 3 Y. Hori, Y. Nagano, H. Uchiyama, Y. Yamada, H. Taniguchi, *Chem. Lett.* **1978**, 73–76.
- 4 C. Wang, Y. Zheng, H. Huo, P. Röse, L. Zhang, K. Harms, G. Hilt, E. Meggers, *Chem. Eur. J.* **2015**, *21*, 7355–7359.
- 5 R. Kombarov, A. Altieri, D. Genis, M. Kirpichenok, V. Kochubey, N. Rakitina, Z. Titarenko, *Mol. Divers.* **2010**, *14*, 193–200.
- 6 (a) M. Zhang, N. Kumagai, M. Shibasaki, *Chem. Eur. J.* **2016**, *22*, 5525–5529. (b) L. Brewitz, F. A. Arteaga, L. Yin, K. Alagiri, N. Kumagai, M. Shibasaki, *J. Am. Chem. Soc.* **2015**, *137*, 15929–15939. (c) K. Weidner, Z. Sun, N. Kumagai, M. Shibasaki, *Angew. Chem. Int. Ed.* **2015**, *54*, 6236–6240.
- 7 (a) D. A. Evans, K. R. Fandrick, H.-J. Song, *J. Am. Chem. Soc.* **2005**, *127*, 8942–8943. (b) D. A. Evans, K. R. Fandrick, *Org. Lett.* **2006**, *8*, 2249–2252. (c) D. A. Evans, H.-J. Song, K. R. Fandrick, *Org. Lett.* **2006**, *8*, 3351–3354. (d) D. A. Evans, K. R. Fandrick, H.-J. Song, K. A. Scheidt, R. Xu, *J. Am. Chem. Soc.* **2007**, *129*, 10029–10041.
- 8 (a) A. Studer, D. P. Curran, *Nature Chem.* **2014**, *6*, 765–773. (b) N. Zhang, S. R. Samanta, B. M. Rosen, V. Percec, *Chem. Rev.* **2014**, *114*, 5848–5958. (c) R. A. Rossi, A. B. Pierini, A. B. Peñéñory, *Chem. Rev.* **2003**, *103*, 71–168.
- 9 M. A. Cismesia, T. P. Yoon, *Chem. Sci.* **2015**, *6*, 5426–5434.
- 10 H. Huo, C. Wang, K. Harms, E. Meggers, *J. Am. Chem. Soc.* **2015**, *137*, 9551–9554.

3.5 Visible-Light-Activated Enantioselective Perfluoroalkylation with a Chiral Iridium Complex

3.5.1 Reaction Design Plan

Recently, Meggers's group reported several examples of cooperative photoredox and asymmetric catalysis using a single chiral iridium¹ or rhodium² complex, which serves both as a photosensitizer precursor to induce and catalyze redox chemistry and at the same time as an asymmetric catalyst (Figure 70). For instance, a visible-light-activated enantioselective α -alkylation of 2-acyl imidazoles with electron deficient benzyl bromides and phenacyl bromides (chapter 3.3),^{1a} as well as an enantioselective, catalytic trichloromethylation of 2-acyl imidazoles and 2-acylpyridines (chapter 3.4).^{1b} Herein the dual function chiral Lewis acid / photoredox catalyst concept is further advanced to develop a photoactivated enantioselective perfluoroalkylation of 2-acyl imidazoles.³ The photoredox chemistry through intermediate perfluoroalkyl radicals occurs at ambient temperature and requires visible light.

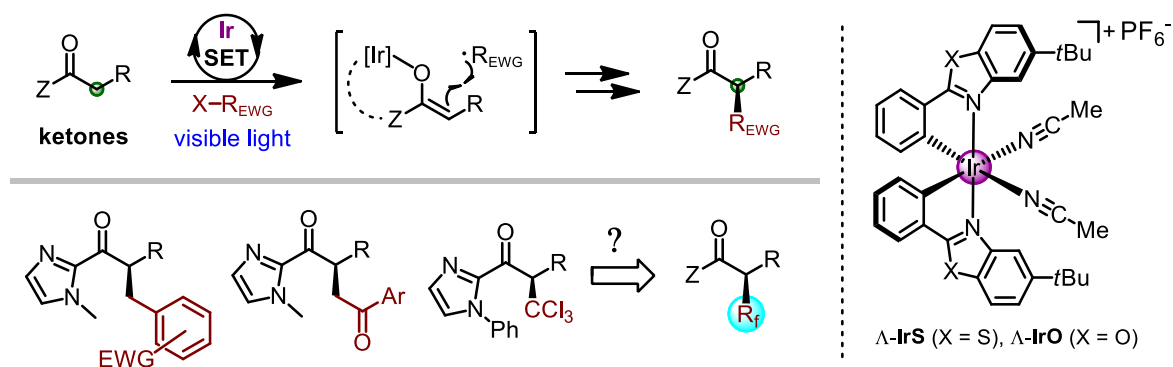


Figure 70 Research plan for the visible-light-driven enantioselective perfluoroalkylation with single iridium photoredox catalyst.

3.5.2 Discovery and Optimization of Visible-Light-Activated Perfluoroalkylation

1) The initial attempts at trifluoromethylation for the viability validation

The study was started by investigating the α -trifluoromethylation of 2-acyl imidazole **24a** with the previously developed protocols, which have been successfully applied in the visible-light-induced α -alkylation (chapter 3.3) and α -trichloromethylation (chapter 3.4). Several typical CF_3 group sources, namely the Togni's reagent **42a-b**, Umemoto's reagent **42c**, trifluoriodomethane **42d** and trifluoromethanesulfonyl chloride **42e**, have been selected for the proposal validation (Figure 71). Disappointingly, when 2-acyl imidazole **24a** reacted with with different CF_3 electrophiles in the presence of Lewis acid **RhS** and Na_2HPO_4 (1.1 equiv) under irradiation with 6 w blue LEDs, no detectable trifluoromethylation product **43** was produced. The decomposition of CF_3 reagents (**42a-c**) could be observed and some unidentified side products were formed.

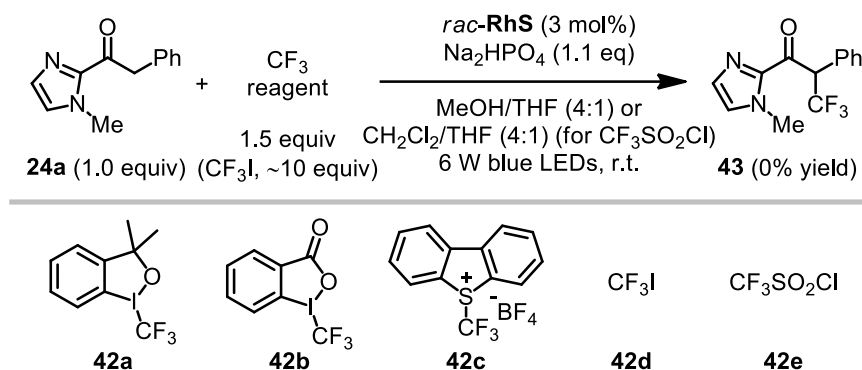


Figure 71 Initial attempts for trifluoromethylation with different CF_3 electrophiles.

Notably, although $\text{CF}_3\text{SO}_2\text{Cl}$ as the CF_3 radical source did not provide any desired product **43** in the presence of Λ -**RhS**, instead it produced the α -chlorination compound **44** in 97% yield and with 21% *ee* (Figure 72, entry 1). The control experiments revealed the light and inert atmosphere were not essential for this transformation, that suggested the α -chlorination was a closed-shell $\text{S}_\text{N}2$ reaction between the formed enolate intermediate and the electrophile $\text{CF}_3\text{SO}_2\text{Cl}$. The low enantioselectivity was highly probably caused by the racemization of product under the basic or acidic condition, which was confirmed by the comparison the *ee* value of crude product (40% *ee*) and the pure compound (22% *ee*) after silica gel purification. The strong withdrawing chloro-substituent increases the acidity of α -carbonyl CH group and thereby facilitates the enolization. Increasing the steric hindrance of the *N*-substituted group improved the enantioselectivities step by step. Finally, the *N*-anthryl imidazole can

provide the chlorination product in 98% yield and with 97% *ee* (entry 6). The *N*-anthryl product did not loss any enantioselectivity after the purification by silica gel column. Whereas, attempts at removing the *N*-anthryl imidazole chelating group have largely been unsuccessful, which have suppressed the extension study for the α -chlorination chemistry.

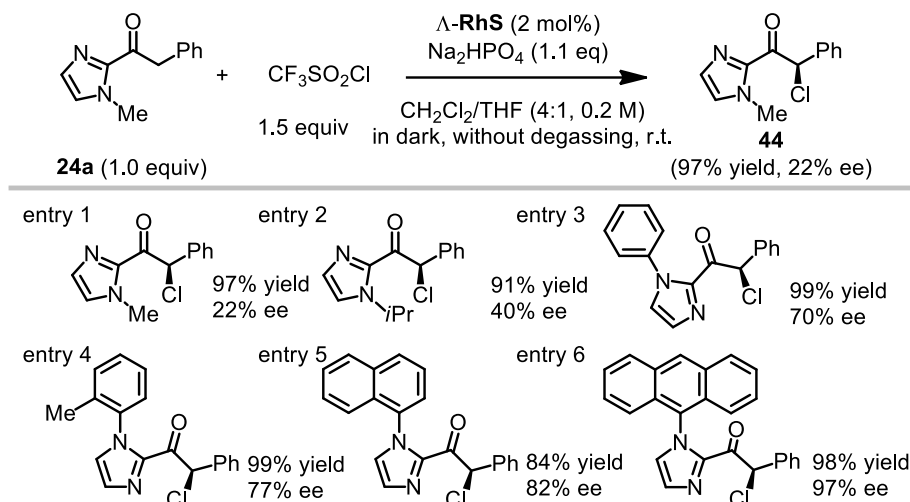


Figure 72 The undesired chlorination of 2-acyl imidazoles in the absence of light. (Results are shown as entries.)

2) The lessons from chlorination of 2-acyl imidazoles.

The exclusive $\text{S}_{\text{N}}2$ chlorination product was produced by the $\Lambda\text{-IrS}$, which indicated the enolate chemistry involved in the reaction process and CF_3 radical formation was suppressed. The $\Lambda\text{-IrS}$ cannot serve as a suitable photosensitizer precursor for these initial experiments. Therefore modifying the photophysical properties of the dual-function catalyst should solve the problem of CF_3 radical generation. Inspired by recent work of MacMillan and coworkers on the asymmetric α -trifluoromethylations of aldehyde *via* photoredox organocatalysis (Figure 73).^{3a} In this dual catalysis strategy, the chiral amine catalyst was applied for enamine formation and stereochemistry induction, the photoredox cycle was relied on an independent sensitizer $\text{Ir}(\text{ppy})_2(\text{dtbbpy})\text{PF}_6$. This photosensitizer has proven to be efficient for CF_3 radical generation from perfluoroalkyl iodides. Thereby, dual catalysts system was considered to get rid of the optimization of the photosensitizer.

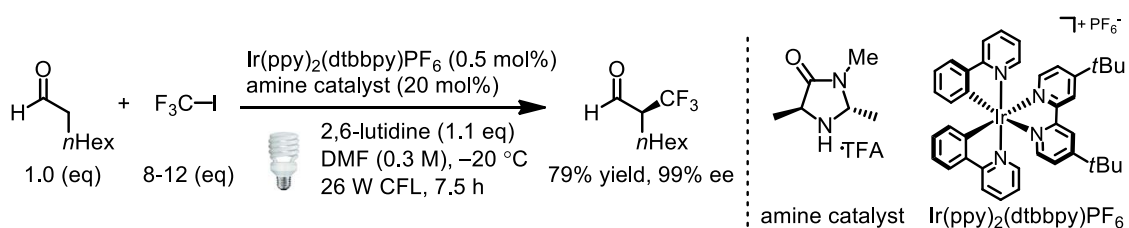


Figure 73 MacMillan's catalyst combination strategy for α -trifluoromethylation of aldehydes.

3) Two catalysts induced the enantioselective trifluoromethylation of 2-acyl imidazoles.

Next, the reaction with two catalysts was design to examine the trifluoromethylation of 2-acyl imidazoles (Table 10). According to MacMillan's reaction conditions, the previous developed Λ -**RhO**⁴ was used as the Lewis acid to facilitate the enolate formation, which is similar to the enamine generation created by chiral amine catalyst in MacMillan's system. Compared to the Λ -**IrO** or Λ -**IrS**, the derivative Λ -**RhO** can tolerate more coordinating polar solvent (DMF, DMSO, NMP, NMA, CH₃CN) for efficient ligand exchange;² the weaker absorbance of Λ -**RhO** at the visible light region reduce the effect of competing light absorbance with photosensitizer.⁵

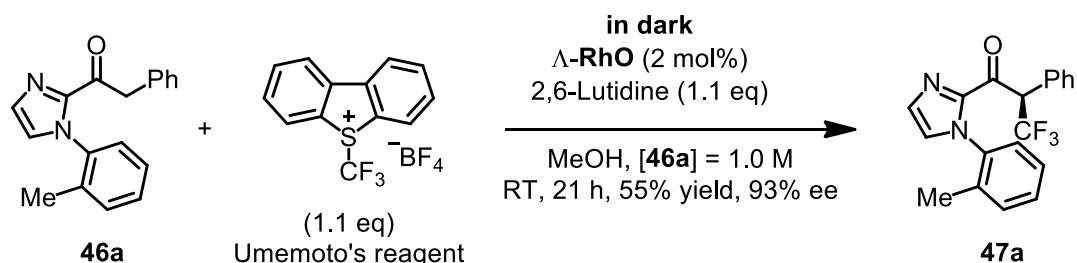
Table 10 Initial experiments to identify an optimal catalyst/sensitizer combination^a

entry	sensitizer/catalyst	conditions	yield ^c	ee ^d	
1	[Ir] (2 mol%) Λ - RhO (2 mol%)	30a (1 eq, 0.4 M), 2,6-lutidine (1.1 eq), RT, 21 h	56%	79%	
2	[Ir] (0.5 mol%) Λ - RhO (2 mol%)	30a (1 eq, 0.4 M), 2,6-lutidine (1.1 eq), RT, 21 h	50%	90%	
3	[Ir] (0.5 mol%) Λ - RhO (2 mol%)	46a (1 eq, 0.4 M), 2,6-lutidine (1.1 eq), RT, 21 h	55%	92%	
4	[Ir] (0.5 mol%) Λ - RhO (2 mol%)	46a (1 eq, 1.0 M), 2,6-lutidine (1.1 eq), RT, 21 h	75%	93%	
5	[Ir] (0.5 mol%) Λ - RhO (2 mol%)	46a (1 eq, 1.0 M), NaHCO ₃ (1.1 eq), RT, 21 h	76%	93%	
6	[Ir] (0.5 mol%) Λ - RhO (2 mol%)	Same as 'entry 4' but in dark	0	n.a.	
7	[Ir] (0 mol%) Λ - RhO (2 mol%)	Same as 'entry 4'	0	n.a.	
8	[Ir] (0.5 mol%) Λ - RhO (4 mol%)	46a (1 eq, 1.0 M), 2,6-lutidine (1.1 eq), RT, 14 h	65%	88%	
9	[Ir] (0.5 mol%) Λ - RhO (1 mol%)	46a (1 eq, 1.0 M), 2,6-lutidine (1.1 eq), RT, 21 h	49%	93%	

^a Conditions: **30a**, **46a** and CF₃I (about 10 eq) with catalyst Λ -**RhO** (1-4 mol%), and photosensitizer (none or 0.5-2 mol%) in DMF at r.t. for 14-21 h under irradiation with visible light. Light source: 20 W compact fluorescence lamp. ^c Isolated yields. ^d Enantioselectivities of **45a** and **47a** determined by HPLC on chiral stationary phase. n.a. = not applicable.

Encouragingly, 2-acyl imidazole **30a** readily react with CF_3I in the presence of rhodium catalyst $\Lambda\text{-RhO}$ and sensitizer $\text{Ir}(\text{ppy})_2(\text{dtbbpy})\text{PF}_6$ under visible light irradiation, trifluoromethylated product **45a** is obtained in 56% yield and with 79% *ee* (table 1, entry 1). Reducing the photosensitizer loading improved the enantioselectivity to 90% *ee* (entry 2). Replacing the *N*-Ph with a 2-MePh substituent and increasing the reaction concentration provided the product **47a** with improved 93% *ee* and in improved 75% yield, respectively (entry 4). The 2-MePh substituent in the imidazole moiety can suppressed the racemization efficiently. The compound **47a** did not loss any *ee* value after purification with silica gel column. When replacing 2,6-lutidine with a weak inorganic base NaHCO_3 , a similar efficiency could be obtained (entry 5). The control experiments confirmed the visible light and the photosensitizer are required for the product formation (entry 6, 7). Furthermore, the higher or lower Lewis acid catalyst loadings cannot provide any improved efficiency (entry 8, 9).

Meanwhile, this dual catalysis protocol has been examined with different CF_3 radical precursors in Figure 71 under the developed conditions (Table 10, entry 4). No traces of trifluoromethylated product **47a** were observed under visible light irradiation. An interesting observation need to be pointed out, with a different reaction condition, the Umemoto's reagent **42c** can provide the product **47a** through a closed-shell $\text{S}_\text{N}2$ reaction with a single catalyst $\Lambda\text{-RhO}$ (Scheme 18). After the optimization of reaction conditions, the compound **47a** can be obtained in 55% yield and with 93% *ee*. Apparently, this protocol in the absence of light and external photosensitizer is a good alternative method for asymmetric trifluoromethylation. Considering there is no other derivative reagents for the corresponding perfluoroalkylation, the photocatalytic technology is still more promising for accessing the perfluoroalkylation with perfluoroalkyl iodides.



Scheme 18 Asymmetric trifluoromethylation with Umemoto's reagent in the absence of light.

4) Single catalyst induced the enantioselective perfluoromethylation of 2-acyl imidazoles.

After accessing the asymmetric trifluoromethylation through visible-light-induced dual catalysis, the perfluoroalkylation with single dual function catalyst Λ -IrS was exploited again (Figure 74). Using the established conditions for dual catalysis, the imidazole **46a** readily reacted with perfluorobutyl iodide (6 equivs) to provide the product **48a** in 74% yield and with 97% yield. Encouragingly, the compound **48a** can also be produced by the previous developed dual-function Lewis acid/photoredox catalyst Λ -IrS in 29% yield and with excellent enantioselectivity of 98% *ee*. Whereas a comparison experiment with CF₃I as the electrophile, no traces of trifluoromethylation compound were produced by the Λ -IrS. This observation can be reasoned that CF₃I cannot be reduced by photoexcited Λ -IrS due to its more negative reduction potential comparing to C₄F₉I. Thereby the optimization of the catalyst structure to adjust the photophysical properties should improve the reaction efficiency.

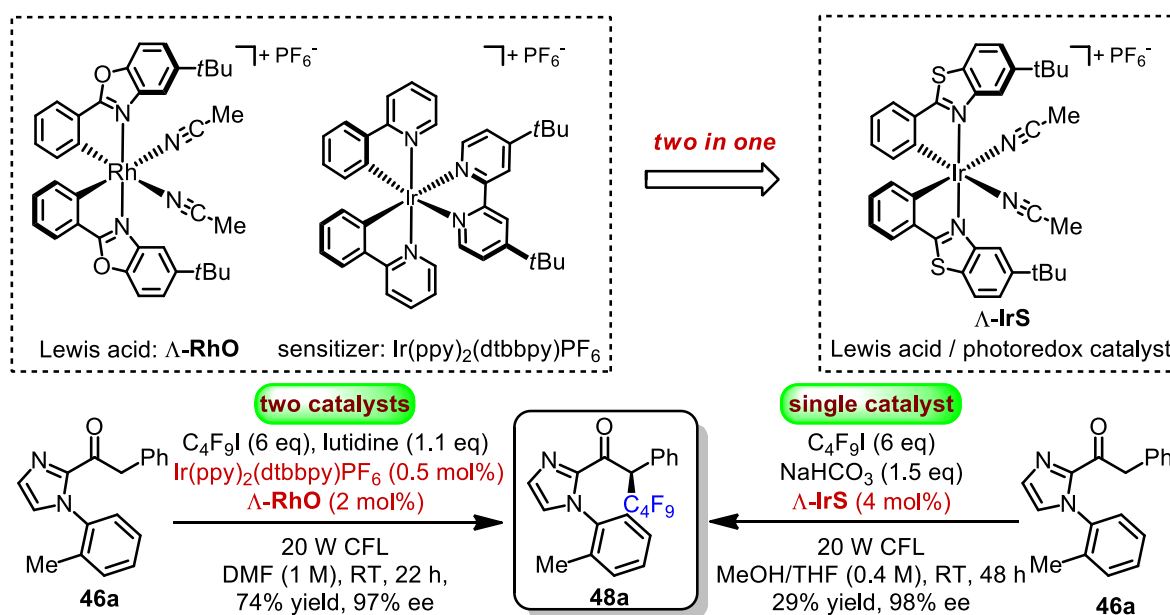


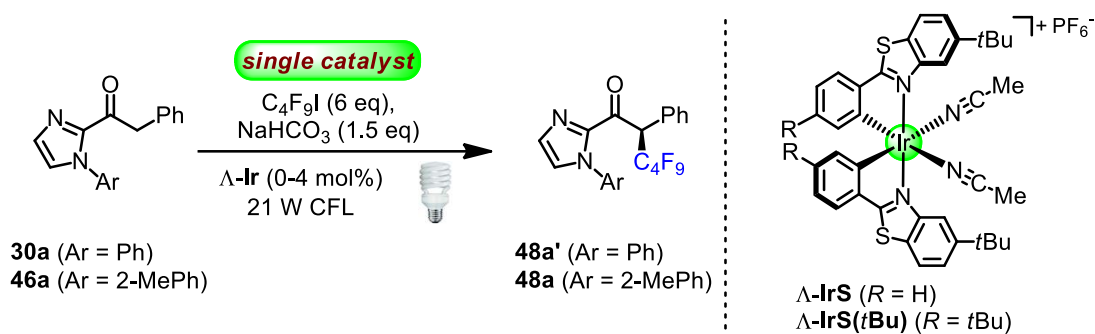
Figure 74 Attempts at extending the two catalysts into single catalyst system for perfluoroalkylation.

The viability of modification of catalyst structure was investigated in Table 11. One new dual function chiral Lewis acid/photoredox catalyst Λ -IrS(*t*Bu) was designed for the enantioselective perfluoroalkylation of 2-acyl imidazoles using the previously established conditions.^{1a-b} When 2-acyl imidazole **30a** reacted with C₄F₉I (6 equiv.) in the presence of NaHCO₃ (1.5 equiv.) and 4 mol% Λ -IrS, the desired α -perfluoroalkylation product **48a'** was provided in a disappointing yield of 24% and with unsatisfactory enantioselectivity of 92% *ee* (entry 1). Increasing the steric congestion of the 2-acyl imidazole by replacing the *N*-Ph substituent (**30a**) with *N*-(2-MePh) (**46a**) improved the

enantioselectivity but the yield remained low (29%) (entry 2, also see in Figure 74).

Surprisingly, replacing Λ -**IrS** with the related catalyst Λ -**IrS**(*t*Bu), this reaction afforded the perfluoroalkylation product **48a** both with a satisfactory yield (78%) and excellent enantioselectivity (99%, entry 3). The catalyst loading of Λ -**IrS**(*t*Bu) could even be reduced to 2 mol% without affecting the performance (entry 4). Control experiments conducted either in the absence of the catalyst or in the dark confirmed that this reaction requires the combined presence of the iridium catalyst and light, otherwise no traces of product were observed (entries 5 and 6). Furthermore, the presence of air completely suppresses the perfluoroalkylation (entry 7), thus supporting the conclusion that this process constitutes a photoredox process that proceeds *via* intermediate perfluoroalkyl radicals.

Table 11 Optimization of the visible-light-driven enantioselective perfluoroalkylation with single chiral iridium complex.^a



entry	Ar	catalyst (mol%) ^b	light ^c	yield (%) ^d	ee (%) ^e
1	Ph	Λ - IrS (4.0)	yes	24	92
2	2-MeC ₆ H ₄	Λ - IrS (4.0)	yes	29	98
3	2-MeC ₆ H ₄	Λ - IrS (<i>t</i> Bu) (4.0)	yes	78	99
4	2-MeC ₆ H ₄	Λ - IrS (<i>t</i> Bu) (2.0)	yes	79	99
5	2-MeC ₆ H ₄	Λ - IrS (<i>t</i> Bu) (2.0)	no	0	n.d.
6	2-MeC ₆ H ₄	none	yes	0	n.d.
7 ^f	2-MeC ₆ H ₄	Λ - IrS (<i>t</i> Bu) (2.0)	yes	0	n.d.

^aReaction conditions: **30a** or **46a** with $\text{C}_4\text{F}_9\text{I}$ (6 eq), NaHCO_3 (1.5 eq) and catalyst (0-4 mol%) in MeOH/THF (4:1) at room temperature for 34-46 h. ^b Catalyst loading (mol%) in brackets. ^c Light source: 21 W compact fluorescent lamp (CFL). ^d Isolated yields. ^e Determined by chiral HPLC. n.d. = not determined. ^f Under air atmosphere.

Figure 75 shows the crystal structure of the catalyst Δ -**IrS(*t*Bu)** (obtained by Xiaoqiang Huang, a graduate student in Meggers group). This complex bears two cyclometalating 2-phenylbenzothiazole ligands in addition to two exchange-labile acetonitrile groups; the chirality originates exclusively from metal centrochirality and thereby creates a C_2 -symmetrical propeller-type coordination sphere.⁶ Compared to **IrS**, **IrS(*t*Bu)** contains two additional *t*Bu-groups serving as the electron donating groups at the phenyl moieties. This modification raises the HOMO and renders **IrS(*t*Bu)** a better electron donor in the ground and excited state,⁷ which is apparently beneficial for perfluoroalkylation described herein. Furthermore, the aliphatic substituent can increase the solubility of catalyst and the corresponding intermediate complexes; the increasing steric repulsion facilitates the ligand exchange that result in faster reaction rate. All these cases can improve the catalytic efficiency of **IrS(*t*Bu)** for the photocatalytic perfluoroalkylation.

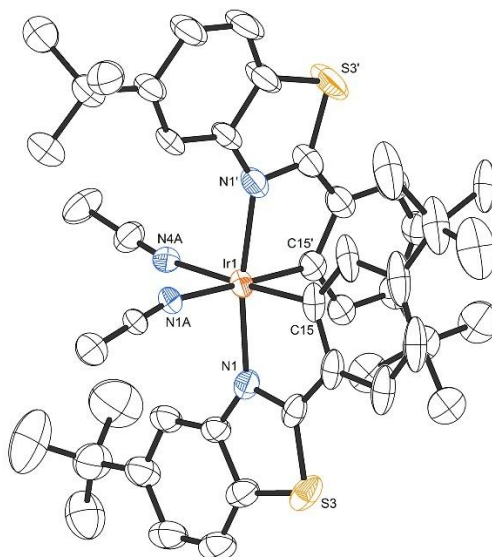


Figure 75 Crystal structure of Δ -**IrS(*t*Bu)**. ORTEP drawing with 30% probability thermal ellipsoids. The counter ion is omitted.

3.5.3 Substrate Scope of Perfluoroalkylation

Along with Xiaoqiang Huang, a graduate student in Meggers group, the substrate scope of this reaction was investigated. The scope with respect to the 2-acyl imidazole substrate is shown in Figure 76. Satisfactory yields (59-90%) and excellent enantioselectivities (96-99% *ee*) were achieved for introducing a C₆F₁₃ substituent into the α -position of the 2-acyl imidazoles, providing the products **49a-h** bearing aromatic (**49a-d**) or aliphatic (**49e-g**) substituents in α -position of the carbonyl group. Even **49h**, bearing an aryl ether, was tolerated. The key feature of this catalytic transformation is the outstanding enantioselectivities, as demonstrated by three of these products were obtained with 99% *ee*.

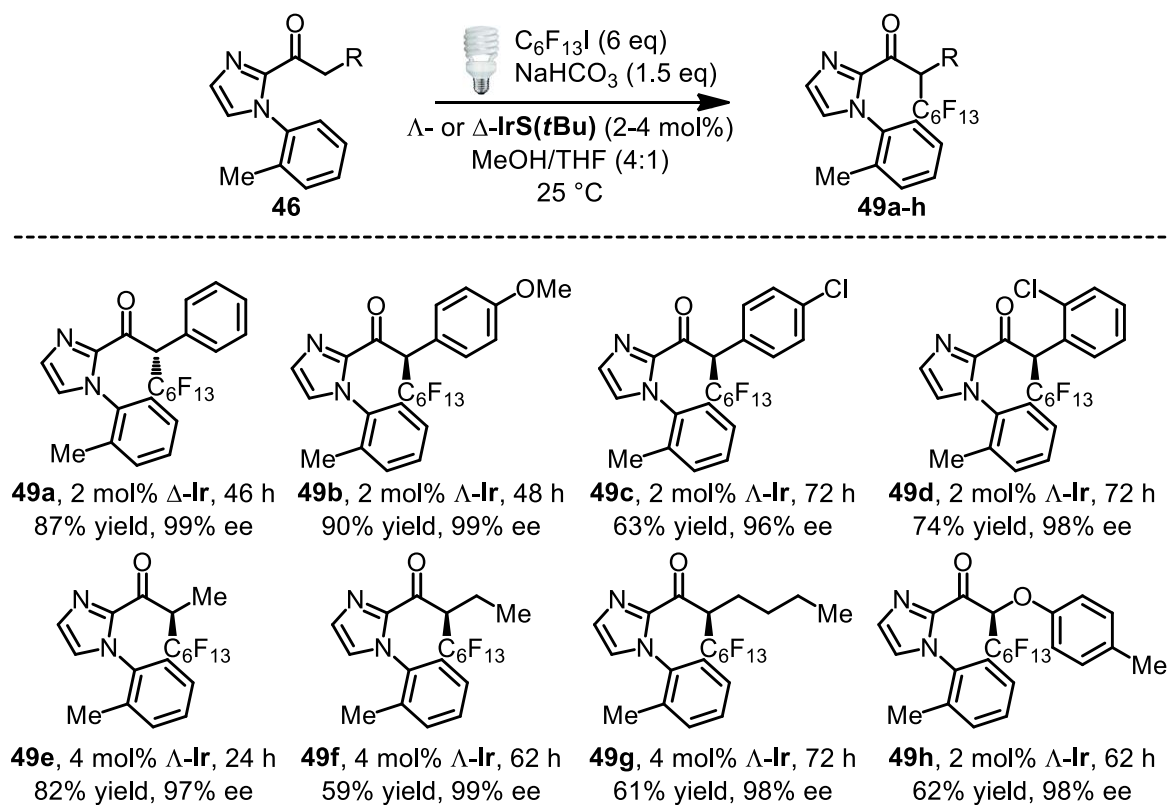


Figure 76 Substrate scope with respect to 2-acyl imidazoles.

The scope of the reaction with respect to the perfluoroalkyl groups was also investigated, synthesizing the perfluoroalkylated products **47a-f**. As shown in Figure 77, CF₃, C₃F₇, C₄F₉, C₆F₁₃ and C₁₀F₂₁ substituents can be introduced in a highly enantioselective fashion (**47a-f**). Furthermore, perfluorobenzylation (**47f**) is achieved in 93% yield, providing virtually only a single enantiomer (>99.5% *ee*), demonstrating the high asymmetric induction that can be achieved by this new developed Λ -Ir(*t*Bu) in this asymmetric photoredox catalysis.

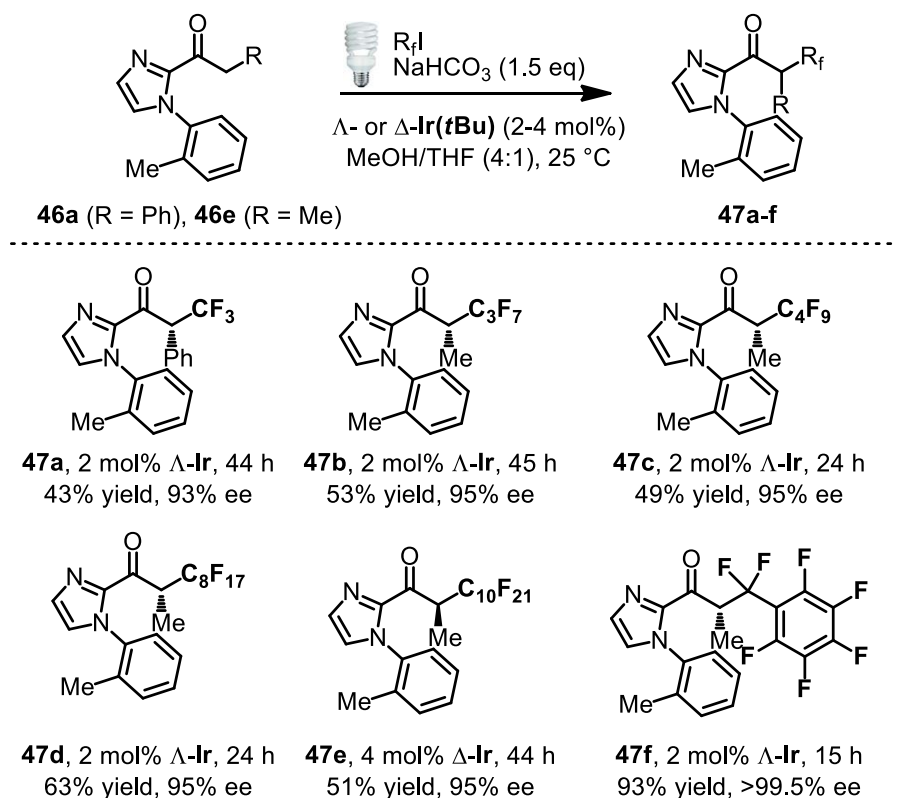


Figure 77 Substrate scope with respect to perfluoroalkyl iodides and perfluorobenzyl iodide.

3.5.4 Proposed Mechanism

The proposed mechanism for the perfluoroalkylation involves the intermediate iridium(III) enolate complex **II** that is highlighted in Figure 78, which is expected to act as the chiral reaction partner for the electron-deficient perfluoroalkyl radicals and, simultaneously, serves as the active photosensitizer (**II** + *hν* → **II*** → **II**⁺ + e⁻). Accordingly, coordination of the 2-acyl imidazole substrate **46** into Λ -Ir(*t*Bu) under release of the two acetonitrile ligands generates the substrate-coordinated intermediate **I**, which upon deprotonation subsequently converts into the key intermediate, namely the enolate complex **II**. The electron-rich π -system of the enolate double bond enables a rapid reaction with the electron-deficient perfluoroalkyl radicals, which themselves are generated by a SET-reduction of the

corresponding perfluoroalkyl halides.⁸ The highly stereoselective radical addition generates an intermediate iridium-coordinated ketyl **III**, which is strongly reducing and converts to iridium-coordinated product **IV** upon oxidation. Release of the product and coordination to a new substrate then leads to a new catalytic cycle. The electron that is released upon oxidation of the ketyl intermediate (**III**→**IV** + e⁻) either flows into the photoredox cycle by regenerating the oxidized enolate photoredox sensitizer (**II**⁺ + e⁻→**II**) or it directly reduces a perfluoroalkyl halide substrate and thereby leads to a chain process. This process can be classified as a redox-neutral, electron-transfer-catalyzed (electron-catalyzed) reaction.⁹

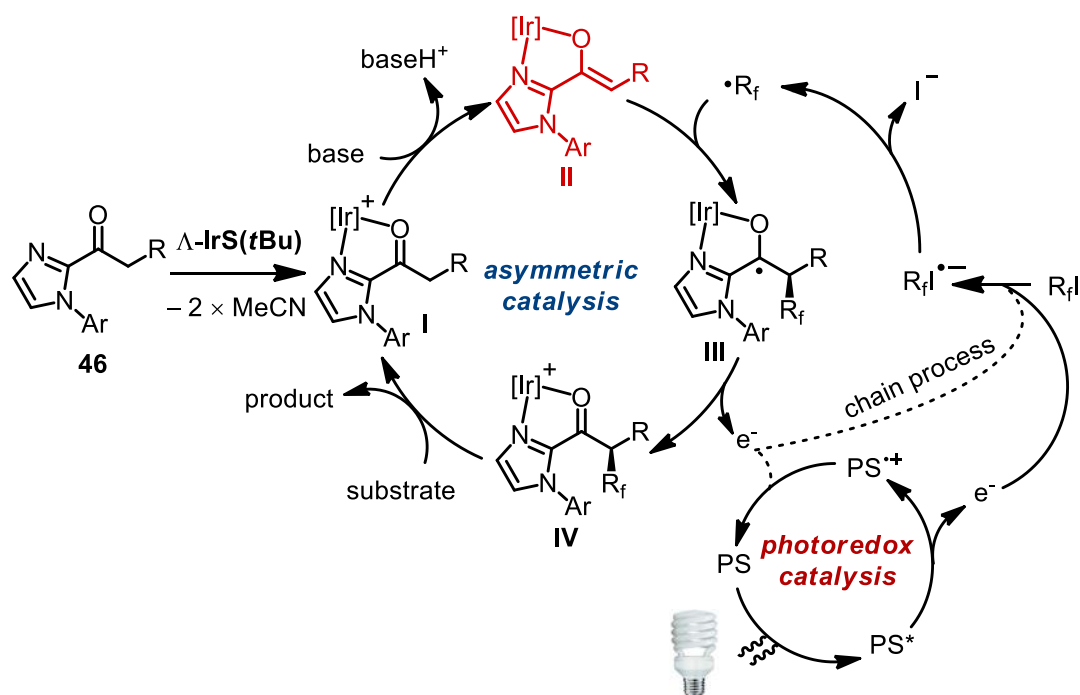


Figure 78 Plausible mechanism for the photoactivated asymmetric perfluoroalkylation of 2-acyl imidazoles. The proposed mechanism involves the highlighted intermediate iridium(III) enolate complex **II**, which most likely serves as the active photosensitizer and the chiral reaction partner for the electron deficient radicals.

3.5.5 Conclusions

In summary, visible-light-activated highly enantioselective perfluoroalkylation of 2-acyl imidazoles with perfluoroalkyl iodides and perfluorobenzyl iodide have been reported.¹⁰ The process uses a dual function chiral Lewis acid / photoredox catalyst at loadings of 2-4 mol% and constitutes a redox-neutral, electron-catalyzed reaction that proceeds *via* intermediate perfluoroalkyl radicals. This work demonstrates the generality of the dual function chiral Lewis acid / photoredox catalyst concept. From the perspective of the catalyst, it is intriguing that the metal center is capable of serving multiple functions at the same time: it constitutes the exclusive center of chirality (only achiral ligands), the catalytically active Lewis acid center, and additionally functions as the key component of the photosensitizer that is formed *in situ*. The facile optimization of catalyst structure has proven to be promising for adjusting the photophysical properties. This chemistry was started with dual catalysts and ended at single catalyst, this research manner provide insights for looking for new reactions. The undesired chlorination of 2-acyl imidazoles *via* closed-shell S_N2 reaction, indeed show the excellent levels of enantioselectivities; unfortunately, these products bearing the imidazole chelating group cannot be converted to any synthetic useful compounds. The **A-RhO** catalyzed trifluoromethylation of 2-acyl imidazole with Umemoto's reagent, has been demonstrated as a closed-shell S_N2 reaction, which provides an alternative method for CF₃ introduction.

References

- 1 (a) H. Huo, X. Shen, C. Wang, L. Zhang, P. Röse, L.-A. Chen, K. Harms, M. Marsch, G. Hilt, E. Meggers, *Nature* **2014**, *515*, 100–103. (b) H. Huo, C. Wang, K. Harms, E. Meggers, *J. Am. Chem. Soc.* **2015**, *137*, 9551–9554. (c) C. Wang, Y. Zheng, H. Huo, P. Röse, L. Zhang, K. Harms, G. Hilt, E. Meggers, *Chem. Eur. J.* **2015**, *21*, 7355–7359. (d) C. Wang, J. Qin, X. Shen, R. Riedel, K. Harms, E. Meggers, *Angew. Chem. Int. Ed.* **2016**, *55*, 685–688.
- 2 Y. Tan, W. Yuan, L. Gong, E. Meggers, *Angew. Chem. Int. Ed.* **2015**, *54*, 13045–13048.

- 3 For perfluoroalkylations through photoredox chemistry, see: (a) D. A. Nagib, M. E. Scott, D. W. MacMillan, *J. Am. Chem. Soc.* **2009**, *131*, 10875–10877. (b) D. A. Nagib, D. W. C. MacMillan, *Nature* **2011**, *480*, 224–228. (c) P. V. Pham, D. A. Nagib, D. W. MacMillan, *Angew. Chem. Int. Ed.* **2011**, *50*, 6119–6122. (d) M. Nappi, G. Bergonzini, P. Melchiorre, *Angew. Chem. Int. Ed.* **2014**, *53*, 4921–4925. (e) V. M. Fernández-Alvarez, M. Nappi, P. Melchiorre, F. Maseras, *Org. Lett.* **2015**, *17*, 2676–2679. (f) F. Sladojevich, E. McNeill, J. Börgel, S. L. Zheng, T. Ritter, *Angew. Chem. Int. Ed.* **2015**, *54*, 3712–3716. (g) G. Filippini, M. Nappi, P. Melchiorre, *Tetrahedron* **2015**, *71*, 4535–4542. (h) J. W. Beatty, J. J. Douglas, K. P. Cole, C. R. Stephenson, *Nat. Commun.* **2015**, *6*, 7919. (i) B. Sahoo, J. L. Li, F. Glorius, *Angew. Chem. Int. Ed.* **2015**, *54*, 11577–11580. (j) Ł. Woźniak, J. J. Murphy, P. Melchiorre, *J. Am. Chem. Soc.* **2015**, *137*, 5678–5681. For a review on metal-mediated radical perfluoroalkylation, see: (k) S. Barata-Vallejo, A. Postigo, *Coord. Chem. Rev.* **2013**, *257*, 3051–3069. For a recent review on radical trifluoromethylation, see: (l) A. Studer, *Angew. Chem. Int. Ed.* **2012**, *51*, 8950–8958.
- 4 C. Wang, L.-A. Chen, H. Huo, X. Shen, K. Harms, L. Gong, E. Meggers, *Chem. Sci.* **2015**, *6*, 1094–1100.
- 5 X. Shen, K. Harms, M. Marsch, E. Meggers, *Chem. Eur. J.* **2016**, DOI: 10.1002/chem.201601572.
- 6 (a) H. Huo, C. Fu, K. Harms, E. Meggers, *J. Am. Chem. Soc.* **2014**, *136*, 2990–2993. (b) X. Shen, H. Huo, C. Wang, B. Zhang, K. Harms, E. Meggers, *Chem. Eur. J.* **2015**, *21*, 9720–9726.
- 7 J. Li, P. I. Djurovich, B. D. Alleyne, M. Yousufuddin, N. N. Ho, J. C. Thomas, J. C. Peters, R. Bau, M. E. Thompson, *Inorg. Chem.* **2005**, *44*, 1713–1727.
- 8 For a diastereoselective addition of perfluoroalkyl radicals to titanium enolates, see: A. T. Herrmann, L. L. Smith, A. Zakarian, *J. Am. Chem. Soc.* **2012**, *134*, 6976–6979.
- 9 (a) M. Chanon, M. L. Tobe, *Angew. Chem. Int. Ed. Engl.* **1982**, *21*, 1–12. (b) A. Studer, D. P. Curran, *Nat. Chem.* **2014**, *6*, 765–773.
- 10 H. Huo, X. Huang, X. Shen, K. Harms, E. Meggers, *Synlett* **2016**, *27*, 749–753.

Chapter 3: Results and Discussion

Part IV: Asymmetric Photoredox Catalysis with a Chiral-at-Metal Rhodium Complex

3.6 Visible-Light-Activated Enantioselective Conjugate Addition

3.6.1 Reaction Design

The newly developed chiral-at-metal iridium complexes (**IrO**, **IrS**, **IrS(*t*Bu)**) catalyzed the enantioselective α -functionalization of carbonyl compounds through visible-light-activated photoredox catalysis. This method allows direct access to α -benzylation/phenacylation (chapter 3.3),¹ α -trichloromethylation (chapter 3.4)² and perfluoroalkylation (sections 3.5).³ However, the satisfactory enantioselectivities are still previously inaccessible for producing β -functionalized ketones in chiral-at-metal catalyst system (see Figure 42 in chapter 3.3).

Despite the conjugate addition of nucleophilic alkyl radicals to electron deficient acceptors is an established and much applied method for the formation of β -functionalized ketones, efficient catalytic enantioselective versions are still limited and this can be pinpointed to the high background (uncatalyzed) reactivity of the involved alkyl radicals.⁴ Sibi and co-workers reported one of the most impressive examples of chiral Lewis acid catalysis in conjugate radical additions, namely using a magnesium bisoxazoline complex at 5 mol% loading for catalyzing the enantioselective conjugate isopropyl radical addition to an oxazolidinone cinnamate (Figure 79).⁵ However, the reaction needs equimolar amounts of a toxic stannane and is executed at $-78\text{ }^{\circ}\text{C}$ to achieve such low catalyst loading. The Yoon group recently reported a catalytic enantioselective addition of α -aminoalkyl radicals to

α,β -unsaturated carbonyl compounds under photoredox conditions (also see Figure 15-16 in Chapter 1.3).⁶ However, catalyst loadings of the employed chiral scandium complex are fairly high and the system is restricted to silanes with amines in α -position. Thus new strategies involved a practical reaction setting will be developed in this chapter to provide new approach for enantioselective radical conjugate addition.

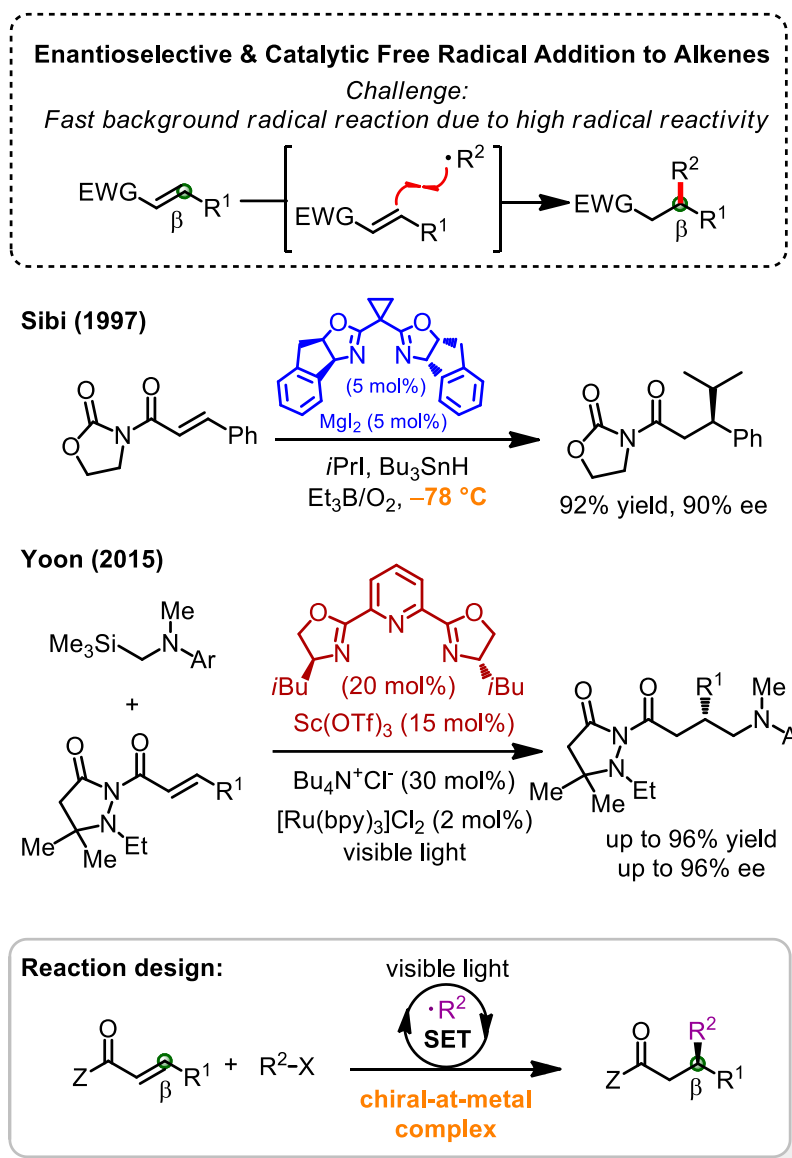
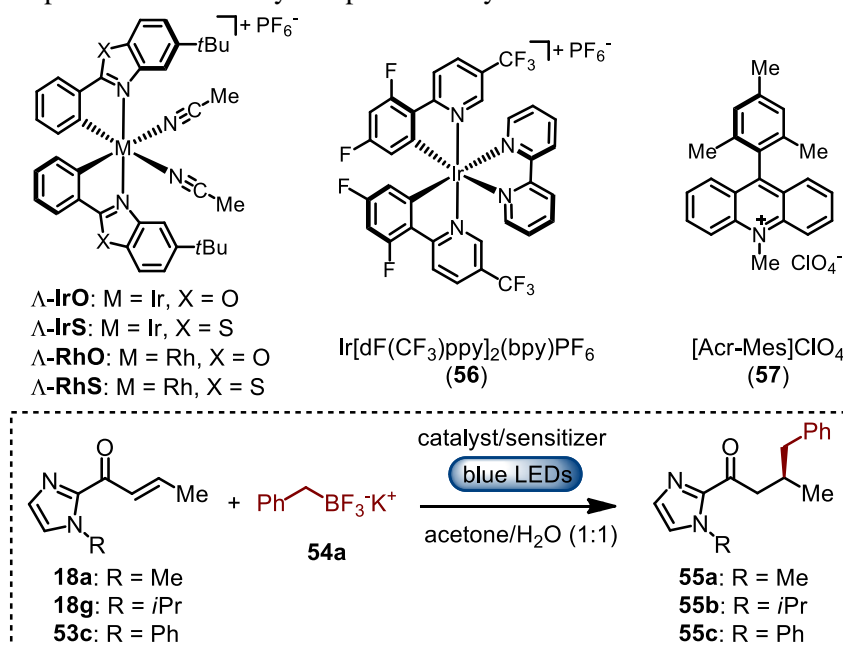


Figure 79 Research plan for catalytic enantioselective radical addition to acceptor substituted alkenes with chiral-at-metal complex.

3.6.2 Reaction Optimization and Substrate Scope

Inspired by recent work of Molander and coworkers on using organotrifluoroborates as precursors for radicals under oxidative photoredox conditions,⁷ this study was started by investigating the reaction of the α,β -unsaturated acyl imidazole **18a** with potassium benzyltrifluoroborate **54a** under photoredox conditions (Table 12).

Table 12 Initial experiments to identify an optimal catalyst/sensitizer combination^a



entry	catalyst	sensitizer	h ν^b	product	yield (%) ^c	ee (%) ^d
1	Λ -IrO	none	yes	55a	0	n.a.
2	Λ -IrS	none	yes	55a	0	n.a.
3	Λ -IrS	56	yes	55a	<5	n.d.
4	Λ -RhO	56	yes	55a	43	79
5	Λ -RhS	56	yes	55a	67	88
6	Λ -RhS	56	yes	55b	66	93
7	Λ -RhS	56	yes	55c	73	94
8	Λ -RhS	57	yes	55c	73	96
9	Λ -RhS	56	no	55c	0	n.a.
10	Λ -RhS	none	yes	55c	0	n.a.
11	none	56	yes	55c	29	0

^a Conditions: **18a**, **18g**, **53c** and **54a** (1.5 eq) with catalyst (none or 4 mol%), and photosensitizer (none or 2 mol%) in acetone/H₂O (1:1) at r.t. for 4–6 h under irradiation with visible light. ^b Light source: 24 W blue LEDs. ^c Isolated yields. ^d Enantioselectivities of **55a–c** determined by HPLC on chiral stationary phase. n.a. = not applicable, n.d. = not determined.

Disappointingly, in the presence of the previously developed dual function photoredox /chiral Lewis acid catalysts Λ -**IrO** or Λ -**IrS** under visible light irradiation,^{1-3, 8} no desired C-C bond formation product **55a** was detectable (entries 1-2). The presence of an additional photosensitizer did not improve the result (entry 3). Encouragingly, when the chiral Lewis acid Λ -**RhO**⁹ in combination with the photosensitizer **56** was applied to this system, the reaction proceeded in 43% yield and with 79% *ee*.¹⁰ The newly developed Lewis acid Λ -**RhS**,¹¹ which provides an increased steric hindrance due to long C-S bonds, afforded the product **55a** with an improved yield of 67% and 88% *ee* (entry 5). An optimization of the imidazole auxiliary by replacing the *N*-methyl (**53a**) with an isopropyl (**53b**) or a phenyl (**53c**) substituent, improved the enantioselectivity to 93% *ee* (**55b**) and 94% *ee* (**55c**), respectively (entries 6 and 7). Using the substrate **53c** in combination with the less expensive organic sensitizer **57**¹² provided the C-C formation product even with 96% *ee* (entry 8). Meanwhile, control experiments verified that the photosensitizer and visible light are essential for product formation (entries 9 and 10). However, in absence of the chiral Lewis acid Λ -**RhS**, the radical addition product **55c** was still generated in 29% yield, albeit as a racemic mixture (entry 11).¹³ This observation demonstrates that Λ -**RhS** must strongly accelerate the radical addition in order to overcome the prevailing racemic background reaction.

Next, the scope of the visible-light-induced enantioselective addition of trifluoroborate **54a** to electron-deficient alkenes **53c-k** was evaluated, providing the C-C bond formation products **55c-k** with 40-90% yields and 83-96% *ee*. Figure 80 summarizes the effect of various alkene substituents. The reaction is tolerant of aliphatic substituents (**55c-f**), an ether (**55g**), and aromatic moieties with electron-rich or electron-deficient groups (**55h-k**). It is noteworthy that depending on the particular alkene, different *N*-imidazole substituents provide the best results as can be seen by the comparison of **55d** with **55d'** (Me favored) and **55e** with **55e'** (*i*Pr favored), which allows for an individual optimization of yields and enantioselectivities.

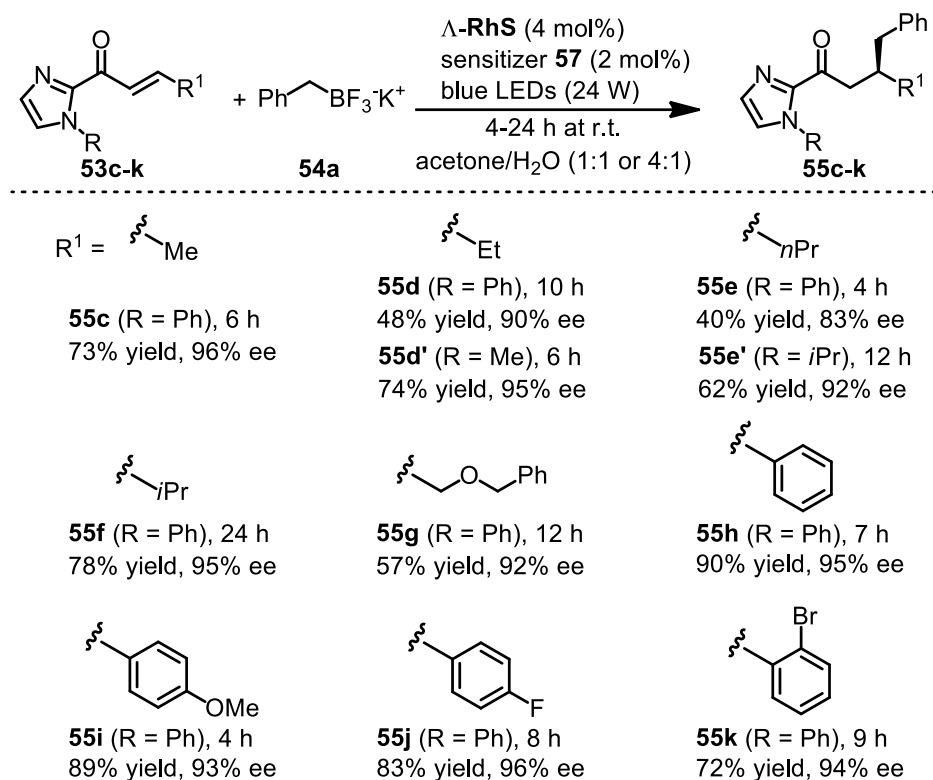


Figure 80 Substrate scope with respect to different 2-acyl imidazoles.

The scope of this reaction with respect to organotrifluoroborates is outlined in Figure 81. A wide range of trifluoroborates (**54b-p**), ranging from benzyltrifluoroborates with electron withdrawing and electron donating substituents, various alkoxyethyltrifluoroborates, secondary alkyltrifluoroborates, and tertiary alkyltrifluoroborates, can be used in this reaction providing the products **55l-z** in yields of 61-97% and with 77-99% *ee*. The addition of the 4-methoxybenzyl radical to **53h** gave **55i** in 97% yield and with perfect 99% *ee*. As shown, the products derived from benzyl radical addition are well tolerated of electron-donating group (**55l-m**), electron-withdrawing group (**55p**), an ortho substituent (**55n**) and a naphthyl (**55o**) group. Likewise, a range of alkoxyethyl radicals can be applied to this protocol (**55q-v**). The potassium alkoxyethylborates bearing a steric *tert*butyl, an ether group, TMS moiety reacted with **53h** to provide **55q** (98% *ee*), **55r** (95% *ee*) and **55v** (94% *ee*), respectively. Furthermore, the secondary (refer to **55w-y**) and tertiary (refer to **55z**) alkyltrifluoroborates, regardless of acyclic or cyclic structures, produced the products in high yields (76-93%) and with excellent enantioselectivities (97-98% *ee*).

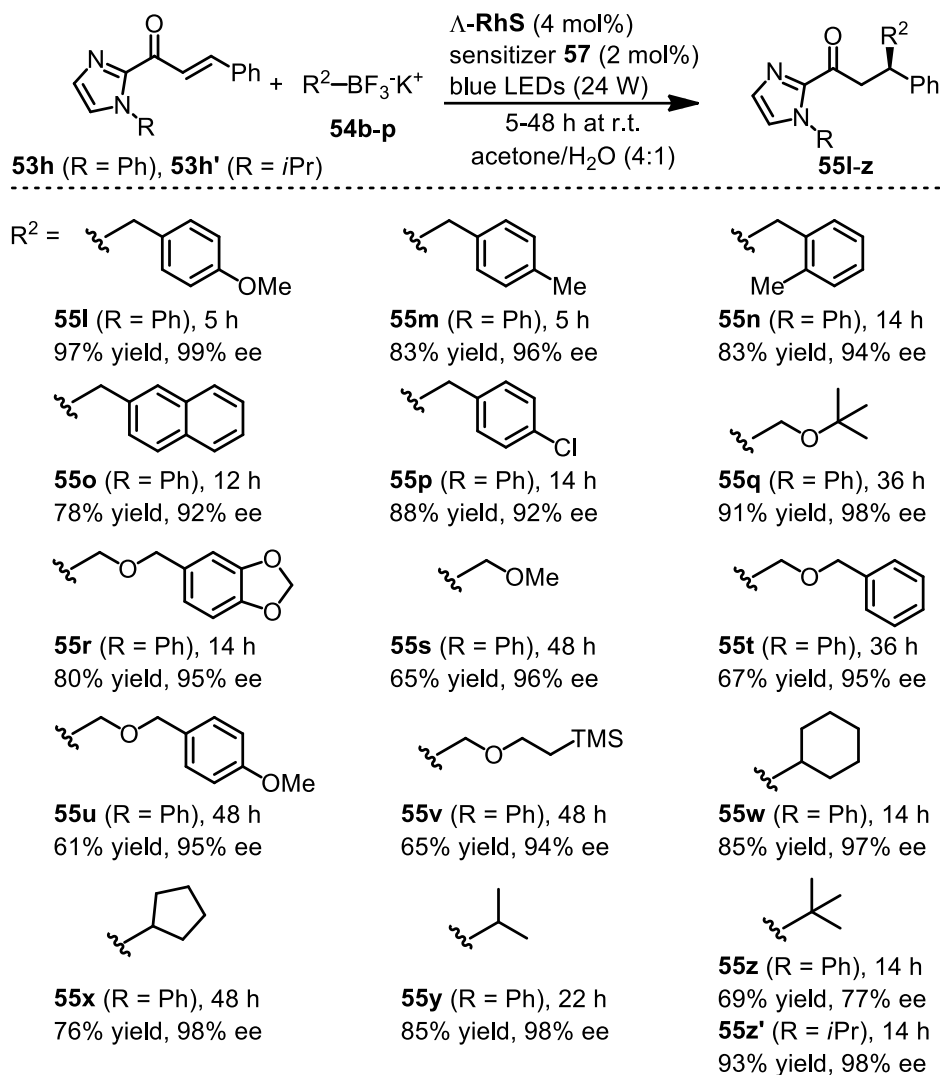


Figure 81 Substrate scope regarding organotrifluoroborates.

Next, to improve the practical utility of this reaction, seeking a synthetically more versatile class of alkene substrates is highly desirable. And α,β -unsaturated *N*-acyl-3,5-dimethylpyrazoles (**58a-e**) were found that they readily react with benzyltrifluoroborates (**54a-e**) under developed reaction conditions to provide the C-C bond formation products **59a-g** in yields of 54-75% and with 83-97% *ee* (Figure 82).

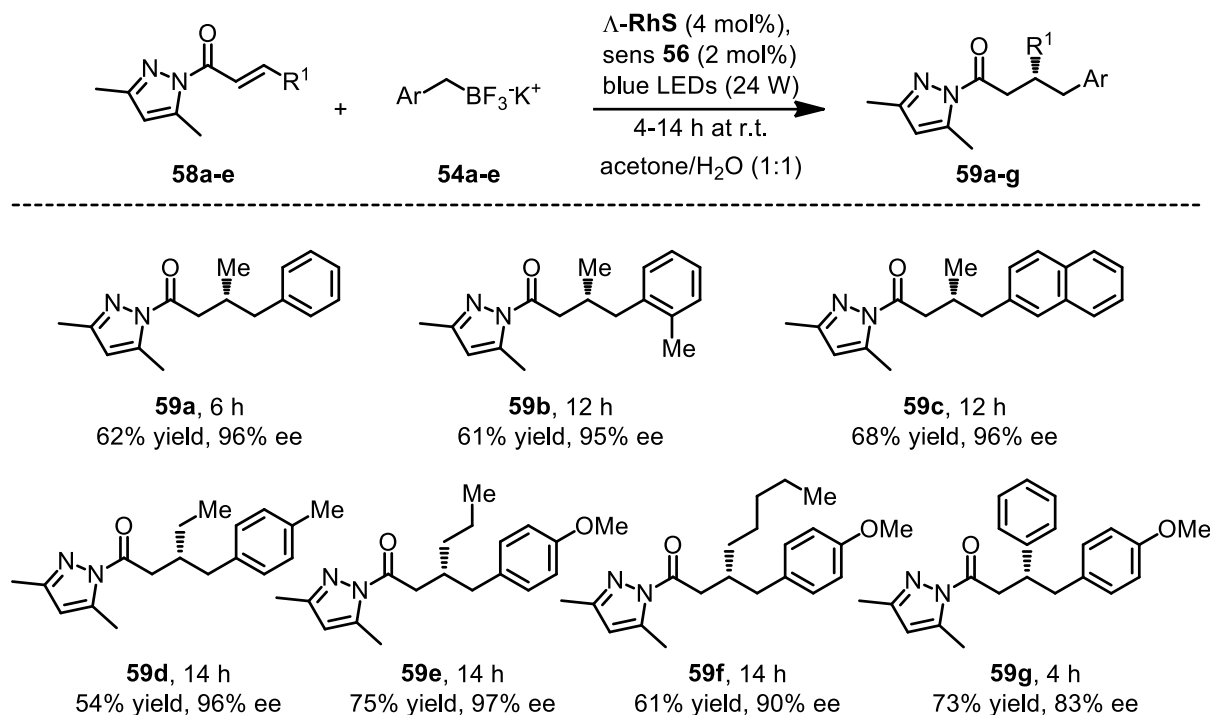


Figure 82 Substrate scope with respect to 2-acyl pyrazoles.

It is worth noting that some reactions have been proven to be unreactive or less efficient for this catalytic system (Figure 83). As shown, the unstabilized primary radical addition only provides adduct in 37% yield (entry 1) and the unreactive alkene acceptor can be recovered, which can be rationalized that the high oxidation potentials of primary trifluoroborate ($E > +1.5$ V) inhibits the alkyl radicals formation.¹⁴ Silicates as C-centered unstabilized primary radical precursors were reported by Fensterbank very recently.¹⁵ The remarkable feature of silicates is the low oxidation potentials ($E \sim +0.75$ V for primary alkylsilicates). Thus alkylsilicates most likely can serve as an alternative precursor to overcome the low reactivity of primary C-centered radical formation. The β -ester substituted alkenes only afforded the radical addition products in moderate enantioselectivities (entry 2). The β -furan substituted alkenes were found to be decomposed under the developed conditions and resulted in the depressed yields (entry 3). For the β -aromatic substituted 2-acyl pyrazoles, unsatisfactory enantioselectivities were obtained due to the strong racemic background reaction (entry 4, see also **59g** in Figure 82). The alkoxyethyltrifluoroborates (entry 5) and secondary / tertiary alkyltrifluoroborates (entry 6) have been proven to be unsuitable for the 2-acyl pyrazole acceptors, only provide unidentified side products.

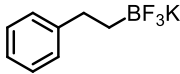
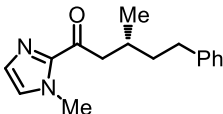
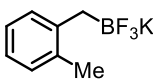
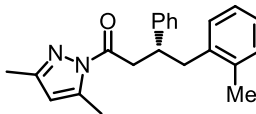
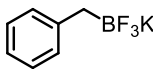
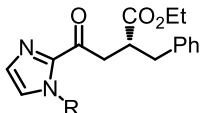
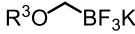
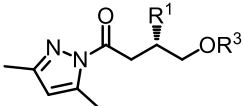
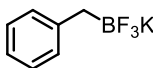
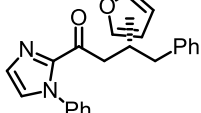
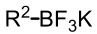
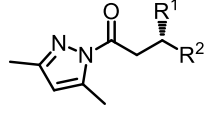
Radical Source	Product	Radical Source	Product
entry 1 	 37% yield, 96% ee	entry 4 	 76% yield, 55% ee
entry 2 	 R = Ph, 21 h, 49% yield, 66% ee R = <i>i</i> Pr, 14 h, 82% yield, 77% ee	entry 5 	 R ¹ = Me or Ph, 0% yield
entry 3 	 2-furan: 28% yield, ee: n.d. 3-furan: 17% yield, ee: n.d.	entry 6 	 R ² = <i>t</i> Bu, cyclohexyl R ¹ = Me or Ph, 0% yield

Figure 83 Some limitations for the developed asymmetric photocatalytic Michael addition. (Results are shown as entries.)

The carboxylic acids have been reported serving as the alkyl radical sources for racemic photocatalytic conjugate addition.¹³ Thus, some carboxylic acids were selected to examine the rhodium catalyzed asymmetric transformation (Figure 84). As shown, these carboxylic acids readily react with the electron-deficient alkene **18a** under the described condition to provide the addition products in 33-51% yields and without any *ee* (entries 2-4). In contrast, potassium *tert*-butyl trifluoroborate afford adduct in 53% yield and with 91% *ee* (entry 1). For the decarboxylative addition, the base is essential for the deprotonation of carboxylic acid to facilitate the single electron oxidation. Whereas the formed conjugate base can coordinate with the rhodium center to result in a neutral complex. The neutral rhodium complex is more stable than the cation complex, and it probably prevent the catalytic turnover leading to a racemic reaction. So trifluoroborates serving as the alkyl precursors are crucial for the asymmetric achievements.

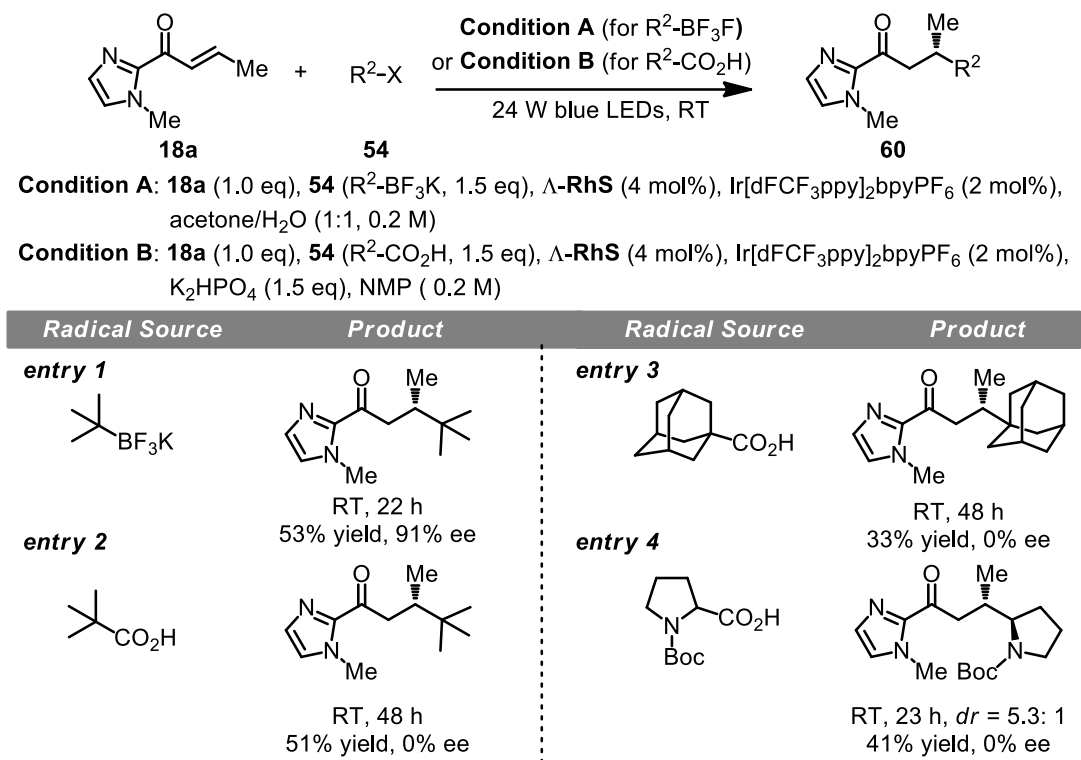
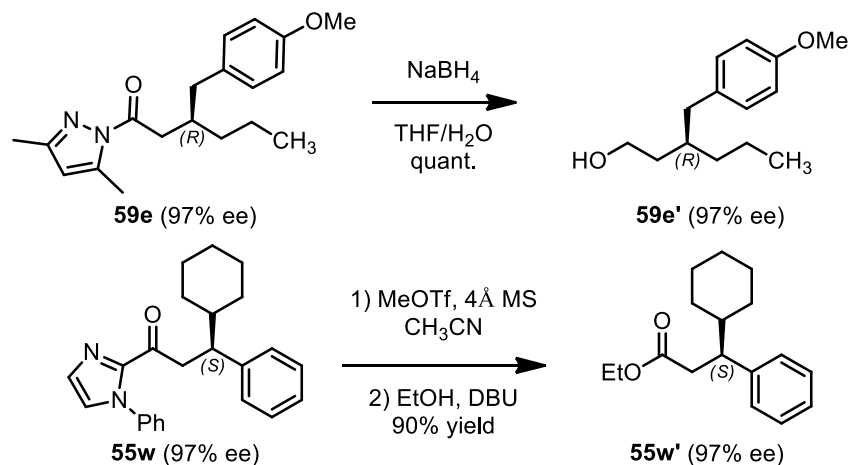


Figure 84 The effect of radical sources for the asymmetric photocatalytic Michael addition. (Results are shown as entries.)

3.6.3 Synthetic Transformations

Finally, the conversion of two typical products, one imidazole and one pyrazole, to useful synthetic building blocks is illustrated in Scheme 19. Cleavage of the pyrazole auxiliary in **59e** under reductive conditions afforded the alcohol **59e'** quantitatively and with unchanged *ee*.¹⁶ On the other hand, the removal of the imidazole moiety of **55w** smoothly proceeded to provide ethyl ester **55w'** in 90% yield and without loss any *ee*.¹⁷



Scheme 19 Transformation of selected products.

3.6.4 Plausible Mechanism

The proposed mechanism is shown in Figure 85. The reaction is initiated by the now well-established photosensitized oxidative conversion of organotrifluoroborates to carbon-centered radicals,^{7,14} which in turn add to *N,O*-rhodium-coordinated 2-acyl imidazole or *N*-acyl pyrazole substrate (intermediate **I**, see experimental section for a crystal structure with an *N*-acyl pyrazole substrate), thereby generating the secondary radical intermediate **II**. Remarkly, Intermediate **II** is subsequently reduced by SET to a rhodium enolate (intermediate **III**), which upon protonation by water provides rhodium-bound product (intermediate **IV**). The formed product is released upon exchange against unreacted starting material, followed by a new catalytic cycle. It is worth noting that the organotrifluoroborates were not only oxidized by the photoexcited sensitizer, but most likely oxidized by the intermediated **II**, thereby leading to a chain process. Except the control experiments in Table 12 reveal visible light and photosensitizer are essential for any product formation, there are still a number of investigations in the mechanism study section which have been executed to verify the proposed mechanism.

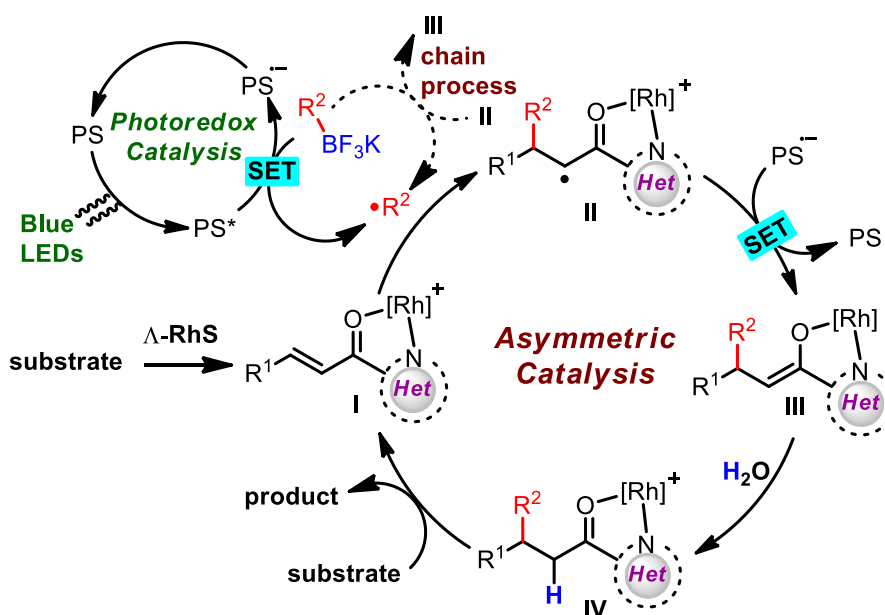


Figure 85 Proposed simplified mechanism without indicating possible chain transfer. SET = single electron transfer, PS = photosensitizer.

3.6.5 Mechanistic Investigations

1) Competition experiments

According to the described mechanism, it is unusual that with catalyst loadings of just 4 mol%, enantioselectivities of up to 99% *ee* can be obtained, and all this even at room temperature. Apparently, the radical addition to the double bond of free substrate (background reaction) cannot compete with the radical addition to rhodium-coordinated substrate (Lewis acid catalyzed reaction). This is counterintuitive considering the high reactivity of alkyl radicals towards acceptor-substituted alkenes combined with the fact that at the beginning of the reaction free substrate is in large excess (25-fold) over rhodium-coordinated substrate. The rhodium-based Lewis acid must therefore provide a strong acceleration of the radical addition. This is indeed the case as determined by competition experiments shown in Figure 86: rhodium coordination increases the radical addition rate by at least a factor of 3×10^4 . This acceleration is obviously the reason for the ability to perform the developed enantioselective radical reaction with low loadings of the chiral Lewis acid.

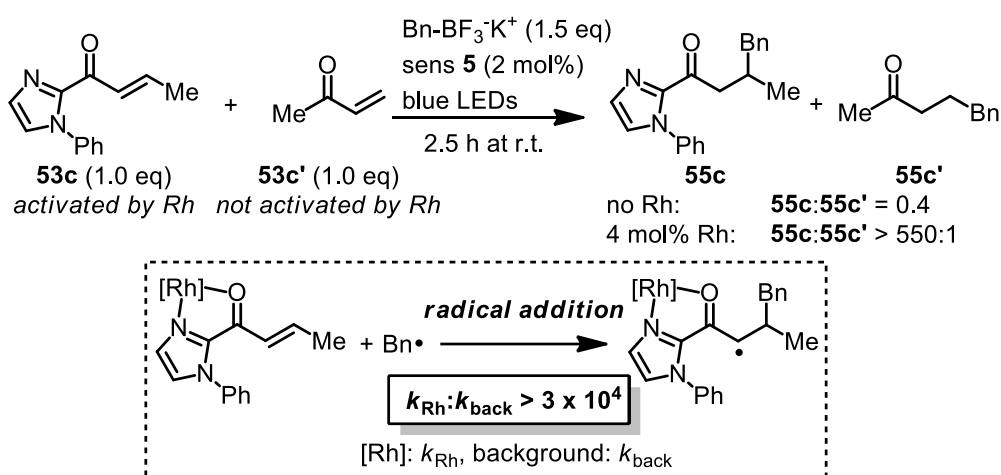
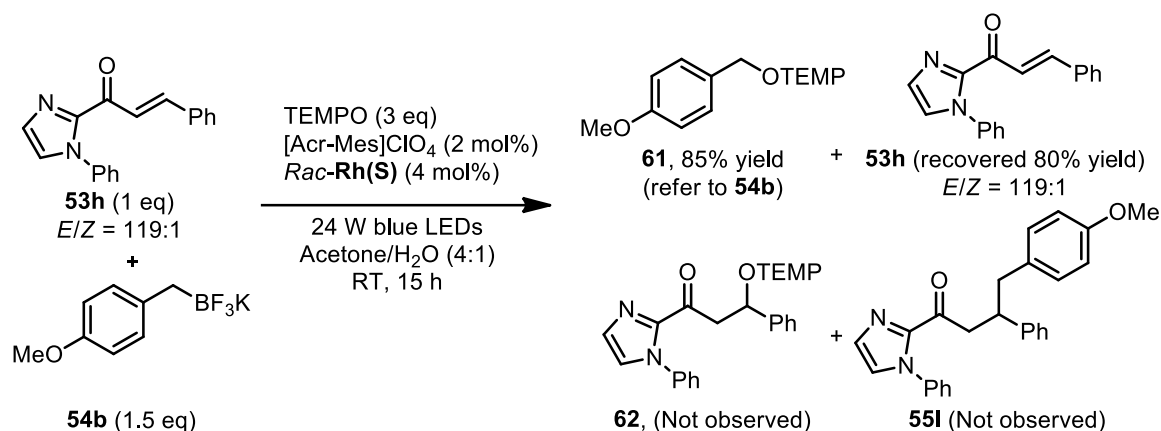


Figure 86 Evaluating the acceleration of the radical addition step by rhodium coordination.

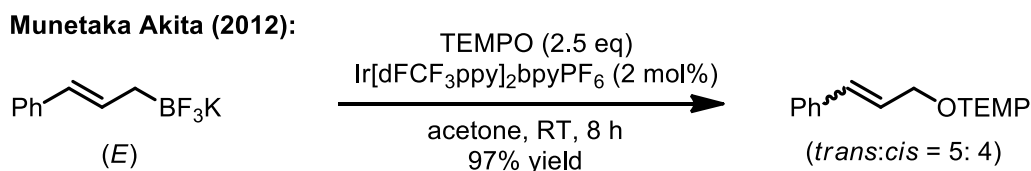
2) Trapping experiment with TEMPO

When two equivalents of TEMPO were added to the reaction after irradiation for 15 h, the radical conjugate addition product **55i** could not be detected (Scheme 20). The formation of oxyaminated product **61** was formed in 85% yield. It was confirmed that this C-O bond formation did not occur either in the dark or in the absence of the photosensitizer [Acr-Mes]ClO₄. Meanwhile, the Michael acceptor **53h** could be recovered in 80% yield and with unchanged *E/Z* value. The C-O coupling product **62** was not observed which does not support the possible involvement of radical-radical coupling pathway.



Scheme 20 Radical trapping experiment with TEMPO.

It's worth noting that one alternative pathway for **61** generation cannot be excluded, in which the formation of **61** involving the nucleophilic addition of trifluoroborates to an oxidatively generated *N*-oxoammonium cation. However, as reported by related investigation (Scheme 21), when the γ -substituted (*E*)-allyltrifluoroborates were examined, the α -oxyaminated products were obtained as a mixture of *E/Z* isomers.^{14(a)} Thus the TEMPO trapping experiments confirm the intermediate generation of alkyl radicals from organotrifluoroborates.



Scheme 21 Photocatalytic coupling of TEMPO and allylic alkyl radical reported by Akita.

3) Control experiments

3.1) Control experiments without degassing

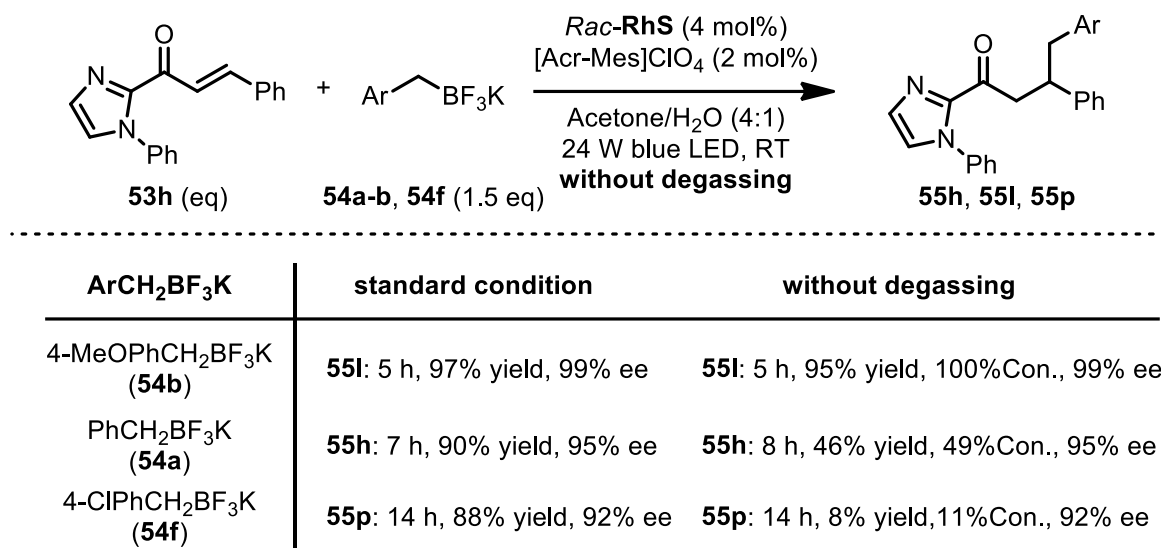


Figure 87 The control experiments in the presence of oxygen.

The described experiments were performed according the general procedure in Figure 80 and Figure 81. The conversion of the photochemical process was determined by ¹H-NMR analysis with 1,3,5-trimethoxybenzene as internal standard. As a result shown above, not degassing caused an obvious inhibition of the formation of **55h** and **55p**. The reaction of trifluoroborate (**54b**) with alkene **53h** is not affected, which seems reasonable considering that the benzyl radical bearing electron donating group serving as a more stabilized radical is not reactive enough to be trapped by oxygen. In contrast, the formation of **55p** using electron deficient substituted trifluoroborate (**54f**) as radical source was inhibited almost completely. Instead a significantly formed aldehyde was observed in the ¹H-NMR spectra of crude product (Figure 88), which also demonstrate the benzyl radicals can be trapped by oxygen resulting in the inhibition of conjugate addition.

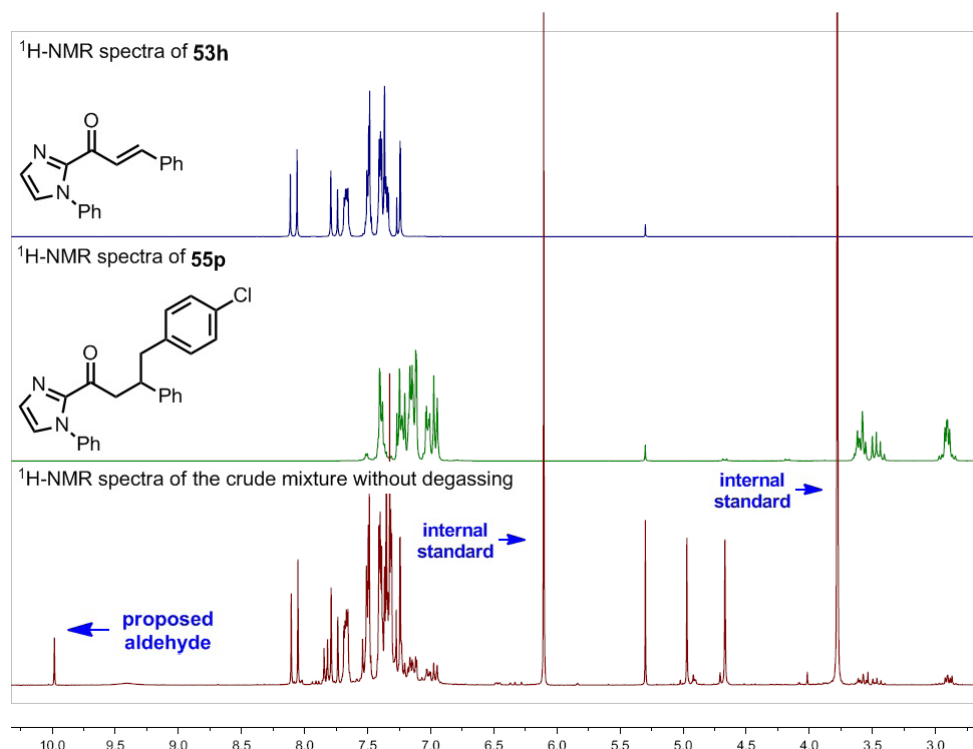


Figure 88 ^1H NMR (300 MHz, in CDCl_3) spectra of **53h**, **55p** (as references) and the crude product from the photolysis. Yield and conversion was inferred by integration ratio.

3.2) Control experiments in deuterated solvent

Two typical substrates, one imidazole, one pyrazole, were selected for the deuterium labeling experiments which were performed under the standard conditions in the indicated solvent system (Figure 89). The ratios of H/D were calculated by ^1H -NMR analysis (Figure 90). Accordingly, the combined solvent of $\text{CD}_3\text{COCD}_3/\text{H}_2\text{O}$ provide the radical adduct with H/D ratio of 99/1, and this ratio does not change in the solvent of $\text{CH}_3\text{COCH}_3/\text{D}_2\text{O}$ in the presence of Lewis acid catalyst **RhS**. In contrast, H/D ratio of 1/1 was observed in the mixed solvent of $\text{CH}_3\text{COCH}_3/\text{D}_2\text{O}$. The product deuteration upon performing the reaction in acetone/ D_2O supports the proposed SET/protonation sequence (Figure 85) as opposed to an alternative H-abstraction from acetone.

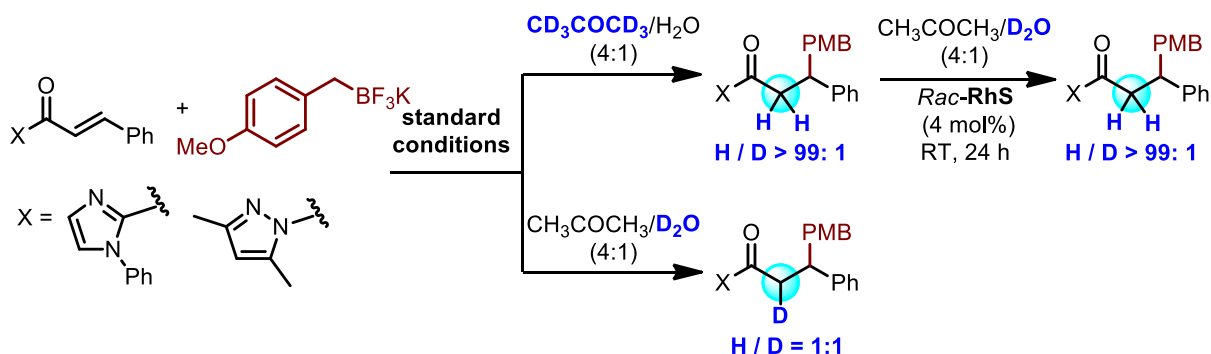


Figure 89 Control experiments in a mixed deuterated solvent system.

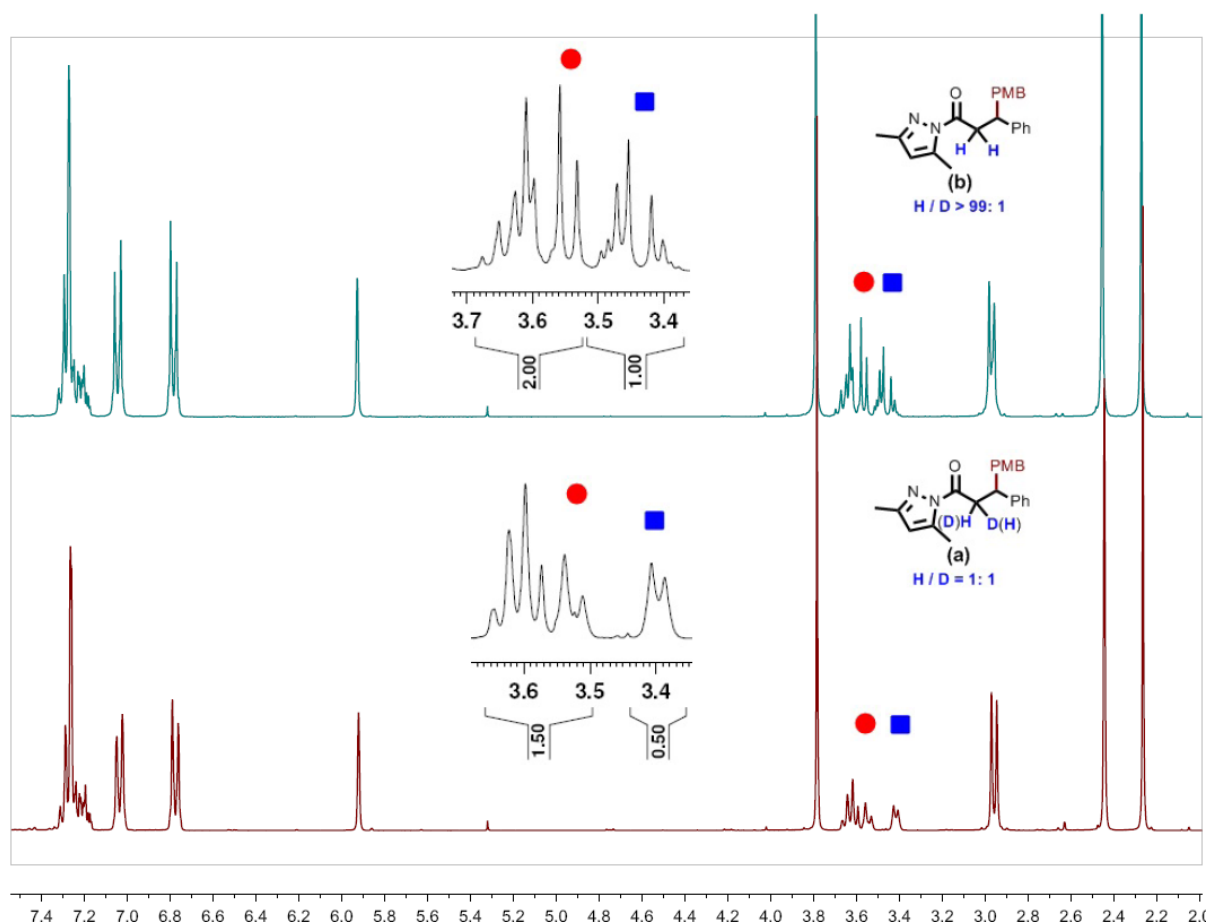


Figure 90 ^1H NMR (300 MHz, in CDCl_3) spectra of illustrated compound (a) and (b). Ratio was inferred by area integration (signals ‘●’ and ‘■’).

4) UV/Vis-absorption spectra

The absorption spectra of the different components of the reaction were measured in solution of acetone/ H_2O (4:1) (Figure 91). The spectra indicate that not only the sensitizers $\text{Ir}[\text{dF}(\text{CF}_3)\text{ppy}]_2(\text{bpy})\text{PF}_6$ ($\lambda_{\text{max}} = 375 \text{ nm}$) and $[\text{Acr-Mes}]\text{ClO}_4$ ($\lambda_{\text{max}} = 420 \text{ nm}$) absorb in the visible region but also the Lewis acid catalyst **RhS** ($\lambda_{\text{max}} = 400 \text{ nm}$) and even more so **RhS** coordinated to the 2-acyl imidazole **53c** (5 equivalents) ($\lambda_{\text{max}} = 390 \text{ nm}$). These absorption spectra suggest a possible interaction between photocatalyst and Lewis acid need to be considered. Such as the static quenching (an inner filter effect) of photocatalyst by **RhS** most likely can be observed.

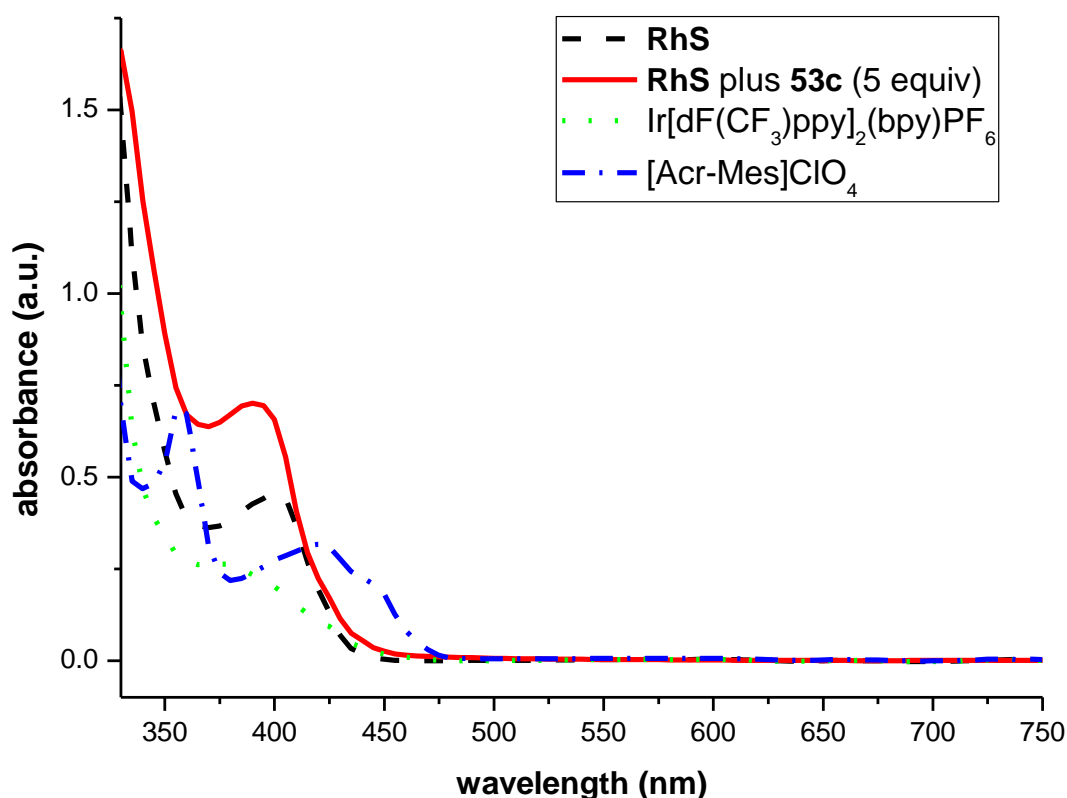


Figure 91 UV/Vis-absorption spectra of the used photoredox catalysts, the Lewis acid catalyst **RhS** and a combination out of **RhS** and the 2-acyl imidazole substrate **53c**. Measured as solutions in acetone/H₂O 4:1 (0.05 mM). a.u. = absorbance units.

5) Luminescence quenching experiments

The luminescence quenching experiments with the photoredox catalyst were investigated both in the presence and absence of **RhS** and olefin. The solutions of Ir[dF(CF₃)ppy]₂(bpy)PF₆ were excited at $\lambda_{\text{max}} = 375$ nm and the emission was measured at 475 nm (emission maximum). The sensitizer Ir[dF(CF₃)ppy]₂(bpy)PF₆ was used for the quenching experiments due to stronger luminescence intensities.

Quenching experiments with Ir[dF(CF₃)ppy]₂(bpy)PF₆ in the absence of RhS and olefin:

The photoexcited iridium sensitizer ($E_{\text{ox}} \approx +1.3$ V)^{7(a)} is quenched by the benzyl and α -oxy trifluoroborates (**54c** and **54h**) in a concentration-dependent fashion (Figure 92). As expected it cannot be quenched by alkyl trifluoroborate **54m** due to its significantly higher oxidation potential ($E_{\text{ox}} \approx +1.5$ V)^{14(f)}. For such alkyl trifluoroborates the alternative sensitizer [Acr-Mes]ClO₄ ($E_{\text{ox}} \approx +2.1$ V)^{14(f)} serves as a stronger and more suitable oxidant and indeed provided efficient transformations (see substrate scope in Figures 80 and 81).

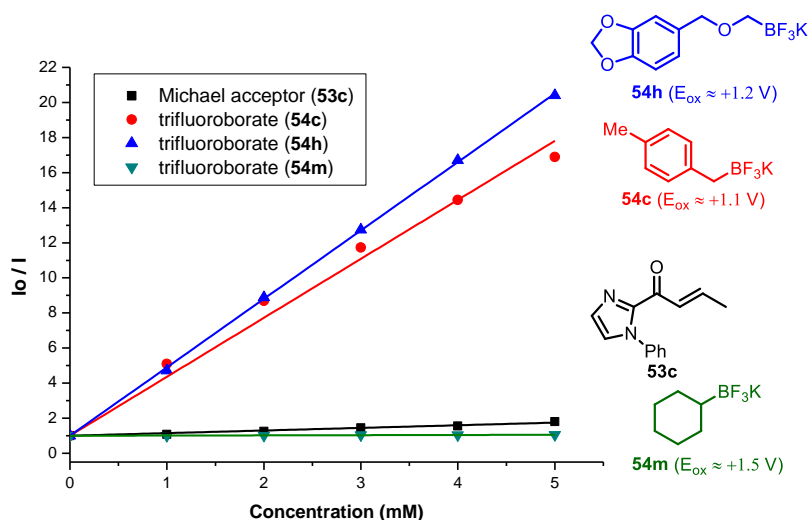


Figure 92 Stern-Volmer plots. I_0 and I are respective luminescence intensities in the absence and presence of the indicated concentrations of the corresponding quencher.

Quenching experiments with Ir[dF(CF₃)ppy]₂(bpy)PF₆ in the presence of RhS and olefin:

When the experiments were performed in the presence of **RhS** and the Michael acceptor **53c**, a decreased luminescence of Ir[dF(CF₃)ppy]₂(bpy)PF₆ was observed, which is demonstrated by the emission intensity of the mixture solution of Ir[dF(CF₃)ppy]₂(bpy)PF₆, **RhS** and alkene **53c** (Figure 93). The ratios of the components were chosen to be analogous to the actual reaction conditions: ([**Ir**]:[**Rh**]:**53c** = 1:2:20). Despite the lower luminescence intensity of the iridium sensitizer, which is apparently due to a static and dynamic quenching caused by **RhS**, the expected concentration-dependent quenching of the photoexcited state of Ir[dF(CF₃)ppy]₂(bpy)PF₆ by the benzyl trifluoroborate **54c** can still be observed (Figure 94).

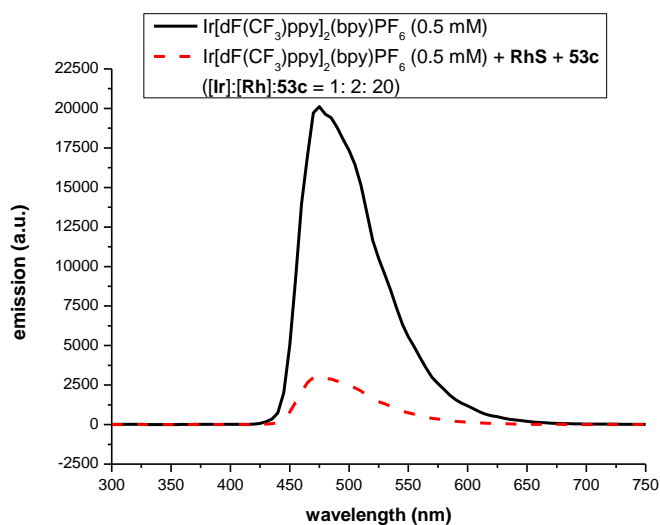


Figure 93 Emission spectra of the photoactive species. The photoactive species were measured as solutions in solvent acetone/H₂O 4:1 (0.05 mM). a.u. = arbitrary unit.

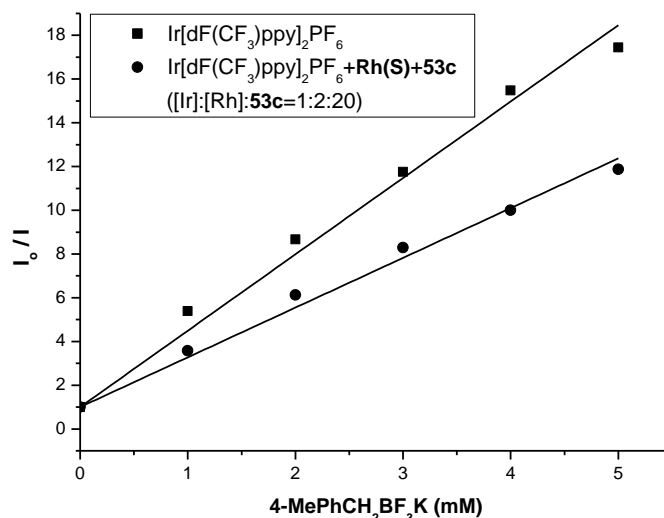
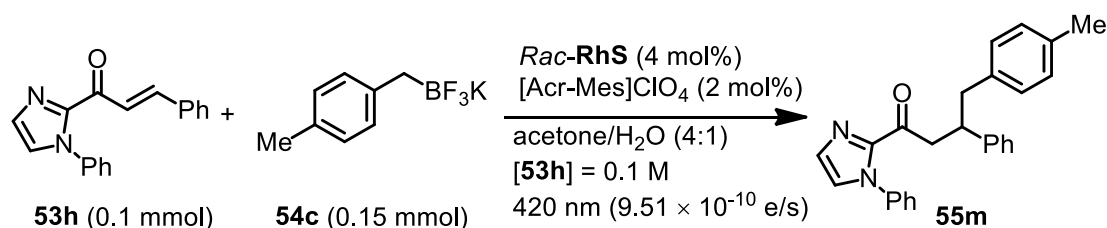


Figure 94 Stern-Volmer plots in the presence and absence of **RhS**. I_0 = luminescence intensity in the absence of 4-MePhCH₂BF₃K. I = luminescence intensity in the presence of the indicated concentrations of 4-MePhCH₂BF₃K.

In summary, these luminescence quenching experiments support the proposed mechanism (Figure 85) in which an initial electron transfer occurs between the excited photoredox sensitizer (acceptor) and the trifluoroborate (donor), while the electron deficient alkene substrates are not involved in this process. The Lewis acid **RhS** reduces the efficiency of this process most likely due to a combination of direct light absorption and quenching of the excited state of the photoredox sensitizer.

6) Quantum yield measurement

The quantum yield was measured by standard ferrioxalate actinometry. A 150 W xenon lamp (50% of light intensity, 420 ± 5 nm bandpass filter) was used as the light source. The potassium ferrioxalate solution measures the decomposition of ferric ions to ferrous ions, which are coordinated to 1,10-phenanthroline and monitored by absorbance at 510 nm. The moles of generated iron-phenanthroline complex is related to moles of incident photons, thus the photon flux was calculated as 9.51×10^{-10} einstein/s (Scheme 22).



Scheme 22 The model reaction for the quantum yield measurement.

6.1) Overall quantum yield:

The model reaction was stirred for specified time intervals (2, 3, 4 h) under the irradiation of 420 nm light. The moles of product formed was measured by GC analysis (FID detector, column: HP-5) using tetradecane as internal standard. Thereby two independent measurements were executed to provide the overall quantum yield (Φ) of the photoreaction as 0.31 and 0.32 respectively. It is important to note that these values present overall quantum yields and do not take into account that there are more than one photoactive species in this system (see Figure 91).

6.2) Evaluating the quantum yield with respect to the photoredox sensitizer [Acr-Mes]ClO₄:

Considering that photons are not only absorbed by the photosensitizer but also by rhodium complexes in solution, the fraction of light that is absorbed directly by [Acr-Mes]ClO₄ was evaluated. Since the absorbance of [Acr-Mes]ClO₄ in acetone/H₂O (4:1) at a concentration of 2 mM, which is a typical concentration for a reaction, showed saturation at 420 nm (Figure 95), the wavelength at which we determined the quantum yield, all investigated samples were 40-fold diluted from the concentration used in a typical reaction (Figure 96).

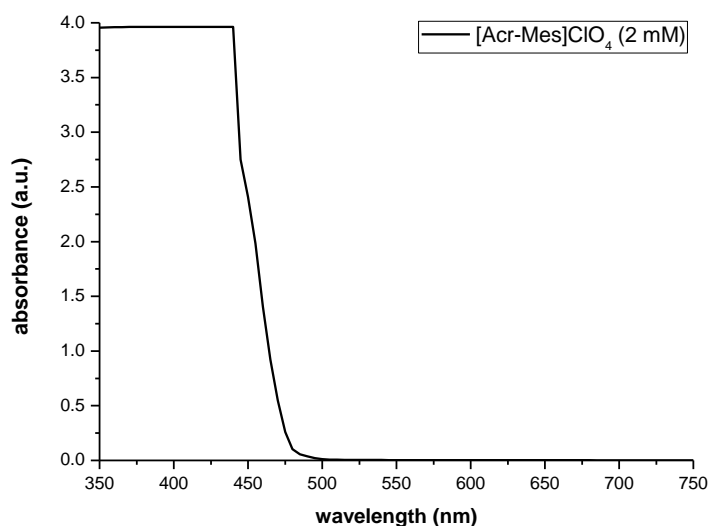


Figure 95 Absorbance of [Acr-Mes]ClO₄ (2 mM in acetone/H₂O 4:1).

The absorbances of the diluted solutions conclude that the photoredox sensitizer absorbs only a fraction of the overall light due to a competing light absorbance from present rhodium complexes. Thus, the quantum yield with respect to the photoredox sensitizer [Acr-Mes]ClO₄ is >0.32 and its exact value is inconclusive.

For the diluted solutions, the following absorption at 420 nm was obtained:

For diluted reaction mixture:

$A_{(420\text{ nm})} = 1.226$, [Rh] = 0.1 mM, [Acr-Mes]ClO₄ = 0.05 mM.

For diluted reaction solution devoid of [Acr-Mes]ClO₄:

$A_{(420\text{ nm})} = 0.908$, [Rh] = 0.1 mM

For the diluted [Acr-Mes]ClO₄ alone:

$A_{(420\text{ nm})} = 0.281$, [Acr-Mes]ClO₄ = 0.05 mM.

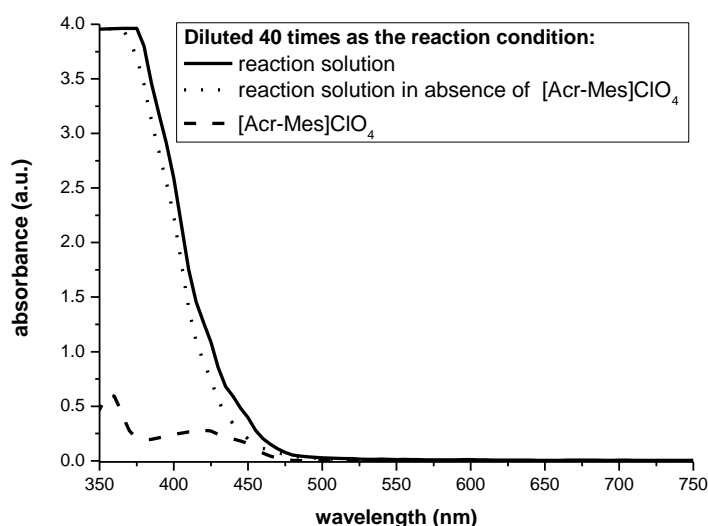


Figure 96 Absorption spectra of the photoactive reaction species. (in acetone/H₂O 4:1, [Rh] = 0.1 mM, [Acr-Mes]ClO₄ = 0.05 mM for the corresponding solution).

6.3) Mechanistic conclusions for quantum yield measurement:

Considering the competing light absorbance of the rhodium complexes, partial quenching of the photoexcited photoredox sensitizer by rhodium complexes (inner filter effect), and further taking into account unproductive processes such as back electron transfer after the initial photoinduced electron transfer from the organotrifluoroborate to the excited photoredox sensitizer, the contribution of chain processes can be expected.

3.6.6 Conclusions

In conclusion, a very efficient and practical catalytic enantioselective conjugate addition has been reported and a broad range of organotrifluoroborates readily react with various acceptor-substituted alkenes under mild photoredox conditions.¹⁸ Key feature is a rhodium-based Lewis acid which not only provides an excellent stereocontrol but also accelerates the involved key radical addition step by at least four to five orders of magnitude, thereby laying the foundation for the low catalyst loadings for this radical reaction. This method for radical generation is much nicer than that used by Sibi,¹⁹ and more general than that used by Yoon.²⁰ The imidazole and pyrazole auxiliary groups are easily cleaved with unchanged *ee*, which has proved the practical utility for this chemistry. The proposed mechanism was supported by an array of mechanistic investigations. Efforts to apply this chemistry to C-centered unstabilized primary radical have met with modest success (37% yield, 96% *ee* for the selected example). Considering the silicates with low oxidation potentials as alternative radical precursors, the proposal in this process should be promising.

References

- 1 H. Huo, X. Shen, C. Wang, L. Zhang, P. Röse, L.-A. Chen, K. Harms, M. Marsch, G. Hilt, E. Meggers, *Nature* **2014**, *515*, 100–103.
- 2 H. Huo, C. Wang, K. Harms, E. Meggers, *J. Am. Chem. Soc.* **2015**, *137*, 9551–9554.
- 3 H. Huo, X. Huang, X. Shen, K. Harms, E. Meggers, *Synlett* **2016**, *27*, 749–753.
- 4 For a review on enantioselective radical reactions, see: J. Zimmerman, M. P. Sibi, *Top. Curr. Chem.* **2006**, *263*, 107–162.
- 5 (a) M. P. Sibi, J. Ji, *J. Org. Chem.* **1997**, *62*, 3800–3801. (b) M. P. Sibi, J. Ji, J. H. Wu, S. Gürtler, N. A. Porter, *J. Am. Chem. Soc.* **1996**, *118*, 9200–9201.
- 6 L. R. Espelt, I. S. McPherson, E. M. Wiensch, T. P. Yoon, *J. Am. Chem. Soc.* **2015**, *137*, 2452–2455.

- 7 (a) J. C. Tellis, D. N. Primer, G. A. Molander, *Science* **2014**, *345*, 433–436. (b) D. N. Primer, I. Karakaya, J. C. Tellis, G. A. Molander, *J. Am. Chem. Soc.* **2015**, *137*, 2195–2198. (c) O. Gutierrez, J. C. Tellis, D. N. Primer, G. A. Molander, M. C. Kozlowski, *J. Am. Chem. Soc.* **2015**, *137*, 4896–4899. (d) I. Karakaya, D. N. Primer, G. A. Molander, *Org. Lett.* **2015**, *17*, 3294–3297. (e) Y. Yamashita, J. C. Tellis, G. A. Molander, *Proc. Natl. Acad. Sci. U. S. A.*, **2015**, *112*, 12026–12029. (f) M. El Khatib, R. A. M. Serafim, G. A. Molander, *Angew. Chem. Int. Ed.* **2016**, *55*, 254–258. (g) D. Ryu, D. N. Primer, J. C. Tellis, G. A. Molander, *Chem. Eur. J.* **2016**, *22*, 120–123. (h) J. Amani, E. Sodagar, G. A. Molander, *Org. Lett.* **2016**, *18*, 732–735.
- 8 (a) C. Wang, Y. Zheng, H. Huo, P. Röse, L. Zhang, K. Harms, G. Hilt, E. Meggers, *Chem. Eur. J.* **2015**, *21*, 7355–7359. (b) C. Wang, J. Qin, X. Shen, R. Riedel, K. Harms, E. Meggers, *Angew. Chem. Int. Ed.* **2016**, *55*, 685–688.
- 9 (a) C. Wang, L.-A. Chen, H. Huo, X. Shen, K. Harms, L. Gong, E. Meggers, *Chem. Sci.* **2015**, *6*, 1094–1100. (b) Y. Tan, W. Yuan, L. Gong, E. Meggers, *Angew. Chem. Int. Ed.* **2015**, *54*, 13045–13048.
- 10 For recent reviews on dual photoredox catalysis, see: M. N. Hopkinson, B. Sahoo, J.-L. Li, F. Glorius, *Chem. Eur. J.* **2014**, *20*, 3874–3886. (b) K. L. Skubi, T. R. Blum, T. P. Yoon, *Chem. Rev.* **2016**, DOI: 10.1021/acs.chemrev.6b00018.
- 11 J. Ma, X. Shen, K. Harms, E. Meggers, *Dalton Trans.* **2016**, *45*, 8320–8323.
- 12 (a) S. Fukuzumi, H. Kotani, K. Ohkubo, S. Ogo, N. V. Tkachenko, H. Lemmetyinen, *J. Am. Chem. Soc.* **2004**, *126*, 1600–1601. (b) A. C. Benniston, A. Harriman, P. Y. Li, J. P. Rostron, H. J. van Ramesdonk, M. M. Groeneveld, H. Zhang, J. W. Verhoeven, *J. Am. Chem. Soc.* **2005**, *127*, 16054–16064. (c) M. Hoshino, H. Uekusa, A. Tomita, S. Koshihara, T. Sato, S. Nozawa, S. Adachi, K. Ohkubo, H. Kotani, S. Fukuzumi, *J. Am. Chem. Soc.* **2012**, *134*, 4569–4572.
- 13 For additions of decarboxylatively generated radicals to electron-deficient alkenes, see: (a) G. L. Lackner, K. W. Quasdorf, L. E. Overman, *J. Am. Chem. Soc.* **2013**, *135*, 15342–15345. (b) L. Chu, C. Ohta, Z. Zuo, D. W. C. MacMillan, *J. Am. Chem. Soc.* **2014**, *136*, 10886–10889. (c) G. L. Lackner, K. W. Quasdorf, G. Pratsch, L. E. Overman, *J. Org. Chem.* **2015**, *80*, 6012–6024. (d) G. Pratsch, G. L. Lackner, L. E. Overman, *J. Org. Chem.* **2015**, *80*, 6025–6036. (e) C. C. Nawrat, C. R. Jamison, Y. Slutskyy, D. W. C. MacMillan, L. E. Overman, *J. Am. Chem. Soc.* **2015**, *137*, 11270–11273.

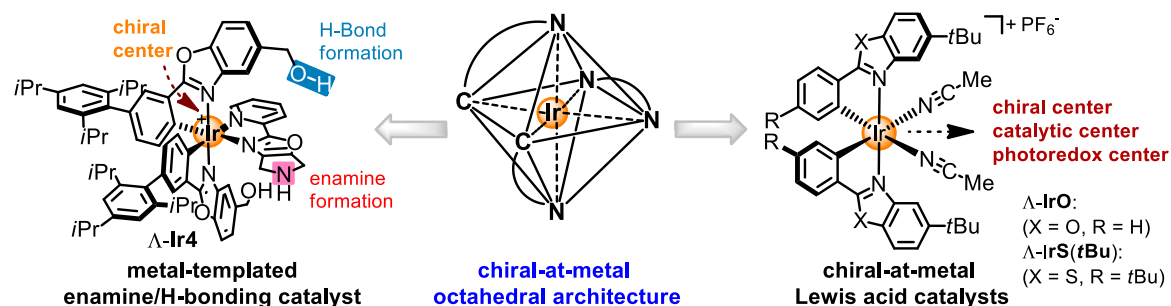
- 14 For organotrifluoroborates as radical precursors, see also: (a) Y. Yasu, T. Koike, M. Akita, *Adv. Synth. Catal.* **2012**, 354, 3414–3420. (b) K. Miyazawa, Y. Yasu, T. Koike, M. Akita, *Chem. Commun.* **2013**, 49, 7249–7251. (c) H. Huang, G. Zhang, L. Gong, S. Zhang, Y. Chen, *J. Am. Chem. Soc.* **2014**, 136, 2280–2283. (d) Y. J. Li, K. Miyazawa, T. Koike, M. Akita, *Org. Chem. Front.* **2015**, 2, 319–323. (e) H. Huang, K. Jia, Y. Chen, *Angew. Chem. Int. Ed.* **2015**, 54, 1881–1884. (f) T. Chinzei, K. Miyazawa, Y. Yasu, T. Koike, M. Akita, *Rsc Adv.* **2015**, 5, 21297–21300. (g) L. Chenneberg, C. Lévêque, V. Corcé, A. Baralle, J.-P. Goddard, C. Ollivier, L. Fensterbank, *Synlett* **2016**, 27, 731–735.
- 15 C. Lévêque, L. Chenneberg, V. Corcé, J.-P. Goddard, C. Ollivier, L. Fensterbank, *Org. Chem. Front.* **2016**, 3, 462–465.
- 16 K. Tokumasu, R. Yazaki, T. Ohshima, *J. Am. Chem. Soc.* **2016**, 138, 2664–2669.
- 17 (a) D. A. Evans, K. R. Fandrick, H.-J. Song, *J. Am. Chem. Soc.* **2005**, 127, 8942–8943. (b) D. A. Evans, K. R. Fandrick, *Org. Lett.* **2006**, 8, 2249–2252. (c) D. A. Evans, H.-J. Song, K. R. Fandrick, *Org. Lett.* **2006**, 8, 3351–3354. (d) D. A. Evans, K. R. Fandrick, H.-J. Song, K. A. Scheidt, R. Xu, *J. Am. Chem. Soc.* **2007**, 129, 10029–10041.
- 18 H. Huo, K. Harms, E. Meggers, *J. Am. Chem. Soc.* **2016**, DOI: 10.1021/jacs.6b03399
- 19 (a) M. P. Sibi, J. Ji, *J. Org. Chem.* **1997**, 62, 3800–3801. (b) M. P. Sibi, J. Ji, J. H. Wu, S. Gürtler, N. A. Porter, *J. Am. Chem. Soc.* **1996**, 118, 9200–9201.
- 20 L. R. Espelt, I. S. McPherson, E. M. Wiensch, T. P. Yoon, *J. Am. Chem. Soc.* **2015**, 137, 2452–2455.

Chapter 4: Summary and Outlook

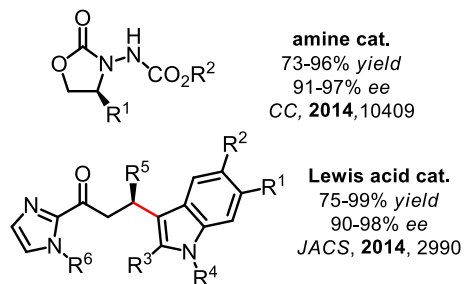
4.1 Summary

Two types of chiral-at-metal octahedral complexes have been developed as exceptionally effective asymmetric catalysts, namely the metal-templated enamine/H-bonding dual catalyst Λ -Ir4 and the active Lewis-acid catalyst Λ -IrO and Λ -IrS(*t*Bu). These novel catalysts or their derivatives have been successfully utilized in a number of enantioselective non-photochemical reactions and visible-light-activated transformations (Figure 97). Remarkably, a single chiral Lewis-acid complex has proven to be capable to serve as photoredox catalyst and at the same time provide very effective asymmetric induction for α -functionalization of carbonyl compounds. These novel asymmetric photoredox catalysts, in which the iridium metal center simultaneously act as the exclusive source of chirality, the catalytically active Lewis acid center, and the photoredox center, offer new opportunities for the economical synthesis of enantioenriched molecules.

catalyst discoveries:



non-photochemical applications:



photoredox applications:

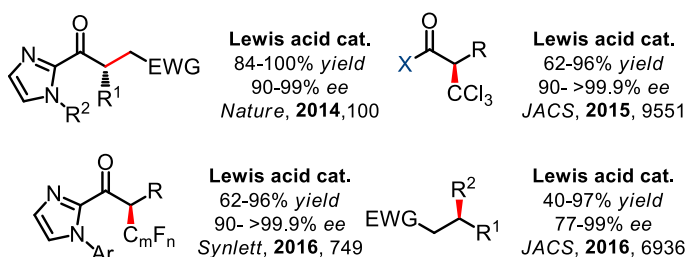
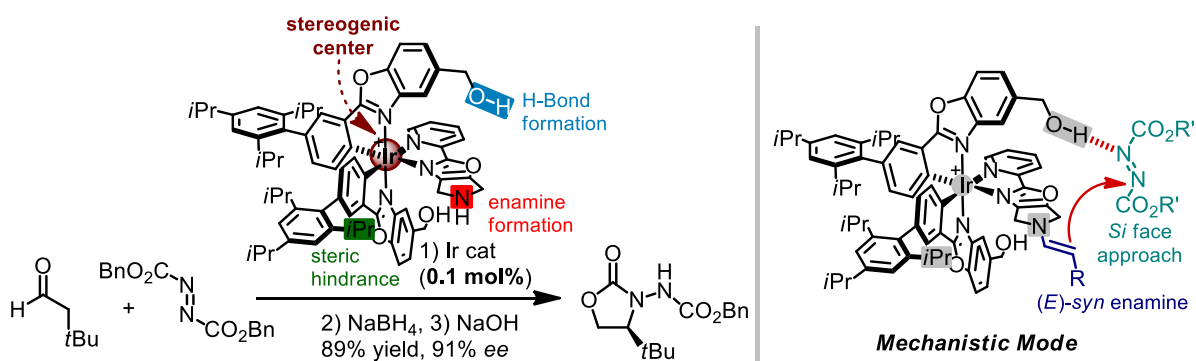
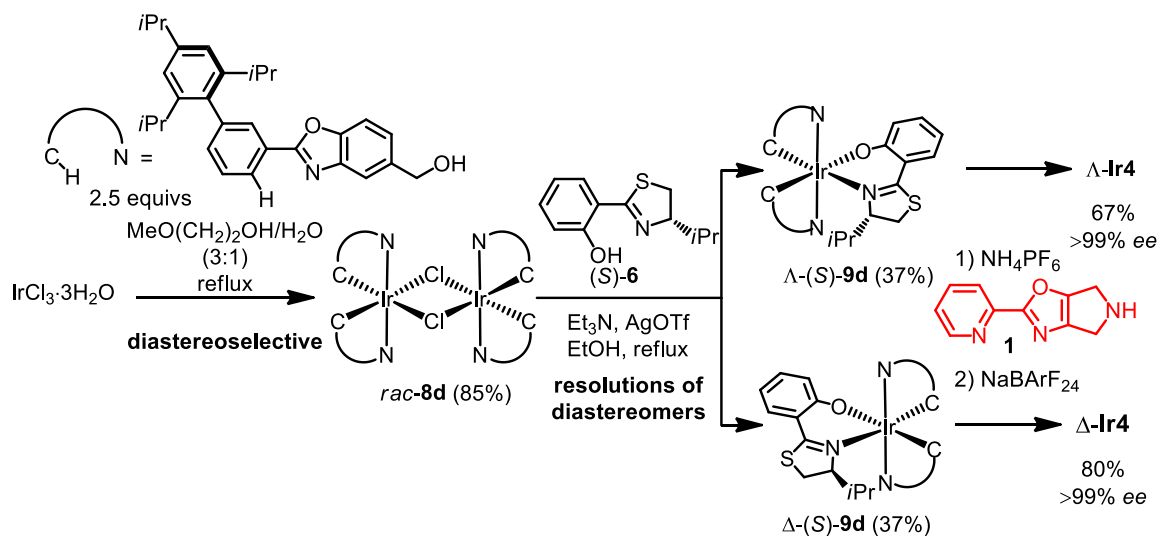


Figure 97 An overview for this thesis: chiral-at-metal catalyst discoveries and their applications in the asymmetric non-photochemical and photoredox catalysis.

1) Metal-templated enantioselective enamine/H-bonding dual activation catalysis


 Figure 98 Enantioselective α -amination of aldehydes with metal-templated iridium complex.

An asymmetric enamine catalyst (Δ -**Ir4**) built from an octahedral chiral-at-metal complex was developed.¹ This complex catalyzed enantioselective α -amination of aldehydes with only 1 mol% catalyst loadings, even down to 0.1 mol% (Figure 98). With respect to catalyst loading in asymmetric organocatalysis, iridium complex Δ -**Ir4** constitutes one of the most efficient catalysts for the enantioselective α -amination of aldehydes to date. Mechanistically, the enamine was produced as (E) -syn form by preventing the unfavorable (E) -anti conformation with a bulky 2,4,6- $i\text{Pr}_3\text{Ph}$ group. The *si* face approach of azodicarboxylate was induced by an H-bonding between of the OH group and a nitrogen or carbonyl oxygen atom of the azodicarboxylate. The catalyst Δ -**Ir4** was synthesized through chiral auxiliary strategy developed in Meggers group.² Two generated diastereomeric complexes Δ -(*S*)-**9** and Δ -(*S*)-**9** (each 37%) which can be resolved by standard silica gel chromatography. The virtually enantiopure Δ -**Ir4** and Δ -**Ir4** (each $>99\%$ ee) were obtained after stereospecific substitution of the chiral auxiliary with secondary amine ligand (**1**).


 Figure 99 Synthesis of the enantiomerically pure enamine/H-bonding catalysts Δ -**Ir4** and Δ -**Ir4**.

2) Asymmetric catalysis with substitutionally labile yet stereochemically stable chiral-at-metal iridium(III) complex: discovery and the non-photochemical application of Λ -IrO/ Δ -IrO

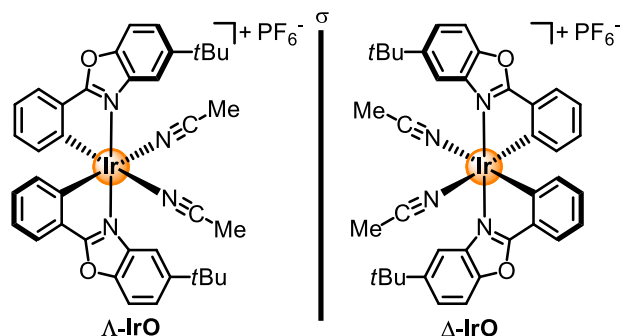


Figure 100 Enantiomers of a substitutionally labile yet configurationally stable chiral-at-metal iridium(III) Lewis acid Λ -IrO and Δ -IrO.

A metal-coordination-based asymmetric catalyst utilizing metal centrochirality as the sole element of chirality was newly developed (Figure 100).³ The Lewis acid complexes Λ -IrO and Δ -IrO were synthesized straightforwardly according to chiral auxiliary strategy developed in Meggers group (Figure 101).² Accordingly, two generated diastereomeric complexes Λ -(S)-**18** and Δ -(S)-**18** which can be resolved by standard silica gel chromatography. The virtually enantiopure Λ -IrO and Δ -IrO (verified by HPLC, each >99% *ee*) were yielded after stereospecific substitution of the chiral auxiliary ligand (upon protonation by NH_4PF_6) by two acetonitrile ligands. Notably, Λ -IrO and Δ -IrO have proven to be bench stable and tolerant to a large range of solvents.

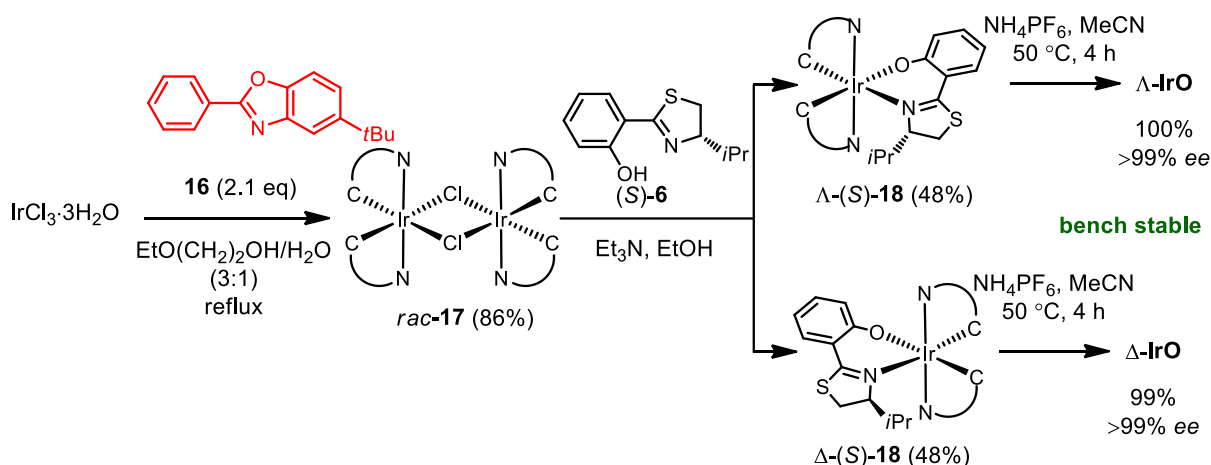


Figure 101 Synthesis of enantiomerically pure Lewis acid complexes Λ -IrO and Δ -IrO.

The introduced substitutionally labile, chiral-at-metal octahedral iridium(III) complex exclusively bears achiral ligands and effectively catalyzes the enantioselective Friedel-Crafts addition of indoles to α,β -unsaturated 2-acylimidazoles (19 examples) with high yields (75%-99%) and high enantioselectivities (90-98% *ee*) at low catalyst loadings (0.25-2 mol%) (Figure 102). Counterintuitively, despite its substitutional lability, which is mechanistically required for coordination to the 2-acylimidazole substrate, the metal-centered chirality is maintained throughout the catalysis. This novel class of reactive chiral-only-at-metal complexes has proven to be of high value for a large variety of asymmetric transformations in Meggers group.

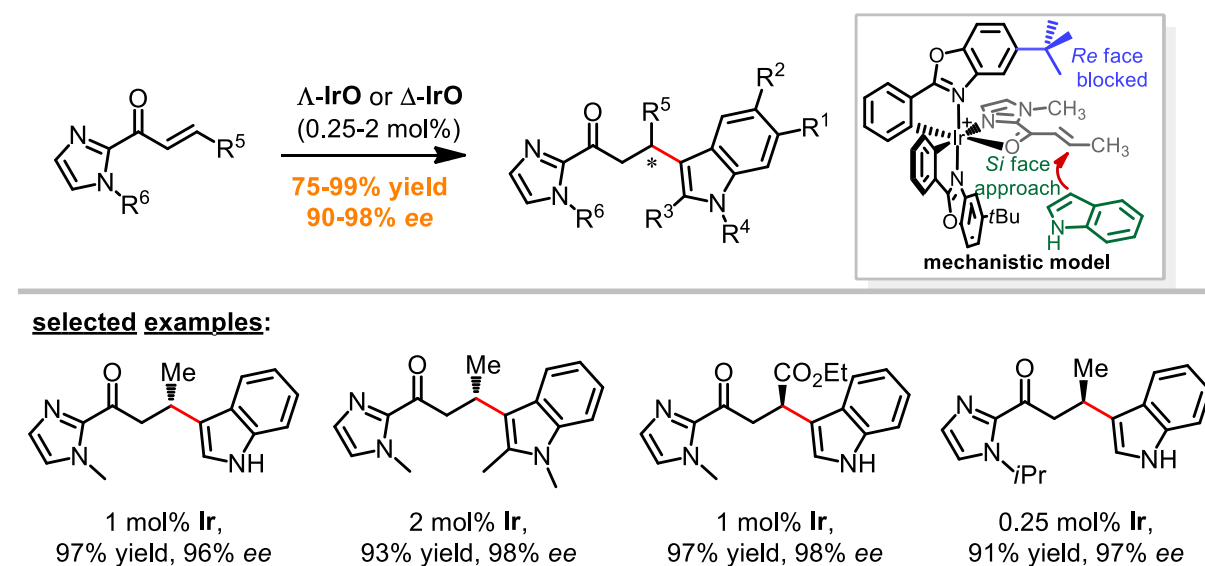


Figure 102 Enantioselective Friedel-Crafts addition of indoles to α,β -unsaturated 2-acyl imidazoles catalyzed by Λ -IrO or Δ -IrO.

crucial asymmetric induction in the catalytic cycle and but at the same time serves as the *in situ* generated active chiral photosensitizer. This process can be classified as redox-neutral, electron-catalyzed reaction.

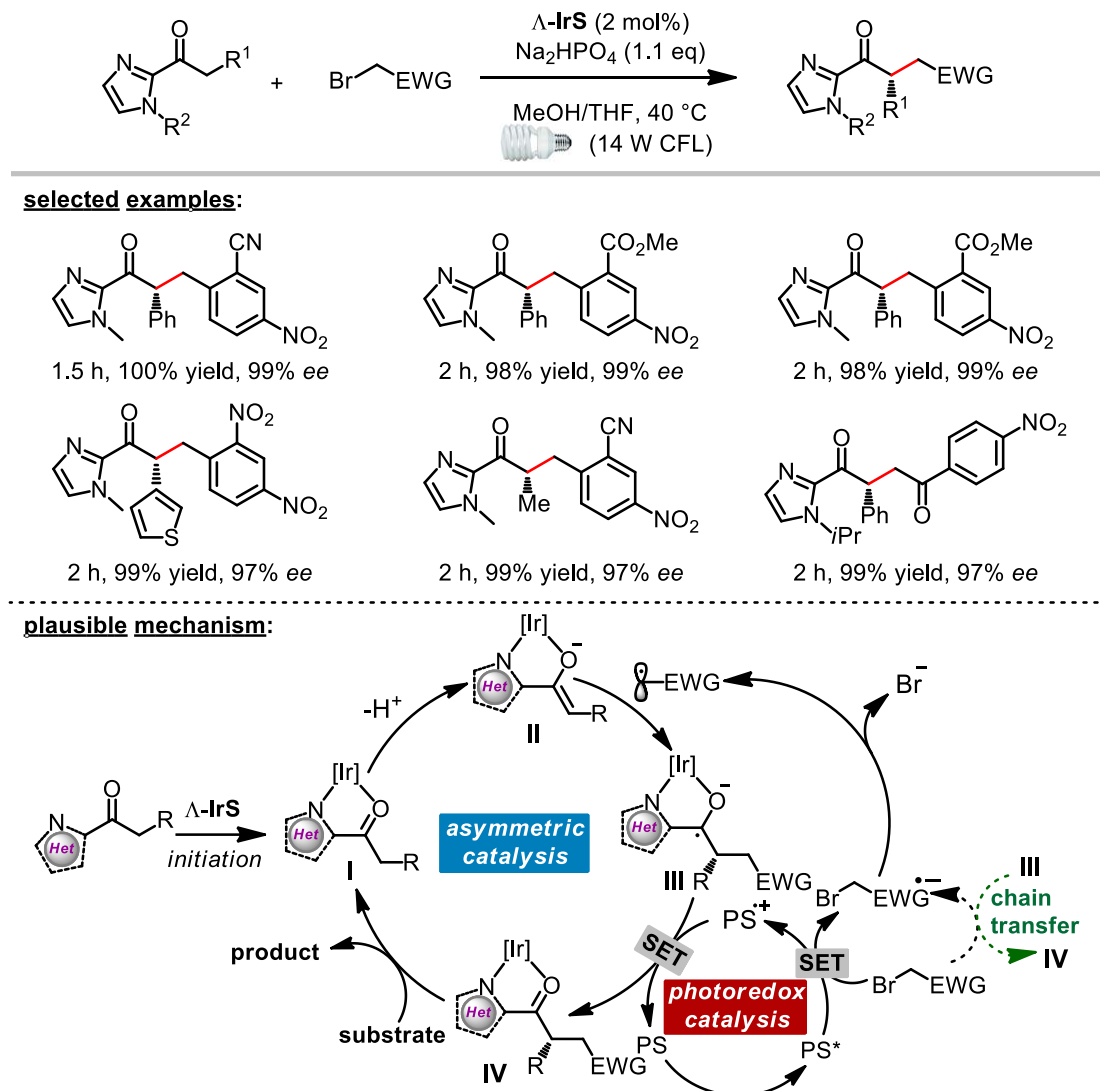


Figure 104 Visible-light-induced enantioselective alkylation of 2-acyl imidazoles with acceptor substituted benzyl bromides and phenacyl bromides.

4) Enantioselective, catalytic trichloromethylation through visible-light-activated photoredox catalysis with a chiral iridium complex

The first example of an enantioselective, catalytic trichloromethylation of 2-acyl imidazoles and 2-acylpyridines has been developed.⁵ Excellent enantioselectivities are often observed with multiple reactions reaching 99% *ee* and even higher (Figure 105). As an extensive research of single catalyst induced photochemical α -functionalization of ketones with electron-deficient alkyl halide, the mechanism is in analogy to the described catalytic cycles in Figure 104. The chiral-at-metal Λ -**IrS** can serve a dual function, as a catalytically active chiral Lewis acid and simultaneously as a precursor for an *in situ* assembled visible-light-triggered photoredox catalyst. However, attempts at extending the achiral templates from imidazole and pyridine to other easily removable moieties have largely been unsuccessful; efforts to the cleavage of the imidazole auxiliary of products met with failure, due to the sensitivity of the CCl_3 group towards HCl elimination under basic conditions.

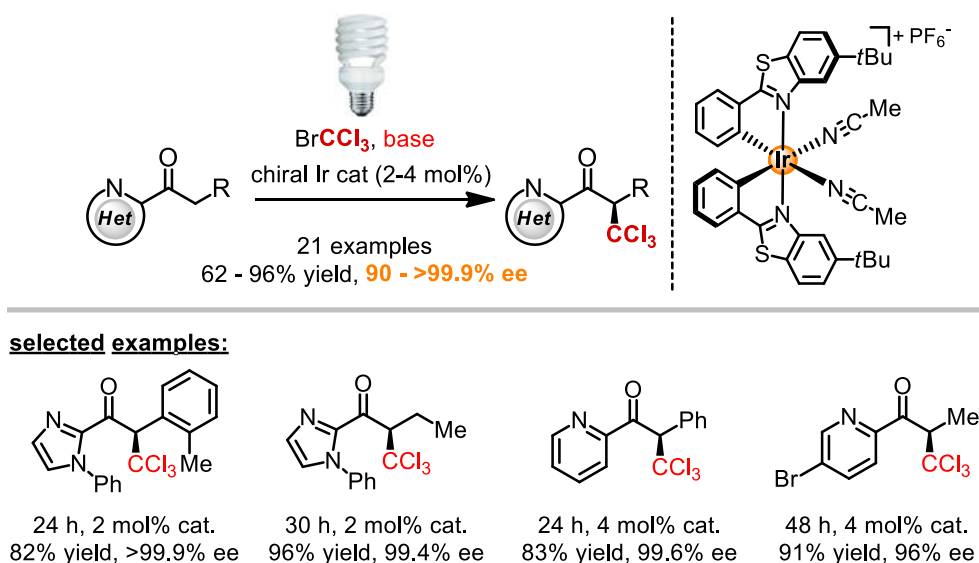
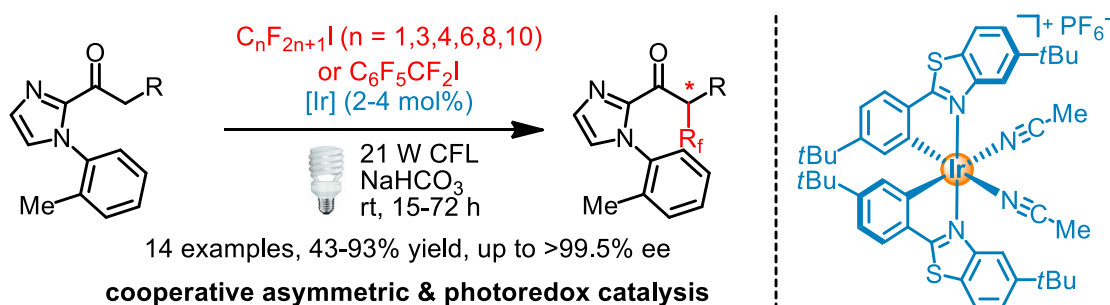


Figure 105 Photocatalytic, asymmetric trichloromethylation of 2-acyl imidazoles and 2-acylpyridines.

5) Visible-light-activated enantioselective perfluoroalkylation with a chiral iridium photoredox catalyst

A visible-light-activated enantioselective radical perfluoroalkylation of 2-acyl imidazoles with perfluoroalkyl iodides and perfluorobenzyl iodide at the α -position of the carbonyl group is developed.⁶ Enantioselectivities with up to >99.5% *ee* are achieved (Figure 106). The process uses a dual function chiral Lewis acid / photoredox catalyst loadings of 2-4 mol% and constitutes a redox-neutral, electron-catalyzed reaction which proceeds through intermediate perfluoroalkyl radicals. This work demonstrates the generality of the dual function chiral Lewis acid / photoredox catalyst concept. The facile optimization of catalyst structure has proven to be promising for adjusting the photophysical properties. This chemistry was started with two catalysts and ended at single catalyst, this research strategy provide insights for looking for new asymmetric photochemical reactions.



selected examples:

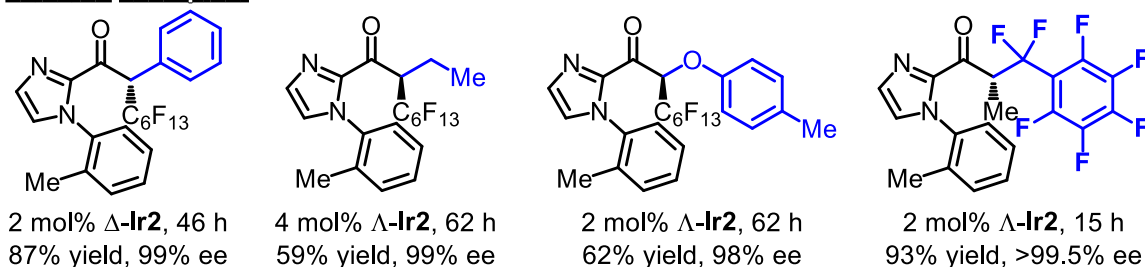


Figure 106 Catalytic, enantioselective perfluoroalkylation through visible-light-activated photoredox catalysis with a chiral iridium complex.

6) Catalytic, enantioselective addition of alkyl radicals to alkenes *via* visible-light-activated photoredox catalysis with a chiral rhodium complex

A very efficient and practical catalytic enantioselective conjugate addition has been developed,⁷ and a broad range of organotrifluoroborates (alkyl, benzyl and alpha-oxy moieties) readily react with various acceptor-substituted alkenes in the presence of only 4 mol% rhodium catalyst (Figure 107). Key feature is this rhodium-based Lewis acid which not only provides an excellent stereocontrol but also accelerates the involved key radical addition step by at least four to five orders of magnitude, thereby laying the foundation for the low catalyst loadings for this radical reaction. This method for radical generation is much nicer and more general than that used by Sibi and Yoon (see also Figure 79).⁸ The imidazole and pyrazole auxiliary groups are easily cleaved with unchanged *ee*, which has proved the practical utility for this chemistry.

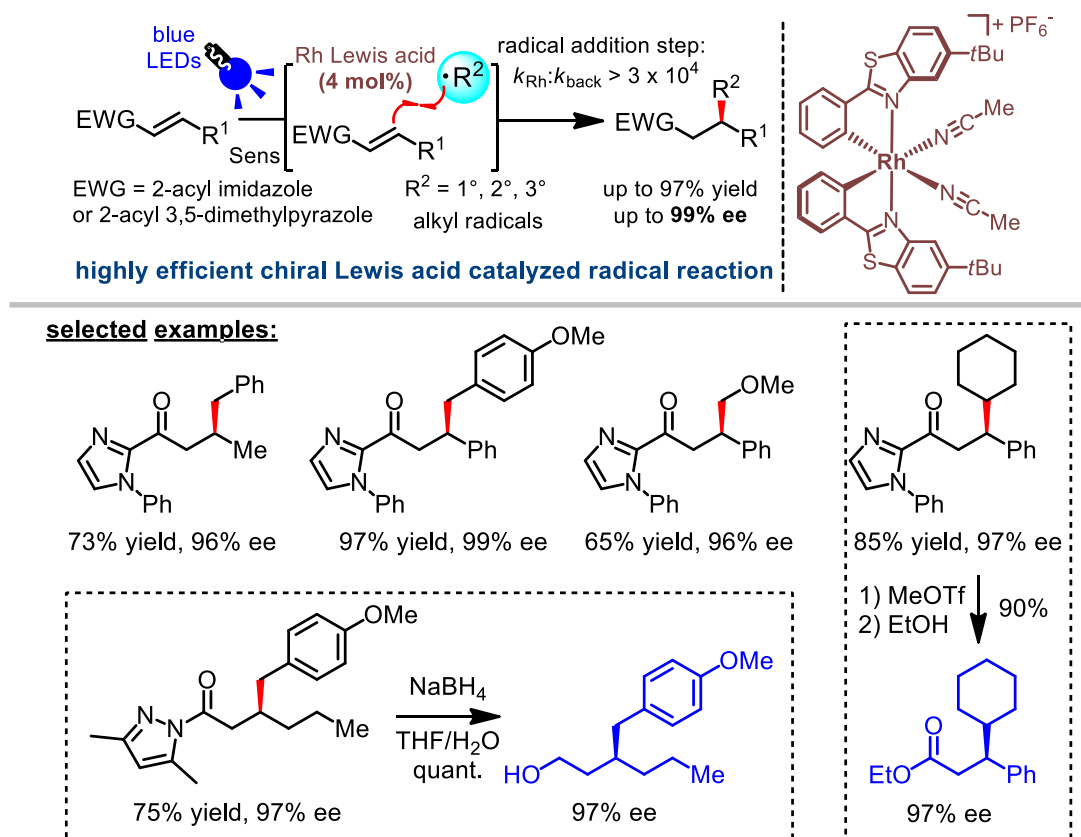


Figure 107 Visible-light-activated enantioselective conjugate addition of alkyl radicals to alkenes.

4.2 Outlook

Considering some unmet need and expected potentials in this thesis, the future investigations can be builded on the following aspects:

1) Simplify the asymmetric synthesis of chiral-at-metal catalysts: Although grams scale synthesis of the chiral Lewis acid Λ -**IrO** and Λ -**IrS** are allowed by the previously established protocol in Meggers group. This strategy relied on the preformed chiral auxiliary and did not get rid of standard silica gel chromatography. The relatively high-cost of synthesis has limited its potential commercial valuable. Thus, the choice of simple, readily available, and easily removable chiral auxiliary is highly desirable for this system, such as the low-cost natural amino acids. Attempts to get various amino-acid-based diastereomers and investigate their differences in solubility would provide a chance to isolate them only relying on recrystallization. The well established directing groups, which have been widely applied in transition-metal catalyzed C-H functionalization, are also rational chiral templates candidates.

2) Measure the redox potentials of chiral-at-metal complexes: With respect to the photoredox catalysis, despite the previous investigations revealed the Λ -**IrO** is more suitable for oxidative chemistry, and Λ -**IrS** is more favorable for reductive chemistry. The general rules of photophysical properties for these iridium complexes are still elusive. The optimization of catalyst structure has proven to be promising in chapter 3.5. Compared to **IrS**, the derivative **IrS(*t*Bu)** contains two additional *t*-Bu behaved as a more stronger reductant. Thus, measuring the redox potentials for all classes of chiral-at-metal complexes in our group, including the intermediate complexes, would provides straightforward insights for catalyst structure optimization. The location of HOMO and LUMO for these complexes will be likely figured out, and then we can adjust the redox potential of catalysts through introducing electron rich or deficient groups at the fixed position of achiral ligand. The previous unmet synthetic applications are highly possible to be realized.

3) Consider the photochemical reactions with enamine/H-bonding catalyst: Attributing to the non-facile synthesis and the sensitive α -amino methylene group of enamine catalyst **Λ -Ir4**, its photoproperties have not been systematically investigated. As a starting point, the sample bis-cyclometalated ligand without H-bonding donors can be selected to synthesize the enamine catalyst. As the model reaction, we can consider the alkylation of aldehydes with electron deficient benzyl bromides and phenacyl bromides. If the direct alkylation of aldehydes can be realized through visible-light-induced photoredox catalysis with **Λ -Ir4** or its derivatives, we would fulfill the synthetic toolbox in Meggers group, and get rid of the necessity of prefunctionalizing the substrates and the subsequent removal of the chelating group.

4) Realize the direct activation of ketones: Considering the substrates for chiral-at-metal Lewis acid catalysis is often limited to the imidazole or pyridine achiral templates, the development of new strategy for chiral-at-metal complexes that allow direct activation of ketones and aldehydes is highly attractive. Except using the well established chiral Ir-based or Rh-based Lewis acid catalysts or their derivatives to look for amenable ketone substrates *via* high throughput screening; exploiting Ru-based chiral-at-metal Lewis acid or metal-templated Brønsted acid catalysts would provide new chances for this unmet activation.

5) Exploit new photoreactions for unmet synthetic applications: Some long-standing challenge transformations for photoredox catalysis are needed to be addressed, Such as the asymmetric conjugate addition of unstabilized primary carbon radicals to alkenes, the enantioselective radical conjugate addition toward the construction of chiral all-carbon quaternary center; enantioselective β - and γ -alkylation of carbonyl compounds based on the enolate/enamine technologies; asymmetric photocatalytic C-H activation based on HAT; photocatalytic multiple metal catalysis; asymmetric photoredox catalysis mediated by the electron shuttles (cocatalysts).

References

- 1 H. Huo, C. Fu, C. Wang, K. Harms, E. Meggers, *Chem. Commun.* **2014**, 50, 10409–10411.
- 2 L. Gong, M. Wenzel, E. Meggers, *Acc. Chem. Res.* **2013**, 46, 2635–2644.
- 3 H. Huo, C. Fu, K. Harms, E. Meggers, *J. Am. Chem. Soc.* **2014**, 136, 2990–2993.
- 4 H. Huo, X. Shen, C. Wang, L. Zhang, P. Röse, L.-A. Chen, K. Harms, M. Marsch, G. Hilt, E. Meggers, *Nature* **2014**, 515, 100–103.
- 5 H. Huo, C. Wang, K. Harms, E. Meggers, *J. Am. Chem. Soc.* **2015**, 137, 9551–9554.
- 6 H. Huo, X. Huang, X. Shen, K. Harms, E. Meggers, *Synlett* **2016**, 27, 749–753.
- 7 H. Huo, K. Harms, E. Meggers, *J. Am. Chem. Soc.* **2016**, 138, 6936–6939.
- 8 (a) M. P. Sibi, J. Ji, *J. Org. Chem.* **1997**, 62, 3800–3801. (b) M. P. Sibi, J. Ji, J. H. Wu, S. Gürtler, N. A. Porter, *J. Am. Chem. Soc.* **1996**, 118, 9200–9201. (c) L. R. Espelt, I. S. McPherson, E. M. Wiensch, T. P. Yoon, *J. Am. Chem. Soc.* **2015**, 137, 2452–2455.

Chapter 5: Experimental Part

5.1 Materials and Methods

All reactions were carried out under an atmosphere of nitrogen or argon with magnetic stirring. The catalysis reactions were performed in a Schlenk tube.

Solvents and Reagents

Solvents were distilled under nitrogen from calcium hydride (CH_3CN , CHCl_3 , CH_2Cl_2 and DMF), magnesium turnings/iodine (MeOH) or sodium/benzophenone (Et_2O , THF). HPLC grade solvents, such as chlorobenzene, 1,2-dichloroethane, ethanol, acetone and toluene were used directly without further drying. All reagents were purchased from Acros, Aldrich, Alfa, TCI, ChemPur, Strem and Fluorochem and used without further purification.

Chromatographic Methods

The course of the reactions and the column chromatographic elutions were traced by thin layer chromatography [Macherey-Nagel (ALUGRAM®Xtra Sil G/UV254) or Merck (aluminum silica gel 60 F254)] with fluorescent indicator UV254 or color developing agent (cerium sulfate / ammonium molybdate solution). For column chromatography silica gel, Merck (particle size 0.040-0.063 mm) was used. The elution was performed at room temperature using a compressed air overpressure. The corresponding mobile phase was specified in the followed procedure. If substance showed poor solubility in eluent solvent, the crude product was firstly absorbed by proper amount of silica gel, and then the adsorbed gel was subjected to the silica gel chromatographic column.

Nuclear Magnetic Resonance Spectroscopy (NMR)

^1H -NMR, proton decoupled ^{13}C -NMR, and proton coupled ^{19}F -NMR spectra were measured on the below spectrometers at ambient temperature.

Bruker Advance 300 MHz (^1H -NMR: 300 MHz, ^{13}C -NMR: 75 MHz, ^{19}F NMR: 282 MHz)

Bruker DRX 400 MHz (^1H -NMR: 400 MHz, ^{13}C -NMR: 100 MHz)

Bruker AM 500 MHz (^1H -NMR: 500 MHz, ^{13}C -NMR: 125 MHz)

Chemical shifts are given in ppm on the δ scale, and were determined after calibration to the residual

signals of the solvents, which were used as an internal standard. NMR standards used are as follows: ^1H -NMR spectroscopy: $\delta = 7.26$ ppm (CDCl_3), $\delta = 5.32$ ppm (CD_2Cl_2), $\delta = 1.94$ ppm (CD_3CN), $\delta = 2.05$ ppm (CD_3COCD_3), $\delta = 2.50$ ppm (CD_3SOCD_3), $\delta = 3.31$ ppm (CD_3OD); ^{13}C -NMR spectroscopy: $\delta = 77.0$ ppm (CDCl_3), $\delta = 53.8$ ppm (CD_2Cl_2), $\delta = 118.26, 1.32$ ppm (CD_3CN), $\delta = 206.26, 29.84$ ppm (CD_3COCD_3), $\delta = 39.52$ ppm (CD_3SOCD_3), $\delta = 49.0$ ppm (CD_3OD). ^{19}F NMR spectroscopy: $\delta = 0$ ppm (CFCl_3). The characteristic signals were specified from the low field to high field with the chemical shifts (δ in ppm). ^1H -NMR spectra peak multiplicities indicated as singlet (s), doublet (d), doublet of doublet (dd), doublet of doublet of doublet (ddd), triplet (t), doublet of triplet (dt), quartet (q), multiplet (m). The coupling constant J indicated in hertz (Hz). And ^1H -NMR spectra and ^{19}F -NMR peak also show the number of protons.

High-Performance Liquid Chromatography (HPLC)

Chiral HPLC was performed with an Agilent 1200 Series or Agilent 1260 Series HPLC System. All the HPLC conditions were detailed in the individual procedures.

Infrared Spectroscopy (IR)

IR measurements were recorded on a Bruker Alpha-P FT-IR spectrometer. The absorption bands were indicated a wave numbers ν (cm^{-1}). All substances were measured as films or solids.

Circular Dichroism Spectroscopy (CD)

CD spectra were recorded on a JASCO J-810 CD spectropolarimeter. The parameters we used as follows: from 600 nm to 200 nm; data pitch (0.5 nm); band width (1 nm); response (1 second); sensitivity (standard); scanning speed (50 nm/min); accumulation (5 times). The concentration of the compounds for the measurements was 0.2 mM. The formula for converting θ to ϵ is shown as below.

$$\Delta\epsilon = \frac{\theta[m\text{deg}]}{32980 \times c(\text{mol}/L) \times L(\text{cm})}$$

C = concentration of the sample; L = thickness of the measurement vessel

Crystal Structure Analysis

Crystal X-ray measurements and the crystal structure analysis were carried out by Dr. Klaus Harms (Chemistry Department, Philipps University of Marburg) on the devices IPDS-II (Mo-K α -irradiation, bis $2\theta = 77^\circ$, Oxford Cryosystem) or IPDS-IIT (Mo-K α -irradiation, bis $2\theta = 135^\circ$, Oxford Cryosystem). The solution and refinement of the structures were carried with the corresponding programs. Details of crystal structures can be found in the Appendix.

UV/Vis Analysis Spectroscopy

UV/Vis measurements were taken on a Spectra Max M5 microplate reader in a 10.0 mm quartz cuvette.

Optical Rotation Polarimeter

Optical rotations were measured on a Krüss P8000-T or Perkin-Elmer 241 polarimeter with $[\alpha]_D^{22}$ values reported in degrees with concentrations reported in g/100 mL.

5.2 Enantioselective α -Amination of Aldehydes with a Chiral-at-Metal

Iridium(III) Complex

5.2.1 Synthesis of the Iridium Catalysts Δ -Ir1-5 and Δ -Ir4

1) Synthesis of benzoxazole ligands

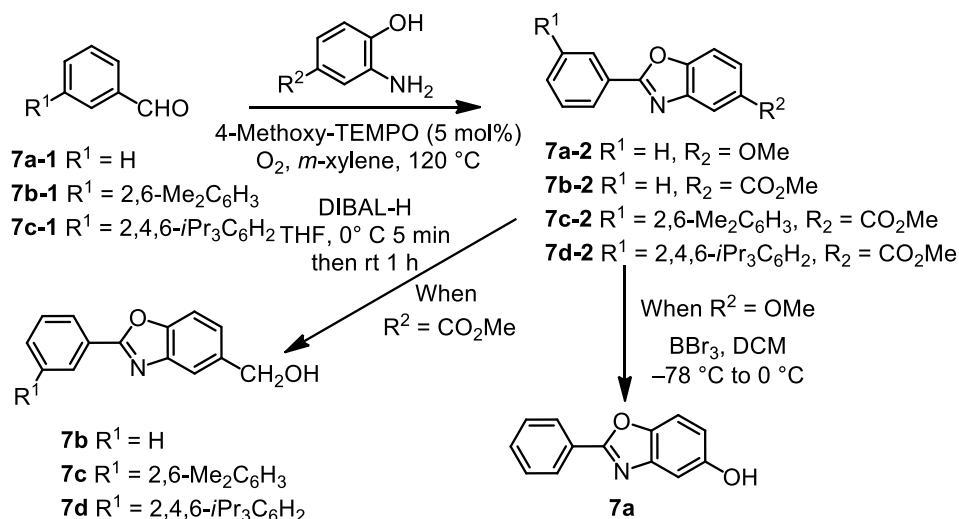


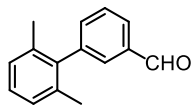
Figure 108 Synthesis of the benzoxazole ligands. Benzoxazole **7b-2**, **7b-1** and **7a-2** were synthesized according to published procedures.

General procedure for synthesis of methyl 2-phenylbenzo[d]oxazole-5-carboxylates (condensation/oxidation procedure):³ A solution of 2-aminophenol (5.0 mmol) and benzaldehyde or substituted benzaldehyde (5.0 mmol) in *m*-xylene (25 mL) was stirred at 120 °C for 0.5 h. Then 4-methoxy-TEMPO (5 mol% in 0.5 mL *m*-xylene) was added to the mixture which was stirred at 120 °C for additional 5 h under an oxygen atmosphere. The reaction mixture was cooled and concentrated under reduced pressure. The residue was purified by flash chromatography on silica gel (eluent: EtOAc/ hexane = 1:20).

General procedure for synthesis of 5-hydroxymethyl-2-phenylbenzo[d]oxazoles (reduction procedure):¹ To a solution of methyl 2-phenylbenzo[d]oxazole-5-carboxylate (4.0 mmol) in THF (20 mL) at 0 °C was added a solution of DIBAL-H (1.0 M in hexane, 10.0 mL, 10.0 mmol) dropwise. After being stirred at 0 °C for 5 min, the reaction was quenched with a saturated aqueous solution of sodium tartrate and stirred vigorously for 1 h at room temperature. The reaction mixture was extracted with EtOAc (4 × 20 mL). The combined organic layers were dried over anhydrous Na₂SO₄, filtered,

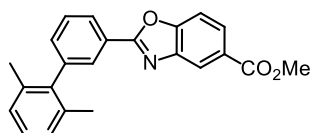
and concentrated under reduced pressure. The residue was purified by flash chromatography on silica gel (eluent: MeOH/CH₂Cl₂ = 1:50).

2',6'-Dimethylbiphenyl-3-carbaldehyde (**7b-1**)



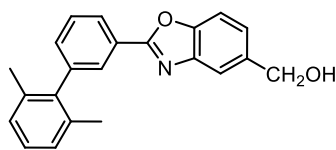
3-Bromobenzaldehyde (2.775 g, 15 mmol) and (2,6-dimethylphenyl)boronic acid (3.150 g, 21 mmol) were dissolved in a mixture of 1 M aqueous sodium carbonate solution (30 mL), toluene (30 mL), and EtOH (15 mL). After degassing with argon for 30 min, Pd(PPh₃)₄ (0.0867 g, 0.75 mmol) was added. The reaction mixture was stirred under argon atmosphere at 80 °C for 20 h. The reaction mixture was cooled to room temperature and water was added to the reaction mixture. The mixture was diluted with EtOAc and the insoluble material was filtered through celite. The combined organic layers were dried over anhydrous Na₂SO₄, filtered, and concentrated under reduced pressure. The residue was purified by flash chromatography on silica gel (eluent: EtOAc/hexane = 1:20) to give compound **7b-1** (2.961 g, yield: 94%) as a colorless oil. ¹H NMR (300 MHz, CDCl₃) δ 10.09 (s, 1H), 7.97–7.88 (m, 1H), 7.76–7.70 (m, 1H), 7.65 (t, *J* = 7.6 Hz, 1H), 7.52–7.43 (m, 1H), 7.31–7.08 (m, 3H), 2.06 (s, 6H). All spectroscopic data were in agreement with the literature.⁴

Methyl 2-(2',6'-dimethylbiphenyl-3-yl)benzo[d]oxazole-5-carboxylate (**7c-2**)



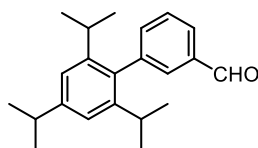
According to the general condensation/oxidation procedure, **7c-2** (1.767 g, yield: 99%) was obtained as a white solid.

¹H NMR (300 MHz, CDCl₃) δ 8.48 (dd, *J* = 1.2, 0.5 Hz, 1H), 8.28 (dt, *J* = 7.8, 1.4 Hz, 1H), 8.19–8.08 (m, 2H), 7.68–7.54 (m, 2H), 7.40 (dt, *J* = 7.6, 1.4 Hz, 1H), 7.27–7.12 (m, 3H), 3.98 (s, 3H), 2.10 (s, 6H). ¹³C NMR (75 MHz, CDCl₃) δ 166.6, 164.3, 153.6, 142.2, 142.1, 140.5, 135.8, 132.8, 129.2, 128.4, 127.5, 127.4, 127.1, 126.9, 126.2, 122.0, 110.3, 52.2, 20.8. IR (film) ν_{max}: 3064, 2952, 2917, 1716, 1618, 1545, 1461, 1431, 1284, 1213, 1188, 1082, 978, 918, 901, 834, 811, 772, 742, 704 cm⁻¹. HRMS (ESI, *m/z*) calcd for C₂₃H₂₀NO₃ [M+H]⁺: 358.1438, found: 358.1438.

(2-(2',6'-Dimethylbiphenyl-3-yl)benzo[d]oxazol-5-yl)methanol (7c)

According to the general reduction procedure, **7c** (1.223 g, yield: 93%) was obtained as a white solid.

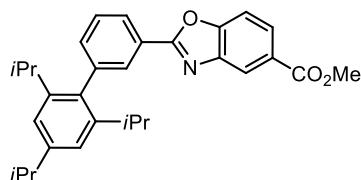
^1H NMR (300 MHz, CDCl_3) δ 8.24 (dt, $J = 7.8, 1.4$ Hz, 1H), 8.07 (t, $J = 1.5$ Hz, 1H), 7.74 (d, $J = 0.6$ Hz, 1H), 7.60 (t, $J = 7.7$ Hz, 1H), 7.51 (d, $J = 8.3$ Hz, 1H), 7.39–7.31 (m, 2H), 7.24–7.08 (m, 3H), 4.80 (s, 2H), 2.53 (br s, 1H), 2.08 (s, 6H). ^{13}C NMR (75 MHz, CDCl_3) δ 163.5, 150.2, 142.1, 142.0, 140.6, 137.9, 135.9, 132.4, 129.2, 128.3, 127.42, 127.39, 127.3, 126.0, 124.4, 118.4, 110.4, 77.4, 77.0, 76.6, 65.2, 20.8. IR (film) ν_{max} : 3422, 3063, 3024, 2931, 2862, 1543, 1456, 1438, 1375, 1324, 1263, 1189, 1051, 979, 905, 801, 761, 726, 702 cm^{-1} . HRMS (ESI, m/z) calcd for $\text{C}_{22}\text{H}_{20}\text{NO}_2$ $[\text{M}+\text{H}]^+$: 330.1489, found: 330.1490.

2',4',6'-Triisopropylbiphenyl-3-carbaldehyde (7c-1)

Synthesized according to a reported method with some modifications.⁵ Accordingly, 2,4,6-triisopropylphenylboronic acid (1.488 g, 6.0 mmol), 3-bromobenzaldehyde (0.0736 g, 4.0 mmol), anhydrous K_3PO_4 (2.544 g, 12.0 mmol) and dicyclohexyl(2',6'-dimethoxybiphenyl-2-yl) phosphine (Sphos, 0.0164 g, 0.4 mmol) were mixed in toluene (40.0 mL). After degassing with argon for 30 min, $\text{Pd}(\text{OAc})_2$ (0.0450 g, 0.2 mmol) was added. The reaction mixture was stirred under argon atmosphere at 110 $^\circ\text{C}$ for 24 h. The reaction mixture was cooled to room temperature, diluted with EtOAc, and the insoluble material was filtered through Celite. The combined organic layers were concentrated under reduced pressure. The residue was purified by flash chromatography on silica gel (eluent: EtOAc/hexane = 1:30) to give compound **7c-1** (1.158 g, yield: 94%) as a white solid. ^1H NMR (300 MHz, CDCl_3) δ 10.05 (s, 1H), 7.89 (dt, $J = 7.6, 1.3$ Hz, 1H), 7.71 (s, 1H), 7.58 (t, $J = 7.6$ Hz, 1H), 7.48 (dt, $J = 7.5, 1.3$ Hz, 1H), 7.08 (s, 2H), 2.96 (hept, $J = 6.9$ Hz, 1H), 2.52 (hept, $J = 6.9$ Hz, 2H), 1.33 (s, 3H), 1.31 (s, 3H), 1.10 (s, 3H), 1.09 (s, 3H), 1.08 (s, 3H), 1.07 (s, 3H). ^{13}C NMR (75 MHz, CDCl_3) δ 192.4, 148.6, 146.4, 142.0, 136.3, 135.9, 135.5, 131.3, 128.7, 127.7, 120.7, 34.3, 30.4, 24.09,

24.05, 24.0. IR (film) ν_{\max} : 2959, 2926, 2868, 1690, 1604, 1572, 1459, 1372, 1282, 1250, 1164, 878, 802, 729, 705, 652 cm^{-1} . HRMS (ESI, m/z) calcd for $\text{C}_{22}\text{H}_{28}\text{ONa}$ $[\text{M}+\text{Na}]^+$: 331.2032, found: 331.2033.

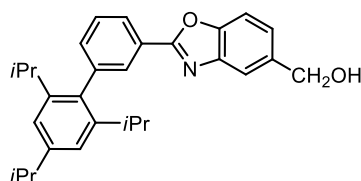
Methyl 2-(2',4',6'-triisopropylbiphenyl-3-yl)benzo[d]oxazole-5-carboxylate (7d-2)



According to the general condensation/oxidation procedure, **7d-2** (2.048 g, yield: 90%) was obtained as a white solid.

^1H NMR (300 MHz, CDCl_3) δ 8.56–8.42 (m, 1H), 8.37–8.22 (m, 1H), 8.14 (t, $J = 1.5$ Hz, 1H), 8.11 (dd, $J = 8.6, 1.7$ Hz, 1H), 7.64–7.55 (m, 2H), 7.49–7.38 (m, 1H), 7.11 (s, 2H), 3.97 (s, 3H), 2.98 (hept, $J = 6.9$ Hz, 1H), 2.64 (hept, $J = 6.8$ Hz, 2H), 1.34 (d, $J = 6.9$ Hz, 6H), 1.14 (d, $J = 6.5$ Hz, 6H), 1.11 (d, $J = 6.5$ Hz, 6H). ^{13}C NMR (75 MHz, CDCl_3) δ 166.7, 164.4, 153.7, 148.5, 146.4, 142.3, 141.9, 135.8, 133.4, 129.1, 128.7, 127.0, 126.5, 126.1, 122.0, 120.7, 110.3, 77.4, 77.0, 76.6, 52.2, 34.3, 30.4, 24.2, 24.13, 24.07. IR (film) ν_{\max} : 2958, 2869, 1722, 1624, 1557, 1460, 1437, 1358, 1294, 1209, 1125, 1085, 1054, 841, 810, 756, 702 cm^{-1} . HRMS (ESI, m/z) calcd for $\text{C}_{30}\text{H}_{34}\text{NO}_3$ $[\text{M}+\text{H}]^+$: 456.2533, found: 456.2529.

(2-(2',4',6'-Triisopropylbiphenyl-3-yl)benzo[d]oxazol-5-yl)methanol (7d)



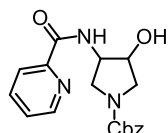
According to the general reduction procedure, **7d** (1.674 g, yield: 98%) was obtained as a white solid.

^1H NMR (300 MHz, CDCl_3) δ 8.26 (dt, $J = 7.8, 1.4$ Hz, 1H), 8.11 (t, $J = 1.5$ Hz, 1H), 7.75 (d, $J = 0.9$ Hz, 1H), 7.57 (t, $J = 7.7$ Hz, 1H), 7.49 (d, $J = 8.3$ Hz, 1H), 7.40 (dt, $J = 7.6, 1.3$ Hz, 1H), 7.34 (dd, $J = 8.4, 1.6$ Hz, 1H), 7.11 (s, 2H), 4.80 (s, 2H), 2.98 (hept, $J = 6.9$ Hz, 1H), 2.64 (hept, $J = 6.8$ Hz, 2H), 2.52 (br s, 1H), 1.34 (d, $J = 6.9$ Hz, 6H), 1.14 (d, $J = 6.6$ Hz, 6H), 1.11 (d, $J = 6.6$ Hz, 6H). ^{13}C NMR (75 MHz, CDCl_3) δ 163.6, 150.2, 148.4, 146.4, 142.2, 141.8, 137.9, 135.9, 133.1, 128.9, 128.6, 126.8,

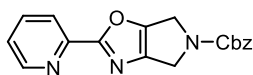
125.9, 124.4, 120.6, 118.4, 110.4, 65.2, 34.3, 30.4, 24.2, 24.13, 24.08. IR (film) ν_{\max} : 3277, 2958, 2929, 2869, 1609, 1554, 1460, 1433, 1257, 1190, 1051, 1022, 877, 810, 781, 704 cm^{-1} . HRMS (ESI, m/z) calcd for $\text{C}_{29}\text{H}_{34}\text{NO}_2$ $[\text{M}+\text{H}]^+$: 428.2584, found: 428.2583.

2) Synthesis of the secondary amine ligand

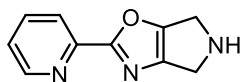
Benzyl 3-hydroxy-4-(picolinamido)pyrrolidine-1-carboxylate (**3**)



To a solution of picolinic acid (4.0 g, 32.8 mmol) in THF (120 mL) at 0 °C was added successively Et_3N (9.1 mL, 65.6 mmol) and ethyl chloroformate (3.1 mL, 32.8 mmol). After being stirred at 0 °C for 1 h, a solution of **2**⁶ (7.1 g, 30.0 mmol) in THF (30 mL) was added. After being stirred at room temperature for overnight, the reaction was quenched with a saturated aqueous solution of NH_4Cl and extracted with CH_2Cl_2 (4 \times 50 mL). The combined organic layers were dried over anhydrous Na_2SO_4 , filtered, and concentrated under reduced pressure. The residue was purified by flash chromatography on silica gel (eluent: $\text{MeOH}/\text{CH}_2\text{Cl}_2 = 1:50$) to give compound **3** (9.5 g, yield: 93%) as a white solid. ^1H NMR (300 MHz, CDCl_3) δ 8.50 (d, $J = 4.5$ Hz, 1H), 8.21 (t, $J = 6.0$ Hz, 1H), 8.11 (d, $J = 7.8$ Hz, 1H), 7.81 (td, $J = 7.7, 1.7$ Hz, 1H), 7.45–7.27 (m, 5H), 5.15 (s, 2H), 4.80 (br, 1H), 4.60–4.45 (m, 1H), 4.40 (s, 1H), 4.11–3.91 (m, 1H), 3.76 (td, $J = 11.4, 5.2$ Hz, 1H), 3.53 (ddd, $J = 15.3, 11.8, 3.2$ Hz, 2H). ^{13}C NMR (75 MHz, CDCl_3) δ 165.1, 164.9, 154.9, 148.8, 148.1, 137.5, 136.5, 128.4, 127.9, 127.82, 127.79, 126.6, 122.2, 74.5, 73.6, 67.0, 56.4, 56.0, 51.7, 51.4, 49.1. IR (film) ν_{\max} : 3346, 3056, 2952, 2884, 1672, 1516, 1426, 1349, 1192, 1108, 738, 695, 595 cm^{-1} . HRMS (ESI, m/z) calcd for $\text{C}_{18}\text{H}_{20}\text{N}_3\text{O}_4$ $[\text{M}+\text{H}]^+$: 342.1448, found: 342.1446.

Benzyl 2-(pyridin-2-yl)-4*H*-pyrrolo[3,4-*d*]oxazole-5(6*H*)-carboxylate (5)

To a solution of **3** (2.0 g, 5.9 mmol) in CH₂Cl₂ (59 mL) at 0 °C was added Dess-Martin reagent (6.1 g, 14.4 mmol). After being stirred at room temperature for overnight, the reaction mixture was diluted with CH₂Cl₂ and washed with NaOH (0.5 M, 3 × 10 mL). The combined organic layers were dried over anhydrous Na₂SO₄, filtered, and concentrated under reduced pressure. The crude product of **4** was used for next step without further purification. The crude **4** (5.9 mmol estimated on the theoretical yield) was dissolved in CHCl₃ (59 mL). PCl₅ (3.7 g, 17.7 mmol) was added at 50 °C and stirring was continued for an additional 3 h. The reaction was quenched with a saturated aqueous solution of Na₂CO₃ and extracted with CH₂Cl₂ (4 × 20 mL). The combined organic layers were dried over anhydrous Na₂SO₄, filtered, and concentrated under reduced pressure. The residue was passed through a short column of silica gel (eluent: MeOH/CH₂Cl₂ = 1:50) to afford the crude product as a black solid. The crude product was washed with MeOH (3 × 3 mL) and centrifuged to afford the **5** (663 mg, 35% in two steps) as a white solid. ¹H NMR (300 MHz, CDCl₃) δ 8.70–8.54 (m, 1H), 8.09–7.92 (m, 1H), 7.72 (tt, *J* = 7.9, 1.5 Hz, 1H), 7.40–7.22 (m, 6H), 5.13 (d, *J* = 0.8 Hz, 2H), 4.63–4.50 (m, 2H), 4.50–4.36 (m, 2H). ¹³C NMR (75 MHz, CDCl₃) δ 164.5, 154.7, 154.6, 149.9, 149.8, 149.4, 149.3, 145.7, 140.3, 140.2, 137.0, 136.9, 136.24, 136.21, 128.4, 128.1, 128.07, 128.02, 127.9, 124.7, 121.7, 121.6, 67.22, 67.20, 45.5, 45.4, 44.9, 44.7. IR (film) ν_{max}: 3053, 2938, 2882, 1696, 1413, 1362, 1295, 1095, 942, 797, 745, 695, 614 cm⁻¹. HRMS (ESI, *m/z*) calcd for C₁₈H₁₆N₃O₃ [M+H]⁺: 322.1186, found: 188.0814.

2-(Pyridin-2-yl)-5,6-dihydro-4H-pyrrolo[3,4-*d*]oxazole (1)

To a solution of **5** (96.3 mg, 0.3 mmol) in CH₃CN/CH₂Cl₂ (3 mL/1 mL) at 0 °C was added TMSI (0.12 mL, 0.9 mmol). After being stirred at room temperature for 1 h, the reaction was quenched with dry MeOH (0.5 mL). The solvent was removed under reduced pressure. The residue was purified by flash chromatography on silica gel (eluent: MeOH/CH₂Cl₂ = 1:10) to give compound **1** (53.0 mg, yield: 95%) as a white solid. ¹H NMR (300 MHz, MeOD) δ 8.68 (d, *J* = 4.6 Hz, 1H), 8.11 (d, *J* = 7.9 Hz, 1H), 8.03 (td, *J* = 7.8, 1.6 Hz, 1H), 7.70–7.47 (m, 1H), 4.33–4.20 (m, 2H), 4.19–4.02 (m, 2H). ¹³C NMR (75 MHz, MeOD) δ 167.0, 154.7, 151.0, 146.3, 145.0, 139.4, 126.8, 123.0, 44.4, 43.8. IR (film) ν_{max}: 3036, 2934, 2882, 1423, 1363, 1296, 1209, 1153, 1095, 956, 738, 696 cm⁻¹. HRMS (ESI, *m/z*) calcd for C₁₀H₁₀N₃O [M+H]⁺: 188.0818, found: 188.0816.

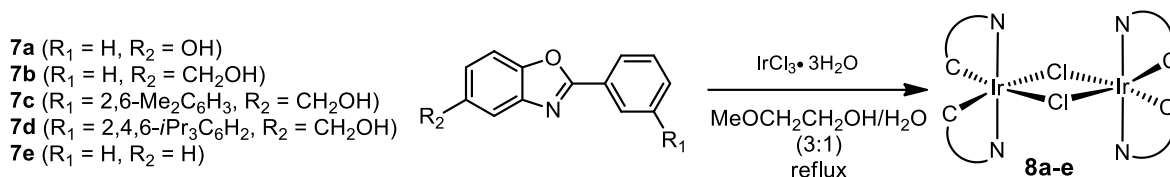
3) Synthesis of iridium complexes

Our developed synthetic strategy⁷ for the generation of enantiomerically pure iridium(III) complexes relies on the use of (*S*)-4-isopropyl-2-(2'-hydroxyphenyl)-2-thiazoline⁸ as a chiral auxiliary. As described in detail below, racemic iridium(III) precursor complexes were converted to diastereomeric phenolato complexes, then resolved into single diastereomers by flash silica gel column chromatography, and followed by an acid-induced substitution of the auxiliary under complete retention of configuration to afford the enantiomerically pure iridium complexes.

3.1) Synthesis of iridium precursor complexes

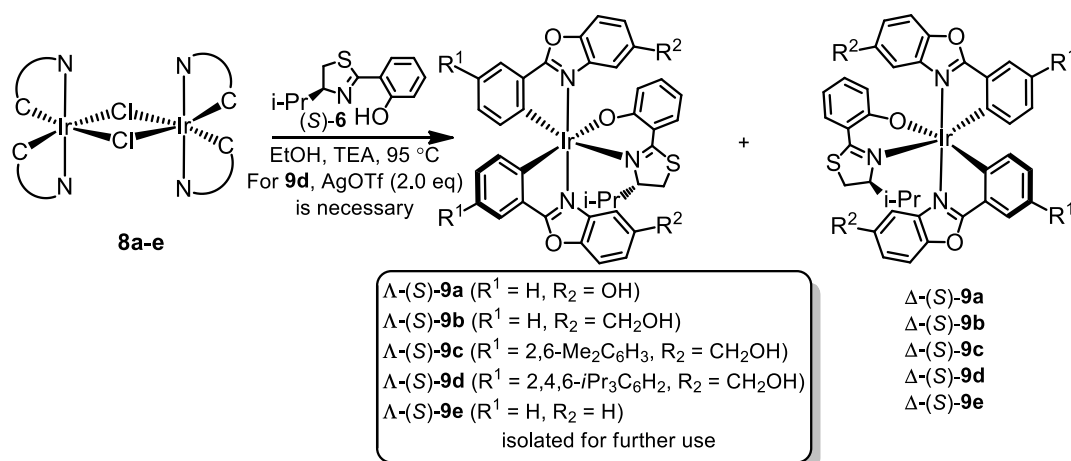
Cyclometalated iridium(III) μ -chloro-bridged dimers of the general formula [(C[^]N)₂Ir(μ -Cl)Ir(C[^]N)₂] (C[^]N = (2-phenylbenzo[*d*]oxazol-5-yl)methanol and its derivatives were synthesized according to a method reported by Nonoyama,⁹ which involves refluxing IrCl₃•*n*H₂O with 2.0–2.5 equiv of cyclometalating ligand in a 3:1 mixture of 2-methoxyethanol and water. Accordingly, (2-phenylbenzo[*d*]oxazol-5-yl)methanol or its derivatives (2.0 mmol) were added to iridium chloride (1.0 mmol) in a mixture of methoxyethanol/water (3:1, 44 mL). The reaction mixture was heated at reflux (120 °C) with constant stirring for 24 h. The resulting precipitate was collected by centrifugation, washed with diethyl ether and dried to yield the product as a yellow powder (60-89%),

which was used without further purification.



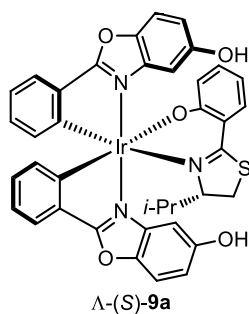
Scheme 23 Synthesis of cyclometalated Ir(III) μ -chloro-bridged dimers **8a-e**.

Preparation of iridium auxiliary complexes



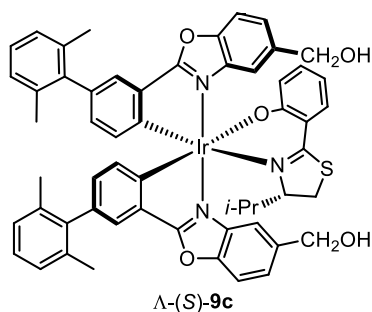
Scheme 24 Preparation of iridium precursor complexes $\Lambda\text{-(S)-9a-e}$. The complexes $\Lambda\text{-(S)-9b}$ and $\Lambda\text{-(S)-9e}$ were synthesized according to published procedures.¹

Preparation of iridium auxiliary complex $\Lambda\text{-(S)-9a}$. A mixture of iridium(III) dimer complex **8a** (259.0 mg, 0.20 mmol), (S)-4-isopropyl-2-(2'-hydroxyphenyl)-2-thiazoline (**S-6**) (110.5 mg, 0.50 mmol), and triethylamine (0.28 mL, 2.0 mmol) in ethanol (20 mL) was purged with argon for 5 min and then heated at reflux overnight. The reaction mixture was cooled to room temperature and concentrated to dryness. The residue was subjected to a flash silica gel chromatography (eluent: EtOAc/CH₂Cl₂ = 1:10) to separate the two diastereomers. Only the first eluting diastereomer (yellow solid, 127.0 mg, 38%) was characterized and used for the synthesis of enantiopure iridium catalyst, which was assigned as Λ -configuration by CD spectroscopy in analogy to reported complexes.¹



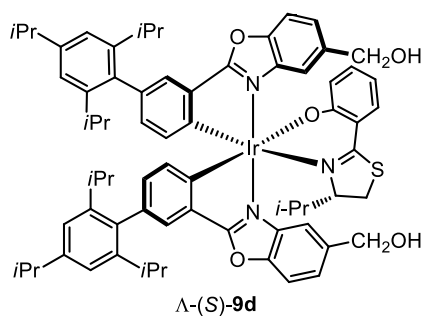
^1H NMR (500 MHz, DMSO) δ 9.86 (s, 1H), 9.78 (s, 1H), 7.76 (d, J = 9.0 Hz, 1H), 7.69 (d, J = 9.0 Hz, 1H), 7.66 (d, J = 6.9 Hz, 1H), 7.56 (d, J = 6.7 Hz, 1H), 7.33 (dd, J = 8.2, 1.7 Hz, 1H), 7.10 (d, J = 2.5 Hz, 1H), 7.07 (ddd, J = 8.6, 6.8, 1.7 Hz, 1H), 6.97 (dd, J = 3.4, 2.6 Hz, 1H), 6.96 (dd, J = 3.4, 2.6 Hz, 1H), 6.90 (t, J = 7.4 Hz, 2H), 6.79 (dtd, J = 8.7, 7.5, 1.3 Hz, 2H), 6.71 (d, J = 2.3 Hz, 1H), 6.52 (d, J = 7.6 Hz, 2H), 6.29–6.21 (m, 1H), 6.18 (d, J = 7.6 Hz, 1H), 4.57 (d, J = 9.8 Hz, 1H), 3.47 (dd, J = 11.8, 10.1 Hz, 1H), 3.17 (d, J = 5.2 Hz, 1H), 0.83–0.70 (m, 1H), 0.21 (d, J = 2.4 Hz, 3H), 0.19 (d, J = 2.4 Hz, 3H). ^{13}C NMR (125 MHz, DMSO) δ 177.7, 177.1, 167.4, 166.9, 156.2, 155.9, 150.6, 148.9, 143.4, 143.0, 138.9, 138.7, 134.3, 133.02, 132.98, 131.6, 131.3, 131.0, 130.6, 130.2, 125.5, 125.0, 123.6, 121.5, 120.6, 117.7, 113.8, 113.7, 112.8, 112.3, 112.0, 102.8, 101.0, 84.1, 31.0, 26.8, 18.6, 13.9. IR (film) ν_{max} : 2958, 2925, 2867, 1592, 1561, 1530, 1440, 1388, 1355, 1299, 1160, 1028, 1003, 944, 816, 741 cm^{-1} . HRMS (ESI, m/z) calcd for $\text{C}_{38}\text{H}_{30}\text{IrN}_3\text{O}_5\text{SNa}$ $[\text{M}+\text{Na}]^+$: 856.1428, found: 856.1422. CD (MeOH): λ , nm ($\Delta\epsilon$, $\text{M}^{-1}\text{cm}^{-1}$) 356 (+40), 289 (−28), 221 (−47).

Preparation of iridium auxiliary complex Λ -(S)-9c A mixture of iridium(III) dimer complex **8c** (265.0 mg, 0.15 mmol), (*S*)-4-isopropyl-2-(2'-hydroxyphenyl)-2-thiazoline (*S*)-**6** (83.0 mg, 0.38 mmol), and triethylamine (0.21 mL, 1.5 mmol) in ethanol (15 mL) was purged with argon for 5 min and then heated at reflux overnight. The reaction mixture was cooled to room temperature and concentrated to dryness. The residue was subjected to a flash silica gel chromatography (eluent: EtOAc/ CH_2Cl_2 = 1:10) to separate the two diastereomers. Only the first eluting diastereomer (orange solid, 120.0 mg, 37%) was characterized and used for the synthesis of enantiopure iridium catalyst, which was assigned as Λ -configuration by CD spectroscopy in analogy to reported complexes.¹

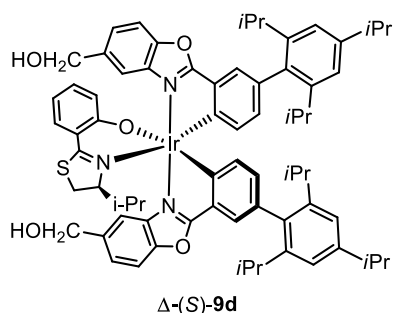


^1H NMR (300 MHz, CDCl_3) δ 7.68 (s, 1H), 7.57 (d, J = 8.5 Hz, 1H), 7.52–7.39 (m, 5H), 7.25–6.98 (m, 8H), 6.90 (d, J = 8.2 Hz, 1H), 6.68–6.56 (m, 2H), 6.53 (dd, J = 7.8, 1.7 Hz, 1H), 6.41 (d, J = 7.8 Hz, 1H), 6.35 (t, J = 7.1 Hz, 1H), 4.96 (d, J = 9.7 Hz, 1H), 4.68–4.40 (m, 4H), 3.57–3.43 (m, 1H), 3.37 (t, J = 5.6 Hz, 1H), 2.79 (d, J = 11.3 Hz, 1H), 2.53 (t, J = 6.1 Hz, 1H), 2.09 (s, 3H), 1.99 (s, 3H), 1.75 (s, 3H), 1.72 (s, 3H), 0.26 (d, J = 6.4 Hz, 3H), 0.24 (d, J = 6.4 Hz, 3H). ^{13}C NMR (75 MHz, CDCl_3) δ 178.5, 178.3, 167.67, 166.73, 149.4, 149.2, 147.9, 147.2, 141.5, 141.4, 139.8, 139.7, 138.8, 138.3, 136.6, 136.4, 136.2, 135.8, 134.1, 133.6, 133.3, 133.2, 133.1, 132.6, 132.5, 131.6, 130.9, 130.2, 127.2, 127.1, 127.03, 126.98, 126.8, 126.7, 126.0, 125.9, 124.1, 124.0, 123.5, 118.7, 116.0, 113.6, 113.4, 111.3, 111.0, 86.0, 64.7, 64.4, 31.0, 27.4, 21.0, 20.9, 20.2, 20.1, 18.7, 14.0. IR (film) ν_{max} : 2958, 2924, 2869, 1598, 1560, 1524, 1463, 1436, 1364, 1253, 1191, 1148, 1031, 1014, 941, 836, 766, 742 cm^{-1} . HRMS (ESI, m/z) calcd for $\text{C}_{56}\text{H}_{51}\text{IrN}_3\text{O}_5\text{S}$ $[\text{M}+\text{H}]^+$: 1070.3176, found: 1070.3189. CD (MeOH): λ , nm ($\Delta\epsilon$, $\text{M}^{-1}\text{cm}^{-1}$) 366 (+26), 328 (+30), 306 (–28), 298 (–28), 230 (–26).

Preparation of iridium auxiliary complex Λ -(S)-9d and Δ -(S)-9d: A mixture of iridium(III) dimer complex **8d** (324.0 mg, 0.15 mmol), (*S*)-4-isopropyl-2-(2'-hydroxyphenyl)-2-thiazoline (*S*)-**6** (83.0 mg, 0.38 mmol), silver triflate (77.1 mg, 0.30 mmol), and triethylamine (0.21 mL, 1.5 mmol) in ethanol (15 mL) was purged with argon for 5 min and then heated at reflux overnight. The reaction mixture was cooled to room temperature and concentrated to dryness. The residue was subjected to a flash silica gel chromatography (eluent: $\text{EtOAc}/\text{CH}_2\text{Cl}_2$ = 1:30) to separate the two diastereomers. Two eluting diastereomers was characterized and can be used for the synthesis of enantiopure iridium catalyst. The first eluting diastereomer (orange solid, 140.0 mg, 37%) was assigned as Λ -configuration by CD spectroscopy in analogy to reported complexes.¹ The second eluting diastereomer (orange solid, 140.0 mg, 37%) was assigned accordingly as Δ -configuration.



^1H NMR (300 MHz, CDCl_3) δ 7.53 (s, 1H), 7.42–7.28 (m, 4H), 7.28–7.17 (m, 3H), 7.05 (dd, J = 8.6, 1.4 Hz, 1H), 6.97 (ddd, J = 8.6, 6.8, 1.7 Hz, 1H), 6.85–6.73 (m, 4H), 6.63 (d, J = 8.5 Hz, 1H), 6.49–6.35 (m, 3H), 6.21 (d, J = 7.8 Hz, 1H), 6.17–6.05 (m, 1H), 4.74 (d, J = 10.3 Hz, 1H), 4.61 (s, 2H), 4.40 (s, 2H), 3.39 (t, J = 10.8 Hz, 1H), 2.86–2.61 (m, 3H), 2.61–2.40 (m, 2H), 2.29–2.14 (m, 2H), 2.06 (s, 1H), 1.68 (br s, 2H), 1.08 (d, J = 3.7 Hz, 6H), 1.06 (d, J = 3.7 Hz, 6H), 0.88 (d, J = 5.3 Hz, 3H), 0.86 (d, J = 5.4 Hz, 3H), 0.80 (dd, J = 6.9, 1.5 Hz, 6H), 0.75 (d, J = 6.9 Hz, 6H), 0.71 (dd, J = 6.8, 1.8 Hz, 6H), 0.13 (d, J = 6.9 Hz, 3H), 0.01 (d, J = 6.9 Hz, 3H). ^{13}C NMR (75 MHz, CDCl_3) δ 178.6, 167.9, 167.4, 149.6, 149.4, 147.7, 147.6, 147.1, 147.0, 146.8, 146.7, 139.6, 139.3, 139.1, 138.6, 136.8, 134.0, 133.5, 133.4, 133.2, 133.1, 132.7, 131.4, 130.6, 129.7, 126.9, 126.6, 124.3, 124.1, 123.0, 120.6, 120.5, 120.4, 120.3, 118.7, 116.1, 113.4, 113.2, 111.5, 111.2, 85.8, 65.0, 64.9, 34.2, 31.2, 30.2, 30.1, 30.0, 27.4, 24.7, 24.4, 24.3, 24.13, 24.05, 24.0, 23.9, 18.6, 14.1. IR (film) ν_{max} : 2958, 2926, 2867, 1599, 1562, 1531, 1464, 1436, 1363, 1334, 1256, 1191, 1155, 1059, 1031, 1012, 942, 788, 748 cm^{-1} . HRMS (ESI, m/z) calcd for $\text{C}_{70}\text{H}_{79}\text{IrN}_3\text{O}_5\text{S}$ $[\text{M}+\text{H}]^+$: 1266.5368, found: 1266.5361. CD (MeOH): λ , nm ($\Delta\epsilon$, $\text{M}^{-1}\text{cm}^{-1}$) 368 (+33), 329 (+41), 306 (−35), 295 (−35), 231 (−26).

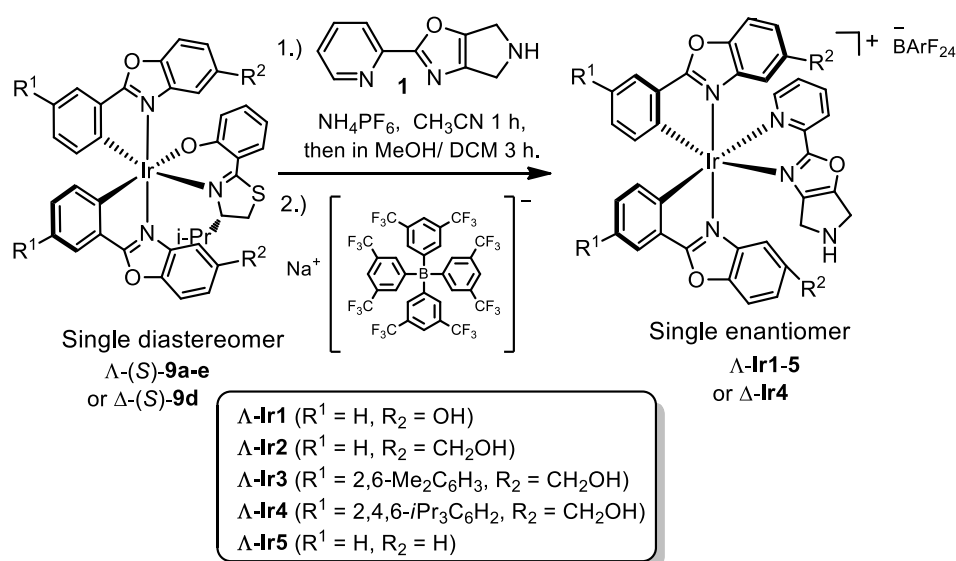


^1H NMR (300 MHz, CDCl_3) δ 7.94 (s, 1H), 7.62–7.58 (m, 2H), 7.56–7.39 (m, 4H), 7.31 (dd, J = 7.9, 1.7 Hz, 1H), 7.27 (d, J = 8.3 Hz, 1H), 7.12–6.96 (m, 4H), 6.88 (ddd, J = 8.6, 7.1, 1.7 Hz, 1H), 6.73 (d, J = 7.8 Hz, 1H), 6.65 (dd, J = 7.8, 1.8 Hz, 1H), 6.62–6.52 (m, 2H), 6.48 (d, J = 7.8 Hz, 1H), 6.34–6.21 (m, 1H), 4.75–4.44 (m, 4H), 3.76 (d, J = 9.5 Hz, 1H), 3.07 (d, J = 11.4 Hz, 1H), 3.01–2.69 (m, 6H),

2.59–2.33 (m, 2H), 2.29–2.10 (m, 1H), 2.02 (t, $J = 5.6$ Hz, 1H), 1.32 (d, $J = 3.3$ Hz, 6H), 1.30 (d, $J = 3.3$ Hz, 6H), 1.17 (d, $J = 6.7$ Hz, 3H), 1.11 (d, $J = 6.9$ Hz, 3H), 1.08 (d, $J = 6.9$ Hz, 3H), 1.06–0.97 (m, 12H), 0.94 (d, $J = 4.3$ Hz, 3H), 0.92 (d, $J = 4.3$ Hz, 3H), 0.34 (d, $J = 6.9$ Hz, 3H). ^{13}C NMR (75 MHz, CDCl_3) δ 179.1, 168.8, 168.5, 149.7, 149.1, 147.9, 147.7, 147.5, 147.2, 147.0, 146.8, 146.5, 146.3, 140.1, 139.4, 138.5, 138.4, 136.7, 135.2, 133.6, 133.4, 133.1, 132.7, 132.6, 132.0, 129.6, 129.5, 129.3, 127.2, 126.5, 124.6, 124.0, 123.7, 121.8, 120.6, 120.5, 120.4, 120.3, 116.0, 115.2, 113.3, 111.3, 111.0, 80.9, 64.9, 64.6, 34.19, 34.17, 31.6, 30.8, 30.1, 30.02, 29.95, 29.86, 24.7, 24.5, 24.4, 24.2, 24.03, 23.96, 23.9, 20.2, 16.4. IR (film) ν_{max} : 2958, 2868, 1599, 1564, 1530, 1437, 1365, 1319, 1252, 1199, 1147, 1028, 942, 877, 816, 749 cm^{-1} . HRMS (ESI, m/z) calcd for $\text{C}_{70}\text{H}_{79}\text{IrN}_3\text{O}_5\text{S}$ $[\text{M}+\text{H}]^+$: 1266.5369, found: 1266.5336. CD (MeOH): λ , nm ($\Delta\epsilon$, $\text{M}^{-1}\text{cm}^{-1}$) 328 (–28), 304 (+24), 288 (+32).

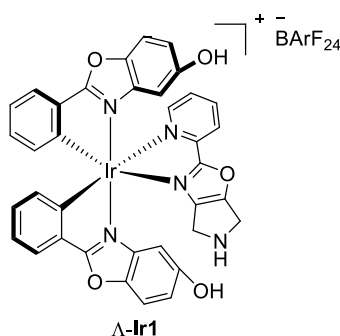
3.2) Synthesis of enantiopure iridium catalysts

The enantiopure iridium catalysts were prepared according to a reported method with some modifications,¹ which relies on the acid-induced substitution of the coordinated phenolato ligand against 2-(pyridin-2-yl)-5,6-dihydro-4*H*-pyrrolo[3,4-*d*]oxazole under retention of configuration and is analogous to previously reported auxiliary-mediated ruthenium(II) chemistry by Meggers et al.¹⁰ The absolute configurations of the obtained Λ -configured iridium(III) complexes were verified by CD spectroscopy in analogy to reported complexes.¹ The enantiomeric purities were verified by chiral HPLC analysis.

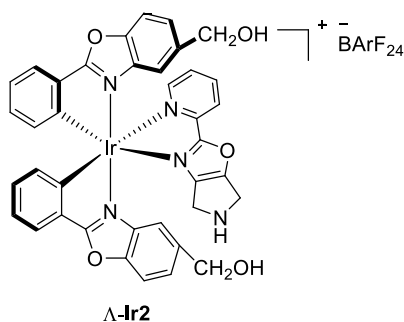


Scheme 25 Synthesis of enantiopure iridium catalysts Λ -Ir1-5 and Δ -Ir4.

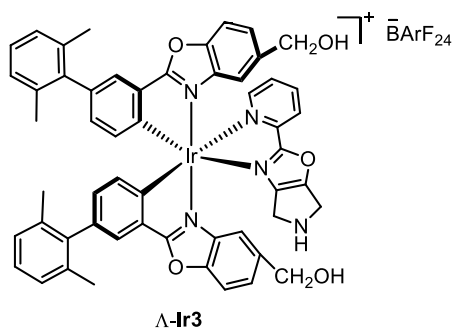
General procedure: A suspension of the iridium auxiliary complexes Λ -(*S*)-**9a-e** or Λ -(*S*)-**9d** (1.0 eq), ligand **1** (2.0 eq), and NH_4PF_6 (5.0 eq) in acetonitrile (10 mM) was stirred at room temperature for 1 h under argon in the dark. Then, the reaction mixture was concentrated to dryness and dissolved in $\text{MeOH}/\text{CH}_2\text{Cl}_2$ (3:1, 10 mM). After being stirred at room temperature for 3 h, the reaction mixture was concentrated to dryness and subjected to a flash silica gel chromatography (eluent: $\text{MeOH}/\text{CH}_2\text{Cl}_2 = 1:30$) to give the pure yellow solid as a hexafluorophosphate salt. The product was directly suspended in CH_2Cl_2 . Sodium tetrakis[(3,5-di-trifluoromethyl)phenyl]borate (NaBArF_{24}) (0.95 eq) was added in one portion and the mixture was stirred at room temperature for 10 min. After removal of the CH_2Cl_2 in vacuo, the residue was taken up in Et_2O (about 2.0 mL) twice and centrifuged. The combined organic layers were dried and concentrated in vacuo to give the pure product as the borate salt.



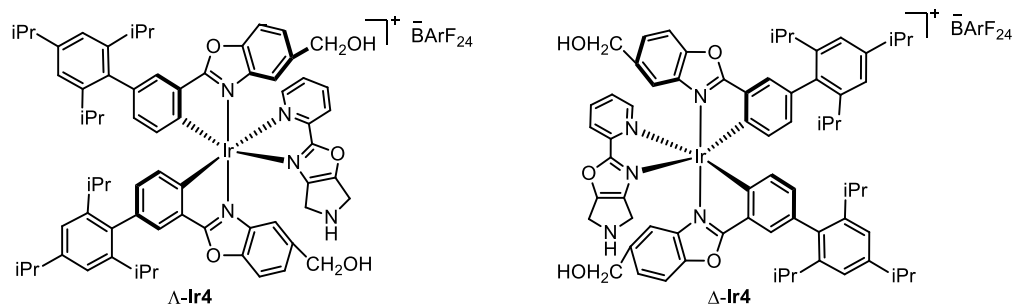
Following the general procedure, Λ -(*S*)-**7a** (83.3 mg, 0.10 mmol) was converted to Λ -**Ir1** (109.7 mg, yield: 66%) as an orange solid. ^1H NMR (400 MHz, CDCl_3) δ 8.11 (d, $J = 5.2$ Hz, 1H), 7.85 (t, $J = 7.8$ Hz, 1H), 7.79 (d, $J = 7.6$ Hz, 1H), 7.76 (d, $J = 7.9$ Hz, 1H), 7.71 (s, 8H), 7.56–7.46 (m, 1H), 7.41 (s, 4H), 7.29 (d, $J = 8.9$ Hz, 1H), 7.14 (t, $J = 7.5$ Hz, 1H), 7.10–6.99 (m, 2H), 6.94 (t, $J = 7.5$ Hz, 1H), 6.82 (dd, $J = 9.0, 2.2$ Hz, 1H), 6.67 (dd, $J = 9.0, 2.3$ Hz, 1H), 6.64 (d, $J = 7.6$ Hz, 1H), 6.54 (d, $J = 7.6$ Hz, 1H), 5.78 (d, $J = 2.1$ Hz, 1H), 5.08 (d, $J = 2.3$ Hz, 1H), 4.01 (d, $J = 13.9$ Hz, 1H), 3.92 (d, $J = 14.7$ Hz, 1H), 3.54 (d, $J = 14.2$ Hz, 1H), 3.25 (d, $J = 13.8$ Hz, 1H). ^{13}C NMR (100 MHz, CDCl_3) δ 178.01, 177.96, 169.9, 162.6, 162.0, 161.3, 160.7, 157.7, 155.4, 154.4, 152.9, 146.1, 144.6, 144.4, 144.0, 143.3, 141.5, 139.7, 138.0, 134.8, 133.5, 133.3, 132.9, 129.8, 129.5, 129.1, 129.0, 128.9, 128.7, 128.3, 126.8, 126.4, 126.2, 123.8, 123.7, 123.4, 122.6, 119.0, 117.5, 114.4, 113.8, 113.2, 112.7, 100.2, 99.6, 43.0, 41.8. IR (film) ν_{max} : 1595, 1451, 1352, 1273, 1115, 888, 831, 738, 708, 672 cm^{-1} . HRMS (ESI, m/z) calcd for $\text{C}_{36}\text{H}_{25}\text{IrN}_5\text{O}_5$ $[\text{M}-\text{BArF}_{24}]^+$: 800.1481, found: 800.1489. CD (MeOH): λ , nm ($\Delta\epsilon$, $\text{M}^{-1}\text{cm}^{-1}$) 337 (+40), 218 (−45).



Following the general procedure, Λ -(*S*)-**7b** (43.3 mg, 0.050 mmol) was converted to Λ -**Ir2** (60.0 mg, yield: 71%) as an orange solid. ^1H NMR (500 MHz, CD_2Cl_2) δ 8.28 (dt, $J = 5.4, 1.2$ Hz, 1H), 8.15–8.09 (m, 2H), 7.87 (ddd, $J = 7.7, 1.3, 0.4$ Hz, 1H), 7.81 (dd, $J = 7.7, 0.9$ Hz, 1H), 7.72 (t, $J = 2.3$ Hz, 8H), 7.67–7.60 (m, 3H), 7.54 (s, 4H), 7.33 (dd, $J = 8.5, 1.7$ Hz, 1H), 7.28 (dd, $J = 8.6, 1.6$ Hz, 1H), 7.19 (td, $J = 7.5, 1.0$ Hz, 1H), 7.12 (td, $J = 7.5, 1.0$ Hz, 1H), 7.06 (td, $J = 7.5, 1.4$ Hz, 1H), 6.97 (td, $J = 7.5, 1.4$ Hz, 1H), 6.70 (d, $J = 7.5$ Hz, 1H), 6.58–6.50 (m, 2H), 5.83 (d, $J = 0.8$ Hz, 1H), 4.77 (d, $J = 14.0$ Hz, 1H), 4.71 (d, $J = 14.0$ Hz, 1H), 4.56 (d, $J = 13.4$ Hz, 1H), 4.52 (d, $J = 13.4$ Hz, 1H), 4.30 (ddd, $J = 15.1, 3.9, 2.1$ Hz, 1H), 4.18 (ddd, $J = 15.0, 3.7, 2.7$ Hz, 1H), 3.74 (s, 3H), 3.62 (ddd, $J = 14.1, 3.9, 2.0$ Hz, 1H), 3.22 (ddd, $J = 14.1, 3.6, 2.6$ Hz, 1H). ^{13}C NMR (126 MHz, CD_2Cl_2) δ 178.3, 177.9, 162.8, 162.4, 162.0, 161.6, 154.0, 149.9, 149.8, 147.0, 144.7, 142.2, 141.0, 140.6, 140.5, 138.1, 137.7, 135.2, 134.0, 133.73, 133.72, 133.3, 129.7, 129.44, 129.42, 129.39, 129.37, 129.19, 129.17, 129.14, 129.12, 128.94, 128.92, 128.89, 128.87, 128.3, 127.4, 127.0, 126.1, 124.8, 124.4, 124.2, 123.9, 121.8, 118.0, 117.94, 117.91, 117.88, 117.85, 112.9, 112.6, 112.2, 111.5, 64.2, 64.1, 44.2, 42.9. IR (film) ν_{max} : 1600, 1520, 1446, 1391, 1354, 1274, 1116, 939, 888, 835, 741, 710 cm^{-1} . HRMS (ESI, m/z) calcd for $\text{C}_{38}\text{H}_{29}\text{IrN}_5\text{O}_5$ $[\text{M}-\text{BArF}_{24}]^+$: 828.1797, found: 828.1789. CD (MeOH): λ , nm ($\Delta\epsilon$, $\text{M}^{-1}\text{cm}^{-1}$) 354 (+26), 330 (+32), 261 (−9), 226 (−27).



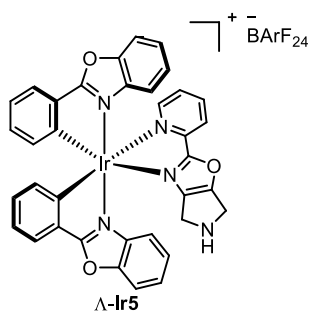
Following the general procedure, Λ -(*S*)-**7c** (64.0 mg, 0.060 mmol) was converted to Λ -**Ir3** (79.8 mg, yield: 70%) as an orange solid. ^1H NMR (300 MHz, CDCl_3) δ 8.20 (d, $J = 5.3$ Hz, 1H), 7.83–7.68 (m, 2H), 7.57 (d, $J = 1.4$ Hz, 9H), 7.52 (d, $J = 1.7$ Hz, 1H), 7.44 (d, $J = 8.5$ Hz, 2H), 7.41–7.35 (m, 1H), 7.32 (s, 4H), 7.16–6.93 (m, 8H), 6.77 (dd, $J = 7.8, 1.8$ Hz, 1H), 6.68 (dd, $J = 7.8, 1.8$ Hz, 1H), 6.64 (d, $J = 7.8$ Hz, 1H), 6.55–6.38 (m, 2H), 5.72 (s, 1H), 4.62 (d, $J = 14.1$ Hz, 1H), 4.54 (d, $J = 14.1$ Hz, 1H), 4.43 (d, $J = 13.5$ Hz, 1H), 4.36 (d, $J = 13.5$ Hz, 1H), 4.07 (d, $J = 15.0$ Hz, 1H), 3.88 (d, $J = 15.1$ Hz, 1H), 3.59 (d, $J = 14.0$ Hz, 1H), 3.18 (d, $J = 14.6$ Hz, 1H), 2.49 (br s, 2H), 2.00 (s, 3H), 1.93 (s, 3H), 1.81 (s, 6H), 1.56 (br s, 1H). ^{13}C NMR (75 MHz, CDCl_3) δ 177.8, 177.5, 169.5, 162.7, 162.0, 161.3, 160.7, 160.5, 153.0, 149.3, 149.2, 145.9, 144.6, 140.6, 140.3, 140.2, 140.0, 139.7, 137.6, 137.4, 136.6, 136.5, 136.2, 135.8, 135.5, 134.7, 134.0, 133.4, 129.9, 129.3, 129.2, 128.6, 127.6, 127.5, 126.9, 126.3, 124.3, 123.8, 123.3, 122.7, 119.0, 117.4, 112.3, 111.5, 110.9, 63.7, 63.4, 43.6, 42.5, 20.9, 20.8, 20.6. IR (film) ν_{max} : 1608, 1446, 1354, 1272, 1116, 1042, 943, 889, 837, 711, 673, 643 cm^{-1} . HRMS (ESI, m/z) calcd for $\text{C}_{54}\text{H}_{45}\text{IrN}_5\text{O}_5$ $[\text{M}-\text{BArF}_{24}]^+$: 1036.3048, found: 1036.3053. CD (MeOH): λ , nm ($\Delta\epsilon$, $\text{M}^{-1}\text{cm}^{-1}$) 360 (+31), 332 (+33), 274 (−15), 241 (−18).



Following the general procedure, Λ -(*S*)-**9d** (140.0 mg, 0.11 mmol) was converted to Λ -**Ir4** (154.4 mg, yield: 67%) and Δ -(*S*)-**9d** (140.0 mg, 0.11 mmol) to Δ -**Ir4** (185.5 mg, yield: 80%). Both complexes are orange solids. NMR spectra of Λ -**Ir4** and Δ -**Ir4** are identical: ^1H NMR (500 MHz, CDCl_3) δ 8.39 (d, J = 5.3 Hz, 1H), 7.92 (d, J = 7.8 Hz, 1H), 7.87 (td, J = 7.8, 1.4 Hz, 1H), 7.74 (d, J = 1.8 Hz, 1H), 7.70 (s, 9H), 7.61–7.49 (m, 3H), 7.44 (s, 4H), 7.25 (d, J = 8.7 Hz, 1H), 7.19 (d, J = 8.7 Hz, 1H), 7.12 (d, J = 1.6 Hz, 1H), 7.09–7.05 (m, 3H), 6.95 (dd, J = 7.8, 1.8 Hz, 1H), 6.87 (dd, J = 7.8, 1.8 Hz, 1H), 6.76 (d, J = 7.8 Hz, 1H), 6.57 (d, J = 7.8 Hz, 1H), 6.54 (s, 1H), 5.85 (s, 1H), 4.73 (d, J = 14.1 Hz, 1H), 4.67 (d, J = 14.1 Hz, 1H), 4.58 (d, J = 13.5 Hz, 1H), 4.50 (d, J = 13.5 Hz, 1H), 4.26 (d, J = 15.2 Hz, 1H), 4.05 (d, J = 15.3 Hz, 1H), 3.76 (d, J = 14.8 Hz, 1H), 3.33 (d, J = 14.0 Hz, 1H), 2.97 (hept, J = 6.8 Hz, 1H), 2.96 (hept, J = 6.8 Hz, 1H), 2.78 (hept, J = 6.9 Hz, 1H), 2.65 (hept, J = 6.9 Hz, 1H), 2.51 (hept, J = 6.9 Hz, 1H), 2.46 (hept, J = 6.8 Hz, 1H), 1.33 (d, J = 6.8 Hz, 6H), 1.31 (d, J = 6.2 Hz, 6H), 1.19 (d, J = 6.8 Hz, 3H), 1.17 (d, J = 6.9 Hz, 3H), 1.14 (d, J = 6.9 Hz, 3H), 1.07 (dd, J = 6.9, 1.9 Hz, 6H), 1.03 (d, J = 6.9 Hz, 3H), 0.98 (d, J = 6.9 Hz, 3H), 0.96 (d, J = 6.9 Hz, 3H). ^{13}C NMR (126 MHz, CDCl_3) δ 177.9, 177.5, 169.9, 162.3, 161.9, 161.5, 161.1, 159.5, 153.2, 149.3, 149.2, 148.6, 148.5, 146.7, 146.6, 146.3, 146.0, 145.2, 144.4, 144.2, 140.4, 140.1, 139.7, 139.5, 137.7, 137.4, 136.3, 135.61, 135.56, 135.5, 134.7, 132.9, 132.7, 129.3, 129.1, 128.9, 128.8, 128.7, 128.6, 128.0, 127.7, 127.6, 125.5, 124.3, 123.8, 123.5, 123.4, 121.2, 120.9, 120.8, 120.7, 120.5, 117.48, 117.45, 117.42, 112.4, 112.3, 111.5, 110.6, 63.7, 63.5, 43.7, 42.6, 34.3, 30.60, 30.56, 30.33, 30.26, 24.24, 24.15, 24.10, 24.02, 23.99, 23.96.

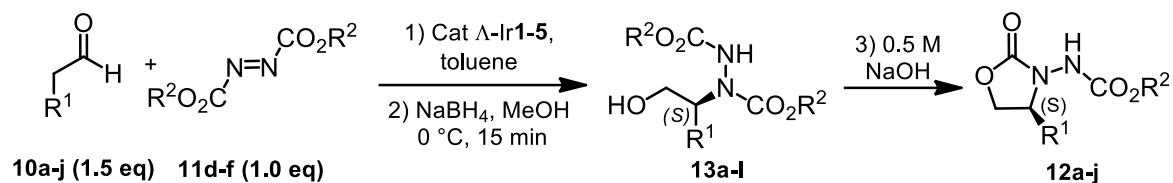
Λ -**Ir4**: IR (film) ν_{max} : 2963, 1606, 1527, 1445, 1354, 1272, 1118, 1040, 886, 836, 711, 673, 640 cm^{-1} . HRMS (ESI, m/z) calcd for $\text{C}_{68}\text{H}_{73}\text{IrN}_5\text{O}_5$ [$\text{M}-\text{BArF}_{24}$] $^+$: 1232.5242, found: 1232.5234. CD (MeOH): λ , nm ($\Delta\epsilon$, $\text{M}^{-1}\text{cm}^{-1}$) 361 (+36), 334 (+37), 269 (−22), 238 (−23).

Δ -**Ir4**: IR (film) ν_{max} : 2961, 2912, 2872, 1606, 1525, 1445, 1353, 1274, 1119, 886, 835, 711, 673 cm^{-1} . HRMS (ESI, m/z) calcd for $\text{C}_{68}\text{H}_{73}\text{IrN}_5\text{O}_5$ [$\text{M}-\text{BArF}_{24}$] $^+$: 1232.5242, found: 1232.5239. CD (MeOH): λ , nm ($\Delta\epsilon$, $\text{M}^{-1}\text{cm}^{-1}$) 361 (−37), 335 (−37), 272 (+21), 241 (+16).



Following the general procedure, Λ -(*S*)-**9e** (40.1 mg, 0.050 mmol) was converted to Λ -**Ir5** (38.0 mg, yield: 46%) as an orange solid. ^1H NMR (500 MHz, CD_2Cl_2) δ 8.20 (dt, $J = 5.4, 1.2$ Hz, 1H), 8.11–8.06 (m, 2H), 7.88 (ddd, $J = 7.7, 1.4, 0.5$ Hz, 1H), 7.83 (ddd, $J = 7.7, 1.4, 0.5$ Hz, 1H), 7.74–7.71 (m, 9H), 7.71–7.69 (m, 1H), 7.59–7.56 (m, 1H), 7.55 (s, 4H), 7.46 (ddd, $J = 8.5, 7.6, 1.2$ Hz, 1H), 7.42 (ddd, $J = 8.5, 7.6, 1.1$ Hz, 1H), 7.35–7.30 (m, 1H), 7.18 (td, $J = 7.5, 1.0$ Hz, 1H), 7.16–7.11 (m, 2H), 7.04 (td, $J = 7.5, 1.4$ Hz, 1H), 6.98 (td, $J = 7.5, 1.4$ Hz, 1H), 6.70–6.64 (m, 1H), 6.62–6.57 (m, 1H), 6.49 (ddd, $J = 8.1, 1.1, 0.6$ Hz, 1H), 5.81 (ddd, $J = 8.1, 1.0, 0.6$ Hz, 1H), 4.25 (ddd, $J = 15.2, 4.3, 2.5$ Hz, 1H), 4.04 (ddd, $J = 15.2, 4.4, 2.6$ Hz, 1H), 3.50 (ddd, $J = 14.2, 4.4, 2.5$ Hz, 1H), 3.02 (ddd, $J = 14.2, 4.3, 2.6$ Hz, 1H), 1.95 (s, 1H). ^{13}C NMR (125 MHz, CD_2Cl_2) δ 178.0, 177.8, 169.9, 162.8, 162.4, 162.0, 161.6, 161.0, 153.5, 150.71, 150.68, 147.4, 146.0, 145.0, 142.6, 140.4, 137.7, 137.5, 135.2, 134.0, 133.8, 133.7, 133.3, 129.7, 129.5, 129.48, 129.46, 129.43, 129.41, 129.39, 129.3, 129.21, 129.18, 129.16, 129.1, 128.9, 128.3, 127.4, 127.3, 127.05, 126.95, 126.7, 126.6, 126.1, 124.1, 124.01, 123.92, 123.7, 121.8, 117.93, 117.90, 117.87, 114.6, 114.5, 113.05, 113.00, 44.2, 42.5. IR (film) ν_{max} : 1673, 1601, 1521, 1453, 1353, 1273, 1116, 937, 889, 743, 711, 673 cm^{-1} . HRMS (ESI, m/z) calcd for $\text{C}_{36}\text{H}_{25}\text{IrN}_5\text{O}_3$ $[\text{M}-\text{BArF}_{24}]^+$: 768.1583, found: 768.1591. CD (MeOH): λ , nm ($\Delta\epsilon$, $\text{M}^{-1}\text{cm}^{-1}$) 354 (+25), 328 (+30), 263 (−10), 227 (−25).

5.2.2 Iridium-Catalyzed Reactions



Scheme 26 Iridium-catalyzed asymmetric α -amination of aldehydes.

General procedure for catalytic reactions of Table 1:

To a solution of dibenzyl azodicarboxylate **11d** (0.2 mmol) and Λ -**Ir1-5** (0.1–4 mol%) in anhydrous toluene (2.0 mL, 0.1 M for entries 1–5, 9 or 200.0 μ L, 1.0 M for entries 6–8) at 0 °C was added the 3,3-dimethylbutyraldehyde **10a** (0.30 mmol). After being stirred at 0 °C (entries 1–4, 5) or RT (entries 5–8) for 1.5 to 36 h under argon atmosphere, MeOH (2.0 mL for entries 1–5, 9 or 200.0 μ L for entries 6–8) was added followed by careful addition of NaBH₄ (10.0 mg, 0.26 mmol) at 0 °C. After 15 min, NaOH (0.5 M, 0.52 mL) was added and after an additional 2 h the mixtures were diluted with water. The aqueous phase was extracted with EtOAc (4 \times 2 mL). The combined organic layers were dried over anhydrous Na₂SO₄, filtered, and concentrated under reduced pressure. The residue was purified by flash chromatography on silica gel (eluent: EtOAc/hexane = 1:4) to give compound **12a**.

General procedure for catalytic reactions of Table 2:

Azodicarboxylates **11d-f** (0.2 mmol) and Λ -**Ir4** (1 mol%) were mixed in a brown glass vial with anhydrous toluene (200.0 μ L, 1.0 M), and the corresponding aldehyde **10a-j** (0.30 mmol) was added at 0 °C. While being stirred at room temperature under argon atmosphere for 12–15 h, the amination products precipitated. MeOH (200.0 μ L) was added followed by a careful addition of NaBH₄ (10.0 mg, 0.26 mmol) at 0 °C. After 15 min, NaOH (0.5 M, 0.52 mL) was added and after an additional 2 h the mixtures were diluted with water (exception for entries 11–12: this NaOH step was skipped). The aqueous phase was extracted with EtOAc (4 \times 2 mL). The combined organic layers were dried over anhydrous Na₂SO₄, filtered, and concentrated under reduced pressure. The residue was purified by flash chromatography on silica gel (eluent: EtOAc:hexane = 1:4 \rightarrow 1:1) to give compounds **13k-l** and **12a-j**.

Catalysis with the PF₆ salt of Λ -Ir4 (in analogy to entry 1 of Table 2):

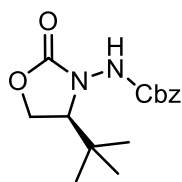
To a solution of Λ -Ir4/PF₆ (2.8 mg, 0.002 mmol) in anhydrous toluene (200.0 μ L) was added sodium tetrakis[(3,5-di-trifluoromethyl)phenyl]borate (NaBArF₂₄) (1.8 mg, 0.002 mmol) in one portion and the mixture was stirred at room temperature for 15 min. Then, dibenzyl azodicarboxylate **11d** (60.0 mg, 0.20 mmol) and 3,3-dimethylbutyraldehyde **10a** (37.6 μ L, 0.30 mmol) were added successively at 0 °C. After being stirred at room temperature for 15 h under argon atmosphere, MeOH (200.0 μ L) was added followed by a careful addition of NaBH₄ (10.0 mg, 0.26 mmol) at 0 °C. After 15 min, NaOH (0.5 M, 0.52 mL) was added and after an additional 2 h the mixtures were diluted with water. The aqueous phase was extracted with EtOAc (4 \times 2 mL). The combined organic layers were dried over anhydrous Na₂SO₄, filtered, and concentrated under reduced pressure. The residue was purified by flash chromatography on silica gel (eluent: EtOAc/hexane = 1:4) to give compound **12a** (50.0 mg, yield: 85%, *ee*: 96%) as a white solid.

Recycling experiments of catalyst Λ -Ir4 (catalysis in analogy to entry 1 of Table 2).

Cycle 1: Dibenzyl azodicarboxylate **11d** (298.3 mg, 1.0 mmol) and Λ -Ir4 (20.9 mg, 0.01 mmol) were mixed in a centrifuge tube with anhydrous toluene (1.0 mL), followed by the addition of 3,3-dimethylbutyraldehyde **10a** (188.0 μ L, 1.5 mmol) at 0 °C. After being stirred at room temperature for 15 h under argon atmosphere, n-hexane (300.0 μ L) was added followed by centrifugation at 4 °C. The mother liquor was transferred out and concentrated under reduced pressure. The residue (TLC showed it contained the catalyst along with a minor amount of amination product) was purified by flash chromatography on silica gel (eluent: MeOH/CH₂Cl₂ = 1:10) to give the pure catalyst Λ -Ir4 (17.0 mg, recovery yield: 81%). MeOH (1.0 mL) was added to the solid in the centrifuge tube followed by careful addition of NaBH₄ (49.4 mg, 1.3 mmol) at 0 °C. After 15 min, NaOH (0.5 M, 2.6 mL) was added and after an additional 2 h the mixtures were diluted with water. The aqueous phase was extracted with EtOAc (4 \times 3 mL). The combined organic layers were dried over anhydrous Na₂SO₄, filtered, and concentrated under reduced pressure. The crude compound **12a** was purified by flash chromatography on silica gel (eluent: EtOAc/hexane = 1:4) to give compound **12a** (222.3 mg, yield: 76%, *ee*: 97%) as a white solid. The recycled catalyst Λ -Ir4 was used for another catalysis reaction (cycle 2).

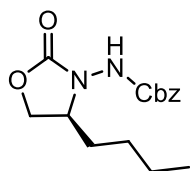
Cycle 2: Dibenzyl azodicarboxylate **11d** (242.1 mg, 0.81 mmol) and the recycled catalyst Λ -**Ir4** (17.0 mg, 0.0081 mmol) were mixed in a centrifuge tube with anhydrous toluene (811.0 μ L), followed by the addition of 3,3-dimethylbutyraldehyde **10a** (152.0 μ L, 1.22 mmol) at 0 °C. After being stirred at room temperature for 15 h under argon atmosphere, n-hexane (250.0 μ L) was added followed by centrifugation at 4 °C. The mother liquor was transferred out and concentrated under reduced pressure. The residue (TLC showed it contained the catalyst along with a minor amount of amination product) was purified by flash chromatography on silica gel (eluent: MeOH/CH₂Cl₂ = 1:10) to give the pure catalyst Λ -**Ir4** (13.2 mg, recovery yield: 78%). MeOH (811.0 μ L) was added to the solid in the centrifuge tube followed by a careful addition of NaBH₄ (40.0 mg, 1.05 mmol) at 0 °C. After 15 min, NaOH (0.5 M, 2.1 mL) was added and after an additional 2 h the mixtures were diluted with water. The aqueous phase extracted with EtOAc (4 \times 3 mL). The combined organic layers were dried over anhydrous Na₂SO₄, filtered, and concentrated under reduced pressure. The crude compound **12a** was purified by flash chromatography on silica gel (eluent: EtOAc/hexane = 1:4) to give compound **12a** (168.0 mg, yield: 71%, *ee*: 95%) as a white solid. The twice recycled catalyst Λ -**Ir4** was used for another catalysis reaction (cycle 3).

Cycle 3: Dibenzyl azodicarboxylate **11d** (188.0 mg, 0.63 mmol) and the twice recycled catalyst Λ -**Ir4** (13.2 mg, 0.0063 mmol) were mixed in a centrifuge tube with anhydrous toluene (630.0 μ L), followed by the addition of 3,3-dimethylbutyraldehyde **10a** (118.0 μ L, 0.95 mmol) at 0 °C. After being stirred at room temperature for 15 h under argon atmosphere, n-hexane (200.0 μ L) was added followed by centrifugation at 4 °C. The mother liquor was transferred out and concentrated under reduced pressure. The residue (TLC showed that it contained the catalyst along with a minor amount of amination product) was purified by flash chromatography on silica gel (eluent: MeOH/CH₂Cl₂ = 1:10) to give the pure catalyst Λ -**Ir4** (MeOH/CH₂Cl₂ = 1:10) (10.0 mg, recovery yield: 76%). MeOH (630.0 μ L) was added to the solid in the centrifuge tube followed by a careful addition of NaBH₄ (31.0 mg, 0.82 mmol) at 0 °C. After 15 min, NaOH (0.5 M, 1.7 mL) was added and after an additional 2 h the mixtures were diluted with water. The aqueous phase extracted with EtOAc (4 \times 3 mL). The combined organic layers were dried over anhydrous Na₂SO₄, filtered, and concentrated under reduced pressure. The crude compound **12a** was purified by flash chromatography on silica gel (eluent: EtOAc/hexane = 1:4) to give compound **12a** (123.0 mg, yield: 67%, *ee*: 96%) as a white solid.

(S)-Benzyl 4-*tert*-butyl-2-oxooxazolidin-3-ylcarbamate (12a)

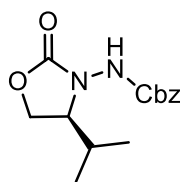
From dibenzyl azodicarboxylate **11d** (60.0 mg, 0.20 mmol) and 3,3-dimethylbutyraldehyde **10a** (37.6 μ L, 0.30 mmol) for 12 h according to the general procedure to give **12a** (56.0 mg, yield: 96%) as a white solid. Enantiomeric excess established by HPLC analysis using a Daicel Chiralpak IB column, *ee* = 97% (HPLC: IB, 254 nm, 40 °C, hexane/ isopropanol = 90/ 10, flow rate 0.5 mL/ min, t_r (major) = 25.0 min, t_r (minor) = 28.7 min); $[\alpha]_D^{20}$ -10.0 (*c* 0.2, CHCl₃).

¹H NMR (300 MHz, CDCl₃) δ 7.33 (s, 5H), 5.15 (q, *J* = 12.2 Hz, 1H), 4.39 (t, *J* = 8.8 Hz, 1H), 4.25–3.98 (m, 1H), 3.83 (s, 1H), 0.93 (s, 9H). ¹³C NMR (75 MHz, CDCl₃) δ 158.9, 155.0, 135.4, 128.5, 128.4, 128.0, 67.9, 64.5, 64.2, 33.3, 25.4. IR (film) ν_{\max} : 3320, 2959, 1762, 1721, 1505, 1410, 1371, 1224, 1118, 1039, 995, 744, 692 cm⁻¹. HRMS (ESI, *m/z*) calcd for C₁₅H₂₀N₂O₄Na [M+Na]⁺: 315.1315, found: 315.1313.

(S)-Benzyl 4-butyl-2-oxooxazolidin-3-ylcarbamate (12b)

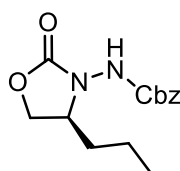
From dibenzyl azodicarboxylate **11d** (60.0 mg, 0.20 mmol) and hexanal **10b** (31.8 μ L, 0.30 mmol) for 15 h according to the general procedure to give **12b** (47.0 mg, yield: 81%) as a colorless oil. Enantiomeric excess established by HPLC analysis using a Daicel Chiralpak IC column, *ee* = 94% (HPLC: IC, 254 nm, 40 °C, hexane/ isopropanol = 70/ 30, flow rate 0.8 mL/ min, t_r (minor) = 23.0 min, t_r (major) = 36.5 min); $[\alpha]_D^{20}$ +27.1 (*c* 1.0, CHCl₃).

¹H NMR (300 MHz, CDCl₃) δ 7.64–6.83 (m, 6H), 5.18–4.91 (m, 2H), 4.36 (s, 1H), 4.08–3.55 (m, 2H), 1.81–1.57 (m, 1H), 1.53–1.31 (m, 1H), 1.30–1.00 (m, 4H), 0.81 (t, *J* = 7.1 Hz, 3H). ¹³C NMR (75 MHz, CDCl₃) δ 157.5, 155.3, 135.3, 128.5, 128.3, 128.0, 67.9, 67.6, 56.7, 31.2, 26.4, 22.5, 13.8. IR (film) ν_{\max} : 3278, 2956, 2931, 2866, 1775, 1729 1503, 1458, 1420, 1227, 1118, 1049, 747, 697 cm⁻¹. HRMS (ESI, *m/z*) calcd for C₁₅H₂₀N₂O₄Na [M+Na]⁺: 315.1315, found: 315.1313.

(S)-Benzyl 4-isopropyl-2-oxooxazolidin-3-ylcarbamate (12c)

From dibenzyl azodicarboxylate **11d** (60.0 mg, 0.20 mmol) and 3-methylbutanal **10c** (32.2 μ L, 0.30 mmol) for 14 h according to the general procedure to give **12c** (49.3 mg, yield: 89%) as a colorless oil. Enantiomeric excess established by HPLC analysis using a Daicel Chiralpak IA column, *ee* = 95% (HPLC: IA, 254 nm, 40 °C, solvent A = 0.1% TFA, solvent B = MeCN, with a linear gradient of 30% to 50% B in 40 min, flow rate 0.5 mL/ min, t_r (major) = 27.9 min, t_r (minor) = 29.8 min); $[\alpha]_D^{20} +14.2$ (*c* 1.0, CHCl₃).

¹H NMR (300 MHz, CDCl₃) δ 7.34 (s, 5H), 7.14 (s, 1H), 5.16 (s, 2H), 4.36 (s, 1H), 4.12–3.66 (m, 2H), 2.07–1.90 (m, 1H), 0.90 (t, *J* = 7.1 Hz, 6H). ¹³C NMR (75 MHz, CDCl₃) δ 157.9, 155.2, 135.3, 128.6, 128.4, 128.1, 68.0, 64.0, 60.8, 28.5, 17.7, 15.8. IR (film) ν_{\max} : 3272, 2963, 1771, 1723, 1505, 1460, 1421, 1395, 1217, 1118, 1046, 744, 698 cm⁻¹. HRMS (ESI, *m/z*) calcd for C₁₄H₁₈N₂O₄Na [M+Na]⁺: 301.1159, found: 301.1157.

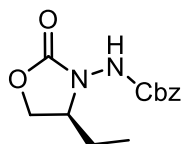
(S)-Benzyl 2-oxo-4-propyloxazolidin-3-ylcarbamate (12d)

From dibenzyl azodicarboxylate **11d** (60.0 mg, 0.20 mmol) and pentanal **10d** (31.8 μ L, 0.30 mmol) for 15 h according to the general procedure to give **12d** (43.2 mg, yield: 78%) as a colorless oil. Enantiomeric excess established by HPLC analysis using a Daicel Chiralpak IA column, *ee* = 96% (HPLC: IA, 254 nm, 40 °C, solvent A = 0.1% TFA, solvent B = MeCN, with a linear gradient of 30% to 45% B in 40 min, flow rate 0.5 mL/ min, t_r (major) = 31.7 min, t_r (minor) = 33.8 min); $[\alpha]_D^{20} +23.4$ (*c* 1.0, CHCl₃).

¹H NMR (300 MHz, CDCl₃) δ 7.35 (s, 5H), 7.21 (s, 1H), 5.15 (s, 2H), 4.43 (s, 1H), 4.06–3.80 (m, 2H), 1.86–1.61 (m, 1H), 1.56–1.37 (m, 1H), 1.36–1.18 (m, 2H), 0.91 (t, *J* = 7.2 Hz, 3H). ¹³C NMR (75 MHz, CDCl₃) δ 157.5, 155.3, 135.3, 128.5, 128.3, 128.1, 67.9, 67.6, 56.6, 33.6, 17.8, 13.9. IR (film)

ν_{\max} : 3300, 2965, 2934, 2875, 1778, 1701, 1512, 1258, 1228, 1202, 1113, 1052, 1010, 744, 694, 621, 579 cm^{-1} . HRMS (ESI, m/z) calcd for $\text{C}_{14}\text{H}_{18}\text{N}_2\text{O}_4\text{Na}$ $[\text{M}+\text{Na}]^+$: 301.1159, found: 301.1157.

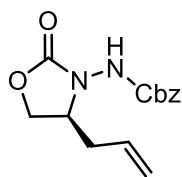
(S)-Benzyl 4-ethyl-2-oxooxazolidin-3-ylcarbamate (12e)



From dibenzyl azodicarboxylate **11d** (60.0 mg, 0.20 mmol) and butyraldehyde **10e** (27.0 μL , 0.30 mmol) for 15 h according to the general procedure to give **12e** (39.2 mg, yield: 73%) as a colorless oil. Enantiomeric excess established by HPLC analysis using a Daicel Chiralpak IA column, $ee = 93\%$ (HPLC: IA, 254 nm, 40 $^{\circ}\text{C}$, solvent A = 0.1% TFA, solvent B = MeCN, with a linear gradient of 30% to 45% B in 40 min, flow rate 0.5 mL/min, $t_r(\text{major}) = 23.8$ min, $t_r(\text{minor}) = 25.3$ min); $[\alpha]_{\text{D}}^{20} +19.2$ (c 1.0, CHCl_3).

^1H NMR (300 MHz, CDCl_3) δ 7.34 (s, 5H), 7.18 (s, 1H), 5.15 (s, 2H), 4.44 (s, 1H), 4.19–3.66 (m, 2H), 1.91–1.66 (m, 1H), 1.65–1.39 (m, 1H), 0.88 (t, $J = 7.5$ Hz, 3H). ^{13}C NMR (75 MHz, CDCl_3) δ 157.5, 155.3, 135.3, 128.5, 128.4, 128.1, 68.0, 67.1, 57.6, 24.3, 8.3. IR (film) ν_{\max} : 3279, 2964, 1768, 1724, 1508, 1218, 1118, 1046, 745, 695 cm^{-1} ; HRMS (ESI, m/z) calcd for $\text{C}_{13}\text{H}_{16}\text{N}_2\text{O}_4\text{Na}$ $[\text{M}+\text{Na}]^+$: 287.1002, found: 287.1003.

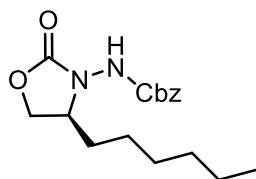
(S)-Benzyl 4-allyl-2-oxooxazolidin-3-ylcarbamate (12f)



From dibenzyl azodicarboxylate **11d** (60.0 mg, 0.20 mmol) and pent-4-enal **10f** (29.6 μL , 0.30 mmol) for 15 h according to the general procedure to give **12f** (48.0 mg, yield: 87%) as a colorless oil. Enantiomeric excess established by HPLC analysis using a Daicel Chiralpak IA column, $ee = 92\%$ (HPLC: IA, 254 nm, 40 $^{\circ}\text{C}$, solvent A = 0.1% TFA, solvent B = MeCN, with a linear gradient of 30% to 45% B in 40 min, flow rate 0.5 mL/min, $t_r(\text{major}) = 28.0$ min, $t_r(\text{minor}) = 29.7$ min); $[\alpha]_{\text{D}}^{20} +36.5$ (c 1.0, CHCl_3). ^1H NMR (300 MHz, CDCl_3) δ 7.27 (s, 5H), 7.07 (s, 1H), 5.60 (td, $J = 17.0, 7.0$ Hz, 1H), 5.09 (s, 3H), 5.05 (s, 1H), 4.34 (t, $J = 7.5$ Hz, 1H), 4.02 (s, 2H), 3.92 (t, $J = 8.1$ Hz, 1H), 2.54–2.34 (m,

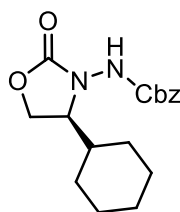
1H), 2.23 (dt, $J = 14.5, 7.3$ Hz, 1H). ^{13}C NMR (75 MHz, CDCl_3) δ 157.3, 155.3, 135.3, 131.2, 128.6, 128.4, 128.1, 119.4, 68.0, 66.8, 55.8, 35.7. IR (film) ν_{max} : 3271, 2912, 1772, 1726, 1502, 1425, 1226, 1119, 1050, 924, 749, 698 cm^{-1} . HRMS (ESI, m/z) calcd for $\text{C}_{14}\text{H}_{16}\text{N}_2\text{O}_4\text{Na}$ $[\text{M}+\text{Na}]^+$: 299.1002, found: 299.1000.

(S)-Benzyl 4-hexyl-2-oxooxazolidin-3-ylcarbamate (12g)



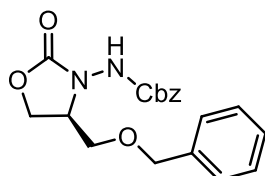
From dibenzyl azodicarboxylate **11d** (60.0 mg, 0.20 mmol) and octanal **10g** (31.8 μL , 0.30 mmol) for 15 h according to the general procedure to give **12g** (48.0 mg, yield: 75%) as a colorless oil. Enantiomeric excess established by HPLC analysis using a Daicel Chiralpak IA column, $ee = 95\%$ (HPLC: IA, 254 nm, 40 $^{\circ}\text{C}$, solvent A = 0.1% TFA, solvent B = MeCN, with a linear gradient of 30% to 60% B in 40 min, flow rate 0.5 mL/min, $t_{\text{r}}(\text{major}) = 33.2$ min, $t_{\text{r}}(\text{minor}) = 35.1$ min); $[\alpha]_{\text{D}}^{20} +24.8$ (c 1.0, CHCl_3).

^1H NMR (300 MHz, CDCl_3) δ 7.26 (s, 6H), 5.07 (d, $J = 2.0$ Hz, 2H), 4.35 (s, 1H), 4.10–3.55 (m, 2H), 1.82–1.54 (m, 1H), 1.40 (s, 1H), 1.18 (s, 8H), 0.80 (t, $J = 6.7$ Hz, 3H). ^{13}C NMR (75 MHz, CDCl_3) δ 157.5, 155.3, 135.3, 128.5, 128.3, 128.0, 67.9, 67.6, 56.7, 31.6, 31.5, 29.0, 24.3, 22.4, 13.9. IR (film) ν_{max} : 3274, 2925, 2857, 1774, 1728, 1502, 1458, 1420, 1220, 1118, 1048, 748, 698 cm^{-1} . HRMS (ESI, m/z) calcd for $\text{C}_{17}\text{H}_{24}\text{N}_2\text{O}_4\text{Na}$ $[\text{M}+\text{Na}]^+$: 343.1628, found: 343.1628.

(S)-Benzyl 4-cyclohexyl-2-oxooxazolidin-3-ylcarbamate (12h)

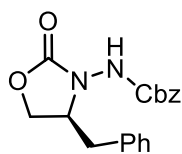
From dibenzyl azodicarboxylate **11d** (60.0 mg, 0.20 mmol) and 2-cyclohexylacetaldehyde **10h** (37.8 mg, 0.30 mmol) for 15 h according to the general procedure to give **12h** (49.0 mg, yield: 77%) as a colorless oil. Enantiomeric excess established by HPLC analysis using a Daicel Chiralpak IC column, *ee* = 95% (HPLC: IC, 254 nm, 40 °C, hexane/ isopropanol = 70/ 30, flow rate 0.8 mL/ min, *t_r*(minor) = 23.9 min, *t_r*(major)= 52.3 min); $[\alpha]_{\text{D}}^{20}$ +24.1 (*c* 1.0, CHCl₃).

¹H NMR (300 MHz, CDCl₃) δ 7.34 (s, 1H), 7.26 (s, 5H), 5.31–4.65 (m, 2H), 4.27 (s, 1H), 3.98 (t, *J* = 8.2 Hz, 1H), 3.85 (s, 1H), 1.88–1.32 (m, 6H), 1.32–0.61 (m, 5H). ¹³C NMR (75 MHz, CDCl₃) δ 158.1, 155.2, 135.3, 128.5, 128.3, 128.0, 67.8, 64.6, 60.3, 38.5, 28.3, 26.3, 26.1, 25.8, 25.5. IR (film) ν_{max} : 3265, 2925, 2854, 1771, 1722, 1504, 1449, 1419, 1213, 1121, 1047, 741, 696 cm⁻¹. HRMS (ESI, *m/z*) calcd for C₁₇H₂₂N₂O₄Na [M+Na]⁺: 341.1472, found: 341.1470.

(S)-Benzyl 4-(benzyloxymethyl)-2-oxooxazolidin-3-ylcarbamate (12i)

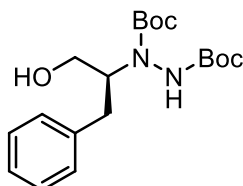
From dibenzyl azodicarboxylate **11d** (60.0 mg, 0.20 mmol) and 3-(benzyloxy)propanal¹¹ **10i** (49.2 mg, 0.30 mmol) for 15 h according to the general procedure to give **12i** (51.2 mg, yield: 75%) as a colorless oil. Enantiomeric excess established by HPLC analysis using a Daicel Chiralpak IC column, *ee* = 91% (HPLC: IC, 254 nm, 40 °C, hexane/ isopropanol = 80/ 20, flow rate 0.5 mL/ min, *t_r*(minor)= 27.4 min, *t_r*(major) = 30.6 min); $[\alpha]_{\text{D}}^{20}$ +13.2 (*c* 1.0, CHCl₃).

¹H NMR (300 MHz, CDCl₃) δ 7.50–7.20 (m, 10H), 7.10 (s, 1H), 5.28–4.96 (m, 2H), 4.52 (s, 2H), 4.44 (t, *J* = 7.8 Hz, 1H), 4.30–4.00 (m, 2H), 3.59 (qd, *J* = 10.2, 3.7 Hz, 2H). ¹³C NMR (75 MHz, CDCl₃) δ 157.1, 155.3, 137.3, 135.2, 128.5, 128.3, 128.1, 128.0, 127.7, 73.3, 67.9, 67.7, 64.8, 55.8. IR (film) ν_{max} : 3273, 3031, 2867, 1774, 1728, 1499, 1453, 1213, 1105, 1038, 742, 697 cm⁻¹. HRMS (ESI, *m/z*) calcd for C₁₉H₂₀N₂O₅Na [M+Na]⁺: 379.1264, found: 379.1262.

(S)-Benzyl 4-benzyl-2-oxooxazolidin-3-ylcarbamate (12j)

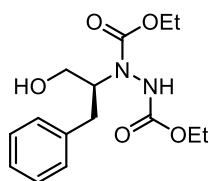
From dibenzyl azodicarboxylate **11d** (60.0 mg, 0.20 mmol) and 3-phenylpropanal **10j** (29.6 μ L, 0.30 mmol) for 22 h (5 °C for 14 h, then up to RT for additional 8 h) according to the general procedure to give **12j** (59.2 mg, yield: 91%) as a colorless oil. Enantiomeric excess established by HPLC analysis using a Daicel Chiralpak IC column, *ee* = 89% (HPLC: IC, 254 nm, 40 °C, hexane/ isopropanol = 70/30, flow rate 0.5 mL/ min, t_r (minor)= 40.0 min, t_r (major) = 50.5 min); $[\alpha]_D^{20}$ +23.5 (*c* 1.0, CHCl₃).

¹H NMR (300 MHz, CDCl₃) δ 7.35–6.91 (m, 10H), 5.07 (s, 2H), 4.20 (s, 2H), 3.95 (s, 1H), 3.05 (dd, *J* = 13.7, 4.1 Hz, 1H), 2.91–2.12 (m, 1H). ¹³C NMR (75 MHz, CDCl₃) δ 157.3, 155.2, 135.3, 135.1, 128.9, 128.6, 128.4, 128.2, 127.2, 68.0, 67.1, 57.7, 37.9. IR (film) ν_{\max} : 3278, 3029, 2938, 1773, 1725, 1496, 1450, 1419, 1221, 1117, 1026, 742, 698 cm⁻¹. HRMS (ESI, *m/z*) calcd for C₁₈H₁₈N₂O₄Na [M+Na]⁺: 349.1159, found: 349.1156.

(S)-Di-tert-butyl 1-(1-hydroxy-3-phenylpropan-2-yl)hydrazine-1,2-dicarboxylate (13k)

From di-*tert*-butyl azodicarboxylate **11e** (46.0 mg, 0.20 mmol) and 3-phenylpropanal **10j** (29.6 μ L, 0.30 mmol) for 15 h according to the general procedure to give **13k** (67.0 mg, yield: 91%) as a white solid. Enantiomeric excess established by HPLC analysis using a Daicel Chiralpak IC column, *ee* = 96% (HPLC: IC, 254 nm, 40 °C, hexane/ isopropanol = 80/ 20, flow rate 0.5 mL/ min, t_r (major) = 13.9 min, t_r (minor)= 16.9 min); $[\alpha]_D^{20}$ –33.7 (*c* 1.0, CHCl₃), (lit¹² $[\alpha]_D^{25}$ +30.8 (*c* 0.53, CHCl₃) product obtained by *L*-proline catalyzed α -amination with *R*-configuration),

¹H NMR (300 MHz, CDCl₃) δ 7.50–6.76 (m, 5H), 6.21–5.78 (m, 1H), 4.94–4.31 (m, 1H), 3.70–3.23 (m, 2H), 2.93–2.14 (m, 2H), 1.43 (s, 9H), 1.23 (m, 9H). ¹³C NMR (75 MHz, CDCl₃) δ 158.7, 155.7, 155.5, 154.7, 137.8, 128.8, 128.5, 126.5, 82.6, 82.3, 81.7, 81.3, 62.2, 61.9, 34.7, 28.1, 28.0, 27.8. IR (film) ν_{\max} : 3419, 3224, 2975, 2930, 1720, 1675, 1531, 1392, 1367, 1333, 1278, 1255, 1160, 1022, 791, 752, 701 cm⁻¹. HRMS (ESI, *m/z*) calcd for C₁₉H₃₀N₂O₅Na [M+Na]⁺: 389.2047, found: 389.2045.

(S)-Diethyl 1-(1-hydroxy-3-phenylpropan-2-yl)hydrazine-1,2-dicarboxylate (13l)

From diethyl azodicarboxylate **11f** (2.2 M in toluene, 90.9 μL , 0.20 mmol) and 3-phenylpropanal **10j** (29.6 μL , 0.30 mmol) for 15 h according to the general procedure to give **13l** (54.6 mg, yield: 88%) as a white solid. Enantiomeric excess established by HPLC analysis using a Daicel Chiralpak IC column, $ee = 95\%$ (HPLC: IC, 254 nm, 40 $^{\circ}\text{C}$, hexane/ isopropanol = 70/ 30, flow rate 0.5 mL/ min, $t_{\text{r}}(\text{minor}) = 31.3$ min, $t_{\text{r}}(\text{major}) = 76.1$ min); $[\alpha]_{\text{D}}^{20} -26.1$ (c 1.0, CHCl_3).

^1H NMR (300 MHz, CDCl_3) δ 7.53–6.78 (m, 5H), 6.59–6.09 (m, 1H), 4.92–4.40 (m, 1H), 4.29–4.09 (m, 2H), 4.08–3.84 (m, 2H), 3.69–3.19 (m, 2H), 2.90–2.30 (m, 2H), 1.23 (t, $J = 7.2$ Hz, 3H), 1.05 (t, $J = 6.9$ Hz, 3H). ^{13}C NMR (75 MHz, CDCl_3) δ 159.4, 156.8, 137.4, 128.7, 128.6, 126.6, 62.9, 62.7, 61.9, 34.6, 14.2. IR (film) ν_{max} : 3428, 3244, 2989, 2922, 2864, 1724, 1678, 1524, 1416, 1254, 1219, 1061, 1025, 776, 753 cm^{-1} . HRMS (ESI, m/z) calcd for $\text{C}_{15}\text{H}_{22}\text{N}_2\text{O}_5\text{Na}$ $[\text{M}+\text{Na}]^+$: 333.1421, found: 333.1417.

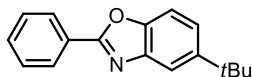
5.2.3 Single Crystal X-Ray Diffraction of Iridium Catalyst *rac*-Ir4

An X-ray crystal structure of the racemic complex Λ/Δ -**Ir4** was obtained as an iodide salt (identification code = cat112_0m_sq). Suitable crystals were obtained by slow diffusion from a solution of Λ/Δ -**Ir4** in $\text{CH}_2\text{Cl}_2/\text{MeOH}$ 5:1 saturated with NaI and layered with Et_2O . The structure information is detailed in Appendices 6.7.

5.3 Metal-Centered Chirality Directs Friedel-Crafts Addition

5.3.1 Synthesis of Iridium Catalysts Λ -IrO and Δ -IrO

5-*tert*-Butyl-2-phenylbenzo[d]oxazole (**16**)

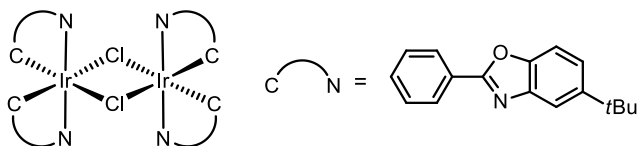


The compound was synthesized following a published procedure with slight modifications.³ A solution of 2-amino-4-*tert*-butylphenol (1.650 g, 10.0 mmol) and benzaldehyde (1.0 mL, 10.0 mmol) in *m*-xylene (33.0 mL) was stirred at 120 °C for 0.5 h. 4-Methoxy-TEMPO (93.0 mg, 5 mol%) was added to the mixture which was stirred at 120 °C for additional 5 h under an oxygen atmosphere. The reaction mixture was cooled and concentrated under reduced pressure. The residue was purified by flash chromatography on silica gel (EtOAc/hexane = 1:20) to afford the desired product **2** (2.380 g, 9.5 mmol, yield: 95%) as a white solid.

¹H NMR (300 MHz, CDCl₃) δ 8.33-8.20 (m, 2H), 7.81 (d, J = 1.8 Hz, 1H), 7.59-7.47 (m, 4H), 7.42 (dd, J = 8.6, 1.9 Hz, 1H), 1.40 (s, 9H).

All spectroscopic data were in agreement with the literature.¹³

Precursor Iridium Complex *rac*-**17**



The new compound *rac*-**17** was synthesized according to a route developed by Nonoyama for iridium(III) μ -chloro-bridged dimers with related cyclometalated ligands,⁹ which involves refluxing IrCl₃·*n*H₂O with 2.0-2.5 equivalents of cyclometalating ligand in a 3:1 mixture of 2-methoxyethanol and water. Accordingly, 5-*tert*-butyl-2-phenylbenzo[d]oxazole **16** (1.030g, 4.1 mmol) was added to iridium chloride hydrate (723.0 mg, 2.0 mmol) in a mixture of 2-ethoxyethanol/water (3:1, 92.0 mL). The reaction mixture was heated at 120 °C for 24 h under argon. The resulting precipitate was collected by centrifugation, washed with diethyl ether and dried to yield the product *rac*-**17** (1.281g, 0.88 mmol, yield: 86% with >95% purity as judged by ¹H-NMR) as a yellow solid.

¹H NMR (300 MHz, CD₂Cl₂) δ 8.40-8.27 (m, 4H), 7.58 (dd, J = 7.6, 1.3 Hz, 4H), 7.36-7.16 (m, 8H),

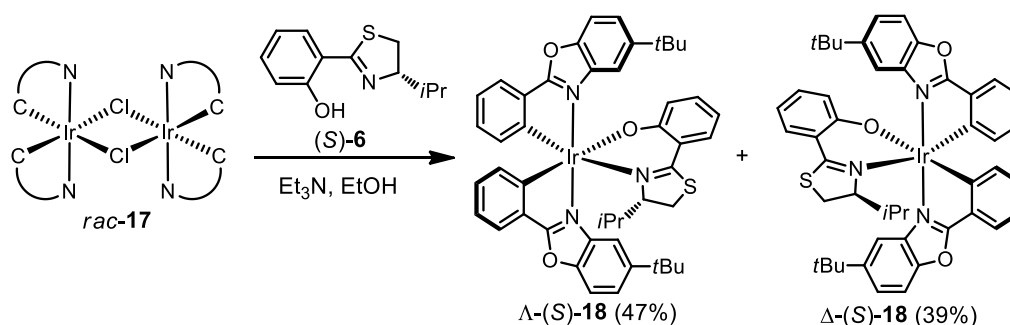
6.88 (dd, $J = 11.0, 3.9$ Hz, 4H), 6.64 (td, $J = 7.5, 1.3$ Hz, 4H), 6.09 (d, $J = 7.8$ Hz, 4H), 1.25 (s, 36H).

^{13}C NMR (75 MHz, CD_2Cl_2) δ 177.0 (4C), 149.2 (4C), 148.2 (4C), 144.4 (4C), 139.8 (4C), 132.9 (4C), 131.6 (4C), 130.5 (4C), 125.8 (4C), 123.7 (4C), 121.9 (4C), 115.1 (4C), 110.6 (4C), 35.3 (4C), 31.8 (12C).

IR (film): ν (cm^{-1}) 3053, 2961, 2870, 1590, 1556, 1517, 1478, 1444, 1382, 1268, 1194, 1123, 1077, 1037, 974, 929, 890, 809, 772, 734, 702, 649, 584, 510, 452, 406.

HRMS (ESI, m/z) calcd for $\text{C}_{68}\text{H}_{64}\text{Cl}_2\text{Ir}_2\text{N}_4\text{O}_4\text{Na}$ $[\text{M}+\text{Na}]^+$: 1479.3442, found: 1479.3444.

Iridium Auxiliary Complexes Λ -(*S*)-**18** and Δ -(*S*)-**18**



A mixture of iridium(III) dimer complex *rac*-**17** (364.0 mg, 0.25 mmol), the chiral auxiliary (*S*)-4-isopropyl-2-(2'-hydroxyphenyl)-2-thiazoline {(*S*)-**6**} (138.0 mg, 0.62 mmol), and triethylamine (348.0 μL , 2.0 mmol) in ethanol (10.0 mL) was purged with argon for 5 min and then heated at reflux overnight. The reaction mixture was cooled to room temperature and concentrated to dryness. The residue was subjected to a flash silica gel chromatography (hexane/ $\text{CH}_2\text{Cl}_2 = 1:2$) to separate the two diastereomers. The first eluting diastereomer (orange solid, 215.0 mg, 0.24 mmol, 47%) was assigned as Λ -(*S*)-**18** and the second eluting diastereomer (orange solid, 177.0 mg, 0.19 mmol, 39%) as Δ -(*S*)-**18** according to CD spectroscopy.¹ The assigned configurations were confirmed by a crystal structure of the catalyst Δ -**IrO**, obtained from Δ -(*S*)-**18** (see below).

Λ -(*S*)-**18**:

^1H NMR (300 MHz, CD_2Cl_2) δ 8.01 (d, $J = 1.7$ Hz, 1H), 7.74 (dd, $J = 7.6, 0.7$ Hz, 1H), 7.71-7.61 (m, 2H), 7.60-7.46 (m, 5H), 7.19 (ddd, $J = 8.6, 6.8, 1.8$ Hz, 1H), 6.96 (dtd, $J = 8.9, 7.5, 1.2$ Hz, 2H), 6.88 (td, $J = 7.5, 1.5$ Hz, 1H), 6.84-6.76 (m, 2H), 6.76-6.71 (m, 1H), 6.42 (d, $J = 7.3$ Hz, 1H), 6.33 (ddd, $J = 8.1, 6.8, 1.2$ Hz, 1H), 4.84-4.70 (dd, $J = 8.1, 2.5$ Hz, 1H), 3.42 (dd, $J = 11.6, 9.8$ Hz, 1H), 3.04 (dd, $J = 11.7, 1.5$ Hz, 1H), 1.49 (s, 9H), 1.24 (s, 9H), 0.87-0.72 (m, 1H), 0.27 (d, $J = 7.0$ Hz, 3H), 0.19 (d, $J =$

7.0 Hz, 3H).

^{13}C NMR (75 MHz, CD_2Cl_2) δ 178.5, 178.1, 168.0, 167.6, 150.9, 150.6, 150.2, 149.9, 148.9, 148.5, 139.4, 138.9, 135.3, 133.7, 131.9, 131.8, 131.6, 131.3, 126.3, 126.0, 124.7, 123.4, 123.2, 122.1, 121.0, 118.5, 115.2, 113.4, 113.2, 111.2, 110.7, 85.2, 35.8, 35.4, 32.1, 31.9, 31.8, 28.2, 19.2, 14.3.

IR (film): ν (cm^{-1}) 2957, 2868, 2032, 1661, 1593, 1556, 1518, 1440, 1380, 1266, 1192, 1150, 1037, 1009, 929, 810, 776, 736, 646, 555, 521, 452.

HRMS (ESI, m/z) calcd for $\text{C}_{46}\text{H}_{46}\text{IrN}_3\text{NaO}_3\text{S}$ $[\text{M}+\text{Na}]^+$: 936.2787, found: 936.2790.

CD (MeOH): λ , nm ($\Delta\epsilon$, $\text{M}^{-1}\text{cm}^{-1}$) 452 (−9), 360 (+29), 323 (+40), 303 (−25), 292 (−28), 263 (+12), 249 (+12), 227 (−33), 216 (−32).

Δ -(*S*)-**18**:

^1H NMR (300 MHz, CD_2Cl_2) δ 7.98 (d, J = 1.8 Hz, 1H), 7.79-7.67 (m, 2H), 7.64 (d, J = 8.8 Hz, 1H), 7.59-7.49 (m, 2H), 7.45 (dd, J = 6.9, 1.8 Hz, 2H), 7.38 (dd, J = 8.0, 1.6 Hz, 1H), 7.04 (ddd, J = 8.6, 6.9, 1.7 Hz, 1H), 6.93 (td, J = 7.3, 0.9 Hz, 2H), 6.88-6.69 (m, 3H), 6.62 (d, J = 8.6 Hz, 1H), 6.46 (d, J = 7.6 Hz, 1H), 6.31 (td, J = 7.5, 0.8 Hz, 1H), 3.64 (d, J = 9.9 Hz, 1H), 2.92 (dd, J = 11.2, 1.7 Hz, 1H), 2.70 (t, J = 10.6 Hz, 1H), 2.34-2.03 (m, 1H), 1.29 (s, 9H), 1.20 (s, 9H), 1.08 (d, J = 6.8 Hz, 3H), 0.06 (d, J = 7.0 Hz, 3H).

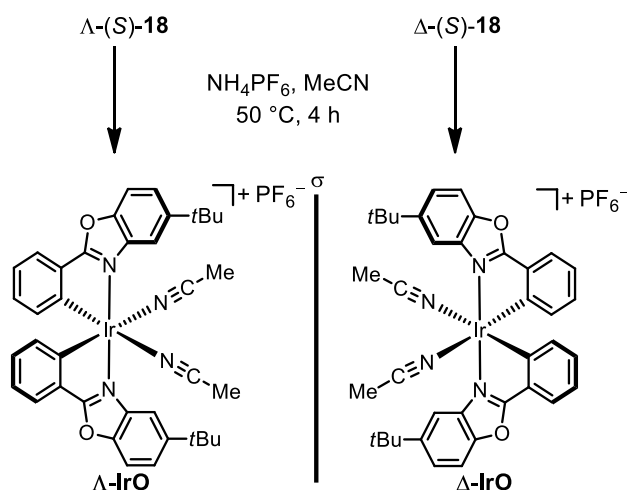
^{13}C NMR (75 MHz, CD_2Cl_2) δ 178.9, 178.9, 167.7, 167.5, 151.3, 150.7, 150.4, 149.6, 149.0, 148.4, 139.8, 138.7, 136.0, 133.2, 132.6, 132.1, 131.6, 131.4, 131.2, 130.6, 126.4, 126.1, 124.2, 123.4, 123.2, 121.8, 120.9, 119.9, 114.9, 114.1, 113.1, 110.9, 110.8, 82.2, 35.6, 35.3, 32.1, 32.0, 31.6, 30.1, 20.4, 17.2.

IR (film): ν (cm^{-1}) 3050, 2956, 2867, 2032, 1732, 1593, 1561, 1518, 1437, 1377, 1270, 1193, 1149, 1124, 1073, 1033, 1010, 930, 809, 734, 648, 591, 555, 521, 451.

HRMS (ESI, m/z) calcd for $\text{C}_{46}\text{H}_{46}\text{IrN}_3\text{NaO}_3\text{S}$ $[\text{M}+\text{Na}]^+$: 936.2787, found: 936.2788.

CD (MeOH): λ , nm ($\Delta\epsilon$, $\text{M}^{-1}\text{cm}^{-1}$) 451 (+11), 404 (+7), 327 (−29), 305 (+23), 300 (+20), 283 (+24), 247 (−9), 210 (−31).

Synthesis of Enantiopure Iridium Catalysts



A suspension of the iridium auxiliary complexes $\Lambda\text{-(S)-18}$ (200.0 mg, 0.22 mmol) or $\Delta\text{-(S)-18}$ (220.0 mg, 0.24 mmol) and NH_4PF_6 (538.0 mg, 3.30 mmol) in acetonitrile (22.0 mL) was heated at 50 °C for 4 h under argon in the dark. The reaction mixture was concentrated to dryness and subjected to a flash silica gel chromatography (100% CH_2Cl_2 to $\text{CH}_2\text{Cl}_2/\text{CH}_3\text{CN} = 10:1$) to give the enantiopure catalysts $\Lambda\text{-IrO}$ (200.3 mg, 0.22 mmol, 99%) or $\Delta\text{-IrO}$ (210.0 mg, 0.23 mmol, 95%) as yellow solids. The absolute configurations of the obtained Λ - and Δ -configured iridium(III) complexes were verified by CD spectroscopy and confirmed by an X-ray crystal structure of $\Delta\text{-IrO}$. The enantiomeric purity was verified by chiral HPLC analysis.

^1H NMR (300 MHz, CD_2Cl_2) δ 7.85 (d, $J = 1.3$ Hz, 2H), 7.82–7.64 (m, 6H), 7.02 (td, $J = 7.5, 1.0$ Hz, 2H), 6.85 (td, $J = 7.5, 1.5$ Hz, 2H), 6.37 (d, $J = 7.4$ Hz, 2H), 2.44 (s, 6H), 1.46 (s, 18H).

^{13}C NMR (75 MHz, CD_2Cl_2) δ 177.4, 151.2, 148.8, 142.0, 138.4, 132.9, 132.6, 130.0, 126.3, 125.0, 123.6, 120.9, 113.0, 112.0, 35.6, 31.8, 30.1, 3.9.

IR (film): ν (cm^{-1}) 2959, 2870, 1594, 1521, 1479, 1453, 1388, 1275, 1194, 1162, 1128, 1084, 1041, 933, 837, 778, 736, 651, 555, 452.

 $\Lambda\text{-IrO}$:

HRMS (ESI, m/z) calcd for $\text{C}_{38}\text{H}_{38}\text{IrN}_4\text{O}_2$ $[\text{M-PF}_6]^+$: 775.2619, found: 775.2622.

CD (MeOH): λ , nm ($\Delta\epsilon$, $\text{M}^{-1}\text{cm}^{-1}$) 436 (−11), 345 (+43), 271 (−37), 208 (+88).

 $\Delta\text{-IrO}$:

HRMS (ESI, m/z) calcd for $\text{C}_{38}\text{H}_{38}\text{IrN}_4\text{O}_2$ $[\text{M-PF}_6]^+$: 775.2619, found: 775.2619.

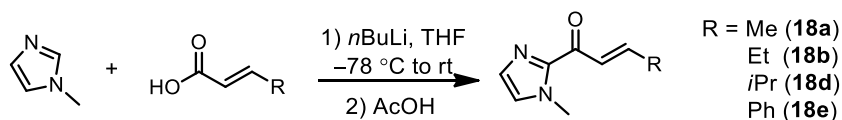
CD (MeOH): λ , nm ($\Delta\epsilon$, $\text{M}^{-1}\text{cm}^{-1}$) 436 (+10), 344 (−35), 272 (+34), 208 (−82).

5.3.2 Synthesis of Substrates

1) Synthesis of α,β -Unsaturated 2-Acyl Imidazoles

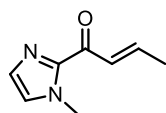
All α,β -unsaturated 2-acylimidazoles were synthesized according to reported procedures with some modifications (methods A-D).¹⁴

Method A



General procedure for method A. To a solution of *N*-methylimidazole (5.2 mL, 66.0 mmol) in THF (100.0 mL) at $-78\text{ }^{\circ}\text{C}$ was added dropwise *n*-BuLi (26.4 mL, 2.5 M in hexane, 66.0 mmol). The reaction was stirred at $-78\text{ }^{\circ}\text{C}$ for 10 min, then stirred at room temperature for additional 30 min. The corresponding carboxylic acid (30.0 mmol) was added to the flask after the reaction was cooled back down to $-78\text{ }^{\circ}\text{C}$. The reaction was allowed to warm to room temperature slowly (over a period of 3-4 h) and stirred overnight. The reaction was quenched with a saturated aqueous solution of Na_2CO_3 and extracted with EtOAc ($4 \times 100\text{ mL}$). The combined organic layers were dried over anhydrous Na_2SO_4 , filtered, and concentrated under reduced pressure. The residue was purified by flash chromatography on silica gel (EtOAc/hexane = 1:1).

(*E*)-1-(1-Methyl-1*H*-imidazol-2-yl)but-2-en-1-one (**18a**)

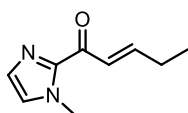


Following the general method A, (*E*)-but-2-enoic acid (2.580 g, 30.0 mmol) was converted to α,β -unsaturated 2-acylimidazole **18a** (1.575 g, 10.5 mmol, yield: 35%) as a white solid.

^1H NMR (300 MHz, CDCl_3) δ 7.39 (dq, $J = 15.7, 1.6\text{ Hz}$, 1H), 7.19-7.03 (m, 2H), 7.02 (s, 1H), 4.01 (s, 3H), 1.96 (dd, $J = 6.9, 1.6\text{ Hz}$, 3H).

^{13}C NMR (75 MHz, CDCl_3) δ 180.6, 143.8, 129.0, 127.8, 127.0, 36.2, 18.4.

All spectroscopic data were in agreement with the literature.¹⁴

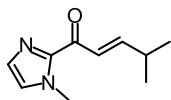
(E)-1-(1-Methyl-1*H*-imidazol-2-yl)pent-2-en-1-one (18b)

Following the general method A, (*E*)-pent-2-enoic acid (3.004 g, 30.0 mmol) was converted to α,β -unsaturated 2-acylimidazole **18b** (1.378 g, 8.4 mmol, yield: 28%) as a colorless oil.

^1H NMR (300 MHz, CDCl_3) δ 7.38 (dt, $J = 15.7, 1.6$ Hz, 1H), 7.22-7.08 (m, 2H), 7.02 (s, 1H), 4.02 (s, 3H), 2.44-2.18 (m, 2H), 1.11 (t, $J = 7.4$ Hz, 3H).

^{13}C NMR (75 MHz, CDCl_3) δ 180.8, 150.1, 143.7, 129.0, 127.0, 125.3, 36.2, 25.6, 12.3.

All spectroscopic data were in agreement with the literature.¹⁴

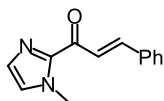
(E)-4-Methyl-1-(1-methyl-1*H*-imidazol-2-yl)pent-2-en-1-one (18d)

Following the general method A, (*E*)-4-methylpent-2-enoic acid (2.280 g, 20.0 mmol) was converted to α,β -unsaturated 2-acylimidazole **18d** (1.440 g, 8.1 mmol, yield: 40%) as a colorless oil.

^1H NMR (300 MHz, CDCl_3) δ 7.33 (dd, $J = 15.7, 1.3$ Hz, 1H), 7.14 (d, $J = 0.8$ Hz, 1H), 7.11-6.99 (m, 2H), 4.01 (s, 3H), 2.69-2.41 (m, 1H), 1.09 (d, $J = 6.8$ Hz, 6H).

^{13}C NMR (75 MHz, CDCl_3) δ 181.0, 154.8, 143.7, 129.0, 127.0, 123.4, 36.2, 31.3, 21.3.

All spectroscopic data were in agreement with the literature.¹⁴

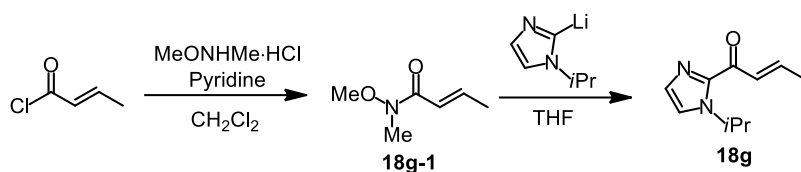
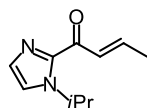
(E)-1-(1-Methyl-1*H*-imidazol-2-yl)-3-phenylprop-2-en-1-one (18e)

Following the general procedure, cinnamic acid (2.960 g, 20.0 mmol) was converted to α,β -unsaturated 2-acylimidazole **18e** (2.417 g, 11.4 mmol, yield: 57%) as a white solid.

^1H NMR (300 MHz, CDCl_3) δ 8.09 (d, $J = 16.0$ Hz, 1H), 7.83 (d, $J = 16.0$ Hz, 1H), 7.77-7.63 (m, 2H), 7.53-7.32 (m, 3H), 7.23 (d, $J = 0.9$ Hz, 1H), 7.08 (s, 1H), 4.10 (s, 3H).

^{13}C NMR (75 MHz, CDCl_3) δ 180.4, 143.9, 143.5, 134.9, 130.5, 129.1, 128.8, 128.8, 127.2, 122.8, 36.4.

All spectroscopic data were in agreement with the literature.¹⁴

Method B**(E)-1-(1-Isopropyl-1H-imidazol-2-yl)but-2-en-1-one (18g)**

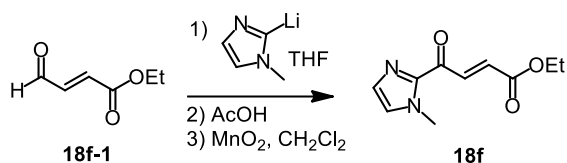
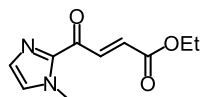
Procedure for the preparation of the Weinreb amide 18g-1. To a solution of *N,O*-dimethylhydroxylamine hydrochloride (3.900 g, 40.0 mmol) in CH_2Cl_2 (80.0 mL) at 0 °C were added *trans*-crotonyl chloride (4.2 mL, 44.0 mmol) and pyridine (7.1 mL, 88.0 mmol) successively. The reaction was stirred at 0 °C for 30 min, then stirred at room temperature for additional 30 min. The reaction was diluted with EtOAc (150 mL). The organic layer was washed with 1 *N* HCl (3 × 30 mL), aqueous saturated NaHCO_3 (3 × 50 mL), and brine (50 mL). The combined organic layers were dried over anhydrous Na_2SO_4 , filtered, and concentrated under reduced pressure. The residue was purified by flash chromatography on silica gel (EtOAc/hexane = 1:3) to give **18g-1** (4.021 g, 31.2 mmol, 78%) as a colorless oil.

Procedure for the preparation of 18g. To a solution of *N*-isopropylimidazole (2.4 mL, 21.4 mmol) in THF (44.0 mL) at −78 °C was added *n*-BuLi (8.6 mL, 2.5 M in hexane, 21.4 mmol) dropwise. The reaction was stirred at −78 °C for 10 min, then stirred at room temperature for 30 min. The Weinreb amide **18g-1** (2.300 g, 17.8 mmol) was added to the flask after the reaction was cooled back down to −78 °C. The reaction was allowed to warm to room temperature slowly (over a period of 3–4 h) and stirred overnight. The reaction was quenched with a saturated aqueous solution of Na_2CO_3 and extracted with EtOAc (4 × 50 mL). The combined organic layers were dried over anhydrous Na_2SO_4 , filtered, and concentrated under reduced pressure. The residue was purified by flash chromatography on silica gel (EtOAc/hexane = 1:1) to produce **18g** (2.376 g, 13.3 mmol, 75%) as a white solid.

^1H NMR (300 MHz, CDCl_3) δ 7.42 (dq, J = 15.5, 1.4 Hz, 1H), 7.24 (s, 1H), 7.15 (s, 1H), 7.11–6.96 (m, 1H), 5.61 (sept., J = 6.5 Hz, 1H), 1.94 (dd, J = 6.8, 1.2 Hz, 3H), 1.41 (d, J = 6.6 Hz, 6H).

^{13}C NMR (75 MHz, CDCl_3) δ 180.6, 143.4, 142.9, 129.5, 128.4, 121.1, 49.1, 23.5, 18.3.

All spectroscopic data were in agreement with the literature.¹⁴

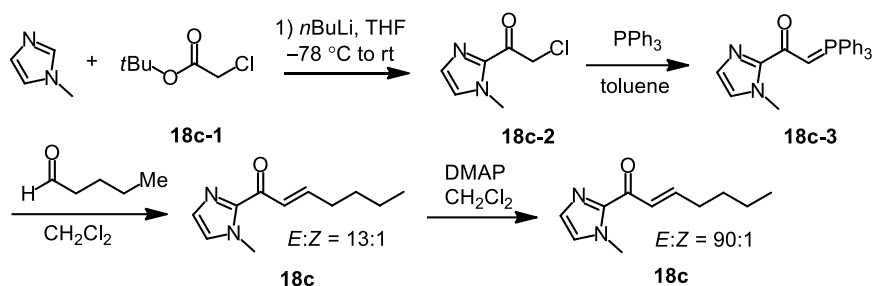
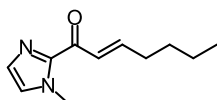
Method C**(E)-Ethyl 4-(1-methyl-1H-imidazol-2-yl)-4-oxobut-2-enoate (18f)**

To a solution of *N*-methylimidazole (2.2 mL, 27.5 mmol) in THF (83.0 mL) at $-78\text{ }^{\circ}\text{C}$ was added dropwise *n*-BuLi (10.0 mL, 2.5 M in hexane, 25.0 mmol). The reaction was stirred at $-78\text{ }^{\circ}\text{C}$ for 10 min, then stirred at room temperature for 30 min. (*E*)-Ethyl 4-oxobut-2-enoate **18f-1** (3.6 mL, 30.0 mmol) was added at $-78\text{ }^{\circ}\text{C}$. After being stirred at $-78\text{ }^{\circ}\text{C}$ for 2 h, the reaction was quenched with H₂O and extracted with EtOAc ($4 \times 100\text{ mL}$). The combined organic layers were dried over anhydrous Na₂SO₄, filtered, and concentrated under reduced pressure. The crude product was dissolved in CH₂Cl₂ (150 mL). Then MnO₂ (34.562 g, 350.0 mmol) was added to the mixture. After being stirred at room temperature for overnight, MnO₂ was removed by filtration. The combined organic layers were concentrated under reduced pressure. The residue was purified by flash chromatography on silica gel (EtOAc/hexane = 1:1) to produce **18f** (619.0 mg, 3.0 mmol, yield: 12%) as a white solid.

¹H NMR (300 MHz, CDCl₃) δ 8.29 (d, $J = 15.9\text{ Hz}$, 1H), 7.22 (s, 1H), 7.11 (s, 1H), 6.91 (d, $J = 15.9\text{ Hz}$, 1H), 4.26 (q, $J = 7.1\text{ Hz}$, 2H), 4.05 (s, 3H), 1.32 (t, $J = 7.1\text{ Hz}$, 2H).

¹³C NMR (75 MHz, CDCl₃) δ 179.4, 165.4, 143.3, 137.0, 131.6, 130.1, 128.1, 61.1, 36.2, 14.1.

All spectroscopic data were in agreement with the literature.¹⁴

Method D**(*E*)-1-(1-Methyl-1*H*-imidazol-2-yl)hept-2-en-1-one (**18c**)**

Preparation of **18c-2.** To a solution of *N*-methylimidazole (1.6 mL, 20.0 mmol) in THF (50.0 mL) at $-78\text{ }^{\circ}\text{C}$ was added dropwise *n*-BuLi (8.0 mL, 2.5 M in hexane, 20.0 mmol). The reaction was stirred at $-78\text{ }^{\circ}\text{C}$ for 10 min, and then stirred at room temperature for additional 30 min. Next, *tert*-butyl 2-chloroacetate **18c-1** (30.0 mmol) was added to the flask at $-78\text{ }^{\circ}\text{C}$. After being stirred at $-78\text{ }^{\circ}\text{C}$ for 2.5 h, the reaction was quenched with H_2O and extracted with EtOAc ($4 \times 50\text{ mL}$). The combined organic layers were dried over anhydrous Na_2SO_4 , filtered, and concentrated under reduced pressure. The residue was purified by flash chromatography on silica gel (EtOAc/hexane = 1:1) to afford **18c-2** (2.519 g, 15.9 mmol, 80%) as a white solid.

Preparation of **18c-3.** To a solution of **18c-2** (2.519 g, 15.9 mmol) in toluene (40.0 mL) at room temperature was added PPh_3 (4.595 g, 17.5 mmol). After being stirred at $95\text{ }^{\circ}\text{C}$ for overnight, the reaction was diluted with 1 *N* HCl (130 mL) and Et_2O (120 mL). The aqueous layer was separated and organic layer was extracted with 1 *N* HCl ($2 \times 30\text{ mL}$). The combined aqueous layers were washed with Et_2O ($2 \times 80\text{ mL}$) and neutralized with aqueous saturated Na_2CO_3 . Then, the aqueous layer was extracted with EtOAc ($3 \times 80\text{ mL}$). The combined organic layers were dried over anhydrous Na_2SO_4 , filtered, and concentrated under reduced pressure to produce Wittig reagent **18c-3** (5.617 g, 14.6 mmol, 92%) as a white solid foam which was used for the next reaction without further purification.

Preparation of **18c.** To a solution of Wittig reagent **18c-3** (3.840 g, 10.0 mmol) in CH_2Cl_2 (50.0 mL) at room temperature was added pentanal (1.3 mL, 12.0 mmol). The reaction was stirred at room temperature overnight. After the solvent was removed in vacuo, the residue was purified by flash chromatography on silica gel (EtOAc/hexane = 1:1) to produce **18c** (0.979 g, 5.1 mmol, 51%) as a mixture of *E*:*Z* isomers (*E*:*Z* = 13:1, determined by ^1H NMR). Then, to a solution of purified **6c** (284.0

mg, 1.48 mmol) in CH_2Cl_2 (5.0 mL) at room temperature was added DMAP (300.0 mg, 2.46 mmol). The reaction was sealed and stored at $-20\text{ }^\circ\text{C}$ (freezer) for 3 days. The mixture was diluted with EtOAc (50 mL) and washed with aqueous saturated NH_4Cl ($2 \times 50\text{ mL}$) followed by brine (50 mL). The combined organic layers were dried over anhydrous Na_2SO_4 , filtered, and concentrated under reduced pressure. The isomerization proceeded well to afford **18c** (280.0 mg, 1.46 mmol, yield = 98% with >97% purity as judged by ^1H NMR) with an improved $E:Z = 90:1$ as determined by ^1H NMR.

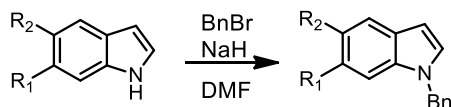
^1H NMR (300 MHz, CDCl_3) δ 7.38 (dt, $J = 15.6, 1.4\text{ Hz}$, 1H), 7.20-6.95 (m, 3H), 4.02 (s, 3H), 2.50-2.02 (m, 2H), 1.58-1.42 (m, 2H), 1.42-1.28 (m, 2H), 0.89 (t, $J = 7.2\text{ Hz}$, 3H).

^{13}C NMR (75 MHz, CDCl_3) δ 180.7, 148.8, 143.7, 129.1, 126.9, 126.1, 36.2, 32.3, 30.2, 22.2, 13.8.

All spectroscopic data were in agreement with the literature.¹⁴

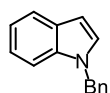
2) Synthesis of Substituted Indoles

The *N*-benzylated indoles **20h-k** were synthesized according to a reported procedure with some modifications.¹⁴ All other indoles were commercially available.



General Procedure for the preparation of *N*-benzylated indoles. To a solution of 1*H*-indole or substituted 1*H*-indole (5.0 mmol) in DMF (10.0 mL) at room temperature was added NaH (220.0 mg, 60% dispersion in mineral oil, 5.5 mmol) and BnBr (1.3 mL, 5.5 mmol) successively. After being stirred at room temperature overnight, the reaction was quenched with aqueous saturated NH_4Cl (5 mL) and extracted with CH_2Cl_2 ($4 \times 10\text{ mL}$). The combined organic layers were dried over anhydrous Na_2SO_4 , filtered, and concentrated under reduced pressure. The residue was purified by flash chromatography on silica gel (EtOAc/hexane = 1:10) to produce **20h-k**.

1-Benzyl-1*H*-indole (**20h**)



Following the general procedure, 1*H*-indole (585.0 mg, 5.0 mmol) was converted to 1-benzyl-1*H*-indole **20h** (983.0 mg, 4.7 mmol, 95%) as a white solid.

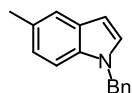
^1H NMR (300 MHz, CDCl_3) δ 8.01-7.90 (m, 1H), 7.57-7.37 (m, 6H), 7.37-7.27 (m, 3H), 6.84 (dd, $J =$

3.2, 0.8 Hz, 1H), 5.44 (s, 2H).

^{13}C NMR (75 MHz, CDCl_3) δ 137.5, 136.2, 128.65, 128.59, 128.1, 127.4, 126.6, 121.6, 120.9, 119.5, 109.6, 101.6, 49.8.

All spectroscopic data were in agreement with the literature.¹⁴

1-Benzyl-5-methyl-1*H*-indole (20i)



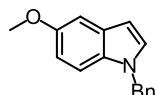
Following the general procedure, 5-methyl-1*H*-indole (656.0 mg, 5.0 mmol) was converted to 1-benzyl-1*H*-indole **20i** (729.0 mg, 3.3 mmol, 66%) as a pale yellow oil.

^1H NMR (300 MHz, CDCl_3) δ 7.35 (d, J = 0.6 Hz, 1H), 7.26-7.11 (m, 3H), 7.07 (d, J = 8.4 Hz, 1H), 7.03-6.96 (m, 3H), 6.90 (dd, J = 8.4, 1.3 Hz, 1H), 6.38 (d, J = 2.8 Hz, 1H), 5.19 (s, 2H), 2.36 (s, 3H).

^{13}C NMR (75 MHz, CDCl_3) δ 137.7, 134.7, 129.0, 128.7, 128.3, 127.5, 126.7, 123.3, 120.6, 109.4, 101.1, 50.1, 21.4.

All spectroscopic data were in agreement with the literature.¹⁴

1-Benzyl-5-methoxy-1*H*-indole (20j)

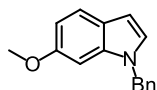


Following the general procedure, 5-methoxy-1*H*-indole (736.0 mg, 5.0 mmol) was converted to 1-benzyl-1*H*-indole **20j** (1.114 g, 4.7 mmol, 94%) as a white solid.

^1H NMR (300 MHz, CDCl_3) δ 7.19-7.08 (m, 3H), 7.05-6.90 (m, 5H), 6.71 (dd, J = 8.8, 2.5 Hz, 1H), 6.35 (d, J = 3.1 Hz, 1H), 5.09 (s, 2H), 3.70 (s, 3H).

^{13}C NMR (75 MHz, CDCl_3) δ 154.1, 137.6, 131.6, 129.1, 128.8, 128.6, 127.5, 126.6, 111.9, 110.4, 102.6, 101.1, 55.7, 50.1.

All spectroscopic data were in agreement with the literature.¹⁴

1-Benzyl-6-methoxy-1H-indole (20k)

Following the general procedure, 6-methoxy-1*H*-indole (736.0 mg, 5.0 mmol) was converted to 1-benzyl-1*H*-indole **20k** (1.078 g, 4.55 mmol, yield: 91%) as a white solid.

¹H NMR (300 MHz, CDCl₃) δ 7.70 (d, J = 8.5 Hz, 1H), 7.51-7.36 (m, 3H), 7.31-7.19 (m, 2H), 7.15 (d, J = 3.2 Hz, 1H), 6.98 (dd, J = 8.6, 2.3 Hz, 1H), 6.91 (d, J = 2.2 Hz, 1H), 6.66 (dd, J = 3.2, 0.8 Hz, 1H), 5.34 (s, 2H), 3.93 (s, 3H).

¹³C NMR (75 MHz, CDCl₃) δ 156.2, 137.4, 137.0, 128.6, 127.4, 127.1, 126.7, 122.9, 121.4, 109.3, 101.5, 93.4, 55.5, 49.8.

All spectroscopic data were in agreement with the literature.¹⁴

5.3.3 Iridium-Catalyzed Reactions

Catalytic Reactions of Table 1. To a solution of catalyst Λ -IrO (1 mol%) in the indicated solvent (entries 1-4: 0.60 mL, 0.5 M; entries 5-8: 0.30 mL, 1.0 M) was added acylimidazole **18a** (45.0 mg, 0.30 mmol) in a glass vial. After being stirred at room temperature for 20 min, 1*H*-indole (entries 1-4: 53.0 mg, 0.45 mmol, 1.5 equiv; entries 5-8: 88.0 mg, 0.75 mmol, 2.5 equiv) was added at room temperature or 0 °C (entries 1-7: room temperature; entry 8: 0 °C). The reaction was stirred at the indicated temperature for 20 or 36 h under argon atmosphere or air as indicated. The conversion was determined by ^1H NMR analysis of the crude product, and *ee* values were determined by chiral HPLC chromatography using a Daicel Chiralpak IC column. Shown below is an example for the calculation of the conversion (Figure 109). It also demonstrates that no significant byproducts are formed in this reaction.

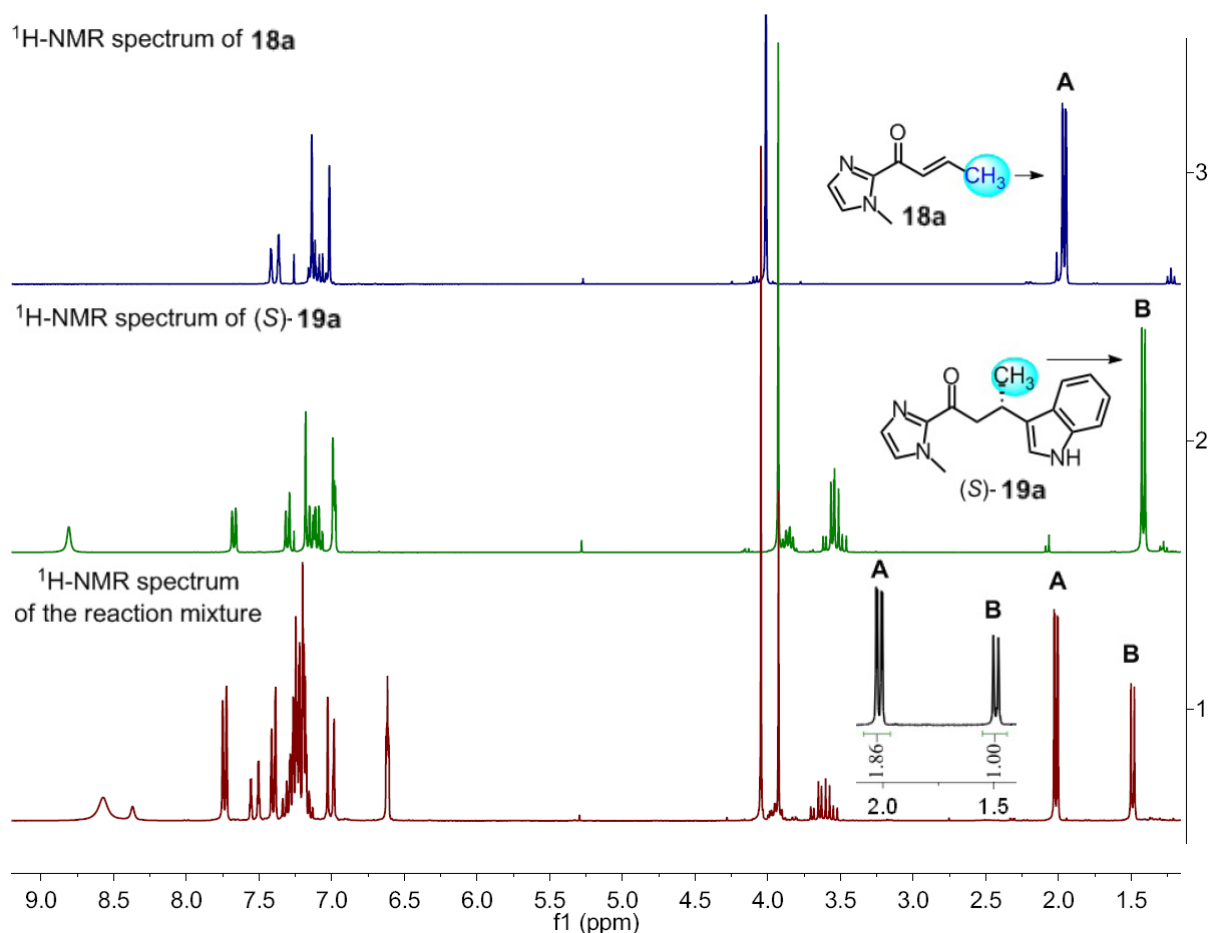
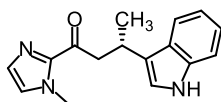


Figure 109 ^1H NMR spectra of **18a**, (*S*)-**19a** (both as reference) and the crude product for the catalysis reaction of entry 1 in Table 1. Area integration ratio = 1.86: 1.00 (conversion = $1.00 / (1.86 + 1.00) \times 100\% = 35\%$).

General Catalysis Procedure (Reactions of Tables 2 and 3). To a solution of catalyst Δ -**IrO** or Δ -**IrO** (0.25-2 mol%) in distilled, anhydrous THF (0.30 mL = 1.0 M, 150.0 μ L = 2.0 M) was added the acylimidazole (0.30 mmol) in a glass vial. After being stirred at room temperature for 20 min, indole or indole derivative (0.75 mmol, 2.5 eq) was added at room temperature or 0 °C. The reaction was stirred at the indicated temperature for the indicated time (conversion monitored by TLC) under argon atmosphere. Afterwards, the mixture was concentrated under reduced pressure. The residue was purified by flash chromatography on silica gel (EtOAc/hexane = 2:3 to 2:1) to afford the products **19a-m** and **21a-f**.

(S)-3-(1*H*-Indol-3-yl)-1-(1-methyl-1*H*-imidazol-2-yl)butan-1-one (19a)



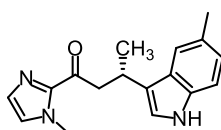
Starting from **18a** (45.0 mg, 0.30 mmol) and 1*H*-indole (88.0 mg, 0.75 mmol) according to the general procedure to give **19a** as a white solid (77.7 mg, 0.291 mmol, yield: 97%). Enantiomeric excess established by HPLC analysis using a Chiralpak IC column, *ee* = 96% (HPLC: IC, 254 nm, hexane/isopropanol = 85:15, flow rate 0.5 mL/min, 40 °C, *t_r* (minor) = 22.5 min, *t_r* (major) = 26.1 min); $[\alpha]_{\text{D}}^{20} = -14.5^{\circ}$ (*c* 2.7, CH₂Cl₂) (Lit.^{S6} $[\alpha]_{\text{D}}^{25} = +9.5^{\circ}$ (*c* 2.4, CH₂Cl₂) for 65% *ee* of product with *R*-configuration).

¹H NMR (300 MHz, CDCl₃) δ 8.81 (br s, 1H), 7.67 (d, *J* = 7.7 Hz, 1H), 7.30 (d, *J* = 7.6 Hz, 1H), 7.22-7.18 (m, 1H), 7.17-7.05 (m, 2H), 6.99 (s, 1H), 6.98-6.95 (m, 1H), 3.93 (s, 3H), 3.91-3.79 (m, 1H), 3.58 (dd, *J* = 16.0, 6.2 Hz, 1H), 3.50 (dd, *J* = 16.0, 8.4 Hz, 1H), 1.42 (d, *J* = 6.9 Hz, 3H).

¹³C NMR (75 MHz, CDCl₃) δ 192.2, 143.2, 136.4, 128.6, 126.8, 126.5, 121.6, 121.2, 120.3, 119.1, 118.9, 111.1, 46.8, 36.1, 27.0, 21.6.

All spectroscopic data were in agreement with the literature.¹⁴

(S)-1-(1-Methyl-1*H*-imidazol-2-yl)-3-(5-methyl-1*H*-indol-3-yl)butan-1-one (19b)



Starting from **18a** (45.0 mg, 0.30 mmol) and 5-methyl-1*H*-indole (98.3 mg, 0.75 mmol) according to

the general procedure to give **19b** as a pale yellow solid (82.6 mg, 0.294 mmol, yield: 98%). Enantiomeric excess established by HPLC analysis using a Chiralpak IC column, *ee* = 94% (HPLC: IC, 254 nm, hexane/isopropanol = 90:10, flow rate 0.5 mL/min, 40 °C, *t_r* (minor) = 34.6 min, *t_r* (major) = 36.5 min); $[\alpha]_{\text{D}}^{20} = -25.1^\circ$ (*c* 1.4, CH₂Cl₂).

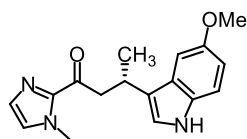
¹H NMR (300 MHz, CDCl₃) δ 8.77 (br s, 1H), 7.44 (d, *J* = 0.6 Hz, 1H), 7.25-7.16 (m, 2H), 7.06-6.96 (m, 2H), 6.94 (d, *J* = 2.3 Hz, 1H), 3.93 (s, 3H), 3.89-3.77 (m, 1H), 3.55 (s, 1H), 3.53 (s, 1H), 2.46 (s, 3H), 1.42 (d, *J* = 6.9 Hz, 3H).

¹³C NMR (75 MHz, CDCl₃) δ 192.3, 143.3, 134.7, 128.7, 127.9, 126.8, 126.7, 123.2, 120.6, 120.4, 118.7, 110.7, 46.8, 36.0, 27.0, 21.6, 21.4.

IR (film): ν (cm⁻¹) 3225, 3136, 3015, 2963, 2917, 2875, 1675, 1446, 1406, 1366, 1288, 1150, 1109, 1079, 983, 921, 868, 792, 765, 695, 667, 630, 546, 427.

HRMS (ESI, *m/z*) calcd for C₁₇H₂₀N₃O [M+H]⁺: 282.1601, found: 282.1603.

(S)-3-(5-Methoxy-1*H*-indol-3-yl)-1-(1-methyl-1*H*-imidazol-2-yl)butan-1-one (19c)



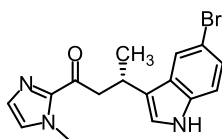
Starting from **18a** (45.0 mg, 0.30 mmol) and 5-methoxy-1*H*-indole (110.3 mg, 0.75 mmol) according to the general procedure to give **19c** as a white solid (88.0 mg, 0.296 mmol, yield: 99%). Enantiomeric excess established by HPLC analysis using a Chiralpak IC column, *ee* = 94% (HPLC: IC, 254 nm, hexane/isopropanol = 85:15, flow rate 0.5 mL/min, 40 °C, *t_r* (minor) = 31.3 min, *t_r* (major) = 37.0 min); $[\alpha]_{\text{D}}^{20} = -11.5^\circ$ (*c* 1.4, CH₂Cl₂).

¹H NMR (300 MHz, CDCl₃) δ 8.85 (br s, 1H), 7.24-7.10 (m, 3H), 7.02-6.97 (m, 1H), 6.95 (d, *J* = 2.3 Hz, 1H), 6.81 (dd, *J* = 8.7, 2.4 Hz, 1H), 3.93 (s, 3H), 3.86 (s, 3H), 3.84-3.73 (m, 1H), 3.58 (dd, *J* = 15.7, 5.8 Hz, 1H), 3.44 (dd, *J* = 15.8, 8.6 Hz, 1H), 1.40 (d, *J* = 6.9 Hz, 3H).

¹³C NMR (75 MHz, CDCl₃) δ 192.2, 153.6, 143.2, 131.5, 128.6, 126.9, 126.8, 121.0, 120.6, 111.9, 111.8, 100.9, 55.8, 46.8, 36.0, 27.0, 21.3.

IR (film): ν (cm⁻¹) 3405, 3224, 2957, 2829, 1668, 1624, 1582, 1479, 1451, 1404, 1280, 1212, 1166, 1112, 1084, 1034, 988, 917, 828, 790, 729, 698, 428.

HRMS (ESI, *m/z*) calcd for C₁₇H₁₉N₃NaO₂ [M+Na]⁺: 320.1369, found: 320.1371.

(S)-3-(5-Bromo-1*H*-indol-3-yl)-1-(1-methyl-1*H*-imidazol-2-yl)butan-1-one (19d)

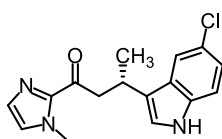
Starting from **18a** (45.0 mg, 0.30 mmol) and 5-bromo-1*H*-indole (146.0 mg, 0.75 mmol) according to the general procedure to give **19d** as a white solid (78.0 mg, 0.226 mmol, yield: 75%). Enantiomeric excess established by HPLC analysis using a Chiralpak IB column, *ee* = 92% (HPLC: IB, 254 nm, solvent A = 0.1% TFA, solvent B = MeCN, with a linear gradient of 30% to 50% B in 40 min, flow rate 0.5 mL/min, 20 °C, *t_r* (minor) = 32.1 min, *t_r* (major) = 33.6 min); $[\alpha]_{\text{D}}^{20} = -23.0^{\circ}$ (*c* 0.5, CH₂Cl₂).

¹H NMR (300 MHz, CDCl₃) δ 8.78 (br s, 1H), 7.75-7.64 (m, 1H), 7.25-7.10 (m, 3H), 7.03 (s, 1H), 6.97 (d, *J* = 2.3 Hz, 1H), 3.93 (s, 3H), 3.85-3.66 (m, 1H), 3.46 (s, 1H), 3.44 (s, 1H), 1.38 (d, *J* = 6.9 Hz, 3H).

¹³C NMR (75 MHz, CDCl₃) δ 191.9, 143.0, 135.0, 128.7, 128.3, 127.0, 124.6, 121.7, 121.5, 121.0, 112.5, 112.3, 47.1, 36.2, 27.0, 21.5.

IR (film): ν (cm⁻¹) 3410, 3151, 2958, 2924, 1667, 1454, 1403, 1330, 1279, 1220, 1153, 1102, 1045, 985, 917, 878, 771, 728, 693, 612, 589, 545, 493, 419.

HRMS (ESI, *m/z*) calcd for C₁₆H₁₆BrN₃NaO [M+Na]⁺: 368.0369, found: 368.0375.

(S)-3-(5-Chloro-1*H*-indol-3-yl)-1-(1-methyl-1*H*-imidazol-2-yl)butan-1-one (19e)

Starting from **18a** (45.0 mg, 0.30 mmol) and 5-chloro-1*H*-indole (114.0 mg, 0.75 mmol) for 48 h according to the general procedure to give **19e** as a white solid (69.6 mg, 0.231 mmol, yield: 77%). Enantiomeric excess established by HPLC analysis using a Chiralpak IB column, *ee* = 94% (HPLC: IB, 254 nm, solvent A = 0.1% TFA, solvent B = MeCN, with a linear gradient of 30% to 45% B in 40 min, flow rate 0.5 mL/min, 20 °C, *t_r* (minor) = 32.0 min, *t_r* (major) = 33.1 min); $[\alpha]_{\text{D}}^{20} = -19.4^{\circ}$ (*c* 0.7, CH₂Cl₂).

¹H NMR (300 MHz, CDCl₃) δ 8.86 (br s, 1H), 7.54 (d, *J* = 1.9 Hz, 1H), 7.25-7.13 (m, 2H), 7.07 (dd, *J* = 8.6, 2.0 Hz, 1H), 7.02 (s, 1H), 6.97 (d, *J* = 2.3 Hz, 1H), 3.93 (s, 3H), 3.84-3.67 (m, 1H), 3.46 (s, 1H),

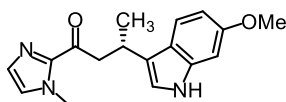
3.44 (d, $J = 1.8$ Hz, 1H), 1.38 (d, $J = 6.9$ Hz, 3H).

^{13}C NMR (75 MHz, CDCl_3) δ 191.9, 143.1, 134.7, 128.8, 127.6, 127.0, 124.7, 122.0, 121.7, 121.1, 118.6, 112.1, 47.0, 36.1, 27.0, 21.5.

IR (film): ν (cm^{-1}) 3162, 3033, 2951, 2903, 1675, 1565, 1451, 1402, 1363, 1292, 1265, 1235, 1154, 1105, 1056, 1009, 967, 922, 888, 861, 818. 771, 728, 693, 636, 566, 538, 415.

HRMS (ESI, m/z) calcd for $\text{C}_{16}\text{H}_{16}\text{ClN}_3\text{NaO}$ $[\text{M}+\text{Na}]^+$: 324.0874, found: 324.0879.

(S)-3-(6-Methoxy-1H-indol-3-yl)-1-(1-methyl-1H-imidazol-2-yl)butan-1-one (19f)



Starting from **18a** (45.0 mg, 0.30 mmol) and 6-methoxy-1H-indole (110.3 mg, 0.75 mmol) according to the general procedure to give **19f** as a white solid (81.0 mg, 0.272 mmol, yield: 91%). Enantiomeric excess established by HPLC analysis using a Chiralpak IC column, $ee = 95\%$ (HPLC: IC, 254 nm, hexane/isopropanol = 80:20, flow rate 0.5 mL/min, 40 °C, t_r (minor) = 27.1 min, t_r (major) = 33.8 min); $[\alpha]_D^{20} = -0.47^\circ$ (c 1.5, CH_2Cl_2).

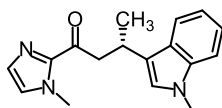
^1H NMR (300 MHz, CDCl_3) δ 8.63 (br s, 1H), 7.65-7.42 (m, 1H), 7.16 (d, $J = 0.9$ Hz, 1H), 7.05-6.93 (m, 1H), 6.85 (d, $J = 1.8$ Hz, 1H), 6.81-6.70 (m, 2H), 3.92 (s, 3H), 3.87-3.72 (m, 4H), 3.55 (dd, $J = 15.9, 6.1$ Hz, 1H), 3.45 (dd, $J = 15.9, 8.4$ Hz, 1H), 1.39 (d, $J = 6.9$ Hz, 3H).

^{13}C NMR (75 MHz, CDCl_3) δ 192.2, 156.2, 143.2, 137.1, 128.7, 126.8, 121.2, 121.0, 119.6, 119.0, 108.8, 94.7, 55.5, 46.8, 36.0, 27.1, 21.6.

IR (film): ν (cm^{-1}) 3402, 3191, 3126, 2957, 2832, 1668, 1625, 1578, 1550, 1502, 1456, 1403, 1299, 1262, 1228, 1197, 1156, 1095, 1019, 985, 917, 779, 697, 655, 596, 550, 513, 460.

HRMS (ESI, m/z) calcd for $\text{C}_{17}\text{H}_{19}\text{N}_3\text{NaO}_2$ $[\text{M}+\text{Na}]^+$: 320.1369, found: 320.1369.

(S)-1-(1-Methyl-1H-imidazol-2-yl)-3-(1-methyl-1H-indol-3-yl)butan-1-one (19g)



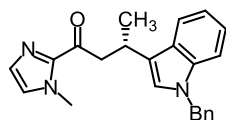
Starting from **18a** (45.0 mg, 0.30 mmol) and 1-methyl-1H-indole (98.3 mg, 0.75 mmol) according to the general procedure to give **19g** as a white solid (83.0 mg, 0.296 mmol, yield: 99%). Enantiomeric excess established by HPLC analysis using a Chiralpak IC column, $ee = 96\%$ (HPLC: IC, 254 nm,

hexane/isopropanol = 85:15, flow rate 0.5 mL/min, 40 °C, t_r (minor) = 21.3 min, t_r (major) = 23.4 min); $[\alpha]_D^{20} = +4.5^\circ$ (c 1.4, CH_2Cl_2). (Lit.^{S6} $[\alpha]_D^{25} = -4.4^\circ$ (c 1.0, CH_2Cl_2) for 93% *ee* of product with *R*-configuration).

^1H NMR (300 MHz, CDCl_3) δ 7.73-7.63 (m, 1H), 7.26 (dd, $J = 7.1, 0.8$ Hz, 1H), 7.24-7.17 (m, 1H), 7.14 (d, $J = 0.9$ Hz, 1H), 7.09 (ddd, $J = 8.0, 6.8, 1.3$ Hz, 1H), 6.97-6.95 (m, 1H), 6.94 (s, 1H), 3.90 (s, 3H), 3.89-3.879 (m, 1H), 3.71 (s, 3H), 3.59 (dd, $J = 15.8, 6.5$ Hz, 1H), 3.46 (dd, $J = 15.8, 8.0$ Hz, 1H), 1.44 (d, $J = 6.9$ Hz, 3H). ^{13}C NMR (75 MHz, CDCl_3) δ 192.2, 143.2, 137.0, 128.7, 126.9, 126.7, 125.0, 121.3, 119.9, 119.3, 118.4, 109.0, 46.8, 36.0, 32.4, 27.1, 21.8.

All spectroscopic data were in agreement with the literature.¹⁴

(S)-3-(1-Benzyl-1*H*-indol-3-yl)-1-(1-methyl-1*H*-imidazol-2-yl)butan-1-one (19h)

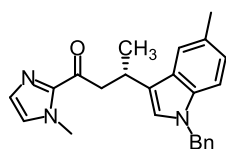


Starting from **18a** (45.0 mg, 0.30 mmol) and 1-benzyl-1*H*-indole (155.3 mg, 0.75 mmol) according to the general procedure to give **19h** as a pale yellow solid (88.0 mg, 0.246 mmol, yield: 82%). Enantiomeric excess established by HPLC analysis using a Chiralpak IC column, *ee* = 95% (HPLC: IC, 254 nm, hexane/isopropanol = 85:15, flow rate 0.5 mL/min, 40 °C, t_r (minor) = 20.0 min, t_r (major) = 23.3 min); $[\alpha]_D^{20} = +3.8^\circ$ (c 1.4, CH_2Cl_2). (Lit.^{S6} $[\alpha]_D^{25} = -2.5^\circ$ (c 4.4, CH_2Cl_2) for 98% *ee* of product with *R*-configuration).

^1H NMR (300 MHz, CDCl_3) δ 7.59 (dd, $J = 7.0, 1.2$ Hz, 1H), 7.22-7.08 (m, 4H), 7.08-6.88 (m, 6H), 6.84 (s, 1H), 5.13 (s, 2H), 3.78 (s, 3H), 3.77-3.68 (m, 1H), 3.48 (dd, $J = 15.7, 6.3$ Hz, 1H), 3.37 (dd, $J = 15.7, 8.3$ Hz, 1H), 1.34 (d, $J = 6.9$ Hz, 3H); ^{13}C NMR (75 MHz, CDCl_3) δ 192.2, 143.2, 137.7, 136.6, 128.9, 128.7, 128.6, 127.4, 127.2, 126.7, 124.5, 121.6, 120.6, 119.4, 118.8, 109.5, 49.8, 46.8, 36.0, 27.2, 21.7.

All spectroscopic data were in agreement with the literature.¹⁴

(S)-3-(1-Benzyl-5-methyl-1*H*-indol-3-yl)-1-(1-methyl-1*H*-imidazol-2-yl)butan-1-one (19i)



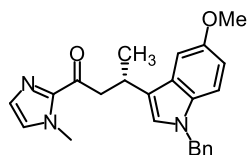
Starting from **18a** (45.0 mg, 0.30 mmol) and 1-benzyl-5-methyl-1*H*-indole (166.0 mg, 0.75 mmol) according to the general procedure to give **19i** as a white solid (102.0 mg, 0.275 mmol, yield: 92%). Enantiomeric excess established by HPLC analysis using a Chiralpak IC column, *ee* = 94% (HPLC: IC, 254 nm, hexane/isopropanol = 90:10, flow rate 0.5 mL/min, 40 °C, *t_r* (minor) = 22.5 min, *t_r* (major) = 24.0 min); $[\alpha]_{\text{D}}^{20} = -7.1^{\circ}$ (*c* 1.7, CH₂Cl₂). (Lit.^{S6} $[\alpha]_{\text{D}}^{25} = +0.13^{\circ}$ (*c* 1.9, CH₂Cl₂) for 93% *ee* of product with *R*-configuration).

¹H NMR (300 MHz, CDCl₃) δ 7.51 (s, 1H), 7.42-7.22 (m, 3H), 7.22-7.07 (m, 4H), 7.06-7.00 (m, 2H), 6.99 (s, 1H), 5.25 (s, 2H), 3.93 (s, 3H), 3.92-3.83 (m, 1H), 3.61 (dd, *J* = 15.7, 6.4 Hz, 1H), 3.54 (dd, *J* = 15.7, 8.2 Hz, 1H), 2.50 (s, 3H), 1.50 (d, *J* = 6.9 Hz, 3H).

¹³C NMR (75 MHz, CDCl₃) δ 192.3, 143.3, 137.9, 135.0, 128.7, 128.5, 127.8, 127.4, 127.3, 126.64, 126.57, 124.6, 123.1, 120.0, 119.0, 109.2, 49.8, 46.8, 35.9, 27.2, 21.7, 21.4.

All spectroscopic data were in agreement with the literature.¹⁴

(S)-3-(1-Benzyl-5-methoxy-1*H*-indol-3-yl)-1-(1-methyl-1*H*-imidazol-2-yl)butan-1-one (19j)

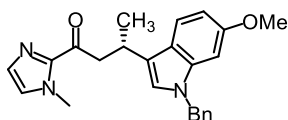


Starting from **18a** (45.0 mg, 0.30 mmol) and 1-benzyl-5-methoxy-1*H*-indole (178.0 mg, 0.75 mmol) according to the general procedure to give **19j** as a white solid (106.0 mg, 0.274 mmol, yield: 91%). Enantiomeric excess established by HPLC analysis using a Chiralpak IC column, *ee* = 94% (HPLC: IC, 254 nm, hexane/isopropanol = 85:15, flow rate 0.5 mL/min, 40 °C, *t_r* (minor) = 25.9 min, *t_r* (major) = 30.2 min); $[\alpha]_{\text{D}}^{20} = +3.6^{\circ}$ (*c* 1.8, CH₂Cl₂). (Lit.⁶ $[\alpha]_{\text{D}}^{25} = -0.06^{\circ}$ (*c* 1.4, CH₂Cl₂) for 97% *ee* of product with *R*-configuration).

¹H NMR (300 MHz, CDCl₃) δ 7.35-7.27 (m, 3H), 7.25 (d, *J* = 2.3 Hz, 1H), 7.19-7.09 (m, 4H), 7.06 (s, 1H), 7.00 (s, 1H), 6.86 (dd, *J* = 8.8, 2.4 Hz, 1H), 5.24 (s, 2H), 3.94 (s, 3H), 3.91 (s, 3H), 3.90-3.84 (m, 1H), 3.66 (dd, *J* = 15.4, 6.1 Hz, 1H), 3.45 (dd, *J* = 15.4, 8.5 Hz, 1H), 1.49 (d, *J* = 6.9 Hz, 3H);

¹³C NMR (75 MHz, CDCl₃) δ 192.3, 153.6, 143.3, 137.8, 131.9, 128.7, 128.5, 127.5, 127.3, 126.7, 126.6, 125.0, 120.1, 111.7, 110.3, 101.3, 55.8, 50.0, 46.8, 35.9, 27.2, 21.4.

All spectroscopic data were in agreement with the literature.¹⁴

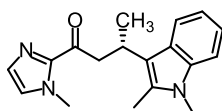
(S)-3-(1-Benzyl-6-methoxy-1*H*-indol-3-yl)-1-(1-methyl-1*H*-imidazol-2-yl)butan-1-one (19k)

Starting from **18a** (45.0 mg, 0.30 mmol) and 1-benzyl-6-methoxy-1*H*-indole (178.0 mg, 0.75 mmol) according to the general procedure to give **19k** as a pale yellow solid (104.0 mg, 0.269 mmol, yield: 90%). Enantiomeric excess established by HPLC analysis using a Chiralpak IC column, *ee* = 95% (HPLC: IC, 254 nm, hexane/isopropanol = 85:15, flow rate 0.5 mL/min, 40 °C, *t_r* (minor) = 30.4 min, *t_r* (major) = 41.1 min); $[\alpha]_{\text{D}}^{20} = +11.0^\circ$ (*c* 1.7, CH₂Cl₂). (Lit.^{S6} $[\alpha]_{\text{D}}^{25} = -0.11^\circ$ (*c* 1.4, CH₂Cl₂) for 95% *ee* of product with *R*-configuration).

¹H NMR (300 MHz, CDCl₃) δ 7.45 (d, *J* = 8.6 Hz, 1H), 7.26-7.09 (m, 3H), 7.01 (d, *J* = 0.9 Hz, 1H), 6.96 (dd, *J* = 7.7, 1.7 Hz, 2H), 6.91-6.82 (m, 1H), 6.79 (d, *J* = 0.4 Hz, 1H), 6.66 (dd, *J* = 8.7, 2.2 Hz, 1H), 6.58 (d, *J* = 2.2 Hz, 1H), 5.07 (s, 2H), 3.78 (s, 3H), 3.76-3.69 (m, 1H), 3.67 (s, 3H), 3.45 (dd, *J* = 15.7, 6.2 Hz, 1H), 3.33 (dd, *J* = 15.7, 8.3 Hz, 1H), 1.31 (d, *J* = 6.9 Hz, 3H).

¹³C NMR (75 MHz, CDCl₃) δ 192.2, 156.2, 143.2, 137.6, 137.4, 128.7, 128.6, 127.3, 126.7, 126.6, 123.3, 121.7, 120.6, 120.0, 108.4, 93.4, 55.6, 49.7, 46.8, 36.0, 27.3, 21.6.

All spectroscopic data were in agreement with the literature.¹⁴

(S)-3-(1,2-Dimethyl-1*H*-indol-3-yl)-1-(1-methyl-1*H*-imidazol-2-yl)butan-1-one (19l)

Starting from **18a** (45.0 mg, 0.30 mmol) and 1,2-dimethyl-1*H*-indole (109.0 mg, 0.75 mmol) for 36 h according to the general procedure to give **19l** as a white solid (82.4 mg, 0.279 mmol, yield: 93%). Enantiomeric excess established by HPLC analysis using a Chiralpak IC column, *ee* = 98% (HPLC: IC, 254 nm, hexane/isopropanol = 85:15, flow rate 0.5 mL/min, 40 °C, *t_r* (major) = 25.9 min, *t_r* (minor) = 32.7 min); $[\alpha]_{\text{D}}^{20} = +65.2^\circ$ (*c* 1.2, CH₂Cl₂). (Lit.^{S6} $[\alpha]_{\text{D}}^{25} = -63.4^\circ$ (*c* 2.2, CH₂Cl₂) for 91% *ee* of product with *R*-configuration).

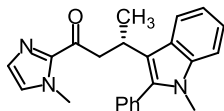
¹H NMR (300 MHz, CDCl₃) δ 7.74 (d, *J* = 7.4 Hz, 1H), 7.21 (d, *J* = 7.6 Hz, 1H), 7.17-6.99 (m, 3H), 6.95-6.82 (m, 1H), 4.00-3.75 (m, 4H), 3.68 (s, 1H), 3.65 (s, 1H), 3.60 (s, 3H), 2.44 (s, 3H), 1.51 (d, *J* = 7.1 Hz, 3H);

¹³C NMR (75 MHz, CDCl₃) δ 192.2, 143.1, 136.6, 132.1, 128.6, 126.5, 126.1, 120.0, 119.2, 118.3,

114.7, 108.5, 46.3, 35.8, 29.2, 27.2, 21.2, 10.5.

All spectroscopic data were in agreement with the literature.¹⁴

(S)-1-(1-Methyl-1*H*-imidazol-2-yl)-3-(1-methyl-2-phenyl-1*H*-indol-3-yl)butan-1-one (19m)



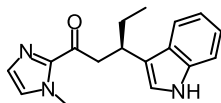
Starting from **18a** (45.0 mg, 0.30 mmol) and 1-methyl-2-phenyl-1*H*-indole (155.5 mg, 0.75 mmol) according to the general procedure to give **19m** as a white solid (104.0 mg, 0.291 mmol, yield: 97%). Enantiomeric excess established by HPLC analysis using a Chiralpak IC column, *ee* = 90% (HPLC: IC, 254 nm, hexane/isopropanol = 85:15, flow rate 0.5 mL/min, 40 °C, *t_r* (major) = 20.7 min, *t_r* (minor) = 36.7 min); [α]_D²⁰ = +20.3° (*c* 1.8, CH₂Cl₂). (Lit.^{S6} [α]_D²⁵ = −0.24° (*c* 1.65, CH₂Cl₂) for 91% *ee* of product with *R*-configuration).

¹H NMR (300 MHz, CDCl₃) δ 7.72 (d, *J* = 7.8 Hz, 1H), 7.42-7.24 (m, 5H), 7.19 (d, *J* = 8.0 Hz, 1H), 7.15-7.06 (m, 1H), 7.01 (ddd, *J* = 8.0, 7.0, 1.2 Hz, 1H), 6.94 (d, *J* = 0.9 Hz, 1H), 6.77 (s, 1H), 3.70 (s, 3H), 3.66-3.53 (m, 2H), 3.50-3.39 (m, 1H), 3.38 (s, 3H), 1.30 (d, *J* = 6.6 Hz, 3H).

¹³C NMR (75 MHz, CDCl₃) δ 192.1, 143.1, 137.2, 137.1, 132.2, 130.8, 128.6, 128.1, 128.0, 126.4, 126.1, 121.2, 120.2, 118.9, 116.8, 109.3, 46.4, 35.8, 30.5, 27.9, 21.5.

All spectroscopic data were in agreement with the literature.¹⁴

(R)-3-(1*H*-Indol-3-yl)-1-(1-methyl-1*H*-imidazol-2-yl)pentan-1-one (21a)



Starting from **18b** (49.0 mg, 0.30 mmol) and 1*H*-indole (88.0 mg, 0.75 mmol) according to the general procedure to give **21a** as a white solid (75.0 mg, 0.267 mmol, yield: 89%). Enantiomeric excess established by HPLC analysis using a Chiralpak IC column, *ee* = 96% (HPLC: IC, 254 nm, hexane/isopropanol = 90:10, flow rate 0.5 mL/min, 40 °C, *t_r* (minor) = 38.4 min, *t_r* (major) = 40.7 min); [α]_D²⁰ = −15.8° (*c* 0.5, CH₂Cl₂).

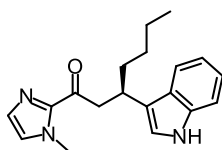
¹H NMR (300 MHz, CDCl₃) δ 8.34 (br s, 1H), 7.55 (d, *J* = 7.8 Hz, 1H), 7.26-7.14 (m, 1H), 7.11-6.94 (m, 3H), 6.92 (d, *J* = 2.3 Hz, 1H), 6.88-6.85 (m, 1H), 3.76 (s, 3H), 3.65-3.51 (m, 1H), 3.51-3.41 (m, 2H), 1.88-1.62 (m, 2H), 0.78 (t, *J* = 7.4 Hz, 3H);

^{13}C NMR (75 MHz, CDCl_3) δ 192.3, 143.2, 136.3, 128.6, 127.0, 126.7, 121.6, 121.2, 119.3, 119.1, 118.9, 111.0, 45.1, 36.0, 33.9, 28.9, 11.9.

IR (film): ν (cm^{-1}) 3409, 3214, 2961, 2925, 2871, 1669, 1456, 1404, 1339, 1287, 1256, 1154, 1100, 1014, 976, 915, 773, 734, 697, 591, 555, 480, 426.

HRMS (ESI, m/z) calcd for $\text{C}_{17}\text{H}_{19}\text{N}_3\text{NaO}$ $[\text{M}+\text{Na}]^+$: 304.1420, found: 304.1421.

(R)-3-(1H-Indol-3-yl)-1-(1-methyl-1H-imidazol-2-yl)heptan-1-one (21b)



Starting from **18c** (58.0 mg, 0.30 mmol) and 1H-indole (88.0 mg, 0.75 mmol) according to the general procedure to give **21b** as a white solid (90.0 mg, 0.291 mmol, yield: 97%). Enantiomeric excess established by HPLC analysis using a Chiralpak IC column, $ee = 91\%$ (HPLC: IC, 254 nm, hexane/isopropanol = 85:15, flow rate 0.5 mL/min, 40 °C, t_r (minor) = 21.5 min, t_r (major) = 23.9 min); $[\alpha]_D^{20} = +5.7^\circ$ (c 1.2, CH_2Cl_2).

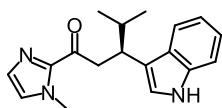
^1H NMR (300 MHz, CDCl_3) δ 8.51 (br s, 1H), 7.54 (d, $J = 7.8$ Hz, 1H), 7.28-7.13 (m, 1H), 7.11-6.92 (m, 3H), 6.88 (d, $J = 2.3$ Hz, 1H), 6.85 (d, $J = 0.5$ Hz, 1H), 3.75 (s, 3H), 3.70-3.54 (m, 1H), 3.47 (s, 1H), 3.45 (d, $J = 1.8$ Hz, 1H), 1.68 (dt, $J = 8.3, 7.4$ Hz, 2H), 1.25-1.04 (m, 4H), 0.71 (t, $J = 6.9$ Hz, 3H).

^{13}C NMR (75 MHz, CDCl_3) δ 192.3, 143.3, 136.3, 128.6, 127.0, 126.7, 121.5, 121.1, 119.5, 119.3, 118.8, 111.0, 45.6, 36.0, 35.9, 32.3, 29.6, 22.7, 14.0.

IR (film): ν (cm^{-1}) 3410, 3215, 3052, 2954, 2925, 2860, 1670, 1458, 1405, 1340, 1285, 1153, 1101, 1016, 977, 915, 771, 736, 698, 425.

HRMS (ESI, m/z) calcd for $\text{C}_{19}\text{H}_{23}\text{N}_3\text{NaO}$ $[\text{M}+\text{Na}]^+$: 332.1733, found: 332.1733.

(S)-3-(1H-Indol-3-yl)-4-methyl-1-(1-methyl-1H-imidazol-2-yl)pentan-1-one (21c)



Starting from **18d** (54.0 mg, 0.30 mmol) and 1H-indole (88.0 mg, 0.75 mmol) according to the general procedure to give **21c** as a pale yellow solid (69.0 mg, 0.234 mmol, yield: 78%). Enantiomeric excess

established by HPLC analysis using a Chiralpak IC column, $ee = 93\%$ (HPLC: IC, 254 nm, hexane/isopropanol = 85:15, flow rate 0.5 mL/min, 40 °C, t_r (minor) = 17.6 min, t_r (major) = 19.8 min); $[\alpha]_D^{20} = +20.3^\circ$ (c 0.8, CH_2Cl_2).

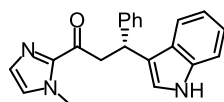
^1H NMR (300 MHz, CDCl_3) δ 8.14 (br s, 1H), 7.68-7.37 (m, 1H), 7.29-7.12 (m, 1H), 7.12-6.89 (m, 4H), 6.83 (s, 1H), 3.67 (s, 3H), 3.64-3.49 (m, 2H), 3.43-3.31 (m, 1H), 2.13-1.93 (m, 1H), 0.86 (d, $J = 4.6$ Hz, 3H), 0.84 (d, $J = 4.6$ Hz, 3H).

^{13}C NMR (75 MHz, CDCl_3) δ 192.5, 143.3, 136.1, 128.5, 127.7, 126.6, 121.8, 121.5, 119.5, 118.9, 118.1, 110.9, 41.9, 38.4, 35.9, 32.9, 20.4, 20.2.

IR (film): ν (cm^{-1}) 3410, 3216, 3053, 2957, 2871, 1670, 1457, 1404, 1339, 1287, 1256, 1225, 1154, 1099, 1029, 988, 918, 769, 738, 692, 610, 476, 425.

HRMS (ESI, m/z) calcd for $\text{C}_{18}\text{H}_{22}\text{N}_3\text{O}$ $[\text{M}+\text{H}]^+$: 296.1757, found: 296.1760.

(*R*)-3-(1*H*-Indol-3-yl)-1-(1-methyl-1*H*-imidazol-2-yl)-3-phenylpropan-1-one (21d)



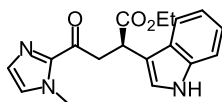
Starting from **18e** (63.6 mg, 0.30 mmol) and 1*H*-indole (88.0 mg, 0.75 mmol) according to the general procedure to give **21d** as a white solid (97.2 mg, 0.295 mmol, yield: 98%). Enantiomeric excess established by HPLC analysis using a Chiralpak IC column, $ee = 93\%$ (HPLC: IC, 254 nm, hexane/isopropanol = 85:15, flow rate 0.5 mL/min, 40 °C, t_r (minor) = 25.4 min, t_r (major) = 35.4 min); $[\alpha]_D^{20} = -92.5^\circ$ (c 0.9, CH_2Cl_2).

^1H NMR (300 MHz, CD_2Cl_2) δ 8.48 (br s, 1H), 7.44 (d, $J = 7.9$ Hz, 1H), 7.40-7.28 (m, 3H), 7.29-7.20 (m, 2H), 7.20-7.07 (m, 4H), 7.04 (s, 1H), 7.02-6.93 (m, 1H), 5.02 (t, $J = 7.6$ Hz, 1H), 4.02 (dd, $J = 16.3, 7.6$ Hz, 1H), 3.88 (s, 3H), 3.78 (dd, $J = 16.3, 7.8$ Hz, 1H);

^{13}C NMR (75 MHz, CD_2Cl_2) δ 191.3, 145.2, 143.7, 137.0, 129.1, 128.7, 128.3, 127.5, 127.2, 126.5, 122.4, 121.9, 119.6, 119.6, 111.5, 45.7, 38.6, 36.4.

IR (film): ν (cm^{-1}) 3218, 3113, 3052, 2903, 1670, 1620, 1548, 1485, 1451, 1409, 1332, 1294, 1262, 1207, 1153, 1107, 1029, 973, 950, 919, 852, 730, 697, 636, 583, 561, 421.

HRMS (ESI, m/z) calcd for $\text{C}_{21}\text{H}_{19}\text{N}_3\text{NaO}$ $[\text{M}+\text{Na}]^+$: 352.1420, found: 352.1422.

(R)-Ethyl 2-(1H-indol-3-yl)-4-(1-methyl-1H-imidazol-2-yl)-4-oxobutanoate (21e)

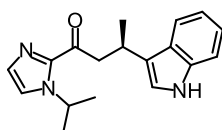
Starting from **18f** (62.0 mg, 0.30 mmol) and 1*H*-indole (88.0 mg, 0.75 mmol) according to the general procedure to give **21e** as a white solid (95.0 mg, 0.292 mmol, yield: 97%). Enantiomeric excess established by HPLC analysis using a Chiralpak IC column, *ee* = 98% (HPLC: IC, 254 nm, hexane/isopropanol = 70:30, flow rate 0.5 mL/min, 40 °C, *t_r* (minor) = 25.8 min, *t_r* (major) = 35.3 min); $[\alpha]_{\text{D}}^{20} = -70.7^{\circ}$ (*c* 1.8, CH₂Cl₂).

¹H NMR (300 MHz, CDCl₃) δ 9.90 (br s, 1H), 7.85-7.73 (m, 1H), 7.37-7.26 (m, 1H), 7.21 (d, *J* = 0.9 Hz, 1H), 7.19-7.07 (m, 3H), 7.04 (d, *J* = 0.4 Hz, 1H), 4.55 (dd, *J* = 11.0, 3.7 Hz, 1H), 4.28 (dd, *J* = 18.2, 11.0 Hz, 1H), 4.14 (dt, *J* = 17.9, 10.8, 7.1 Hz, 2H), 3.98 (s, 3H), 3.60 (dd, *J* = 18.2, 3.8 Hz, 1H), 1.20 (t, *J* = 7.1 Hz, 3H).

¹³C NMR (75 MHz, CDCl₃) δ 190.4, 173.9, 142.4, 136.2, 128.7, 127.0, 126.3, 122.2, 121.8, 119.3, 119.1, 112.3, 111.3, 60.8, 42.0, 37.4, 36.0, 14.0.

IR (film): ν (cm⁻¹) 3223, 2990, 2917, 1716, 1678, 1448, 1408, 1362, 1347, 1269, 1238, 1212, 1170, 1096, 1056, 1019, 980, 919, 898, 864, 782, 750, 727, 682, 618, 565, 519, 485, 462, 421.

HRMS (ESI, *m/z*) calcd for C₁₈H₁₉N₃NaO₃ [M+Na]⁺: 348.1319, found: 348.1319.

(R)-3-(1H-Indol-3-yl)-1-(1-isopropyl-1H-imidazol-2-yl)butan-1-one (21f)

Starting from **18g** (54.0 mg, 0.30 mmol) and 1*H*-indole (88.0 mg, 0.75 mmol) according to the general procedure to give **21f** as a white solid (88.0 mg, 0.298 mmol, yield: 99%). Enantiomeric excess established by HPLC analysis using a Chiralpak IC column, *ee* = 97% (HPLC: IC, 254 nm, hexane/isopropanol = 90:10, flow rate 0.5 mL/min, 40 °C, *t_r* (major) = 30.8 min, *t_r* (minor) = 33.6 min); $[\alpha]_{\text{D}}^{20} = +5.4^{\circ}$ (*c* 1.2, CH₂Cl₂).

¹H NMR (300 MHz, CDCl₃) δ 8.87 (br s, 1H), 7.57 (d, *J* = 7.6 Hz, 1H), 7.18 (d, *J* = 8.1 Hz, 1H), 7.12 (dd, *J* = 7.9, 0.9 Hz, 2H), 7.00 (dtd, *J* = 14.6, 7.0, 1.2 Hz, 2H), 6.84 (d, *J* = 2.2 Hz, 1H), 5.40 (hept, *J* = 6.7 Hz, 1H), 3.86-3.67 (m, 1H), 3.45 (dd, *J* = 7.3, 2.5 Hz, 2H), 1.30 (d, *J* = 4.8 Hz, 3H), 1.28 (d, *J* =

2.4 Hz, 3H), 1.26 (d, $J = 4.6$ Hz, 3H);

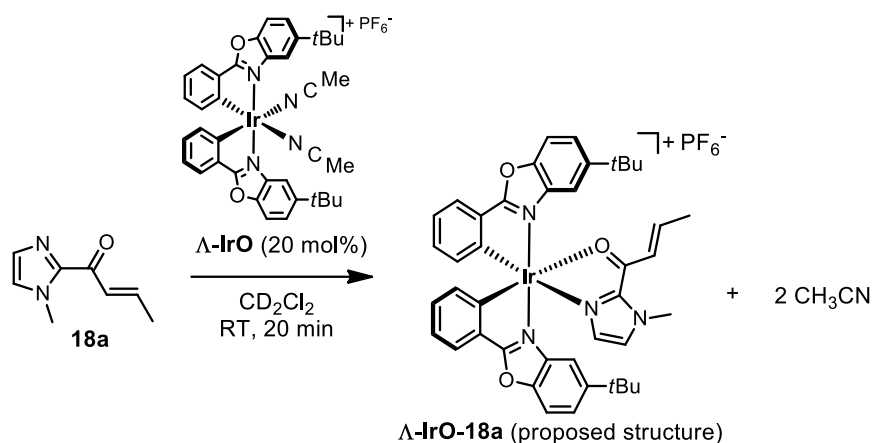
^{13}C NMR (75 MHz, CDCl_3) δ 192.4, 142.5, 136.4, 129.1, 126.5, 121.5, 121.2, 121.0, 120.3, 119.0, 118.8, 111.1, 49.1, 47.4, 27.1, 23.43, 23.39, 21.5.

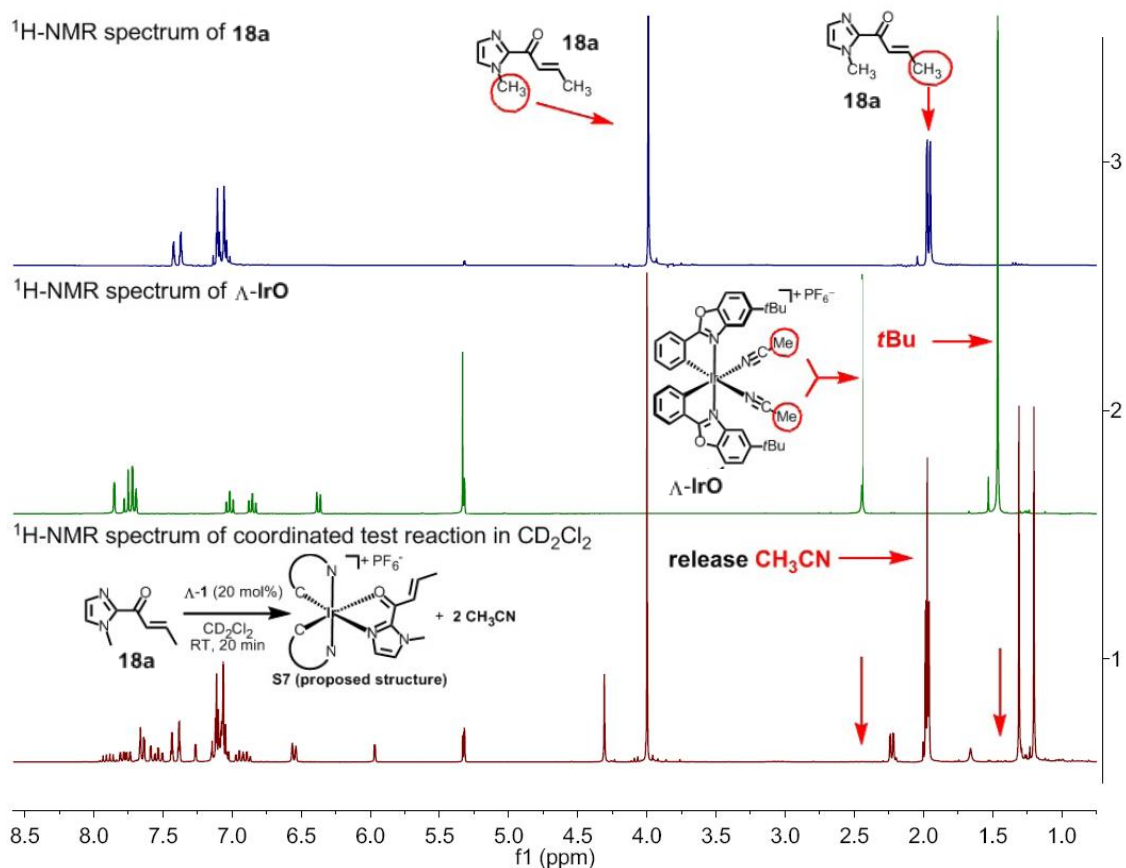
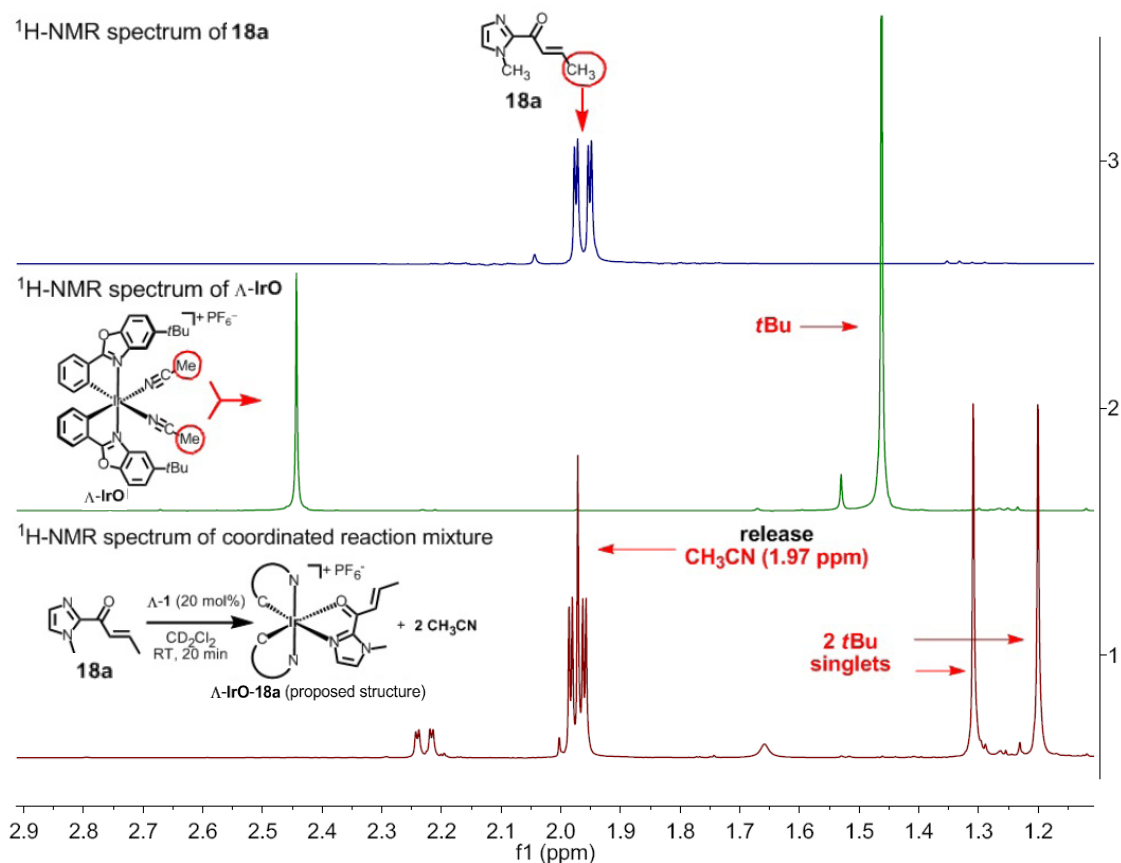
IR (film): ν (cm^{-1}) 3175, 3106, 3070, 2974, 2950, 2923, 2868, 1660, 1456, 1387, 1341, 1257, 1223, 1157, 1132, 1092, 1044, 1001, 927, 878, 816, 782, 745, 708, 679, 638, 578, 482, 428.

HRMS (ESI, m/z) calcd for $\text{C}_{18}\text{H}_{21}\text{N}_3\text{NaO}$ $[\text{M}+\text{Na}]^+$: 318.1577, found: 318.1580.

5.3.4 Investigation of the Proposed Substrate-Coordinated Catalyst

To a solution of $\Lambda\text{-IrO}$ (10.0 mg, 0.011 mmol) in CD_2Cl_2 (1.0 mL) at room temperature was added **18a** (8.2 mg, 0.054 mmol). The reaction was stirred at room temperature for 20 min and then analyzed by ^1H NMR spectroscopy. The fast bidentate coordination of **18a** to the catalyst could be found, and the released CH_3CN was obvious (see Figure 110, 111). When used 1.0 equivalent **18a**, the proposed intermediate $\Lambda\text{-IrO-18a}$ was obtained as a black solid (90% purity as judged by ^1H NMR). The ^1H NMR and ^{13}C NMR spectra were also consistent with the hypothesis structure $\Lambda\text{-IrO-18a}$. When tried to purify the intermediate $\Lambda\text{-IrO-18a}$ by flash silica gel column chromatography, it decomposed on the silica gel column.



Figure 110 ¹H-NMR spectra of substrate-coordinated catalyst.Figure 111 Partial ¹H-NMR spectra of substrate-coordinated catalyst.

5.3.5 Investigation of the Stability of Iridium Catalyst Λ -IrO

1) Catalyst Stability Investigated by ^1H NMR

The iridium complex Λ -IrO (12.0 mg) was dissolved in CD_2Cl_2 and kept in the NMR tube at room temperature under reduced light. ^1H -NMR spectra were recorded after 2, 4, 6, and 8 days (see Figure 112).

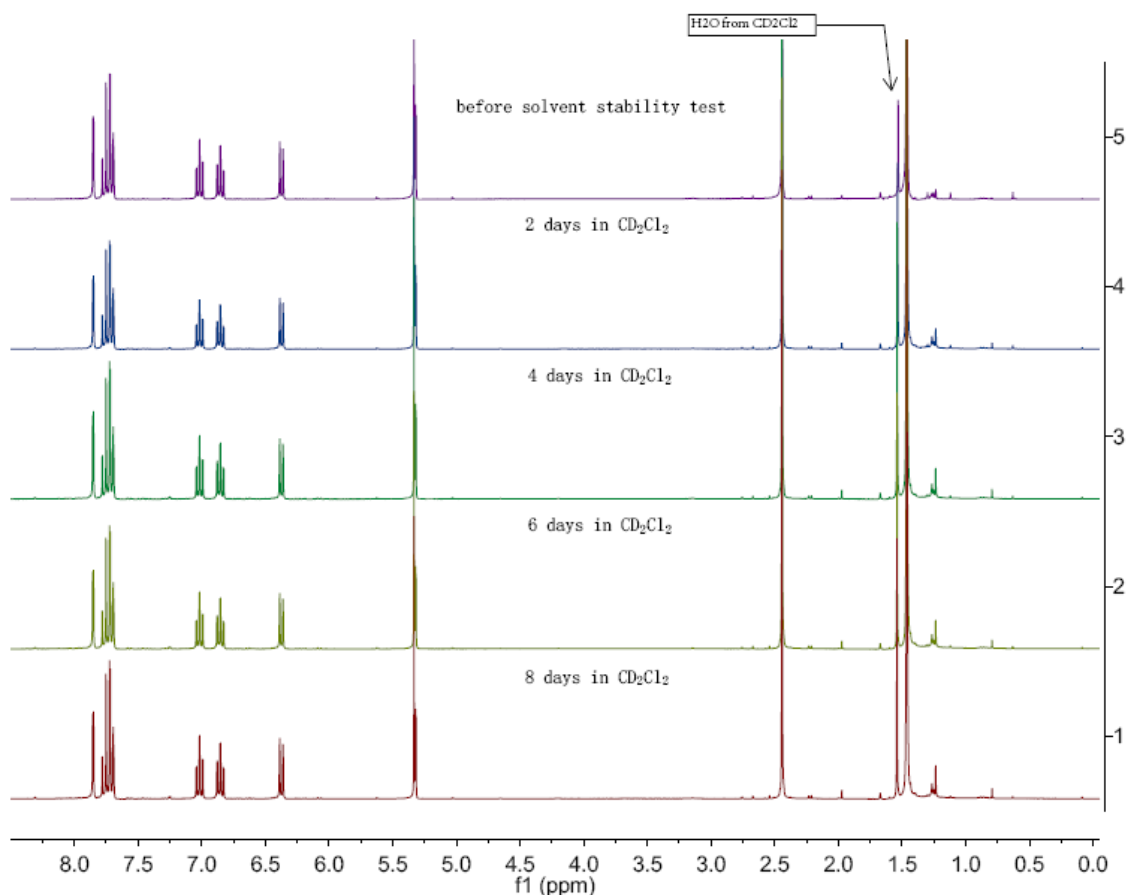


Figure 112 ^1H NMR of Λ -IrO recorded in CD_2Cl_2 over 8 days.

2) Catalyst Stability Investigated by Chiral HPLC

Enantiopure iridium complexes Λ -IrO (2.0 mg) and Δ -IrO (2.0 mg) were dissolved in CH_2Cl_2 (1.0 mL, HPLC grade). A solution containing 99.5% Λ -IrO (995.0 μL) and 0.5% Δ -IrO (5.0 μL) was prepared and the enantiomeric ratio was then monitored over time while kept in a brown glass vial at room temperature. The HPLC spectra were collected after 2-8 days. HPLC conditions: Daicel Chiralpak IB (250 \times 4.6 mm) HPLC column, the column temperature was 20 $^\circ\text{C}$ and UV-absorption was measured at 254 nm. Solvent A = 0.1% TFA, solvent B = MeCN with a linear gradient of 20% to 43% B in 60 min at a flow rate = 0.5 mL/min (Figures 113-117).

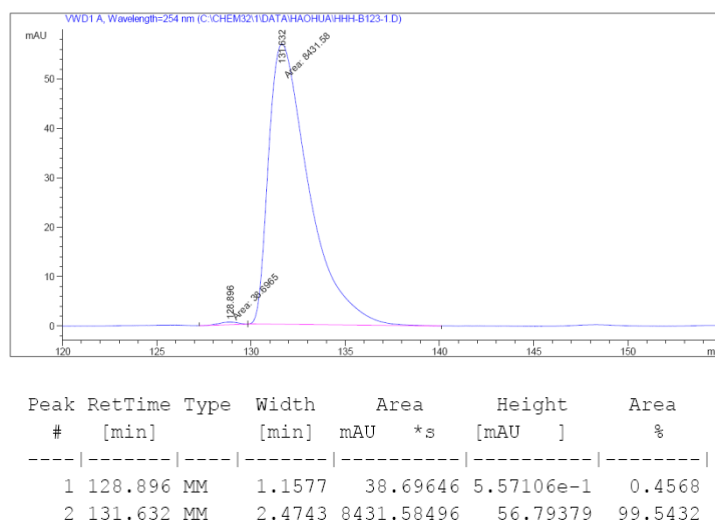


Figure 113 HPLC trace of the freshly prepared mixture Λ -IrO: Δ -IrO. Area integration = 99.5:0.5 (99.0% *ee*)

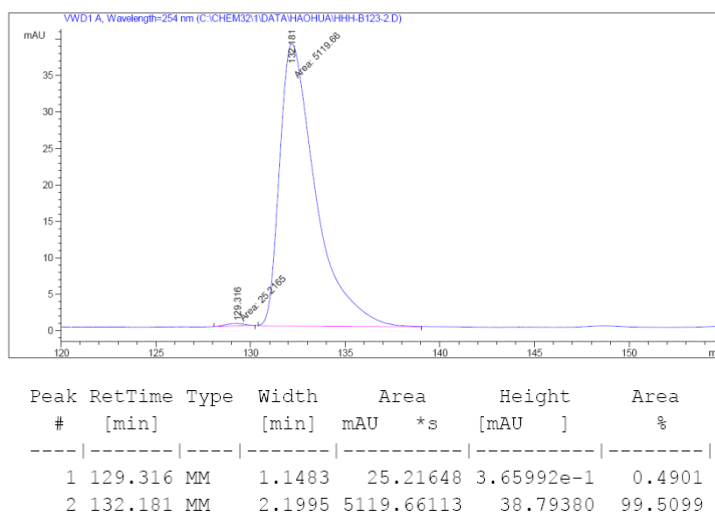


Figure 114 HPLC trace after 2 days in CH_2Cl_2 . Area integration = 99.5:0.5 (99.0% *ee*)

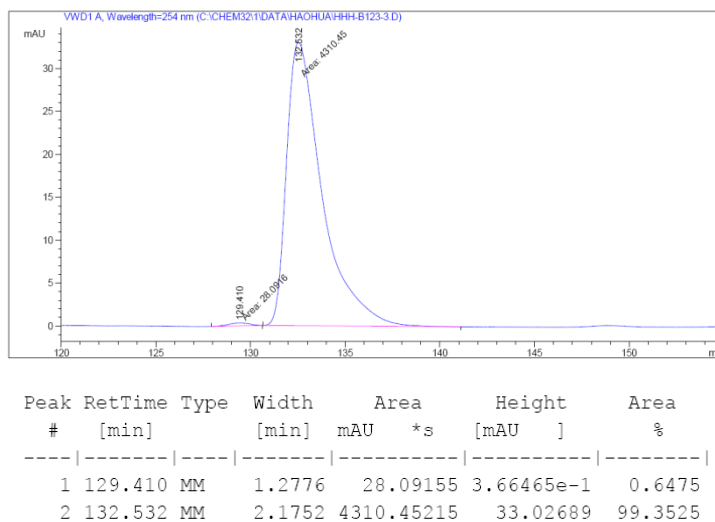


Figure 115 HPLC trace after 4 days in CH_2Cl_2 . Area integration = 99.4:0.6 (98.8% *ee*)

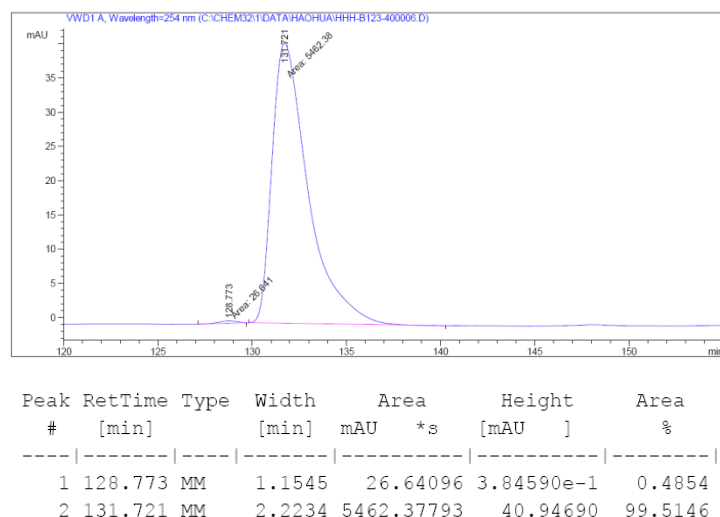


Figure 116 HPLC trace after 6 days in CH₂Cl₂. Area integration = 99.5:0.5 (99.0% *ee*)

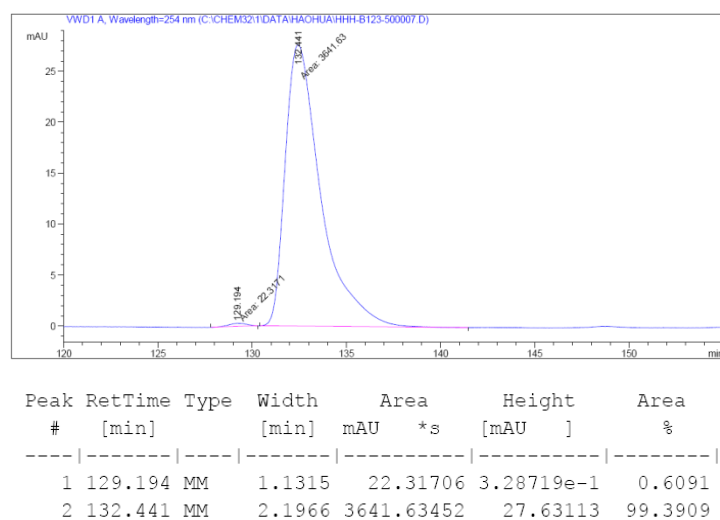


Figure 117 HPLC trace after 8 days in CH₂Cl₂. Area integration = 99.4:0.6 (98.8% *ee*)

5.3.6 Single Crystal X-Ray Diffraction of Iridium Catalyst Δ -IrO

Crystals of Δ -IrO were obtained by slow diffusion from a solution of Δ -IrO in CH₂Cl₂ layered with Et₂O. Data were collected on a STOE-IPDS2T diffractometer employing graphite-monochromated Mo-K α radiation ($\lambda = 0.71073$ Å) at a temperature of 100 K. The structure was solved by direct methods (SIR92). Refinement was done by full-matrix least squares based on F² data of one twin domain using SHELXS-97, SHELXL-2013. The absolute configuration was determined. The structure information is shown Appendices 6.7.

5.4 Visible-Light-Activated Asymmetric Alkylation of 2-Acyl Imidazoles

5.4.1 Synthesis of Substrates

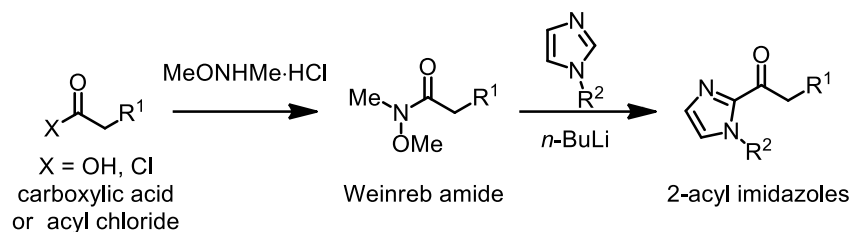
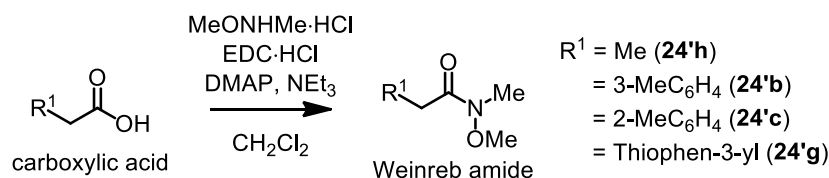


Figure 118 Synthesis of the 2-acyl imidazoles.

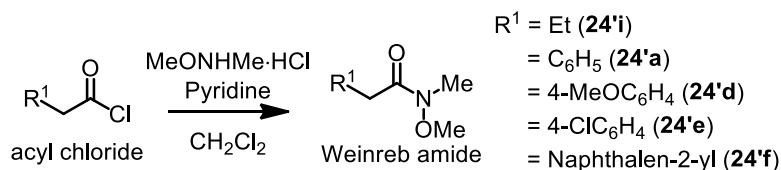
1) Synthesis of Weinreb Amides

All Weinreb amides were synthesized according to reported procedures with some modifications (methods A-B).¹⁵

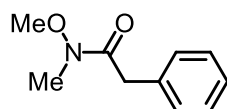
Method A:



To a mixture of the corresponding carboxylic acid (10.0 mmol), *N,O*-dimethylhydroxylamine hydrochloride (1.268 g, 13.0 mmol) and DMAP (0.122 g, 1.0 mmol) in CH₂Cl₂ (50.0 mL) at 0 °C were added NEt₃ (1.8 mL, 13.3 mmol) and EDC (2.492 g, 13.0 mmol) successively. The reaction mixture was stirred at 0 °C for 1 h, then allowed to warm to room temperature and stirred overnight. The reaction was diluted with EtOAc (100 mL). The organic layer was washed with 1 *N* HCl (3 × 10 mL), aqueous saturated NaHCO₃ (3 × 10 mL), and brine (20 mL). The combined organic layers were dried over anhydrous Na₂SO₄, filtered, and concentrated under reduced pressure. The residue was purified by flash chromatography on silica gel (EtOAc/hexane = 1:3).

Method B:

To a solution of *N,O*-dimethylhydroxylamine hydrochloride (1.073 g, 11.0 mmol) in CH_2Cl_2 (20.0 mL) at 0 °C were added the corresponding acyl chloride (10.0 mmol) and pyridine (2.0 mL, 25.0 mmol) successively. The reaction was stirred at 0 °C for 30 min, then stirred at room temperature for additional 30 min. The reaction was diluted with EtOAc (100 mL). The organic layer was washed with 1 *N* HCl (3 × 10 mL), aqueous saturated NaHCO_3 (3 × 10 mL), and brine (20 mL). The combined organic layers were dried over anhydrous Na_2SO_4 , filtered, and concentrated under reduced pressure. The residue was purified by flash chromatography on silica gel (EtOAc/hexane = 1:3).

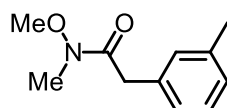
***N*-Methoxy-*N*-methyl-2-phenylacetamide (**24'a**)**

Following the general method B, 2-phenylacetyl chloride (1.546 g, 10.0 mmol) was converted to Weinreb amide **24'a** (1.790 g, 9.5 mmol, yield: 95%) as a colorless oil.

^1H NMR (300 MHz, CDCl_3) δ 7.46-7.15 (m, 5H), 3.79 (s, 2H), 3.62 (s, 3H), 3.21 (s, 3H).

^{13}C NMR (75 MHz, CDCl_3) δ 172.3, 134.9, 129.2, 128.4, 126.7, 61.2, 39.3, 32.2.

All spectroscopic data were in agreement with the literature.¹⁶

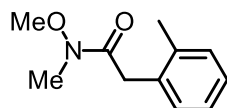
***N*-Methoxy-*N*-methyl-2-(*m*-tolyl)acetamide (**24'b**)**

Following the general method A, 2-(*m*-tolyl)acetic acid (1.500 g, 10.0 mmol) was converted to Weinreb amide **24'b** (1.776 g, 9.2 mmol, yield: 92%) as a colorless oil.

^1H NMR (300 MHz, CDCl_3) δ 7.27-6.83 (m, 4H), 3.66 (s, 2H), 3.53 (s, 3H), 3.11 (s, 3H), 2.26 (s, 3H).

^{13}C NMR (75 MHz, CDCl_3) δ 172.4, 138.0, 134.8, 129.9, 128.3, 127.5, 126.3, 61.2, 39.3, 32.2, 21.3.

All spectroscopic data were in agreement with the literature.¹⁵

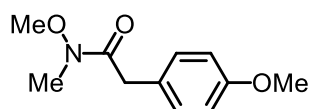
***N*-Methoxy-*N*-methyl-2-(*o*-tolyl)acetamide (**24'**c)**

Following the general method A, 2-(*o*-tolyl)acetic acid (1.500 g, 10.0 mmol) was converted to Weinreb amide **24'**c (1.821 g, 9.4 mmol, yield: 94%) as a colorless oil.

^1H NMR (300 MHz, CDCl_3) δ 7.16-6.96 (m, 4H), 3.70 (s, 2H), 3.52 (s, 3H), 3.13 (s, 3H), 2.23 (s, 3H).

^{13}C NMR (75 MHz, CDCl_3) δ 172.5, 136.8, 133.6, 130.2, 129.8, 126.9, 126.0, 61.1, 37.1, 32.4, 19.6.

All spectroscopic data were in agreement with the literature.¹⁵

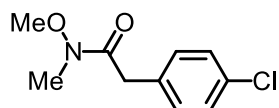
***N*-Methoxy-2-(4-methoxyphenyl)-*N*-methylacetamide (**24'**d)**

Following the general method B, 2-(4-methoxyphenyl)acetyl chloride (1.846 g, 10.0 mmol) was converted to Weinreb amide **24'**d (1.861 g, 8.9 mmol, yield: 89%) as a colorless oil.

^1H NMR (300 MHz, CDCl_3) δ 7.23 (d, J = 8.8 Hz, 2H), 6.87 (d, J = 8.7 Hz, 2H), 3.80 (s, 3H), 3.72 (s, 2H), 3.63 (s, 3H), 3.20 (s, 3H).

^{13}C NMR (75 MHz, CDCl_3) δ 172.7, 158.4, 130.2, 126.9, 113.9, 61.2, 55.2, 38.4, 32.2.

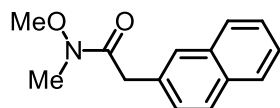
All spectroscopic data were in agreement with the literature.¹⁷

2-(4-Chlorophenyl)-*N*-methoxy-*N*-methylacetamide (24'**e)**

Following the general method B, 2-(4-chlorophenyl)acetyl chloride (1.880 g, 10.0 mmol) was converted to Weinreb amide **24'**e (2.051 g, 9.6 mmol, yield: 96%) as pale yellow solid.

^1H NMR (300 MHz, CDCl_3) δ 7.31 (d, J = 8.6 Hz, 2H), 7.24 (d, J = 8.6 Hz, 2H), 3.76 (s, 2H), 3.65 (s, 3H), 3.21 (s, 3H).

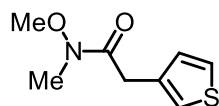
All spectroscopic data were in agreement with the literature.¹⁸

***N*-Methoxy-*N*-methyl-2-(naphthalen-2-yl)acetamide (24'f)**

Following the general method B, 2-(naphthalen-2-yl)acetyl chloride (2.040 g, 10.0 mmol) was converted to Weinreb amide **24'f** (2.130 g, 9.3 mmol, yield: 93%) as a yellow oil.

^1H NMR (300 MHz, CDCl_3) δ 7.97-7.65 (m, 4H), 7.56-7.35 (m, 3H), 3.97 (s, 2H), 3.63 (s, 3H), 3.24 (s, 3H).

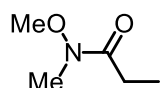
All spectroscopic data were in agreement with the literature.¹⁹

***N*-Methoxy-*N*-methyl-2-(thiophen-3-yl)acetamide (24'g)**

Following the general method A, 2-(thiophen-3-yl)acetic acid (1.421 g, 10.0 mmol) was converted to Weinreb amide **24'g** (1.702 g, 9.2 mmol, yield: 92%) as a colorless oil.

^1H NMR (300 MHz, CDCl_3) δ 7.30 (dd, J = 4.9, 3.0 Hz, 1H), 7.19-7.12 (m, 1H), 7.08 (dd, J = 4.9, 1.2 Hz, 1H), 3.82 (s, 2H), 3.65 (s, 3H), 3.22 (s, 3H).

All spectroscopic data were in agreement with the literature.²⁰

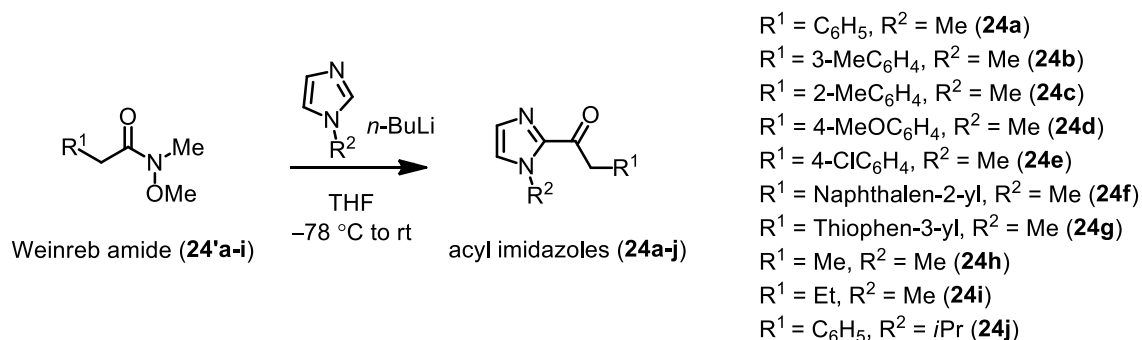
***N*-Methoxy-*N*-methylpropionamide (24'h)**

Following the general method A, propionic acid (1.421 g, 10.0 mmol) was converted to Weinreb amide **24'h** (1.030 g, 8.8 mmol, yield: 88%) as a colorless oil.

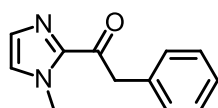
^1H NMR (300 MHz, CDCl_3) δ 3.77-3.51 (m, 3H), 3.19 (s, 3H), 2.46 (q, J = 7.5 Hz, 2H), 1.15 (t, J = 7.5 Hz, 2H).

All spectroscopic data were in agreement with the literature.²¹

2) Synthesis of 2-Acyl Imidazoles



General procedure for the preparation of the 2-acyl imidazoles. To a solution of *N*-methylimidazole or *N*-isopropylimidazole (1.1 eq) in THF (0.4 M referring to the Weinreb amide **24'a-i**) at $-78\text{ }^\circ\text{C}$ was added *n*-BuLi (1.1 eq) dropwise. The reaction was stirred at $-78\text{ }^\circ\text{C}$ for 30 min, then stirred at room temperature for 30 min. The corresponding Weinreb amide **24'** (1.0 eq in THF) was added dropwise to the flask after the reaction was cooled back down to $-78\text{ }^\circ\text{C}$. The reaction was allowed to warm to room temperature slowly (over a period of 3-4 h) and stirred overnight. The reaction was quenched with AcOH (6.0 eq) at room temperature and extracted with EtOAc. The organic layer was washed with aqueous saturated NaHCO_3 and brine. The combined organic layers were dried over anhydrous Na_2SO_4 , filtered, and concentrated under reduced pressure. The residue was purified by flash chromatography on silica gel (EtOAc/hexane = 1:3) to produce **24a-j**.

1-(1-Methyl-1*H*-imidazol-2-yl)-2-phenylethanone (**24a**)

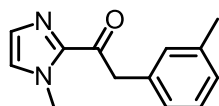
Following the general procedure, Weinreb amide **24'a** (3.580 g, 20.0 mmol) was converted to 2-acyl imidazole **24a** (3.721 g, 18.6 mmol, yield: 93%) as a colorless oil.

^1H NMR (300 MHz, CDCl_3) δ 7.32-7.13 (m, 5H), 7.11 (d, $J = 0.8\text{ Hz}$, 1H), 6.96 (s, 1H), 4.36 (s, 2H), 3.88 (s, 3H).

^{13}C NMR (75 MHz, CDCl_3) δ 190.1, 142.8, 134.6, 129.9, 129.2, 128.4, 127.3, 126.8, 45.4, 36.1.

IR (film): ν (cm^{-1}) 3109, 3061, 3029, 2954, 1670, 1459, 1399, 1284, 1153, 1077, 992, 913, 774, 731, 694, 468.

HRMS (ESI, m/z) calcd for $\text{C}_{12}\text{H}_{12}\text{N}_2\text{ONa}$ $[\text{M}+\text{Na}]^+$: 223.0842, found: 223.0843.

1-(1-Methyl-1H-imidazol-2-yl)-2-(*m*-tolyl)ethanone (24b)

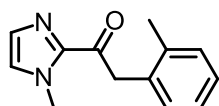
Following the general procedure, Weinreb amide **24'b** (1.776 g, 9.2 mmol) was converted to 2-acyl imidazole **24b** (1.702 g, 8.0 mmol, yield: 87%) as a colorless oil.

^1H NMR (300 MHz, CDCl_3) δ 7.33-6.94 (m, 6H), 4.42 (s, 2H), 3.99 (s, 3H), 2.36 (s, 3H).

^{13}C NMR (75 MHz, CDCl_3) δ 190.2, 142.8, 138.0, 134.4, 130.6, 129.2, 128.3, 127.6, 127.3, 126.9, 45.3, 36.2, 21.3.

IR (film): ν (cm^{-1}) 3108, 3019, 2919, 1672, 1605, 1464, 1399, 1285, 1153, 1085, 1027, 994, 913, 766, 696.

HRMS (ESI, m/z) calcd for $\text{C}_{12}\text{H}_{15}\text{N}_2\text{O}$ $[\text{M}+\text{H}]^+$: 215.1179, found: 215.1176.

1-(1-Methyl-1H-imidazol-2-yl)-2-(*o*-tolyl)ethanone (24c)

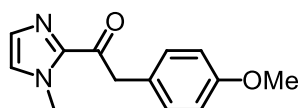
Following the general procedure, Weinreb amide **24'c** (1.821 g, 9.4 mmol) was converted to 2-acyl imidazole **24c** (1.627 g, 7.6 mmol, yield: 81%) as a colorless oil.

^1H NMR (300 MHz, CDCl_3) δ 7.23-7.04 (m, 5H), 6.97 (d, J = 0.4 Hz, 1H), 4.42 (s, 2H), 3.89 (s, 3H), 2.24 (s, 3H).

^{13}C NMR (75 MHz, CDCl_3) δ 190.0, 142.8, 137.2, 133.3, 130.7, 130.2, 129.1, 127.2, 127.1, 125.9, 43.2, 36.1, 19.8.

IR (film): ν (cm^{-1}) 3108, 3017, 2954, 1672, 1463, 1399, 1285, 1153, 993, 913, 775, 742, 686, 603.

HRMS (ESI, m/z) calcd for $\text{C}_{12}\text{H}_{15}\text{N}_2\text{O}$ $[\text{M}+\text{H}]^+$: 215.1179, found: 215.1178.

2-(4-Methoxyphenyl)-1-(1-methyl-1H-imidazol-2-yl)ethanone (24d)

Following the general procedure, Weinreb amide **24'd** (1.861 g, 8.9 mmol) was converted to 2-acyl imidazole **24d** (1.476 g, 6.4 mmol, yield: 72%) as a white solid.

^1H NMR (300 MHz, CDCl_3) δ 7.29 (d, J = 8.5 Hz, 2H), 7.20 (d, J = 0.7 Hz, 1H), 7.05 (s, 1H), 6.88 (d,

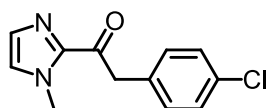
$J = 8.7$ Hz, 2H), 4.38 (s, 2H), 3.97 (s, 3H), 3.79 (s, 3H).

^{13}C NMR (75 MHz, CDCl_3) δ 190.4, 158.5, 142.7, 130.8, 129.2, 127.2, 126.6, 113.9, 55.2, 44.5, 36.1.

IR (film): ν (cm^{-1}) 3112, 3010, 2954, 2833, 1666, 1607, 1504, 1395, 1241, 1156, 1109, 1081, 1026, 911, 822, 782, 716, 664, 631, 602, 521, 418.

HRMS (ESI, m/z) calcd for $\text{C}_{13}\text{H}_{15}\text{N}_2\text{O}_2$ $[\text{M}+\text{H}]^+$: 231.1128, found: 231.1133.

2-(4-Chlorophenyl)-1-(1-methyl-1H-imidazol-2-yl)ethanone (**24e**)



Following the general procedure, Weinreb amide **24'e** (1.819 g, 8.5 mmol) was converted to 2-acyl imidazole **24e** (1.595 g, 6.8 mmol, yield: 80%) as a white solid.

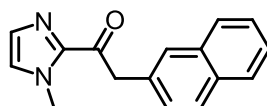
^1H NMR (300 MHz, CDCl_3) δ 7.21 (s, 4H), 7.11 (d, $J = 0.9$ Hz, 1H), 6.98 (s, 1H), 4.32 (s, 2H), 3.89 (s, 3H).

^{13}C NMR (75 MHz, CDCl_3) δ 189.5, 142.5, 133.0, 132.8, 131.2, 129.3, 128.5, 127.5, 44.6, 36.1.

IR (film): ν (cm^{-1}) 3102, 2961, 2909, 1670, 1484, 1401, 1316, 1289, 1226, 1197, 1150, 1083, 990, 908, 857, 828, 802, 766, 681, 532, 496, 419.

HRMS (ESI, m/z) calcd for $\text{C}_{12}\text{H}_{12}\text{ClN}_2\text{O}$ $[\text{M}+\text{H}]^+$: 235.0633, found: 235.0635.

1-(1-Methyl-1H-imidazol-2-yl)-2-(naphthalen-2-yl)ethanone (**24f**)



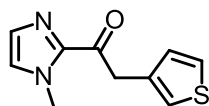
Following the general procedure, Weinreb amide **24'f** (2.061 g, 9.0 mmol) was converted to 2-acyl imidazole **24f** (1.959 g, 7.8 mmol, yield: 87%) as a pale yellow oil.

^1H NMR (300 MHz, CDCl_3) δ 8.00-7.74 (m, 4H), 7.52 (dd, $J = 8.4, 1.7$ Hz, 1H), 7.50-7.41 (m, 2H), 7.23 (d, $J = 0.9$ Hz, 1H), 7.03 (s, 1H), 4.62 (s, 2H), 3.96 (s, 3H).

^{13}C NMR (75 MHz, CDCl_3) δ 190.0, 142.7, 133.4, 132.3, 132.1, 129.2, 128.5, 128.0, 127.9, 127.6, 127.5, 127.4, 125.9, 125.5, 45.5, 36.1.

IR (film): ν (cm^{-1}) 3122, 3053, 2932, 1665, 1504, 1465, 1396, 1263, 1148, 1076, 1028, 951, 910, 837, 788, 680, 627, 591, 475.

HRMS (ESI, m/z) calcd for $\text{C}_{16}\text{H}_{15}\text{N}_2\text{O}$ $[\text{M}+\text{H}]^+$: 251.1179, found: 251.1177.

1-(1-Methyl-1H-imidazol-2-yl)-2-(thiophen-3-yl)ethanone (24g)

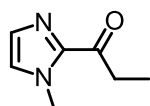
Following the general procedure, Weinreb amide **24'g** (1.300 g, 7.0 mmol) was converted to 2-acyl imidazole **24g** (1.150 g, 5.6 mmol, yield: 80%) as a white solid.

^1H NMR (300 MHz, CDCl_3) δ 7.28 (dd, $J = 4.7, 3.2$ Hz, 1H), 7.25-7.15 (m, 2H), 7.10 (dd, $J = 4.9, 1.2$ Hz, 1H), 7.05 (s, 1H), 4.47 (s, 2H), 3.98 (s, 3H).

^{13}C NMR (75 MHz, CDCl_3) δ 189.4, 142.5, 134.1, 129.2, 129.0, 127.3, 125.3, 123.1, 39.8, 36.1.

IR (film): ν (cm^{-1}) 3099, 2952, 1665, 1466, 1401, 1280, 1225, 1142, 1073, 1029, 943, 915, 858, 819, 774, 689, 606, 516.

HRMS (ESI, m/z) calcd for $\text{C}_{10}\text{H}_{11}\text{N}_2\text{OS}$ $[\text{M}+\text{H}]^+$: 207.0587, found: 207.0585.

1-(1-Methyl-1H-imidazol-2-yl)propan-1-one (24h)

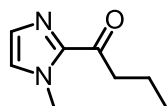
Following the general procedure, Weinreb amide **24'h** (0.960 g, 8.2 mmol) was converted to 2-acyl imidazole **24h** (0.872 g, 6.3 mmol, yield: 77%) as a colorless oil.

^1H NMR (300 MHz, CDCl_3) δ 7.09 (d, $J = 0.7$ Hz, 1H), 7.00 (s, 1H), 3.97 (s, 3H), 3.11 (q, $J = 7.4$ Hz, 2H), 1.16 (t, $J = 7.4$ Hz, 3H).

^{13}C NMR (75 MHz, CDCl_3) δ 193.7, 142.9, 128.8, 126.6, 36.0, 32.2, 8.0.

IR (film): ν (cm^{-1}) 3108, 2976, 2939, 2879, 1672, 1460, 1404, 1289, 1227, 1154, 1090, 1011, 948, 911, 768, 696, 683.

HRMS (ESI, m/z) calcd for $\text{C}_7\text{H}_{10}\text{N}_2\text{ONa}$ $[\text{M}+\text{Na}]^+$: 161.0685, found: 161.0685.

1-(1-Methyl-1H-imidazol-2-yl)butan-1-one (24i)

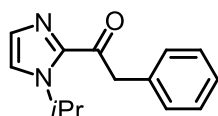
Following the general procedure, Weinreb amide **24'i** (1.049 g, 8.0 mmol) was converted to 2-acyl imidazole **24i** (0.876 g, 5.8 mmol, yield: 72%) as a colorless oil.

^1H NMR (300 MHz, CDCl_3) δ 7.14 (s, 1H), 7.03 (s, 1H), 4.01 (s, 3H), 3.28-3.01 (m, 2H), 1.87-1.65 (m, 2H), 1.01 (t, $J = 7.4$ Hz, 3H).

^{13}C NMR (75 MHz, CDCl_3) δ 193.2, 143.0, 128.8, 126.7, 41.0, 36.2, 17.7, 13.8.

IR (film): ν (cm^{-1}) 3108, 2962, 2874, 1671, 1463, 1405, 1285, 1225, 1154, 1113, 1081, 1044, 991, 914, 891, 769, 693.

HRMS (ESI, m/z) calcd for $\text{C}_8\text{H}_{12}\text{N}_2\text{O}[\text{M}+\text{Na}]^+$: 175.0842, found: 175.0842.

1-(1-Isopropyl-1H-imidazol-2-yl)-2-phenylethanone (24j)

Following the general procedure, Weinreb amide **24'a** (1.790 g, 10.0 mmol) was converted to 2-acyl imidazole **24j** (2.032 g, 8.9 mmol, yield: 89%) as a colorless oil.

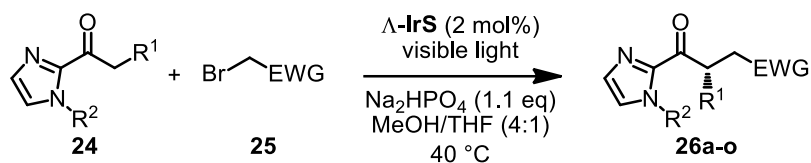
^1H NMR (300 MHz, CDCl_3) δ 7.39-7.23 (m, 7H), 5.77-5.33 (m, 1H), 4.49 (s, 2H), 1.43 (d, $J = 6.7$ Hz, 6H).

^{13}C NMR (75 MHz, CDCl_3) δ 190.2, 142.0, 134.7, 129.9, 129.6, 128.4, 126.7, 121.5, 49.3, 46.0, 23.5.

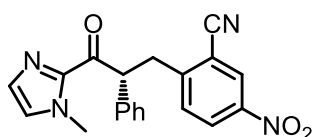
IR (film): ν (cm^{-1}) 3061, 3029, 2977, 2934, 1671, 1494, 1456, 1390, 1255, 1215, 1139, 1080, 1010, 984, 914, 772, 730, 696, 617, 544, 518, 477.

HRMS (ESI, m/z) calcd for $\text{C}_{14}\text{H}_{17}\text{N}_2\text{O}[\text{M}+\text{H}]^+$: 229.1335, found: 229.1333.

5.4.2 Iridium-Catalyzed Photoredox Reactions



General catalysis procedure. A dried 10 mL Schlenk tube was charged with the catalyst $\Delta\text{-IrS}$ (2 mol%), Na_2HPO_4 (31.2 mg, 0.22 mmol, 1.1 eq) and the corresponding bromide (0.2 mmol, 1.0 eq). The tube was purged with argon and MeOH/THF (4:1, 0.5 mL) was added via syringe, followed by the corresponding 2-acyl imidazoles (0.6 mmol, 3.0 eq). The reaction mixture was degassed via freeze-pump-thaw for three cycles. After the mixture was thoroughly degassed, the vial was sealed and positioned approximately 5 cm from a 14 w white light energy saving lamp. The reaction was stirred at 40 °C for the indicated time (monitored by TLC) under argon atmosphere. Afterwards, the mixture was diluted with CH_2Cl_2 (8 mL), the inorganic salt was removed by centrifugation. The combined organic layers were concentrated under reduced pressure. The residue was purified by flash chromatography on silica gel (EtOAc/hexane = 1:5 to 1:3) to afford the products **26a-o**. Racemic samples were obtained by carrying out the reactions with *rac*-**IrS**. The enantiomeric excess was determined by chiral HPLC analysis.

(R)-2-(3-(1-Methyl-1H-imidazol-2-yl)-3-oxo-2-phenylpropyl)-5-nitrobenzonitrile (26a)

Starting from 2-acyl imidazole **24a** (120.0 mg, 0.60 mmol) and 2-(bromomethyl)-5-nitrobenzonitrile (48.0 mg, 0.20 mmol) according to the general procedure to give **26a** as a white solid (72.0 mg, 0.20 mmol, yield: 100%). Enantiomeric excess established by HPLC analysis using a Chiralpak AD-H column, *ee* = 99% (HPLC: AD-H, 254 nm, hexane/isopropanol = 90:10, flow rate 0.8 mL/min, 25 °C, t_r (minor) = 44.6 min, t_r (major) = 49.8 min). $[\alpha]_D^{25} = -145.9^\circ$ (*c* 1.0, CH_2Cl_2).

^1H NMR (300 MHz, CDCl_3) δ 8.34 (d, *J* = 2.4 Hz, 1H), 8.14 (dd, *J* = 8.6, 2.4 Hz, 1H), 7.43 (d, *J* = 8.6 Hz, 1H), 7.37-7.29 (m, 2H), 7.26-7.11 (m, 3H), 7.01 (d, *J* = 0.8 Hz, 1H), 6.89 (s, 1H), 5.52 (t, *J* = 7.7

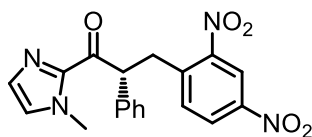
Hz, 1H), 3.86 (s, 3H), 3.72 (dd, $J = 14.2, 8.3$ Hz, 1H), 3.40 (dd, $J = 14.2, 7.2$ Hz, 1H).

^{13}C NMR (75 MHz, CDCl_3) δ 189.6, 150.7, 146.2, 142.1, 137.2, 131.4, 129.6, 128.9, 128.5, 127.7, 127.6, 126.9, 115.8, 114.6, 53.0, 37.1, 36.0.

IR (film): ν (cm^{-1}) 3058, 2959, 2867, 1663, 1591, 1522, 1478, 1445, 1398, 1354, 1272, 1078, 1037, 735, 694.

HRMS (ESI, m/z) calcd for $\text{C}_{20}\text{H}_{16}\text{N}_4\text{O}_3\text{Na}$ $[\text{M}+\text{Na}]^+$: 383.1115, found: 383.1110.

(R)-3-(2,4-Dinitrophenyl)-1-(1-methyl-1H-imidazol-2-yl)-2-phenylpropan-1-one (26b)



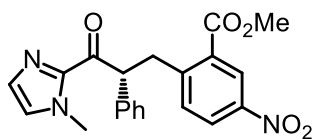
Starting from 2-acyl imidazole **24a** (120.0 mg, 0.60 mmol) and 1-(bromomethyl)-2,4-dinitrobenzene (52.2 mg, 0.20 mmol) according to the general procedure to give **26b** as a white solid (73.7 mg, 0.194 mmol, yield: 97%). Enantiomeric excess established by HPLC analysis using a Chiralpak AD-H column, $ee = 99\%$ (HPLC: AD-H, 254 nm, hexane/isopropanol = 85:15, flow rate 0.8 mL/min, 25 °C, t_r (major) = 27.4 min, t_r (minor) = 29.0 min). $[\alpha]_{\text{D}}^{25} = -138.6^\circ$ (c 1.0, CH_2Cl_2).

^1H NMR (300 MHz, CDCl_3) δ 8.66 (d, $J = 2.4$ Hz, 1H), 8.14 (dd, $J = 8.5, 2.4$ Hz, 1H), 7.41 (d, $J = 8.6$ Hz, 1H), 7.36-7.26 (m, 2H), 7.26-7.10 (m, 3H), 6.99 (d, $J = 0.8$ Hz, 1H), 6.88 (s, 1H), 5.51 (dd, $J = 8.0, 6.9$ Hz, 1H), 3.86 (s, 3H), 3.80 (dd, $J = 13.8, 8.1$ Hz, 1H), 3.44 (dd, $J = 13.8, 6.7$ Hz, 1H).

^{13}C NMR (75 MHz, CDCl_3) δ 190.0, 149.5, 146.4, 142.2, 141.8, 137.7, 134.0, 129.6, 128.9, 128.5, 127.6, 126.5, 120.3, 53.1, 36.1, 35.7.

IR (film): ν (cm^{-1}) 3111, 2957, 2863, 1663, 1602, 1525, 1399, 1344, 1287, 903, 776, 731, 699, 533.

HRMS (ESI, m/z) calcd for $\text{C}_{19}\text{H}_{16}\text{N}_4\text{O}_5\text{Na}$ $[\text{M}+\text{Na}]^+$: 403.1013, found: 403.1025.

(R)-Methyl 2-(3-(1-methyl-1H-imidazol-2-yl)-3-oxo-2-phenylpropyl)-5-nitrobenzoate (26c)

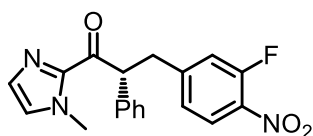
Starting from 2-acyl imidazole **24a** (120.0 mg, 0.60 mmol) and methyl 2-(bromomethyl)-5-nitrobenzoate (54.6 mg, 0.20 mmol) according to the general procedure to give **26c** as a white solid (76.6 mg, 0.195 mmol, yield: 98%). Enantiomeric excess established by HPLC analysis using a Chiralpak OD-H column, *ee* = 99% (HPLC: OD-H, 254 nm, hexane/isopropanol = 90:10, flow rate 1.0 mL/min, 25 °C, *t_r* (major) = 17.0 min, *t_r* (minor) = 20.5 min). $[\alpha]_{\text{D}}^{25} = -119.0^{\circ}$ (*c* 1.0, CH₂Cl₂).

¹H NMR (300 MHz, CDCl₃) δ 8.63 (d, *J* = 2.5 Hz, 1H), 8.00 (dd, *J* = 8.5, 2.5 Hz, 1H), 7.33-7.25 (m, 2H), 7.24-7.06 (m, 4H), 6.95 (d, *J* = 0.8 Hz, 1H), 6.84 (s, 1H), 5.44 (t, *J* = 7.4 Hz, 1H), 3.90-3.78 (m, 7H), 3.50 (dd, *J* = 13.1, 7.2 Hz, 1H).

¹³C NMR (75 MHz, CDCl₃) δ 190.9, 165.7, 148.9, 146.1, 142.4, 138.3, 133.0, 131.0, 129.3, 128.59, 128.58, 127.3, 127.2, 125.8, 125.7, 53.8, 52.6, 37.1, 36.0.

IR (film): ν (cm⁻¹) 3112, 2949, 2853, 1720, 1660, 1607, 1514, 1444, 1399, 1341, 1249, 1125, 1067, 905, 746, 697, 535.

HRMS (ESI, *m/z*) calcd for C₂₁H₁₉N₃O₅Na [M+Na]⁺: 416.1217, found: 416.1215.

(R)-3-(3-Fluoro-4-nitrophenyl)-1-(1-methyl-1H-imidazol-2-yl)-2-phenylpropan-1-one (26d)

Starting from 2-acyl imidazole **24a** (120.0 mg, 0.60 mmol) and methyl 4-(bromomethyl)-2-fluoro-1-nitrobenzene (46.6 mg, 0.20 mmol) according to the general procedure to give **26d** as a white solid (68.5 mg, 0.194 mmol, yield: 97%). Enantiomeric excess established by HPLC analysis using a Chiralpak OD-H column, *ee* = 95% (HPLC: OD-H, 254 nm, hexane/isopropanol = 90:10, flow rate 1.0 mL/min, 25 °C, *t_r* (minor) = 18.5 min, *t_r* (major) = 21.6 min). $[\alpha]_{\text{D}}^{25} = -118.4^{\circ}$ (*c* 1.0, CH₂Cl₂).

¹H NMR (300 MHz, CDCl₃) δ 7.80 (t, *J* = 8.2 Hz, 1H), 7.35-7.28 (m, 2H), 7.26-7.08 (m, 3H),

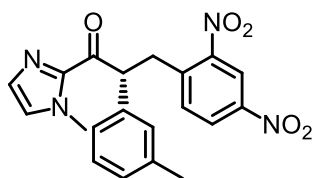
7.06-7.00 (m, 2H), 6.99 (s, 1H), 6.89 (s, 1H), 5.41 (t, $J = 7.8$ Hz, 1H), 3.83 (s, 3H), 3.48 (dd, $J = 13.9$, 8.4 Hz, 1H), 3.10 (dd, $J = 13.9$, 7.3 Hz, 1H).

^{13}C NMR (75 MHz, CDCl_3) δ 190.3, 157.0, 153.5, 149.4, 149.3, 142.3, 137.7, 129.5, 128.8, 128.5, 127.7, 127.4, 125.9, 125.8, 125.20, 125.15, 118.9, 118.7, 53.4, 38.4, 36.0.

IR (film): ν (cm^{-1}) 3031, 2957, 1664, 1602, 1518, 1397, 1336, 1286, 1242, 1156, 1080, 946, 907, 835, 778, 739, 692, 512.

HRMS (ESI, m/z) calcd for $\text{C}_{19}\text{H}_{16}\text{FN}_3\text{O}_3\text{Na}$ $[\text{M}+\text{Na}]^+$: 376.1068, found: 376.1070.

(R)-3-(2,4-Dinitrophenyl)-1-(1-methyl-1H-imidazol-2-yl)-2-(*m*-tolyl)propan-1-one (26e)



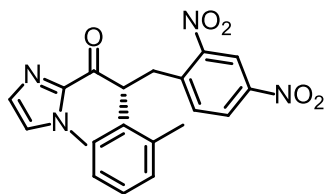
Starting from 2-acyl imidazole **24b** (128.4 mg, 0.60 mmol) and 1-(bromomethyl)-2,4-dinitrobenzene (52.2 mg, 0.20 mmol) according to the general procedure to give **26e** as a white solid (78.0 mg, 0.198 mmol, yield: 99%). Enantiomeric excess established by HPLC analysis using a Chiralpak IB column, $ee = 99\%$ (HPLC: IB, 254 nm, hexane/isopropanol = 90:10, flow rate 1.0 mL/min, 25 °C, t_r (major) = 16.5 min, t_r (minor) = 18.9 min). $[\alpha]_{\text{D}}^{25} = -151.9^\circ$ (c 1.0, CH_2Cl_2).

^1H NMR (300 MHz, CDCl_3) δ 8.64 (d, $J = 2.4$ Hz, 1H), 8.13 (dd, $J = 8.5$, 2.4 Hz, 1H), 7.43 (d, $J = 8.6$ Hz, 1H), 7.16-7.03 (m, 3H), 7.01-6.90 (m, 2H), 6.90-6.81 (m, 1H), 5.46 (dd, $J = 8.3$, 6.6 Hz, 1H), 3.84 (s, 3H), 3.77 (dd, $J = 13.8$, 8.3 Hz, 1H), 3.42 (dd, $J = 13.8$, 6.5 Hz, 1H), 2.22 (s, 3H).

^{13}C NMR (75 MHz, CDCl_3) δ 190.1, 149.5, 146.4, 142.2, 141.9, 138.6, 137.5, 134.0, 129.5, 129.0, 128.7, 128.4, 127.6, 126.4, 125.6, 120.2, 53.0, 36.0, 35.6, 21.3.

IR (film): ν (cm^{-1}) 3109, 2951, 1664, 1601, 1527, 1462, 1398, 1342, 1151, 1056, 977, 942, 906, 833, 780, 739, 696, 511.

HRMS (ESI, m/z) calcd for $\text{C}_{20}\text{H}_{18}\text{N}_4\text{O}_5\text{Na}$ $[\text{M}+\text{Na}]^+$: 417.1169, found: 417.1170.

(R)-3-(2,4-Dinitrophenyl)-1-(1-methyl-1*H*-imidazol-2-yl)-2-(*o*-tolyl)propan-1-one (26f)

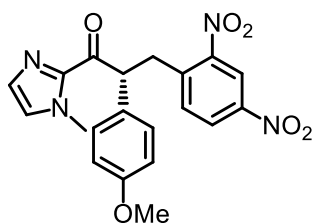
Starting from 2-acyl imidazole **24c** (128.4 mg, 0.60 mmol) and 1-(bromomethyl)-2,4-dinitrobenzene (52.2 mg, 0.20 mmol) according to the general procedure to give **26f** as a white solid (73.3 mg, 0.186 mmol, yield: 93%). Enantiomeric excess established by HPLC analysis using a Chiralpak AD-H column, *ee* = 99% (HPLC: AD-H, 254 nm, hexane/isopropanol = 70:30, flow rate 1.0 mL/min, 25 °C, *t_r* (major) = 7.6 min, *t_r* (minor) = 9.0 min). $[\alpha]_{\text{D}}^{25} = -166.1^\circ$ (*c* 1.0, CH₂Cl₂).

¹H NMR (300 MHz, CDCl₃) δ 8.64 (d, *J* = 2.4 Hz, 1H), 8.11 (dd, *J* = 8.5, 2.4 Hz, 1H), 7.36-7.25 (m, 2H), 7.16-6.96 (m, 3H), 6.94 (d, *J* = 0.8 Hz, 1H), 6.86 (s, 1H), 5.71 (t, *J* = 7.5 Hz, 1H), 3.85 (s, 3H), 3.74 (dd, *J* = 13.6, 7.8 Hz, 1H), 3.36 (dd, *J* = 13.6, 7.2 Hz, 1H), 2.33 (s, 3H).

¹³C NMR (75 MHz, CDCl₃) δ 190.7, 149.6, 146.4, 142.5, 141.8, 137.5, 136.1, 134.2, 131.0, 129.5, 127.52, 127.48, 127.0, 126.33, 126.28, 120.1, 48.7, 36.0, 35.9, 19.7.

IR (film): ν (cm⁻¹) 3126, 2950, 2866, 1663, 1602, 1527, 1399, 1341, 943, 907, 735, 692, 547.

HRMS (ESI, *m/z*) calcd for C₂₀H₁₈N₄O₅Na [M+Na]⁺: 417.1169, found: 417.1170.

(R)-3-(2,4-Dinitrophenyl)-2-(4-methoxyphenyl)-1-(1-methyl-1*H*-imidazol-2-yl)propan-1-one (26g)

Starting from 2-acyl imidazole **24d** (138.0 mg, 0.60 mmol) and 1-(bromomethyl)-2,4-dinitrobenzene (52.2 mg, 0.20 mmol) according to the general procedure to give **26g** as a white solid (79.5 mg, 0.194 mmol, yield: 97%). Enantiomeric excess established by HPLC analysis using a Chiralpak AD-H column, *ee* = 97% (HPLC: AD-H, 254 nm, hexane/isopropanol = 70:30, flow rate 1.0 mL/min, 25 °C, *t_r* (minor) = 16.6 min, *t_r* (major) = 20.8 min). $[\alpha]_{\text{D}}^{25} = -152.5^\circ$ (*c* 1.0, CH₂Cl₂).

¹H NMR (300 MHz, CDCl₃) δ 8.64 (d, *J* = 2.2 Hz, 1H), 8.13 (dd, *J* = 8.5, 2.2 Hz, 1H), 7.40 (d, *J* = 8.5

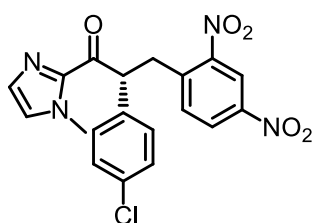
Hz, 1H), 7.21 (d, $J = 8.6$ Hz, 2H), 6.98 (s, 1H), 6.88 (s, 1H), 6.73 (d, $J = 8.6$ Hz, 2H), 5.44 (t, $J = 7.4$ Hz, 1H), 3.85 (s, 3H), 3.76 (dd, $J = 13.8, 7.9$ Hz, 1H), 3.67 (s, 3H), 3.41 (dd, $J = 13.8, 7.0$ Hz, 1H).

^{13}C NMR (75 MHz, CDCl_3) δ 190.2, 159.0, 149.5, 146.4, 142.2, 141.9, 134.0, 129.6, 129.5, 127.5, 126.4, 120.2, 114.3, 55.2, 52.2, 36.0, 35.6.

IR (film): ν (cm^{-1}) 3107, 2956, 2837, 1669, 1604, 1530, 1400, 1344, 1248, 1178, 1031, 874, 834, 786, 730, 544.

HRMS (ESI, m/z) calcd for $\text{C}_{20}\text{H}_{18}\text{N}_4\text{O}_6\text{Na}$ $[\text{M}+\text{Na}]^+$: 433.1119, found: 433.1116.

(R)-2-(4-Chlorophenyl)-3-(2,4-dinitrophenyl)-1-(1-methyl-1H-imidazol-2-yl)propan-1-one (26h)



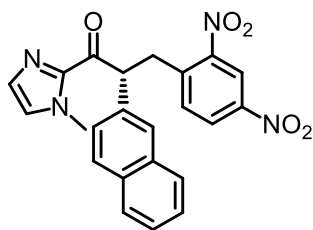
Starting from 2-acyl imidazole **24e** (140.4 mg, 0.60 mmol) and 1-(bromomethyl)-2,4-dinitrobenzene (52.2 mg, 0.20 mmol) according to the general procedure to give **26h** as a white solid (81.1 mg, 0.196 mmol, yield: 98%). Enantiomeric excess established by HPLC analysis using a Chiralpak AD-H column, $ee = 96\%$ (HPLC: AD-H, 254 nm, hexane/isopropanol = 80:20, flow rate 1.0 mL/min, 25 °C, t_r (minor) = 17.6 min, t_r (major) = 20.8 min). $[\alpha]_{\text{D}}^{25} = -126.2^\circ$ (c 1.0, CH_2Cl_2).

^1H NMR (300 MHz, CDCl_3) δ 8.66 (d, $J = 1.7$ Hz, 1H), 8.16 (dd, $J = 8.5, 1.5$ Hz, 1H), 7.43 (d, $J = 8.5$ Hz, 1H), 7.26 (d, $J = 8.3$ Hz, 2H), 7.17 (d, $J = 8.0$ Hz, 2H), 6.98 (s, 1H), 6.90 (s, 1H), 5.49 (t, $J = 7.3$ Hz, 1H), 3.86 (s, 3H), 3.78 (dd, $J = 13.7, 8.3$ Hz, 1H), 3.40 (dd, $J = 13.8, 6.4$ Hz, 1H).

^{13}C NMR (75 MHz, CDCl_3) δ 189.6, 149.4, 146.5, 142.0, 141.5, 136.3, 134.0, 133.6, 129.9, 129.7, 129.1, 127.8, 126.6, 120.3, 52.4, 36.1, 35.5.

IR (film): ν (cm^{-1}) 3296, 3105, 2954, 1670, 1603, 1530, 1486, 1401, 1345, 1285, 908, 874, 833, 774.

HRMS (ESI, m/z) calcd for $\text{C}_{19}\text{H}_{15}\text{ClN}_4\text{O}_5\text{Na}$ $[\text{M}+\text{Na}]^+$: 437.0623, found: 437.0621.

(R)-3-(2,4-Dinitrophenyl)-1-(1-methyl-1*H*-imidazol-2-yl)-2-(naphthalen-2-yl)propan-1-one (26i)

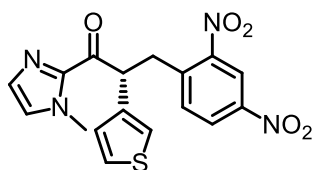
Starting from 2-acyl imidazole **24f** (150.0 mg, 0.60 mmol) and 1-(bromomethyl)-2,4-dinitrobenzene (52.2 mg, 0.20 mmol) according to the general procedure to give **26i** as a white solid (84.3 mg, 0.196 mmol, yield: 98%). Enantiomeric excess established by HPLC analysis using a Chiralpak AD-H column, *ee* = 98% (HPLC: AD-H, 254 nm, hexane/isopropanol = 70:30, flow rate 1.0 mL/min, 25 °C, *t_r* (minor) = 16.6 min, *t_r* (major) = 24.4 min). $[\alpha]_{\text{D}}^{25} = -198.4^{\circ}$ (*c* 1.0, CH₂Cl₂).

¹H NMR (300 MHz, CDCl₃) δ 8.62 (d, *J* = 2.4 Hz, 1H), 8.05 (dd, *J* = 8.5, 2.4 Hz, 1H), 7.82-7.60 (m, 4H), 7.53-7.26 (m, 4H), 6.95 (d, *J* = 0.8 Hz, 1H), 6.83 (s, 1H), 5.67 (dd, *J* = 7.9, 6.8 Hz, 1H), 3.88 (dd, *J* = 13.8, 8.1 Hz, 1H), 3.83 (s, 3H), 3.51 (dd, *J* = 13.8, 6.7 Hz, 1H).

¹³C NMR (75 MHz, CDCl₃) δ 189.9, 149.4, 146.4, 142.2, 141.7, 135.1, 134.0, 133.4, 132.6, 129.5, 128.7, 127.8, 127.59, 127.55, 126.5, 126.24, 126.22, 126.1, 120.2, 53.2, 36.0, 35.6.

IR (film): ν (cm⁻¹) 3109, 3048, 2954, 1671, 1602, 1528, 1399, 1340, 908, 750, 688, 542, 475.

HRMS (ESI, *m/z*) calcd for C₂₃H₁₈N₄O₅Na [M+Na]⁺: 453.1169, found: 453.1161.

(R)-3-(2,4-Dinitrophenyl)-1-(1-methyl-1*H*-imidazol-2-yl)-2-(thiophen-3-yl)propan-1-one (26j)

Starting from 2-acyl imidazole **24g** (124.1 mg, 0.60 mmol) and 1-(bromomethyl)-2,4-dinitrobenzene (52.2 mg, 0.20 mmol) according to the general procedure to give **26j** as a white solid (76.4 mg, 0.198 mmol, yield: 99%). Enantiomeric excess established by HPLC analysis using a Chiralpak OD-H column, *ee* = 97% (HPLC: OD-H, 254 nm, hexane/isopropanol = 70:30, flow rate 1.0 mL/min, 25 °C, *t_r* (minor) = 17.8 min, *t_r* (major) = 22.0 min). $[\alpha]_{\text{D}}^{25} = -85.5^{\circ}$ (*c* 1.0, CH₂Cl₂).

¹H NMR (300 MHz, CDCl₃) δ 8.65 (d, *J* = 2.4 Hz, 1H), 8.15 (dd, *J* = 8.5, 2.4 Hz, 1H), 7.41 (d, *J* = 8.5 Hz, 1H), 7.21-7.14 (m, 1H), 7.11 (dd, *J* = 2.9, 1.2 Hz, 1H), 7.03 (dd, *J* = 5.0, 1.3 Hz, 1H), 7.01 (d, *J* =

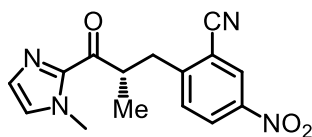
0.8 Hz, 1H), 6.92 (s, 1H), 5.67 (t, $J = 7.4$ Hz, 1H), 3.87 (s, 3H), 3.74 (dd, $J = 13.8, 7.9$ Hz, 1H), 3.48 (dd, $J = 13.8, 7.0$ Hz, 1H).

^{13}C NMR (75 MHz, CDCl_3) δ 189.6, 149.4, 146.4, 142.0, 141.6, 137.6, 133.9, 129.5, 127.8, 127.2, 126.5, 126.2, 123.3, 120.2, 48.3, 36.1, 35.5.

IR (film): ν (cm^{-1}) 3108, 2956, 1665, 1604, 1526, 1398, 1345, 944, 905, 772, 731, 683.

HRMS (ESI, m/z) calcd for $\text{C}_{17}\text{H}_{14}\text{N}_4\text{O}_5\text{SNa}$ $[\text{M}+\text{Na}]^+$: 409.0577, found: 409.0580.

(S)-2-(2-Methyl-3-(1-methyl-1H-imidazol-2-yl)-3-oxopropyl)-5-nitrobenzonitrile (26k)



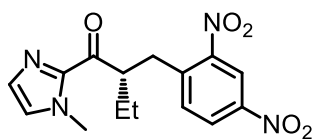
Starting from 2-acyl imidazole **24h** (82.8 mg, 0.60 mmol) and 2-(bromomethyl)-5-nitrobenzonitrile (48.0 mg, 0.20 mmol) according to the general procedure to give **26k** as a pale yellow oil (51.8 mg, 0.174 mmol, yield: 87%). Enantiomeric excess established by HPLC analysis using a Chiralpak AD-H column, $ee = 97\%$ (HPLC: AD-H, 254 nm, hexane/isopropanol = 85:15, flow rate 0.8 mL/min, 25 °C, t_r (minor) = 19.2 min, t_r (major) = 27.1 min). $[\alpha]_{\text{D}}^{25} = +70.6^\circ$ (c 0.5, CH_2Cl_2).

^1H NMR (300 MHz, CDCl_3) δ 8.38 (d, $J = 2.4$ Hz, 1H), 8.23 (dd, $J = 8.6, 2.4$ Hz, 1H), 7.56 (d, $J = 8.7$ Hz, 1H), 7.05 (d, $J = 0.9$ Hz, 1H), 6.97 (s, 1H), 4.43-4.17 (m, 1H), 3.91 (s, 3H), 3.39 (dd, $J = 14.1, 8.0$ Hz, 1H), 3.04 (dd, $J = 14.1, 6.4$ Hz, 1H), 1.26 (d, $J = 7.0$ Hz, 3H).

^{13}C NMR (75 MHz, CDCl_3) δ 193.6, 151.2, 146.2, 141.9, 131.4, 129.3, 127.7, 127.5, 127.0, 115.9, 114.6, 42.4, 37.0, 36.2, 17.8.

IR (film): ν (cm^{-1}) 3081, 2962, 2928, 2869, 2231, 1670, 1525, 1460, 1405, 1348, 972, 910, 839, 791, 734.

HRMS (ESI, m/z) calcd for $\text{C}_{15}\text{H}_{14}\text{N}_4\text{O}_3\text{Na}$ $[\text{M}+\text{Na}]^+$: 321.0958, found: 321.0954.

(S)-2-(2,4-Dinitrobenzyl)-1-(1-methyl-1H-imidazol-2-yl)butan-1-one (26l)

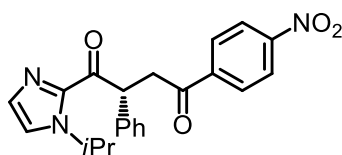
Starting from 2-acyl imidazole **24i** (91.2 mg, 0.60 mmol) and 1-(bromomethyl)-2,4-dinitrobenzene (52.2 mg, 0.20 mmol) according to the general procedure to give **26l** as a pale yellow oil (55.8 mg, 0.168 mmol, yield: 84%). Enantiomeric excess established by HPLC analysis using a Chiralpak AD-H column, *ee* = 91% (HPLC: AD-H, 254 nm, hexane/isopropanol = 80:20, flow rate 1.0 mL/min, 25 °C, *t_r* (minor) = 9.0 min, *t_r* (major) = 11.5 min). $[\alpha]_{\text{D}}^{25} = +35.0^\circ$ (*c* 0.5, CH₂Cl₂).

¹H NMR (300 MHz, CDCl₃) δ 8.65 (d, *J* = 2.4 Hz, 1H), 8.18 (dd, *J* = 8.5, 2.4 Hz, 1H), 7.57 (d, *J* = 8.6 Hz, 1H), 6.98 (d, *J* = 0.8 Hz, 1H), 6.93 (s, 1H), 4.32-4.11 (m, 1H), 3.87 (s, 3H), 3.42-3.15 (m, 2H), 1.99-1.75 (m, 1H), 1.74-1.53 (m, 1H), 0.90 (t, *J* = 7.5 Hz, 3H).

¹³C NMR (75 MHz, CDCl₃) δ 194.0, 149.4, 146.3, 142.7, 142.5, 133.8, 129.2, 127.5, 126.5, 120.2, 48.6, 36.2, 33.6, 26.2, 11.3.

IR (film): ν (cm⁻¹) 3107, 2964, 2874, 1668, 1604, 1530, 1456, 1406, 1345, 1287, 1153, 1069, 1004, 908, 836, 778, 735, 528.

HRMS (ESI, *m/z*) calcd for C₁₅H₁₆N₄O₅Na [M+Na]⁺: 355.1013, found: 355.1015.

(R)-1-(1-Isopropyl-1H-imidazol-2-yl)-4-(4-nitrophenyl)-2-phenylbutane-1,4-dione (26m)

Starting from 2-acyl imidazole **24j** (136.8 mg, 0.60 mmol) and 2-bromo-1-(4-nitrophenyl)ethanone (48.8 mg, 0.20 mmol) according to the general procedure to give **26m** as a white solid (71.2 mg, 0.182 mmol, yield: 91%). Enantiomeric excess established by HPLC analysis using a Chiralpak IB column, *ee* = 90% (HPLC: IB, 254 nm, hexane/isopropanol = 70:30, flow rate 1.0 mL/min, 25 °C, *t_r* (major) = 14.9 min, *t_r* (minor) = 18.0 min). $[\alpha]_{\text{D}}^{25} = -154.6^\circ$ (*c* 1.0, CH₂Cl₂).

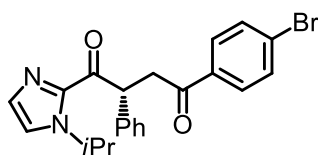
¹H NMR (300 MHz, CDCl₃) δ 8.38-8.13 (m, 2H), 8.12-7.92 (m, 2H), 7.47-7.35 (m, 2H), 7.29-7.19 (m, 2H), 7.19-7.07 (m, 3H), 5.73 (dd, *J* = 10.8, 3.8 Hz, 1H), 5.53-5.15 (m, 1H), 4.08 (dd, *J* = 18.2, 10.8 Hz, 1H), 3.32 (dd, *J* = 18.2, 3.8 Hz, 1H), 1.34 (d, *J* = 6.7 Hz, 3H), 1.24 (d, *J* = 6.7 Hz, 3H).

^{13}C NMR (75 MHz, CDCl_3) δ 196.4, 190.7, 150.3, 141.8, 140.9, 138.1, 130.0, 129.1, 128.8, 128.4, 127.2, 123.7, 121.3, 49.1, 48.5, 43.4, 23.4.

IR (film): ν (cm^{-1}) 3109, 2977, 2922, 1670, 1600, 1523, 1455, 1394, 1341, 1248, 1197, 996, 945, 909, 853, 744, 695, 583, 520.

HRMS (ESI, m/z) calcd for $\text{C}_{22}\text{H}_{22}\text{N}_3\text{O}_4$ $[\text{M}+\text{H}]^+$: 392.1605, found: 392.1604.

(R)-4-(4-Bromophenyl)-1-(1-isopropyl-1H-imidazol-2-yl)-2-phenylbutane-1,4-dione (26o)



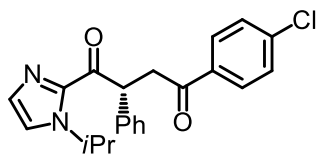
Starting from 2-acyl imidazole **24j** (136.8 mg, 0.60 mmol) and 2-bromo-1-(4-bromophenyl)ethanone (55.6 mg, 0.20 mmol) according to the general procedure to give **26o** as a pale yellow oil (73.0 mg, 0.172 mmol, yield: 86%). Enantiomeric excess established by HPLC analysis using a Chiralpak IB column, ee = 91% (HPLC: IB, 254 nm, hexane/isopropanol = 80:20, flow rate 1.0 mL/min, 25 °C, t_r (major) = 7.3 min, t_r (minor) = 9.2 min). $[\alpha]_{\text{D}}^{25} = -160.4^\circ$ (c 1.0, CH_2Cl_2).

^1H NMR (300 MHz, CDCl_3) δ 7.83-7.68 (m, 2H), 7.55-7.44 (m, 2H), 7.45-7.34 (m, 2H), 7.27-7.09 (m, 5H), 5.70 (dd, J = 10.9, 3.7 Hz, 1H), 5.55-5.25 (m, 1H), 4.02 (dd, J = 18.0, 10.9 Hz, 1H), 3.26 (dd, J = 18.0, 3.8 Hz, 1H), 1.34 (d, J = 6.7 Hz, 3H), 1.23 (d, J = 6.7 Hz, 3H).

^{13}C NMR (75 MHz, CDCl_3) δ 196.8, 191.0, 141.9, 138.5, 135.2, 131.8, 129.9, 129.6, 128.7, 128.5, 128.2, 127.1, 121.1, 49.1, 48.5, 43.0, 23.4.

IR (film): ν (cm^{-1}) 3155, 3068, 3028, 2980, 2921, 1666, 1578, 1488, 1457, 1394, 1205, 1151, 1123, 1092, 1068, 987, 946, 909, 830, 795, 771, 745, 695, 580, 524.

HRMS (ESI, m/z) calcd for $\text{C}_{22}\text{H}_{22}\text{BrN}_2\text{O}_2$ $[\text{M}+\text{H}]^+$: 425.0859, found: 425.0855.

(R)-4-(4-Chlorophenyl)-1-(1-isopropyl-1H-imidazol-2-yl)-2-phenylbutane-1,4-dione (26p)

Starting from 2-acyl imidazole **24j** (136.8 mg, 0.60 mmol) and 2-bromo-1-(4-chlorophenyl)ethanone (37.6 mg, 0.20 mmol) according to the general procedure to give **26p** as a pale red oil (69.2 mg, 0.182 mmol, yield: 91%). Enantiomeric excess established by HPLC analysis using a Chiralpak IB column, *ee* = 91% (HPLC: IB, 254 nm, hexane/isopropanol = 80:20, flow rate 1.0 mL/min, 25 °C, *t_r* (major) = 7.2 min, *t_r* (minor) = 9.4 min). $[\alpha]_D^{25} = -147.5^\circ$ (*c* 1.0, CH₂Cl₂).

¹H NMR (300 MHz, CDCl₃) δ 7.89-7.77 (m, 2H), 7.51-7.37 (m, 2H), 7.36-7.28 (m, 2H), 7.27-7.07 (m, 5H), 5.70 (dd, *J* = 10.9, 3.7 Hz, 1H), 5.38 (hept, *J* = 6.7 Hz, 1H), 4.03 (dd, *J* = 18.0, 10.9 Hz, 1H), 3.27 (dd, *J* = 18.0, 3.8 Hz, 1H), 1.35 (d, *J* = 6.7 Hz, 3H), 1.24 (d, *J* = 6.7 Hz, 3H).

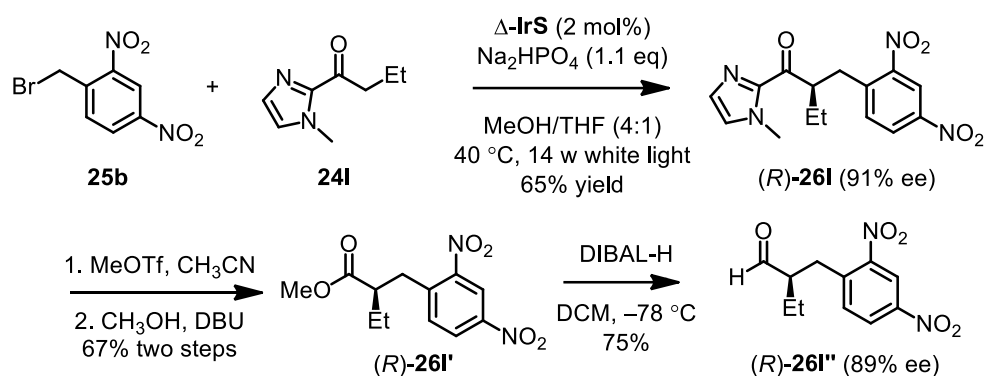
¹³C NMR (75 MHz, CDCl₃) δ 196.6, 191.1, 141.9, 139.5, 138.5, 134.8, 129.9, 129.5, 128.8, 128.7, 128.5, 127.1, 121.1, 49.1, 48.5, 43.0, 23.4.

IR (film): ν (cm⁻¹) 3159, 3071, 3028, 2982, 2922, 1668, 1583, 1489, 1457, 1396, 1248, 1205, 1156, 1089, 988, 946, 910, 834, 771, 747, 696, 666, 550, 521.

HRMS (ESI, *m/z*) calcd for C₂₂H₂₂ClN₂O₂ [M+H]⁺: 381.1364, found: 381.1361.

5.4.3 Assignment of Absolute Configurations for Asymmetric Catalysis Products

The absolute configuration of the product **26l** (synthesized through catalysis with Δ -**IrS**) was assigned by converting it to the corresponding reported non-racemic aldehyde **26l''** for which the absolute configuration has been established.²² As shown below, the (*R*)-configuration was assigned by comparison with published optical rotation and chiral HPLC retention time data.²² Thus, it can be concluded for the results of Figure 41-43 in which the catalyst Δ -**IrS** was employed, that **26l** was provided as (*S*)-**26l**. All other products were assigned accordingly.



Optical rotation of (*R*)-**26l''**:

$[\alpha]_{\text{D}}^{25} = +67.8$ (*c* 1.0, CHCl_3 , 89% *ee*)

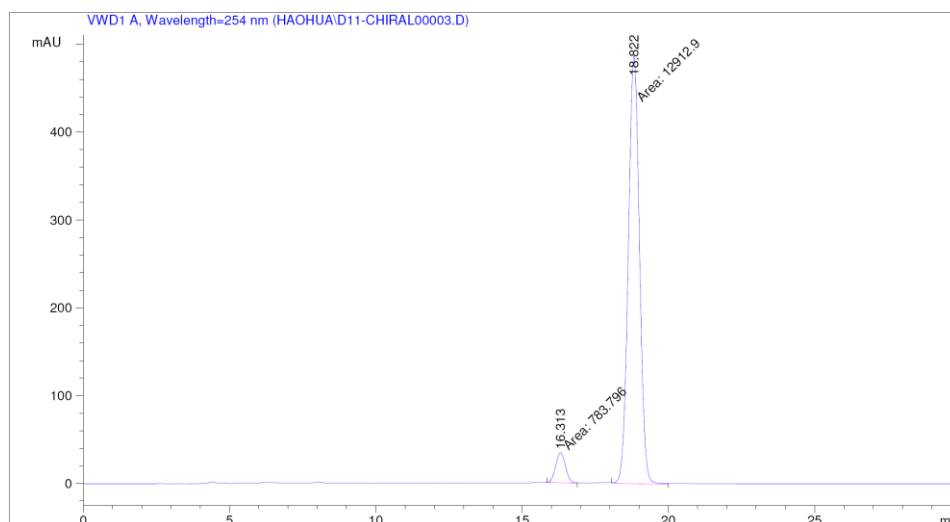
Lit.²²: $[\alpha]_{\text{D}}^{29} = +59.3$ (*c* 1.0, CHCl_3 , 92% *ee* for *R*-configuration)

Chiral HPLC with (*R*)-**26l''**:

(Daicel Chiralpak IC column, 254 nm, hexane/isopropanol = 70:30, flow rate 1.0 mL/min, 25 °C)

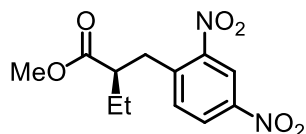
t_{r} (minor) = 16.3 min, t_{r} (major) = 18.8 min

Lit.²²: t_{r} (minor) = 16.7 min, t_{r} (major) = 19.9 min



Peak #	RetTime [min]	Type	Width [min]	Area mAU * s	Height [mAU]	Area %
1	16.313	MM	0.3843	783.79620	33.98812	5.7225
2	18.822	MM	0.4423	1.29129e4	486.59186	94.2775

(*R*)-Methyl 2-(2,4-dinitrobenzyl)butanoate (26l')



The compound was synthesized following a published procedure with some modifications.^[12] To a solution of (*R*)-**3l** (160 mg, 0.48 mmol) in CH₃CN (2.4 mL) was added methyl trifluoromethanesulfonate (158 μ L, 1.44 mmol) at room temperature. After being stirred at room temperature for 8 h, MeOH (2.4 mL) and DBU (1.0 mL) were added to the reaction mixture. After being stirred at room temperature for 30 min, the reaction was quenched with a saturated aqueous solution of Na₂HCO₃ and extracted with EtOAc (4 \times 4 mL). The combined organic layers were dried over anhydrous Na₂SO₄, filtered, and concentrated under reduced pressure. The residue was purified by flash chromatography on silica gel (EtOAc/hexane = 1:10) to give **3l'** (91.2 mg, 0.32 mmol, yield: 67%) as a colorless oil.

¹H NMR (300 MHz, CDCl₃) δ 8.73 (d, *J* = 2.4 Hz, 1H), 8.28 (dd, *J* = 8.5, 2.4 Hz, 1H), 7.53 (d, *J* = 8.5 Hz, 1H), 3.51 (s, 3H), 3.29-3.00 (m, 2H), 2.91-2.55 (m, 1H), 1.97- 1.42 (m, 2H), 0.91 (t, *J* = 7.4 Hz, 3H).

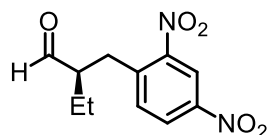
¹³C NMR (75 MHz, CDCl₃) δ 174.8, 149.2, 146.7, 141.8, 134.0, 126.8, 120.5, 51.7, 47.7, 34.9, 26.2,

11.4.

IR (film): ν (cm⁻¹) 3104, 2963, 2876, 1730, 1604, 1530, 1454, 1345, 1265, 1203, 1168, 1096, 1062, 1012, 910, 832, 801, 737.

HRMS (ESI, m/z) calcd for C₁₂H₁₄N₂O₆Na [M+Na]⁺: 305.0744, found: 305.0747.

(*R*)-2-(2,4-Dinitrobenzyl)butanal (26l'')



To a solution of (*R*)-**3l'** (91.2 mg, 0.32 mmol) in CH₂Cl₂ (3.2 mL) was added DIBAL-H (0.8 mL, 1.0 M in toluene, 0.80 mmol) at -78 °C. After being stirred at -78 °C for 2 h, the reaction was quenched with a saturated aqueous solution of Na₂HCO₃ and extracted with EtOAc (4 × 5 mL). The combined organic layers were dried over anhydrous Na₂SO₄, filtered, and concentrated under reduced pressure. The residue was purified by flash chromatography on silica gel (EtOAc/hexane = 1:10) to give **3l''** (59.3 mg, 0.24 mmol, yield: 75%) as a pale yellow oil. $[\alpha]_D^{25} = +67.8^\circ$ (c 1.0, CHCl₃) (Lit.^[11] $[\alpha]_D^{29} = +59.3^\circ$ (c 1.0, CHCl₃) for 92% *ee* of product with *R*-configuration).

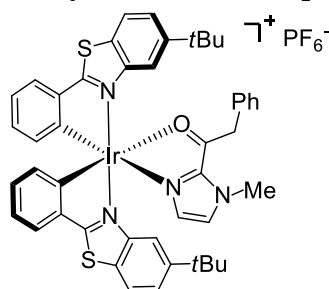
¹H NMR (300 MHz, CDCl₃) δ 9.64 (d, $J = 1.4$ Hz, 1H), 8.78 (s, 1H), 8.35 (dd, $J = 8.5, 2.3$ Hz, 1H), 7.68 (d, $J = 8.5$ Hz, 1H), 3.36 (dd, $J = 13.7, 8.9$ Hz, 1H), 3.09 (dd, $J = 13.7, 4.8$ Hz, 1H), 2.87-2.62 (m, 1H), 1.94-1.60 (m, 2H), 1.02 (t, $J = 7.5$ Hz, 3H).

¹³C NMR (75 MHz, CDCl₃) δ 202.5, 149.2, 146.6, 141.9, 134.6, 126.8, 120.4, 53.6, 31.2, 22.5, 10.9.

All spectroscopic data were in agreement with the literature.²²

5.4.4 Mechanistic Experiments

1) Synthesis of the Proposed Intermediate Complexes I and II



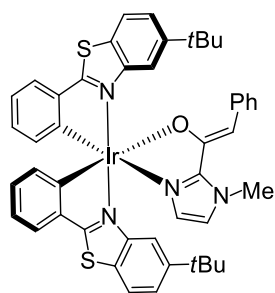
intermediate complex I

The racemic complex **I** was obtained by reacting substrate **24a** (14.2 mg, 0.071 mmol) with racemic Δ/Λ -**IrS** (45 mg, 0.047 mmol) at room temperature overnight in CH_2Cl_2 (1.0 mL). After the slow addition of hexane (5.0 mL), crystals were collected after several days (37.7 mg, yield: 65%).

^1H NMR (300 MHz, CD_2Cl_2) δ 7.98 (d, $J = 8.6$ Hz, 1H), 7.92 (d, $J = 8.6$ Hz, 1H), 7.85 (dd, $J = 7.7$, 0.9 Hz, 1H), 7.78 (dd, $J = 7.7$, 1.1 Hz, 1H), 7.61 (dd, $J = 8.6$, 1.8 Hz, 1H), 7.57-7.49 (m, 3H), 7.11-7.02 (m, 3H), 6.94 (d, $J = 1.0$ Hz, 1H), 6.88-6.75 (m, 4H), 6.55-6.48 (m, 3H), 6.38 (d, $J = 7.5$ Hz, 1H), 6.30 (d, $J = 1.6$ Hz, 1H), 4.48 (dd, $J = 31.5$, 14.7 Hz, 3H), 4.05 (s, 2H), 1.34 (s, 9H), 0.85 (s, 9H).

^{13}C NMR (75 MHz, CD_2Cl_2) δ 195.1, 183.4, 179.4, 152.8, 152.6, 150.0, 149.0, 147.7, 147.4, 141.9, 140.1, 137.9, 134.8, 134.0, 133.4, 131.9, 131.7, 131.6, 130.2, 129.7, 128.9, 128.8, 128.6, 128.5, 126.7, 126.6, 125.1, 124.6, 123.8, 123.4, 123.3, 115.5, 115.3, 45.8, 37.7, 35.4, 35.0, 31.6, 31.2.

IR (film): ν (cm^{-1}) 3146, 3053, 2959, 1576, 1522, 1464, 1439, 1409, 1296, 1249, 1039, 995, 836, 730, 553.



enolate complex II

To a solution of catalyst Δ/Λ -**IrS** (100.0 mg, 0.105 mmol) in CH_2Cl_2 (3 mL) was added substrate **24a** (31.8 mg, 0.159 mmol). The reaction mixture was concentrated after around 12 hours. The residue was purified by flash chromatography on silica gel ($\text{CH}_2\text{Cl}_2/\text{EtOAc} = 50:1$) to afford the enolate complex

II as a red solid (90.0 mg, 0.097 mmol, yield: 93%).

^1H NMR (300 MHz, CD_2Cl_2) δ 8.80 (d, J = 1.6 Hz, 1H), 7.82-7.73 (m, 5H), 7.71 (dd, J = 7.7, 0.9 Hz, 1H), 7.43 (dt, J = 8.5, 1.8 Hz, 2H), 7.14 (d, J = 1.6 Hz, 1H), 7.10 (dd, J = 10.7, 4.8 Hz, 2H), 7.00-6.80 (m, 3H), 6.76-6.63 (m, 3H), 6.59-6.50 (m, 1H), 6.48-6.36 (m, 2H), 5.46 (s, 1H), 3.79 (s, 3H), 1.13 (s, 9H), 1.07 (s, 9H).

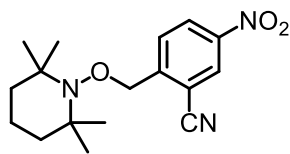
^{13}C NMR (75 MHz, CD_2Cl_2) δ 181.6, 179.7, 156.0, 155.4, 154.7, 152.4, 151.4, 151.32, 151.28, 149.9, 142.4, 142.0, 140.3, 135.2, 134.5, 130.6, 130.4, 129.1, 128.8, 127.8, 127.6, 126.1, 126.0, 125.0, 124.6, 123.5, 123.3, 123.2, 122.4, 121.7, 121.3, 120.9, 119.3, 117.1, 102.8, 37.0, 35.21, 35.17, 31.6, 31.4.

IR (film): ν (cm^{-1}) 3048, 2953, 2866, 1480, 1462, 1421, 1375, 1282, 1241, 1165, 1089, 1026, 990, 931, 728, 692, 457.

2) Trapping Experiment with TEMPO

With excess TEMPO as shown in Scheme 7: A dried 10 mL Schlenk tube was charged with the catalyst *rac*-**IrS** (2 mol%), Na_2HPO_4 (31.2 mg, 0.22 mmol), TEMPO (78.0 mg, 0.5 mmol) and the 2-(bromomethyl)-5-nitrobenzonitrile (48.0 mg, 0.2 mmol). The tube was purged with argon and MeOH/THF (4:1, 0.5 mL) was added via syringe, followed by the 2-acyl imidazole **24a** (34.0 μL , 0.2 mmol). The reaction mixture was degassed via freeze-pump-thaw for three cycles. After the mixture was thoroughly degassed, the vial was sealed and positioned approximately 5 cm from a 14 w white light energy saving lamp. The reaction was stirred at 40 °C for 22 h under argon atmosphere. Afterwards, the mixture was diluted with CH_2Cl_2 (8 mL), the inorganic salt was removed by centrifugation. The combined organic layers were concentrated under reduced pressure. The residue was purified by flash chromatography on silica gel (EtOAc/hexane = 1:20 to 1:5) to afford the products **27** (55.0 mg, 0.174 mmol, yield: 87%) as a white solid and **28** (65.1 mg, 0.183 mmol, yield: 92%) as a white solid.

With 5 mol% TEMPO as shown in Scheme 8: The experiment was executed as describe above but with only 0.05 equivalents of TEMPO. As a result, TEMPO was consumed within 15 min and products **27** and **28** were observed by ^1H -NMR analysis of the crude reaction mixture.

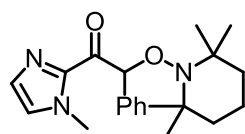
5-Nitro-2-(((2,2,6,6-tetramethylpiperidin-1-yl)oxy)methyl)benzonitrile (27)

^1H NMR (300 MHz, CDCl_3) δ 8.43 (d, $J = 2.2$ Hz, 1H), 8.38 (dd, $J = 8.6, 2.3$ Hz, 1H), 7.84 (d, $J = 8.5$ Hz, 1H), 5.07 (s, 2H), 1.57-1.25 (m, 6H), 1.14 (s, 6H), 1.11 (s, 6H).

^{13}C NMR (75 MHz, CDCl_3) δ 149.0, 146.7, 128.9, 127.6, 127.4, 115.1, 111.6, 75.5, 60.3, 39.6, 32.8, 20.3, 16.9.

IR (film): ν (cm^{-1}) 2969, 2931, 1610, 1583, 1529, 1472, 1447, 1348, 1132, 1057, 959, 926, 906, 820, 734.

HRMS (ESI, m/z) calcd for $\text{C}_{17}\text{H}_{24}\text{N}_3\text{O}_3$ $[\text{M}+\text{H}]^+$: 318.1812, found: 318.1805.

1-(1-Methyl-1H-imidazol-2-yl)-2-phenyl-2-(((2,2,6,6-tetramethylpiperidin-1-yl)oxy)ethanone (28)

^1H NMR (400 MHz, CDCl_3) δ 7.61 (d, $J = 6.8$ Hz, 2H), 7.37-7.10 (m, 4H), 7.00 (s, 1H), 6.67 (s, 1H), 3.93 (s, 3H), 1.65-1.20 (m, 9H), 1.12 (s, 3H), 1.06 (s, 3H), 0.78 (s, 3H).

^{13}C NMR (101 MHz, CDCl_3) δ 190.4, 141.9, 138.3, 129.3, 127.9, 127.8, 127.2, 127.1, 88.97, 59.6, 59.4, 39.9, 35.7, 33.6, 33.1, 20.0, 17.0.

IR (film): ν (cm^{-1}) 2925, 2861, 1686, 1455, 1405, 1373, 1257, 1052, 969, 919, 881, 833, 787, 751, 693, 614, 514.

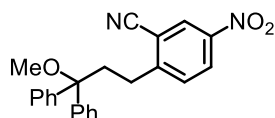
HRMS (ESI, m/z) calcd for $\text{C}_{21}\text{H}_{30}\text{N}_3\text{O}_2$ $[\text{M}+\text{H}]^+$: 356.2333, found: 356.2342.

3) Trapping Experiment with 1,1-Diphenylethylene

As shown in Scheme 9, A dried 10 mL Schlenk tube was charged with the catalyst *rac*-**IrS** (2 mol%), Na_2HPO_4 (31.2 mg, 0.22 mmol), 1,1-diphenylethylene (88.0 μL , 0.5 mmol) and the 2-(bromomethyl)-5-nitrobenzonitrile **25a** (48.0 mg, 0.2 mmol). The tube was purged with argon and MeOH/THF (4:1, 0.5 mL) was added via syringe, followed by the 2-acyl imidazole **24a** (102.0 μL , 0.6 mmol). The reaction mixture was degassed via freeze-pump-thaw for three cycles. After the mixture

was thoroughly degassed, the vial was sealed and positioned approximately 5 cm from a 14 w white light energy saving lamp. The reaction was stirred at 40 °C for 22 h under argon atmosphere. Afterwards, the mixture was diluted with CH₂Cl₂ (8 mL), the inorganic salt was removed by centrifugation. The combined organic layers were concentrated under reduced pressure. The residue was purified by flash chromatography on silica gel (EtOAc/hexane = 1:20) to afford the products **29** (42.4 mg, 0.114 mmol, yield: 57%) as a white solid and **26a** (4.2 mg, 0.012 mmol, yield: 6%) as a white solid.

2-(3-Methoxy-3,3-diphenylpropyl)-5-nitrobenzonitrile (**29**)



¹H NMR (300 MHz, CDCl₃) δ 8.37 (d, J = 2.4 Hz, 1H), 8.19 (dd, J = 8.6, 2.4 Hz, 1H), 7.34-7.09 (m, 11H), 3.08 (s, 3H), 2.71 (ddd, J = 6.3, 5.6, 2.5 Hz, 2H), 2.61 (ddd, J = 9.5, 5.6, 2.5 Hz, 2H).

¹³C NMR (75 MHz, CDCl₃) δ 154.0, 146.1, 144.4, 131.1, 128.2, 127.9, 127.2, 127.1, 126.8, 115.9, 113.8, 82.1, 50.4, 36.3, 29.0.

IR (film): ν (cm⁻¹) 3079, 2929, 2817, 2230, 2152, 1609, 1530, 1485, 1447, 1346, 1301, 1182, 1073, 1031, 910, 850, 746, 698, 498.

HRMS (ESI, m/z) calcd for C₂₃H₂₀N₂O₃Na [M+Na]⁺: 395.1366, found: 395.1372.

4) Luminescence Quenching Experiments

Emission intensities were recorded on a Spectra Max M5 microplate reader in a 10.0 mm quartz cuvette. Catalyst Δ/Λ -**IrS** solutions were excited at $\lambda_{\text{max}} = 425$ nm and the emission was measured at 560 nm (emission maximum). The enolate complex **II** solutions were excited at $\lambda_{\text{max}} = 440$ nm and the emission measured at 550 nm (emission maximum). The concentration of iridium complex (**IrS** and enolate complex **II**) was 0.5 mM in MeOH/THF (4:1). The concentration of the quencher (benzyl bromide **25a**) stock solution was 200 mM in MeOH/THF (4:1). For each quenching experiment, 5 μ L of this stock solution were titrated to a solution (1 mL) of iridium complex in a screw-top 10.0 mm quartz cuvette. The addition of 5 μ L stock solution refers to an increase of the quencher concentration of 1 mM. After degassing with an argon stream for 5 minutes, the emission intensity was collected. See Figure 53 for the obtained Stern-Volmer plots.

5.4.5 Cyclic Voltammetry

Cyclic voltammetry was carried out on a BAS C3 Cell Stand and a BAS 100 series Electrochemical Analyzer using a platinum disk anode (2.0 mm diameter) and a platinum wire cathode (0.5 mm diameter) at r.t. in acetonitrile containing 0.1 M Bu₄NBF₄. Potentials were referred to a saturated Ag/AgCl reference electrode. Before each experiment the surface of the anode was polished followed by thorough rinsing with distilled water. The solution was purged with nitrogen before each measurement. See Figure 54 for the results.

5.4.6 Single-Crystal X-Ray Diffraction Studies

Single crystals of Λ -**IrS** suitable for X-ray diffraction were obtained by slow diffusion from a solution of Λ -**IrS** (30 mg) in CH₂Cl₂ (0.5 mL) layered with *n*-hexane (1.5 mL) at room temperature for several days in an NMR-tube. Single crystals suitable for X-ray diffraction of the substrate coordinated iridium catalyst (intermediate **I**, here denoted as zll3) were obtained by reacting substrate **24a** (14.2 mg, 0.071 mmol) with Δ/Λ -**IrS** (45 mg, 0.047 mmol) overnight at room temperature in CH₂Cl₂ (1.0 mL). After the slow addition of *n*-hexane (5.0 mL), crystals were collected after several days (65% yield). Single crystals of the intermediate enolate complex **II** (zll4) were obtained as follows: To a solution of Δ/Λ -**IrS** catalyst (100.0 mg, 0.105 mmol) in CH₂Cl₂ (3 mL) was added substrate **24a** (31.8 mg, 0.159 mmol). The reaction mixture was concentrated after around 12 hours, purified by chromatography over silica gel using CH₂Cl₂-EtOAc (50:1), affording compound as red solid (90.0 mg, 0.097 mmol). Single crystals suitable for X-ray diffraction were obtained by slow diffusion from a solution of the compound in CH₂Cl₂ layered with *n*-hexane at room temperature for several days. Crystal data and details of the structure determination are presented in the Appendices (Chapter 6.7).

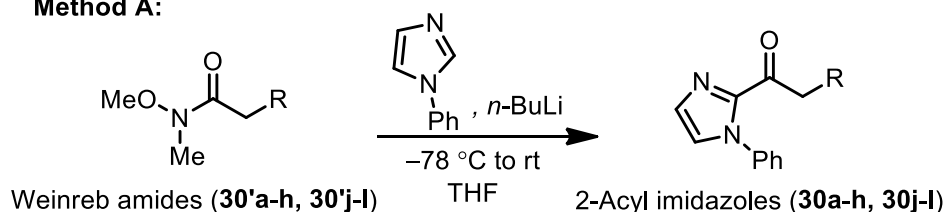
5.5 Visible-Light-Activated Enantioselective Trichloromethylation

5.5.1 Synthesis of Substrates

1) Synthesis of 2-Acyl Imidazoles

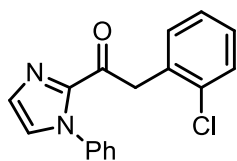
2-Acyl imidazoles **30a-h**, **30j-l** and the corresponding Weinreb amides were synthesized according to our recently published procedures (method A).²³ 2-Acyl imidazole **30i** was synthesized according to a reported procedure with some modifications (method B).²⁴

Method A:



General procedure for method A. To a solution of *N*-phenylimidazole (1.1 eq) in THF at $-78\text{ }^{\circ}\text{C}$ was added *n*-BuLi (1.1 eq) dropwise. The reaction was stirred at $-78\text{ }^{\circ}\text{C}$ for 30 min, and then stirred at room temperature for 30 min. The corresponding Weinreb amide (1.0 eq in THF) was added dropwise to the flask after the reaction was cooled back down to $-78\text{ }^{\circ}\text{C}$. The overall concentration of Weinreb amide was 0.4 M. The reaction was allowed to warm to room temperature slowly (over a period of 3-4 h) and stirred overnight. The reaction was quenched with AcOH (6.0 eq) at room temperature and extracted with EtOAc. The organic layer was washed with aqueous saturated NaHCO_3 and brine. The combined organic layers were dried over anhydrous Na_2SO_4 , filtered, and concentrated under reduced pressure. The residue was purified by flash chromatography on silica gel (EtOAc/hexane = 1:3) to produce **30a-h**, **30j-l**.

The experimental data of **30f** and **30l** are shown below. The other 2-acyl imidazoles (**30a-e**, **30g-h**, **30j-k**) have been reported previously.²³

2-(2-Chlorophenyl)-1-(1-phenyl-1H-imidazol-2-yl)ethanone (30f)

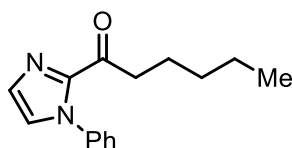
Following the general procedure, Weinreb amide **30f** (852 mg, 4.0 mmol) was converted to 2-acyl imidazole **30f** (890 mg, 3.0 mmol, yield: 75%) as a white solid.

^1H NMR (300 MHz, CDCl_3) δ 7.64-6.99 (m, 12H), 4.69 (s, 2H).

^{13}C NMR (75 MHz, CDCl_3) δ 187.1, 142.7, 138.2, 134.8, 133.0, 132.2, 129.7, 129.4, 128.9, 128.7, 128.4, 127.3, 126.7, 125.9, 43.8.

IR (film): ν (cm^{-1}) 3136, 3069, 3014, 2914, 1727, 1677, 1590, 1484, 1442, 1393, 1306, 1141, 1032, 957, 909, 744, 685, 538, 503, 442.

HRMS (ESI, m/z) calcd for $\text{C}_{17}\text{H}_{14}\text{ClN}_2\text{O}$ $[\text{M}+\text{H}]^+$: 297.0789, found: 297.0789.

1-(1-Phenyl-1H-imidazol-2-yl)hexan-1-one (30l)

Following the general procedure, Weinreb amide **30l** (636 mg, 4.0 mmol) was converted to 2-acyl imidazole **30l** (808 mg, 3.4 mmol, yield: 84%) as a colorless oil.

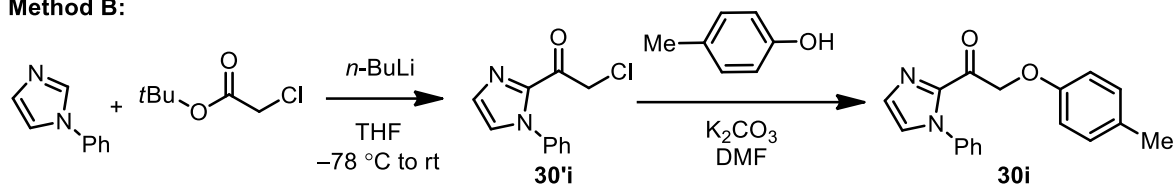
^1H NMR (300 MHz, CDCl_3) δ 7.57-7.40 (m, 3H), 7.37-7.23 (m, 3H), 7.19 (d, $J = 0.9$ Hz, 1H), 3.16 (t, $J = 7.5$ Hz, 2H), 1.88-1.47 (m, 2H), 1.58-1.11 (m, 4H), 0.91 (t, $J = 7.1$ Hz, 3H).

^{13}C NMR (75 MHz, CDCl_3) δ 191.7, 143.2, 138.5, 129.4, 128.9, 128.6, 126.9, 125.9, 39.2, 31.4, 23.7, 22.4, 13.9.

IR (film): ν (cm^{-1}) 3109, 3062, 2954, 2928, 2863, 1683, 1596, 1496, 1446, 1404, 1306, 1040, 957, 910, 761, 691, 554, 515.

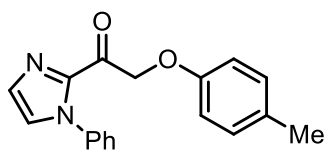
HRMS (ESI, m/z) calcd for $\text{C}_{15}\text{H}_{19}\text{N}_2\text{O}$ $[\text{M}+\text{H}]^+$: 243.1492, found: 243.1493.

Method B:



Procedure for the preparation of 30i. To a solution of *N*-phenylimidazole (864 mg, 6.0 mmol) in THF (15 mL) at $-78\text{ }^{\circ}\text{C}$ was added *n*-BuLi (2.4 mL, 2.5 M in hexane, 6.0 mmol) dropwise. The reaction was stirred at $-78\text{ }^{\circ}\text{C}$ for 1 h, and then stirred at room temperature for 30 min. The *tert*-butyl chloroacetate (1.3 mL, 7.5 mmol) was added at one portion to the flask after the reaction was cooled back down to $-78\text{ }^{\circ}\text{C}$. The reaction was allowed to warm to room temperature slowly (over a period of 3–4 h) and stirred overnight. The reaction was quenched with water at room temperature and extracted with EtOAc. The combined organic layers were dried over anhydrous Na_2SO_4 , filtered, and concentrated under reduced pressure. The residue was purified by flash chromatography on silica gel (EtOAc/hexane = 1:3) to produce **30'i** (960 mg, 4.4 mmol, yield: 73%) as a white solid.

To a mixture of **30'i** (880 mg, 4.0 mmol) and K_2CO_3 (552 mg, 4.0 mmol) in DMF (8.0 mL) at $0\text{ }^{\circ}\text{C}$ were added *p*-cresol (648 mg, 6.0 mmol). The reaction mixture was stirred at room temperature for overnight. The reaction was quenched with water (8 mL) at room temperature and extracted with DCM ($4 \times 10\text{ mL}$). The combined organic layers were dried over anhydrous Na_2SO_4 , filtered, and concentrated under reduced pressure. The residue was purified by flash chromatography on silica gel (EtOAc/hexane = 1:3) to afford **1i** (595 mg, 2.0 mmol, yield: 50%) as a white solid.

1-(1-Phenyl-1*H*-imidazol-2-yl)-2-(*p*-tolylloxy)ethanone (30i)


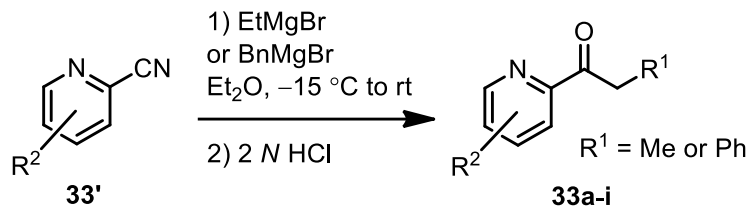
^1H NMR (300 MHz, CDCl_3) δ 7.53–7.39 (m, 3H), 7.39–7.30 (m, 3H), 7.28 (d, $J = 1.0\text{ Hz}$, 1H), 7.07 (d, $J = 8.2\text{ Hz}$, 2H), 6.87 (d, $J = 8.6\text{ Hz}$, 2H), 5.50 (s, 2H), 2.28 (s, 3H).

^{13}C NMR (75 MHz, CDCl_3) δ 184.8, 156.0, 140.8, 137.6, 130.5, 130.0, 129.9, 129.0, 128.9, 127.3, 125.9, 114.5, 70.1, 20.4.

All spectroscopic data were in agreement with the literature.²⁴

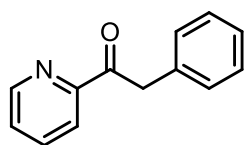
2) Synthesis of 2-Acyl Pyridines

All 2-acyl pyridines (**33a-i**) were synthesized according to reported procedures with some modifications.²⁵



General procedure for the synthesis of 2-acyl pyridines. To a solution of the corresponding 2-pyridinecarbonitrile **33'** (1.0 eq) in Et₂O (0.5 M) at $-15\text{ }^\circ\text{C}$ were added ethylmagnesium bromide or benzylmagnesium bromide (1.2 eq, 1.0 M in THF). The reaction mixture was stirred at $-15\text{ }^\circ\text{C}$ for 30 min, then allowed to warm to room temperature and stirred for a further 2.5 h. The mixture was added 2 N HCl (2.4 eq) and stirred at room temperature for 15 min. The reaction was neutralized with 2 N NaOH to pH 8 and diluted with EtOAc. The organic layer was washed with aqueous saturated NaHCO₃ and brine (20 mL). The combined organic layers were dried over anhydrous Na₂SO₄, filtered, and concentrated under reduced pressure. The residue was purified by flash chromatography on silica gel (EtOAc/hexane = 1:10) to obtain the pure compounds **33a-i**.

2-Phenyl-1-(pyridin-2-yl)ethanone (**33a**)



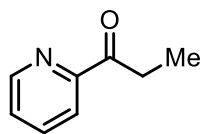
Following the general procedure, 2-pyridinecarbonitrile (1.5 mL, 16.0 mmol) was converted to 2-acyl pyridine **33a** (2.648 g, 13.4 mmol, yield: 84%) as a white solid.

¹H NMR (300 MHz, CDCl₃) δ 8.65 (ddd, $J = 4.7, 1.7, 0.9$ Hz, 1H), 8.06-7.88 (m, 1H), 7.74 (td, $J = 7.7, 1.7$ Hz, 1H), 7.39 (ddd, $J = 7.6, 4.8, 1.2$ Hz, 1H), 7.32-7.07 (m, 5H), 4.48 (s, 2H).

¹³C NMR (75 MHz, CDCl₃) δ 199.1, 153.1, 148.9, 136.9, 134.8, 129.9, 128.4, 127.1, 126.6, 122.3, 43.9.

IR (film): ν (cm⁻¹) 3058, 3032, 2890, 1698, 1578, 1494, 1435, 1396, 1333, 1219, 991, 769, 737, 697, 562.

HRMS (ESI, m/z) calcd for C₁₃H₁₂NO [M+H]⁺: 198.0913, found: 198.0917.

1-(Pyridin-2-yl)propan-1-one (33b)

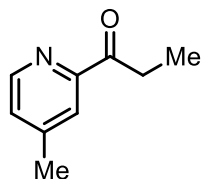
Following the general procedure, 2-pyridinecarbonitrile (1.5 mL, 16.0 mmol) was converted to 2-acyl pyridine **4b** (1.837 g, 13.6 mmol, yield: 85%) as a colorless oil.

^1H NMR (300 MHz, CDCl_3) δ 8.60 (ddd, $J = 4.7, 1.6, 0.8$ Hz, 1H), 8.03-7.86 (m, 1H), 7.75 (td, $J = 7.7, 1.7$ Hz, 1H), 7.38 (ddd, $J = 7.5, 4.8, 1.2$ Hz, 1H), 3.17 (q, $J = 7.3$ Hz, 2H), 1.14 (t, $J = 7.3$ Hz, 3H).

^{13}C NMR (75 MHz, CDCl_3) δ 202.5, 153.5, 148.9, 136.8, 126.9, 121.7, 31.0, 7.9.

IR (film): ν (cm^{-1}) 3057, 2977, 2938, 2881, 1696, 1580, 1459, 1353, 1222, 1093, 996, 954, 756, 667, 617, 568.

HRMS (ESI, m/z) calcd for $\text{C}_8\text{H}_{10}\text{NO}$ $[\text{M}+\text{H}]^+$: 136.0757, found: 136.0758.

1-(4-Methylpyridin-2-yl)propan-1-one (33c)

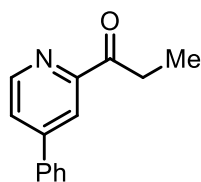
Following the general procedure, 4-methyl-2-pyridinecarbonitrile (733 mg, 6.2 mmol) was converted to 2-acyl pyridine **33c** (711 mg, 4.8 mmol, yield: 77%) as a colorless oil.

^1H NMR (300 MHz, CDCl_3) δ 8.53 (d, $J = 4.9$ Hz, 1H), 8.16-7.57 (m, 1H), 7.46-7.00 (m, 1H), 3.23 (q, $J = 7.3$ Hz, 2H), 2.43 (s, 3H), 1.22 (t, $J = 7.3$ Hz, 3H).

^{13}C NMR (75 MHz, CDCl_3) δ 202.8, 153.4, 148.7, 148.1, 127.7, 122.5, 31.1, 21.0, 8.0.

IR (film): ν (cm^{-1}) 3052, 2976, 2936, 2879, 1696, 1599, 1457, 1408, 1345, 1266, 1165, 1032, 996, 972, 841, 801, 672, 577, 526, 481.

HRMS (ESI, m/z) calcd for $\text{C}_9\text{H}_{11}\text{NONa}$ $[\text{M}+\text{Na}]^+$: 172.0733, found: 172.0733.

1-(4-Phenylpyridin-2-yl)propan-1-one (33d)

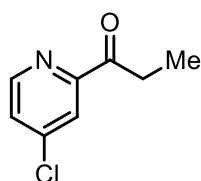
Following the general procedure, 4-phenyl-2-pyridinecarbonitrile (900 mg, 5.0 mmol) was converted to 2-acyl pyridine **33d** (847 mg, 4.0 mmol, yield: 80%) as a colorless oil.

^1H NMR (300 MHz, CDCl_3) δ 8.70 (d, $J = 5.1$ Hz, 1H), 8.38-8.20 (m, 1H), 7.81-7.59 (m, 3H), 7.58-7.39 (m, 3H), 3.28 (q, $J = 7.3$ Hz, 2H), 1.25 (t, $J = 7.3$ Hz, 3H).

^{13}C NMR (75 MHz, CDCl_3) δ 202.6, 154.0, 149.4, 137.5, 129.4, 129.2, 127.0, 124.6, 119.6, 31.3, 8.0.

IR (film): ν (cm^{-1}) 2975, 2933, 2898, 1696, 1589, 1543, 1501, 1454, 1402, 1342, 1282, 1196, 964, 760, 683, 609, 449.

HRMS (ESI, m/z) calcd for $\text{C}_{14}\text{H}_{13}\text{NONa}$ $[\text{M}+\text{Na}]^+$: 234.0889, found: 234.0890.

1-(4-Chloropyridin-2-yl)propan-1-one (33e)

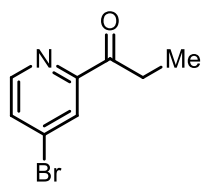
Following the general procedure, 4-chloro-2-pyridinecarbonitrile (889 mg, 6.4 mmol) was converted to 2-acyl pyridine **33e** (898 mg, 5.3 mmol, yield: 83%) as a pale yellow oil.

^1H NMR (300 MHz, CDCl_3) δ 8.49 (dd, $J = 5.2, 0.4$ Hz, 1H), 7.95 (dd, $J = 2.1, 0.5$ Hz, 1H), 7.38 (dd, $J = 5.2, 2.1$ Hz, 1H), 3.14 (q, $J = 7.3$ Hz, 2H), 1.14 (t, $J = 7.3$ Hz, 3H).

^{13}C NMR (75 MHz, CDCl_3) δ 201.3, 154.7, 149.8, 145.4, 127.0, 122.2, 31.2, 7.8.

IR (film): ν (cm^{-1}) 3056, 2978, 2939, 2907, 2880, 1700, 1562, 1458, 1399, 1346, 1279, 1221, 1095, 1022, 971, 899, 841, 793, 706, 487.

HRMS (ESI, m/z) calcd for $\text{C}_8\text{H}_8\text{NOCINa}$ $[\text{M}+\text{Na}]^+$: 192.0187, found: 192.0188.

1-(4-Bromopyridin-2-yl)propan-1-one (33f)

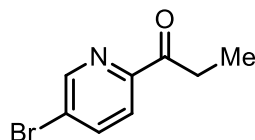
Following the general procedure, 4-bromo-2-pyridinecarbonitrile (819 mg, 4.5 mmol) was converted to 2-acyl pyridine **33f** (776 mg, 3.4 mmol, yield: 76%) as a white solid.

^1H NMR (300 MHz, CDCl_3) δ 8.59-8.38 (m, 1H), 8.32-8.02 (m, 1H), 7.71-7.53 (m, 1H), 3.42-2.92 (m, 2H), 1.38-1.11 (m, 2H).

^{13}C NMR (75 MHz, CDCl_3) δ 201.2, 154.3, 149.7, 134.0, 130.0, 125.2, 31.2, 7.8.

IR (film): ν (cm^{-1}) 3051, 2976, 2937, 2907, 2879, 1699, 1554, 1455, 1392, 1344, 1215, 1082, 1020, 967, 899, 837, 801, 777, 684, 576, 478.

HRMS (ESI, m/z) calcd for $\text{C}_8\text{H}_8\text{NOBrNa}$ $[\text{M}+\text{Na}]^+$: 235.9681 and 237.9661, found: 235.9684 and 237.9664.

1-(5-Bromopyridin-2-yl)propan-1-one (33g)

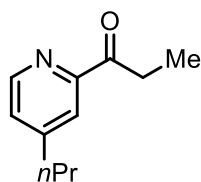
Following the general procedure, 5-bromo-2-pyridinecarbonitrile (819 mg, 4.5 mmol) was converted to 2-acyl pyridine **33g** (796 mg, 3.5 mmol, yield: 78%) as a white solid.

^1H NMR (300 MHz, CDCl_3) δ 8.69 (dd, $J = 2.1, 0.9$ Hz, 1H), 7.94 (dd, $J = 8.4, 2.1$ Hz, 1H), 7.90 (dd, $J = 8.4, 0.9$ Hz, 1H), 3.17 (q, $J = 7.3$ Hz, 2H), 1.18 (t, $J = 7.3$ Hz, 3H).

^{13}C NMR (75 MHz, CDCl_3) δ 201.6, 151.7, 150.0, 139.5, 125.0, 122.9, 31.0, 7.8.

IR (film): ν (cm^{-1}) 3113, 2912, 2867, 1693, 1556, 1454, 1369, 1342, 1253, 1208, 1122, 1079, 997, 949, 862, 800, 728, 620, 559, 497.

HRMS (ESI, m/z) calcd for $\text{C}_8\text{H}_8\text{NOBrNa}$ $[\text{M}+\text{Na}]^+$: 235.9681 and 237.9661, found: 235.9686 and 237.9666.

1-(4-Propylpyridin-2-yl)propan-1-one (33h)

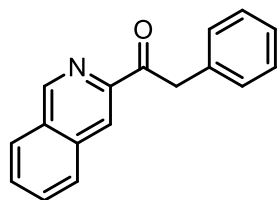
Following the general procedure, 4-*n*-propyl-2-pyridinecarbonitrile (819 mg, 4.0 mmol) was converted to 2-acyl pyridine **33h** (572 mg, 3.2 mmol, yield: 80%) as a colorless oil.

^1H NMR (300 MHz, CDCl_3) δ 8.34 (d, $J = 4.9$ Hz, 1H), 7.67 (d, $J = 1.0$ Hz, 1H), 7.07 (dd, $J = 4.9, 1.7$ Hz, 1H), 3.03 (q, $J = 7.3$ Hz, 2H), 2.64-2.19 (m, 2H), 1.80-1.25 (m, 2H), 1.01 (t, $J = 7.3$ Hz, 3H), 0.75 (t, $J = 7.3$ Hz, 3H).

^{13}C NMR (75 MHz, CDCl_3) δ 202.9, 153.4, 152.6, 148.7, 127.1, 121.8, 37.3, 31.2, 23.3, 13.6, 8.0.

IR (film): ν (cm^{-1}) 3051, 2965, 2934, 2872, 1697, 1598, 1460, 1412, 1347, 1254, 1164, 1023, 993, 862, 833, 801, 492.

HRMS (ESI, m/z) calcd for $\text{C}_{11}\text{H}_{15}\text{NONa}$ $[\text{M}+\text{Na}]^+$: 200.1046, found: 200.1046.

1-(Isoquinolin-3-yl)-2-phenylethanone (33i)

Following the general procedure, isoquinoline-3-carbonitrile (363 mg, 2.4 mmol) was converted to 2-acyl pyridine **33i** (248 mg, 1.0 mmol, yield: 42%) as a white solid.

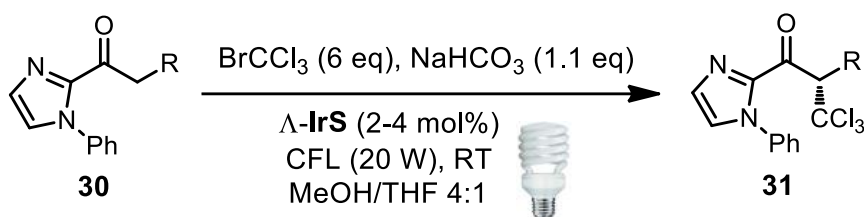
^1H NMR (300 MHz, CD_2Cl_2) δ 9.33 (s, 1H), 8.49 (s, 1H), 8.17-7.92 (m, 2H), 7.85- 7.67 (m, 2H), 7.49-7.17 (m, 5H), 4.69 (s, 2H).

^{13}C NMR (75 MHz, CDCl_3) δ 199.3, 151.8, 147.4, 135.6, 135.1, 130.9, 130.2, 130.0, 129.4, 128.6, 128.4, 127.5, 126.6, 121.0, 44.7.

IR (film): ν (cm^{-1}) 3083, 3027, 2924, 1683, 1618, 1584, 1489, 1448, 1381, 1264, 1222, 1115, 1030, 945, 902, 834, 755, 719, 686, 557, 481.

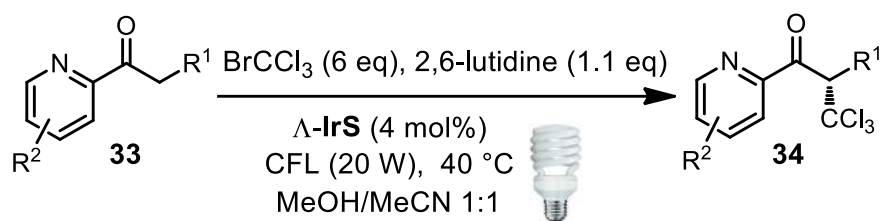
HRMS (ESI, m/z) calcd for $\text{C}_{17}\text{H}_{14}\text{NO}$ $[\text{M}+\text{H}]^+$: 248.1070, found: 248.1070.

5.5.2 Iridium-Catalyzed Photoredox Reactions



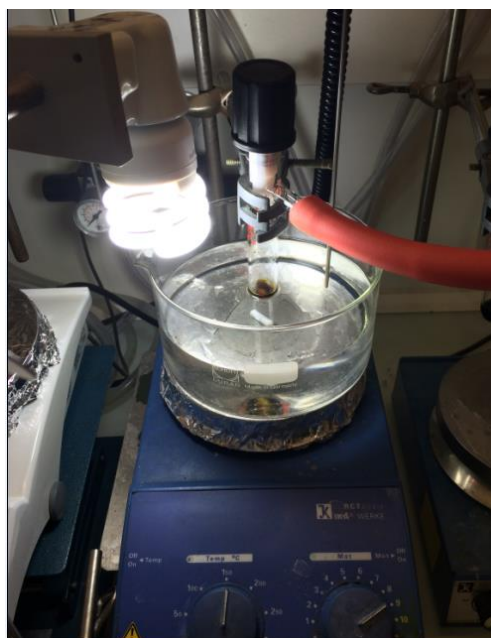
General procedure A: α -trichloromethylation of 2-acyl imidazoles. A dried 10 mL Schlenk tube was charged with the catalyst $\Delta\text{-IrS}$ (2 or 4 mol%), NaHCO_3 (18.5 mg, 0.22 mmol, 1.1 eq) and the corresponding 2-acyl imidazole **30a-l** (0.2 mmol, 1.0 eq). The tube was purged with argon and MeOH/THF (4:1, 0.5 mL) was added *via* syringe, followed by bromotrichloromethane (118.0 μL , 1.2 mmol, 6.0 eq). The reaction mixture was degassed *via* freeze-pump-thaw for three cycles. After the mixture was thoroughly degassed, the vial was sealed and positioned approximately 5 cm from a 20 W white light energy saving lamp. The reaction was stirred at room temperature for the indicated time (monitored by TLC) under nitrogen atmosphere. Afterwards, the mixture was diluted with CH_2Cl_2 (8 mL), the inorganic salt was removed by centrifugation. The combined organic layers were concentrated under reduced pressure. The residue was purified by flash chromatography on silica gel (EtOAc/hexane = 1:15 to 1:10) to afford the products **31a-l**. Racemic samples were obtained by carrying out the reactions with *rac*- IrS . The enantiomeric excess was determined by chiral HPLC analysis.

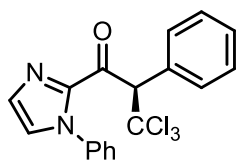
Exemplary reaction setup:



General procedure B: α -trichloromethylation of 2-acylpyridines. A dried 10 mL Schlenk tube was charged with the catalyst Δ -IrS (4 mol%) and the corresponding 2-acyl pyridine **33a-i** (0.2 mmol, 1.0 eq). The tube was purged with nitrogen and MeOH/MeCN (1:1, 0.5 mL) was added *via* syringe, followed by 2,6-lutidine (25.0 μ L, 0.22 mmol, 1.1 eq) and bromotrichloromethane (118.0 μ L, 1.2 mmol, 6.0 eq). The reaction mixture was degassed *via* freeze-pump-thaw for three cycles. After the mixture was thoroughly degassed, the vial was sealed and positioned approximately 5 cm from a 20 W white light energy saving lamp. The reaction was stirred at 40 °C (silicone oil bath) for the indicated time (monitored by TLC) under nitrogen atmosphere. Afterwards, the mixture was concentrated under reduced pressure. The residue was purified by flash chromatography on silica gel (EtOAc/hexane = 1:30 to 1:15) to afford the products **34a-i**. Racemic samples were obtained by carrying out the reactions with *rac*-IrS. The enantiomeric excess was determined by chiral HPLC analysis.

Exemplary reaction setup:



(R)-3,3,3-Trichloro-2-phenyl-1-(1-phenyl-1*H*-imidazol-2-yl)propan-1-one (31a)

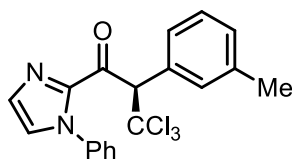
Starting from 2-acyl imidazole **30a** (52.4 mg, 0.20 mmol) according to the general procedure A to give **31a** as a white solid (58.3 mg, 0.154 mmol, yield: 77%). Enantiomeric excess established by HPLC analysis using a Chiralpak OD-H column, *ee* = 99.7% (HPLC: OD-H, 254 nm, hexane/isopropanol = 99:1, flow rate 1.0 mL/min, 25 °C, *t_r* (minor) = 12.3 min, *t_r* (major) = 13.0 min). [α]_D²² = −206.4° (*c* 0.7, CH₂Cl₂).

¹H NMR (300 MHz, CD₂Cl₂) δ 7.76-7.63 (m, 2H), 7.58-7.46 (m, 3H), 7.45-7.36 (m, 3H), 7.31-7.19 (m, 4H), 6.58 (s, 1H).

¹³C NMR (75 MHz, CD₂Cl₂) δ 183.5, 142.8, 138.5, 132.5, 132.1, 130.5, 129.6, 129.5, 129.4, 128.9, 128.8, 126.1, 98.9, 67.7.

IR (film): ν (cm^{−1}) 1686, 1592, 1494, 1448, 1392, 1304, 1153, 1062, 1032, 958, 914, 871, 760, 740, 691, 634, 547.

HRMS (ESI, *m/z*) calcd for C₁₈H₁₃Cl₃N₂ONa [M+Na]⁺: 400.9997 and 402.9969, found: 401.0000 and 402.9971.

(R)-3,3,3-Trichloro-1-(1-phenyl-1*H*-imidazol-2-yl)-2-(*m*-tolyl)propan-1-one (31b)

Starting from 2-acyl imidazole **30b** (55.2 mg, 0.20 mmol) according to the general procedure A to give **31b** as a white solid (71.0 mg, 0.181 mmol, yield: 91%). Enantiomeric excess established by HPLC analysis using a Chiralpak OD-H column, *ee* = 99.0% (HPLC: OD-H, 254 nm, hexane/isopropanol = 99:1, flow rate 1.0 mL/min, 25 °C, *t_r* (minor) = 12.6 min, *t_r* (major) = 11.2 min). [α]_D²² = −229.4° (*c* 0.7, CH₂Cl₂).

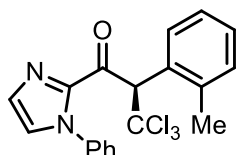
¹H NMR (300 MHz, CD₂Cl₂) δ 7.66-7.46 (m, 5H), 7.40-7.06 (m, 6H), 6.54 (s, 1H), 2.38 (s, 3H).

¹³C NMR (75 MHz, CD₂Cl₂) δ 183.5, 142.8, 138.7, 138.5, 132.6, 132.3, 130.5, 130.4, 129.5, 129.3, 129.1, 128.9, 128.6, 126.1, 98.9, 67.8, 21.6.

IR (film): ν (cm⁻¹) 3125, 3064, 2966, 2919, 2856, 1685, 1594, 1492, 1447, 1393, 1306, 1145, 1050, 968, 877, 823, 761, 716, 638, 556, 517.

HRMS (ESI, m/z) calcd for C₁₉H₁₆Cl₃N₂O [M+H]⁺: 393.0323 and 395.0295, found: 393.0326 and 395.0295.

(R)-3,3,3-Trichloro-1-(1-phenyl-1*H*-imidazol-2-yl)-2-(*o*-tolyl)propan-1-one (31c)



Starting from 2-acyl imidazole **30c** (55.2 mg, 0.20 mmol) according to the general procedure A to give **31c** as a white solid (64.3 mg, 0.164 mmol, yield: 82%). Enantiomeric excess established by HPLC analysis using a Chiralpak OD-H column, $ee > 99.9\%$ (HPLC: OD-H, 254 nm, hexane/isopropanol = 99:1, flow rate 1.0 mL/min, 25 °C, t_r (minor) = 8.7 min, t_r (major) = 9.9 min). $[\alpha]_D^{22} = -270.8^\circ$ (c 0.7, CH₂Cl₂).

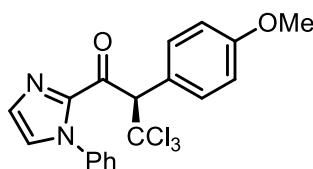
¹H NMR (300 MHz, CD₂Cl₂) δ 7.77 (d, J = 7.6 Hz, 1H), 7.60-7.39 (m, 3H), 7.29 (dd, J = 5.2, 1.1 Hz, 2H), 7.27-7.12 (m, 5H), 6.89 (s, 1H), 2.84 (s, 3H).

¹³C NMR (75 MHz, CD₂Cl₂) δ 183.8, 143.0, 140.6, 138.5, 131.7, 131.2, 130.5, 130.4, 129.6, 129.5, 129.3, 128.9, 126.1, 126.0, 99.6, 63.0, 20.9.

IR (film): ν (cm⁻¹) 3118, 3061, 2978, 1691, 1596, 1494, 1449, 1393, 1307, 1057, 960, 916, 872, 725, 693, 635, 543.

HRMS (ESI, m/z) calcd for C₁₉H₁₆Cl₃N₂O [M+H]⁺: 393.0323 and 395.0295, found: 393.0326 and 395.0296.

(R)-3,3,3-Trichloro-2-(4-methoxyphenyl)-1-(1-phenyl-1*H*-imidazol-2-yl)propan-1-one (31d)



Starting from 2-acyl imidazole **30d** (58.4 mg, 0.20 mmol) according to the general procedure A to give **31d** as a white solid (73.1 mg, 0.179 mmol, yield: 90%). Enantiomeric excess established by HPLC analysis using a Chiralpak IC column, $ee = 99.4\%$ (HPLC: IC, 254 nm, hexane/isopropanol = 95:5,

flow rate 1.0 mL/min, 25 °C, t_r (minor) = 11.2 min, t_r (major) = 8.1 min). $[\alpha]_D^{22} = -236.4^\circ$ (c 0.7, CH_2Cl_2).

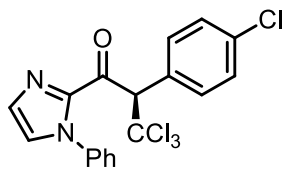
^1H NMR (300 MHz, CD_2Cl_2) δ 7.60 (d, J = 8.9 Hz, 2H), 7.55-7.46 (m, 3H), 7.35-7.16 (m, 4H), 6.92 (d, J = 8.9 Hz, 2H), 6.51 (s, 1H), 3.80 (s, 3H).

^{13}C NMR (75 MHz, CD_2Cl_2) δ 183.8, 160.9, 142.8, 138.6, 133.3, 130.5, 129.5, 129.4, 128.8, 126.2, 124.4, 114.2, 99.4, 67.1, 55.7.

IR (film): ν (cm^{-1}) 3135, 2967, 2927, 2842, 1687, 1602, 1505, 1451, 1392, 1308, 1254, 1179, 1072, 1024, 952, 767, 723, 627, 535.

HRMS (ESI, m/z) calcd for $\text{C}_{19}\text{H}_{15}\text{Cl}_3\text{N}_2\text{O}_2$ $[\text{M}+\text{Na}]^+$: 431.0091 and 433.0064, found: 431.0094 and 433.0065.

(*R*)-3,3,3-Trichloro-2-(4-chlorophenyl)-1-(1-phenyl-1*H*-imidazol-2-yl)propan-1-one (31e)



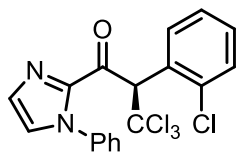
Starting from 2-acyl imidazole **30e** (59.2 mg, 0.20 mmol) according to the general procedure A to give **31e** as a white solid (56.2 mg, 0.136 mmol, yield: 68%). Enantiomeric excess established by HPLC analysis using a Chiralpak OD-H column, ee = 99.4% (HPLC: OD-H, 254 nm, hexane/isopropanol = 99:1, flow rate 1.0 mL/min, 25 °C, t_r (minor) = 11.5 min, t_r (major) = 10.5 min). $[\alpha]_D^{22} = -222.8^\circ$ (c 0.5, CH_2Cl_2).

^1H NMR (300 MHz, CD_2Cl_2) δ 7.66 (d, J = 8.5 Hz, 2H), 7.57-7.46 (m, 3H), 7.38 (d, J = 8.6 Hz, 2H), 7.32-7.20 (m, 4H), 6.58 (s, 1H).

^{13}C NMR (75 MHz, CD_2Cl_2) δ 183.2, 142.7, 138.5, 135.9, 133.4, 131.2, 130.7, 129.6, 129.5, 129.1, 129.0, 126.2, 98.5, 66.9.

IR (film): ν (cm^{-1}) 2965, 2927, 2880, 1691, 1594, 1492, 1448, 1394, 1307, 1092, 1062, 957, 764, 717, 691, 645, 543, 438.

HRMS (ESI, m/z) calcd for $\text{C}_{18}\text{H}_{12}\text{Cl}_4\text{N}_2\text{ONa}$ $[\text{M}+\text{Na}]^+$: 434.9596, 436.9568 and 438.9541, found: 434.9597, 436.9567 and 438.9539.

(R)-3,3,3-Trichloro-2-(2-chlorophenyl)-1-(1-phenyl-1H-imidazol-2-yl)propan-1-one (31f)

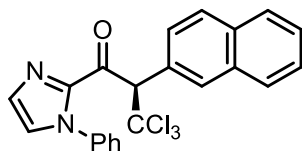
Starting from 2-acyl imidazole **30f** (59.2 mg, 0.20 mmol) according to the general procedure A to give **31f** as a white solid (68.0 mg, 0.165 mmol, yield: 83%). Enantiomeric excess established by HPLC analysis using a Chiralpak OD-H column, *ee* = 99.6% (HPLC: OD-H, 254 nm, hexane/isopropanol = 99:1, flow rate 1.0 mL/min, 25 °C, *t_r* (minor) = 12.5 min, *t_r* (major) = 13.6 min). [α]_D²² = −269.6° (*c* 0.7, CH₂Cl₂).

¹H NMR (300 MHz, CD₂Cl₂) δ 7.92 (dd, *J* = 7.7, 1.9 Hz, 1H), 7.62-7.43 (m, 4H), 7.43-7.15 (m, 7H).

¹³C NMR (75 MHz, CD₂Cl₂) δ 183.1, 142.9, 138.5, 137.5, 132.2, 130.9, 130.83, 130.78, 130.5, 129.6, 129.4, 129.2, 126.9, 126.2, 98.8, 62.2.

IR (film): ν (cm^{−1}) 3132, 3090, 3037, 2852, 1686, 1591, 1486, 1443, 1395, 1301, 1147, 1051, 961, 863, 759, 716, 687, 630, 540.

HRMS (ESI, *m/z*) calcd for C₁₈H₁₂Cl₄N₂ONa [M+Na]⁺: 434.9596, 436.9568 and 438.9541, found: 434.9595, 436.9566 and 438.9537.

(R)-3,3,3-Trichloro-2-(naphthalen-2-yl)-1-(1-phenyl-1H-imidazol-2-yl)propan-1-one (31g)

Starting from 2-acyl imidazole **30g** (62.4 mg, 0.20 mmol) according to the general procedure A to give **31g** as a white solid (61.2 mg, 0.143 mmol, yield: 71%). Enantiomeric excess established by HPLC analysis using a Chiralpak OD-H column, *ee* = 99.2% (HPLC: OD-H, 254 nm, hexane/isopropanol = 98:2, flow rate 1.0 mL/min, 25 °C, *t_r* (minor) = 10.5 min, *t_r* (major) = 13.6 min). [α]_D²² = −279.2° (*c* 0.5, CH₂Cl₂).

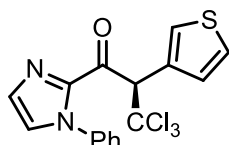
¹H NMR (300 MHz, CD₂Cl₂) δ 8.19 (d, *J* = 1.1 Hz, 1H), 7.99-7.77 (m, 4H), 7.63-7.46 (m, 5H), 7.33-7.22 (m, 3H), 7.21 (d, *J* = 0.9 Hz, 1H), 6.76 (s, 1H).

¹³C NMR (75 MHz, CD₂Cl₂) δ 183.4, 142.8, 138.5, 133.8, 133.4, 131.8, 130.5, 129.9, 129.5, 129.4, 129.2, 128.9, 128.7, 128.3, 128.0, 127.4, 126.8, 126.2, 99.0, 67.8.

IR (film): ν (cm⁻¹) 2969, 2927, 2884, 1686, 1596, 1498, 1449, 1392, 1306, 1152, 1056, 950, 817, 761, 724, 690, 477.

HRMS (ESI, m/z) calcd for C₂₂H₁₅Cl₃N₂ONa [M+Na]⁺: 451.0142 and 453.0116, found: 451.0143 and 453.0114.

(R)-3,3,3-Trichloro-1-(1-phenyl-1*H*-imidazol-2-yl)-2-(thiophen-3-yl)propan-1-one (31h)



Starting from 2-acyl imidazole **30h** (53.6 mg, 0.20 mmol) according to the general procedure A to give **31h** as a white solid (48.0 mg, 0.125 mmol, yield: 62%). Enantiomeric excess established by HPLC analysis using a Chiralpak AD-H column, $ee = 96\%$ (HPLC: AD-H, 254 nm, hexane/isopropanol = 95:5, flow rate 1.0 mL/min, 25 °C, t_r (minor) = 8.6 min, t_r (major) = 11.2 min). $[\alpha]_D^{22} = -158.8^\circ$ (c 0.3, CH₂Cl₂).

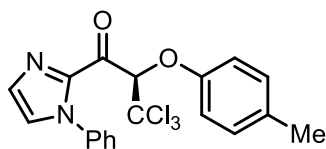
¹H NMR (300 MHz, CD₂Cl₂) δ 7.62 (dd, $J = 2.8, 1.4$ Hz, 1H), 7.57-7.45 (m, 3H), 7.35 (qd, $J = 5.0, 2.1$ Hz, 2H), 7.30-7.22 (m, 4H), 6.74 (s, 1H).

¹³C NMR (75 MHz, CD₂Cl₂) δ 183.4, 142.8, 138.6, 132.7, 130.6, 130.2, 129.6, 129.4, 129.1, 128.4, 126.2, 125.6, 98.7, 63.3.

IR (film): ν (cm⁻¹) 3144, 3107, 3067, 2847, 1686, 1491, 1444, 1394, 1302, 1148, 1062, 966, 761, 713, 671, 532.

HRMS (ESI, m/z) calcd for C₁₆H₁₁Cl₃N₂OSNa [M+Na]⁺: 406.9550 and 408.9521, found: 406.9552 and 408.9523.

(R)-3,3,3-Trichloro-1-(1-phenyl-1*H*-imidazol-2-yl)-2-(*p*-tolxyloxy)propan-1-one (31i)



Starting from 2-acyl imidazole **30i** (58.4 mg, 0.20 mmol) according to the general procedure A to give **31i** as a colorless oil (52.1 mg, 0.128 mmol, yield: 64%). Enantiomeric excess established by HPLC analysis using a Chiralpak OD-H column, $ee = 92\%$ (HPLC: OD-H, 254 nm, hexane/isopropanol =

97:3, flow rate 1.0 mL/min, 25 °C, t_r (minor) = 8.4 min, t_r (major) = 9.7 min). $[\alpha]_D^{22} = -92.8^\circ$ (c 1.0, CH_2Cl_2).

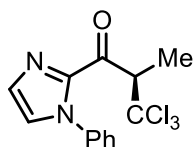
^1H NMR (300 MHz, CD_2Cl_2) δ 7.54-7.45 (m, 3H), 7.41 (d, J = 0.9 Hz, 1H), 7.35 (d, J = 0.9 Hz, 1H), 7.32-7.25 (m, 2H), 7.10 (br s, 4H), 6.93 (s, 1H), 2.28 (s, 3H).

^{13}C NMR (75 MHz, CD_2Cl_2) δ 181.6, 155.6, 143.3, 137.9, 133.0, 131.2, 130.55, 129.60, 129.5, 129.0, 126.0, 116.7, 96.5, 83.4, 20.7.

IR (film): ν (cm^{-1}) 3121, 3036, 2924, 2862, 1698, 1598, 1503, 1447, 1398, 1303, 1218, 1060, 946, 901, 809, 766, 727, 689, 580, 521.

HRMS (ESI, m/z) calcd for $\text{C}_{19}\text{H}_{15}\text{Cl}_3\text{N}_2\text{O}_2\text{Na}$ $[\text{M}+\text{Na}]^+$: 431.0091 and 433.0064, found: 431.0092 and 433.0062.

(*R*)-3,3,3-Trichloro-2-methyl-1-(1-phenyl-1*H*-imidazol-2-yl)propan-1-one (31j)



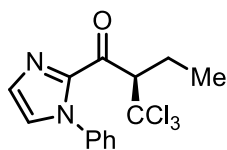
Starting from 2-acyl imidazole **30j** (40.0 mg, 0.20 mmol) according to the general procedure A to give **31j** as a white solid (46.0 mg, 0.146 mmol, yield: 73%). Enantiomeric excess established by HPLC analysis using a Chiralpak IC column, ee = 98.8% (HPLC: IC, 254 nm, hexane/isopropanol = 99:1, flow rate 1.0 mL/min, 25 °C, t_r (minor) = 9.4 min, t_r (major) = 8.2 min). $[\alpha]_D^{22} = +25.2^\circ$ (c 0.5, CH_2Cl_2).

^1H NMR (300 MHz, CD_2Cl_2) δ 7.49-7.33 (m, 3H), 7.28-7.12 (m, 4H), 5.30 (q, J = 6.8 Hz, 1H), 1.50 (d, J = 6.8 Hz, 3H).

^{13}C NMR (75 MHz, CD_2Cl_2) δ 186.6, 142.9, 138.6, 130.5, 129.5, 129.3, 128.9, 126.2, 100.5, 58.3, 16.0.

IR (film): ν (cm^{-1}) 3154, 3122, 3065, 2961, 2930, 1688, 1591, 1492, 1449, 1399, 1299, 1151, 1078, 1012, 953, 905, 831, 767, 687, 601, 532.

HRMS (ESI, m/z) calcd for $\text{C}_{13}\text{H}_{11}\text{Cl}_3\text{N}_2\text{ONa}$ $[\text{M}+\text{Na}]^+$: 338.9829 and 340.9801, found: 338.9830 and 340.9800.

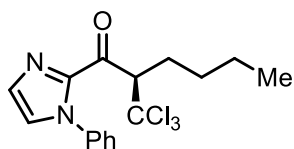
(R)-1-(1-Phenyl-1H-imidazol-2-yl)-2-(trichloromethyl)butan-1-one (31k)

Starting from 2-acyl imidazole **30k** (42.8 mg, 0.20 mmol) according to the general procedure A to give **31k** as a white solid (63.3 mg, 0.192 mmol, yield: 96%). Enantiomeric excess established by HPLC analysis using a Chiralpak IC column, *ee* = 99.4% (HPLC: IC, 254 nm, hexane/isopropanol = 99:1, flow rate 1.0 mL/min, 25 °C, *t_r* (minor) = 7.3 min, *t_r* (major) = 6.3 min). $[\alpha]_D^{22} = -1.6^\circ$ (*c* 0.6, CH₂Cl₂). ¹H NMR (300 MHz, CDCl₃) δ 7.50-7.35 (m, 3H), 7.27 (d, *J* = 0.9 Hz, 1H), 7.26-7.15 (m, 3H), 5.23 (dd, *J* = 8.7, 5.2 Hz, 1H), 2.25-1.92 (m, 2H), 0.91 (t, *J* = 7.5 Hz, 3H).

¹³C NMR (75 MHz, CDCl₃) δ 186.6, 144.0, 138.1, 130.3, 129.2, 128.9, 128.1, 125.6, 99.2, 63.9, 24.3, 11.6.

IR (film): ν (cm⁻¹) 3120, 3059, 2971, 2878, 1735, 1686, 1495, 1448, 1399, 1308, 1201, 1148, 1113, 1073, 1031, 961, 762, 684.

HRMS (ESI, *m/z*) calcd for C₁₄H₁₃Cl₃N₂ONa [M+Na]⁺: 352.9986 and 354.9957, found: 352.9986 and 354.9958.

(R)-1-(1-Phenyl-1H-imidazol-2-yl)-2-(trichloromethyl)hexan-1-one (31l)

Starting from 2-acyl imidazole **30l** (48.4 mg, 0.20 mmol) according to the general procedure A to give **31l** as a colorless oil (54.4 mg, 0.152 mmol, yield: 76%). Enantiomeric excess established by HPLC analysis using a Chiralpak OD-H column, *ee* = 98.8% (HPLC: OD-H, 254 nm, hexane/isopropanol = 99:1, flow rate 1.0 mL/min, 25 °C, *t_r* (minor) = 6.3 min, *t_r* (major) = 6.8 min). $[\alpha]_D^{22} = -28.0^\circ$ (*c* 0.5, CH₂Cl₂).

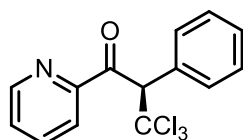
¹H NMR (300 MHz, CD₂Cl₂) δ 7.58-7.44 (m, 3H), 7.40-7.20 (m, 4H), 5.36 (dd, *J* = 10.3, 3.4 Hz, 1H), 2.22-1.96 (m, 2H), 1.51-1.17 (m, 4H), 0.87 (t, *J* = 7.1 Hz, 3H).

¹³C NMR (75 MHz, CD₂Cl₂) δ 186.9, 144.3, 138.7, 130.6, 129.5, 129.3, 128.9, 126.2, 100.0, 62.6, 31.2, 29.5, 23.0, 13.9.

IR (film): ν (cm⁻¹) 3113, 3064, 2957, 2930, 2865, 1688, 1596, 1497, 1448, 1399, 1310, 1039, 905, 854, 761, 685, 547.

HRMS (ESI, m/z) calcd for C₁₆H₁₇Cl₃N₂ONa [M+Na]⁺: 381.0299 and 383.0271, found: 381.0298 and 383.0269.

(R)-3,3,3-Trichloro-2-phenyl-1-(pyridin-2-yl)propan-1-one (34a)



Starting from 2-acyl pyridine **33a** (39.4 mg, 0.20 mmol) according to the general procedure B to give **34a** as a white solid (52.0 mg, 0.166 mmol, yield: 83%). Enantiomeric excess established by HPLC analysis using a Chiralpak IC column, $ee = 99.6\%$ (HPLC: IC, 254 nm, hexane/isopropanol = 99:1, flow rate 1.0 mL/min, 25 °C, t_r (minor) = 9.6 min, t_r (major) = 7.6 min). $[\alpha]_D^{22} = -85.0^\circ$ (c 0.3, CH₂Cl₂).

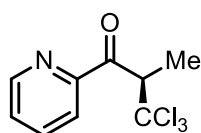
¹H NMR (300 MHz, CD₂Cl₂) δ 8.64 (ddd, $J = 4.7, 1.7, 0.9$ Hz, 1H), 8.10 (dt, $J = 7.9, 1.1$ Hz, 1H), 7.84 (td, $J = 7.7, 1.7$ Hz, 1H), 7.78-7.66 (m, 2H), 7.46 (ddd, $J = 7.6, 4.8, 1.2$ Hz, 1H), 7.40-7.33 (m, 3H), 6.89 (s, 1H).

¹³C NMR (75 MHz, CD₂Cl₂) δ 194.3, 152.6, 149.4, 137.7, 132.4, 129.5, 128.7, 128.2, 123.2, 99.3, 65.8.

IR (film): ν (cm⁻¹) 3057, 2949, 1704, 1580, 1436, 1324, 1248, 1213, 1067, 992, 893, 871, 809, 742, 699, 616, 560.

HRMS (ESI, m/z) calcd for C₁₄H₁₀Cl₃N₂ONa [M+Na]⁺: 335.9720 and 337.9692, found: 335.9722 and 337.9692.

(R)-3,3,3-Trichloro-2-methyl-1-(pyridin-2-yl)propan-1-one (34b)



Starting from 2-acyl pyridine **33b** (27.0 mg, 0.20 mmol) according to the general procedure B to give **34b** as a colorless oil (33.6 mg, 0.134 mmol, yield: 67%). Enantiomeric excess established by HPLC

analysis using a Chiralpak OD-H column, $ee = 95\%$ (HPLC: OD-H, 254 nm, hexane/isopropanol = 99:1, flow rate 1.0 mL/min, 25 °C, t_r (minor) = 7.8 min, t_r (major) = 6.7 min). $[\alpha]_D^{22} = +40.3^\circ$ (c 0.4, CH_2Cl_2).

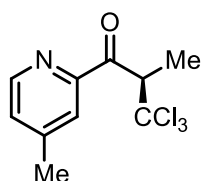
^1H NMR (300 MHz, CDCl_3) δ 8.65 (ddd, $J = 4.7, 1.7, 0.9$ Hz, 1H), 8.05 (dt, $J = 7.9, 1.0$ Hz, 1H), 7.82 (td, $J = 7.7, 1.7$ Hz, 1H), 7.46 (ddd, $J = 7.6, 4.8, 1.2$ Hz, 1H), 5.60 (q, $J = 6.9$ Hz, 1H), 1.55 (d, $J = 6.9$ Hz, 3H).

^{13}C NMR (75 MHz, CDCl_3) δ 197.1, 152.3, 149.0, 137.3, 127.7, 122.7, 100.0, 55.5, 15.7.

IR (film): ν (cm^{-1}) 3288, 3170, 3130, 3061, 2957, 2924, 1701, 1578, 1443, 1333, 1213, 968, 923, 810, 768, 741, 665, 582, 408.

HRMS (ESI, m/z) calcd for $\text{C}_9\text{H}_8\text{Cl}_3\text{NONa}$ $[\text{M}+\text{Na}]^+$: 273.9564 and 275.9535, found: 273.9565 and 275.9535.

(R)-3,3,3-Trichloro-2-methyl-1-(4-methylpyridin-2-yl)propan-1-one (34c)



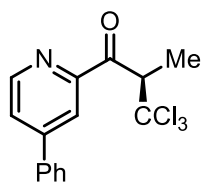
Starting from 2-acyl pyridine **33c** (29.8 mg, 0.20 mmol) according to the general procedure B to give **34c** as a colorless oil (34.2 mg, 0.129 mmol, yield: 65%). Enantiomeric excess established by HPLC analysis using a Chiralpak OD-H column, $ee = 93\%$ (HPLC: OD-H, 254 nm, hexane/isopropanol = 99:1, flow rate 1.0 mL/min, 25 °C, t_r (minor) = 11.1 min, t_r (major) = 7.5 min). $[\alpha]_D^{22} = +43.1^\circ$ (c 0.4, CH_2Cl_2).

^1H NMR (300 MHz, CDCl_3) δ 8.58-8.32 (m, 1H), 7.98-7.68 (m, 1H), 7.26 (ddd, $J = 4.9, 1.7, 0.7$ Hz, 1H), 5.59 (q, $J = 6.9$ Hz, 1H), 2.38 (s, 3H), 1.54 (d, $J = 6.9$ Hz, 3H).

^{13}C NMR (75 MHz, CDCl_3) δ 197.4, 152.2, 148.8, 128.6, 123.5, 100.0, 55.5, 21.1, 15.7.

IR (film): ν (cm^{-1}) 3112, 3055, 2989, 2952, 2878, 1702, 1598, 1497, 1451, 1400, 1317, 1158, 1019, 981, 934, 842, 817, 771, 727, 671, 584, 514, 427.

HRMS (ESI, m/z) calcd for $\text{C}_{10}\text{H}_{10}\text{Cl}_3\text{NONa}$ $[\text{M}+\text{Na}]^+$: 287.9720 and 289.9691, found: 287.9722 and 289.9693.

(R)-3,3,3-Trichloro-2-methyl-1-(4-phenylpyridin-2-yl)propan-1-one (34d)

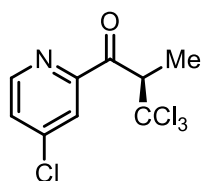
Starting from 2-acyl pyridine **33d** (42.2 mg, 0.20 mmol) according to the general procedure B to give **34d** as a white solid (46.5 mg, 0.142 mmol, yield: 71%). Enantiomeric excess established by HPLC analysis using a Chiralpak OD-H column, *ee* = 94% (HPLC: OD-H, 254 nm, hexane/isopropanol = 99:1, flow rate 1.0 mL/min, 25 °C, *t_r* (minor) = 14.4 min, *t_r* (major) = 10.0 min). $[\alpha]_D^{22} = +48.7^\circ$ (*c* 0.4, CH₂Cl₂).

¹H NMR (300 MHz, CDCl₃) δ 8.68 (dd, *J* = 5.1, 0.6 Hz, 1H), 8.27 (dd, *J* = 1.8, 0.7 Hz, 1H), 7.66 (dd, *J* = 5.1, 1.9 Hz, 1H), 7.61 (dt, *J* = 8.5, 2.3 Hz, 2H), 7.53-7.31 (m, 3H), 1.58 (d, *J* = 6.9 Hz, 3H).

¹³C NMR (75 MHz, CDCl₃) δ 197.2, 152.9, 149.9, 149.5, 137.2, 129.6, 129.3, 127.1, 125.4, 120.5, 100.0, 55.6, 15.7.

IR (film): ν (cm⁻¹) 3062, 3034, 2962, 2927, 1699, 1591, 1455, 1401, 1324, 1262, 1188, 1087, 1027, 984, 930, 825, 768, 707, 667, 578, 507, 428.

HRMS (ESI, *m/z*) calcd for C₁₅H₁₂Cl₃NONa [M+Na]⁺: 349.9877 and 351.9849, found: 349.9879 and 351.9849.

(R)-3,3,3-Trichloro-1-(4-chloropyridin-2-yl)-2-methylpropan-1-one (34e)

Starting from 2-acyl pyridine **33e** (33.8 mg, 0.20 mmol) according to the general procedure B to give **34e** as a colorless oil (46.0 mg, 0.161 mmol, yield: 81%). Enantiomeric excess established by HPLC analysis using a Chiralpak OD-H column, *ee* = 95% (HPLC: OD-H, 254 nm, hexane/isopropanol = 99:1, flow rate 1.0 mL/min, 25 °C, *t_r* (minor) = 9.9 min, *t_r* (major) = 6.7 min). $[\alpha]_D^{22} = +44.4^\circ$ (*c* 0.5, CH₂Cl₂).

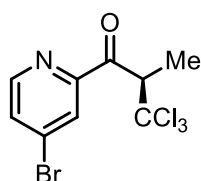
¹H NMR (300 MHz, CDCl₃) δ 8.55 (d, *J* = 5.2 Hz, 1H), 8.02 (d, *J* = 2.0 Hz, 1H), 7.46 (dd, *J* = 5.2, 2.0 Hz, 1H), 5.52 (q, *J* = 6.8 Hz, 1H), 1.54 (d, *J* = 6.9 Hz, 3H).

^{13}C NMR (75 MHz, CDCl_3) δ 196.0, 153.5, 149.9, 145.9, 127.8, 123.1, 99.6, 55.7, 15.6.

IR (film): ν (cm^{-1}) 3083, 3057, 2992, 2952, 2879, 1709, 1562, 1454, 1395, 1322, 1214, 1094, 993, 930, 829, 777, 700, 666, 583, 517, 425.

HRMS (ESI, m/z) calcd for $\text{C}_9\text{H}_8\text{Cl}_4\text{NO}$ $[\text{M}+\text{H}]^+$: 285.9355, 287.9325 and 289.9297, found: 285.9356, 287.9327 and 289.9297.

(R)-1-(4-Bromopyridin-2-yl)-3,3,3-trichloro-2-methylpropan-1-one (34f)



Starting from 2-acyl pyridine **33f** (42.6 mg, 0.20 mmol) according to the general procedure B to give **34f** as a colorless oil (44.8 mg, 0.136 mmol, yield: 68%). Enantiomeric excess established by HPLC analysis using a Chiralpak OD-H column, $ee = 92\%$ (HPLC: OD-H, 254 nm, hexane/isopropanol = 99:1, flow rate 1.0 mL/min, 25 °C, t_r (minor) = 10.5 min, t_r (major) = 6.8 min). $[\alpha]_{\text{D}}^{22} = +36.9^\circ$ (c 0.3, CH_2Cl_2).

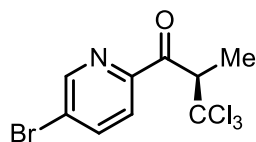
^1H NMR (300 MHz, CDCl_3) δ 8.53 (d, $J = 5.2$ Hz, 1H), 8.25 (dd, $J = 1.9, 0.4$ Hz, 1H), 7.69 (dd, $J = 5.2, 1.9$ Hz, 1H), 5.58 (q, $J = 6.9$ Hz, 1H), 1.61 (d, $J = 6.9$ Hz, 3H).

^{13}C NMR (75 MHz, CDCl_3) δ 195.9, 153.2, 149.7, 134.4, 130.8, 126.2, 99.6, 55.7, 15.6.

IR (film): ν (cm^{-1}) 3091, 3055, 2991, 2961, 2879, 1707, 1555, 1453, 1386, 1326, 1205, 1086, 989, 931, 829, 778, 674, 581, 509, 425.

HRMS (ESI, m/z) calcd for $\text{C}_9\text{H}_8\text{BrCl}_3\text{NO}$ $[\text{M}+\text{H}]^+$: 329.8849, 331.8825, 333.8798 and 335.8771, found: 329.8852, 331.8827, 333.8800 and 335.8773.

(R)-1-(5-Bromopyridin-2-yl)-3,3,3-trichloro-2-methylpropan-1-one (34g)



Starting from 2-acyl pyridine **33g** (42.6 mg, 0.20 mmol) according to the general procedure B to give **34g** as a colorless oil (60.1 mg, 0.182 mmol, yield: 91%). Enantiomeric excess established by HPLC analysis using a Chiralpak OD-H column, $ee = 96\%$ (HPLC: OD-H, 254 nm, hexane/isopropanol =

99:1, flow rate 1.0 mL/min, 25 °C, t_r (minor) = 10.5 min, t_r (major) = 8.5 min). $[\alpha]_D^{22} = +24.8^\circ$ (c 0.6, CH_2Cl_2).

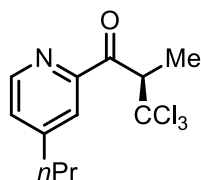
^1H NMR (300 MHz, CDCl_3) δ 8.70 (dd, $J = 1.9, 0.9$ Hz, 1H), 8.04-7.91 (m, 2H), 5.49 (q, $J = 6.8$ Hz, 1H), 1.54 (d, $J = 6.9$ Hz, 3H).

^{13}C NMR (75 MHz, CDCl_3) δ 196.3, 150.5, 150.2, 140.1, 126.1, 123.9, 99.7, 55.4, 15.6.

IR (film): ν (cm^{-1}) 3053, 2983, 2942, 2879, 1703, 1560, 1453, 1370, 1329, 1208, 1086, 1006, 967, 826, 777, 676, 625, 583.

HRMS (ESI, m/z) calcd for $\text{C}_9\text{H}_8\text{BrCl}_3\text{NO}$ $[\text{M}+\text{H}]^+$: 329.8849, 331.8825, 333.8798 and 335.8771, found: 329.8853, 331.8828, 333.8803 and 335.8774.

(R)-3,3,3-Trichloro-2-methyl-1-(4-propylpyridin-2-yl)propan-1-one (34h)



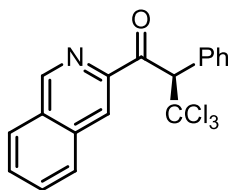
Starting from 2-acyl pyridine **33h** (35.4 mg, 0.20 mmol) according to the general procedure B to give **34h** as a colorless oil (39.3 mg, 0.134 mmol, yield: 67%). Enantiomeric excess established by HPLC analysis using a Chiralpak OD-H column, $ee = 94\%$ (HPLC: OD-H, 254 nm, hexane/isopropanol = 99:1, flow rate 1.0 mL/min, 25 °C, t_r (minor) = 7.8 min, t_r (major) = 6.0 min). $[\alpha]_D^{22} = +44.3^\circ$ (c 0.4, CH_2Cl_2).

^1H NMR (300 MHz, CDCl_3) δ 8.58 (d, $J = 4.9$ Hz, 1H), 7.93 (s, 1H), 7.33 (dd, $J = 4.9, 1.6$ Hz, 1H), 5.66 (q, $J = 6.9$ Hz, 1H), 2.87-2.50 (m, 2H), 1.70 (dq, $J = 14.8, 7.5$ Hz, 2H), 1.61 (d, $J = 6.9$ Hz, 3H), 0.96 (t, $J = 7.3$ Hz, 3H).

^{13}C NMR (75 MHz, CDCl_3) δ 197.4, 153.2, 152.3, 148.8, 127.9, 122.8, 100.1, 55.6, 37.3, 23.3, 15.7, 13.6.

IR (film): ν (cm^{-1}) 2961, 2934, 2871, 1706, 1597, 1414, 1324, 1159, 1003, 934, 825, 779, 731, 669, 580, 428.

HRMS (ESI, m/z) calcd for $\text{C}_{12}\text{H}_{14}\text{Cl}_3\text{NONa}$ $[\text{M}+\text{Na}]^+$: 316.0033, 318.0005 and 319.9977, found: 316.0034, 318.0005 and 319.9977.

(R)-3,3,3-Trichloro-1-(isoquinolin-3-yl)-2-phenylpropan-1-one (34i)

Starting from 2-acyl pyridine **33i** (49.4 mg, 0.20 mmol) according to the general procedure B to give **34i** as a white solid (52.3 mg, 0.144 mmol, yield: 72%). Enantiomeric excess established by HPLC analysis using a Chiralpak OD-H column, *ee* = 90% (HPLC: OD-H, 254 nm, hexane/isopropanol = 98:2, flow rate 1.0 mL/min, 25 °C, *t_r* (minor) = 11.1 min, *t_r* (major) = 7.5 min). $[\alpha]_D^{22} = -102.0^\circ$ (*c* 0.4, CH₂Cl₂).

¹H NMR (300 MHz, CD₂Cl₂) δ 9.22 (s, 1H), 8.56 (s, 1H), 8.10-7.90 (m, 2H), 7.86-7.64 (m, 4H), 7.47-7.25 (m, 3H), 7.01 (s, 1H).

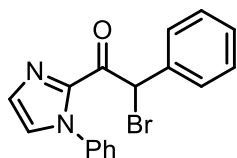
¹³C NMR (75 MHz, CD₂Cl₂) δ 194.5, 152.3, 146.8, 136.0, 132.6, 132.5, 131.7, 130.9, 130.5, 129.5, 129.1, 128.7, 128.0, 122.3, 99.5, 66.5.

IR (film): ν (cm⁻¹) 3058, 2947, 2855, 1963, 1694, 1490, 1444, 1384, 1309, 1245, 1161, 1124, 1060, 939, 908, 864, 737, 697, 622, 562, 485.

HRMS (ESI, *m/z*) calcd for C₁₈H₁₂Cl₃NONa [M+Na]⁺: 385.9877, 387.9849 and 389.9823, found: 385.9878, 387.9849 and 389.9820.

5.5.3 Mechanistic Experiments**1) Control Experiments for Table 9**

As shown in Scheme 11-12 and Figure 65-66, the experiment data of compound **32** and **36** are shown below.

2-Bromo-2-phenyl-1-(1-phenyl-1H-imidazol-2-yl)ethanone (32)

White solid.

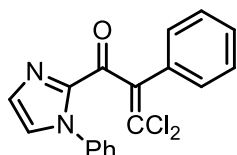
¹H NMR (300 MHz, CD₂Cl₂) δ 7.55-7.45 (m, 2H), 7.44-7.34 (m, 3H), 7.31-7.13 (m, 7H), 6.90 (s, 1H).

¹³C NMR (75 MHz, CD₂Cl₂) δ 182.3, 141.1, 138.4, 136.3, 130.6, 130.0, 129.5, 129.4, 129.1, 129.0, 126.2, 50.2.

IR (film): ν (cm⁻¹) 1686, 1591, 1492, 1446, 1394, 1304, 1148, 1064, 1028, 955, 914, 867, 741, 690, 633, 547.

HRMS (ESI, m/z) calcd for C₁₇H₁₄BrN₂O [M+H]⁺: 341.0284 and 343.0265, found: 341.0297 and 343.0277.

3,3-Dichloro-2-phenyl-1-(1-phenyl-1*H*-imidazol-2-yl)prop-2-en-1-one (36)



White solid.

¹H NMR (300 MHz, CD₂Cl₂) δ 7.47-7.36 (m, 5H), 7.34-7.24 (m, 4H), 7.24-7.15 (m, 3H).

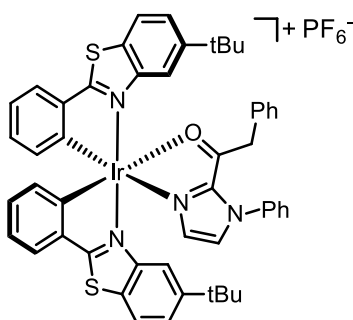
¹³C NMR (75 MHz, CD₂Cl₂) δ 181.6, 142.1, 140.5, 138.2, 134.4, 131.6, 130.0, 129.6, 129.4, 129.3, 129.2, 129.0, 128.4, 126.1, 122.7.

IR (film): ν (cm⁻¹) 1669, 1597, 1494, 1446, 1389, 1301, 1252, 1203, 1150, 1073, 1029, 996, 937, 913, 839, 802, 756, 692, 643, 576, 536.

HRMS (ESI, m/z) calcd for C₁₈H₁₃Cl₂N₂O [M+H]⁺: 343.0399 and 345.0373, found: 343.0414 and 345.0388.

2) Synthesis of the Proposed Intermediate Complex I and II

Intermediate I



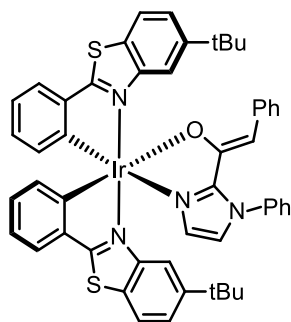
The racemic complex **I** was obtained by reacting substrate **30a** (31.4 mg, 0.12 mmol) with racemic Δ/Λ -**IrS** (95.2 mg, 0.10 mmol) at room temperature overnight in CH₂Cl₂ (2.0 mL). Afterwards, the mixture was concentrated under vacuum. The residue black solid was washed by Et₂O (4 \times 1 mL), the yellow solid was obtained (110.0 mg, yield: 97%).

¹H NMR (300 MHz, CD₂Cl₂) δ 7.98 (dd, J = 8.6, 1.4 Hz, 2H), 7.83 (ddd, J = 11.8, 7.7, 1.0 Hz, 2H),

7.75 (tt, $J = 7.5, 1.1$ Hz, 1H), 7.70-7.58 (m, 4H), 7.54 (dd, $J = 8.6, 1.8$ Hz, 1H), 7.50 (d, $J = 1.5$ Hz, 1H), 7.16 (d, $J = 1.2$ Hz, 1H), 7.08 (dddd, $J = 9.3, 8.2, 4.7, 3.6$ Hz, 4H), 6.94 (t, $J = 7.4$ Hz, 1H), 6.84 (dtd, $J = 8.8, 7.5, 1.4$ Hz, 2H), 6.72-6.56 (m, 3H), 6.50 (d, $J = 7.4$ Hz, 1H), 6.41 (d, $J = 7.3$ Hz, 1H), 5.92 (d, $J = 7.5$ Hz, 2H), 4.02 (d, $J = 14.0$ Hz, 1H), 3.76 (d, $J = 14.0$ Hz, 1H), 1.38 (s, 9H), 0.99 (s, 9H).

^{13}C NMR (75 MHz, CD_2Cl_2) δ 196.4, 183.2, 179.9, 152.9, 152.6, 149.8, 149.1, 147.3, 146.8, 141.9, 140.0, 137.4, 134.8, 134.1, 133.2, 132.7, 131.93, 131.88, 131.86, 129.9, 129.22, 129.18, 128.9, 128.5, 128.4, 126.9, 126.6, 125.2, 124.8, 124.1, 123.8, 123.6, 123.5, 115.4, 114.9, 45.8, 35.5, 35.2, 31.8, 31.5. IR (film): ν (cm^{-1}) 3214, 3060, 2962, 2868, 1578, 1503, 1444, 1404, 1360, 1289, 1245, 1161, 1113, 1025, 994, 838, 760, 731, 694, 554, 455.

Intermediate II



To a mixture of catalyst Δ/Λ -**IrS** (95.2 mg, 0.10 mmol) and NaHCO_3 (16.8 mg, 0.20 mmol) in CH_2Cl_2 (5 mL) was added substrate **30a** (52.4 mg, 0.20 mmol). The reaction mixture was concentrated after around 12 hours. The residue was purified by flash chromatography on activated basic aluminum oxide (EtOAc / hexane = 1:10) to afford the enolate complex **II** as a red solid (89.8 mg, 0.091 mmol, yield: 91%).

^1H NMR (300 MHz, CD_2Cl_2) δ 8.84 (d, $J = 1.7$ Hz, 1H), 7.86-7.68 (m, 4H), 7.59-7.38 (m, 6H), 7.29 (d, $J = 7.3$ Hz, 2H), 7.16 (d, $J = 6.9$ Hz, 2H), 7.05-6.88 (m, 4H), 6.86 (d, $J = 1.4$ Hz, 1H), 6.71 (td, $J = 8.5, 1.2$ Hz, 3H), 6.64-6.53 (m, 2H), 6.45 (d, $J = 7.5$ Hz, 1H), 4.59 (s, 1H), 1.21 (s, 9H), 1.07 (s, 9H).

^{13}C NMR (75 MHz, CD_2Cl_2) δ 181.4, 179.8, 155.8, 154.6, 154.3, 152.4, 151.4, 151.3, 149.6, 142.4, 142.1, 139.9, 138.3, 135.2, 134.5, 130.6, 130.4, 129.7, 129.1, 128.9, 127.5, 127.4, 127.3, 126.1, 126.0, 125.3, 124.8, 123.7, 123.3, 123.1, 122.4, 121.7, 121.4, 120.9, 119.0, 117.1, 104.6, 35.3, 35.2, 31.8, 31.4.

IR (film): ν (cm⁻¹) 3112, 3049, 2956, 2903, 2864, 1584, 1492, 1462, 1421, 1378, 1285, 1243, 1196, 1156, 1096, 1018, 991, 926, 909, 868, 810, 781, 760, 733, 692, 666, 502, 466.

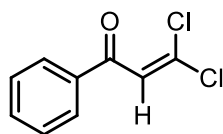
3) Luminescence Quenching Experiments (Figure 68)

Emission intensities were recorded on a Spectra Max M5 microplate reader in a 10.0 mm quartz cuvette. The methyl imidazole derivatives were used due to higher stability of the enolate complex. Catalyst Δ/Λ -**IrS** solutions were excited at $\lambda_{\text{max}} = 420$ nm and the emission was measured at 550 nm (emission maximum). The enolate complex **I** ($N = \text{Me}$) solutions were excited at $\lambda_{\text{max}} = 420$ nm and the emission measured at 550 nm (emission maximum). The enolate complex **II** ($N = \text{Me}$) solutions were excited at $\lambda_{\text{max}} = 440$ nm and the emission measured at 550 nm (emission maximum). The concentration of iridium complex (**IrS** and intermediate complex **I** and **II**) was 0.2 mM in MeOH/THF (4:1). The concentration of the quencher (BrCCl_3) stock solution was 200 mM in MeOH/THF (4:1). For each quenching experiment, 5 μL of this stock solution were titrated to a solution (1 mL) of iridium complex in a screw-top 10.0 mm quartz cuvette. The addition of 5 μL stock solution refers to an increase of the quencher concentration of 1 mM. After degassing with an argon stream for 5 minutes, the emission intensity was collected. See Figure 65 for the obtained Stern-Volmer plots.

4) Trapping Experiments

As shown in Scheme 15-16, the experiment data of compound **40** and **41** are shown below.

3,3-Dichloro-1-phenylprop-2-en-1-one (**40**)



Colorless oil.

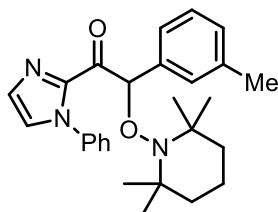
¹H NMR (300 MHz, CDCl_3) δ 7.94-7.78 (m, 2H), 7.58-7.49 (m, 1H), 7.48-7.35 (m, 2H), 7.19 (s, 1H).

¹³C NMR (75 MHz, CDCl_3) δ 186.6, 137.0, 135.4, 133.7, 128.8, 128.5, 124.1.

IR (film): ν (cm⁻¹) 1668, 1595, 1563, 1447, 1318, 1293, 1265, 1216, 1181, 1011, 935, 843, 794, 769, 690, 624, 491.

HRMS (ESI, m/z) calcd for $\text{C}_9\text{H}_6\text{Cl}_2\text{ONa}$ $[\text{M}+\text{Na}]^+$: 222.9688 and 224.9659, found: 222.9688 and 224.9659.

1-(1-Phenyl-1*H*-imidazol-2-yl)-2-((2,2,6,6-tetramethylpiperidin-1-yl)oxy)-2-(*m*-tolyl)ethanone
(41)



^1H NMR (300 MHz, CD_2Cl_2) δ 7.47-7.35 (m, 3H), 7.34-7.24 (m, 3H), 7.23-7.13 (m, 2H), 7.11-6.97 (m, 3H), 6.58 (s, 1H), 2.32 (s, 3H), 1.45 (s, 6H), 1.17 (s, 3H), 1.05 (s, 6H), 0.78 (s, 3H).

^{13}C NMR (75 MHz, CD_2Cl_2) δ 189.3, 142.9, 138.6, 138.37, 138.35, 130.2, 129.3, 129.0, 128.9, 128.7, 128.4, 127.6, 125.9, 125.8, 90.0, 60.2, 60.0, 40.6, 34.1, 33.6, 21.6, 20.3, 17.6.

IR (film): ν (cm^{-1}) 3139, 2969, 2926, 1688, 1496, 1493, 1448, 1398, 1303, 1252, 1140, 1062, 1012, 959, 916, 862, 762, 693, 632, 546, 442.

HRMS (APCI, m/z) calcd for $\text{C}_{27}\text{H}_{33}\text{N}_3\text{O}_2\text{Na}$ $[\text{M}+\text{Na}]^+$: 454.2465, found:454.2468.

5) Quantum Yield Measurement

The quantum yield was measured by standard ferrioxalate actinometry. A 6 W blue LED lamp (420 nm) was used as the light source. The measured method was designed according to published procedures with slight modifications.²⁶

The solutions were prepared and stored in the dark:

Potassium ferrioxalate solution (0.15 M): 736.9 mg of potassium ferrioxalate hydrate was dissolved in 10 mL of 0.05 M H_2SO_4 .

Buffered solution of phenanthroline: 50 mg of 1,10-phenanthroline and 11.25 g of sodium acetate were dissolved in 50 mL of 0.5 M H_2SO_4 .

a) Measurement of light intensity at 420 nm

1 mL of the ferrioxalate solution was added to a quartz cuvette ($l = 10$ mm). The actinometry solution was irradiated with 6 W blue LED lamp ($420 \text{ nm} \pm 10 \text{ nm}$) for 90.0 seconds. After irradiation, 175 μL of the phenanthroline solution was added to the cuvette. The solution was kept in dark for 30 min to make sure the complete coordination. The absorbance of the actinometry solution was monitored at 510 nm. The absorbance of a non-irradiated (in dark) sample was also measured at 510 nm.

The moles of Fe^{2+} formed were determined using Beer's Law:

$$\text{moles Fe}^{2+} = \frac{V_1 \times V_3 \times \Delta A(510\text{nm})}{10^3 \times V_2 \times l \times \varepsilon(510\text{nm})}$$

Where V_1 (1 mL) is the irradiated volume, V_2 (1 mL) is the aliquot of the irradiated solution taken for the determination of the ferrous ions. V_3 (1.175 mL) is the final volume after complexation with phenanthroline (all in mL), l is the path length (1 cm), and $\Delta A(510\text{nm})$ is the optical difference in absorbance between the irradiated and non-irradiated solutions, $\varepsilon(510\text{ nm})$ is the molar absorptivity of $\text{Fe}(\text{phen})_3^{2+}$ ($11100\text{ L mol}^{-1}\text{ cm}^{-1}$).

The photon flux can be calculated as:

$$\text{photon flux (einstein s}^{-1}\text{)} = \frac{\text{moles Fe}^{2+}}{\Phi \cdot t \cdot f}$$

Where Φ is the quantum yield for the ferrioxalate actinometer (1.05 for a 0.15 solution at 412 nm; 1.04 for a 0.15 solution at 422 nm; 1.03 for a 0.15 solution at 433 nm),²⁷ t is the irradiated time (90.0 s), and f is the fraction of light absorbed at $\lambda = 420\text{ nm}$ ($f = 1 - 10^{-A}$, A is the absorbance of above ferrioxalate solution at 420 nm is > 3 , indicating f is > 0.999).

The calculations were done as follows:

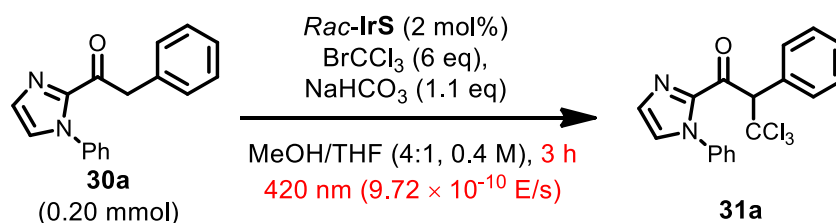
$\Delta A(510\text{nm})$ was calculated (average of three cycles) to be 0.860.

$$\text{moles Fe}^{2+} = \frac{1\text{mL} \times 1.175\text{mL} \times 0.860}{10^3 \times 1\text{mL} \times 1\text{cm} \times 11100\text{ L} \cdot \text{mol}^{-1} \cdot \text{cm}^{-1}} = 9.103 \times 10^{-8}\text{ mol}$$

$$\text{photon flux} = \frac{9.103 \times 10^{-8}\text{ mol}}{1.04 \times 90\text{s} \times 1.0} = 9.72 \times 10^{-10}\text{ einstein/s}$$

b) Measurement of quantum yield:

Model reaction:



A screw-top cuvette (10.0 mm) was charged with the catalyst *rac-IrS* (2 mol%), 2-acyl imidazole **30a** (0.2 mmol, 1.0 eq), NaHCO_3 (0.22 mmol, 1.1 eq), 0.5 mL MeOH/THF (4:1, 0.4 M), bromotrichloromethane (1.2 mmol, 6.0 eq) and a small magnetic stir bar. The cuvette was degassed

with an argon stream for 10 min. After the mixture was thoroughly degassed, the vial was sealed and positioned approximately 8 cm from a 6 W blue lamp. The reaction mixture was stirred and irradiated for 10800 s (3 h). After irradiation, the reaction mixture was passed through a short silica gel column. The yield of product formed was measured by ^1H -NMR with trimethyl(phenyl)silane as internal standard.

Experiment 1: *Rac*-**IrS** (3.8 mg, 0.004 mmol), 2-acyl imidazole **30a** (52.4 mg, 0.2 mmol), NaHCO_3 (18.5 mg, 0.22 mmol), MeOH/THF (4:1, 0.4 M, 0.5 mL), bromotrichloromethane (118.0 μL , 1.2 mmol). After irradiation for 10800 s, the product **31a** was formed in 26.8% yield. The quantum yield calculation as following:

$$\Phi = \frac{\text{moles of product formed}}{\text{einsteins of light absorbed}} = \frac{0.2 \times 10^{-3} \times 0.268 \text{ mol}}{9.72 \times 10^{-10} \text{ einstein} \cdot \text{s}^{-1} \times 10800 \text{ s}} = 5.1$$

Experiment 2: *Rac*-**IrS** (3.8 mg, 0.004 mmol), 2-acyl imidazole **30a** (52.5 mg, 0.2 mmol), NaHCO_3 (18.4 mg, 0.22 mmol), MeOH/THF (4:1, 0.4 M, 0.5 mL), bromotrichloromethane (118.0 μL , 1.2 mmol). After irradiation for 10800 s, the product **31a** was formed in 28.5% yield. The quantum yield calculation as following:

$$\Phi = \frac{\text{moles of product formed}}{\text{einsteins of light absorbed}} = \frac{0.2 \times 10^{-3} \times 0.285 \text{ mol}}{9.72 \times 10^{-10} \text{ einstein} \cdot \text{s}^{-1} \times 10800 \text{ s}} = 5.4$$

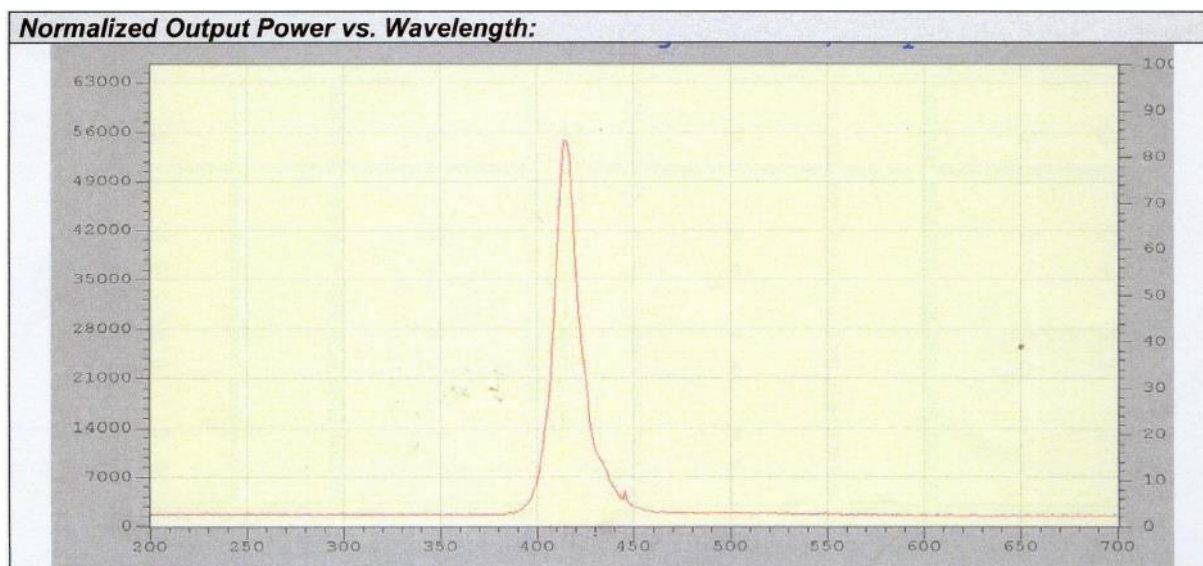
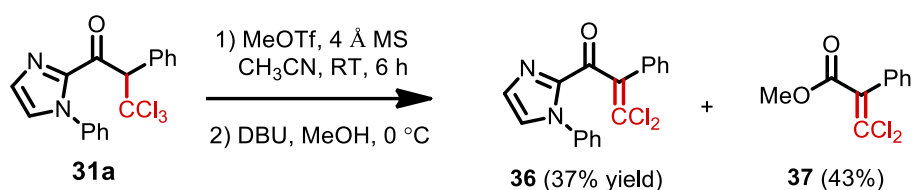
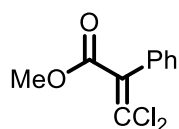


Figure 119 The output wavelength of the used 6 w blue LED (420 nm \pm 10 nm).

5.5.4 Efforts towards Removal of Imidazole Moieties



To a solution of *rac*-**2a** (151.2 mg, 0.4 mmol) in CH₃CN (2.0 mL) was added 4 Å MS (200 mg, 50 mg/0.1 mmol of **2a**) under nitrogen atmosphere. The suspension was stirred vigorously under a positive pressure of nitrogen for 2 h at room temperature, and then methyl trifluoromethanesulfonate (88 µL, 0.8 mmol) was added at room temperature. After being stirred at room temperature for 6 h, MeOH (0.32 mL, 8.0 mmol) and DBU (90 µL, 0.6 mmol) were added to the reaction mixture at 0 °C. After being stirred at 0 °C for 60 min, the solvent was evaporated and the residue was purified by flash chromatography on silica gel (EtOAc/hexane = 1:50) to give **S5** (50.2 mg, 0.15 mmol, yield: 37%) as a white solid and **S8** (40.0 mg, 0.17 mmol, yield: 43%) as a colorless oil.

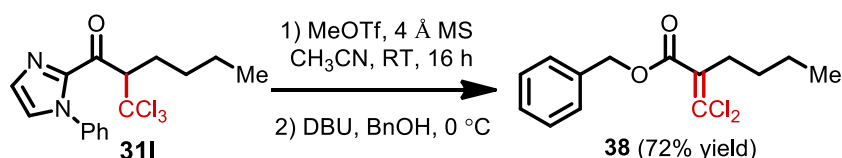
Methyl 3,3-dichloro-2-phenylacrylate (**37**)

¹H NMR (300 MHz, CD₂Cl₂) δ 7.57-7.23 (m, 5H), 3.79 (s, 3H).

¹³C NMR (75 MHz, CD₂Cl₂) δ 165.8, 134.5, 134.3, 129.4, 129.0, 129.0, 127.5, 53.2.

IR (film): ν (cm⁻¹) 3059, 3027, 2952, 2844, 1729, 1599, 1490, 1435, 1272, 1211, 1073, 1034, 954, 881, 839, 706, 589.

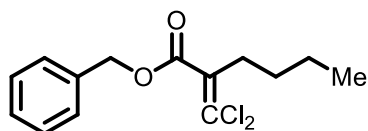
HRMS (ESI, *m/z*) calcd for C₁₀H₈Cl₂O₂Na [M+Na]⁺: 252.9794 and 254.9765, found: 252.9799 and 254.9766.



To a solution of *rac*-**311** (107.0 mg, 0.3 mmol) in CH₃CN (1.5 mL) was added 4 Å MS (150 mg, 50 mg/0.1 mmol of **311**) under nitrogen atmosphere. The suspension was stirred vigorously under a positive pressure of nitrogen for 2 h at room temperature, and then methyl trifluoromethanesulfonate

(98 μ L, 0.9 mmol) was added at room temperature. After being stirred at room temperature for 16 h, BnOH (0.31 mL, 3.0 mmol) and DBU (90 μ L, 0.6 mmol) were added to the reaction mixture at 0 $^{\circ}$ C. After being stirred at 0 $^{\circ}$ C for 60 min, the solvent was evaporated and the residue was purified by flash chromatography on silica gel (EtOAc/hexane = 1:50) to give **38** (62.1 mg, 0.22 mmol, yield: 72%) as a colorless oil.

Benzyl 2-(dichloromethylene)hexanoate (38)



^1H NMR (300 MHz, CD_2Cl_2) δ 7.52-7.20 (m, 5H), 5.24 (s, 2H), 2.66-2.35 (m, 2H), 1.51-1.20 (m, 4H), 0.89 (t, J = 7.2 Hz, 3H).

^{13}C NMR (75 MHz, CD_2Cl_2) δ 165.9, 135.9, 134.3, 129.0, 128.9, 128.8, 128.6, 67.8, 32.8, 29.8, 22.6, 13.9.

IR (film): ν (cm^{-1}) 3066, 3033, 2958, 2929, 2866, 1725, 1588, 1496, 1455, 1374, 1267, 1203, 1135, 946, 907, 741, 695.

HRMS (ESI, m/z) calcd for $\text{C}_{14}\text{H}_{16}\text{Cl}_2\text{O}_2\text{Na}$ $[\text{M}+\text{Na}]^+$: 309.0420 and 311.0391, found: 309.0422 and 311.0395.

5.5.5 Single-Crystal X-Ray Diffraction Studies

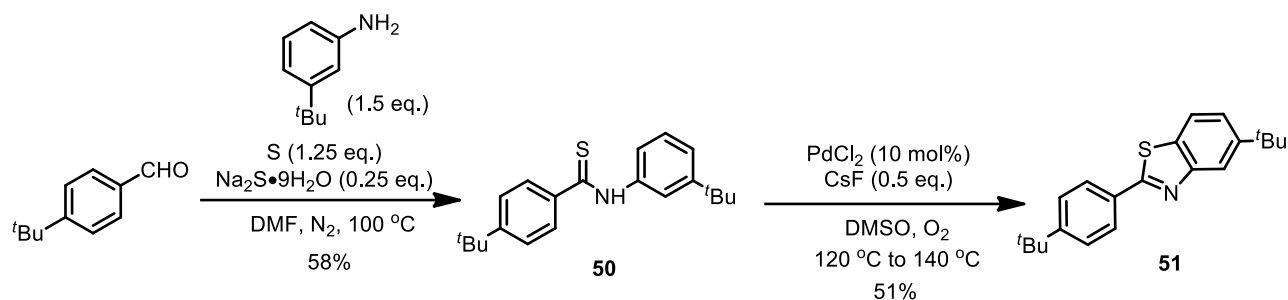
Single crystals of (*R*)-**31a** (3hnb) suitable for X-ray diffraction were obtained by slow diffusion from a solution of (*R*)-**31a** (30 mg) in CH_2Cl_2 (0.5 mL) layered with *n*-hexane (2.5 mL) at room temperature for several days in a glass tube. The absolute configurations of compound (*R*)-**31a** (3hnb) has been determined. Crystal data and details of the structure determination are presented in the Appendices (Chapter 6.7).

5.6 Visible-Light-Activated Enantioselective Perfluoroalkylation

5.6.1 Synthesis of Catalysts

The Catalysts **A-IrS(*t*Bu)** and **Δ -IrS(*t*Bu)** were synthesized according to the following route.

1) Synthesis of Ligand



4-(*tert*-Butyl)-*N*-(3-(*tert*-butyl)phenyl)benzothioamide (**50**)

Compound **50** was synthesized following a published procedure with slight modifications.²⁸ Na₂S·9H₂O (1.5 g, 6.25 mmol) was added to a mixture of sulfur (1.0 g, 31.2 mmol) and 3-(*tert*-butyl)aniline (5.6 g, 37.5 mmol) in DMF (25 mL). The suspension was stirred at 115 °C for 0.5 h under nitrogen. Afterwards, the mixture was cooled to room temperature, 4-(*tert*-butyl)benzaldehyde (4.1 g, 25 mmol) was added and the mixture was stirred at 115 °C for 24 h under nitrogen. After cooling to room temperature, the resulting solution was quenched with saturated NH₄Cl aqueous solution and extracted with ethyl acetate. The organic fraction was thoroughly washed with water and dried with Na₂SO₄. After concentration, the residue was purified by silica gel column (*n*-hexane/EtOAc = 40:1) to yield thioamide **50** as a yellow solid (4.72 g, 58%).

¹H NMR (300 MHz, CDCl₃) δ 9.06 (brs, 1H), 7.83-7.76 (m, 3H), 7.72-7.62 (m, 1H), 7.51-7.27 (m, 4H), 1.35 (s, 18H).

¹³C NMR (75 MHz, CDCl₃) δ 197.8, 154.7, 152.3, 140.6, 138.9, 128.5, 126.5, 125.5, 123.7, 120.6, 120.5, 34.83, 34.78, 31.2, 31.1.

IR (film): ν (cm⁻¹) 3173, 2957, 2867, 1595, 1512, 1472, 1419, 1336, 1274, 1240, 1199, 1112, 999, 907, 843, 747, 701.

Hz, 4H), 1.19 (s, 36H), 0.71 (s, 36H).

^{13}C NMR (75 MHz, CD_2Cl_2) δ 179.6, 152.9, 152.6, 150.4, 144.9, 139.3, 129.3, 128.0, 125.1, 123.3, 121.3, 120.1, 119.4, 35.5, 34.5, 32.0, 30.9.

IR (film): ν (cm^{-1}) 3108, 3054, 2958, 2904, 2867, 1582, 1551, 1437, 1366, 1289, 1260, 1199, 1147, 1109, 991, 928, 884, 804, 731, 670, 594, 459.

Rac-IrS(*t*Bu) complex

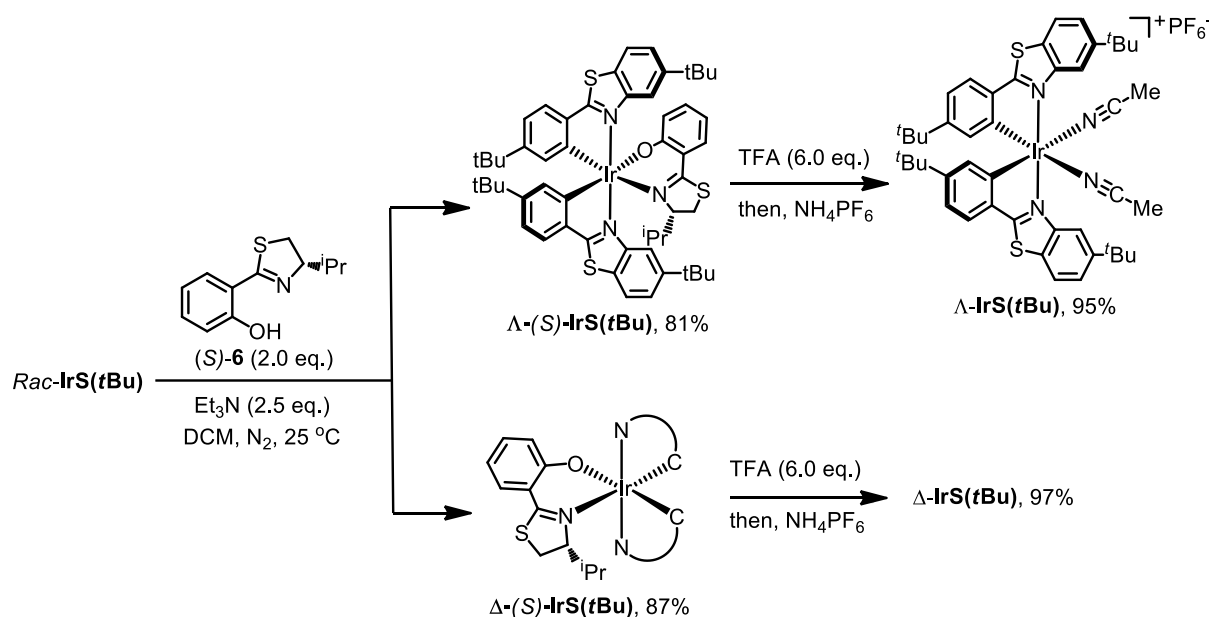
A mixture of iridium dimer (**52**) (583 mg, 0.335 mmol) and AgPF_6 (253 mg, 1.0 mmol) in CH_3CN (22.4 mL) was purged with nitrogen for 5 min and then heated at 60 °C overnight. The reaction mixture was cooled to room temperature and concentrated to dryness. The residue was subjected to a flash silica gel chromatography (DCM/MeCN = 500:1 to 50:1) to obtain the racemic catalyst *rac-IrS(*t*Bu)* as a yellow solid (711 mg, 100% yield).

^1H NMR (300 MHz, CD_2Cl_2) δ 8.40 (d, J = 1.5 Hz, 2H), 8.00 (d, J = 9.0 Hz, 2H), 7.71 (dd, J_1 = 8.7 Hz, J_2 = 1.8 Hz, 2H), 7.58 (d, J = 8.1 Hz, 2H), 7.01 (dd, J_1 = 8.1 Hz, J_2 = 1.8 Hz, 2H), 6.14 (d, J = 1.5 Hz, 2H), 2.39 (s, 6H), 1.45 (s, 18H), 0.88 (s, 18H).

^{13}C NMR (75 MHz, CD_2Cl_2) δ 181.3, 155.3, 152.9, 150.5, 142.4, 138.6, 129.8, 128.7, 125.8, 125.1, 123.1, 121.5, 121.0, 116.9, 35.6, 34.9, 31.7, 31.0, 4.1.

IR (film): ν (cm^{-1}) 2957, 2869, 1584, 1463, 1435, 1366, 1295, 1267, 1203, 1151, 1111, 995, 935, 839, 730, 673, 641, 598, 556, 458.

3) Synthesis of chiral catalyst

**Auxiliary complexes Λ -(*S*)-***IrS(tBu)*** and Δ -(*S*)-***IrS(tBu)*****

A mixture of *rac-IrS(tBu)* (400.0 mg, 0.376 mmol), the chiral auxiliary *(S)*-**6** (166.4 mg, 0.752 mmol) and triethylamine (95.1 mg, 0.940 mmol) in DCM (37.6 mL) was purged with argon for 5 min and then stirred for 4 hours. The reaction mixture was concentrated to dryness. The residue was subjected to a flash silica gel chromatography ($\text{EtOAc}/n\text{-hexane} = 1:10$) to separate the two diastereomers. The first eluting diastereomer was assigned as Λ -(*S*)-***IrS(tBu)*** (an orange solid, 161 mg, 41%) and the second eluting diastereomer as Δ -(*S*)-***IrS(tBu)*** (an orange solid, 173 mg, 44%). The absolute configurations of Λ -(*S*)-***IrS(tBu)*** and Δ -(*S*)-***IrS(tBu)*** were assigned by comparison with CD spectra of the published analogous complexes³⁰ and further confirmed by an X-ray crystal structure of Δ -***IrS(tBu)*** which was obtained by the follow-up transformation.

 Λ -(*S*)-*IrS(tBu)***:**

^1H NMR (300 MHz, CD_2Cl_2) δ 9.01 (d, $J = 1.5$ Hz, 1H), 7.88-7.82 (m, 2H), 7.74 (d, $J = 8.4$ Hz, 1H), 7.66 (d, $J = 8.1$ Hz, 1H), 7.56 (d, $J = 8.4$ Hz, 1H), 7.51 (d, $J = 2.1$ Hz, 1H), 7.49 (d, $J = 2.1$ Hz, 1H), 7.22 (dd, $J_1 = 7.8$ Hz, $J_2 = 1.8$ Hz, 1H), 7.00-6.90 (m, 4H), 6.59 (dd, $J_1 = 8.4$ Hz, $J_2 = 1.2$ Hz, 1H), 6.15-6.07 (m, 1H), 6.06 (d, $J = 1.8$ Hz, 1H), 4.44 (dt, $J_1 = 10.2$ Hz, $J_2 = 2.4$ Hz, 1H), 3.37 (dd, $J_1 = 11.4$ Hz, $J_2 = 9.9$ Hz, 1H), 3.00 (dt, $J_1 = 11.7$ Hz, $J_2 = 2.1$ Hz, 1H), 1.50 (s, 9H), 1.20 (s, 9H), 1.01 (s, 9H), 0.97 (s, 9H), 0.90-0.80 (m, 1H), 0.34 (d, $J = 6.9$ Hz, 3H), 0.15 (d, $J = 6.9$ Hz, 3H).

^{13}C NMR (75 MHz, CD_2Cl_2) δ 181.0, 180.1, 169.8, 169.4, 154.0, 152.8, 152.3, 151.9, 151.5, 151.0,

150.1, 140.4, 140.1, 133.2, 133.1, 132.6, 129.0, 128.4, 128.3, 126.0, 125.7, 124.3, 123.7, 123.3, 122.3, 121.5, 120.0, 119.8, 119.5, 118.6, 116.1, 113.2, 83.8, 35.4, 35.3, 34.8, 34.7, 32.1, 31.5, 31.3, 31.1, 30.1, 28.3, 19.8, 14.9.

IR (film): ν (cm^{-1}) 3059, 2955, 2965, 1729, 1583, 1555, 1523, 1435, 1356, 1288, 1259, 1195, 1145, 1110, 997, 931, 878, 846, 806, 746, 672, 639, 598, 567, 462.

CD (MeOH): λ , nm ($\Delta\epsilon$, $\text{M}^{-1}\text{cm}^{-1}$) 461 (−19), 343 (+66), 319 (−22), 268 (+10), 253 (−4), 242 (+13), 229 (−45), 216 (+131).

Δ -(S)-IrS(*t*Bu):

^1H NMR (300 MHz, CD_2Cl_2) δ 8.86 (d, $J = 1.5$ Hz, 1H), 7.92 (d, $J = 1.5$ Hz, 1H), 7.86 (d, $J = 8.4$ Hz, 1H), 7.79 (d, $J = 8.4$ Hz, 1H), 7.62-7.48 (m, 3H), 7.47 (dd, $J_1 = 8.4$ Hz, $J_2 = 1.8$ Hz, 1H), 7.04-6.90 (m, 3H), 6.60-6.53 (m, 2H), 6.31-6.22 (m, 2H), 3.67-3.59 (m, 1H), 2.93 (dd, $J_1 = 11.4$ Hz, $J_2 = 4.8$ Hz, 1H), 2.59 (dd, $J_1 = 11.4$ Hz, $J_2 = 9.6$ Hz, 1H), 1.95-1.83 (m, 1H), 1.28 (s, 9H), 1.17 (s, 9H), 1.05 (s, 9H), 1.01 (s, 9H), 0.94-0.88 (m, 1H), 0.86 (d, $J = 6.9$ Hz, 3H), 0.12 (d, $J = 6.9$ Hz, 3H).

^{13}C NMR (75 MHz, CD_2Cl_2) δ 181.3, 180.5, 169.3, 168.2, 153.59, 153.55, 152.7, 152.4, 151.9, 151.7, 151.0, 150.3, 140.3, 139.6, 133.3, 132.4, 132.2, 129.3, 128.4, 128.3, 126.1, 125.5, 124.2, 123.9, 123.7, 122.1, 121.7, 121.2, 119.3, 118.9, 118.4, 117.6, 112.9, 83.3, 35.5, 35.3, 34.7, 34.6, 31.8, 31.4, 31.2, 31.1, 30.1, 21.0, 17.8.

IR (film): ν (cm^{-1}) 3058, 2955, 2966, 1582, 1556, 1523, 1436, 1356, 1288, 1258, 1196, 1147, 1108, 994, 934, 882, 845, 806, 746, 671, 637, 596, 555, 463.

CD (MeOH): λ , nm ($\Delta\epsilon$, $\text{M}^{-1}\text{cm}^{-1}$) 488 (+12), 348 (−48), 325 (+38), 271 (−4), 256 (+7), 245 (+2), 228 (+66), 216 (−96).

Chiral catalysts Λ -IrS(*t*Bu) and Δ -IrS(*t*Bu)

A suspension of the auxiliary complex Λ -(S)-IrS(*t*Bu) (150 mg, 0.142 mmol) or Δ -(S)-IrS(*t*Bu) (150 mg, 0.142 mmol) in MeCN (5.7 ml, 25 mM) was added trifluoroacetic acid (97.2 mg, 0.852 mmol) under argon in the dark. The reaction mixture was concentrated to dryness and dissolved in MeCN. NH_4PF_6 (462.9 mg, 2.84 mmol) was added to the solution. After stirring for 15 min, the reaction mixture was concentrated to dryness and subjected to a flash silica gel chromatography ($\text{CH}_2\text{Cl}_2/\text{CH}_3\text{CN} = 100:1$ to $30:1$) to give the enantiopure catalyst Λ -IrS(*t*Bu) (143.7 mg, 95%) or

Δ -**IrS**(*t*Bu) (146.3 mg, 97%) as a yellow solid. The absolute configurations were verified by CD spectroscopy and confirmed by a crystal structure of Δ -**IrS**(*t*Bu).

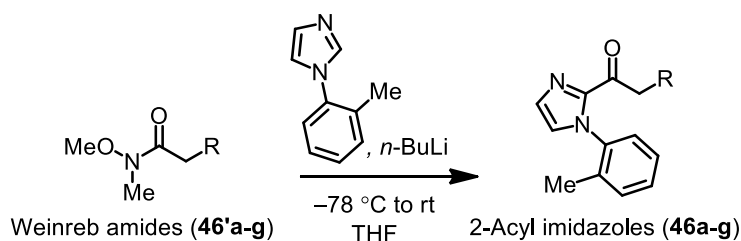
CD (MeOH) for Δ -**IrS**(*t*Bu): λ , nm ($\Delta\epsilon$, M⁻¹cm⁻¹) 465 (−12), 363 (+56), 347 (+39), 338 (+47), 293 (−53), 259 (+6), 242 (−35), 236 (−25), 229 (−45), 216 (+216).

CD (MeOH) for Δ -**IrS**(*t*Bu): λ , nm ($\Delta\epsilon$, M⁻¹cm⁻¹) 465 (+10), 363 (−44), 348 (−31), 339 (−34), 294 (+44), 259 (−4), 242 (+29), 237 (+20), 229 (+36), 215 (−171).

5.6.2 Synthesis of Substrates

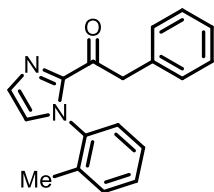
The 2-Acyl imidazoles **30a**, **46a-g** and the corresponding Weinreb amides were synthesized according to our recently published procedures (method A).³¹ 2-Acyl imidazole **46h** was synthesized according to a reported procedure with some modifications (method B).³²

Method A:



General procedure for method A. To a solution of *N*-phenylimidazole (1.1 eq.) in THF at −78 °C was added *n*-BuLi (1.1 eq.) dropwise. The reaction was stirred at −78 °C for 30 min, then stirred at room temperature for 30 min. The corresponding Weinreb amide (1.0 eq. in THF) was added dropwise to the flask after the reaction was cooled back down to −78 °C. The overall concentration of Weinreb amide was 0.4 M. The reaction was allowed to warm to room temperature slowly (over a period of 3–4 h) and stirred overnight. The reaction was quenched with AcOH (6.0 eq.) at room temperature and extracted with EtOAc. The organic layer was washed with aqueous saturated NaHCO₃ and brine. The combined organic layers were dried over anhydrous Na₂SO₄, filtered, and concentrated under reduced pressure. The residue was purified by flash chromatography on silica gel (EtOAc/hexane = 1:3) to produce **46a-g**.

The experimental data of **46a-d**, **46e-g** are shown below. The other 2-acyl imidazoles (**30a**³², **46e**³³) have been reported previously.

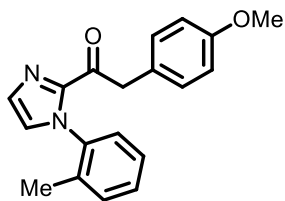
2-Phenyl-1-(1-(*o*-tolyl)-1*H*-imidazol-2-yl)ethanone (46a)

75% yield. A white solid.

^1H NMR (300 MHz, CDCl_3) δ 7.30-7.09 (m, 9H), 7.03-6.96 (m, 2H), 6.89-6.80 (m, 2H), 4.41 (q, J = 15.0 Hz, 1H), 4.31 (q, J = 15.0 Hz, 1H), 1.81 (s, 3H).

^{13}C NMR (75 MHz, CDCl_3) δ 188.3, 143.2, 137.7, 134.4, 134.3, 130.6, 129.9, 129.8, 128.9, 128.3, 126.71, 126.67, 126.5, 126.2, 45.3, 16.9.

IR (film): ν (cm^{-1}) 3105, 3030, 2914, 1685, 1592, 1494, 1452, 1390, 1340, 1307, 1208, 1147, 1079, 1023, 991, 958, 912, 887, 840, 789, 761, 721, 696, 590, 542, 512, 480, 454.

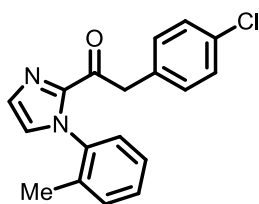
2-(4-Methoxyphenyl)-1-(1-(*o*-tolyl)-1*H*-imidazol-2-yl)ethanone (46b)

72% yield. A white solid.

^1H NMR (300 MHz, CDCl_3) δ 7.40-7.21 (m, 6H), 7.14-7.07 (m, 2H), 6.89-6.80 (m, 2H), 4.45 (d, J = 15.0 Hz, 1H), 4.35 (d, J = 15.6 Hz, 1H), 3.79 (s, 3H), 1.92 (s, 3H).

^{13}C NMR (75 MHz, CDCl_3) δ 188.7, 158.6, 143.3, 137.9, 134.5, 130.9, 130.7, 129.8, 129.0, 126.7, 126.5, 126.4, 126.3, 113.9, 55.2, 44.5, 17.0.

IR (film): ν (cm^{-1}) 3158, 2916, 1668, 1607, 1583, 1509, 1488, 1460, 1447, 1421, 1394, 1302, 1261, 1239, 1179, 1146, 1114, 1087, 1057, 1037, 975, 941, 916, 830, 818, 787, 768, 714, 671, 615, 567, 549, 530, 518, 458, 445, 419.

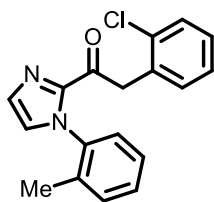
2-(4-Chlorophenyl)-1-(1-(*o*-tolyl)-1*H*-imidazol-2-yl)ethanone (46c)

72% yield. A white solid.

^1H NMR (300 MHz, CDCl_3) δ 7.37 (d, $J = 1.0$ Hz, 1H), 7.35-7.31 (m, 1H), 7.30-7.20 (m, 6H), 7.11 (d, $J = 1.0$ Hz, 1H), 7.08 (dd, $J_1 = 7.7$ Hz, $J_2 = 1.4$ Hz, 1H), 4.45 (d, $J = 15.3$ Hz, 1H), 4.36 (d, $J = 15.4$ Hz, 1H), 1.90 (s, 3H).

^{13}C NMR (75 MHz, CDCl_3) δ 187.8, 143.0, 137.7, 134.4, 132.79, 132.75, 131.2, 130.7, 130.0, 129.1, 128.5, 126.9, 126.6, 126.2, 44.7, 17.0.

IR (film): ν (cm^{-1}) 3111, 3029, 2913, 1684, 1591, 1494, 1451, 1392, 1306, 1207, 1145, 1079, 1023, 958, 912, 841, 788, 764, 718, 591, 543, 454.

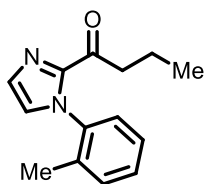
2-(2-Chlorophenyl)-1-(1-(*o*-tolyl)-1*H*-imidazol-2-yl)ethanone (46d)

62% yield. A white solid.

^1H NMR (300 MHz, CDCl_3) δ 7.39 (d, $J = 1.0$ Hz, 1H), 7.37-7.20 (m, 5H), 7.20-7.14 (m, 3H), 7.13 (d, $J = 1.0$ Hz, 1H), 4.77 (d, $J = 17.6$ Hz, 1H), 4.57 (d, $J = 17.7$ Hz, 1H), 1.99 (s, 3H).

^{13}C NMR (75 MHz, CDCl_3) δ 187.0, 143.0, 137.7, 134.7, 134.5, 132.9, 132.1, 130.7, 129.9, 129.3, 129.0, 128.4, 126.6, 126.5, 126.2, 43.6, 17.1.

IR (film): ν (cm^{-1}) 3089, 1683, 1501, 1488, 1472, 1460, 1444, 1400, 1344, 1309, 1150, 1094, 1050, 1032, 963, 948, 915, 811, 802, 787, 766, 751, 717, 692, 678, 598, 573, 554, 535, 504, 459, 448, 436.

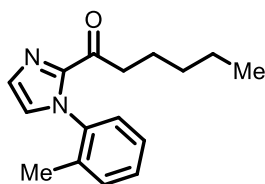
1-(1-(*o*-Tolyl)-1*H*-imidazol-2-yl)butan-1-one (46f)

93% yield. A white solid.

^1H NMR (300 MHz, CDCl_3) δ 7.34-7.15 (m, 4H), 7.07-6.96 (m, 2H), 3.12-2.94 (m, 2H), 1.90 (s, 3H), 1.68-1.52 (m, 2H), 0.88 (t, $J = 7.4$ Hz, 3H).

^{13}C NMR (75 MHz, CDCl_3) δ 191.4, 143.5, 138.0, 134.4, 130.7, 129.6, 129.0, 126.5, 126.24, 126.17, 40.9, 17.4, 17.1, 13.7.

IR (film): ν (cm^{-1}) 3102, 2961, 2877, 1685, 1496, 1457, 1407, 1400, 1301, 1211, 1149, 1025, 967, 886, 766, 699.

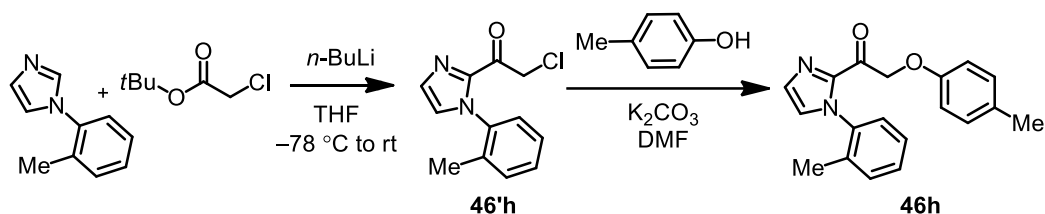
1-(1-(*o*-Tolyl)-1*H*-imidazol-2-yl)hexan-1-one (46g)

91% yield. A colorless liquid.

^1H NMR (300 MHz, CDCl_3) δ 7.43-7.24 (m, 4H), 7.16-7.05 (m, 2H), 3.22-3.04 (m, 2H), 1.99 (s, 3H), 1.70-1.61 (m, 2H), 1.38-1.28 (m, 4H), 0.92-0.84 (m, 3H).

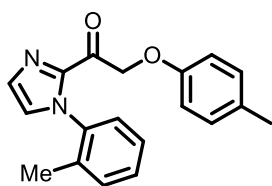
^{13}C NMR (75 MHz, CDCl_3) δ 191.6, 143.5, 138.1, 134.5, 130.7, 129.6, 129.0, 126.5, 126.3, 126.2, 38.9, 31.4, 23.6, 22.4, 17.1, 13.8.

IR (film): ν (cm^{-1}) 3108, 2927, 2862, 1681, 1496, 1452, 1404, 1303, 1141, 1037, 956, 910, 762, 714.

Method B:

Procedure for the preparation of 46h. To a solution of 1-(*o*-tolyl)-1*H*-imidazole (948 mg, 6.0 mmol) in THF (15 mL) at -78°C was added *n*-BuLi (2.4 mL, 2.5 M in hexane, 6.0 mmol) dropwise. The reaction was stirred at -78°C for 1 h, then stirred at room temperature for 30 min. The *tert*-butyl chloroacetate (1.3 mL, 7.5 mmol) was added at one portion to the flask after the reaction was cooled back down to -78°C . The reaction was allowed to warm to room temperature slowly (over a period of 3-4 h) and stirred overnight. The reaction was quenched with water at room temperature and extracted with EtOAc. The combined organic layers were dried over anhydrous Na_2SO_4 , filtered, and concentrated under reduced pressure. The residue was purified by flash chromatography on silica gel (EtOAc/hexane = 1:3) to produce **46'h** (1.0 g, yield: 72%) as a white solid.

To a mixture of **46'h** (936 mg, 4.0 mmol) and K_2CO_3 (552 mg, 4.0 mmol) in DMF (8.0 mL) at 0°C were added *p*-cresol (648 mg, 6.0 mmol). The reaction mixture was stirred at room temperature for overnight. The reaction was quenched with water (8 mL) at room temperature and extracted with DCM (4×10 mL). The combined organic layers were dried over anhydrous Na_2SO_4 , filtered, and concentrated under reduced pressure. The residue was purified by flash chromatography on silica gel (EtOAc/hexane = 1:3) to afford **46h** (713 mg, yield: 58%) as a white solid.

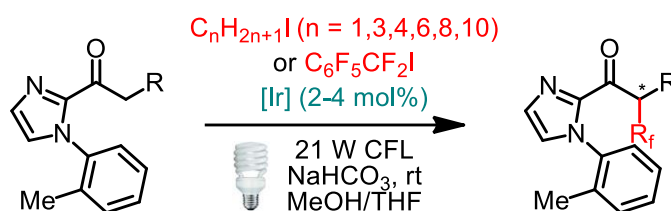
1-(1-(*o*-Tolyl)-1*H*-imidazol-2-yl)-2-(*p*-tolylloxy)ethanone (46h)

^1H NMR (300 MHz, CDCl_3) δ 7.28-7.10 (m, 4H), 7.06-6.98 (m, 2H), 6.94 (d, $J = 8.4$ Hz, 2H), 6.72 (d, $J = 8.7$ Hz, 2H), 5.42 (d, $J = 17.7$ Hz, 1H), 5.31 (d, $J = 17.7$ Hz, 1H), 2.15 (s, 3H), 1.88 (s, 3H).

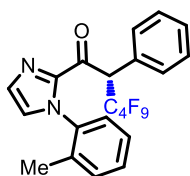
^{13}C NMR (75 MHz, CDCl_3) δ 184.5, 155.9, 141.2, 137.1, 134.4, 130.7, 130.4, 130.1, 129.8, 129.2, 126.7, 126.5, 126.3, 114.4, 69.8, 20.3, 17.0.

IR (film): ν (cm^{-1}) 3134, 2922, 1697, 1506, 1459, 1424, 1404, 1337, 1295, 1262, 1214, 1178, 1144, 1081, 1013, 946, 911, 822, 803, 787, 771, 720, 704, 678, 561, 536, 508, 459, 448.

5.6.3 Iridium-Catalyzed Photoredox Reactions



General procedure: A dried 10 mL Schlenk tube was charged with the catalyst Δ -**IrS**(*t*Bu) or Δ -**IrS**(*t*Bu) (2 or 4 mol%), NaHCO₃ (25.2 mg, 0.3 mmol, 1.5 equiv) and the corresponding 2-acyl imidazole **46** (0.2 mmol, 1.0 equiv). The tube was purged with nitrogen and MeOH/THF (4:1, 0.5 mL) was added via syringe, followed by CnFmI. The reaction mixture was degassed via freeze-pump-thaw for three cycles. After the mixture was thoroughly degassed, the vial was sealed and positioned approximately 5 cm from a 21 W white light energy saving lamp. The reaction was stirred at room temperature for the indicated time (monitored by TLC) under nitrogen atmosphere. Afterwards, the mixture was diluted with CH₂Cl₂ (8 mL). The combined organic layers were concentrated under reduced pressure. The residue was purified by flash chromatography on silica gel (hexane/EtOAc = 30:1 to 10:1) to afford the products **49a-h** and **47a-f**. Racemic samples were obtained by carrying out the reactions with *rac*-**IrS**(*t*Bu). The enantiomeric excess was determined by chiral HPLC analysis.

(S)-3,3,4,4,5,5,6,6,6-Nonafluoro-2-phenyl-1-(1-(*o*-tolyl)-1*H*-imidazol-2-yl)hexan-1-one (**48a**)

According to the general procedure, the reaction of 2-acyl imidazole **46a** (55.3 mg, 0.20 mmol) and C₄F₉I (415.1 mg, 1.20 mmol) catalyzed by Δ -**Ir**(*t*Bu) (4.3 mg, 0.004 mol) gave **48a** as a yellow liquid (78.3 mg, yield: 79%) after 46 hours. Enantiomeric excess established by HPLC analysis using a Chiralpak AD-H column, *ee* = 99% (HPLC: AD-H, 254 nm, hexane/isopropanol = 99:1, flow rate 1 mL/min, 25 °C, *t_r* (major) = 5.7 min, *t_r* (minor) = 5.0 min). [α]_D²² = −134.6° (*c* 0.4, CH₂Cl₂).

¹H NMR (300 MHz, CD₂Cl₂) δ 7.59-7.54 (m, 2H), 7.46-6.94 (m, 9H), 6.44-6.27 (m, 1H), 2.00 (s, 3H), 1.62 (s, 3H, other rotamer).

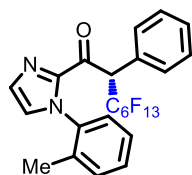
^{13}C NMR (75 MHz, CD_2Cl_2) δ 181.6, 142.3, 137.9 (d, $J = 3.3$ Hz), 135.1 (d, $J = 27.5$ Hz), 131.2 (d, $J = 5.9$ Hz), 131.1, 131.0 (d, $J = 3.5$ Hz), 129.7 (d, $J = 3.9$ Hz), 129.3 (d, $J = 12.5$ Hz), 129.2, 128.7 (d, $J = 9.6$ Hz), 127.1 (d, $J = 9.7$ Hz), 126.6 (d, $J = 21.6$ Hz), 52.4-51.6 (m), 16.9 (d, $J = 15.4$ Hz).

^{19}F NMR (282 MHz, CD_2Cl_2) δ -81.92 - -82.44 (m, 3F), -110.84 - -115.21 (m, 2F), -121.21 - -122.07 (m, 2F), -125.66 - -128.36 (m, 2F).

IR (film): ν (cm^{-1}) 3115, 3067, 3036, 2978, 1694, 1497, 1456, 1401, 1350, 1214, 1129, 1026, 971, 866, 813, 763, 739, 707, 645, 578, 550, 525, 455.

HRMS (FD, m/z) calcd for $\text{C}_{22}\text{H}_{15}\text{F}_9\text{N}_2\text{O}$ $[\text{M}]^+$: 494.1041, found: 494.1028.

(S)-3,3,4,4,5,5,6,6,7,7,8,8,8-Tridecafluoro-2-phenyl-1-(1-(*o*-tolyl)-1*H*-imidazol-2-yl)octan-1-one (49a)



According to the general procedure, the reaction of 2-acyl imidazole **46a** (55.3 mg, 0.20 mmol) and $\text{C}_6\text{F}_{13}\text{I}$ (535.2 mg, 1.20 mmol) catalyzed by Δ -**Ir(*t*Bu)** (4.3 mg, 0.004 mol) gave **49a** as a yellow liquid (103.5 mg, yield: 87%) after 46 hours. Enantiomeric excess established by HPLC analysis using a Chiralpak AD-H column, $ee = 99\%$ (HPLC: AD-H, 254 nm, hexane/isopropanol = 99:1, flow rate 1 mL/min, 25 °C, t_r (major) = 4.2 min, t_r (minor) = 4.8 min). $[\alpha]_{\text{D}}^{22} = -100.9^\circ$ (c 0.3, CH_2Cl_2).

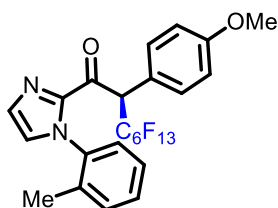
^1H NMR (300 MHz, CD_2Cl_2) δ 7.59-7.51 (m, 2H), 7.46-6.93 (m, 9H), 6.42-6.24 (m, 1H), 1.99 (s, 3H), 1.67 (s, 3H, other rotamer).

^{13}C NMR (75 MHz, CD_2Cl_2) δ 181.6, 142.9 (d, $J = 3.6$ Hz), 137.9 (d, $J = 2.6$ Hz), 135.1 (d, $J = 27.0$ Hz), 131.2 (d, $J = 7.6$ Hz), 131.1, 131.0 (d, $J = 4.3$ Hz), 129.7 (d, $J = 3.5$ Hz), 129.3 (d, $J = 11.7$ Hz), 129.2, 128.7 (d, $J = 9.2$ Hz), 127.1 (d, $J = 9.5$ Hz), 126.7 (d, $J = 21.8$ Hz), 52.6-51.8 (m), 16.9 (d, $J = 9.1$ Hz).

^{19}F NMR (282 MHz, CD_2Cl_2) δ -81.97 - -82.11 (m, 3F), -110.62 - -114.90 (m, 2F), -120.62 - -120.94 (m, 2F), -122.43 - -123.11 (m, 2F), -123.57 - -124.12 (m, 2F), -126.98 - -127.43 (m, 2F).

IR (film): ν (cm^{-1}) 3068, 3037, 2973, 1695, 1497, 1457, 1401, 1234, 1196, 1142, 1027, 975, 910, 862, 810, 766, 736, 703, 633, 527, 454.

HRMS (FD, m/z) calcd for $\text{C}_{24}\text{H}_{15}\text{F}_{13}\text{N}_2\text{O}$ $[\text{M}]^+$: 594.0977, found: 594.0992.

(R)-3,3,4,4,5,5,6,6,7,7,8,8,8-Tridecafluoro-2-(4-methoxyphenyl)-1-(1-(*o*-tolyl)-1*H*-imidazol-2-yl)octan-1-one (49b)

According to the general procedure, the reaction of 2-acyl imidazole **46b** (61.3 mg, 0.20 mmol) and $\text{C}_6\text{F}_{13}\text{I}$ (535.2 mg, 1.20 mmol) catalyzed by $\Lambda\text{-Ir}(\text{tBu})$ (4.3 mg, 0.004 mol) gave **49b** as a yellow liquid (111.8 mg, yield: 90%) after 48 hours. Enantiomeric excess established by HPLC analysis using a Chiralpak AD-H column, $ee = 99\%$ (HPLC: AD-H, 254 nm, hexane/isopropanol = 99:1, flow rate 1 mL/min, 25 °C, t_r (major) = 4.4 min, t_r (minor) = 5.4 min). $[\alpha]_{\text{D}}^{22} = -123.5^\circ$ (c 1.1, CH_2Cl_2).

^1H NMR (300 MHz, CD_2Cl_2) δ 7.52-6.85 (m, 10H), 6.37-6.18 (m, 1H), 3.78 (s, 3H), 1.99 (s, 3H), 1.64 (s, 3H, other rotamer).

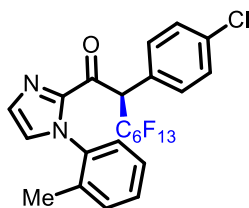
^{13}C NMR (75 MHz, CD_2Cl_2) δ 181.9 (d, $J = 4.2$ Hz), 160.8, 143.1-142.9 (m), 138.1, 135.2 (d, $J = 28.6$ Hz), 132.4, 131.2 (d, $J = 6.1$ Hz), 130.9 (d, $J = 2.1$ Hz), 129.7 (d, $J = 3.5$ Hz), 128.6 (d, $J = 7.8$ Hz), 127.1 (d, $J = 9.5$ Hz), 126.7 (d, $J = 21.6$ Hz), 121.4 (d, $J = 3.4$ Hz), 114.7, 55.6, 51.8-51.1 (m), 16.9 (d, $J = 9.3$ Hz).

^{19}F NMR (282 MHz, CD_2Cl_2) δ -80.95 - -82.05 (m, 3F), -109.85 - -115.05 (m, 2F), -119.05 - -120.90 (m, 2F), -120.95 - -122.55 (m, 2F), -122.60 - -124.70 (m, 2F), -125.15 - -127.80 (m, 2F).

IR (film): ν (cm^{-1}) 2926, 2850, 1695, 1610, 1509, 1458, 1402, 1355, 1303, 1235, 1190, 1142, 1031, 976, 944, 911, 863, 841, 768, 734, 654, 627, 529, 452.

HRMS (FD, m/z) calcd for $\text{C}_{24}\text{H}_{17}\text{F}_{13}\text{N}_2\text{O}_2$ $[\text{M}]^+$: 624.1082, found: 624.1107.

(R)-2-(4-Chlorophenyl)-3,3,4,4,5,5,6,6,7,7,8,8,8-tridecafluoro-1-(1-(*o*-tolyl)-1*H*-imidazol-2-yl)octan-1-one (49c)



According to the general procedure, the reaction of 2-acyl imidazole **46c** (62.2 mg, 0.20 mmol) and $C_6F_{13}I$ (535.2 mg, 1.20 mmol) catalyzed by Λ -**Ir(*t*Bu)** (4.3 mg, 0.004 mol) gave **49c** as a yellow liquid (78.6 mg, yield: 63%) after 72 hours. Enantiomeric excess established by HPLC analysis using a Chiralpak AD-H column, *ee* = 96% (HPLC: AD-H, 254 nm, hexane/isopropanol = 99:1, flow rate 1 mL/min, 25 °C, t_r (major) = 4.2 min, t_r (minor) = 4.9 min). $[\alpha]_D^{22} = -96.9^\circ$ (*c* 0.9, CH_2Cl_2).

1H NMR (300 MHz, CD_2Cl_2) δ 7.57-7.50 (m, 2H), 7.48-6.95 (m, 8H), 6.44-6.26 (m, 1H), 1.99 (s, 3H), 1.65 (s, 3H, other rotamer).

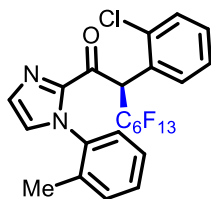
^{13}C NMR (75 MHz, CD_2Cl_2 , mixture of rotamers) δ 181.3, 142.7, 137.8 (d, $J = 2.9$ Hz), 135.6 (d, $J = 1.7$ Hz), 135.1, 135.0 (d, $J = 29.0$ Hz), 132.5, 132.2, 131.3, 131.2, 131.1, 129.9, 129.8, 129.7, 129.5, 129.4, 129.0, 128.9, 128.6, 128.3, 127.2, 127.1, 127.0, 126.8, 126.5, 51.7-51.0 (m), 16.9 (d, $J = 4.8$ Hz).

^{19}F NMR (282 MHz, CD_2Cl_2) δ -81.03 - -81.32 (m, 3F), -109.92 - -114.91 (m, 2F), -119.69 - -120.19 (m, 2F), -121.45 - -122.62 (m, 2F), -122.81 - -123.43 (m, 2F), -126.11 - -126.65 (m, 2F).

IR (film): ν (cm^{-1}) 3116, 2964, 2928, 2860, 1694, 1610, 1494, 1456, 1400, 1309, 1233, 1196, 1142, 1055, 1021, 976, 859, 769, 714, 657, 552, 452.

HRMS (FD, m/z) calcd for $C_{24}H_{14}ClF_{13}N_2O$ $[M]^+$: 628.0587, found: 628.0573.

(R)-2-(2-Chlorophenyl)-3,3,4,4,5,5,6,6,7,7,8,8,8-tridecafluoro-1-(1-(*o*-tolyl)-1*H*-imidazol-2-yl)octan-1-one (49d)



According to the general procedure, the reaction of 2-acyl imidazole **46d** (62.2 mg, 0.20 mmol) and $C_6F_{13}I$ (535.2 mg, 1.20 mmol) catalyzed by Λ -**Ir(*t*Bu)** (4.3 mg, 0.004 mol) gave **49d** as a yellow liquid (93.1 mg, yield: 74%) after 72 hours. Enantiomeric excess established by HPLC analysis using a Chiralpak OD-H column, *ee* = 98% (HPLC: OD-H, 254 nm, hexane/isopropanol = 99:1, flow rate 1 mL/min, 25 °C, t_r (major) = 6.9 min, t_r (minor) = 6.3 min). $[\alpha]_D^{22} = -152.6$ (*c* 1.0, CH_2Cl_2).

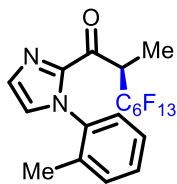
1H NMR (300 MHz, CD_2Cl_2) δ 7.74-7.67 (m, 1H), 7.52-6.94 (m, 10H), 2.00 (s, 3H), 1.69 (s, 3H, other rotamer).

^{13}C NMR (75 MHz, CD_2Cl_2) δ 181.4-181.1 (m), 143.1 (d, $J = 2.8$ Hz), 137.9 (d, $J = 2.6$ Hz), 136.5 (d, $J = 4.1$ Hz), 135.1 (d, $J = 35.6$ Hz), 131.7 (d, $J = 10.8$ Hz), 131.3 (d, $J = 2.6$ Hz), 131.2 (d, $J = 5.2$ Hz), 130.7 (d, $J = 3.9$ Hz), 130.5 (d, $J = 7.4$ Hz), 129.7 (d, $J = 2.0$ Hz), 129.0 (d, $J = 7.5$ Hz), 127.6 (d, $J = 2.2$ Hz), 127.4 (d, $J = 4.7$ Hz), 127.1 (d, $J = 11.9$ Hz), 126.7 (d, $J = 23.7$ Hz), 47.8-46.8 (m), 16.9.

^{19}F NMR (282 MHz, CD_2Cl_2) δ -80.95 - -81.40 (m, 3F), -109.16 - -114.44 (m, 2F), -119.23 - -121.05 (m, 2F), -121.58 - -122.31 (m, 2F), -122.82 - -123.38 (m, 2F), -126.17 - -126.74 (m, 2F).

IR (film): ν (cm^{-1}) 3070, 2978, 2930, 1694, 1496, 1459, 1401, 1353, 1311, 1233, 1196, 1141, 1029, 974, 865, 812, 754, 709, 653, 547.

HRMS (FD, m/z) calcd for $C_{24}H_{14}ClF_{13}N_2O$ $[M]^+$: 628.0587, found: 628.0614.

(R)-3,3,4,4,5,5,6,6,7,7,8,8,8-Tridecafluoro-2-methyl-1-(1-(*o*-tolyl)-1*H*-imidazol-2-yl)octan-1-one(4 9e)

According to the general procedure, the reaction of 2-acyl imidazole **46e** (42.9 mg, 0.20 mmol) and C₆F₁₃I (535.2 mg, 1.20 mmol) catalyzed by Λ -**Ir(*t*Bu)** (8.6 mg, 0.008 mol) gave **49e** as a yellow liquid (86.0 mg, yield: 82%) after 24 hours. Enantiomeric excess established by HPLC analysis using a Chiralpak OJ-H column, *ee* = 97% (HPLC: OJ-H, 254 nm, hexane/isopropanol = 99:1, flow rate 1.0 mL/min, 25 °C, *t_r* (major) = 4.4 min, *t_r* (minor) = 7.0 min). [α]_D²² = -1.5° (*c* 1.1, CH₂Cl₂).

¹H NMR (300 MHz, CD₂Cl₂) δ 7.46-7.26 (m, 4H), 7.22-7.08 (m, 2H), 5.23-5.05 (m, 1H), 1.99 (s, 3H), 1.94 (s, 3H, other rotamer), 1.41 (t, *J* = 7.4 Hz, 3H).

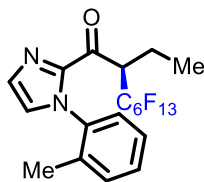
¹³C NMR (75 MHz, CD₂Cl₂) δ 185.2, 143.1, 138.1 (d, *J* = 5.1 Hz), 135.2 (d, *J* = 22.7 Hz), 131.2 (d, *J* = 5.0 Hz), 130.9 (d, *J* = 4.4 Hz), 129.7, 128.6 (d, *J* = 6.1 Hz), 127.1 (d, *J* = 13.3 Hz), 126.8 (d, *J* = 8.0 Hz), 42.2-41.5 (m), 17.1 (d, *J* = 30.3 Hz) 11.3 (d, *J* = 5.1 Hz).

¹⁹F NMR (282 MHz, CD₂Cl₂) δ -81.15 (t, *J* = 9.7 Hz, 3F), -113.35 - -116.35 (m, 2F), -120.38 - -121.25 (m, 2F), -121.65 - -122.30 (m, 2F), -122.75 - -123.35 (m, 2F), -126.05 - -126.50 (m, 2F).

IR (film): ν (cm⁻¹) 2925, 2859, 1693, 1497, 1457, 1404, 1351, 1309, 1234, 1197, 1143, 1018, 948, 905, 766, 704, 626, 529, 465.

HRMS (FD, *m/z*) calcd for C₁₉H₁₃F₁₃N₂O [M]⁺: 532.0820, found: 532.0832.

(R)-2-Ethyl-3,3,4,4,5,5,6,6,7,7,8,8,8-tridecafluoro-1-(1-(*o*-tolyl)-1*H*-imidazol-2-yl)octan-1-one
(49f)



According to the general procedure, the reaction of 2-acyl imidazole **46f** (5.7 mg, 0.20 mmol) and $C_6F_{13}I$ (535.2 mg, 1.20 mmol) Λ -**Ir(*t*Bu)** (8.6 mg, 0.008 mol) gave **49f** as a yellow liquid (64.3 mg, yield: 59%) after 62 hours. Enantiomeric excess established by HPLC analysis using a Chiralpak OD-H column, $ee = 99\%$ (HPLC: OD-H, 254 nm, hexane/isopropanol = 99:1, flow rate 1.0 mL/min, 25 °C, t_r (major) = 4.5 min, t_r (minor) = 4.9 min). $[\alpha]_D^{22} = -22.1^\circ$ (c 0.8, CH_2Cl_2).

1H NMR (300 MHz, CD_2Cl_2) δ 7.46-7.24 (m, 4H), 7.22-7.18 (m, 1H), 7.17-7.06 (m, 1H), 5.15-4.96 (m, 1H), 2.04-1.90 (m, 2H), 1.99 (s, 3H), 1.94 (s, 3H, other rotamer), 0.92 (q, $J = 8.0$ Hz, 3H).

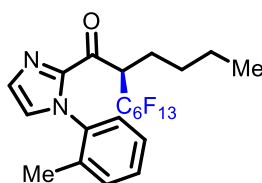
^{13}C NMR (75 MHz, CD_2Cl_2) δ 185.2, 144.3, 138.2 (d, $J = 3.4$ Hz), 135.2 (d, $J = 21.6$ Hz), 131.2 (d, $J = 9.0$ Hz), 131.0 (d, $J = 3.5$ Hz), 129.7, 128.6, 127.0 (d, $J = 11.6$ Hz), 126.8 (d, $J = 8.0$ Hz), 48.5-47.8 (m), 20.2-20.0 (m), 17.1 (d, $J = 34.5$ Hz), 11.6 (d, $J = 5.4$ Hz).

^{19}F NMR (282 MHz, CD_2Cl_2) δ -81.89 (t, $J = 9.7$ Hz, 3F), -113.45 - -115.64 (m, 2F), -120.38 - -121.25 (m, 2F), -121.65 - -122.30 (m, 2F), -122.75 - -123.35 (m, 2F), -126.75 - -126.45 (m, 2F).

IR (film): ν (cm^{-1}) 2928, 2861, 1691, 1498, 1457, 1405, 1317, 1233, 1196, 1142, 1024, 964, 905, 850, 764, 714, 647, 531, 459.

HRMS (FD, m/z) calcd for $C_{20}H_{15}F_{13}N_2O$ $[M]^+$: 546.0977, found: 546.1001.

(R)-2-Butyl-3,3,4,4,5,5,6,6,7,7,8,8,8-tridecafluoro-1-(1-(*o*-tolyl)-1*H*-imidazol-2-yl)octan-1-one
(49g)



According to the general procedure, the reaction of 2-acyl imidazole **46g** (51.3 mg, 0.20 mmol) and $C_6F_{13}I$ (535.2 mg, 1.20 mmol) Λ -**Ir(*t*Bu)** (8.6 mg, 0.008 mol) gave **49g** as a yellow liquid (70.2 mg, yield: 61%) after 72 hours. Enantiomeric excess established by HPLC analysis using a Chiralpak

OD-H column, *ee* = 98% (HPLC: OD-H, 254 nm, hexane/isopropanol = 99.5:0.5, flow rate 0.5 mL/min, 25 °C, *t_r* (major) = 13.5 min, *t_r* (minor) = 14.5 min). $[\alpha]_{\text{D}}^{22} = -34.5^\circ$ (*c* 0.4, CH₂Cl₂).

¹H NMR (300 MHz, CD₂Cl₂) δ 7.46-7.25 (m, 4H), 7.22-7.07 (m, 2H), 5.22-5.03 (m, 1H), 2.03-1.82 (m, 2H), 1.99 (s, 3H), 1.94 (s, 3H, other rotamer), 1.45-1.15 (m, 4H), 0.85 (t, *J* = 7.1 Hz, 3H).

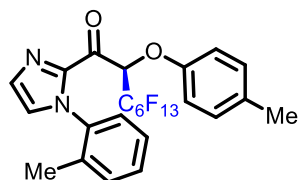
¹³C NMR (75 MHz, CD₂Cl₂) δ 185.3, 144.2, 138.1 (d, *J* = 3.8 Hz), 135.2 (d, *J* = 24.5 Hz), 131.2 (d, *J* = 8.4 Hz), 131.0 (d, *J* = 2.8 Hz), 129.7, 128.6 (d, *J* = 1.6 Hz), 127.0 (d, *J* = 12.4 Hz), 126.8 (d, *J* = 8.6 Hz), 47.1-46.4 (m), 29.4 (d, *J* = 9.4 Hz), 26.4-26.2 (m), 22.9 (d, *J* = 1.2 Hz), 17.1 (d, *J* = 34.2 Hz) 13.8.

¹⁹F NMR (282 MHz, CD₂Cl₂) δ -81.30 (t, *J* = 9.9 Hz, 3F), -110.60 - -115.40 (m, 2F), -119.38 - -121.25 (m, 2F), -121.65 - -122.40 (m, 2F), -122.75 - -123.35 (m, 2F), -126.20 - -126.65 (m, 2F).

IR (film): ν (cm⁻¹) 2961, 2930, 2869, 1691, 1498, 1457, 1405, 1234, 1197, 1142, 1053, 904, 766, 716, 644, 531.

HRMS (FD, *m/z*) calcd for C₂₂H₁₉F₁₃N₂O [M]⁺: 574.1290, found: 574.1263.

(*R*)-3,3,4,4,5,5,6,6,7,7,8,8,8-Tridecafluoro-1-(1-(*o*-tolyl)-1*H*-imidazol-2-yl)-2-(*p*-tolylloxy)octan-1-one (49h)



According to the general procedure, the reaction of 2-acyl imidazole **46h** (61.3 mg, 0.20 mmol) and C₆F₁₃I (535.2 mg, 1.20 mmol) catalyzed by Λ -**Ir**(*t*Bu) (4.3 mg, 0.004 mol) gave **49h** as a yellow liquid (78.1 mg, yield: 62%) after 62 hours. Enantiomeric excess established by HPLC analysis using a Chiralpak AD-H column, *ee* = 98% (HPLC: AD-H, 254 nm, hexane/isopropanol = 99:1, flow rate 1 mL/min, 25 °C, *t_r* (major) = 6.0 min, *t_r* (minor) = 5.0 min). $[\alpha]_{\text{D}}^{22} = -30.6^\circ$ (*c* 1.0, CH₂Cl₂).

¹H NMR (300 MHz, CD₂Cl₂) δ 7.49-7.26 (m, 5H), 7.22-7.03 (m, 3H), 6.97-6.84 (m, 3H), 2.27 (s, 3H), 1.949 (s, 3H), 1.87 (s, 3H, other rotamer).

¹³C NMR (75 MHz, CD₂Cl₂) δ 180.3, 154.6, 143.2, 137.3, 135.3, 134.9, 132.9, 132.1, 131.8, 131.4, 131.3, 131.2, 130.6, 130.0, 129.9, 129.0, 128.2, 127.2, 127.03, 126.98, 126.9, 126.7, 118.0, 115.7, 73.5,

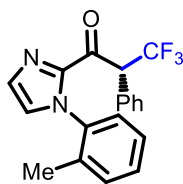
37.6, 32.4, 30.5, 30.2, 29.9, 27.6, 23.2, 20.6, 17.2, 16.8, 14.3.

^{19}F NMR (282 MHz, CD_2Cl_2) δ -81.65 - -82.65 (m, 3F), -115.20 - -118.05 (m, 2F), -121.50 - -124.90 (m, 6F), -125.90 - -128.45 (m, 2F).

IR (film): ν (cm^{-1}) 3118, 3035, 2928, 2865, 1702, 1610, 1506, 1456, 1403, 1315, 1197, 1144, 902, 812, 766, 714, 525.

HRMS (FD, m/z) calcd for $\text{C}_{25}\text{H}_{17}\text{F}_{13}\text{N}_2\text{O}_2$ $[\text{M}]^+$: 624.1082, found: 624.1103.

(*R*)-3,3,3-Trifluoro-2-phenyl-1-(1-(*o*-tolyl)-1*H*-imidazol-2-yl)propan-1-one (47a)



According to the general procedure, the reaction of 2-acyl imidazole **46a** (53.3 mg, 0.20 mmol) and trifluoriodomethane (391.8 mg, 2.00 mmol) catalyzed by Λ -**Ir(*t*Bu)** (4.3 mg, 0.004 mol) gave **47a** as a yellow liquid (29.8 mg, yield: 43%) after 44 hours. Enantiomeric excess established by HPLC analysis using a Chiralpak IC column, $ee = 93\%$ (HPLC: IC, 254 nm, hexane/isopropanol = 99:1, flow rate 1 mL/min, 25 °C, t_r (major) = 6.1 min, t_r (minor) = 5.7 min). $[\alpha]_{\text{D}}^{22} = -303.0^\circ$ (c 0.4, CH_2Cl_2).

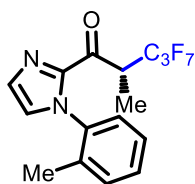
^1H NMR (300 MHz, CD_2Cl_2) δ 7.54-7.47 (m, 2H), 7.46-6.97 (m, 9H), 6.17-6.04 (m, 1H), 2.03 (s, 3H), 1.70 (s, 3H, other rotamer).

^{13}C NMR (75 MHz, CD_2Cl_2) δ 182.1, 137.9, 135.2, 134.9, 131.3, 131.2, 131.0, 130.5, 130.3, 129.7, 129.4, 129.3, 128.9, 128.5, 127.1, 127.0, 126.9, 126.8, 126.5, 123.0, 56.2-55.2 (m), 17.1 (d, $J = 20.8$ Hz).

^{19}F NMR (282 MHz, CD_2Cl_2) δ -67.33 (d, $J = 7.9$ Hz, 3F).

IR (film): ν (cm^{-1}) 3114, 3065, 3035, 2963, 2928, 1692, 1497, 1455, 1402, 1328, 1257, 1153, 1120, 1027, 976, 861, 822, 764, 739, 698, 674, 588, 522, 455.

HRMS (FD, m/z) calcd for $\text{C}_{19}\text{H}_{15}\text{F}_3\text{N}_2\text{O}$ $[\text{M}]^+$: 344.1137, found: 344.1120.

(R)-3,3,4,4,5,5,5-Heptafluoro-2-methyl-1-(1-(*o*-tolyl)-1*H*-imidazol-2-yl)pentan-1-one (47b)

According to the general procedure, the reaction of 2-acyl imidazole **46e** (42.9 mg, 0.20 mmol) and 1,1,1,2,2,3,3-heptafluoro-3-iodopropane (355.1 mg, 1.20 mmol) catalyzed by Λ -**Ir(*t*Bu)** (4.3 mg, 0.004 mol) gave **47b** as a yellow liquid (40.7 mg, yield: 53%) after 45 hours. Enantiomeric excess established by HPLC analysis using a Chiralpak OJ-H column, *ee* = 95% (HPLC: OJ-H, 254 nm, hexane/isopropanol = 99:1, flow rate 1 mL/min, 25 °C, *t_r* (major) = 14.6 min, *t_r* (minor) = 20.6 min). $[\alpha]_D^{22} = -11.5^\circ$ (*c* 0.5, CH₂Cl₂).

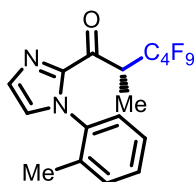
¹H NMR (300 MHz, CD₂Cl₂) δ 7.45-7.25 (m, 4H), 7.22-7.08 (m, 2H), 5.20-5.02 (m, 1H), 1.98 (s, 3H), 1.93 (s, 3H, other rotamer), 1.40 (t, *J* = 7.4 Hz, 3H).

¹³C NMR (75 MHz, CD₂Cl₂) δ 185.1, 142.9, 138.0 (d, *J* = 5.3 Hz), 135.1 (d, *J* = 23.2 Hz), 131.1 (d, *J* = 4.2 Hz), 130.8 (d, *J* = 5.1 Hz), 129.6, 128.6 (d, *J* = 5.7 Hz), 127.0 (d, *J* = 13.3 Hz), 126.7 (d, *J* = 8.6 Hz), 41.9-41.1 (m), 17.0 (d, *J* = 27.1 Hz), 11.2 (d, *J* = 5.0 Hz).

¹⁹F NMR (282 MHz, CD₂Cl₂) δ -80.47 - -81.47 (td, *J*₂ = 11.0 Hz, *J*₂ = 1.7 Hz, 3F), -114.45 - -117.36 (m, 2F), -125.09 - -125.36 (m, 2F).

IR (film): ν (cm⁻¹) 3114, 2924, 2855, 1693, 1497, 1457, 1404, 1346, 1306, 1222, 1180, 1116, 1070, 1008, 949, 914, 762, 711, 672, 631, 535, 453.

HRMS (FD, *m/z*) calcd for C₁₆H₁₃F₇N₂O [M]⁺: 382.0916, found: 382.0904.

(R)-3,3,4,4,5,5,6,6,6-Nonafluoro-2-methyl-1-(1-(*o*-tolyl)-1*H*-imidazol-2-yl)hexan-1-one (47c)

According to the general procedure, the reaction of 2-acyl imidazole **46e** (42.9 mg, 0.20 mmol) and 1,1,1,2,2,3,3,4,4-nonafluoro-4-iodobutane (345.9 mg, 1.20 mmol) catalyzed by Λ -**Ir(*t*Bu)** (4.3 mg, 0.004 mol) gave **47c** as a yellow liquid (42.2 mg, yield: 49%) after 24 hours. Enantiomeric excess established by HPLC analysis using a Chiralpak OJ-H column, *ee* = 95% (HPLC: OJ-H, 254 nm,

hexane/isopropanol = 99:1, flow rate 1 mL/min, 25 °C, t_r (major) = 14.6 min, t_r (minor) = 20.6 min).

$[\alpha]_D^{22} = -4.5^\circ$ (c 0.5, CH_2Cl_2).

^1H NMR (300 MHz, CD_2Cl_2) δ 7.45-7.26 (m, 4H), 7.18-7.08 (m, 2H), 5.22-5.04 (m, 1H), 1.98 (s, 3H), 1.93 (s, 3H, other rotamer), 1.40 (t, $J = 7.4$ Hz, 3H).

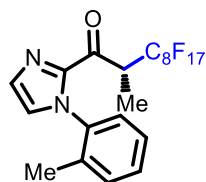
^{13}C NMR (75 MHz, CD_2Cl_2) δ 185.1, 143.0, 138.1 (d, $J = 4.7$ Hz), 135.1 (d, $J = 23.9$ Hz), 131.2 (d, $J = 5.0$ Hz), 130.9 (d, $J = 4.6$ Hz), 129.7, 128.6 (d, $J = 5.2$ Hz), 127.0 (d, $J = 13.9$ Hz), 126.7 (d, $J = 7.6$ Hz), 42.1-41.2 (m), 17.0 (d, $J = 29.1$ Hz), 11.2 (d, $J = 5.3$ Hz).

^{19}F NMR (282 MHz, CD_2Cl_2) δ -80.47 - -81.47 (m, 3F), -113.64 - -116.76 (m, 2F), -121.07 - -122.98 (m, 2F), -125.06 - -127.62 (m, 2F).

R (film): ν (cm^{-1}) 3116, 2956, 2928, 1693, 1497, 1458, 1405, 1346, 1307, 1212, 1131, 1016, 946, 907, 874, 840, 762, 712, 527, 458.

HRMS (FD, m/z) calcd for $\text{C}_{17}\text{H}_{13}\text{F}_9\text{N}_2\text{O}$ $[\text{M}]^+$: 432.0884 found: 432.0883.

(*R*)-3,3,4,4,5,5,6,6,7,7,8,8,9,9,10,10,10-Heptadecafluoro-2-methyl-1-(1-(*o*-tolyl)-1*H*-imidazol-2-yl) decan-1-one (47d)



According to the general procedure, the reaction of 2-acyl imidazole **46e** (42.9 mg, 0.20 mmol) and 1,1,1,2,2,3,3,4,4,5,5,6,6,7,7,8,8,8-heptadecafluoro-8-iodooctane (655.0 mg, 1.20 mmol) catalyzed by Λ -**Ir(*t*Bu)** (4.3 mg, 0.004 mol) gave **47d** as a yellow liquid (80.0 mg, yield: 63%) after 24 hours. Enantiomeric excess established by HPLC analysis using a Chiralpak OJ-H column, $ee = 95\%$ (HPLC: OJ-H, 254 nm, hexane/isopropanol = 99:1, flow rate 1 mL/min, 25 °C, t_r (major) = 4.2 min, t_r (minor) = 6.1 min). $[\alpha]_D^{22} = +2.5^\circ$ (c 0.9, CH_2Cl_2).

^1H NMR (300 MHz, CD_2Cl_2) δ 7.45-7.25 (m, 4H), 7.22-7.08 (m, 2H), 5.22-5.04 (m, 1H), 1.98 (s, 3H), 1.93 (s, 3H, other rotamer), 1.41 (t, $J = 7.4$ Hz, 3H).

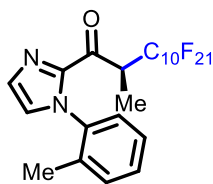
^{13}C NMR (75 MHz, CD_2Cl_2) δ 185.1, 143.0, 138.1 (d, $J = 5.7$ Hz), 135.1 (d, $J = 22.8$ Hz), 131.2 (d, $J = 4.3$ Hz), 130.9 (d, $J = 5.0$ Hz), 129.7, 128.6 (d, $J = 5.9$ Hz), 127.0 (d, $J = 13.4$ Hz), 126.7 (d, $J = 7.8$ Hz), 42.2-41.4 (m), 17.0 (d, $J = 31.4$ Hz), 11.3 (d, $J = 5.7$ Hz).

^{19}F NMR (282 MHz, CD_2Cl_2) δ -88.14 - -88.33 (m, 3F), -113.41 - -116.53 (m, 2F), -119.37 - -121.79 (m, 2F), -121.66 - -123.68 (m, 6F), -122.75 - -123.19 (m, 2F), -126.15 - -126.58 (m, 2F).

IR (film): ν (cm^{-1}) 3115, 2924, 2854, 1694, 1498, 1458, 1405, 1202, 1144, 1011, 950, 908, 766, 708, 652, 529, 459.

HRMS (FD, m/z) calcd for $\text{C}_{21}\text{H}_{13}\text{F}_{17}\text{N}_2\text{O}$ $[\text{M}]^+$: 632.0756, found: 632.0785.

(S)-3,3,4,4,5,5,6,6,7,7,8,8,9,9,10,10,11,11,12,12,12-Henicosafuoro-2-methyl-1-(1-(*o*-tolyl)-1*H*-imidazol-2-yl)dodecan-1-one (47e)



According to the general procedure, the reaction of 2-acyl imidazole **46e** (42.9 mg, 0.20 mmol) and 1,1,1,2,2,3,3,4,4,5,5,6,6,7,7,8,8,9,9,10,10-henicosafuoro-10-iododecane (775.2 mg, 1.20 mmol) catalyzed by Δ -**Ir(*t*Bu)** (8.6 mg, 0.008 mol) in MeOH/THF (0.8mL/0.2mL) gave **47e** as a yellow solid (75.1 mg, yield: 51%) after 44 hours. Enantiomeric excess established by HPLC analysis using a Chiralpak OJ-H column, $ee = 95\%$ (HPLC: OJ-H, 254 nm, hexane/isopropanol = 99:1, flow rate 1 mL/min, 25 °C, t_r (major) = 5.4 min, t_r (minor) = 3.8 min). $[\alpha]_D^{22} = +4.6^\circ$ (c 0.8, CH_2Cl_2).

^1H NMR (300 MHz, CD_2Cl_2) δ 7.45-7.26 (m, 4H), 7.22-7.07 (m, 2H), 5.22-5.05 (m, 1H), 1.98 (s, 3H), 1.93 (s, 3H, other rotamer), 1.41 (t, $J = 7.2$ Hz, 3H).

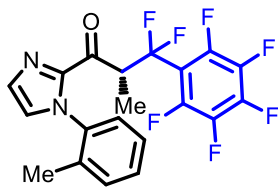
^{13}C NMR (75 MHz, CD_2Cl_2) δ 185.2, 143.0, 138.1 (d, $J = 4.7$ Hz), 135.1 (d, $J = 23.5$ Hz), 131.2 (d, $J = 5.1$ Hz), 130.9 (d, $J = 4.9$ Hz), 129.7, 128.6 (d, $J = 6.1$ Hz), 127.0 (d, $J = 13.1$ Hz), 126.8 (d, $J = 7.4$ Hz), 42.2-41.4 (m), 17.0 (d, $J = 32.3$ Hz), 11.3 (d, $J = 7.9$ Hz).

^{19}F NMR (282 MHz, CD_2Cl_2) δ -81.14 - -81.38 (m, 3F), -113.04 - -116.95 (m, 2F), -119.47 - -121.12 (m, 2F), -121.66 - -122.38 (m, 10F), -122.71 - -123.18 (m, 2F), -126.18 - -126.60 (m, 2F).

IR (film): ν (cm^{-1}) 3145, 2923, 2854, 1688, 1461, 1404, 1203, 1144, 1066, 950, 911, 761, 527, 524.

HRMS (FD, m/z) calcd for $\text{C}_{23}\text{H}_{13}\text{F}_{21}\text{N}_2\text{O}$ $[\text{M}]^+$: 732.0693, found: 732.0720.

(R)-3,3-Difluoro-2-methyl-3-(perfluorophenyl)-1-(1-(*o*-tolyl)-1H-imidazol-2-yl)propan-1-one
(47f)



According to the general procedure, the reaction of 2-acyl imidazole **46e** (42.9 mg, 0.20 mmol) and 1-(difluoriodomethyl)-2,3,4,5,6-pentafluorobenzene (413.0 mg, 1.20 mmol) catalyzed by Λ -**Ir(*t*Bu)** (4.3 mg, 0.004 mol) gave **47f** as a yellow liquid (80.0 mg, yield: 93%) after 15 hours. Enantiomeric excess established by HPLC analysis using a Chiralpak OD-H column, *ee* > 99.5% (HPLC: OD-H, 254 nm, hexane/isopropanol = 99:1, flow rate 1 mL/min, 25 °C, *t_r* (major) = 8.6 min, *t_r* (minor) = 9.5 min). $[\alpha]_D^{22} = +70.6^\circ$ (*c* 0.9, CH₂Cl₂).

¹H NMR (300 MHz, CD₂Cl₂) δ 7.44-7.22 (m, 4H), 7.16-7.02 (m, 2H), 5.16-4.98 (m, 1H), 1.95 (s, 3H), 1.89 (s, 3H, other rotamer), 1.39 (t, *J* = 6.9 Hz, 3H).

¹³C NMR (75 MHz, CD₂Cl₂) δ 186.6, 143.1, 138.0 (d, *J* = 5.9 Hz), 131.1 (d, *J* = 8.4 Hz), 130.7 138.0 (d, *J* = 3.9 Hz), 129.6, 128.3 (d, *J* = 12.4 Hz), 127.0 (d, *J* = 10.7 Hz), 126.6 (d, *J* = 7.1 Hz), 49.0-47.9 (m), 17.0 (d, *J* = 37.3 Hz), 11.0 (dt, *J₁* = 20.1, *J₂* = 4.6 Hz).

¹⁹F NMR (282 MHz, CD₂Cl₂) δ -87.75 - -93.05 (m, 1F), -95.75 - -98.85 (m, 1F), -119.05 - -120.90 (m, 2F), -137.40 - -141.55 (m, 2F), -150.60 - -152.70 (m, 1F), -160.45 - -163.80 (m, 2F).

IR (film): ν (cm⁻¹) 3117, 2926, 2891, 1688, 1654, 1498, 1457, 1402, 1336, 1190, 1084, 988, 943, 908, 832, 764, 710, 546, 458.

HRMS (FD, *m/z*) calcd for C₂₀H₁₃F₇N₂O [M]⁺: 430.0916, found: 430.0920.

5.6.4 Single-Crystal X-Ray Diffraction Studies

Single crystals of Δ -**IrS(*t*Bu)** suitable for X-ray diffraction were obtained by slow diffusion from a solution of Δ -**IrS(*t*Bu)** (20 mg) in toluene (2.0 mL) layered with *n*-hexane (0.5 mL) at room temperature for several days in a glass tube. The absolute configurations of compound Δ -**IrS(*t*Bu)** has been determined. Crystal data and details of the structure determination are presented in the Appendices (Chapter 6.7).

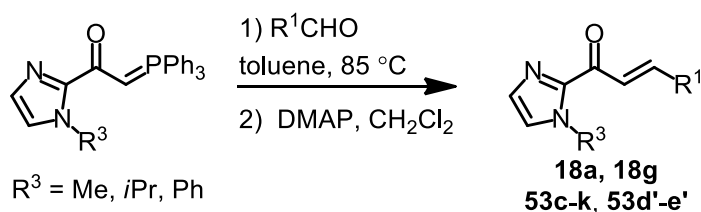
5.7 Visible-Light-Activated Enantioselective Addition of Alkyl Radicals to Alkenes with a Chiral Rhodium Complex

5.7.1 Synthesis of Substrates

1) Synthesis of α,β -Unsaturated Alkenes

α,β -Unsaturated 2-acyl pyrazoles (**58a-e**) were synthesized according to published procedures without any further change,³⁴ while α,β -unsaturated 2-acyl imidazoles (**18a**, **18g**, **53c-k**, **53d'** and **53e'**) were synthesized according to reported procedures with some modifications (shown as following).³⁵

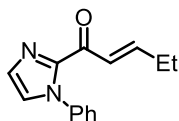
General procedure for the synthesis of α,β -unsaturated 2-acyl imidazoles.



To a solution of Wittig reagent³⁵ (2.4 mmol) in toluene (12.0 mL) at room temperature was added the corresponding aldehyde (2 to 10 equiv). The reaction was stirred at 85 °C overnight. After the solvent was removed in vacuo, the residue was purified by flash chromatography on silica gel (EtOAc/hexane = 1/5 to 1/3) to produce the unsaturated alkenes as a mixture of *E*:*Z* isomers. Then, to a solution of purified alkene in CH_2Cl_2 (0.2 M) at room temperature was added DMAP (0.1 equiv). The reaction was sealed and stored at 4 °C (fridge) for 24 hours. After isomerization, the solution was passed through a short silica column. The isomerization proceeded well to afford **18a**, **18g**, **53c-k**, **53d'-e'** with an improved *E*/*Z* value (*E*/*Z* > 50/1, as judged by ^1H NMR).

The experimental data of **53d-g**, **53j-k** and **53e'** are shown below. The other 2-acyl imidazoles (**18a**, **18g**, **53c**,³⁵ **53h-i**,³⁶ **53d'**³⁵) have been reported previously.

(*E*)-1-(1-Phenyl-1*H*-imidazol-2-yl)pent-2-en-1-one (**53d**)



Following the general procedure, propionaldehyde (1.7 mL, 24.0 mmol, 10 equiv) was converted to α,β -Unsaturated 2-acyl imidazole **53d** (462.1 mg, 2.04 mmol, yield: 85%) as a white solid.

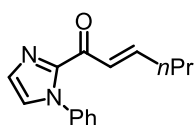
^1H NMR (300 MHz, CDCl_3) δ 7.53 – 7.46 (m, 3H), 7.42 (dt, J = 15.6, 1.6 Hz, 1H), 7.36 – 7.28 (m, 3H), 7.22 (d, J = 0.9 Hz, 1H), 7.14 (dt, J = 15.6, 6.4 Hz, 1H), 2.44 – 2.25 (m, 2H), 1.15 (t, J = 7.4 Hz, 3H).

^{13}C NMR (75 MHz, CDCl_3) δ 179.5, 150.7, 143.8, 138.6, 129.6, 128.9, 128.6, 127.0, 125.9, 125.3, 25.8, 12.3.

IR (film): ν (cm^{-1}) 1665, 1613, 1492, 1446, 1399, 1299, 1060, 971, 806, 761, 691.

HRMS (ESI, m/z) calcd for $\text{C}_{14}\text{H}_{15}\text{N}_2\text{O}$ $[\text{M}+\text{H}]^+$: 227.1179, found: 227.1181.

(*E*)-1-(1-Phenyl-1*H*-imidazol-2-yl)hex-2-en-1-one (53e)



Following the general procedure, butyraldehyde (1.1 mL, 12.0 mmol, 5 equiv) was converted to α,β -unsaturated 2-acyl imidazole **53e** (440.0 mg, 1.83 mmol, yield: 76%) as a white solid.

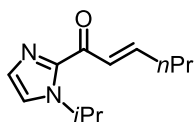
^1H NMR (300 MHz, CDCl_3) δ 7.53 – 7.38 (m, 4H), 7.37 – 7.26 (m, 3H), 7.22 (s, 1H), 7.09 (dt, J = 15.6, 7.0 Hz, 1H), 2.31 (qd, J = 7.2, 1.4 Hz, 2H), 1.64 – 1.48 (m, 2H), 0.97 (t, J = 7.4 Hz, 3H).

^{13}C NMR (75 MHz, CDCl_3) δ 179.4, 149.2, 143.8, 138.6, 129.6, 128.9, 128.6, 127.0, 126.3, 125.9, 34.7, 21.4, 13.7.

IR (film): ν (cm^{-1}) 3113, 2958, 2926, 2870, 1666, 1617, 1495, 1446, 1398, 1303, 1148, 1063, 972, 826, 798, 763, 692.

HRMS (ESI, m/z) calcd for $\text{C}_{15}\text{H}_{17}\text{N}_2\text{O}$ $[\text{M}+\text{H}]^+$: 241.1335, found: 241.1338.

(*E*)-1-(1-Isopropyl-1*H*-imidazol-2-yl)hex-2-en-1-one (53e')



Following the general procedure, butyraldehyde (1.1 mL, 12.0 mmol, 5 equiv) was converted to α,β -Unsaturated 2-acyl imidazole **53e'** (381.2 mg, 1.85 mmol, yield: 77%) as a white solid.

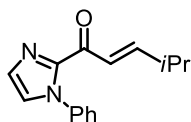
^1H NMR (300 MHz, CDCl_3) δ 7.46 (dd, J = 15.6, 1.0 Hz, 1H), 7.28 (s, 1H), 7.21 (s, 1H), 7.17 – 7.04 (m, 1H), 5.67 (hept, J = 6.8 Hz, 1H), 2.31 (q, J = 7.2 Hz, 2H), 1.65 – 1.50 (m, 2H), 1.47 (dd, J = 6.7, 1.0 Hz, 6H), 0.97 (t, J = 7.4 Hz, 3H).

^{13}C NMR (75 MHz, CDCl_3) δ 180.9, 148.3, 143.1, 129.6, 127.1, 121.1, 49.2, 34.7, 23.6, 21.5, 13.7.

IR (film): ν (cm⁻¹) 2962, 2931, 2873, 1665, 1616, 1391, 1253, 1013, 977, 809, 764, 649.

HRMS (ESI, m/z) calcd for C₁₂H₁₉N₂O [M+H]⁺: 207.1492, found: 207.1494.

(*E*)-4-Methyl-1-(1-phenyl-1*H*-imidazol-2-yl)pent-2-en-1-one (53f)



Following the general procedure, isobutyraldehyde (2.2 mL, 24.0 mmol, 10 equiv) was converted to α,β -Unsaturated 2-acyl imidazole **53f** (505.0 mg, 2.10 mmol, yield: 88%) as a white solid.

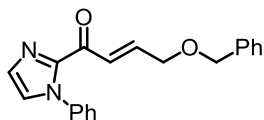
¹H NMR (300 MHz, CDCl₃) δ 7.53 – 7.43 (m, 3H), 7.43 – 7.27 (m, 4H), 7.22 (d, J = 1.0 Hz, 1H), 7.06 (dd, J = 15.7, 6.7 Hz, 1H), 2.70 – 2.47 (m, 1H), 1.13 (d, J = 6.8 Hz, 6H).

¹³C NMR (75 MHz, CDCl₃) δ 179.7, 155.4, 143.9, 138.6, 129.6, 128.9, 128.6, 127.0, 125.9, 123.3, 31.4, 21.3.

IR (film): ν (cm⁻¹) 3141, 3061, 2961, 2926, 2876, 1665, 1612, 1491, 1439, 1397, 1299, 1141, 1043, 1003, 963, 918, 863, 777, 688, 651, 607, 532.

HRMS (ESI, m/z) calcd for C₁₅H₁₇N₂O [M+H]⁺: 241.1335, found: 241.1338.

(*E*)-4-(Benzyloxy)-1-(1-phenyl-1*H*-imidazol-2-yl)but-2-en-1-one (53g)



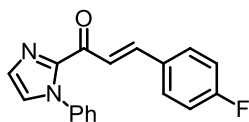
Following the general procedure, 2-(benzyloxy)acetaldehyde (674.0 μ L, 4.8 mmol, 2 equiv) was converted to α,β -Unsaturated 2-acyl imidazole **53g** (560.4 mg, 1.76 mmol, yield: 73%) as a white solid.

¹H NMR (300 MHz, CDCl₃) δ 7.68 (dt, J = 15.8, 1.9 Hz, 1H), 7.58 – 7.45 (m, 3H), 7.44 – 7.29 (m, 8H), 7.24 (d, J = 0.8 Hz, 1H), 7.10 (dt, J = 15.8, 4.6 Hz, 1H), 4.62 (s, 2H), 4.29 (dd, J = 4.6, 1.9 Hz, 2H).

¹³C NMR (75 MHz, CDCl₃) δ 179.1, 143.9, 143.7, 138.5, 137.9, 129.9, 129.0, 128.7, 128.4, 127.7, 127.2, 126.2, 125.9, 72.7, 69.2.

IR (film): ν (cm⁻¹) 3121, 3032, 2838, 2783, 1665, 1620, 1495, 1442, 1399, 1353, 1304, 1263, 1209, 1125, 1030, 974, 912, 832, 791, 759, 739, 692, 638, 605, 561, 513, 469.

HRMS (ESI, m/z) calcd for C₂₀H₁₉N₂O₂ [M+H]⁺: 319.1441, found: 319.1446.

(E)-3-(4-Fluorophenyl)-1-(1-phenyl-1H-imidazol-2-yl)prop-2-en-1-one (53j)

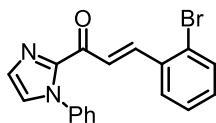
Following the general procedure, 4-fluorobenzaldehyde (515.0 μ L, 4.8 mmol, 2 equiv) was converted to α,β -Unsaturated 2-acyl imidazole **53j** (632.0 mg, 2.16 mmol, yield: 90%) as a white solid.

^1H NMR (300 MHz, CDCl_3) δ 8.00 (d, J = 16.0 Hz, 1H), 7.78 – 7.58 (m, 3H), 7.54 – 7.41 (m, 3H), 7.40 – 7.28 (m, 3H), 7.23 (d, J = 1.0 Hz, 1H), 7.08 (t, J = 8.6 Hz, 2H).

^{13}C NMR (75 MHz, CDCl_3) δ 179.0, 165.7, 162.4, 144.0, 142.5, 138.5, 131.21, 131.16, 130.7, 130.6, 129.8, 129.0, 128.8, 127.3, 125.9, 122.5, 122.4, 116.1, 115.9.

IR (film): ν (cm^{-1}) 3110, 3048, 1658, 1584, 1496, 1410, 1300, 1215, 1156, 1039, 975, 822, 756, 690, 503, 451.

HRMS (ESI, m/z) calcd for $\text{C}_{18}\text{H}_{14}\text{FN}_2\text{O}$ $[\text{M}+\text{H}]^+$: 293.1085, found: 293.1085.

(E)-3-(2-Bromophenyl)-1-(1-phenyl-1H-imidazol-2-yl)prop-2-en-1-one (53k)

Following the general procedure, 2-bromobenzaldehyde (883.0 mg, 4.8 mmol, 2 equiv) was converted to α,β -Unsaturated 2-acyl imidazole **53k** (826.3 mg, 2.35 mmol, yield: 98%) as a white solid.

^1H NMR (300 MHz, CDCl_3) δ 8.15 (d, J = 15.9 Hz, 1H), 8.04 (d, J = 15.9 Hz, 1H), 7.86 (dd, J = 7.8, 1.6 Hz, 1H), 7.60 (dd, J = 8.0, 1.2 Hz, 1H), 7.54 – 7.44 (m, 3H), 7.42 – 7.28 (m, 4H), 7.29 – 7.16 (m, 2H).

^{13}C NMR (75 MHz, CDCl_3) δ 178.6, 143.9, 141.9, 138.5, 134.9, 133.5, 131.3, 129.9, 129.0, 128.8, 128.1, 127.6, 127.5, 126.2, 126.0, 125.1.

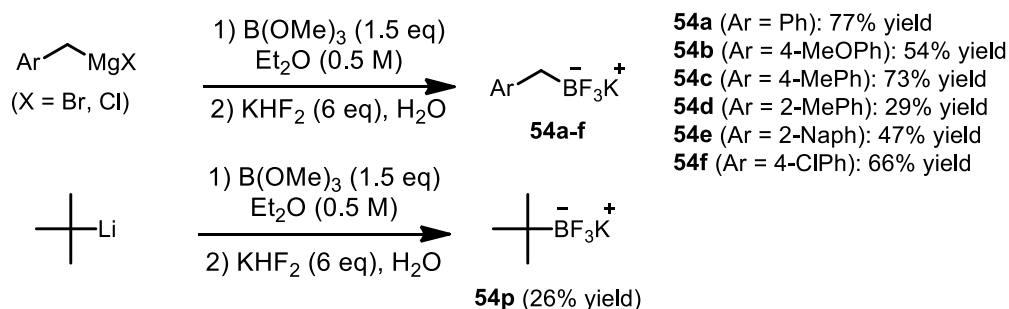
IR (film): ν (cm^{-1}) 1662, 1592, 1495, 1444, 1403, 1342, 1307, 1048, 1032, 975, 776, 743, 687, 580, 516.

HRMS (ESI, m/z) calcd for $\text{C}_{18}\text{H}_{14}\text{BrN}_2\text{O}$ $[\text{M}+\text{H}]^+$: 353.0284 and 355.0265, found: 353.0289 and 355.0268.

2) Synthesis of Potassium Organotrifluoroborates

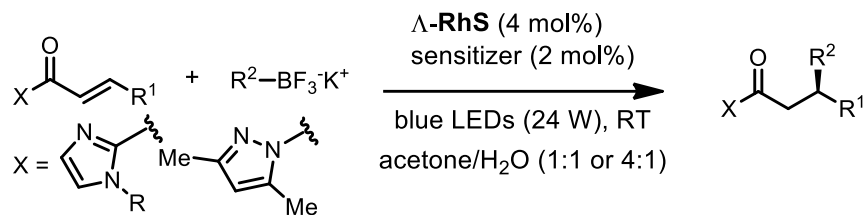
Potassium benzyltrifluoroborates (**54a-f**), potassium *tert*-butyltrifluoroborate (**54p**), potassium alkoxymethyltrifluoroborates (**54h-l**) were synthesized according to reported procedures with some modifications.³⁷ The other trifluoroborates were purchased commercially.

General procedure for the synthesis of potassium benzyltrifluoroborates (54a-f**) and potassium *tert*-butyltrifluoroborate (**54p**).**^{37a}



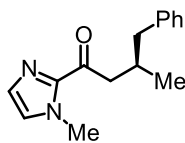
To a solution of fresh prepared Grignard reagent ArCH_2MgX (25.0 mmol, 1.0 eq) or *tert*-BuLi (25.0 mmol, 1.0 eq) in Et_2O (50.0 mL, 0.5 M) at -78°C were added trimethyl borate (4.2 mL, 37.5 mmol, 1.5 eq). The reaction mixture was stirred at -78°C for 30 min, then allowed to warm to room temperature and stirred for a further 1 h. After the reaction was cooled to 0°C , KHF_2 (11.7 g, 150.0 mmol) was added at one portion followed by the addition of H_2O (20.0 mL) over 20 min. After stirring at room temperature for 1 h, the solution was evaporated and the resulting solid was dried under high vacuum at 40°C for 1 h. The solid was extracted in hot acetone ($4 \times 100 \text{ mL}$), filtered and the solvent was concentrated under reduced pressure. The crude solid was recrystallized in acetone/ Et_2O to afford benzylic trifluoroborates (**54a-f**) and *tert*-butyltrifluoroborate (**54p**) as a white solid (26-77% yield).

5.7.2 Rhodium-Catalyzed Photoredox Reactions



General procedure for conjugate additions of alkyl radicals to alkenes. A dried 10 mL Schlenk tube was charged with the catalyst $\Delta\text{-RhS}$ (4 mol%), photosensitizer [Acr-Mes] ClO_4 (2 mol%, applied for α,β -unsaturated 2-acyl imidazoles) or $\text{Ir}[\text{dF}(\text{CF}_3)\text{ppy}]_2(\text{bpy})\text{PF}_6$ (2 mol%, applied for α,β -unsaturated 2-acyl pyrazoles), and the corresponding α,β -unsaturated alkene (0.2 mmol, 1.0 eq). The tube was purged with nitrogen and acetone/ H_2O (4:1 or 1:1, 1.0 mL) was added via syringe, followed by potassium trifluoroborate (0.3 mmol, 1.5 eq). The reaction mixture was degassed via freeze-pump-thaw for three cycles. After the mixture was thoroughly degassed, the vial was sealed and positioned approximately 10 cm from a 24 W blue LEDs lamp. The reaction was stirred at room temperature for the indicated time (monitored by TLC) under nitrogen atmosphere. Afterwards, the reaction was quenched with aqueous saturated NaHCO_3 at room temperature and extracted with CH_2Cl_2 (5×5 mL). The combined organic layers were dried over anhydrous Na_2SO_4 , filtered, and concentrated under reduced pressure. The residue was purified by flash chromatography on silica gel ($\text{EtOAc}/\text{hexane} = 1:15$ to 1:5) to afford the radical addition products. Racemic samples were obtained by carrying out the reactions with *rac*- RhS . The enantiomeric excess was determined by chiral HPLC analysis.

Exemplary reaction setup:

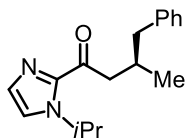
(R)-3-Methyl-1-(1-methyl-1H-imidazol-2-yl)-4-phenylbutan-1-one (55a)

According to the condition in table 12 (entry 5), α,β -unsaturated acyl imidazole **18a** (30.0 mg, 0.2 mmol) reacted with potassium benzyltrifluoroborate **54a** (59.4 mg, 0.30 mmol) in acetone/H₂O (1:1, 1.0 mL) to give **55a** as a colorless oil (32.5 mg, 0.134 mmol, yield: 67%). Enantiomeric excess established by HPLC analysis using a Chiralpak AD-H column, *ee* = 88% (HPLC: AD-H, 254 nm, hexane/isopropanol = 95:5, flow rate 1.0 mL/min, 25 °C, *t_r* (minor) = 7.8 min, *t_r* (major) = 11.7 min). $[\alpha]_D^{22} = -24.4^\circ$ (*c* 0.20, CH₂Cl₂).

¹H NMR (300 MHz, CDCl₃) δ 7.24 – 7.06 (m, 5H), 7.05 (d, *J* = 0.8 Hz, 1H), 6.92 (s, 1H), 3.88 (s, 3H), 3.01 (d, *J* = 6.5 Hz, 2H), 2.71 – 2.53 (m, 1H), 2.53 – 2.25 (m, 2H), 0.89 (d, *J* = 6.3 Hz, 3H).

¹³C NMR (75 MHz, CDCl₃) δ 192.7, 143.4, 140.7, 129.3, 128.7, 128.1, 126.8, 125.8, 45.6, 43.3, 36.2, 31.6, 19.9.

HRMS (ESI, *m/z*) calcd for C₁₅H₁₉N₂O [M+H]⁺: 243.1492, found: 243.1494.

(R)-1-(1-Isopropyl-1H-imidazol-2-yl)-3-methyl-4-phenylbutan-1-one (55b)

According to the condition in table 12 (entry 6), α,β -unsaturated acyl imidazole **18g** (35.6 mg, 0.2 mmol) reacted with potassium benzyltrifluoroborate **54a** (59.4 mg, 0.30 mmol) in acetone/H₂O (1:1, 1.0 mL) to give **55b** as a colorless oil (35.7 mg, 0.132 mmol, yield: 66%). Enantiomeric excess established by HPLC analysis using a Chiralpak AD-H column, *ee* = 93% (HPLC: AD-H, 254 nm, hexane/isopropanol = 95:5, flow rate 1.0 mL/min, 25 °C, *t_r* (minor) = 7.0 min, *t_r* (major) = 13.0 min). $[\alpha]_D^{22} = -26.7^\circ$ (*c* 0.21, CH₂Cl₂).

¹H NMR (300 MHz, CDCl₃) δ 7.28 – 6.94 (m, 7H), 5.44 (hept, *J* = 6.8 Hz, 1H), 3.03 (d, *J* = 6.5 Hz, 2H), 2.72 – 2.55 (m, 1H), 2.54 – 2.35 (m, 2H), 1.36 (d, *J* = 5.0 Hz, 3H), 1.34 (d, *J* = 5.0 Hz, 3H), 0.88 (d, *J* = 6.3 Hz, 3H).

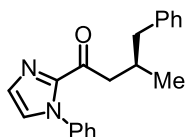
¹³C NMR (75 MHz, CDCl₃) δ 192.8, 142.6, 140.7, 129.3, 129.2, 128.1, 125.8, 120.9, 49.2, 46.2, 43.3,

31.7, 23.6, 23.6, 19.8.

IR (film): ν (cm⁻¹) 3061, 3026, 2964, 2925, 1670, 1455, 1396, 1254, 1203, 1151, 1087, 996, 912, 771, 737, 699, 498.

HRMS (ESI, m/z) calcd for C₁₇H₂₃N₂O [M+H]⁺: 271.1805, found: 271.1806.

(R)-3-Methyl-4-phenyl-1-(1-phenyl-1H-imidazol-2-yl)butan-1-one (55c)



According to the general procedure, α,β -unsaturated acyl imidazole **53c** (42.4 mg, 0.2 mmol) reacted with potassium benzyltrifluoroborate **54a** (59.4 mg, 0.30 mmol) in acetone/H₂O (1:1, 1.0 mL) to give **55c** as a white solid (44.4 mg, 0.146 mmol, yield: 73%). Enantiomeric excess established by HPLC analysis using a Chiralpak AD-H column, ee = 96% (HPLC: AD-H, 254 nm, hexane/isopropanol = 95:5, flow rate 1.0 mL/min, 25 °C, t_r (minor) = 10.0 min, t_r (major) = 11.1 min). $[\alpha]_D^{22}$ = -11.1° (c 0.37, CH₂Cl₂).

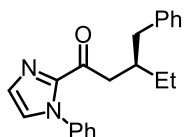
¹H NMR (300 MHz, CDCl₃) δ 7.44 – 7.32 (m, 3H), 7.23 – 7.12 (m, 5H), 7.12 – 7.03 (m, 4H), 3.13 – 2.92 (m, 2H), 2.68 – 2.52 (m, 1H), 2.51 – 2.28 (m, 2H), 0.85 (d, J = 6.4 Hz, 3H).

¹³C NMR (75 MHz, CDCl₃) δ 191.0, 143.3, 140.6, 138.5, 129.30, 129.25, 128.9, 128.7, 128.1, 126.9, 125.9, 125.8, 45.6, 43.3, 31.3, 19.8.

IR (film): ν (cm⁻¹) 3110, 3056, 3025, 2963, 2916, 2856, 1682, 1596, 1496, 1449, 1406, 1305, 1025, 970, 909, 777, 749, 694, 502.

HRMS (ESI, m/z) calcd for C₂₀H₂₁N₂O [M+H]⁺: 305.1648, found: 305.1649.

(R)-3-Benzyl-1-(1-phenyl-1H-imidazol-2-yl)pentan-1-one (55d)



According to the general procedure, α,β -unsaturated acyl imidazole **53d** (45.2 mg, 0.2 mmol) reacted with potassium benzyltrifluoroborate **54a** (59.4 mg, 0.30 mmol) in acetone/H₂O (1:1, 1.0 mL) to give **55d** as a colorless oil (30.5 mg, 0.096 mmol, yield: 48%). Enantiomeric excess established by HPLC

analysis using a Chiralpak AD-H column, $ee = 90\%$ (HPLC: AD-H, 254 nm, hexane/isopropanol = 99:1, flow rate 1.0 mL/min, 25 °C, t_r (minor) = 14.6 min, t_r (major) = 16.3 min). $[\alpha]_D^{22} = -24.4^\circ$ (c 0.20, CH_2Cl_2). $[\alpha]_D^{22} = -30.3^\circ$ (c 0.20, CH_2Cl_2).

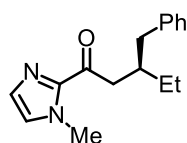
^1H NMR (300 MHz, CDCl_3) δ 7.44 – 7.31 (m, 3H), 7.23 – 7.12 (m, 5H), 7.11 – 7.03 (m, 4H), 3.12 (dd, $J = 17.0, 6.9$ Hz, 1H), 2.96 (dd, $J = 16.9, 6.4$ Hz, 1H), 2.60 (dd, $J = 13.5, 7.1$ Hz, 1H), 2.48 (dd, $J = 13.5, 7.4$ Hz, 1H), 2.34 – 2.18 (m, 1H), 1.38 – 1.20 (m, 2H), 0.83 (t, $J = 7.4$ Hz, 3H).

^{13}C NMR (75 MHz, CDCl_3) δ 191.2, 143.4, 140.8, 138.5, 129.3, 128.9, 128.7, 128.1, 126.9, 125.9, 125.8, 42.7, 40.2, 37.3, 26.5, 11.1.

IR (film): ν (cm^{-1}) 2960, 2925, 2868, 1683, 1597, 1496, 1448, 1404, 1307, 1035, 963, 912, 765, 735, 696.

HRMS (ESI, m/z) calcd for $\text{C}_{21}\text{H}_{23}\text{N}_2\text{O}$ $[\text{M}+\text{H}]^+$: 319.1805, found: 319.1807.

(*R*)-3-Benzyl-1-(1-methyl-1*H*-imidazol-2-yl)pentan-1-one (55d')



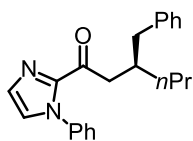
According to the general procedure, α,β -unsaturated acyl imidazole **53d'** (32.8 mg, 0.2 mmol) reacted with potassium benzyltrifluoroborate **54a** (59.4 mg, 0.30 mmol) in acetone/ H_2O (1:1, 1.0 mL) to give **55d'** as a colorless oil (38.0 mg, 0.148 mmol, yield: 74%). Enantiomeric excess established by HPLC analysis using a Chiralpak AD-H column, $ee = 95\%$ (HPLC: AD-H, 254 nm, hexane/isopropanol = 90:10, flow rate 1.0 mL/min, 25 °C, t_r (minor) = 7.7 min, t_r (major) = 11.3 min). $[\alpha]_D^{22} = -33.7^\circ$ (c 0.66, CH_2Cl_2).

^1H NMR (300 MHz, CDCl_3) δ 7.22 – 7.05 (m, 5H), 7.04 (d, $J = 0.7$ Hz, 1H), 6.90 (s, 1H), 3.83 (s, 3H), 3.07 (dd, $J = 16.6, 6.7$ Hz, 1H), 2.96 (dd, $J = 16.6, 6.8$ Hz, 1H), 2.62 (dd, $J = 13.5, 7.0$ Hz, 1H), 2.50 (dd, $J = 13.5, 7.4$ Hz, 1H), 2.41 – 2.25 (m, 1H), 1.45 – 1.20 (m, 2H), 0.86 (t, $J = 7.4$ Hz, 3H).

^{13}C NMR (75 MHz, CDCl_3) δ 192.9, 143.4, 140.8, 129.3, 128.7, 128.0, 126.7, 125.7, 42.6, 40.3, 37.7, 36.1, 26.6, 11.1.

IR (film): ν (cm^{-1}) 3025, 2959, 2924, 2871, 1669, 1404, 1285, 1152, 1018, 911, 768, 734, 696.

HRMS (ESI, m/z) calcd for $\text{C}_{16}\text{H}_{21}\text{N}_2\text{O}$ $[\text{M}+\text{H}]^+$: 257.1648, found: 257.1651.

(R)-3-Benzyl-1-(1-phenyl-1H-imidazol-2-yl)hexan-1-one (55e)

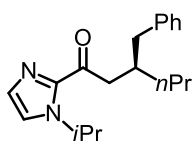
According to the general procedure, α,β -unsaturated acyl imidazole **53e** (48.0 mg, 0.2 mmol) reacted with potassium benzyltrifluoroborate **54a** (59.4 mg, 0.30 mmol) in acetone/H₂O (1:1, 1.0 mL) to give **55e** as a colorless oil (26.9 mg, 0.081 mmol, yield: 40%). Enantiomeric excess established by HPLC analysis using a Chiralpak AD-H column, *ee* = 83% (HPLC: AD-H, 254 nm, hexane/isopropanol = 95:5, flow rate 1.0 mL/min, 25 °C, *t_r* (minor) = 10.2 min, *t_r* (major) = 11.0 min). $[\alpha]_D^{22} = -12.4^\circ$ (*c* 0.24, CH₂Cl₂).

¹H NMR (300 MHz, CDCl₃) δ 7.42 – 7.31 (m, 3H), 7.21 – 7.10 (m, 5H), 7.10 – 7.00 (m, 4H), 3.10 (dd, *J* = 16.9, 6.7 Hz, 1H), 2.96 (dd, *J* = 16.9, 6.4 Hz, 1H), 2.59 (dd, *J* = 13.5, 6.9 Hz, 1H), 2.48 (dd, *J* = 13.5, 7.4 Hz, 1H), 2.41 – 2.24 (m, 1H), 1.37 – 1.10 (m, 4H), 0.76 (t, *J* = 6.6 Hz, 3H).

¹³C NMR (75 MHz, CDCl₃) δ 191.2, 143.4, 140.8, 138.5, 129.3, 128.9, 128.6, 128.1, 126.9, 125.9, 125.7, 43.1, 40.7, 36.3, 35.7, 19.9, 14.2.

IR (film): ν (cm⁻¹) 2955, 2923, 2864, 1681, 1595, 1494, 1446, 1402, 1038, 962, 911, 761, 695.

HRMS (ESI, *m/z*) calcd for C₂₂H₂₅N₂O [M+H]⁺: 333.1961, found: 333.1965.

(R)-3-Benzyl-1-(1-isopropyl-1H-imidazol-2-yl)hexan-1-one (55e')

According to the general procedure, α,β -unsaturated acyl imidazole **53e'** (41.2 mg, 0.2 mmol) reacted with potassium benzyltrifluoroborate **54a** (59.4 mg, 0.30 mmol) in acetone/H₂O (1:1, 1.0 mL) to give **55e'** as a colorless oil (37.1 mg, 0.125 mmol, yield: 62%). Enantiomeric excess established by HPLC analysis using a Chiralpak OD-H column, *ee* = 92% (HPLC: OD-H, 254 nm, hexane/isopropanol = 98:2, flow rate 1.0 mL/min, 25 °C, *t_r* (major) = 6.6 min, *t_r* (minor) = 7.3 min). $[\alpha]_D^{22} = -26.5^\circ$ (*c* 0.24, CH₂Cl₂).

¹H NMR (300 MHz, CDCl₃) δ 7.33 – 7.01 (m, 7H), 5.47 (hept, *J* = 6.7 Hz, 1H), 3.18 (dd, *J* = 16.7, 6.6 Hz, 1H), 3.06 (dd, *J* = 16.7, 6.6 Hz, 1H), 2.69 (dd, *J* = 13.4, 7.0 Hz, 1H), 2.59 (dd, *J* = 13.4, 7.2 Hz,

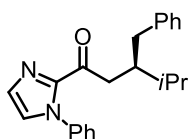
¹H), 2.48 (dq, $J = 12.2, 6.1$ Hz, 1H), 1.54 – 1.21 (m, 10H), 0.87 (t, $J = 6.7$ Hz, 3H).

¹³C NMR (75 MHz, CDCl₃) δ 193.0, 142.8, 140.9, 129.3, 129.2, 128.1, 125.7, 120.8, 49.1, 43.7, 40.9, 36.4, 36.0, 23.6, 23.5, 19.9, 14.2.

IR (film): ν (cm⁻¹) 3060, 3027, 2956, 2873, 1682, 1597, 1495, 1446, 1402, 1306, 1034, 961, 911, 760, 693.

HRMS (ESI, m/z) calcd for C₁₉H₂₇N₂O [M+H]⁺: 299.2118, found: 299.2119.

(R)-3-Benzyl-4-methyl-1-(1-phenyl-1H-imidazol-2-yl)pentan-1-one (55f)



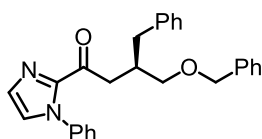
According to the general procedure, α,β -unsaturated acyl imidazole **53f** (48.0 mg, 0.2 mmol) reacted with potassium benzyltrifluoroborate **54a** (59.4 mg, 0.30 mmol) in acetone/H₂O (1:1, 1.0 mL) to give **55f** as a colorless oil (51.8 mg, 0.156 mmol, yield: 78%). Enantiomeric excess established by HPLC analysis using a Chiralpak AD-H column, $ee = 95\%$ (HPLC: AD-H, 254 nm, hexane/isopropanol = 98:2, flow rate 1.0 mL/min, 25 °C, t_r (minor) = 8.5 min, t_r (major) = 9.9 min). $[\alpha]_D^{22} = -20.2^\circ$ (c 0.52, CH₂Cl₂).

¹H NMR (300 MHz, CDCl₃) δ 7.51 – 7.36 (m, 3H), 7.31 – 7.06 (m, 9H), 3.18 (dd, $J = 17.1, 5.9$ Hz, 1H), 3.05 (dd, $J = 17.1, 6.8$ Hz, 1H), 2.70 (dd, $J = 13.3, 6.4$ Hz, 1H), 2.56 – 2.44 (m, 1H), 2.45 – 2.32 (m, 1H), 1.83 – 1.64 (m, 1H), 0.96 (d, $J = 6.9$ Hz, 3H), 0.92 (d, $J = 6.9$ Hz, 3H).

¹³C NMR (75 MHz, CDCl₃) δ 191.2, 143.4, 141.1, 138.5, 129.3, 128.8, 128.6, 128.1, 126.9, 125.9, 125.7, 41.4, 39.6, 37.7, 29.6, 19.6, 18.5.

HRMS (ESI, m/z) calcd for C₂₂H₂₅N₂O [M+H]⁺: 333.1961, found: 333.1964.

(R)-3-Benzyl-4-(benzyloxy)-1-(1-phenyl-1H-imidazol-2-yl)butan-1-one (55g)



According to the general procedure, α,β -unsaturated acyl imidazole **53g** (63.6 mg, 0.2 mmol) reacted with potassium benzyltrifluoroborate **54a** (59.4 mg, 0.30 mmol) in acetone/H₂O (4:1, 2.0 mL) to give

55g as a colorless oil (46.9 mg, 0.114 mmol, yield: 57%). Enantiomeric excess established by HPLC analysis using a Chiralpak OD-H column, $ee = 92\%$ (HPLC: OD-H, 254 nm, hexane/isopropanol = 90:10, flow rate 1.0 mL/min, 25 °C, t_r (major) = 10.6 min, t_r (minor) = 12.0 min). $[\alpha]_D^{22} = -27.8^\circ$ (c 0.16, CH_2Cl_2).

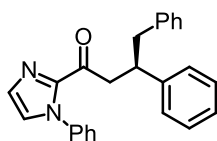
^1H NMR (300 MHz, CDCl_3) δ 7.47 – 7.36 (m, 3H), 7.34 – 7.21 (m, 8H), 7.21 – 7.15 (m, 3H), 7.15 – 7.05 (m, 3H), 4.41 (s, 2H), 3.56 – 3.26 (m, 3H), 3.04 (dd, $J = 16.6, 5.0$ Hz, 1H), 2.93 – 2.54 (m, 3H).

^{13}C NMR (75 MHz, CDCl_3) δ 190.6, 143.3, 140.0, 138.6, 138.5, 129.3, 128.8, 128.5, 128.20, 128.17, 127.6, 127.3, 126.8, 125.9, 125.8, 72.9, 72.7, 41.0, 37.8, 36.9.

IR (film): ν (cm^{-1}) 3060, 3028, 2918, 2856, 1682, 1596, 1495, 1447, 1404, 1306, 1097, 1026, 971, 910, 738, 695.

HRMS (ESI, m/z) calcd for $\text{C}_{27}\text{H}_{26}\text{N}_2\text{ONa}$ $[\text{M}+\text{Na}]^+$: 433.1886, found: 433.1894.

(R)-3,4-Diphenyl-1-(1-phenyl-1H-imidazol-2-yl)butan-1-one (55h)



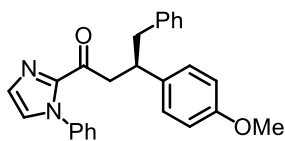
According to the general procedure, α,β -unsaturated acyl imidazole **53h** (54.8 mg, 0.2 mmol) reacted with potassium benzyltrifluoroborate **54a** (59.4 mg, 0.30 mmol) in acetone/ H_2O (4:1, 1.0 mL) to give **55h** as a colorless oil (66.0 mg, 0.180 mmol, yield: 90%). Enantiomeric excess established by HPLC analysis using a Chiralpak OJ-H column, $ee = 95\%$ (HPLC: OJ-H, 254 nm, hexane/isopropanol = 50:50, flow rate 1.0 mL/min, 25 °C, t_r (minor) = 13.7 min, t_r (major) = 22.6 min). $[\alpha]_D^{22} = -11.4^\circ$ (c 0.68, CH_2Cl_2).

^1H NMR (300 MHz, CDCl_3) δ 7.46 – 7.34 (m, 3H), 7.32 – 7.15 (m, 9H), 7.15 – 7.07 (m, 3H), 7.07 – 6.97 (m, 2H), 3.79 – 3.60 (m, 2H), 3.51 – 3.36 (m, 1H), 2.99 (d, $J = 7.1$ Hz, 2H).

^{13}C NMR (75 MHz, CDCl_3) δ 190.0, 143.9, 143.3, 139.8, 138.2, 129.4, 129.3, 128.8, 128.5, 128.2, 128.0, 127.8, 126.8, 126.2, 125.9, 125.6, 44.4, 43.5, 43.0.

IR (film): ν (cm^{-1}) 3059, 3027, 2921, 2852, 1683, 1597, 1495, 1446, 1403, 1306, 1065, 1031, 964, 911, 759, 694, 518.

HRMS (ESI, m/z) calcd for $\text{C}_{25}\text{H}_{23}\text{N}_2\text{O}$ $[\text{M}+\text{H}]^+$: 367.1805, found: 367.1810.

(R)-3-(4-Methoxyphenyl)-4-phenyl-1-(1-phenyl-1*H*-imidazol-2-yl)butan-1-one (55i)

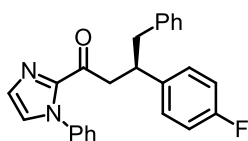
According to the general procedure, α,β -unsaturated acyl imidazole **53i** (60.8 mg, 0.2 mmol) reacted with potassium benzyltrifluoroborate **54a** (59.4 mg, 0.30 mmol) in acetone/H₂O (4:1, 1.0 mL) to give **55i** as a colorless oil (70.7 mg, 0.179 mmol, yield: 89%). Enantiomeric excess established by HPLC analysis using a Chiralpak AD-H column, *ee* = 93% (HPLC: AD-H, 254 nm, hexane/isopropanol = 90:10, flow rate 1.0 mL/min, 25 °C, *t_r* (minor) = 17.4 min, *t_r* (major) = 19.0 min). [α]_D²² = −15.5° (*c* 0.62, CH₂Cl₂).

¹H NMR (300 MHz, CDCl₃) δ 7.42 – 7.33 (m, 3H), 7.28 – 6.94 (m, 11H), 6.77 (d, *J* = 8.7 Hz, 2H), 3.76 (s, 3H), 3.70 – 3.51 (m, 2H), 3.45 – 3.26 (m, 1H), 2.92 (d, *J* = 7.1 Hz, 2H).

¹³C NMR (75 MHz, CDCl₃) δ 190.1, 158.0, 143.3, 139.9, 138.2, 136.1, 129.4, 129.3, 128.82, 128.76, 128.5, 128.1, 126.8, 125.9, 125.7, 113.6, 55.2, 44.7, 43.7, 42.3.

IR (film): ν (cm^{−1}) 3059, 3028, 2923, 2839, 1682, 1603, 1503, 1403, 1302, 1244, 1032, 963, 827, 757, 694, 544, 514.

HRMS (ESI, *m/z*) calcd for C₂₆H₂₅N₂O₂ [M+H]⁺: 397.1911, found: 397.1916.

(R)-3-(4-Fluorophenyl)-4-phenyl-1-(1-phenyl-1*H*-imidazol-2-yl)butan-1-one (55j)

According to the general procedure, α,β -unsaturated acyl imidazole **53j** (58.4 mg, 0.2 mmol) reacted with potassium benzyltrifluoroborate **54a** (59.4 mg, 0.30 mmol) in acetone/H₂O (4:1, 1.0 mL) to give **55j** as a white solid (63.7 mg, 0.179 mmol, yield: 83%). Enantiomeric excess established by HPLC analysis using a Chiralpak OJ-H column, *ee* = 96% (HPLC: OJ-H, 254 nm, hexane/isopropanol = 70:30, flow rate 1.0 mL/min, 25 °C, *t_r* (minor) = 15.2 min, *t_r* (major) = 26.6 min). [α]_D²² = −6.3° (*c* 0.76, CH₂Cl₂).

¹H NMR (300 MHz, CDCl₃) δ 7.46 – 7.36 (m, 3H), 7.27 (d, *J* = 0.8 Hz, 1H), 7.25 – 7.11 (m, 6H), 7.11 – 7.01 (m, 4H), 6.92 (t, *J* = 8.7 Hz, 2H), 3.78 – 3.58 (m, 2H), 3.56 – 3.31 (m, 1H), 3.07 – 2.81 (m,

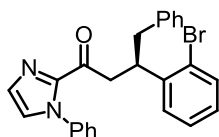
2H).

^{13}C NMR (75 MHz, CDCl_3) δ 189.7, 163.0, 159.7, 143.2, 139.51, 139.49, 138.2, 129.4, 129.3, 129.21, 129.15, 128.8, 128.6, 128.1, 126.9, 126.0, 125.6, 115.0, 114.8, 44.5, 43.5, 42.3.

IR (film): ν (cm^{-1}) 3109, 3060, 3030, 2923, 2854, 1682, 1599, 1501, 1446, 1404, 1305, 1222, 1154, 964, 912, 830, 758, 694, 540.

HRMS (ESI, m/z) calcd for $\text{C}_{25}\text{H}_{22}\text{FN}_2\text{O}$ $[\text{M}+\text{H}]^+$: 385.1711, found: 385.1717.

(R)-3-(2-Bromophenyl)-4-phenyl-1-(1-phenyl-1H-imidazol-2-yl)butan-1-one (55k)



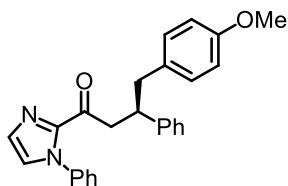
According to the general procedure, α,β -unsaturated acyl imidazole **53k** (70.4 mg, 0.2 mmol) reacted with potassium benzyltrifluoroborate **54a** (59.4 mg, 0.30 mmol) in acetone/ H_2O (4:1, 1.0 mL) to give **55k** as a white solid (63.9 mg, 0.144 mmol, yield: 72%). Enantiomeric excess established by HPLC analysis using a Chiralpak OJ-H column, $ee = 94\%$ (HPLC: OJ-H, 254 nm, hexane/isopropanol = 70:30, flow rate 1.0 mL/min, 25 °C, t_r (minor) = 10.7 min, t_r (major) = 16.0 min). $[\alpha]_D^{22} = +7.8^\circ$ (c 0.56, CH_2Cl_2).

^1H NMR (300 MHz, CDCl_3) δ 7.50 (dd, $J = 8.0, 1.2$ Hz, 1H), 7.42 – 7.30 (m, 4H), 7.28 – 7.13 (m, 7H), 7.12 (d, $J = 0.9$ Hz, 1H), 7.08 – 6.97 (m, 3H), 4.32 – 4.13 (m, 1H), 3.64 (dd, $J = 16.8, 8.1$ Hz, 1H), 3.46 (dd, $J = 16.8, 6.8$ Hz, 1H), 3.05 (dd, $J = 13.6, 6.3$ Hz, 1H), 2.82 (dd, $J = 13.6, 8.4$ Hz, 1H).

^{13}C NMR (75 MHz, CDCl_3) δ 189.3, 143.2, 142.8, 139.2, 138.2, 133.0, 129.4, 128.9, 128.5, 128.2, 128.1, 127.7, 127.4, 126.9, 126.1, 125.7, 125.0, 43.0, 42.1, 41.2.

IR (film): ν (cm^{-1}) 3055, 3025, 2909, 2850, 1683, 1593, 1492, 1444, 1410, 1300, 1020, 961, 911, 857, 753, 694.

HRMS (ESI, m/z) calcd for $\text{C}_{25}\text{H}_{21}\text{BrN}_2\text{ONa}$ $[\text{M}+\text{Na}]^+$: 467.0729 and 469.0712, found: 467.0734 and 469.0714.

(R)-4-(4-Methoxyphenyl)-3-phenyl-1-(1-phenyl-1*H*-imidazol-2-yl)butan-1-one (55l)

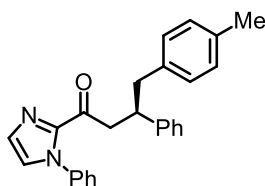
According to the general procedure, α,β -unsaturated acyl imidazole **53h** (54.8 mg, 0.2 mmol) reacted with potassium trifluoro(4-methoxybenzyl)borate **54b** (68.4 mg, 0.30 mmol) in acetone/H₂O (4:1, 1.0 mL) to give **55l** as a white solid (77.0 mg, 0.194 mmol, yield: 97%). Enantiomeric excess established by HPLC analysis using a Chiralpak OJ-H column, *ee* = 99% (HPLC: OJ-H, 254 nm, hexane/isopropanol = 50:50, flow rate 1.0 mL/min, 25 °C, *t_r* (minor) = 17.4 min, *t_r* (major) = 44.8 min). $[\alpha]_D^{22} = +4.3^\circ$ (*c* 0.92, CH₂Cl₂).

¹H NMR (300 MHz, CDCl₃) δ 7.46 – 7.33 (m, 3H), 7.31 – 7.14 (m, 6H), 7.11 (d, *J* = 0.8 Hz, 2H), 7.01 (d, *J* = 8.3 Hz, 4H), 6.76 (d, *J* = 8.6 Hz, 2H), 3.77 (s, 3H), 3.72 – 3.56 (m, 2H), 3.54 – 3.35 (m, 1H), 2.92 (d, *J* = 7.1 Hz, 2H).

¹³C NMR (75 MHz, CDCl₃) δ 190.0, 157.8, 144.1, 143.2, 138.2, 131.8, 130.2, 129.3, 128.8, 128.5, 128.2, 127.8, 126.7, 126.2, 125.6, 113.5, 55.1, 44.3, 43.2, 42.7.

IR (film): ν (cm⁻¹) 3060, 3028, 2916, 2839, 1682, 1603, 1504, 1446, 1403, 1303, 1243, 1176, 1032, 826, 759, 693, 522.

HRMS (ESI, *m/z*) calcd for C₂₆H₂₄N₂O₂Na [M+Na]⁺: 419.1730, found: 419.1735.

(R)-3-Phenyl-1-(1-phenyl-1*H*-imidazol-2-yl)-4-(*p*-tolyl)butan-1-one (55m)

According to the general procedure, α,β -unsaturated acyl imidazole **53h** (54.8 mg, 0.2 mmol) reacted with potassium trifluoro(4-methylbenzyl)borate **54c** (63.6 mg, 0.30 mmol) in acetone/H₂O (4:1, 1.0 mL) to give **55m** as a white solid (63.0 mg, 0.166 mmol, yield: 83%). Enantiomeric excess established by HPLC analysis using a Chiralpak OJ-H column, *ee* = 96% (HPLC: OJ-H, 254 nm, hexane/isopropanol = 50:50, flow rate 1.0 mL/min, 25 °C, *t_r* (minor) = 11.6 min, *t_r* (major) = 22.5 min). $[\alpha]_D^{22} = -2.3^\circ$ (*c* 0.75, CH₂Cl₂).

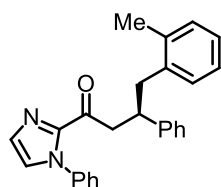
^1H NMR (300 MHz, CDCl_3) δ 7.47 – 7.34 (m, 3H), 7.33 – 7.15 (m, 6H), 7.12 (d, $J = 1.0$ Hz, 1H), 7.09 – 6.95 (m, 6H), 3.79 – 3.59 (m, 2H), 3.52 – 3.34 (m, 1H), 3.10 – 2.86 (m, 2H), 2.32 (s, 3H).

^{13}C NMR (75 MHz, CDCl_3) δ 190.0, 144.1, 143.3, 138.2, 136.7, 135.3, 129.3, 129.1, 128.8, 128.7, 128.4, 128.2, 127.8, 126.7, 126.2, 125.6, 44.4, 43.09, 43.05, 20.9.

IR (film): ν (cm^{-1}) 3127, 3025, 2918, 1675, 1592, 1494, 1440, 1401, 1308, 1062, 1034, 972, 918, 863, 787, 759, 696, 531.

HRMS (ESI, m/z) calcd for $\text{C}_{26}\text{H}_{25}\text{N}_2\text{O}$ $[\text{M}+\text{H}]^+$: 381.1961, found: 381.1966.

(R)-3-Phenyl-1-(1-phenyl-1H-imidazol-2-yl)-4-(o-tolyl)butan-1-one (55n)



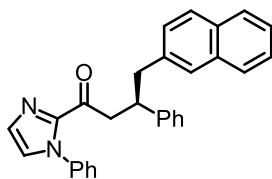
According to the general procedure, α,β -unsaturated acyl imidazole **53h** (54.8 mg, 0.2 mmol) reacted with potassium trifluoro(2-methylbenzyl)borate **54d** (63.6 mg, 0.30 mmol) in acetone/ H_2O (4:1, 1.0 mL) to give **55n** as a colorless oil (63.2 mg, 0.166 mmol, yield: 83%). Enantiomeric excess established by HPLC analysis using a Chiralpak AD-H column, $ee = 94\%$ (HPLC: AD-H, 254 nm, hexane/isopropanol = 90:10, flow rate 1.0 mL/min, 25 °C, t_r (minor) = 8.5 min, t_r (major) = 9.7 min). $[\alpha]_{\text{D}}^{22} = -13.4^\circ$ (c 0.38, CH_2Cl_2).

^1H NMR (300 MHz, CDCl_3) δ 7.44 – 7.31 (m, 3H), 7.31 – 7.15 (m, 6H), 7.13 – 6.93 (m, 7H), 3.76 (dd, $J = 15.8, 8.7$ Hz, 1H), 3.70 – 3.56 (m, 1H), 3.41 (dd, $J = 15.8, 5.5$ Hz, 1H), 2.95 (d, $J = 7.4$ Hz, 2H), 2.25 (s, 3H).

^{13}C NMR (75 MHz, CDCl_3) δ 190.0, 144.2, 143.3, 138.2, 138.0, 136.4, 130.20, 130.15, 129.4, 128.8, 128.5, 128.2, 127.8, 126.8, 126.3, 126.1, 125.6, 125.5, 44.2, 41.8, 41.1, 19.4.

IR (film): ν (cm^{-1}) 3060, 3024, 2924, 2863, 1683, 1494, 1447, 1306, 964, 911, 757, 694, 521.

HRMS (ESI, m/z) calcd for $\text{C}_{26}\text{H}_{25}\text{N}_2\text{O}$ $[\text{M}+\text{H}]^+$: 381.1961, found: 381.1966.

(R)-4-(Naphthalen-2-yl)-3-phenyl-1-(1-phenyl-1H-imidazol-2-yl)butan-1-one (55o)

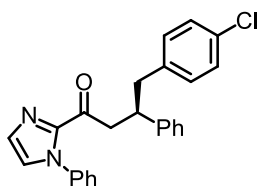
According to the general procedure, α,β -unsaturated acyl imidazole **53h** (54.8 mg, 0.2 mmol) reacted with potassium trifluoro(naphthalen-2-ylmethyl)borate **54e** (74.4 mg, 0.30 mmol) in acetone/H₂O (4:1, 1.0 mL) to give **55o** as pale yellow solid (65.1 mg, 0.156 mmol, yield: 78%). Enantiomeric excess established by HPLC analysis using a Chiralpak AD-H column, *ee* = 92% (HPLC: AD-H, 254 nm, hexane/isopropanol = 90:10, flow rate 1.0 mL/min, 25 °C, *t_r* (minor) = 13.2 min, *t_r* (major) = 14.8 min). $[\alpha]_D^{22} = +30.0^\circ$ (*c* 0.81, CH₂Cl₂).

¹H NMR (300 MHz, CDCl₃) δ 7.84 – 7.64 (m, 3H), 7.55 (s, 1H), 7.51 – 7.30 (m, 5H), 7.30 – 7.12 (m, 7H), 7.07 (s, 1H), 6.96 – 6.82 (m, 2H), 3.79 (p, *J* = 7.4 Hz, 1H), 3.67 (dd, *J* = 16.5, 7.9 Hz, 1H), 3.53 (dd, *J* = 16.5, 6.5 Hz, 1H), 3.13 (d, *J* = 7.5 Hz, 2H).

¹³C NMR (75 MHz, CDCl₃) δ 189.7, 144.2, 143.2, 138.2, 137.4, 133.4, 132.1, 129.3, 128.8, 128.5, 128.3, 127.9, 127.8, 127.7, 127.6, 127.51, 127.47, 126.8, 126.3, 125.7, 125.6, 125.2, 44.4, 43.8, 42.9.

IR (film): ν (cm⁻¹) 3053, 2921, 2853, 1682, 1596, 1496, 1445, 1402, 1335, 1305, 1064, 1024, 961, 907, 857, 817, 753, 693, 649, 518, 475.

HRMS (ESI, *m/z*) calcd for C₂₉H₂₄N₂ONa [M+Na]⁺: 439.1781, found: 439.1788.

(R)-4-(4-Chlorophenyl)-3-phenyl-1-(1-phenyl-1H-imidazol-2-yl)butan-1-one (55p)

According to the general procedure, α,β -unsaturated acyl imidazole **53h** (54.8 mg, 0.2 mmol) reacted with potassium (4-chlorobenzyl)trifluoroborate **54f** (69.6 mg, 0.30 mmol) in acetone/H₂O (4:1, 1.0 mL) to give **55p** as a white solid (70.5 mg, 0.176 mmol, yield: 88%). Enantiomeric excess established by HPLC analysis using a Chiralpak OD-H column, *ee* = 91% (HPLC: OD-H, 254 nm, hexane/isopropanol = 95:5, flow rate 1.0 mL/min, 25 °C, *t_r* (minor) = 13.5 min, *t_r* (major) = 16.9 min). $[\alpha]_D^{22} = +62.6^\circ$ (*c* 0.78, CH₂Cl₂).

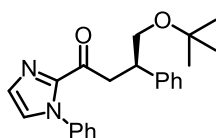
^1H NMR (300 MHz, CDCl_3) δ 7.46 – 7.33 (m, 3H), 7.30 – 7.19 (m, 3H), 7.19 – 7.09 (m, 6H), 7.07 – 6.99 (m, 2H), 6.96 (d, J = 8.3 Hz, 2H), 3.69 – 3.53 (m, 2H), 3.53 – 3.36 (m, 1H), 3.02 – 2.79 (m, 2H).

^{13}C NMR (75 MHz, CDCl_3) δ 189.7, 143.6, 143.2, 138.3, 138.2, 131.8, 130.6, 129.4, 128.9, 128.6, 128.3, 128.1, 127.8, 126.9, 126.4, 125.7, 44.5, 42.9, 42.8.

IR (film): ν (cm^{-1}) 3059, 3029, 2922, 2855, 1682, 1596, 1492, 1446, 1403, 1306, 1090, 1014, 964, 911, 760, 730, 694, 517.

HRMS (ESI, m/z) calcd for $\text{C}_{25}\text{H}_{21}\text{ClN}_2\text{ONa}$ $[\text{M}+\text{Na}]^+$: 423.1235, 424.1268 and 425.1205, found: 423.1240, 424.1272 and 425.1209.

(*R*)-4-(*tert*-Butoxy)-3-phenyl-1-(1-phenyl-1*H*-imidazol-2-yl)butan-1-one (55q)



According to the general procedure, α,β -unsaturated acyl imidazole **53h** (54.8 mg, 0.2 mmol) reacted with potassium (*tert*-butoxymethyl)trifluoroborate **54g** (58.2 mg, 0.30 mmol) in acetone/ H_2O (4:1, 1.0 mL) to give **55q** as a white solid (66.2 mg, 0.183 mmol, yield: 91%). Enantiomeric excess established by HPLC analysis using a Chiralpak OJ-H column, ee = 98% (HPLC: OJ-H, 254 nm, hexane/isopropanol = 50:50, flow rate 1.0 mL/min, 25 °C, t_r (minor) = 5.6 min, t_r (major) = 8.3 min). $[\alpha]_D^{22} = -58.4^\circ$ (c 0.83, CH_2Cl_2).

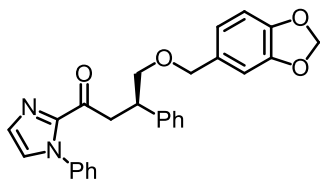
^1H NMR (300 MHz, CDCl_3) δ 7.46 – 7.35 (m, 3H), 7.35 – 7.17 (m, 6H), 7.17 – 7.07 (m, 3H), 3.79 (dd, J = 15.8, 6.0 Hz, 1H), 3.67 – 3.37 (m, 4H), 1.12 (s, 9H).

^{13}C NMR (75 MHz, CDCl_3) δ 190.2, 143.4, 142.4, 138.4, 129.2, 128.8, 128.4, 128.2, 128.1, 126.6, 126.4, 125.7, 72.7, 66.4, 42.3, 42.1, 27.4.

IR (film): ν (cm^{-1}) 2969, 2902, 2862, 1688, 1603, 1495, 1603, 1495, 1449, 1405, 1188, 1087, 974, 764, 696, 561, 524.

HRMS (ESI, m/z) calcd for $\text{C}_{23}\text{H}_{27}\text{N}_2\text{O}_2$ $[\text{M}+\text{H}]^+$: 363.2067, found: 363.2067.

(R)-4-(Benzo[d][1,3]dioxol-5-ylmethoxy)-3-phenyl-1-(1-phenyl-1*H*-imidazol-2-yl)butan-1-one (55r)



According to the general procedure, α,β -unsaturated acyl imidazole **53h** (54.8 mg, 0.2 mmol) reacted with potassium ((benzo[d][1,3]dioxol-5-ylmethoxy)methyl)trifluoroborate **54h** (81.6 mg, 0.30 mmol) in acetone/H₂O (4:1, 1.0 mL) to give **55r** as a colorless oil (70.7 mg, 0.161 mmol, yield: 80%). Enantiomeric excess established by HPLC analysis using a Chiralpak AD-H column, *ee* = 95% (HPLC: AD-H, 254 nm, hexane/isopropanol = 80:20, flow rate 1.0 mL/min, 25 °C, *t_r* (minor) = 14.0 min, *t_r* (major) = 17.2 min). $[\alpha]_D^{22} = -34.5^\circ$ (*c* 0.86, CH₂Cl₂).

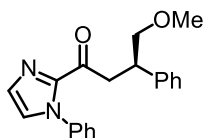
¹H NMR (300 MHz, CDCl₃) δ 7.47 – 7.35 (m, 3H), 7.35 – 7.18 (m, 6H), 7.15 (d, *J* = 0.8 Hz, 1H), 7.12 – 6.97 (m, 2H), 6.79 – 6.58 (m, 3H), 5.92 (dd, *J* = 6.0, 1.3 Hz, 2H), 4.36 (s, 2H), 3.88 – 3.70 (m, 2H), 3.70 – 3.55 (m, 2H), 3.44 (dd, *J* = 15.1, 5.8 Hz, 1H).

¹³C NMR (75 MHz, CDCl₃) δ 189.7, 147.6, 146.9, 143.2, 141.8, 138.3, 132.2, 129.3, 128.8, 128.4, 128.3, 128.0, 126.8, 126.6, 125.6, 121.2, 108.4, 107.8, 100.8, 74.6, 72.8, 42.3, 41.7.

IR (film): ν (cm⁻¹) 3061, 3029, 2859, 1683, 1598, 1493, 1443, 1404, 1242, 1091, 1034, 969, 923, 809, 762, 696, 523.

HRMS (ESI, *m/z*) calcd for C₂₇H₂₄N₂O₄Na [M+Na]⁺: 463.1628, found: 463.1635.

(R)-4-Methoxy-3-phenyl-1-(1-phenyl-1*H*-imidazol-2-yl)butan-1-one (55s)



According to the general procedure, α,β -unsaturated acyl imidazole **53h** (54.8 mg, 0.2 mmol) reacted with potassium trifluoro(methoxymethyl)borate **54i** (45.6 mg, 0.30 mmol) in acetone/H₂O (4:1, 1.0 mL) to give **55s** as a white solid (41.7 mg, 0.130 mmol, yield: 65%). Enantiomeric excess established by HPLC analysis using a Chiralpak AD-H column, *ee* = 96% (HPLC: AD-H, 254 nm, hexane/isopropanol = 95:5, flow rate 1.0 mL/min, 25 °C, *t_r* (minor) = 17.5 min, *t_r* (major) = 19.0 min). $[\alpha]_D^{22} = -64.5^\circ$ (*c* 0.47, CH₂Cl₂).

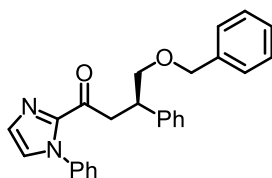
^1H NMR (300 MHz, CDCl_3) δ 7.49 – 7.36 (m, 3H), 7.35 – 7.19 (m, 6H), 7.19 – 7.08 (m, 3H), 3.76 – 3.43 (m, 5H), 3.29 (s, 3H).

^{13}C NMR (75 MHz, CDCl_3) δ 189.8, 143.3, 141.8, 138.3, 129.4, 128.9, 128.5, 128.4, 127.9, 126.7, 126.6, 125.7, 77.1, 58.7, 42.4, 41.5.

IR (film): ν (cm^{-1}) 3059, 3029, 2922, 2876, 2823, 1688, 1495, 1446, 1403, 1306, 1112, 909, 760, 695, 526.

HRMS (ESI, m/z) calcd for $\text{C}_{20}\text{H}_{21}\text{N}_2\text{O}_2$ $[\text{M}+\text{H}]^+$: 321.1598, found: 321.1598.

(R)-4-(Benzyloxy)-3-phenyl-1-(1-phenyl-1H-imidazol-2-yl)butan-1-one (55t)



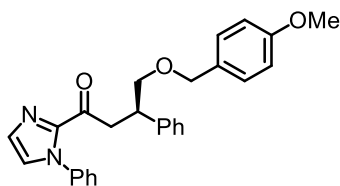
According to the general procedure, α,β -unsaturated acyl imidazole **53h** (54.8 mg, 0.2 mmol) reacted with potassium ((benzyloxy)methyl)trifluoroborate **54j** (68.4 mg, 0.30 mmol) in acetone/ H_2O (4:1, 1.0 mL) to give **55t** as a colorless oil (53.3 mg, 0.135 mmol, yield: 67%). Enantiomeric excess established by HPLC analysis using a Chiralpak OD-H column, $ee = 95\%$ (HPLC: OD-H, 254 nm, hexane/isopropanol = 95:5, flow rate 1.0 mL/min, 25 $^\circ\text{C}$, t_r (minor) = 22.1 min, t_r (major) = 24.8 min). $[\alpha]_{\text{D}}^{22} = -38.0^\circ$ (c 0.28, CH_2Cl_2).

^1H NMR (300 MHz, CDCl_3) δ 7.42 – 7.32 (m, 3H), 7.32 – 7.24 (m, 8H), 7.24 – 7.16 (m, 3H), 7.12 (d, $J = 0.8$ Hz, 1H), 7.07 – 6.93 (m, 2H), 4.45 (s, 2H), 3.86 – 3.56 (m, 4H), 3.55 – 3.34 (m, 1H).

^{13}C NMR (75 MHz, CDCl_3) δ 189.8, 143.3, 141.9, 138.3, 129.3, 128.8, 128.5, 128.4, 128.2, 128.0, 127.6, 127.4, 126.8, 126.6, 125.7, 74.9, 73.0, 42.3, 41.7.

IR (film): ν (cm^{-1}) 3060, 3029, 2919, 2855, 1683, 1599, 1495, 1447, 1403, 1306, 1093, 1030, 969, 909, 756, 693, 524.

HRMS (ESI, m/z) calcd for $\text{C}_{26}\text{H}_{25}\text{N}_2\text{O}_2$ $[\text{M}+\text{H}]^+$: 397.1911, found: 397.1917.

(R)-4-((4-Methoxybenzyl)oxy)-3-phenyl-1-(1-phenyl-1*H*-imidazol-2-yl)butan-1-one (55u)

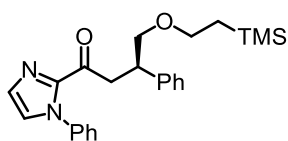
According to the general procedure, α,β -unsaturated acyl imidazole **53h** (54.8 mg, 0.2 mmol) reacted with potassium trifluoro(((4-methoxybenzyl)oxy)methyl)borate **54k** (77.4 mg, 0.30 mmol) in acetone/H₂O (4:1, 1.0 mL) to give **55u** as a colorless oil (51.8 mg, 0.122 mmol, yield: 61%). Enantiomeric excess established by HPLC analysis using a Chiralpak AD-H column, *ee* = 95% (HPLC: AD-H, 254 nm, hexane/isopropanol = 90:10, flow rate 1.0 mL/min, 25 °C, *t_r* (minor) = 19.4 min, *t_r* (major) = 21.2 min). $[\alpha]_D^{22} = -34.2^\circ$ (*c* 0.32, CH₂Cl₂).

¹H NMR (300 MHz, CDCl₃) δ 7.45 – 7.32 (m, 3H), 7.32 – 7.17 (m, 6H), 7.17 – 7.07 (m, 3H), 7.07 – 6.94 (m, 2H), 6.82 (d, *J* = 8.7 Hz, 2H), 4.39 (s, 2H), 3.85 – 3.68 (m, 5H), 3.68 – 3.53 (m, 2H), 3.51 – 3.34 (m, 1H).

¹³C NMR (75 MHz, CDCl₃) δ 189.8, 159.1, 143.3, 141.9, 138.3, 130.5, 129.3, 129.2, 128.8, 128.4, 128.3, 128.0, 126.7, 126.6, 125.7, 74.5, 72.6, 55.2, 42.3, 41.7.

IR (film): ν (cm⁻¹) 2906, 2849, 1683, 1605, 1503, 1447, 1403, 1303, 1243, 1174, 1085, 1031, 969, 910, 819, 761, 697, 522.

HRMS (ESI, *m/z*) calcd for C₂₇H₂₆N₂O₃Na [M+Na]⁺: 449.1836, found: 449.1843.

(R)-3-Phenyl-1-(1-phenyl-1*H*-imidazol-2-yl)-4-(2-(trimethylsilyl)ethoxy)butan-1-one (55v)

According to the general procedure, α,β -unsaturated acyl imidazole **53h** (54.8 mg, 0.2 mmol) reacted with potassium trifluoro((2-(trimethylsilyl)ethoxy)methyl)borate **54l** (71.4 mg, 0.30 mmol) in acetone/H₂O (4:1, 1.0 mL) to give **55v** as a colorless oil (53.0 mg, 0.130 mmol, yield: 65%). Enantiomeric excess established by HPLC analysis using a Chiralpak AD-H column, *ee* = 94% (HPLC: AD-H, 254 nm, hexane/isopropanol = 95:5, flow rate 1.0 mL/min, 25 °C, *t_r* (minor) = 8.3 min, *t_r* (major) = 9.1 min). $[\alpha]_D^{22} = -49.2^\circ$ (*c* 0.40, CH₂Cl₂).

¹H NMR (300 MHz, CDCl₃) δ 7.47 – 7.33 (m, 3H), 7.32 – 7.15 (m, 6H), 7.15 – 7.04 (m, 3H), 3.85 –

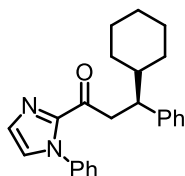
3.21 (m, 7H), 0.98 – 0.59 (m, 2H), -0.03 (s, 9H).

^{13}C NMR (75 MHz, CDCl_3) δ 190.0, 143.4, 142.1, 138.4, 129.3, 128.8, 128.5, 128.3, 128.0, 126.7, 126.5, 125.7, 74.7, 68.1, 42.4, 41.8, 18.0, -1.4.

IR (film): ν (cm^{-1}) 2950, 2855, 1685, 1495, 1447, 1405, 1247, 1094, 834, 758, 693, 525.

HRMS (ESI, m/z) calcd for $\text{C}_{24}\text{H}_{30}\text{N}_2\text{O}_2\text{SiNa}$ $[\text{M}+\text{Na}]^+$: 429.1969, found: 429.1976.

(S)-3-Cyclohexyl-3-phenyl-1-(1-phenyl-1*H*-imidazol-2-yl)propan-1-one (55w)



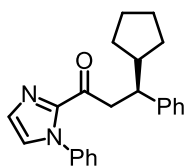
According to the general procedure, α,β -unsaturated acyl imidazole **53h** (54.8 mg, 0.2 mmol) reacted with potassium cyclohexyltrifluoroborate **54m** (57.0 mg, 0.30 mmol) in acetone/ H_2O (4:1, 1.0 mL) to give **55w** as a colorless oil (58.1 mg, 0.162 mmol, yield: 81%). Enantiomeric excess established by HPLC analysis using a Chiralpak AD-H column, $ee = 97\%$ (HPLC: AD-H, 254 nm, hexane/isopropanol = 98:2, flow rate 1.0 mL/min, 25 $^\circ\text{C}$, t_r (minor) = 16.5 min, t_r (major) = 19.6 min). $[\alpha]_D^{22} = -64.6^\circ$ (c 0.70, CH_2Cl_2).

^1H NMR (300 MHz, CDCl_3) δ 7.31 – 7.19 (m, 3H), 7.18 – 7.10 (m, 3H), 7.10 – 7.01 (m, 3H), 6.99 (d, $J = 1.0$ Hz, 1H), 6.85 – 6.72 (m, 2H), 3.58 – 3.34 (m, 2H), 3.07 (dd, $J = 15.0, 7.8$ Hz, 1H), 1.87 – 1.32 (m, 6H), 1.24 – 0.66 (m, 5H).

^{13}C NMR (75 MHz, CDCl_3) δ 190.8, 143.5, 143.4, 138.2, 129.3, 128.8, 128.7, 128.4, 127.9, 126.5, 125.9, 125.5, 47.2, 43.5, 42.7, 31.0, 30.8, 26.5, 26.47, 26.36.

IR (film): ν (cm^{-1}) 2922, 2850, 1683, 1595, 1494, 1445, 1403, 1305, 1047, 960, 911, 759, 734, 695, 527.

HRMS (ESI, m/z) calcd for $\text{C}_{24}\text{H}_{27}\text{N}_2\text{O}$ $[\text{M}+\text{H}]^+$: 359.2118, found: 359.2122.

(S)-3-Cyclopentyl-3-phenyl-1-(1-phenyl-1H-imidazol-2-yl)propan-1-one (55x)

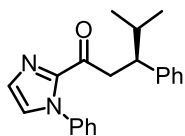
According to the general procedure, α,β -unsaturated acyl imidazole **53h** (54.8 mg, 0.2 mmol) reacted with potassium cyclopentyltrifluoroborate **54n** (52.8 mg, 0.30 mmol) in acetone/H₂O (4:1, 1.0 mL) to give **55x** as a colorless oil (52.4 mg, 0.152 mmol, yield: 76%). Enantiomeric excess established by HPLC analysis using a Chiralpak AD-H column, *ee* = 98% (HPLC: AD-H, 254 nm, hexane/isopropanol = 95:5, flow rate 1.0 mL/min, 25 °C, *t_r* (minor) = 10.4 min, *t_r* (major) = 12.8 min). $[\alpha]_D^{22} = -72.0^\circ$ (*c* 0.44, CH₂Cl₂).

¹H NMR (300 MHz, CDCl₃) δ 7.44 – 7.30 (m, 3H), 7.29 – 7.11 (m, 6H), 7.08 (d, *J* = 1.0 Hz, 1H), 6.91 (dd, *J* = 8.0, 1.7 Hz, 2H), 3.66 (dd, *J* = 16.0, 10.0 Hz, 1H), 3.46 (dd, *J* = 16.0, 5.0 Hz, 1H), 3.15 (td, *J* = 9.9, 5.0 Hz, 1H), 2.24 – 2.01 (m, 1H), 1.91 (dtd, *J* = 10.7, 7.3, 3.5 Hz, 1H), 1.77 – 1.19 (m, 6H), 1.17 – 0.97 (m, 1H).

¹³C NMR (75 MHz, CDCl₃) δ 190.5, 144.5, 143.4, 138.2, 129.3, 128.8, 128.4, 128.2, 128.0, 126.5, 125.9, 125.5, 47.1, 46.9, 44.9, 31.32, 31.26, 25.2, 24.9.

IR (film): ν (cm⁻¹) 3027, 2948, 2864, 1683, 1597, 1495, 1446, 1403, 1305, 1146, 1051, 964, 912, 759, 695, 530.

HRMS (ESI, *m/z*) calcd for C₂₃H₂₅N₂O [M+H]⁺: 345.1961, found: 345.1967.

(S)-4-Methyl-3-phenyl-1-(1-phenyl-1H-imidazol-2-yl)pentan-1-one (55y)

According to the general procedure, α,β -unsaturated acyl imidazole **53h** (54.8 mg, 0.2 mmol) reacted with potassium trifluoro(isopropyl)borate **54o** (45.0 mg, 0.30 mmol) in acetone/H₂O (4:1, 1.0 mL) to give **55y** as a colorless oil (53.8 mg, 0.169 mmol, yield: 85%). Enantiomeric excess established by HPLC analysis using a Chiralpak AD-H column, *ee* = 98% (HPLC: AD-H, 254 nm, hexane/isopropanol = 95:5, flow rate 1.0 mL/min, 25 °C, *t_r* (minor) = 9.4 min, *t_r* (major) = 11.9 min). $[\alpha]_D^{22} = -76.2^\circ$ (*c* 0.64, CH₂Cl₂).

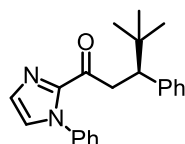
^1H NMR (300 MHz, CDCl_3) δ 7.43 – 7.30 (m, 3H), 7.31 – 7.22 (m, 3H), 7.22 – 7.14 (m, 3H), 7.10 (d, J = 0.9 Hz, 1H), 6.91 (dd, J = 8.0, 1.6 Hz, 2H), 3.64 (dd, J = 16.1, 9.6 Hz, 1H), 3.49 (dd, J = 16.1, 5.6 Hz, 1H), 3.16 (ddd, J = 9.6, 7.5, 5.7 Hz, 1H), 2.03 – 1.81 (m, 1H), 1.00 (d, J = 6.7 Hz, 3H), 0.81 (d, J = 6.7 Hz, 3H).

^{13}C NMR (75 MHz, CDCl_3) δ 190.7, 143.4, 143.3, 138.2, 129.3, 128.8, 128.7, 128.4, 127.9, 126.6, 126.0, 125.5, 48.1, 42.7, 33.7, 20.7, 20.3.

IR (film): ν (cm^{-1}) 2958, 2871, 1683, 1595, 1494, 1446, 1403, 1307, 1249, 1050, 967, 912, 859, 760, 697, 538.

HRMS (ESI, m/z) calcd for $\text{C}_{21}\text{H}_{23}\text{N}_2\text{O}$ $[\text{M}+\text{H}]^+$: 319.1805, found: 319.1809.

(S)-4,4-Dimethyl-3-phenyl-1-(1-phenyl-1*H*-imidazol-2-yl)pentan-1-one (55z)



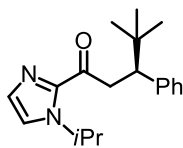
According to the general procedure, α,β -unsaturated acyl imidazole **53h** (54.8 mg, 0.2 mmol) reacted with potassium *tert*-butyltrifluoroborate **54p** (49.2 mg, 0.30 mmol) in acetone/ H_2O (4:1, 1.0 mL) to give **55z** as a colorless oil (45.5 mg, 0.137 mmol, yield: 69%). Enantiomeric excess established by HPLC analysis using a Chiralpak AD-H column, ee = 77% (HPLC: AD-H, 254 nm, hexane/isopropanol = 95:5, flow rate 1.0 mL/min, 25 $^\circ\text{C}$, t_r (minor) = 7.4 min, t_r (major) = 10.3 min). $[\alpha]_{\text{D}}^{22} = -49.4^\circ$ (c 0.55, CH_2Cl_2).

^1H NMR (300 MHz, CDCl_3) δ 7.40 – 7.12 (m, 9H), 7.07 (d, J = 0.9 Hz, 1H), 6.77 (dd, J = 8.1, 1.4 Hz, 2H), 3.84 (dd, J = 15.8, 11.0 Hz, 1H), 3.38 (dd, J = 15.9, 4.5 Hz, 1H), 3.24 (dd, J = 10.9, 4.5 Hz, 1H), 0.95 (s, 9H).

^{13}C NMR (75 MHz, CDCl_3) δ 191.1, 143.6, 141.9, 138.1, 129.9, 129.2, 128.8, 128.3, 127.5, 126.4, 126.0, 125.4, 51.6, 40.0, 33.8, 28.0.

IR (film): ν (cm^{-1}) 3060, 3029, 2958, 2904, 2870, 1684, 1596, 1495, 1447, 1403, 1304, 1063, 1032, 965, 913, 759, 696, 530.

HRMS (ESI, m/z) calcd for $\text{C}_{22}\text{H}_{25}\text{N}_2\text{O}$ $[\text{M}+\text{H}]^+$: 333.1961, found: 333.1965.

(S)-1-(1-Isopropyl-1H-imidazol-2-yl)-4,4-dimethyl-3-phenylpentan-1-one (55z')

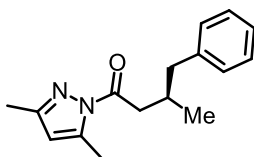
According to the general procedure, α,β -unsaturated acyl imidazole **53h'** (48.0 mg, 0.2 mmol) reacted with potassium *tert*-butyltrifluoroborate **54p** (49.2 mg, 0.30 mmol) in acetone/H₂O (4:1, 1.0 mL) to give **55z'** as a colorless oil (55.4 mg, 0.186 mmol, yield: 93%). Enantiomeric excess established by HPLC analysis using a Chiralpak AD-H column, *ee* = 98% (HPLC: AD-H, 254 nm, hexane/isopropanol = 95:5, flow rate 1.0 mL/min, 25 °C, *t_r* (major) = 7.8 min, *t_r* (minor) = 9.1 min). $[\alpha]_D^{22} = +5.7^\circ$ (*c* 0.68, CH₂Cl₂).

¹H NMR (300 MHz, CDCl₃) δ 7.18 – 6.97 (m, 7H), 5.19 (hept, *J* = 6.7 Hz, 1H), 3.79 (dd, *J* = 16.6, 10.9 Hz, 1H), 3.32 (dd, *J* = 16.6, 4.2 Hz, 1H), 3.15 (dd, *J* = 10.9, 4.2 Hz, 1H), 1.20 (d, *J* = 6.7 Hz, 3H), 1.11 (d, *J* = 6.7 Hz, 3H), 0.86 (s, 9H).

¹³C NMR (75 MHz, CDCl₃) δ 192.6, 142.8, 142.2, 129.6, 129.1, 127.3, 125.9, 120.6, 51.3, 48.8, 40.4, 33.8, 28.1, 23.4, 23.2.

IR (film): ν (cm⁻¹) 2960, 2905, 2870, 1673, 1455, 1396, 1254, 1224, 1140, 1081, 1018, 981, 915, 763, 707.

HRMS (ESI, *m/z*) calcd for C₁₉H₂₇N₂O [M+H]⁺: 299.2118, found: 299.2120.

(R)-1-(3,5-Dimethyl-1H-pyrazol-1-yl)-3-methyl-4-phenylbutan-1-one (59a)

According to the general procedure, α,β -unsaturated acyl pyrazole **58a** (32.8 mg, 0.2 mmol) reacted with potassium benzyltrifluoroborate **54a** (59.4 mg, 0.30 mmol) in acetone/H₂O (1:1, 1.0 mL) to give **59a** as a colorless oil (31.8 mg, 0.124 mmol, yield: 62%). Enantiomeric excess established by HPLC analysis using a Chiralpak AD-H column, *ee* = 96% (HPLC: AD-H, 254 nm, hexane/isopropanol = 99.5:0.5, flow rate 1.0 mL/min, 25 °C, *t_r* (minor) = 6.8 min, *t_r* (major) = 7.3 min). $[\alpha]_D^{22} = -53.8^\circ$ (*c* 0.28, CH₂Cl₂).

¹H NMR (300 MHz, CDCl₃) δ 7.33 – 7.23 (m, 2H), 7.23 – 7.13 (m, 3H), 5.94 (s, 1H), 3.11 (dd, *J* =

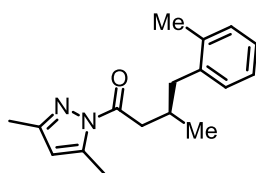
16.6, 5.9 Hz, 1H), 3.01 (dd, $J = 16.6, 7.3$ Hz, 1H), 2.83 – 2.65 (m, 1H), 2.62 – 2.40 (m, 5H), 2.24 (s, 3H), 1.00 (d, $J = 6.4$ Hz, 3H).

^{13}C NMR (75 MHz, CDCl_3) δ 173.4, 151.6, 144.0, 140.5, 129.2, 128.2, 125.9, 111.0, 43.1, 41.7, 31.7, 19.8, 14.6, 13.8.

IR (film): ν (cm^{-1}) 3061, 3027, 2960, 2925, 1724, 1582, 1378, 1335, 993, 963, 745, 700.

HRMS (ESI, m/z) calcd for $\text{C}_{16}\text{H}_{21}\text{N}_2\text{O}$ $[\text{M}+\text{H}]^+$: 257.1648, found: 257.1651.

(R)-1-(3,5-Dimethyl-1H-pyrazol-1-yl)-3-methyl-4-(*o*-tolyl)butan-1-one (59b)



According to the general procedure, α,β -unsaturated acyl pyrazole **58a** (32.8 mg, 0.2 mmol) reacted with potassium trifluoro(2-methylbenzyl)borate **54d** (63.6 mg, 0.30 mmol) in acetone/ H_2O (1:1, 1.0 mL) to give **59b** as a colorless oil (33.0 mg, 0.122 mmol, yield: 61%). Enantiomeric excess established by HPLC analysis using a Chiralpak OJ-H column, $ee = 95\%$ (HPLC: OJ-H, 254 nm, hexane/isopropanol = 99:1, flow rate 1.0 mL/min, 25 °C, t_r (minor) = 6.4 min, t_r (major) = 6.8 min). $[\alpha]_D^{22} = -44.1^\circ$ (c 0.28, CH_2Cl_2).

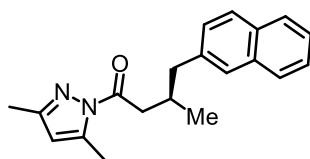
^1H NMR (300 MHz, CDCl_3) δ 7.23 – 6.96 (m, 4H), 5.94 (s, 1H), 3.15 (dd, $J = 16.2, 5.6$ Hz, 1H), 3.03 (dd, $J = 16.3, 7.2$ Hz, 1H), 2.83 – 2.65 (m, 1H), 2.64 – 2.39 (m, 5H), 2.34 (s, 3H), 2.24 (s, 3H), 1.01 (d, $J = 6.2$ Hz, 3H).

^{13}C NMR (75 MHz, CDCl_3) δ 173.4, 151.6, 143.9, 138.8, 136.4, 130.2, 130.1, 126.1, 125.6, 110.9, 42.2, 40.5, 30.5, 19.9, 19.4, 14.5, 13.8.

IR (film): ν (cm^{-1}) 2958, 2926, 2867, 1722, 1580, 1375, 1331, 960, 741.

HRMS (ESI, m/z) calcd for $\text{C}_{17}\text{H}_{22}\text{N}_2\text{ONa}$ $[\text{M}+\text{Na}]^+$: 293.1624, found: 293.1628.

(R)-1-(3,5-Dimethyl-1H-pyrazol-1-yl)-3-methyl-4-(naphthalen-2-yl)butan-1-one (59c)



According to the general procedure, α,β -unsaturated acyl pyrazole **58a** (32.8 mg, 0.2 mmol) reacted

with potassium trifluoro(naphthalen-2-ylmethyl)borate **54e** (74.4 mg, 0.30 mmol) in acetone/H₂O (1:1, 1.0 mL) to give **59c** as a colorless oil (41.8 mg, 0.137 mmol, yield: 68%). Enantiomeric excess established by HPLC analysis using a Chiralpak OJ-H column, *ee* = 96% (HPLC: OJ-H, 254 nm, hexane/isopropanol = 90:10, flow rate 1.0 mL/min, 25 °C, *t_r* (minor) = 8.4 min, *t_r* (major) = 12.9 min). $[\alpha]_D^{22} = -42.0^\circ$ (*c* 0.39, CH₂Cl₂).

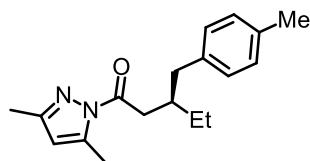
¹H NMR (300 MHz, CDCl₃) δ 7.89 – 7.69 (m, 3H), 7.63 (s, 1H), 7.55 – 7.30 (m, 3H), 5.91 (s, 1H), 3.17 (dd, *J* = 16.6, 6.0 Hz, 1H), 3.05 (dd, *J* = 16.5, 7.3 Hz, 1H), 2.91 (dd, *J* = 13.0, 6.4 Hz, 1H), 2.78 – 2.53 (m, 2H), 2.48 (s, 3H), 2.24 (s, 3H), 1.04 (d, *J* = 6.5 Hz, 3H).

¹³C NMR (75 MHz, CDCl₃) δ 173.3, 151.6, 143.9, 138.1, 133.5, 132.1, 127.9, 127.7, 127.54, 127.47, 127.46, 125.8, 125.1, 111.0, 43.3, 41.7, 31.6, 19.9, 14.5, 13.8.

IR (film): ν (cm⁻¹) 3052, 2960, 2924, 2872, 1721, 1582, 1375, 1330, 960, 893, 859, 809, 745, 474.

HRMS (ESI, *m/z*) calcd for C₂₀H₂₂N₂ONa [M+Na]⁺: 329.1624, found: 329.1629.

(R)-1-(3,5-Dimethyl-1H-pyrazol-1-yl)-3-(4-methylbenzyl)pentan-1-one (59d)



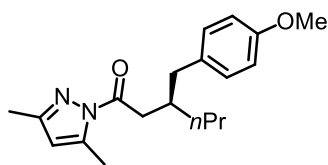
According to the general procedure, α,β -unsaturated acyl pyrazole **58b** (35.6 mg, 0.2 mmol) reacted with potassium trifluoro(4-methylbenzyl)borate **54c** (63.6 mg, 0.30 mmol) in acetone/H₂O (1:1, 1.0 mL) to give **59d** as a white solid (30.8 mg, 0.109 mmol, yield: 54%). Enantiomeric excess established by HPLC analysis using a Chiralpak OJ-H column, *ee* = 96% (HPLC: OJ-H, 254 nm, hexane/isopropanol = 90:10, flow rate 1.0 mL/min, 25 °C, *t_r* (minor) = 4.4 min, *t_r* (major) = 5.8 min). $[\alpha]_D^{22} = -45.2^\circ$ (*c* 0.35, CH₂Cl₂).

¹H NMR (300 MHz, CDCl₃) δ 7.11 – 7.02 (m, 4H), 5.92 (s, 1H), 3.09 (dd, *J* = 16.9, 6.8 Hz, 1H), 3.01 (dd, *J* = 16.9, 6.8 Hz, 1H), 2.66 (dd, *J* = 13.6, 7.2 Hz, 1H), 2.58 (dd, *J* = 13.7, 7.3 Hz, 1H), 2.49 (s, 3H), 2.40 – 2.25 (m, 5H), 2.23 (s, 3H), 1.51 – 1.32 (m, 2H), 0.94 (t, *J* = 7.4 Hz, 3H).

¹³C NMR (75 MHz, CDCl₃) δ 173.8, 151.5, 143.9, 137.5, 135.2, 129.2, 128.8, 110.9, 39.7, 38.7, 38.0, 26.4, 21.0, 14.5, 13.8, 11.1.

IR (film): ν (cm⁻¹) 2962, 2925, 2866, 1724, 1581, 1513, 1450, 1410, 1378, 1340, 962, 805, 745.

HRMS (ESI, *m/z*) calcd for C₁₈H₂₄N₂ONa [M+Na]⁺: 307.1781, found: 307.1786.

(R)-1-(3,5-Dimethyl-1H-pyrazol-1-yl)-3-(4-methoxybenzyl)hexan-1-one (59e)

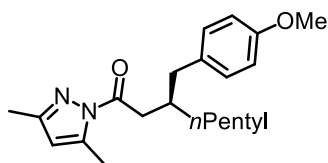
According to the general procedure, α,β -unsaturated acyl pyrazole **58c** (38.4 mg, 0.2 mmol) reacted with potassium trifluoro(4-methoxybenzyl)borate **54b** (68.4 mg, 0.30 mmol) in acetone/H₂O (1:1, 1.0 mL) to give **59e** as a colorless oil (47.2 mg, 0.150 mmol, yield: 75%). Enantiomeric excess established by HPLC analysis using a Chiralpak OJ-H column, $ee = 97\%$ (HPLC: OJ-H, 254 nm, hexane/isopropanol = 99.5:0.5, flow rate 1.0 mL/min, 25 °C, t_r (major) = 14.1 min, t_r (minor) = 17.4 min). $[\alpha]_D^{22} = -57.0^\circ$ (c 0.56, CH₂Cl₂).

¹H NMR (300 MHz, CDCl₃) δ 7.10 (d, $J = 8.6$ Hz, 2H), 6.79 (d, $J = 8.6$ Hz, 2H), 5.92 (s, 1H), 3.77 (s, 3H), 3.08 (dd, $J = 15.0, 4.7$ Hz, 1H), 3.00 (dd, $J = 14.9, 4.8$ Hz, 1H), 2.65 (dd, $J = 13.6, 7.0$ Hz, 1H), 2.55 (dd, $J = 13.6, 7.3$ Hz, 1H), 2.48 (s, 3H), 2.46 – 2.30 (m, 1H), 2.23 (s, 3H), 1.50 – 1.23 (m, 4H), 0.88 (t, $J = 6.6$ Hz, 3H).

¹³C NMR (75 MHz, CDCl₃) δ 173.7, 157.8, 151.4, 143.9, 132.6, 130.1, 113.6, 110.9, 55.2, 39.7, 39.1, 36.3, 36.2, 19.9, 14.5, 14.2, 13.7.

IR (film): ν (cm⁻¹) 2956, 2925, 2866, 1722, 1611, 1581, 1510, 1457, 1410, 1377, 1335, 1242, 1174, 1034, 960, 805, 741, 521.

HRMS (ESI, m/z) calcd for C₁₉H₂₆N₂O₂Na [M+Na]⁺: 337.1886, found: 337.1891.

(R)-1-(3,5-Dimethyl-1H-pyrazol-1-yl)-3-(4-methoxybenzyl)octan-1-one (59f)

According to the general procedure, α,β -unsaturated acyl pyrazole **58d** (44.0 mg, 0.2 mmol) reacted with potassium trifluoro(4-methoxybenzyl)borate **54b** (68.4 mg, 0.30 mmol) in acetone/H₂O (1:1, 1.0 mL) to give **59f** as a colorless oil (41.9 mg, 0.122 mmol, yield: 61%). Enantiomeric excess established by HPLC analysis using a Chiralpak OJ-H column, $ee = 90\%$ (HPLC: OJ-H, 254 nm, hexane/isopropanol = 99.5:0.5, flow rate 1.0 mL/min, 25 °C, t_r (major) = 10.5 min, t_r (minor) = 13.1 min). $[\alpha]_D^{22} = -31.8^\circ$ (c 0.45, CH₂Cl₂).

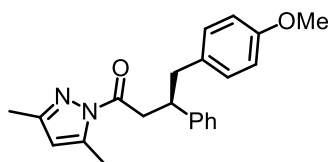
^1H NMR (300 MHz, CDCl_3) δ 7.10 (d, $J = 8.6$ Hz, 2H), 6.79 (d, $J = 8.6$ Hz, 2H), 5.92 (s, 1H), 3.77 (s, 3H), 3.07 (dd, $J = 14.5, 4.4$ Hz, 1H), 3.00 (dd, $J = 14.5, 4.4$ Hz, 1H), 2.65 (dd, $J = 13.6, 7.0$ Hz, 1H), 2.55 (dd, $J = 13.7, 7.3$ Hz, 1H), 2.48 (s, 3H), 2.44 – 2.28 (m, 1H), 2.23 (s, 3H), 1.47 – 1.14 (m, 8H), 0.86 (t, $J = 6.8$ Hz, 3H).

^{13}C NMR (75 MHz, CDCl_3) δ 173.7, 157.8, 151.4, 143.9, 132.6, 130.2, 113.6, 110.9, 55.2, 39.7, 39.1, 36.6, 33.8, 32.0, 26.4, 22.6, 14.5, 14.0, 13.8.

IR (film): ν (cm^{-1}) 2925, 2856, 1723, 1510, 1377, 1336, 1242, 1175, 1035, 961, 804, 747, 521.

HRMS (ESI, m/z) calcd for $\text{C}_{21}\text{H}_{30}\text{N}_2\text{ONa}$ $[\text{M}+\text{Na}]^+$: 365.2199, found: 365.2205.

(R)-1-(3,5-Dimethyl-1H-pyrazol-1-yl)-4-(4-methoxyphenyl)-3-phenylbutan-1-one (59g)



According to the general procedure, α,β -unsaturated acyl pyrazole **58e** (45.2 mg, 0.2 mmol) reacted with potassium trifluoro(4-methoxybenzyl)borate **54b** (68.4 mg, 0.30 mmol) in acetone/ H_2O (1:1, 1.0 mL) to give **59g** as a white solid (51.0 mg, 0.147 mmol, yield: 73%). Enantiomeric excess established by HPLC analysis using a Chiralpak AD-H column, $ee = 83\%$ (HPLC: AD-H, 254 nm, hexane/isopropanol = 98:2, flow rate 1.0 mL/min, 25 °C, t_r (minor) = 7.7 min, t_r (major) = 8.6 min). $[\alpha]_D^{22} = +45.6^\circ$ (c 0.31, CH_2Cl_2).

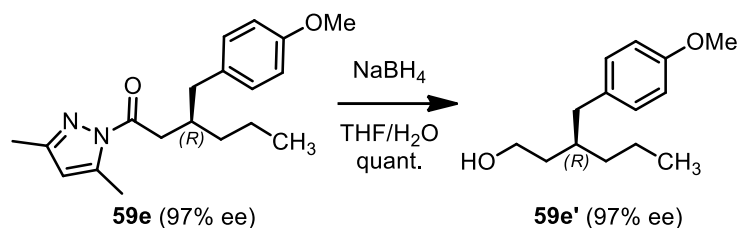
^1H NMR (300 MHz, CDCl_3) δ 7.34 – 7.14 (m, 5H), 7.02 (d, $J = 8.6$ Hz, 2H), 6.76 (d, $J = 8.6$ Hz, 2H), 5.91 (s, 1H), 3.77 (s, 3H), 3.71 – 3.52 (m, 2H), 3.51 – 3.37 (m, 1H), 2.95 (d, $J = 7.1$ Hz, 2H), 2.43 (s, 3H), 2.25 (s, 3H).

^{13}C NMR (75 MHz, CDCl_3) δ 172.5, 157.9, 151.6, 144.0, 143.9, 131.8, 130.1, 128.2, 127.7, 126.3, 113.5, 110.9, 55.1, 43.4, 42.3, 40.6, 14.4, 13.7.

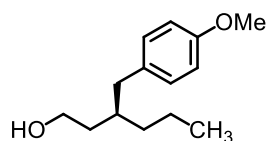
IR (film): ν (cm^{-1}) 3060, 2990, 2921, 2834, 1707, 1510, 1377, 1309, 1241, 1170, 963, 809, 757, 700, 594, 523.

HRMS (ESI, m/z) calcd for $\text{C}_{22}\text{H}_{24}\text{N}_2\text{O}_2\text{Na}$ $[\text{M}+\text{Na}]^+$: 371.1730, found: 371.1735.

5.7.3 Synthetic Transformations



To a solution of **5e** (46.0 mg, 0.146 mmol) in THF/H₂O (4/1, 1.5 mL, 0.1 M) at 0 °C was added NaBH₄ (56.0 mg, 1.5 mmol). The reaction mixture was stirred at room temperature for overnight. The reaction was quenched with aqueous 2 N HCl (1.0 mL) at room temperature and extracted with DCM (4 × 10 mL). The combined organic layers were dried over anhydrous Na₂SO₄, filtered, and concentrated under reduced pressure. The residue was purified by flash chromatography on silica gel (EtOAc/hexane = 1:5) to afford **5e'** (32.5 mg, 0.146 mmol, yield: 100%) as a colorless oil.

(R)-3-(4-Methoxybenzyl)hexan-1-ol (59e')

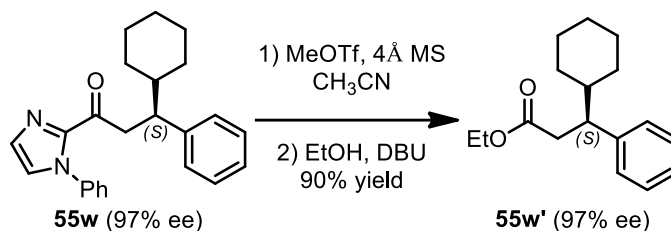
Enantiomeric excess established by HPLC analysis using a Chiralpak OD-H column, *ee* = 97% (HPLC: OD-H, 254 nm, hexane/isopropanol = 96:4, flow rate 1.0 mL/min, 25 °C, *t_r* (major) = 11.7 min, *t_r* (minor) = 13.0 min). $[\alpha]_D^{22} = -6.9^\circ$ (*c* 0.40, CH₂Cl₂).

¹H NMR (300 MHz, CDCl₃) δ 7.07 (d, *J* = 8.5 Hz, 2H), 6.83 (d, *J* = 8.6 Hz, 2H), 3.79 (s, 3H), 3.65 (pd, *J* = 10.5, 6.9 Hz, 2H), 2.57 (dd, *J* = 13.7, 6.7 Hz, 1H), 2.46 (dd, *J* = 13.7, 7.3 Hz, 1H), 1.84 – 1.67 (m, 1H), 1.53 (dd, *J* = 13.5, 6.8 Hz, 2H), 1.46 – 1.21 (m, 5H), 0.89 (t, *J* = 7.0 Hz, 3H).

¹³C NMR (75 MHz, CDCl₃) δ 157.8, 133.2, 130.0, 113.6, 61.1, 55.2, 39.8, 36.54, 36.45, 35.9, 19.7, 14.3.

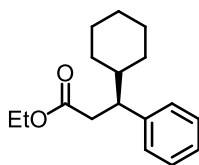
IR (film): ν (cm⁻¹) 3336, 2922, 2867, 1611, 1510, 1456, 1242, 1176, 1034, 822, 520.

HRMS (ESI, *m/z*) calcd for C₁₄H₂₂O₂Na [M+Na]⁺: 245.1512, found: 245.1515.



To a solution of (*S*)-**3w** (90.0 mg, 0.25 mmol) in CH₃CN (2.5 mL) was added 4 Å MS (250 mg, 100 mg/0.1 mmol of **3w**) under nitrogen atmosphere. The suspension was stirred vigorously under a positive pressure of nitrogen for 2 h at room temperature, and then methyl trifluoromethanesulfonate (41 µL, 0.38 mmol) was added at room temperature. After being stirred at room temperature for 2 h, EtOH (1.25 mL) and DBU (0.50 mL) were subsequently added to the reaction mixture at 0 °C. After being stirred at 0 °C for 60 min, the solvent was evaporated and the residue was purified by flash chromatography on silica gel (EtOAc/hexane = 1:50) to give **3w'** (58.6 mg, 0.225 mmol, yield: 90%) as a colorless oil.

(*S*)-Ethyl 3-cyclohexyl-3-phenylpropanoate (55w'**)**



Enantiomeric excess established by HPLC analysis using a Chiralpak OD-H column, *ee* = 97% (HPLC: OD-H, 254 nm, hexane/isopropanol = 98:2, flow rate 0.5 mL/min, 25 °C, *t_r* (major) = 9.6 min, *t_r* (minor) = 14.2 min). $[\alpha]_{\text{D}}^{22} = -21.4^\circ$ (*c* 0.64, CH₂Cl₂).

¹H NMR (300 MHz, CDCl₃) δ 7.25 – 7.14 (m, 2H), 7.14 – 7.00 (m, 3H), 3.88 (q, *J* = 7.1 Hz, 2H), 2.89 – 2.77 (m, 1H), 2.72 (dd, *J* = 14.8, 5.6 Hz, 1H), 2.47 (dd, *J* = 14.8, 9.8 Hz, 1H), 1.80 – 1.62 (m, 2H), 1.62 – 1.47 (m, 2H), 1.48 – 1.31 (m, 2H), 1.24 – 0.92 (m, 6H), 0.92 – 0.65 (m, 2H).

¹³C NMR (75 MHz, CDCl₃) δ 172.9, 143.2, 128.3, 128.0, 126.2, 60.0, 48.2, 42.9, 38.5, 31.0, 30.8, 26.5, 26.4, 14.00.

IR (film): ν (cm⁻¹) 2979, 2924, 2852, 1732, 1448, 1371, 1251, 1153, 1033, 758, 700.

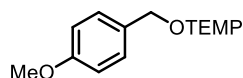
HRMS (ESI, *m/z*) calcd for C₁₇H₂₄O₂Na [M+Na]⁺: 283.1669, found: 283.1669.

5.7.4 Mechanistic Experiments

1) Trapping Experiment with TEMPO

As shown in Scheme 20-21, the experiment data of compound **61** are shown below.

1-((4-Methoxybenzyl)oxy)-2,2,6,6-tetramethylpiperidine (**61**)



^1H NMR (300 MHz, CDCl_3) δ 7.21 (d, J = 8.6 Hz, 2H), 6.79 (d, J = 8.6 Hz, 2H), 4.66 (s, 2H), 3.72 (s, 3H), 1.64 – 1.22 (m, 6H), 1.18 (s, 6H), 1.05 (s, 6H).

^{13}C NMR (75 MHz, CDCl_3) δ 159.0, 130.5, 129.1, 113.7, 78.4, 59.9, 55.2, 39.7, 33.2, 20.3, 17.1.

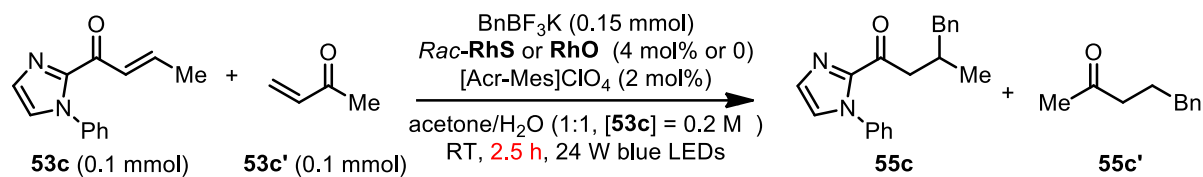
All spectroscopic data were in agreement with the literature.³⁸

2) Control Experiments

See Figure 87-90

3) Competition Experiment (Figure 86)

A dried 10 mL Schlenk tube was charged with the catalyst *rac*-**RhS** or *rac*-**RhO** (0 or 4 mol%), sensitizer [Acr-Mes] ClO_4 (2 mol%), α,β -unsaturated 2-acyl imidazole **53c** (21.2 mg, 0.1 mmol, 1.0 eq), 3-buten-2-one **53c'** (8.1 μL , 0.1 mmol, 1.0 eq), BnBF_3K (0.15 mmol, 1.5 eq), 0.5 mL acetone/ H_2O (1:1, 0.1 M). The reaction mixture was degassed *via* freeze-pump-thaw for three cycles. After the mixture was thoroughly degassed, the vial was sealed and positioned approximately 10 cm from a 24 W blue LEDs lamp. After being irradiated for 2.5 h, the reaction mixture was passed through a short silica gel column. The yield of product formed was measured by ^1H -NMR analysis with 1,1,2,2-tetrachloroethane (0.1 mmol/mL in CDCl_3) as internal standard.



	yield (55c)	yield (55c')	55c : 55c'
no Rh	8%	20%	0.4 : 1
RhS (4% mol)	55%	not observed	> 550 : 1
RhO (4% mol)	61%	not observed	> 610 : 1

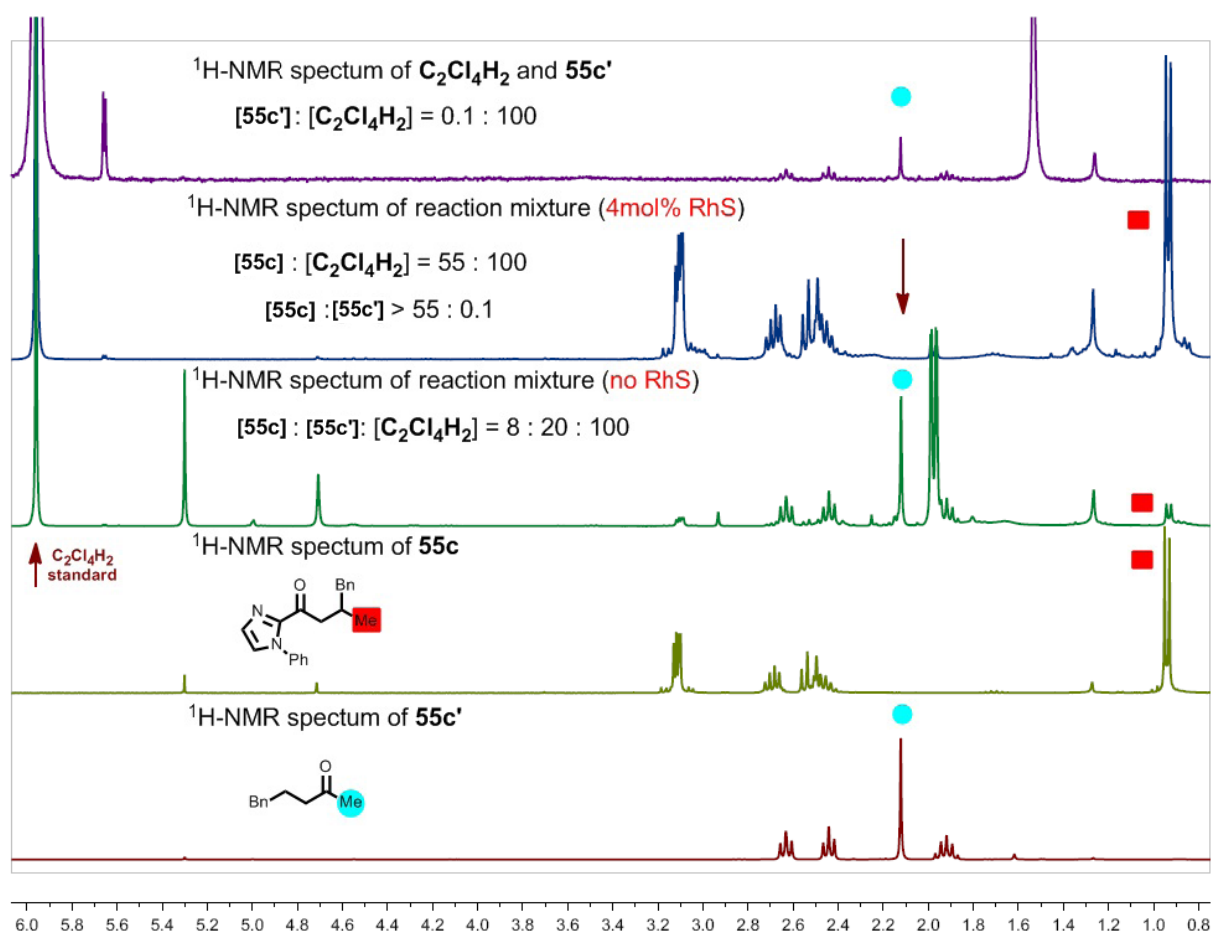


Figure 120 ¹H NMR (300 MHz, in CDCl₃) spectra of **55c**, **55c'** (as references) and the crude product from the photolysis. Yield was inferred by integration ratio (signals '●' and '■').

4) Luminescence Quenching Experiments

As shown in Figure 92-94, the luminescence quenching experiments with the photoredox catalyst were investigated both in the presence and absence of **RhS** and olefin. Emission intensities were recorded on a Spectra Max M5 microplate reader in a 10.0 mm quartz cuvette. The solutions of Ir[dF(CF₃)ppy]₂(bpy)PF₆ were excited at $\lambda_{\text{max}} = 375$ nm and the emission was measured at 475 nm (emission maximum). The sensitizer Ir[dF(CF₃)ppy]₂(bpy)PF₆ was used for the quenching experiments due to stronger luminescence intensities. The concentration of the photoredox catalyst solution (iridium sensitizer or iridium sensitizer in presence of **RhS** and Michael acceptor **53c**) was 0.5 mM in acetone/H₂O (4:1). The concentration of the quencher (potassium trifluoroborates **54c**, **54h**, **54m**, Michael acceptor **53c**) stock solution was 200 mM in acetone/H₂O (4:1). For each quenching experiment, 5 μ L of this stock solution were titrated to a solution (1 mL) of iridium complex in a screw-top 10.0 mm quartz cuvette. The addition of 5 μ L stock solution refers to an increase of the quencher concentration of 1 mM. After degassing with an argon stream for 5 minutes, the emission intensity was collected.

5) Quantum Yield Measurement

The quantum yield was measured by standard ferrioxalate actinometry. A 150 W xenon lamp (50% of light intensity, 420 \pm 5 nm bandpass filter) was used as the light source. The measured method was designed according to a published procedure with slight modifications.³⁹ All the light sensitive operations were processed in the darkroom under red light.

The solutions were prepared and stored in the dark:

Potassium ferrioxalate solution (0.15 M): 736.9 mg of potassium ferrioxalate hydrate was dissolved in 10 mL of 0.05 M H₂SO₄.

Buffered solution of phenanthroline: 50 mg of 1,10-phenanthroline and 11.25 g of sodium acetate were dissolved in 50 mL of 0.5 M H₂SO₄.

5.1) Measurement of light intensity at 420 nm

1000 μ L of the ferrioxalate solution was added to a quartz cuvette (l = 10 mm). The actinometry solution was irradiated with 150 W Xenon Lamp (50% of light intensity, 420 nm \pm 5 nm) for specified time intervals (30, 60, 90, 120 seconds). After irradiation, 175 μ L of the phenanthroline

solution was added to the cuvette. The solution was kept in dark for 30 min to make sure the complete coordination. The absorbance of the actinometry solution was monitored at 510 nm. The absorbance of a non-irradiated (in dark) sample was also measured at 510 nm.

The moles of Fe^{2+} formed were determined using Beer's Law:

$$\text{moles Fe}^{2+} = \frac{V_1 \times V_3 \times \Delta A(510 \text{ nm})}{10^3 \times V_2 \times l \times \varepsilon(510 \text{ nm})}$$

Where V_1 (1 mL) is the irradiated volume, V_2 (1 mL) is the aliquot of the irradiated solution taken for the determination of the ferrous ions. V_3 (1.175 mL) is the final volume after complexation with phenanthroline (all in mL), l is the path length (1 cm), and $\Delta A(510 \text{ nm})$ is the optical difference in absorbance between the irradiated and non-irradiated solutions, $\varepsilon(510 \text{ nm})$ is the molar absorptivity of $\text{Fe}(\text{phen})_3^{2+}$ ($11100 \text{ L mol}^{-1} \text{ cm}^{-1}$).

One calculation example of moles Fe^{2+} (when $t = 30 \text{ s}$) was shown below:

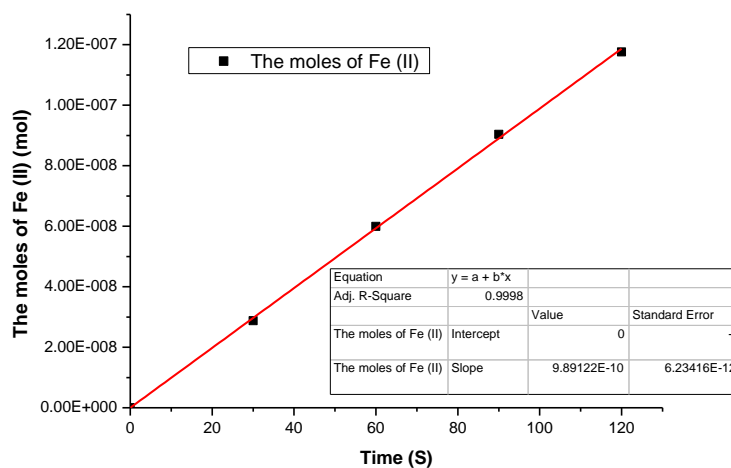
$$\text{moles Fe}^{2+} = \frac{V_1 \times V_3 \times \Delta A(510 \text{ nm})}{10^3 \times V_2 \times l \times \varepsilon(510 \text{ nm})} = \frac{1 \text{ mL} \times 1.175 \text{ mL} \times 0.272}{10^3 \times 1 \text{ mL} \times 1 \text{ cm} \times 11100 \text{ L} \cdot \text{mol}^{-1} \cdot \text{cm}^{-1}} = 2.879 \times 10^{-8} \text{ mol}$$

The moles of Fe^{2+} formed for each sample (30, 60, 90, 120 s) are listed as follows:

irradiation time	30 s	60 s	90 s	120 s
ΔA	0.272	0.566	0.854	1.111
Fe^{2+} (10^{-8} mol)	2.879	5.991	9.040	11.760

The moles of Fe^{2+} formed are plotted as a function of time (t). The slope is shown as:

$$d(\text{moles Fe}^{2+})/dt = 9.891 \times 10^{-10}$$



The photon flux can be calculated as:

$$\text{photon flux (einstein s}^{-1}\text{)} = \frac{\text{moles Fe}^{2+}}{\Phi \cdot t \cdot f} = \frac{d(\text{moles Fe}^{2+})/dt}{\Phi \cdot f} = \frac{9.891 \times 10^{-10}}{1.04 \times 1.0} = 9.51 \times 10^{-10} \text{ einstein/s}$$

Where Φ is the quantum yield for the ferrioxalate actinometer (1.05 for a 0.15 solution at 412 nm; 1.04 for a 0.15 solution at 422 nm; 1.03 for a 0.15 solution at 433 nm),⁴⁰ t is the irradiated time, and f is the fraction of light absorbed at $\lambda = 420$ nm ($f = 1 - 10^{-A}$). The measurement of the fraction of the light at 420 nm for the ferrioxalate solution was shown in Figure 120. The absorbance of the ferrioxalate solution at 420 nm is >3 indicating f ($f = 1 - 10^{-A}$) is >0.999 .

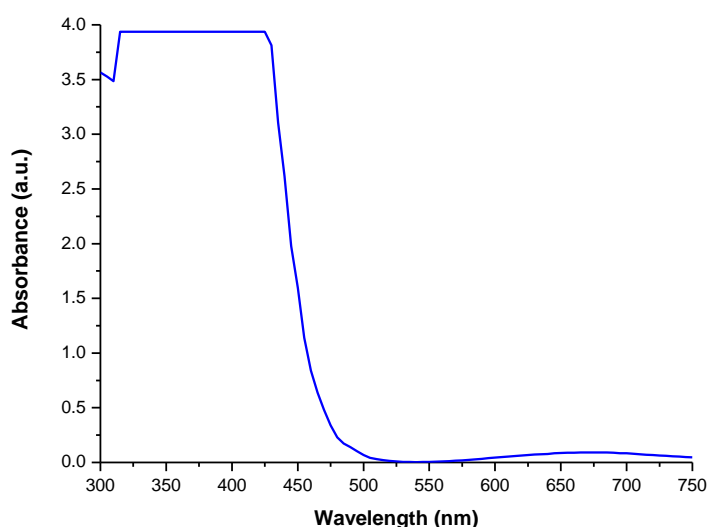
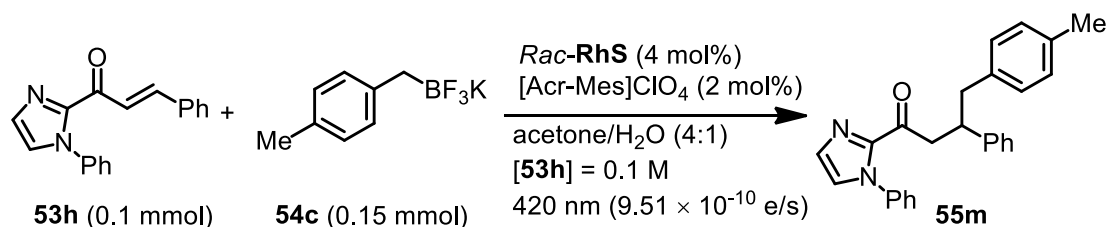


Figure 121 Absorbance of the ferrioxalate actinometer solution (0.15 M).

5.2) Measurement of quantum yield:

Model reaction:

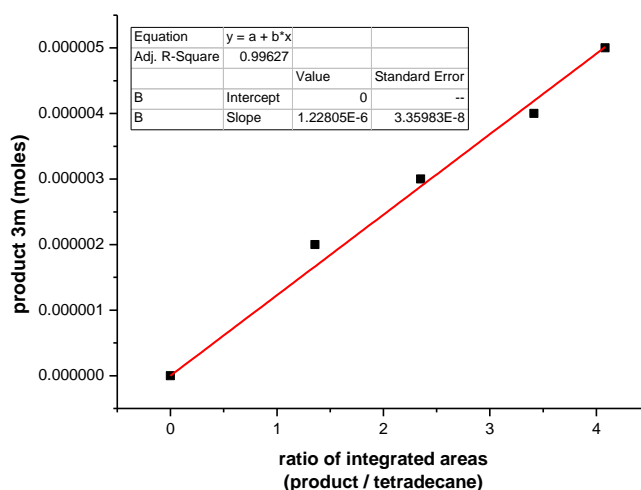


The Newport instrument for quantum yield determination was set up at a fixed position in a dark room (red light). A screw-top cuvette (10.0 mm) was charged with the Lewis acid catalyst *rac*-**RhS** (4 mol%), sensitizer [Acr-Mes]ClO₄ (2 mol%), α,β -unsaturated 2-acyl imidazole **53h** (0.1 mmol, 1.0 eq), trifluoroborate **54c** (0.15 mmol, 1.5 eq), 1.0 mL acetone/H₂O (4:1, 0.1 M) and a small magnetic stir

bar. The cuvette was degassed with an argon stream for 10 min. After the mixture was thoroughly degassed, the vial was sealed and fixed at the same position as the measurement of photon flux. The reaction mixture was stirred and irradiated for specified time intervals (2, 3, 4 h). After irradiation, the reaction mixture was passed through a short silica gel column. The moles of product formed was measured by GC analysis (FID detector, column: HP-5) using tetradecane as internal standard.

Determination of response factor for GC analysis:

The internal standard remained constant for every measurement. The number of moles of products is related to the ratios of integrated areas (product/internal standard). The relation formula was yielded as $y = 1.228\text{E-}6 * x$ (y is the moles of product **55m**, x is the ratio of integrated areas).

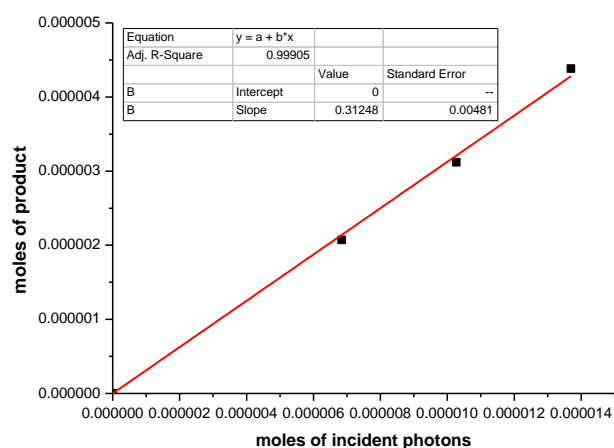


The relation between the produced molecules and incident photons:

After irradiation for specified time (2, 3, 4 h), the moles of formed product **55m** was calculated below ($y = 1.228\text{E-}6 * x$):

irradiation time (S)	7200	10800	14400
ratio of integrated areas (55m / tetradecane)	1.687	2.539	3.568
product (10^{-6} mol)	2.072	3.118	4.382

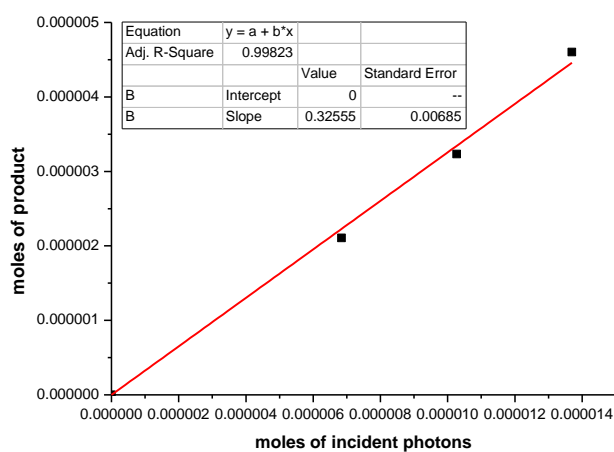
The number of molecules generated is related to the number of photons absorbed. The number of photons absorbed is correlated to the number of incident photons. The relation between the number of formed molecules and the number of incident photons was shown below ($y = 0.31x$).



The measurements were repeated a second time to provide the moles of product as below ($y = 1.228\text{E-}6 \cdot x$):

irradiation time (S)	7200	10800	14400
ratio of integrated areas (55m / tetradecane)	1.715	2.634	3.748
product (10^{-6} mol)	2.106	3.234	4.602

The relation between the number of formed molecules and the number of incident photons was shown below ($y = 0.32x$).



Overall quantum yield:

$$\Phi = \frac{\text{moles of product}}{\text{moles of absorbed photons}} = \frac{\text{moles of product}}{\text{moles of incident photons} \times (1 - 10^{-A(420\text{nm})})}$$

The slope yields the value of d (moles of product)/ d (moles of incident photons). Absorbance at 420 nm is >3 (Figure 121) demonstrating that the fraction of light absorbed is >0.999 ($f = 1 - 10^{-A}$). The absorbance of reaction mixture in acetone/H₂O (4:1) was measured at a dilute concentration (10% of the reaction conditions above).

Due to the fraction of light absorbed is >0.999, the slopes provide the overall quantum yield (Φ) of the photoreaction as 0.31 and 0.32 respectively for these two independent measurements. It is important to note that these values present overall quantum yields and do not take into account that there are more than one photoactive species in this system (see Figure 91).

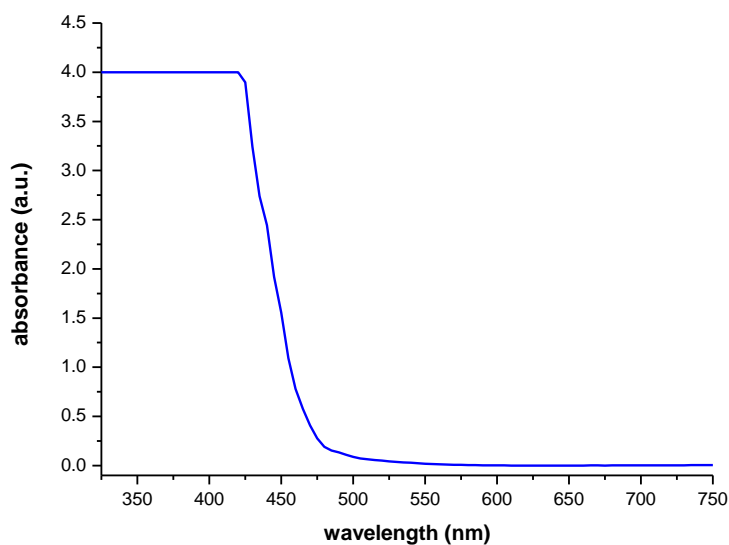
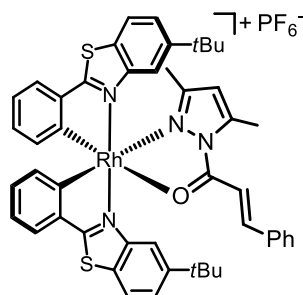


Figure 122 Absorbance of the reaction solution (**RhS** = 0.4 mM, [Acr-Mes]ClO₄ = 0.2 mM in acetone/H₂O (4:1)).

6) Synthesis of Intermediate Complex I

intermediate I (*RhS-Py*)

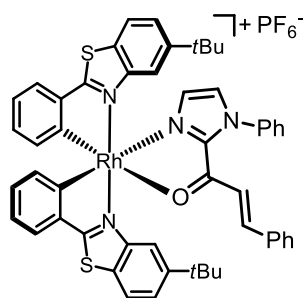
The racemic complex **RhS-Py** was obtained by reacting Michael acceptor **6e** (9.0 mg, 0.04 mmol) with racemic Δ/Λ -**RhS** (34.5 mg, 0.04 mmol) at room temperature for 5 min in CH_2Cl_2 (2.0 mL). Afterwards, the solution was evaporated and the resulting solid was dissolved in CH_2Cl_2 (2.0 mL) followed by concentrated under vacuum. The labile ligands (CH_3CN) were completely removed *via* dissolved-evaporated for five cycles. The residue yellow solid was washed by Et_2O (4×1 mL), the pure yellow solid was obtained (41.4 mg, yield: 100%).

^1H NMR (300 MHz, CD_2Cl_2) δ 8.44 (d, $J = 15.3$ Hz, 1H), 8.00 (dd, $J = 8.3, 7.3$ Hz, 2H), 7.89 – 7.78 (m, 2H), 7.75 (d, $J = 1.4$ Hz, 1H), 7.70 (d, $J = 7.1$ Hz, 2H), 7.67 – 7.58 (m, 3H), 7.54 (t, $J = 7.3$ Hz, 2H), 7.29 (d, $J = 15.3$ Hz, 1H), 7.24 – 7.11 (m, 2H), 7.06 (d, $J = 1.4$ Hz, 1H), 6.97 (qd, $J = 7.7, 1.3$ Hz, 2H), 6.52 (s, 1H), 6.47 (d, $J = 7.9$ Hz, 1H), 6.36 (d, $J = 7.8$ Hz, 1H), 2.82 (s, 3H), 1.84 (s, 3H), 1.26 (s, 9H), 1.22 (s, 9H).

^{13}C NMR (75 MHz, CD_2Cl_2) δ 178.1, 175.9, 169.4, 162.3, 161.9, 161.1, 160.7, 160.3, 156.5, 152.9, 152.8, 150.1, 150.0, 145.9, 141.0, 140.2, 134.4, 134.2, 134.1, 133.2, 131.7, 131.6, 130.1, 130.0, 129.4, 129.3, 127.1, 126.7, 125.4, 124.9, 124.7, 123.3, 117.9, 115.5, 115.0, 112.5, 35.5, 35.3, 31.7, 31.5, 16.2, 13.6.

IR (film): ν (cm^{-1}) 3057, 2959, 2868, 1632, 1564, 1442, 1410, 1354, 1321, 1291, 1249, 1080, 1031, 987, 833, 758, 726, 671, 579, 552, 489, 455.

HRMS (APCI, m/z) calcd for $\text{C}_{48}\text{H}_{46}\text{N}_4\text{ORhS}_2$ $[\text{M}]^+$: 861.2163 and 862.2194, found: 861.2168 and 862.2202.

intermediate I (**RhS-Im**)

The racemic complex **RhS-Im** was obtained by reacting Michael acceptor **53h** (21.9 mg, 0.08 mmol) with racemic Δ/Λ -**RhS** (69.0 mg, 0.08 mmol) at room temperature for 5 min in CH_2Cl_2 (2.0 mL). Afterwards, the solution was evaporated and the resulting solid was dissolved in CH_2Cl_2 (2.0 mL) followed by concentrated under vacuum. The labile ligands (CH_3CN) were completely removed *via* dissolved-evaporated for five cycles. The residue orange solid was washed by Et_2O (4×1 mL), the pure orange solid was obtained (84.0 mg, yield: 99%).

^1H NMR (300 MHz, CD_2Cl_2) δ 8.15 (d, $J = 15.4$ Hz, 1H), 7.94 (t, $J = 8.8$ Hz, 2H), 7.84 (td, $J = 7.5$, 1.0 Hz, 2H), 7.77 (d, $J = 7.5$ Hz, 1H), 7.72 – 7.62 (m, 4H), 7.58 (ddd, $J = 17.4$, 8.6, 1.6 Hz, 2H), 7.47 (t, $J = 7.4$ Hz, 1H), 7.40 – 7.11 (m, 7H), 7.08 (d, $J = 7.5$ Hz, 2H), 6.96 (t, $J = 7.6$ Hz, 3H), 6.49 (dd, $J = 14.6$, 7.8 Hz, 2H), 6.33 (d, $J = 15.4$ Hz, 1H), 1.19 (s, 9H), 1.18 (s, 9H).

^{13}C NMR (75 MHz, CD_2Cl_2) δ 182.5, 178.33, 178.28, 175.44, 175.40, 164.0, 163.6, 160.3, 159.9, 153.1, 152.6, 152.4, 150.0, 149.3, 146.0, 141.4, 139.9, 135.8, 135.2, 134.4, 133.9, 133.3, 132.3, 131.5, 131.3, 131.1, 129.9, 129.8, 129.5, 129.4, 126.9, 126.8, 126.6, 125.2, 124.8, 124.7, 124.5, 123.4, 123.2, 118.9, 115.8, 115.7, 35.39, 35.37, 31.6.

IR (film): ν (cm^{-1}) 2956, 2920, 2863, 1615, 1580, 1529, 1486, 1443, 1404, 1294, 1158, 1114, 1079, 1026, 990, 928, 831, 769, 728, 691, 554, 458, 407.

HRMS (APCI, m/z) calcd for $\text{C}_{52}\text{H}_{46}\text{N}_4\text{ORhS}_2$ $[\text{M}]^+$: 909.2163 and 910.2194, found: 909.2169 and 910.2203.

5.7.5 Single-Crystal X-Ray Diffraction Studies

Single crystals of (*R*)-**55k** (H53) suitable for X-ray diffraction were obtained by slow diffusion from a solution of (*R*)-**55k** (20 mg) in CH₂Cl₂ (0.3 mL) layered with Et₂O (2.5 mL) at –20 °C for several days in a glass tube. The absolute configuration of compound (*R*)-**55k** (H53) has been determined.

Single crystals of intermediate **I** (**RhS-Py**) suitable for X-ray diffraction were obtained by slow diffusion from a solution of **RhS-Py** (20 mg) in CH₂Cl₂ (0.5 mL) layered with Et₂O (1.5 mL) at room temperature for several days in a glass tube.

Crystal data and details of the structure determination are presented in the Appendices (Chapter 6.7).

References

- 1 L.-A. Chen, W. Xu, B. Huang, J. Ma,; L. Wang, J. Xi, K. Harms, L. Gong, E. Meggers, *J. Am. Chem. Soc.* **2013**, *135*, 10598–10601.
- 2 S. Ueda, H. Nagasawa, *J. Org. Chem.* **2009**, *74*, 4272–4277.
- 3 Y. X. Chen, L. F. Qian, W. Zhang, B. Han, *Angew. Chem. Int. Ed.* **2008**, *47*, 9330–9333.
- 4 N. Negoro, S. Sasaki, M. Ito, S. Kitamura, Y. Tsujihata, R. Ito, M. Suzuki, K. Takeuchi, N. Suzuki, J. Miyazaki, T. Santou, T. Odani, N. Kanzaki, M. Funami, T. Tanaka, T. Yasuma, Y. Momose, *J. Med. Chem.* **2012**, *55*, 1538–1552.
- 5 T. E. Barder, S. D. Walker, J. R. Martinelli, S. L. Buchwald, *J. Am. Chem. Soc.* **2005**, *127*, 4685–4696.
- 6 D. F. Burdi, R. Hunt, L. Fan, T. Hu, J. Wang, Z. Guo, Z. Huang, C. Wu, L. Hardy, M. Detheux, M. A. Orsini, M. S. Quinton, R. Lew, K. Spear, *J. Med. Chem.* **2010**, *53*, 7107–7118.
- 7 M. Helms, Z. Lin, L. Gong, K. Harms, E. Meggers, *Eur. J. Inorg. Chem.* **2013**, 4164–4172.
- 8 G. Mercey, D. Bregeon, A.-C. Gaumont, J. Levillain, M. Gulea, *Tetrahedron Lett.* **2008**, *49*, 6553–6555.
- 9 G. Nonoyama, *Bull. Chem. Soc. Jpn.* **1974**, *47*, 767–768.
- 10 L. Gong, M. Wenzel, E. Meggers, *Acc. Chem. Res.* **2013**, *46*, 2635–2644.
- 11 J. S. Yadav, S. Aravind, G. M. Kumar, B. V. S. Reddy, *Tetrahedron Lett.* **2012**, *53*, 6163–6166.

- 12 (a) A. Bøgevig, K. Juhl, N. Kumaragurubaran, W. Zhuang, K. A. Jørgensen, *Angew. Chem. Int. Ed.* **2002**, *41*, 1790–1793. (b) T. B. Poulsen, C. Alemparte, K. A. Jørgensen, *J. Am. Chem. Soc.* **2005**, *127*, 11614–11615.
- 13 R. G. Xing, Y. N. Li, Q. A. Liu, Q. Y. Meng, J. Li, X. X. Shen, Z. G. Liu, B. Zhou, X. J. Yao, Z. L. Liu, *Eur. J. Org. Chem.* **2010**, 6627–6632.
- 14 D. A. Evans, K. R. Fandrick, H. J. Song, *J. Am. Chem. Soc.* **2005**, *127*, 8942–8943.
- 15 H. A. Duong, R. E. Gilligan, M. L. Cooke, R. J. Phipps, M. J. Gaunt, *Angew. Chem. Int. Ed.* **2011**, *50*, 463–466.
- 16 T. Niu, W. M. Zhang, D. F. Huang, C. M. Xu, H. F. Wang, Y. L. Hu, *Org. Lett.* **2009**, *11*, 4474–4477.
- 17 M. K. Gupta, Z. Li, T. S. Snowden, *Org. Lett.* **2014**, *16*, 1602–1605.
- 18 J. R. Denton, H. M. Davies, *Org. Lett.* **2009**, *11*, 787–790.
- 19 H. Wang, J. R. Denton, H. M. Davies, *Org. Lett.* **2011**, *13*, 4316–4319.
- 20 B. M. Trost, K. Lehr, D. J. Michaelis, J. Xu, A. K. Buckl, *J. Am. Chem. Soc.* **2010**, *132*, 8915–8917.
- 21 S. Ueno, R. Shimizu, R. Kuwano, *Angew. Chem. Int. Ed.* **2009**, *48*, 4543–4545.
- 22 E. Arceo, I. D. Jurberg, A. Álvarez-Fernández, P. Melchiorre, *Nat. Chem.* **2013**, *5*, 750–756.
- 23 C. Wang, Y. Zheng, H. Huo, P. Rose, L. Zhang, K. Harms, G. Hilt, E. Meggers, *Chem. Eur. J.* **2015**, *21*, 7355–7359.
- 24 D. Yang, D. Li, L. Wang, D. Zhao, R. Wang, *J. Org. Chem.* **2015**, *80*, 4336–4348.
- 25 J. Easmon, G. Purstinger, K. S. Thies, G. Heinisch, J. Hofmann, *J. Med. Chem.* **2006**, *49*, 6343–6350.
- 26 M. A. Cismesia, T. P. Yoon, *Chem. Sci.* **2015**, *6*, 5426–5434.
- 27 S. L. Murov, I. Carmichael, G. L. Hug, *Handbook of Photochemistry (Second Edition)*, Marcel Dekker: New York, **1993**.
- 28 K. Okamoto, T. Yamamoto, T. Kanbara, *Synlett* **2007**, 2687–2690.
- 29 K. Inamoto, C. Hasegawa, J. Kawasaki, K. Hiroya, T. Doi, *Adv. Synth. Catal.* **2010**, *352*, 2643–2655.
- 30 H. Huo, X. Shen, C. Wang, L. Zhang, P. Röse, L.-A. Chen, K. Harms, M. Marsch, G. Hilt, E. Meggers, *Nature* **2014**, *515*, 100–103.

- 31 C. Wang, Y. Zheng, H. Huo, P. Röse, L. Zhang, K. Harms, G. Hilt, E. Meggers, *Chem. Eur. J.* **2015**, *21*, 7355–7359.
- 32 H. Huo, C. Wang, K. Harms, E. Meggers, *J. Am. Chem. Soc.* **2015**, *137*, 9551–9554.
- 33 B. M. Trost, K. Lehr, D. J. Michaelis, J. Xu, A. K. Buckl, *J. Am. Chem. Soc.* **2010**, *132*, 8915–8917.
- 34 Q. Yao, Z. Wang, Y. Zhang, X. Liu, L. Lin, X. Feng, *J. Org. Chem.* **2015**, *80*, 5704–5712.
- 35 (a) D. A. Evans, K. R. Fandrick, H.-J. Song, K. A. Scheidt, R. Xu, *J. Am. Chem. Soc.* **2007**, *129*, 10029–10041. (b) D. A. Evans, K. R. Fandrick, *Org. Lett.* **2006**, *8*, 2249–2252.
- 36 B. M. Trost, T. M. Lam, *J. Am. Chem. Soc.* **2012**, *134*, 11319–11321.
- 37 (a) G. Sorin, R. M. Mallorquin, Y. Contie, A. Baralle, M. Malacria, J. P. Goddard, L. Fensterbank, *Angew. Chem. Int. Ed.* **2010**, *49*, 8721–8723. (b) J. C. Tellis, D. N. Primer, G. A. Molander, *Science* **2014**, *345*, 433–436. (c) I. Karakaya, D. N. Primer, G. A. Molander, *Org. Lett.* **2015**, *17*, 3294–3297.
- 38 Y. Yasu, T. Koike, M. Akita, *Adv. Synth. Catal.* **2012**, *354*, 3414–3420.
- 39 M. A. Cismesia, T. P. Yoon, *Chem. Sci.* **2015**, *6*, 5426–5434.
- 40 Murov, S. L.; Carmichael, I.; Hug, G. L. *Handbook of Photochemistry (Second Edition)*, Marcel Dekker, New York, **1993**.

Chapter 6. Appendices

6.1 List of Abbreviations

^1H NMR	proton nuclear magnetic resonance spectroscopy
^{13}C NMR	carbon nuclear magnetic resonance spectroscopy
^9F NMR	fluorine nuclear magnetic resonance spectroscopy
δ	chemical shift
J	coupling constant
br	broad
s	singlet
d	doublet
t	triplet
q	quartet
m	multiplet
ppm	parts per million
AcOH	acetic acid
ada	adamantane
aq	aqueous
Ar	argon
BArF_{24}	tetrakis[(3,5-di-trifluoromethyl)phenyl]borate
bpy	2,2'-bipyridine
CD	circular dichroism
CH_2Cl_2 / DCM	dichloromethane
CD_2Cl_2	dideuteromethylenechloride
CHCl_3	chloroform
CDCl_3	deuteriochloroform
CH_3CN / MeCN	acetonitrile
conc	concentrated
DBU	1,8-diazabicycloundec-7-ene
DIPEA	<i>N,N</i> -diisopropylethylamine
DMAc	dimethylacetamide
DMAP	4-dimethylaminopyridine

DMF	dimethylformamide
DMSO	dimethyl sulfoxide
DNB	dinitrobenzene
DTBP	2,6-Di- <i>tert</i> -butylpyridine
dr	diastereomeric ratio
EDA	electron donor-acceptor
EDC	1-ethyl-3-(3-dimethylaminopropyl)carbodiimide hydrochloride
ee	enantiomeric excesses
e.g.	exempli gratia (lat.: for example)
en	ethylenediamine
er	enantiomeric ratio
et al.	et alii (lat.: and others)
ESI	electrospray ionization
EtOH	ethanol
Et ₂ O	diethyl ether
Et ₂ NH	diethyl amine
Et ₃ N	triethyl amine
EtOAc	ethyl acetate
EWG	electron withdrawing group
HAT	hydrogen atom transfer
h	hour(s)
HPLC	high performance liquid chromatography
HRMS	high resolution mass spectrometry
Hz	Hertz
IR spectra	infrared spectra
Ir	iridium
L	liter(s)
M	mol/liter
<i>m</i>	meta-
min	minute(s)
mL	milliliter(s)
MLCT	metal-to-ligand charge transfer
mmol	millimole
MS	mass spectroscopy
N ₂	nitrogen

NBS	<i>N</i> -bromosuccinimide
Nu	nucleophile
PCET	proton-coupled electron transfer
Ph	phenyl
PPh ₃	triphenylphosphine
ppm	parts per million
ppy	2-phenylpyridine
PS	photosensitizer
<i>rac</i>	racemate
RCM	ring closing metathesis
Rh	rhodium
rt	room temperature
<i>sec</i>	secondary
SET	single-electron transfer
TEMPO	2,2,6,6-tetramethyl-1-piperidinyloxy
4-MeO-TEMPO	4-methoxy-2,2,6,6-tetramethyl-1-piperidinyloxy
TFA	trifluoroacetic acid
THF	tetrahydrofuran
TLC	thin layer chromatography
UV	ultraviolet

6.2 List of Figures

Figure 1 The interaction between light and matter constitutes one of the most active areas of scientific research (Image with respect to Nobel Prize winners was taken from the official web site of the Nobel Prize with permission).....	1
Figure 2 Typical chiral organocatalysts and metal-based catalysts for asymmetric catalysis.	2
Figure 3 Fontecave's asymmetric oxidation with chiral-at-metal Ru(II) complex.....	3
Figure 4 Gladysz's asymmetric Michael addition with chiral-at-metal Co(III) Werner complex.	4
Figure 5 Chiral-at-metal iridium(III) complex catalyzed asymmetric transfer hydrogenation.	4
Figure 6 The proposed mechanistic model for asymmetric transfer hydrogenation with a chiral-at-metal iridium(III) complex.....	5
Figure 7 Chiral-at-metal iridium(III) complex catalyzed asymmetric Friedel-Crafts alkylation.	6
Figure 8 Asymmetric Brønsted base catalysis with chiral-at-metal Ir(III) complexes.	6
Figure 9 Traditional Lewis acid catalyst and the prospect of a chiral-only-at-metal complex.....	7
Figure 10 MacMillan's dual catalysis strategies for visible-light-induced asymmetric catalysis.....	8
Figure 11 Proposed mechanism for merging photoredox catalysis with asymmetric organocatalysis. PS, photosensitizer; SET, single electron transfer; EWG, electron withdrawing group. The chain mechanism is not shown here for simplification.	9
Figure 12 Luo's asymmetric α -photoalkylation of β -ketocarboxyls by primary amine catalysis.	10
Figure 13 Yoon's asymmetric Lewis acid catalyzed [2+2]-cycloaddition of α,β -unsaturated ketones <i>via</i> photoredox catalysis.	10
Figure 14 Yoon's proposed mechanism for asymmetric Lewis acid catalyzed [2+2]-cycloaddition <i>via</i> photoredox catalysis.	11
Figure 15 Yoon's dual Lewis acid/photoredox catalysis system for the enantioselective aminoalkylation of α,β -unsaturated carbonyl compounds.....	11
Figure 16 The proposed mechanism for Yoon's enantioselective addition of photogenerated α -amino radicals to Michael acceptors.	12
Figure 17 Knowles' asymmetric aza-pinacol cyclization by merged photoredox catalysis and chiral brønsted acid catalysis.....	13
Figure 18 Asymmetric iminium nucleophilic addition <i>via</i> sequential catalysis through photoinduced oxidation followed by asymmetric counterion binding catalysis with a chiral thiourea.	13
Figure 19 Rovis' asymmetric α -acylation of <i>N</i> -aryltetrahydroisoquinolines <i>via</i> N-heterocyclic carbene/photoredox combination.	14
Figure 20 Molander's asymmetric cross-coupling by photoredox/nickel dual catalysis.....	15
Figure 21 MacMillan and Fu's asymmetric decarboxylative cross-coupling <i>via</i> photoredox/nickel dual catalysis.	16
Figure 22 Bach's photoinduced asymmetric [2+2] intramolecular cycloaddition <i>via</i> energy transfer.	17
Figure 23 Melchiorre's stereoselective catalytic α -alkylation of aldehydes driven by photoactive electron donor-acceptor complex.	18
Figure 24 Melchiorre's enantioselective α -alkylation of cyclic ketones by means of photo-organocatalysis.....	19
Figure 25 MacMillan's enantioselective α -amination of aldehydes <i>via</i> a photoredox mechanism.....	20
Figure 26 Organic versus metal-templated (this study) bifunctional asymmetric enamine catalysts for	

enantioselective α -functionalizations of aldehydes.....	29
Figure 27 Metal-templated chiral-at-metal enamine/H-bonding catalysts.	30
Figure 28 Attempts toward the α -functionalizations of aldehydes with the newly developed metal-templated catalyst Λ - Ir1	33
Figure 29 Proposed enamine/H-bonding mechanism of the α -amination of aldehydes (blue) with azodicarboxylates (green) catalyzed by iridium complex Λ - Ir4	36
Figure 30 Structure of Λ - Ir4 (ORTEP drawing with 30% probability thermal ellipsoids). The iridium complex was crystallized as an iodide salt in its racemic form. The iodide counterions and the Δ -isomer are omitted from the unit cell for clarity.....	37
Figure 31 Catalyst design for the substitutionally labile yet configurationally stable chiral-at-metal iridium complex.	40
Figure 32 Initial design plan for directing asymmetric catalysis with metal-centered chirality.	41
Figure 33 <i>Rac</i> - Ir6 catalyzed Friedel-Crafts additions of indole to α,β -unsaturated 2-acyl pyrazoles.	42
Figure 34 Enantiomers of a substitutionally labile yet configurationally stable chiral-at-metal iridium(III) complex.....	43
Figure 35 Crystal structure of Δ - IrO . The hexafluorophosphate counteranion is omitted for clarity. ORTEP drawing with 50% probability thermal ellipsoids.	46
Figure 36 Chiral HPLC traces demonstrating the enantiopurity of synthesized Λ - IrO and Δ - IrO . HPLC conditions: Daicel Chiralcel IB, 250 \times 4.6 mm, flow rate = 0.5 ml/min, 0.1% aq. TFA with MeCN as eluent (20-43% in 60 min).....	47
Figure 37 Substrate design results in improved reaction efficiency.	47
Figure 38 Proposed model for the asymmetric induction in the transition state in which one face of the alkene is shielded by the C_2 -symmetrical catalyst.....	51
Figure 39 An intermediate crystal structure of α,β -unsaturated 2-acyl imidazole complexes with IrO . The hexafluorophosphate counteranion is omitted for clarity. ORTEP drawing with 50% probability thermal ellipsoids.	51
Figure 40 A series of asymmetric reactions were found to be catalyzed by Λ - IrO	53
Figure 41 Initial design plan for asymmetric photoredox catalysis with chiral-at-metal Λ - IrO	56
Figure 42 Initial experiments to the photoinduced reaction of α,β -unsaturated 2-acyl imidazole 7 with α -silylamine 22 catalyzed by Λ - IrO	57
Figure 43 New strategy for photoredox catalysis based on the enolate activation mode.	58
Figure 44 Substrate scope of the photoinduced enantioselective alkylation of 2-acyl imidazoles with acceptor substituted benzyl bromides and phenacyl bromides.....	63
Figure 45 Examples of the photoinduced enantioselective alkylation of 2-acyl imidazoles without acceptor substituted phenacyl bromides.	64
Figure 46 Comparison of the catalytic efficiency of Λ - IrO and Λ - IrS	64
Figure 47 Comparison of the structures of IrO and IrS . a,b) Distances between the quaternary carbon atoms of the <i>tert</i> -butyl groups and the nitrile carbons of the neighboring MeCN ligands in Δ - IrO and Λ - IrS . c) Superimposed structures of the cationic complexes of Λ - IrO and Λ - IrS . Λ - IrO was obtained by mirror imaging the previous crystal structure of Δ - IrO	65
Figure 48 Plausible mechanism for a combined photoredox and asymmetric catalysis. SET = single electron transfer, EWG = electron withdrawing group, PS = photosensitizer in form of enolate complex II	66
Figure 49 X-Ray crystal structures of the proposed Ir(III) intermediate complex I (the left one) and II	

(the right one). These compounds were crystallized as a racemic mixture, and only the Λ -enantiomer is shown here, as an ORTEP drawing with 30% probability ellipsoids.	67
Figure 50 Proposed model for the asymmetric induction of photoredox alkylation reactions.	67
Figure 51 Light-dark interval experiment for the reaction 24a + 25a \rightarrow 26a	70
Figure 52 ^1H NMR (300 MHz, in CDCl_3) spectra of 25a , 26a (both as reference) and the crude product from the light-dark interval experiment.	71
Figure 53 Luminescence quenching experiments. I_0 and I are respectively luminescence intensities in the absence and presence of the indicated concentrations of the electron deficient benzyl bromide 25a	72
Figure 54 Cyclic voltammetry. Cyclic voltammograms and differential pulse voltammograms of the catalyst IrS (0.25 mM) and the enolate iridium complex II (0.25 mM) in CH_2Cl_2 containing 0.1 M $n\text{Bu}_4\text{NBF}_4$	73
Figure 55 Absorption and emission properties of the catalyst IrS and the intermediate iridium enolate complex II . The complexes were measured as solutions in solvent MeOH/THF 4:1 (0.1 mM).	74
Figure 56 Investigation of the influence of bromide substrates on the optical absorption spectra of enolate complex II . Recorded in MeOH/THF 4:1 with enolate complex II at a concentration of 0.1 mM and an excess of substrate (0.2 M).	74
Figure 57 Mechanistical variations based on radical-radical recombination for the combined photoredox and asymmetric catalysis.	75
Figure 58 The redox required chemistry induced by visible-light-activated photoredox catalysis with chiral iridium complexes.	78
Figure 59 Substrate scope with 2-acyl imidazoles. ^a Higher catalyst loading to increase yield and enantioselectivity.	81
Figure 60 Some limitations of the substrate scope with respect to 2-acyl imidazoles.	82
Figure 61 Substrate scope with 2-acyl pyridines.	83
Figure 62 Some limitations of the substrate scope with respect to 2-acylpyridines.	84
Figure 63 Efforts to extend the coordinating auxiliary scope.	84
Figure 64 Putative mechanism for the visible light activated asymmetric catalysis. SET = single electron transfer, PS = photosensitizer in form of enolate intermediate II	86
Figure 65 ^1H NMR (300 MHz, in CD_2Cl_2) spectra of 30a , 31a , 32 (as references) and the crude product from the photolysis. Conversion was inferred by integration ratio (signals H^1 and H^3).	88
Figure 66 The effect of base for the photocatalytic trichloromethylation.	89
Figure 67 Plausible mechanism for explaining the suppressed bromination and exclusive formation of the trichloromethylated product in the presence of visible light.	91
Figure 68 Luminescence quenching experiments. I_0 and I = luminescence intensities in the absence and presence of the indicated concentrations of BrCCl_3 , respectively.	92
Figure 69 ^1H NMR (300 MHz, in CD_2Cl_2) spectra of reactions 1-3	94
Figure 70 Research plan for the visible-light-driven enantioselective perfluoroalkylation with single iridium photoredox catalyst.	97
Figure 71 Initial attempts for trifluoromethylation with different CF_3 electrophiles.	98
Figure 72 The undesired chlorination of 2-acyl imidazoles in the absence of light.	99
Figure 73 MacMillan's catalyst combination strategy for α -trifluoromethylation of aldehydes.	99
Figure 74 Attempts at extending the two catalysts into single catalyst system for perfluoroalkylation.	102

Figure 75 Crystal structure of Δ -IrS(<i>t</i> Bu). ORTEP drawing with 30% probability thermal ellipsoids. The counter ion is omitted.	104
Figure 76 Substrate scope with respect to 2-acyl imidazoles.	105
Figure 77 Substrate scope with respect to perfluoroalkyl iodides and perfluorobenzyl iodide.	106
Figure 78 Plausible mechanism for the photoactivated asymmetric perfluoroalkylation of 2-acyl imidazoles. The proposed mechanism involves the highlighted intermediate iridium(III) enolate complex II , which most likely serves as the active photosensitizer and the chiral reaction partner for the electron deficient radicals.	107
Figure 79 Research plan for catalytic enantioselective radical addition to acceptor substituted alkenes with chiral-at-metal complex.	111
Figure 80 Substrate scope with respect to different 2-acyl imidazoles.	114
Figure 81 Substrate scope regarding organotrifluoroborates.	115
Figure 82 Substrate scope with respect to 2-acyl pyrazoles.	116
Figure 83 Some limitations for the developed asymmetric photocatalytic Michael addition.	117
Figure 84 The effect of radical sources for the asymmetric photocatalytic Michael addition.	118
Figure 85 Proposed simplified mechanism without indicating possible chain transfer. SET = single electron transfer, PS = photosensitizer.	119
Figure 86 Evaluating the acceleration of the radical addition step by rhodium coordination.	120
Figure 87 The control experiments in the presence of oxygen.	122
Figure 88 ^1H NMR (300 MHz, in CDCl_3) spectra of 53h , 55p (as references) and the crude product from the photolysis. Yield and conversion was inferred by integration ratio.	123
Figure 89 Control experiments in a mixed deuterated solvent system.	123
Figure 90 ^1H NMR (300 MHz, in CDCl_3) spectra of illustrated compound (a) and (b).	124
Figure 91 UV/Vis-absorption spectra of the used photoredox catalysts, the Lewis acid catalyst RhS and a combination out of RhS and the 2-acyl imidazole substrate 53c . Measured as solutions in acetone/ H_2O 4:1 (0.05 mM). a.u. = absorbance units.	125
Figure 92 Stern-Volmer plots. I_0 and I are respective luminescence intensities in the absence and presence of the indicated concentrations of the corresponding quencher.	126
Figure 93 Emission spectra of the photoactive species. The photoactive species were measured as solutions in solvent acetone/ H_2O 4:1 (0.05 mM). a.u. = arbitrary unit.	126
Figure 94 Stern-Volmer plots in the presence and absence of RhS . I_0 = luminescence intensity in the absence of 4-MePhCH $_2$ BF $_3$ K. I = luminescence intensity in the presence of the indicated concentrations of 4-MePhCH $_2$ BF $_3$ K.	127
Figure 95 Absorbance of [Acr-Mes]ClO $_4$ (2 mM in acetone/ H_2O 4:1).	128
Figure 96 Absorption spectra of the photoactive reaction species. (in acetone/ H_2O 4:1, [Rh] = 0.1 mM, [Acr-Mes]ClO $_4$ = 0.05 mM for the corresponding solution).	129
Figure 97 An overview for this thesis: chiral-at-metal catalyst discoveries and their applications in the asymmetric non-photochemical and photoredox catalysis.	133
Figure 98 Enantioselective α -amination of aldehydes with metal-templated iridium complex.	134
Figure 99 Synthesis of the enantiomerically pure enamine/H-bonding catalysts Λ -Ir4 and Δ -Ir4.	134
Figure 100 Enantiomers of a substitutionally labile yet configurationally stable chiral-at-metal iridium(III) Lewis acid Λ -IrO and Δ -IrO.	135
Figure 101 Synthesis of enantiomerically pure Lewis acid complexes Λ -IrO and Δ -IrO.	135
Figure 102 Enantioselective Friedel-Crafts addition of indoles to α,β -unsaturated 2-acyl imidazoles	

catalyzed by Λ -IrO or Δ -IrO.....	136
Figure 103 Chiral iridium complexes for asymmetric photoredox catalysis. (S, substrate; I, intermediate; P*, enantioenriched product.).....	137
Figure 104 Visible-light-induced enantioselective alkylation of 2-acyl imidazoles with acceptor substituted benzyl bromides and phenacyl bromides.	138
Figure 105 Photocatalytic, asymmetric trichloromethylation of 2-acyl imidazoles and 2-acylpyridines.	139
Figure 106 Catalytic, enantioselective perfluoroalkylation through visible-light-activated photoredox catalysis with a chiral iridium complex.	140
Figure 107 Visible-light-activated enantioselective conjugate addition of alkyl radicals to alkenes.	141
Figure 108 Synthesis of the benzoxazole ligands. Benzoxazole 7b-2 , 7b and 7a were synthesized according to published procedures.	148
Figure 109 ^1H NMR spectra of 18a , (<i>S</i>)- 19a (both as reference) and the crude product for the catalysis reaction of entry 1 in Table 1. Area integration ratio = 1.86: 1.00 (conversion = $1.00/(1.86 + 1.00) \times 100\% = 35\%$).....	187
Figure 110 ^1H -NMR spectra of substrate-coordinated catalyst.	200
Figure 111 Partial ^1H -NMR spectra of substrate-coordinated catalyst.	200
Figure 112 ^1H NMR of Λ -IrO recorded in CD_2Cl_2 over 8 days.....	201
Figure 113 HPLC trace of the freshly prepared mixture Λ -IrO: Δ -IrO. Area integration = 99.5:0.5 (99.0% <i>ee</i>)	202
Figure 114 HPLC trace after 2 days in CH_2Cl_2 . Area integration = 99.5:0.5 (99.0% <i>ee</i>).....	202
Figure 115 HPLC trace after 4 days in CH_2Cl_2 . Area integration = 99.4:0.6 (98.8% <i>ee</i>).....	202
Figure 116 HPLC trace after 6 days in CH_2Cl_2 . Area integration = 99.5:0.5 (99.0% <i>ee</i>).....	203
Figure 117 HPLC trace after 8 days in CH_2Cl_2 . Area integration = 99.4:0.6 (98.8% <i>ee</i>).....	203
Figure 118 Synthesis of the 2-acyl imidazoles.	204
Figure 119 The output wavelength of the used 6 w blue LED (420 nm \pm 10 nm).	260
Figure 120 ^1H NMR (300 MHz, in CDCl_3) spectra of 55c , 55c' (as references) and the crude product from the photolysis.....	319
Figure 121 Absorbance of the ferrioxalate actinometer solution (0.15 M).	322
Figure 122 Absorbance of the reaction solution ($\text{RhS} = 0.4 \text{ mM}$, $[\text{Acr-Mes}]\text{ClO}_4 = 0.2 \text{ mM}$ in acetone/ H_2O (4:1)).	325
Figure 123 ^1H -NMR and ^{13}C -NMR spectrum of Λ -(<i>S</i>)- 7a	352
Figure 124 ^1H -NMR and ^{13}C -NMR spectrum of Λ -(<i>S</i>)- 7c	353
Figure 125 ^1H -NMR and ^{13}C -NMR spectrum of Λ -(<i>S</i>)- 7d	354
Figure 126 ^1H -NMR and ^{13}C -NMR spectrum of Δ -(<i>S</i>)- 7d	355
Figure 127 ^1H -NMR and ^{13}C -NMR spectrum of Λ -Ir1.	356
Figure 128 ^1H -NMR and ^{13}C -NMR spectrum of Λ -Ir2.	357
Figure 129 ^1H -NMR and ^{13}C -NMR spectrum of Λ -Ir3.	358
Figure 130 ^1H -NMR and ^{13}C -NMR spectrum of Λ -Ir4.	359
Figure 131 ^1H -NMR and ^{13}C -NMR spectrum of Λ -Ir5.	360
Figure 132 ^1H -NMR and ^{13}C -NMR spectrum of <i>rac</i> - 17	361
Figure 133 ^1H -NMR and ^{13}C -NMR spectrum of Λ -(<i>S</i>)- 18	362
Figure 134 ^1H -NMR and ^{13}C -NMR spectrum of Δ -(<i>S</i>)- 18	363
Figure 135 ^1H -NMR and ^{13}C -NMR spectrum of Λ -IrO.	364

Figure 136 ^1H -NMR and ^{13}C -NMR spectrum of racemic intermediate complex I	365
Figure 137 ^1H -NMR and ^{13}C -NMR spectrum of racemic intermediate enolate complex II	366
Figure 138 ^1H -NMR and ^{13}C -NMR spectrum of racemic intermediate complex I -(NPh).	367
Figure 139 ^1H -NMR and ^{13}C -NMR spectrum of racemic intermediate complex II -(NPh).....	368
Figure 140 ^1H -NMR and ^{13}C -NMR spectrum of dimer- IrS (<i>t</i> Bu).....	369
Figure 141 ^1H -NMR and ^{13}C -NMR spectrum of Λ -(<i>S</i>)- IrS (<i>t</i> Bu).....	370
Figure 142 ^1H -NMR and ^{13}C -NMR spectrum of Δ -(<i>S</i>)- IrS (<i>t</i> Bu).....	371
Figure 143 ^1H -NMR and ^{13}C -NMR spectrum of Λ - IrS (<i>t</i> Bu).....	372
Figure 144 ^1H -NMR and ^{13}C -NMR spectrum of intermediate I (RhS -Py).....	373
Figure 145 ^1H -NMR and ^{13}C -NMR spectrum of intermediate I (RhS -Im).	374
Figure 146 CD spectrum of complex Λ -(<i>S</i>)- 9a recorded in CH_3OH (0.2 mM).....	375
Figure 147 CD spectrum of complex Λ -(<i>S</i>)- 9b recorded in CH_3OH (0.2 mM).	375
Figure 148 CD spectrum of complex Λ -(<i>S</i>)- 9c recorded in CH_3OH (0.2 mM).....	376
Figure 149 CD spectra of complexes Λ -(<i>S</i>)- 9d and Δ -(<i>S</i>)- 9d recorded in CH_3OH (0.2 mM).....	376
Figure 150 CD spectrum of complex Λ -(<i>S</i>)- 9e recorded in CH_3OH (0.2 mM).....	377
Figure 151 CD spectrum of catalyst Λ - Ir1 recorded in CH_3OH (0.2 mM).....	377
Figure 152 CD spectrum of catalyst Λ - Ir2 recorded in CH_3OH (0.2 mM).....	378
Figure 153 CD spectrum of catalyst Λ - Ir3 recorded in CH_3OH (0.2 mM).....	378
Figure 154 CD spectra of catalyst Λ - Ir4 and Δ - Ir4 recorded in CH_3OH (0.2 mM).	379
Figure 155 CD spectrum of catalyst Λ - Ir5 recorded in CH_3OH (0.2 mM).....	379
Figure 156 CD spectrum of auxiliary complex Λ -(<i>S</i>)- 18 recorded in CH_3OH (0.2 mM).....	380
Figure 157 CD spectrum of auxiliary complex Δ -(<i>S</i>)- 18 recorded in CH_3OH (0.2 mM).....	380
Figure 158 CD spectra of complexes Λ - IrO and Δ - IrO recorded in CH_3OH (0.2 mM).	381
Figure 159 CD spectra of complexes Λ -(<i>S</i>)- IrS (<i>t</i> Bu) and Δ -(<i>S</i>)- IrS (<i>t</i> Bu) recorded in CH_3OH (0.2 mM).	382
Figure 160 CD spectra of complexes Λ - IrS (<i>t</i> Bu) and Δ - IrS (<i>t</i> Bu) recorded in CH_3OH (0.2 mM)....	382
Figure 161 HPLC traces of the reference <i>rac</i> - Ir4 , Λ - Ir4 , and Δ - Ir4 (all as their PF_6 salt). Integration of peak areas > 99% <i>ee</i> (Daicel Chiralpak IA, with a linear gradient of 30% to 60% B in 25 min, flow rate = 0.5 mL/min).	383
Figure 162 HPLC traces for the complex <i>rac</i> - IrO , Λ - IrO , Δ - IrO . Integration of peak areas > 100:1 e.r. (Daicel Chiralpak IB with a linear gradient of 20% to 43% B in 60 min, flow rate = 0.5 mL/min)..	384
Figure 163 Crystal structure of the racemic catalyst Λ/Δ - Ir4	385
Figure 164 Crystal structure of Δ - IrO	387
Figure 165 Crystal structure of intermediate complex I	389
Figure 166 Crystal structure of enolate complex II	391
Figure 167 Crystal structure of (<i>R</i>)- 31a	393
Figure 168 Crystal structure of Δ - IrS (<i>t</i> Bu).....	395
Figure 169 Crystal structure of (<i>R</i>)- 55k	397
Figure 170 Crystal structure of intermediate I (RhS -Py).....	399

6.3 List of Schemes

Scheme 1 Synthesis of secondary amine ligand (1).....	31
Scheme 2 Outline of the synthesis of the enantiomerically pure catalysts Λ - Ir1-5 and Δ - Ir4 . NaBArF ₂₄ = sodium tetrakis[(3,5-di-trifluoromethyl)phenyl]borate.	31
Scheme 3 Evaluation of Friedel-Crafts addition with <i>rac</i> - Ir7	42
Scheme 4 Synthesis of the enantiomerically pure complexes Λ - IrO and Δ - IrO	44
Scheme 5 The transformation of impure complexes derived from the auxiliary complex Λ -(<i>S</i>)- 5	46
Scheme 6 Evaluation of the catalytic activity of enolate complex II	68
Scheme 7 Trapping experiment with excess TEMPO.....	68
Scheme 8 Trapping experiment with catalytic amount of TEMPO.	69
Scheme 9 Trapping experiment with electron rich alkene.....	69
Scheme 10 Efforts towards removal of imidazole auxiliary.	85
Scheme 11 Control experiments for the comparison of the dark reaction and photoreaction.	87
Scheme 12 The effect of aerobic conditions for the photocatalytic trichloromethylation.	89
Scheme 13 The comparison of rates for the formation of 32 and 31a	90
Scheme 14 Evaluating the possible transformation of bromination product 32	90
Scheme 15 Trapping experiments with electron rich silyl enolether 39	93
Scheme 16 Trapping experiment with TEMPO.	93
Scheme 17 The model reaction for the quantum yield measurement.	93
Scheme 18 Asymmetric trifluoromethylation with Umemoto's reagent in the absence of light.	101
Scheme 19 Transformation of selected products.	118
Scheme 20 Radical trapping experiment with TEMPO.	121
Scheme 21 Photocatalytic coupling of TEMPO and allylic alkyl radical reported by Akita.	121
Scheme 22 The model reaction for the quantum yield measurement.	127
Scheme 23 Synthesis of cyclometalated Ir(III) μ -chloro-bridged dimers 8a-e	155
Scheme 24 Preparation of iridium precursor complexes Λ -(<i>S</i>)- 9a-e . The complexes Λ -(<i>S</i>)- 9b and Λ -(<i>S</i>)- 9e were synthesized according to published procedures.....	155
Scheme 25 Synthesis of enantiopure iridium catalysts Λ - Ir1-5 and Δ - Ir4	159
Scheme 26 Iridium-catalyzed asymmetric α -amination of aldehydes.....	165

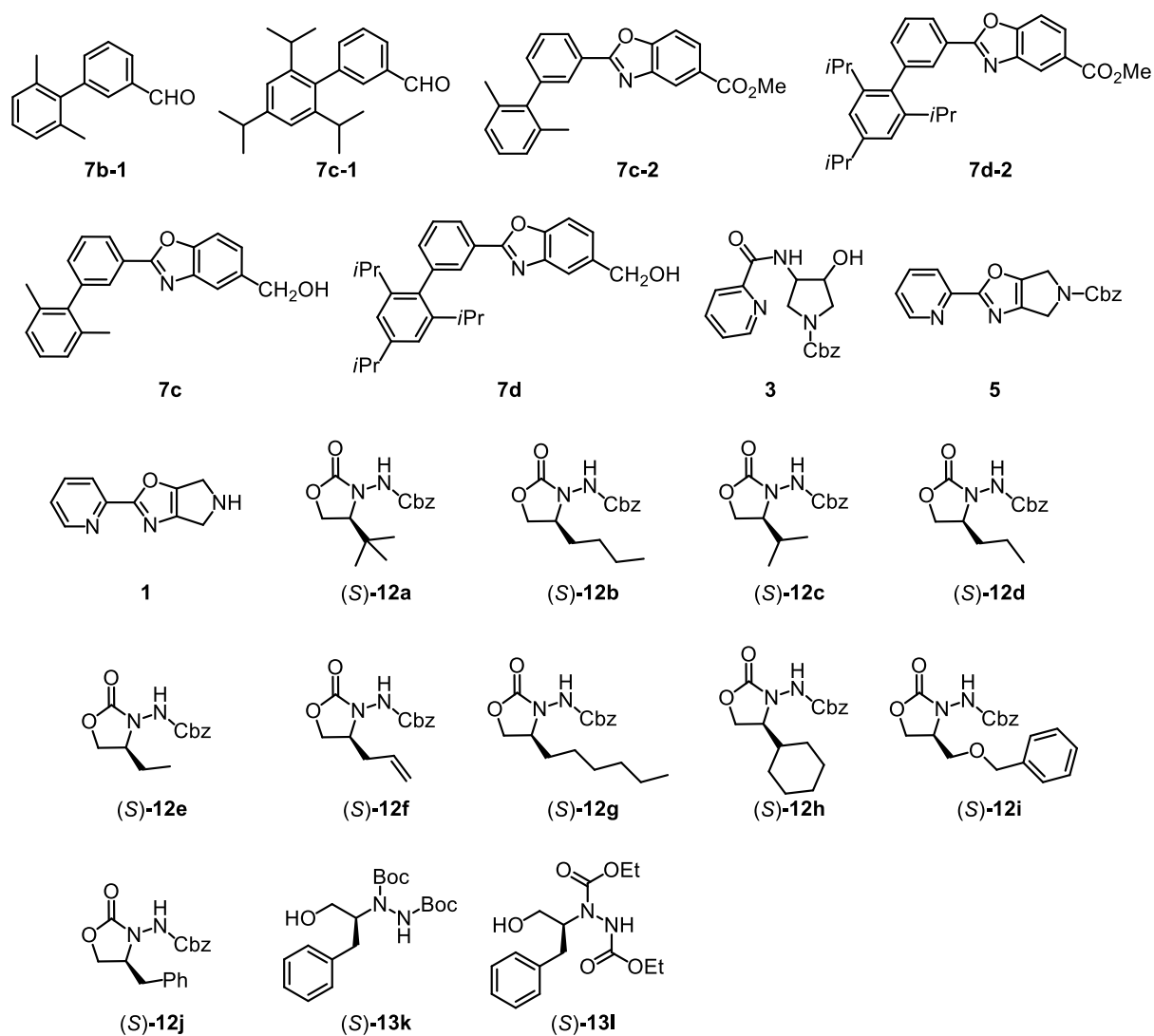
6.4 List of Tables

Table 1 Development of a chiral-at-metal iridium(III) catalyst for the enantioselective α -amination of aldehydes with azodicarboxylates	34
Table 2 Substrate scope of the enantioselective α -amination of aldehydes with iridium catalyst Λ - Ir4	35
Table 3 The optimization toward the synthesis of enantiopure catalyst Λ - IrO	45
Table 4 Enantioselective Friedel-Crafts addition of indole to α,β -unsaturated 2-acyl imidazole 18a catalyzed by Λ - IrO	48
Table 5 Enantioselective Friedel-Crafts addition of substituted indoles to α,β -unsaturated 2-acyl imidazole 18a catalyzed by Λ - IrO	49
Table 6 Enantioselective Friedel-Crafts addition of indole to α,β -unsaturated 2-acyl imidazoles 18b-g catalyzed by Λ - IrO or Δ - IrO	50
Table 7 Initial evaluation and optimization of the photoinduced enantioselective alkylation of acyl imidazole 24a with benzyl bromide 25a catalyzed by Λ - IrO or Λ - IrS	60
Table 8 Screening of different bases in the photoinduced alkylation reaction	61
Table 9 Initial experiments for the catalytic enantioselective α -trichloromethylation activated by visible light	80
Table 10 Initial experiments to identify an optimal catalyst/sensitizer combination	100
Table 11 Optimization of the visible-light-driven enantioselective perfluoroalkylation with single chiral iridium complex.	103
Table 12 Initial experiments to identify an optimal catalyst/sensitizer combination	112

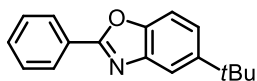
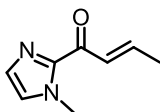
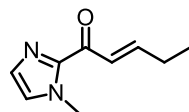
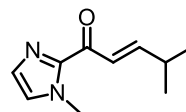
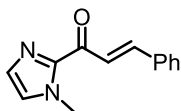
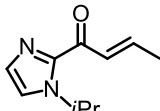
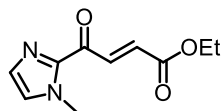
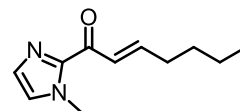
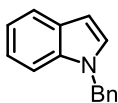
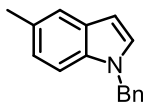
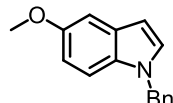
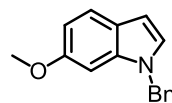
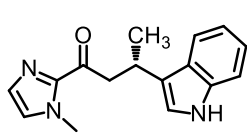
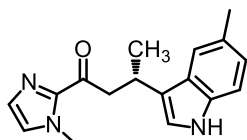
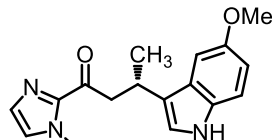
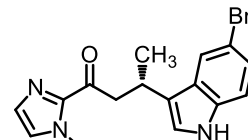
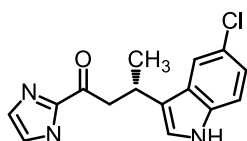
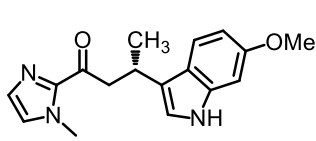
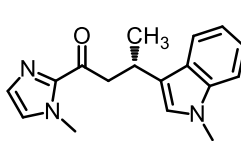
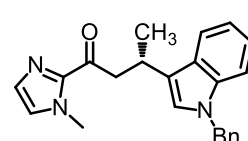
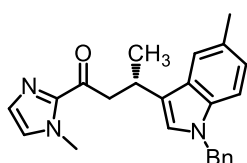
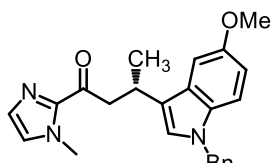
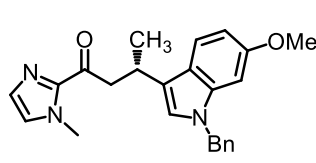
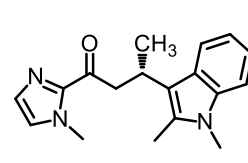
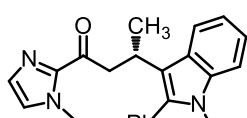
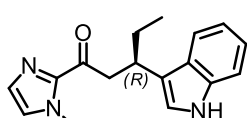
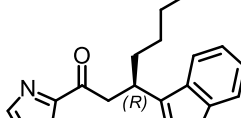
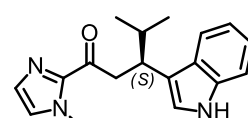
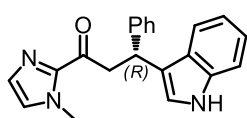
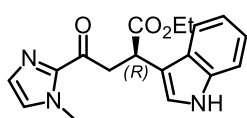
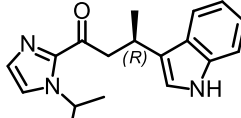
6.5 List of Synthesized Compounds

6.5.1 List of Organic Compounds

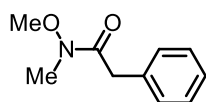
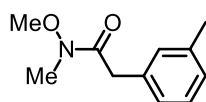
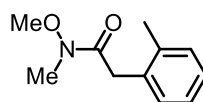
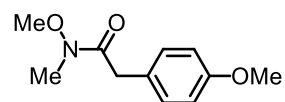
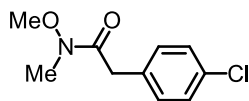
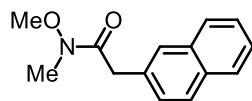
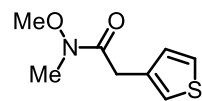
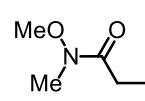
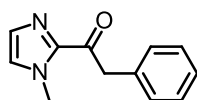
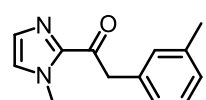
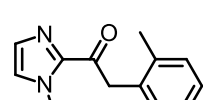
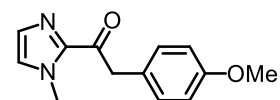
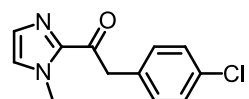
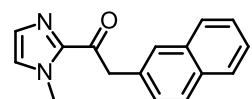
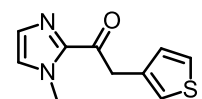
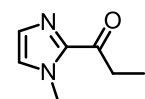
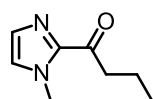
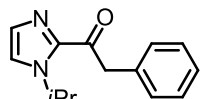
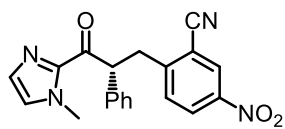
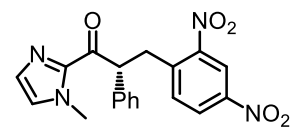
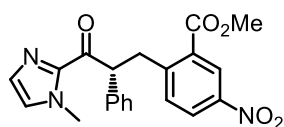
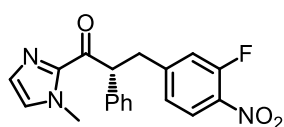
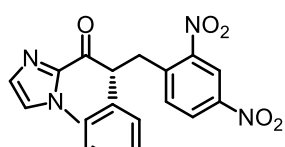
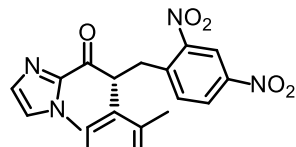
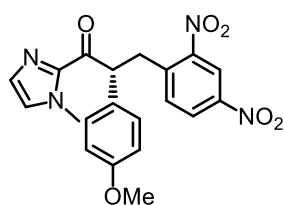
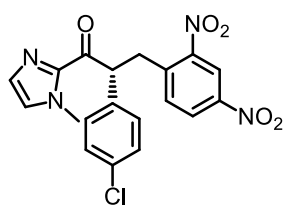
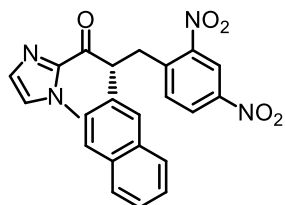
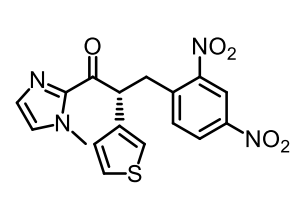
Chapter 3.1 and its experimental part Chapter 5.2:

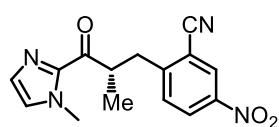


Chapter 3.2 and its experimental part Chapter 5.3:

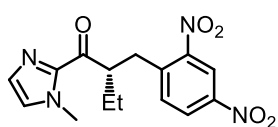
**16****18a****18b****18d****18e****18g****18f****18c****20h****20i****20j****20k****(S)-19a****(S)-19b****(S)-19c****(S)-19d****(S)-19e****(S)-19f****(S)-19g****(S)-19h****(S)-19i****(S)-19j****(S)-19k****(S)-19l****(S)-19m****(R)-21a****(R)-21b****(S)-21c****(R)-21d****(R)-21e****(R)-21f**

Chapter 3.3 and its experimental part Chapter 5.4:

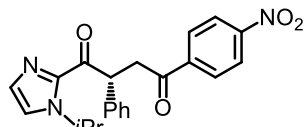
**24'a****24'b****24'c****24'd****24'e****24'f****24'g****24'h****24a****24b****24c****24d****24e****24f****24g****24h****24i****24j****(R)-26a****(R)-26b****(R)-26c****(R)-26d****(R)-26e****(R)-26f****(R)-26g****(R)-26h****(R)-26i****(R)-26j**



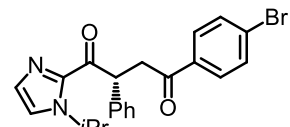
(S)-26k



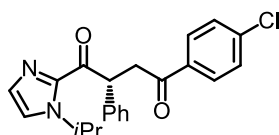
(S)-26l



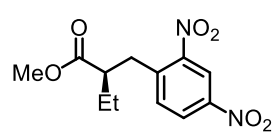
(R)-26m



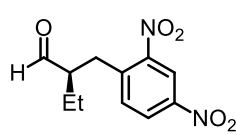
(R)-26n



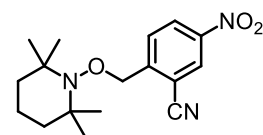
(R)-26o



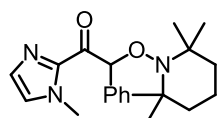
(R)-26l'



(R)-26l''



27

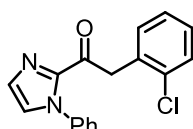


28

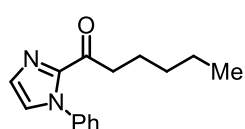


29

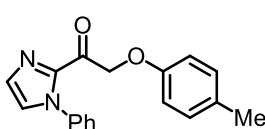
Chapter 3.4 and its experimental part Chapter 5.5:



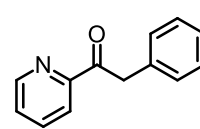
30f



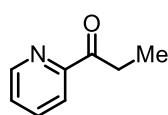
30l



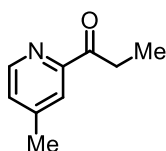
30i



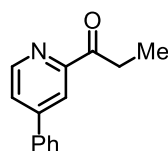
33a



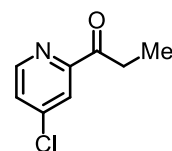
33b



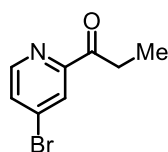
33c



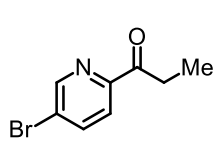
33d



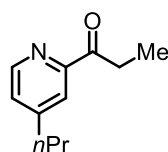
33e



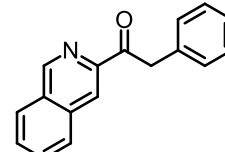
33f



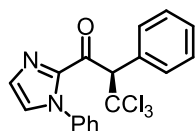
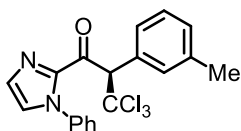
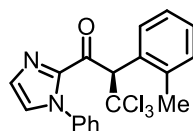
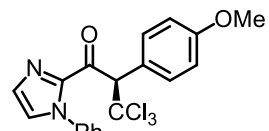
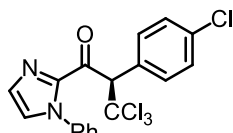
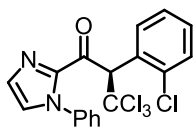
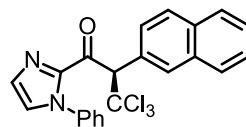
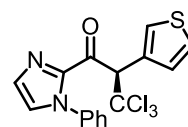
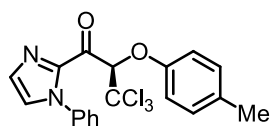
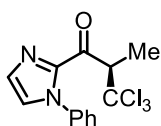
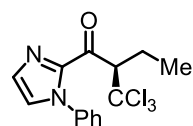
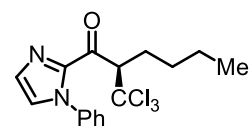
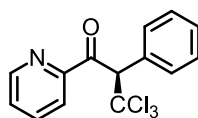
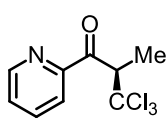
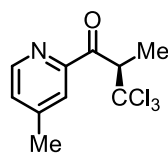
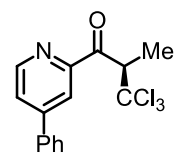
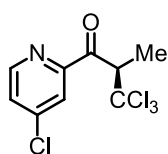
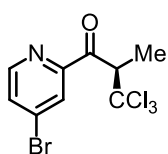
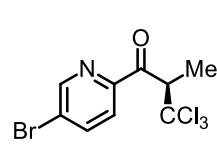
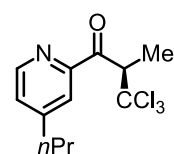
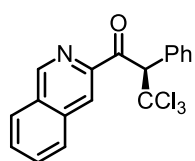
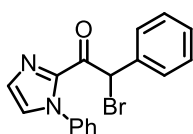
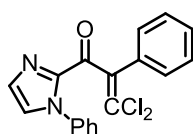
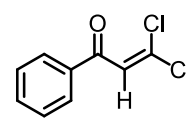
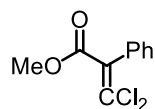
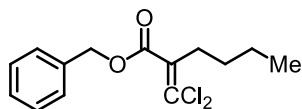
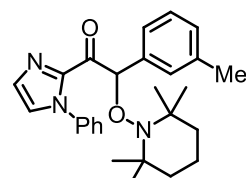
33g



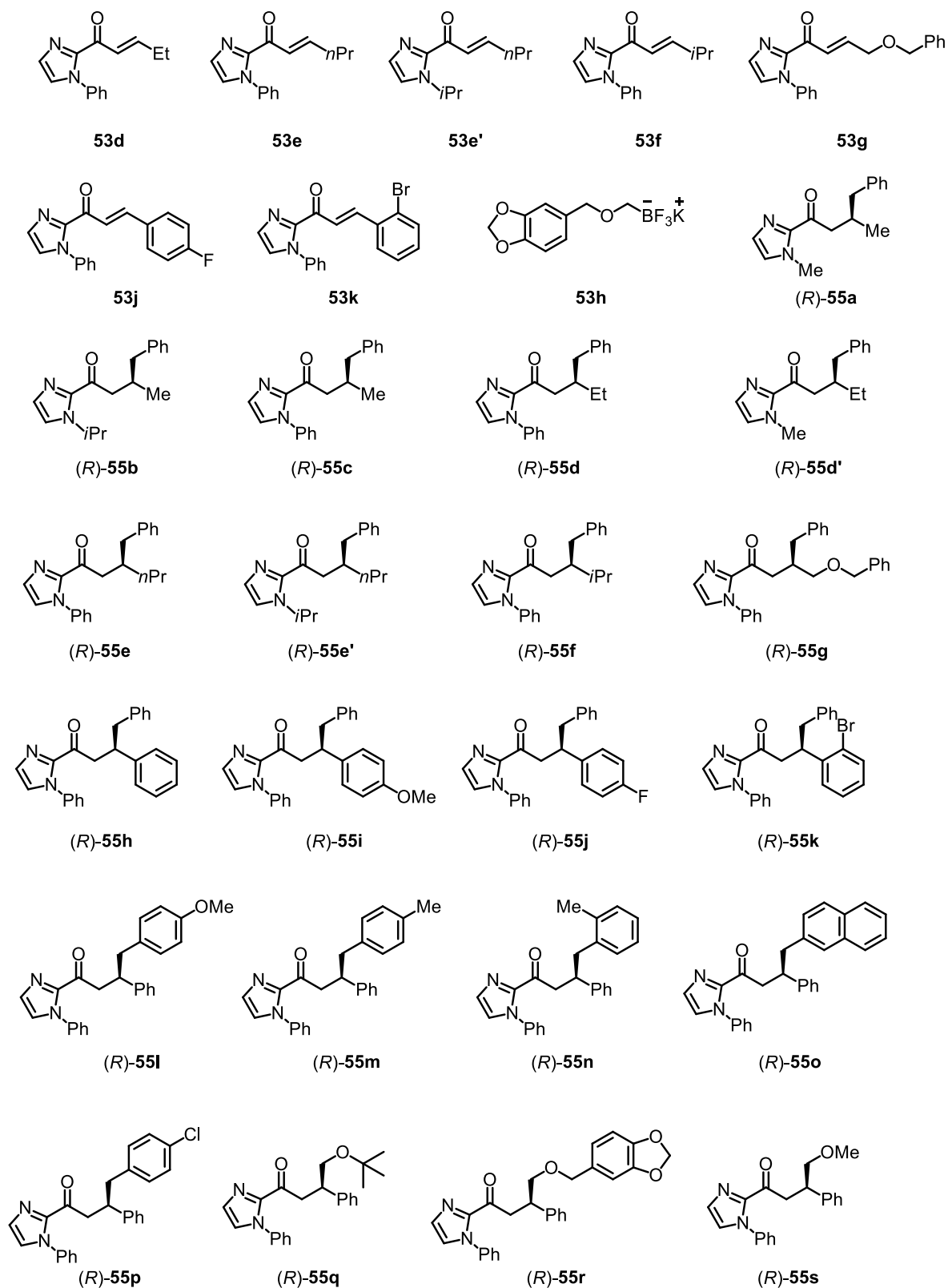
33h

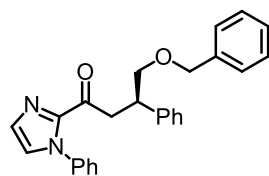
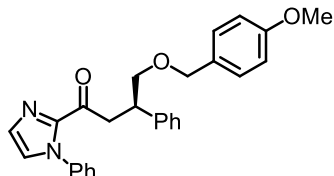
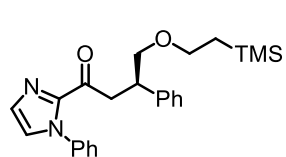
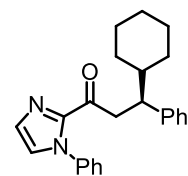
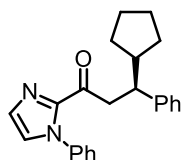
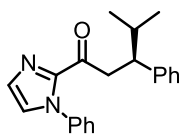
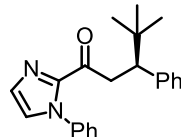
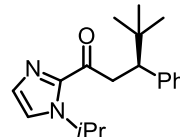
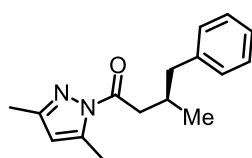
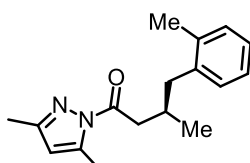
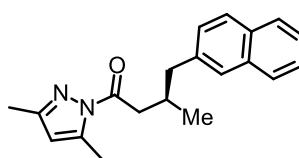
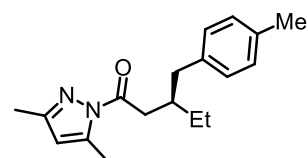
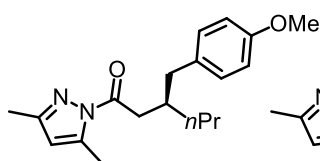
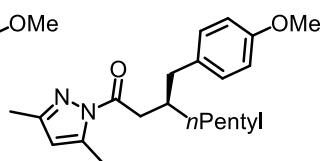
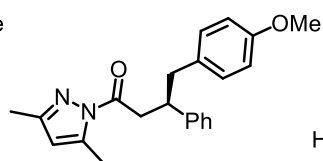
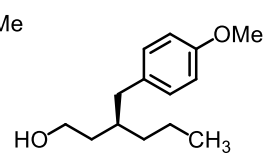
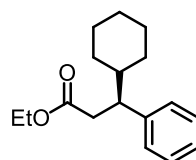
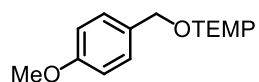


33i

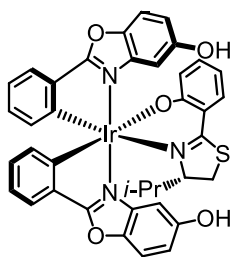
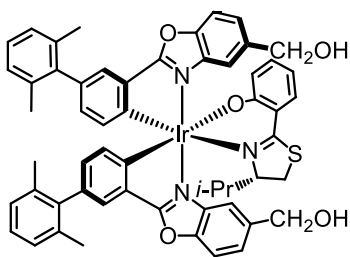
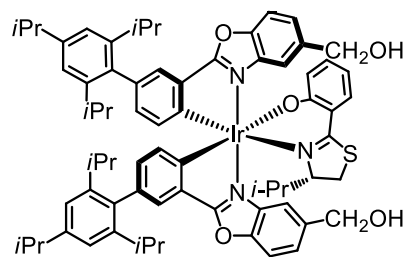
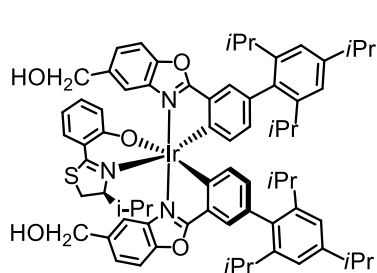
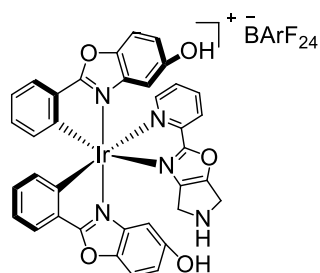
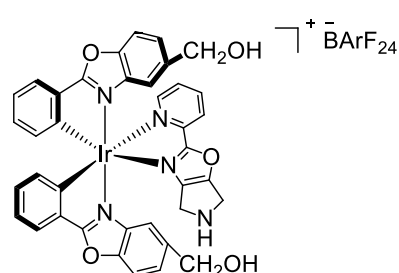
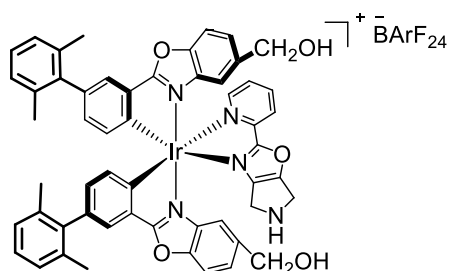
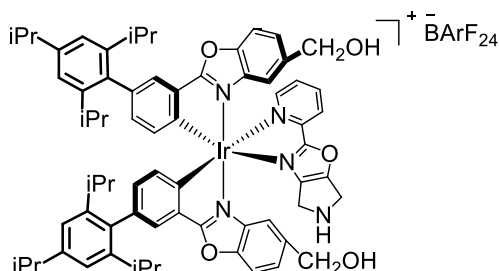
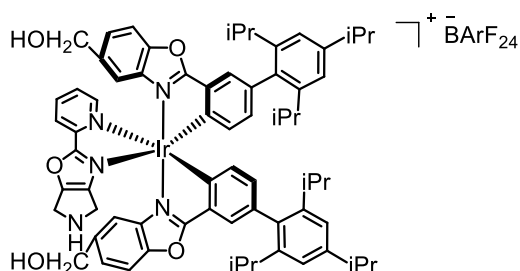
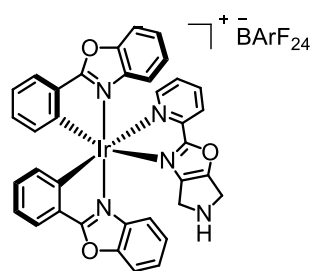
**(R)-31a****(R)-31b****(R)-31c****(R)-31d****(R)-31e****(R)-31f****(R)-31g****(R)-31h****(R)-31i****(R)-31j****(R)-31k****(R)-31l****(R)-34a****(R)-34b****(R)-34c****(R)-34d****(R)-34e****(R)-34f****(R)-34g****(R)-34h****(R)-34i****32****36****40****37****38****41**

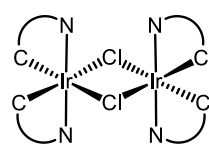
Chapter 3.6 and its experimental part Chapter 5.7:



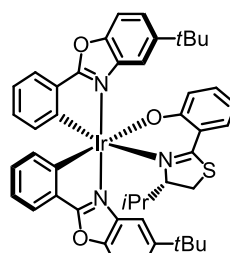
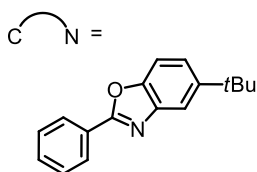
**(R)-55t****(R)-55u****(R)-55v****(S)-55w****(S)-55x****(S)-55y****(S)-55z****(S)-55z'****(R)-59a****(R)-59b****(R)-59c****(R)-59d****(R)-59e****(R)-59f****(R)-59g****(R)-59e'****(R)-55w'****61**

6.5.2 List of Iridium/Rhodium Complexes

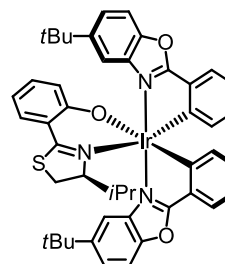
 Δ -(S)-9a Δ -(S)-9c Δ -(S)-9d Δ -(S)-9d Δ -Ir1 Δ -Ir2 Δ -Ir3 Δ -Ir4 Δ -Ir4 Δ -Ir5



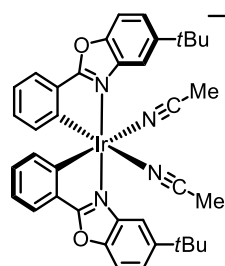
dimer-IrO



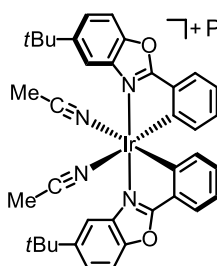
Δ-(S)-18



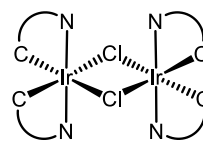
Δ-(S)-18



Δ-IrO

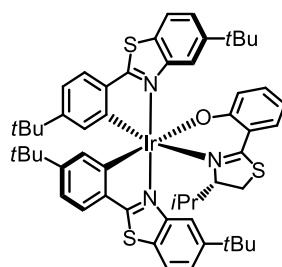
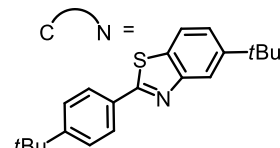


Δ-IrO

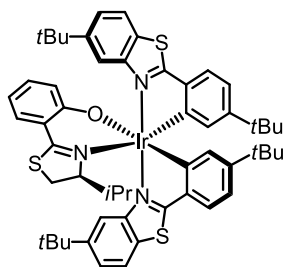


dimer-IrS(tBu)

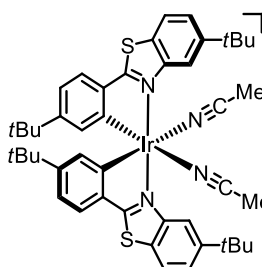
rac-17



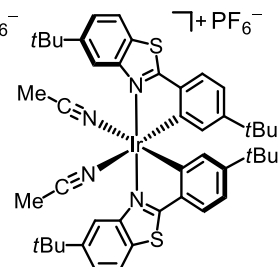
Δ-(S)-IrS(tBu)



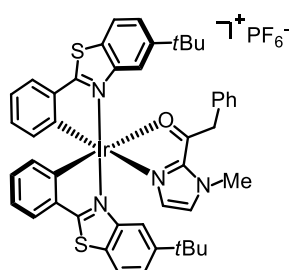
Δ-(S)-IrS(tBu)



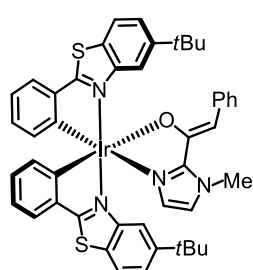
Δ-IrS(tBu)



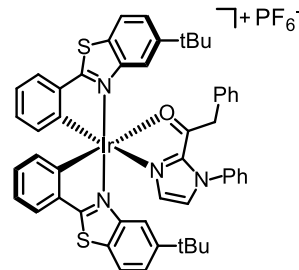
Δ-IrS(tBu)



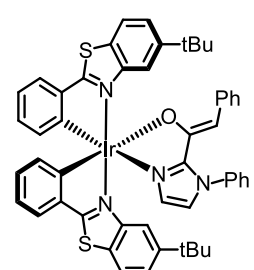
intermediate complex I-(NMe)



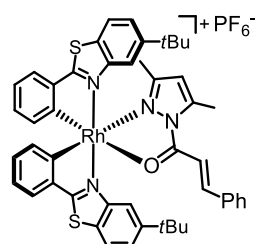
enolate complex II-(NMe)



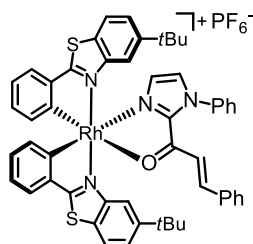
intermediate complex I-(NPh)



enolate complex II-(NPh)



intermediate I (RhS-Py)



intermediate I (RhS-Im)

6.6 List of Spectra of Iridium/Rhodium Complexes

6.6.1 NMR Spectra of Iridium/Rhodium Complexes

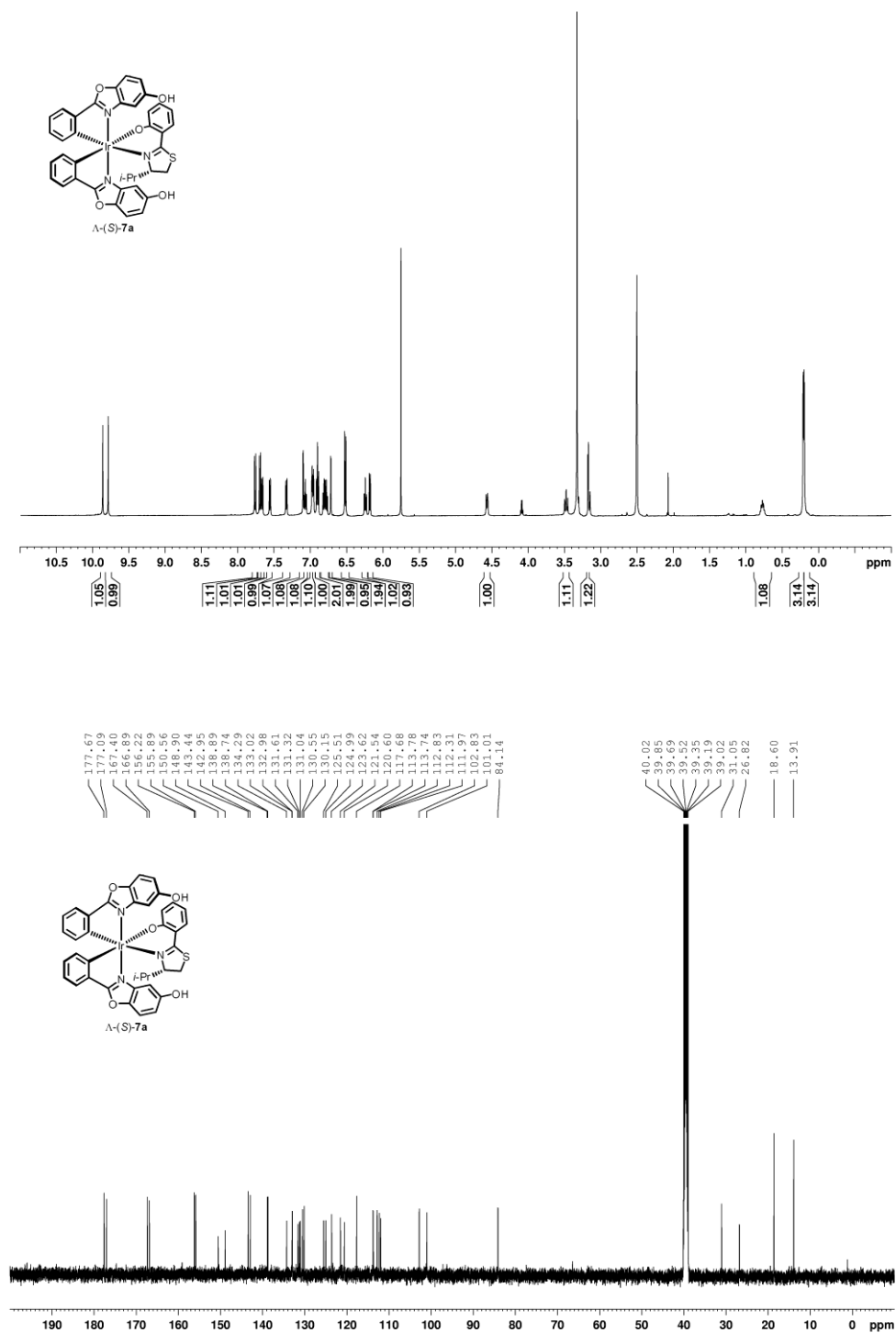


Figure 123 ^1H -NMR and ^{13}C -NMR spectrum of Λ -(S)-7a.

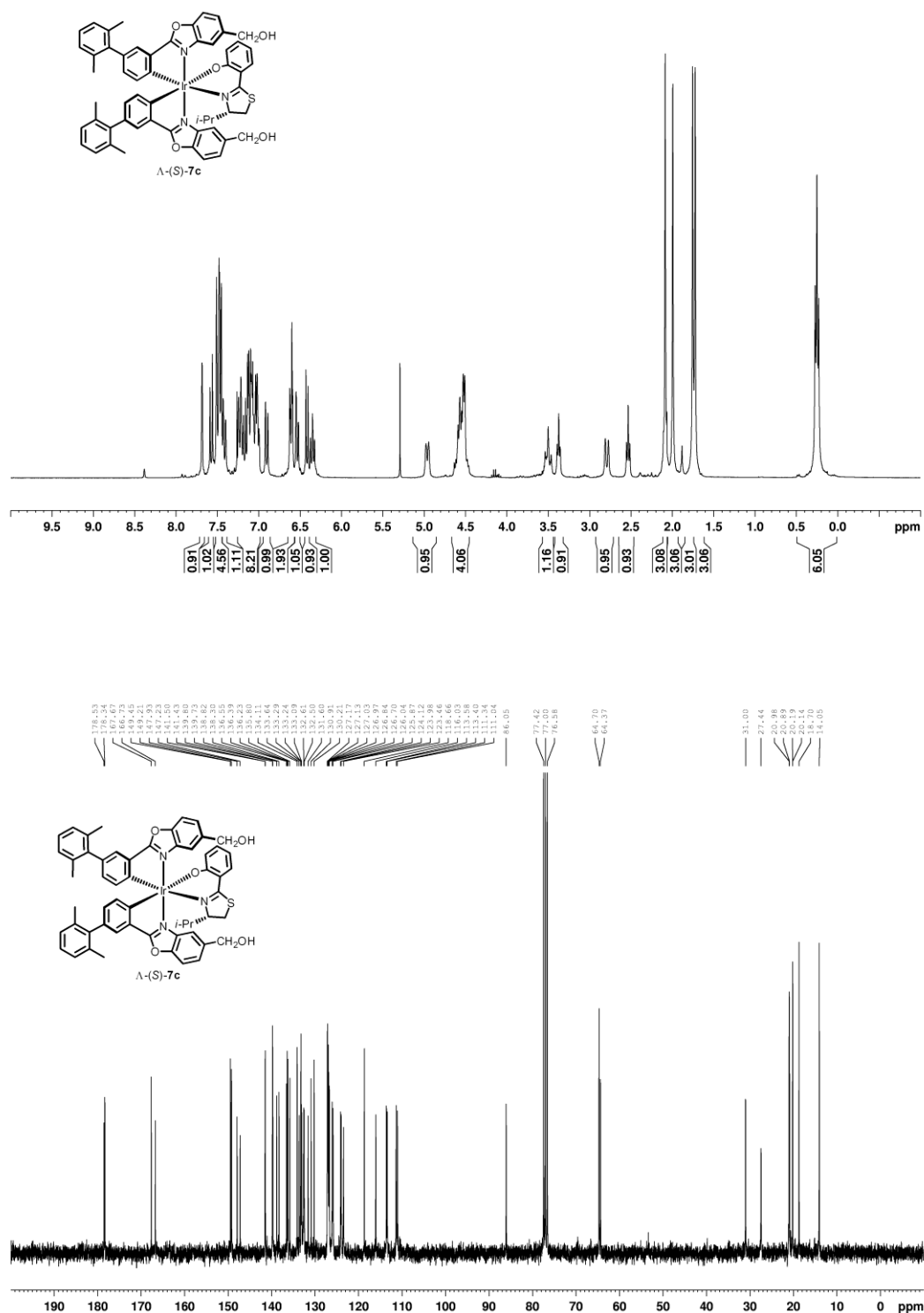
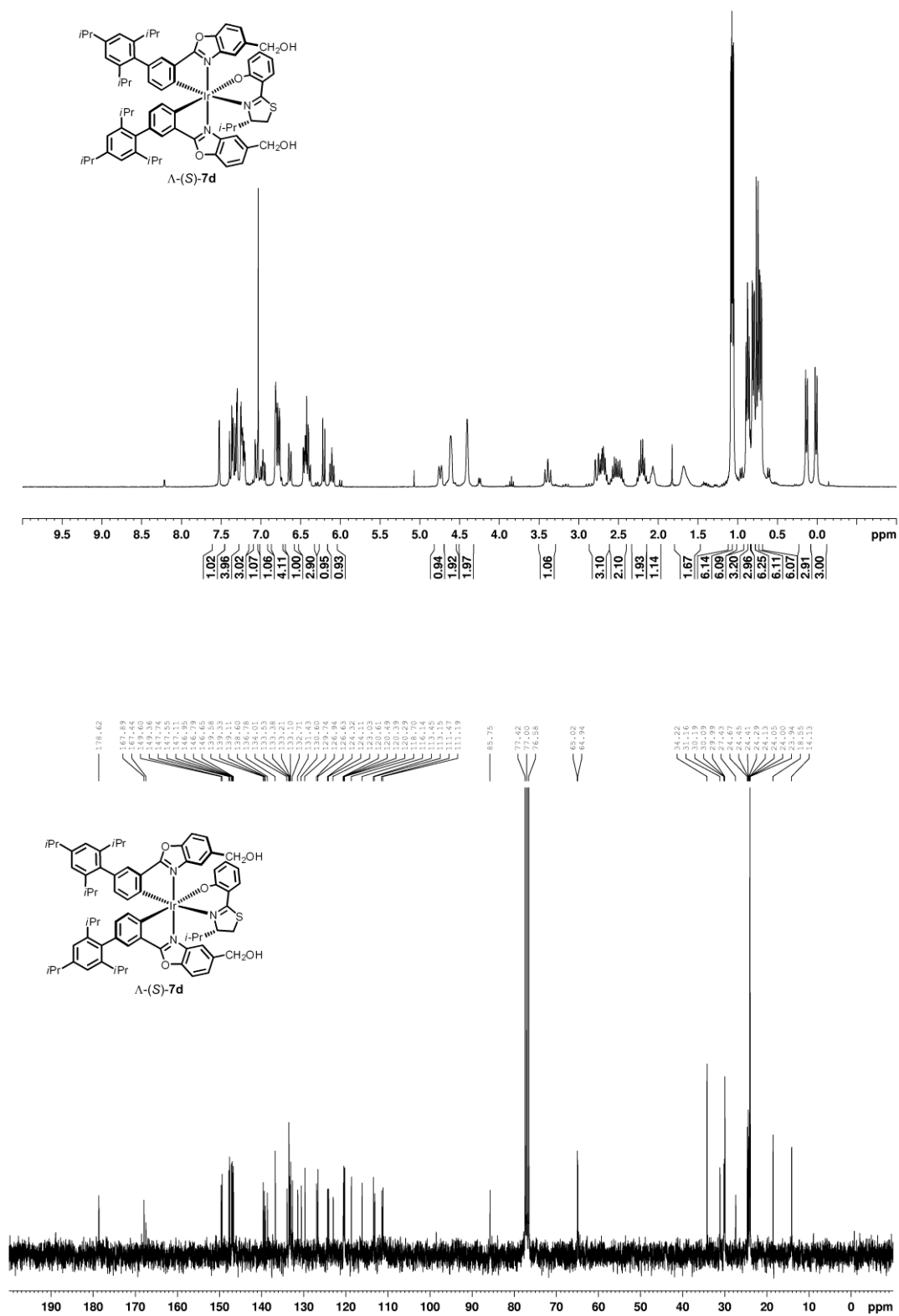
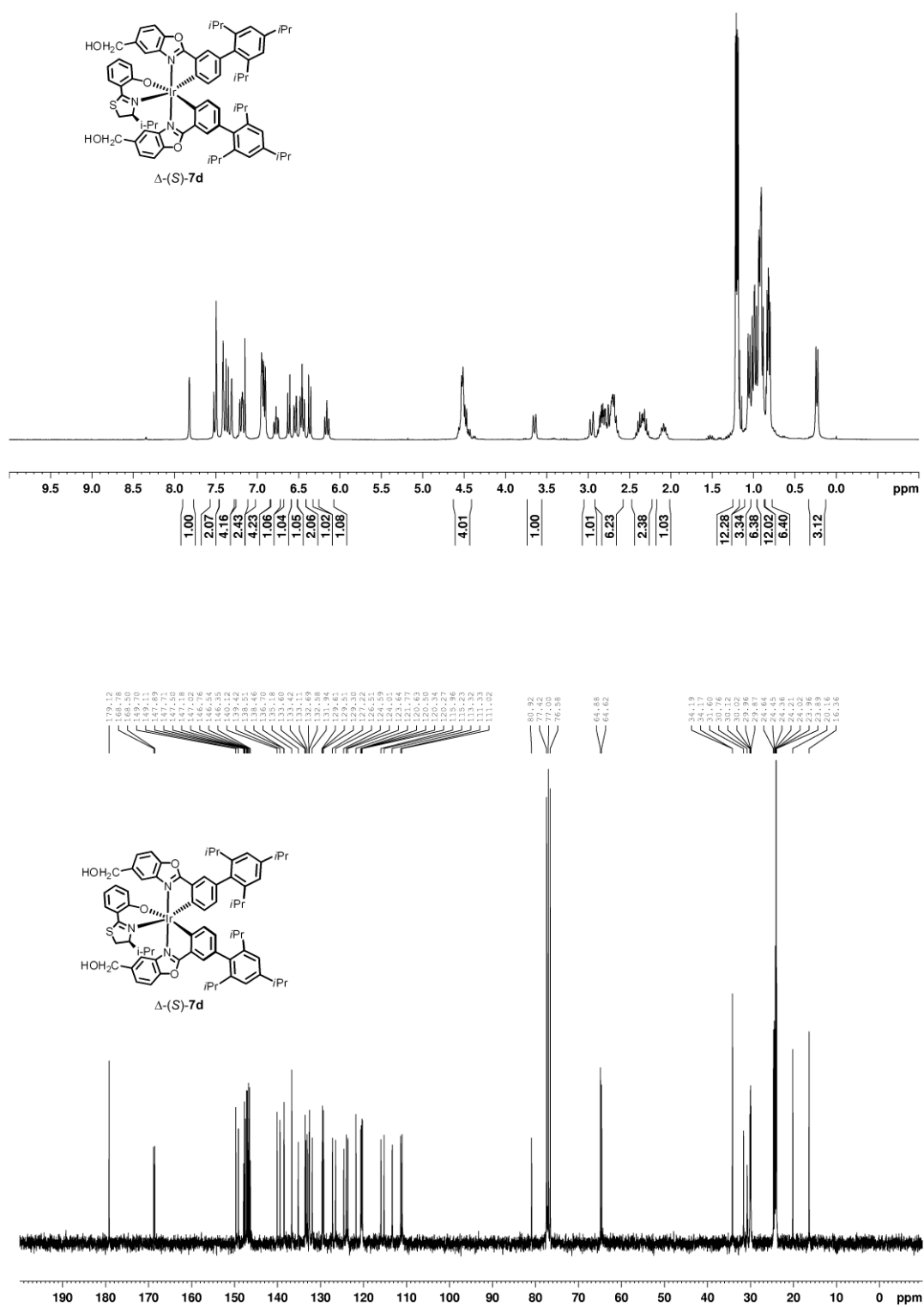
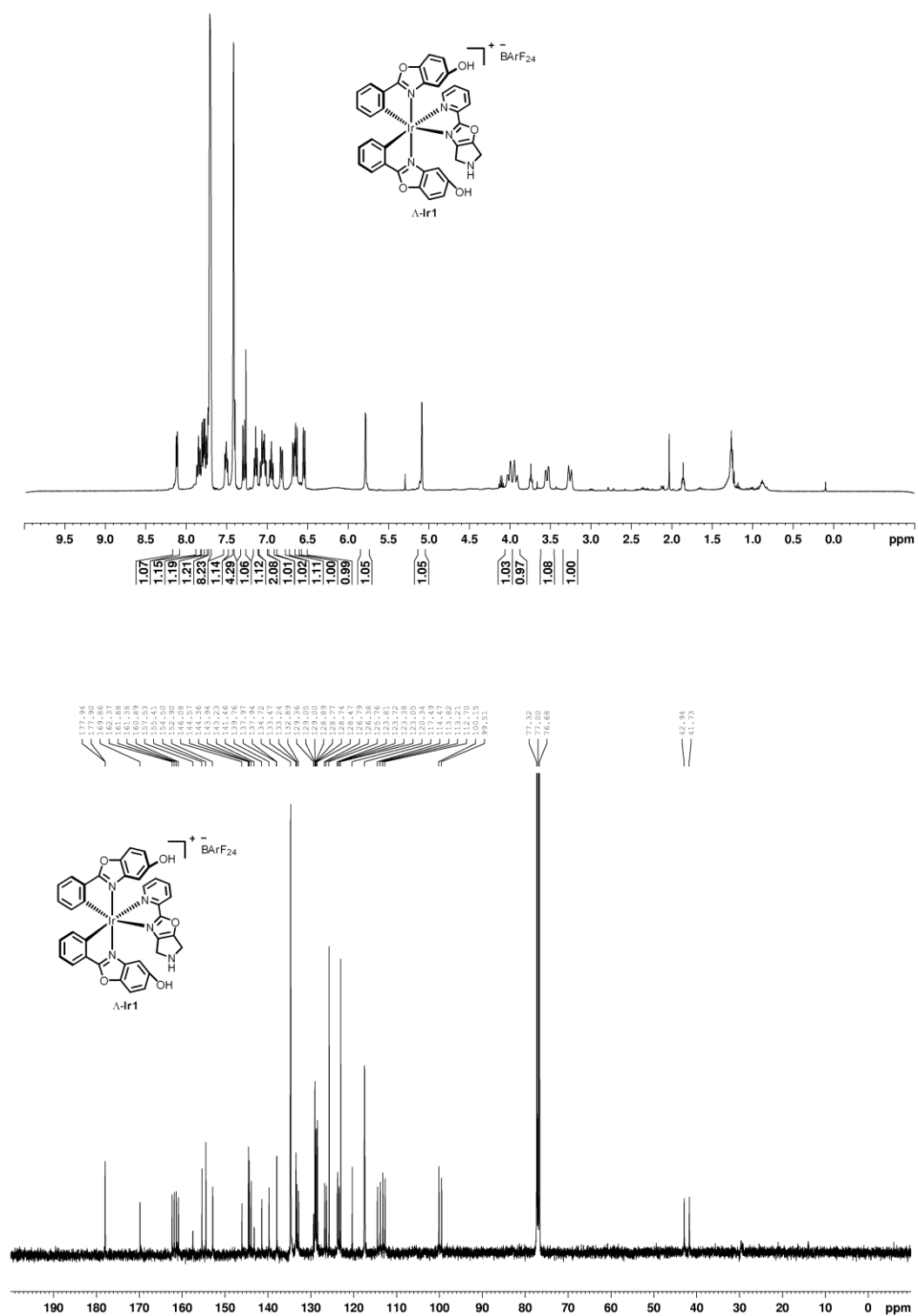


Figure 124 ^1H -NMR and ^{13}C -NMR spectrum of Λ -(S)-7c.

Figure 125 ^1H -NMR and ^{13}C -NMR spectrum of Λ -(S)-7d.

Figure 126 ^1H -NMR and ^{13}C -NMR spectrum of Δ -(S)-7d.

**Figure 127** ^1H -NMR and ^{13}C -NMR spectrum of Λ -Ir1.

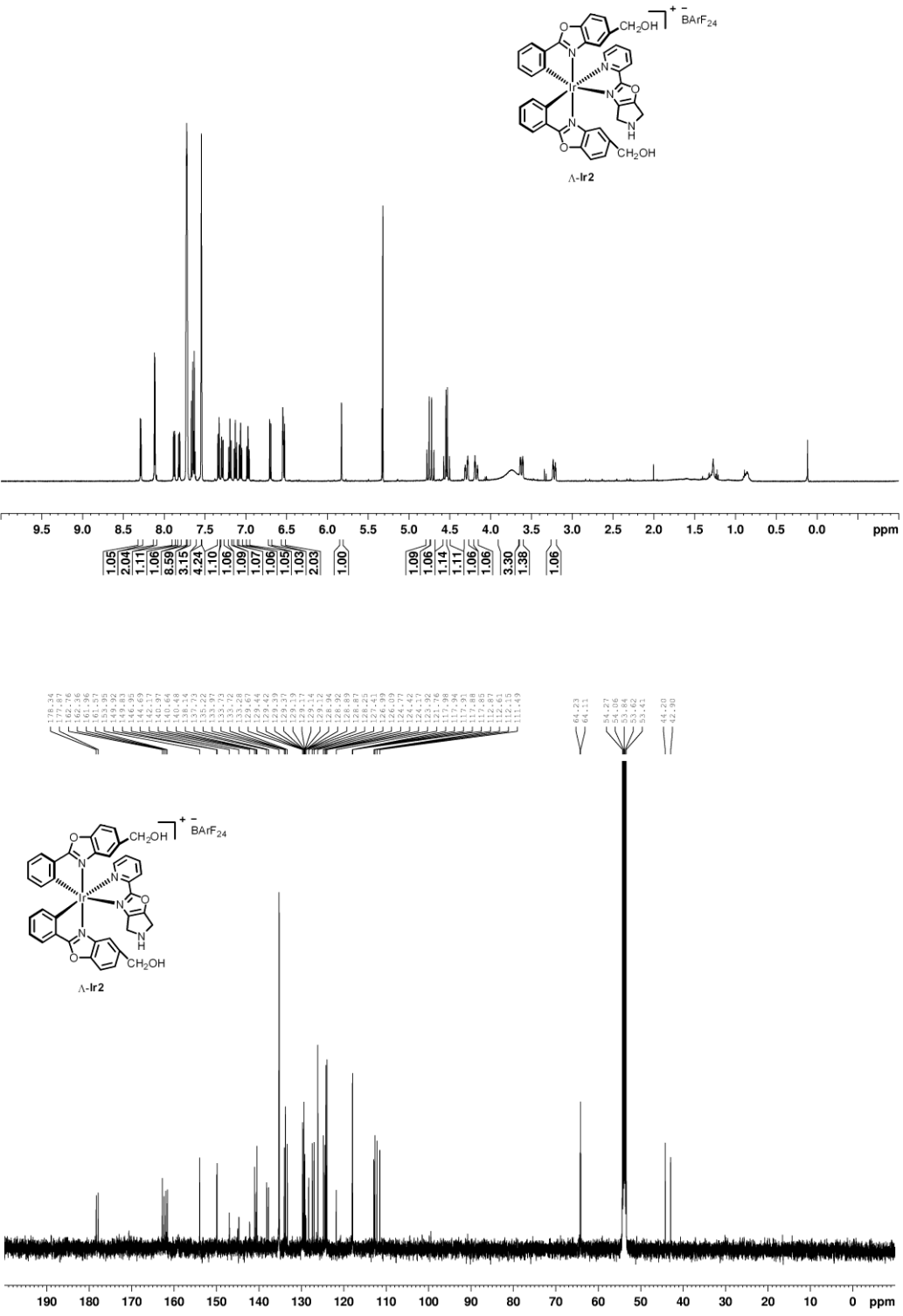
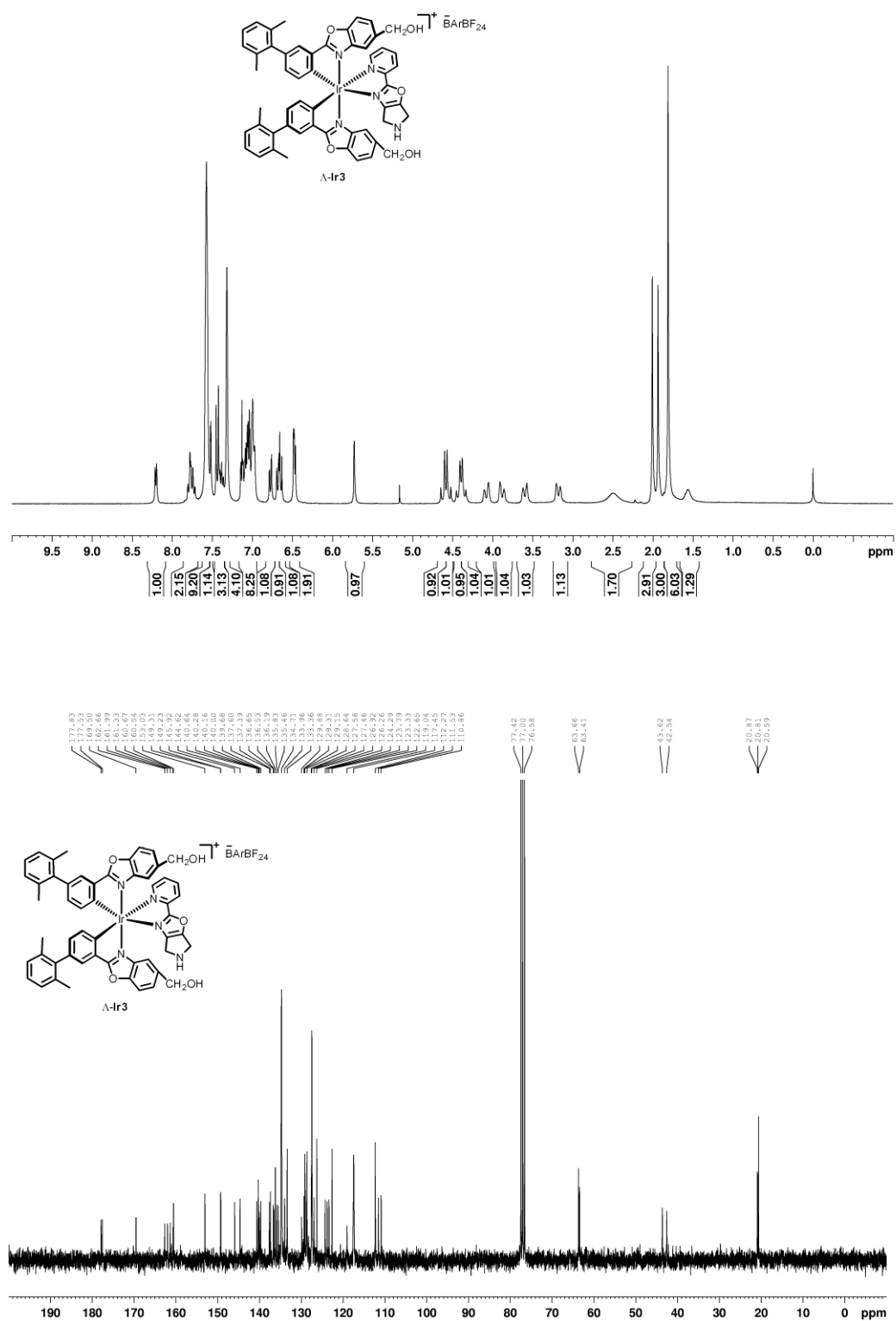
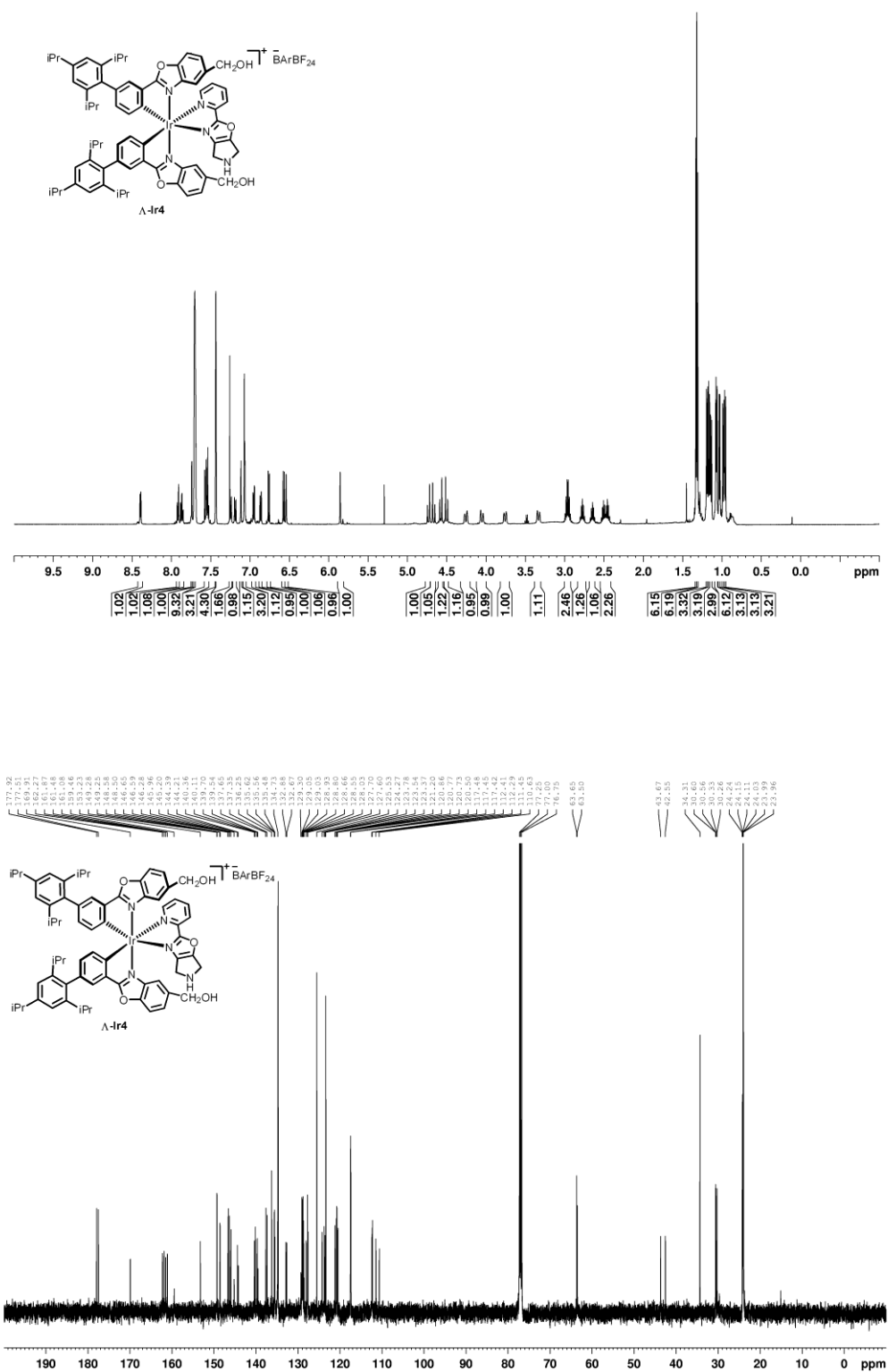
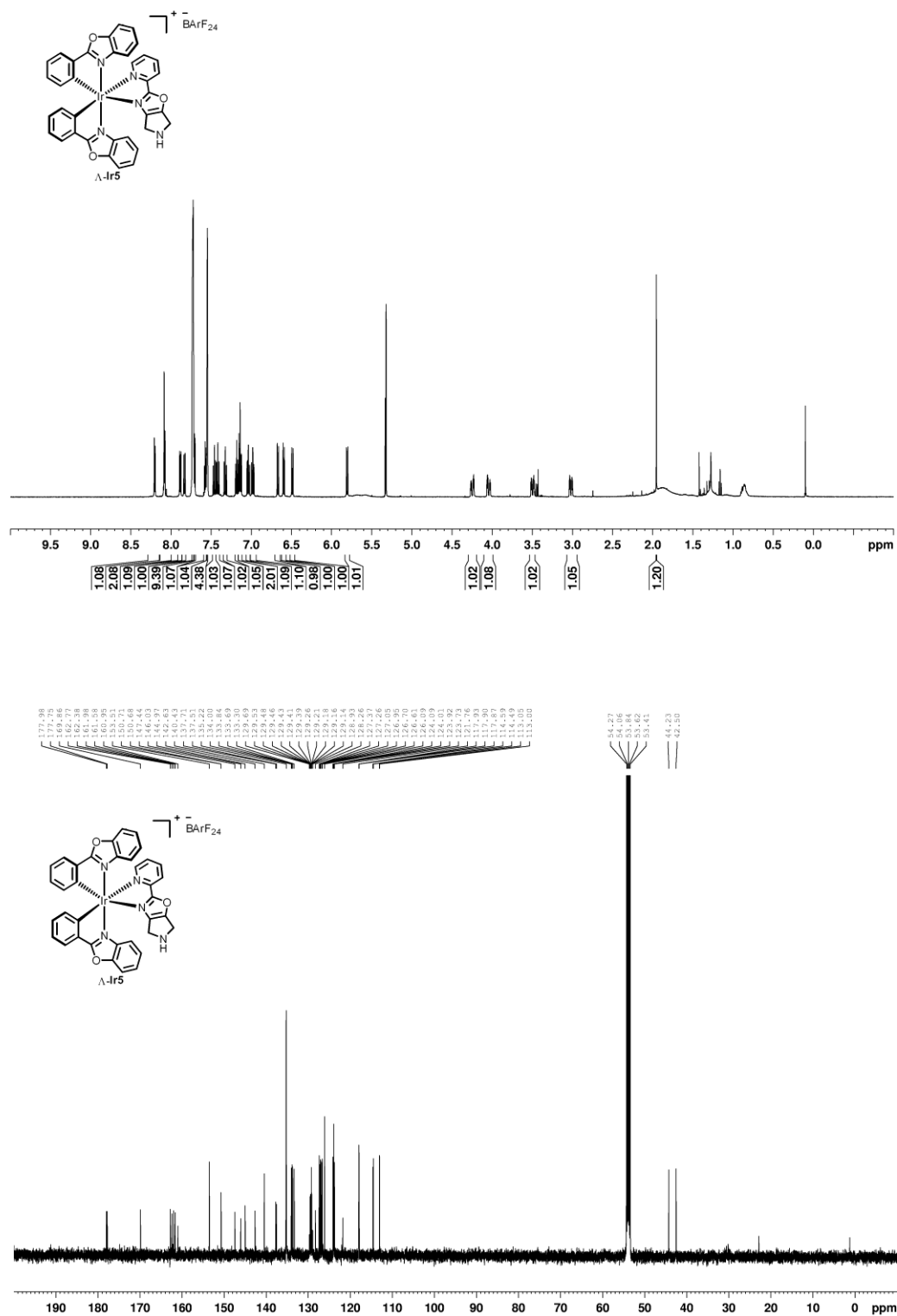
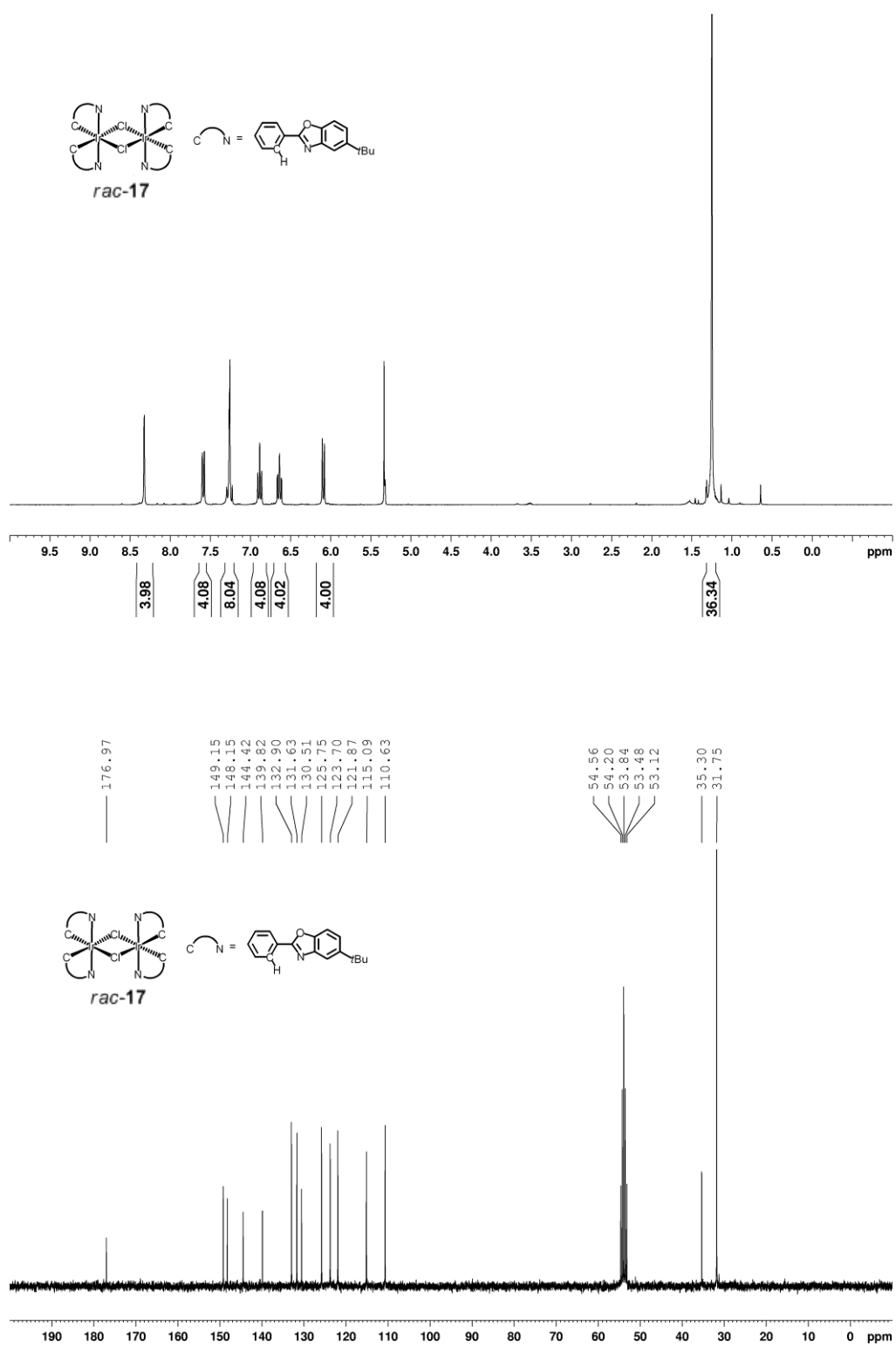


Figure 128 ^1H -NMR and ^{13}C -NMR spectrum of Λ -Ir2

Figure 129 ^1H -NMR and ^{13}C -NMR spectrum of Λ -Ir3.

**Figure 130** ^1H -NMR and ^{13}C -NMR spectrum of Λ -Ir4.

**Figure 131** ^1H -NMR and ^{13}C -NMR spectrum of Λ -Ir5.

Figure 132 ¹H-NMR and ¹³C-NMR spectrum of *rac-17*

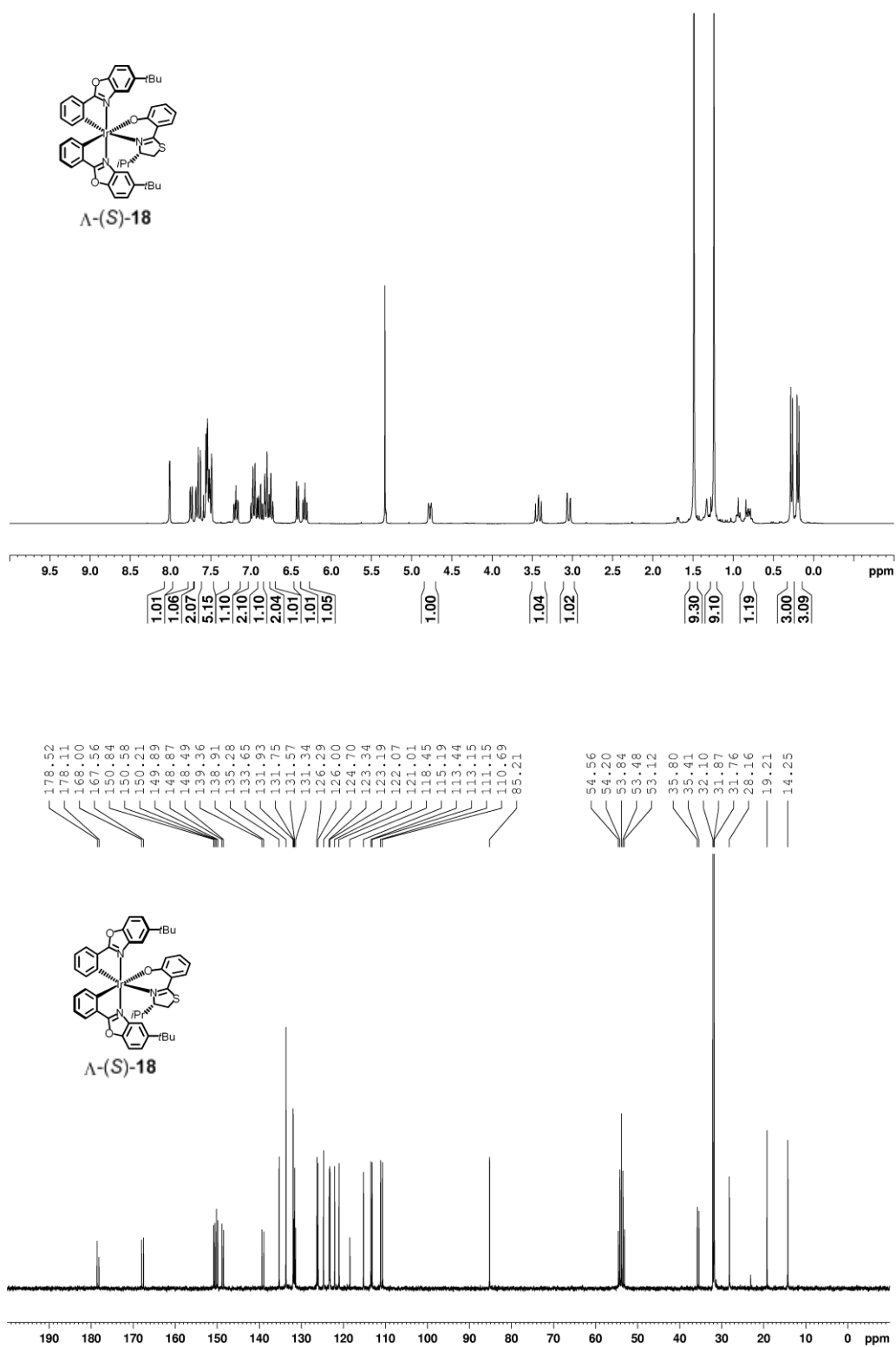


Figure 133 ^1H -NMR and ^{13}C -NMR spectrum of Λ -(S)-18.

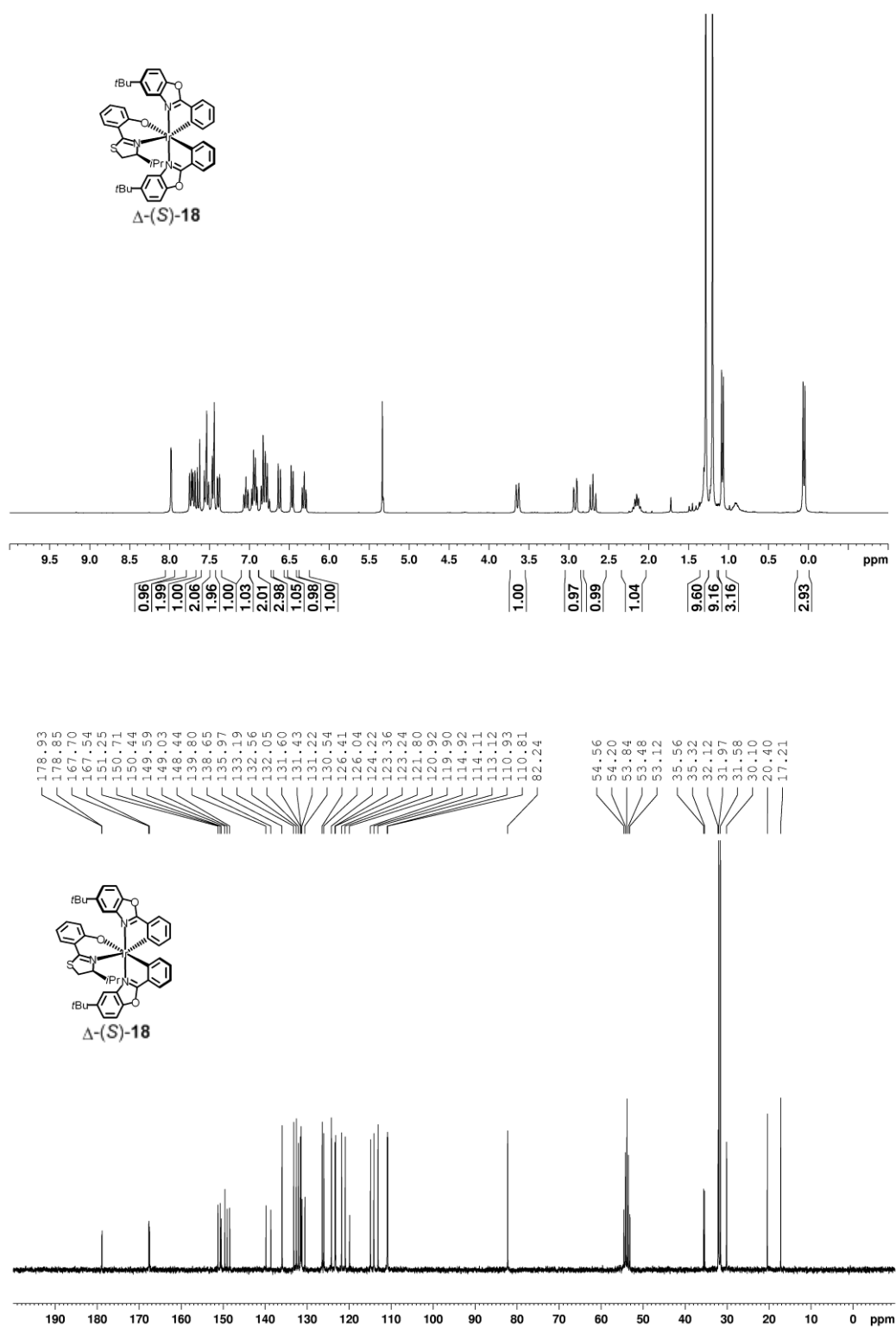


Figure 134 ^1H -NMR and ^{13}C -NMR spectrum of Δ -(S)-18.

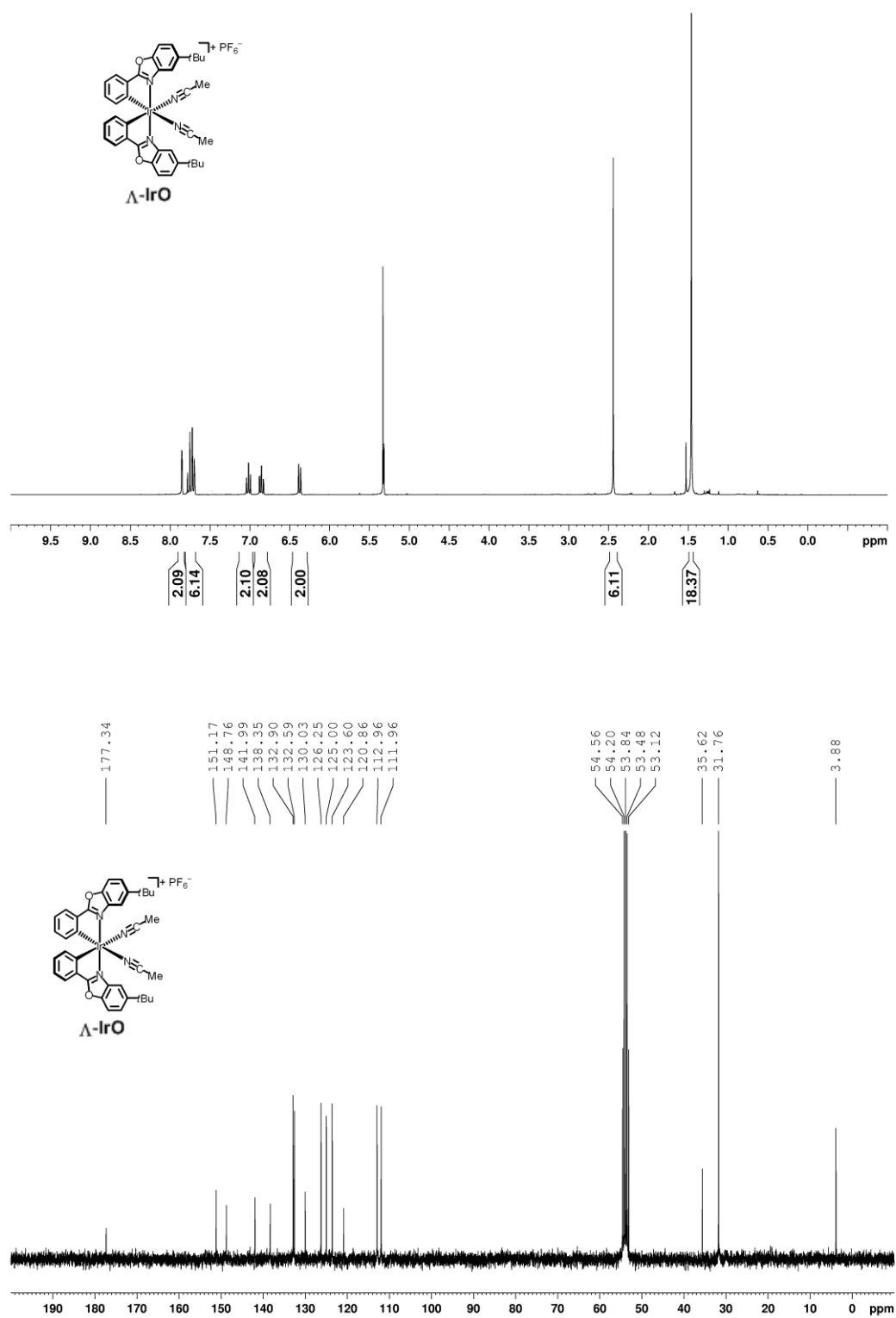


Figure 135 ^1H -NMR and ^{13}C -NMR spectrum of Λ -IrO.

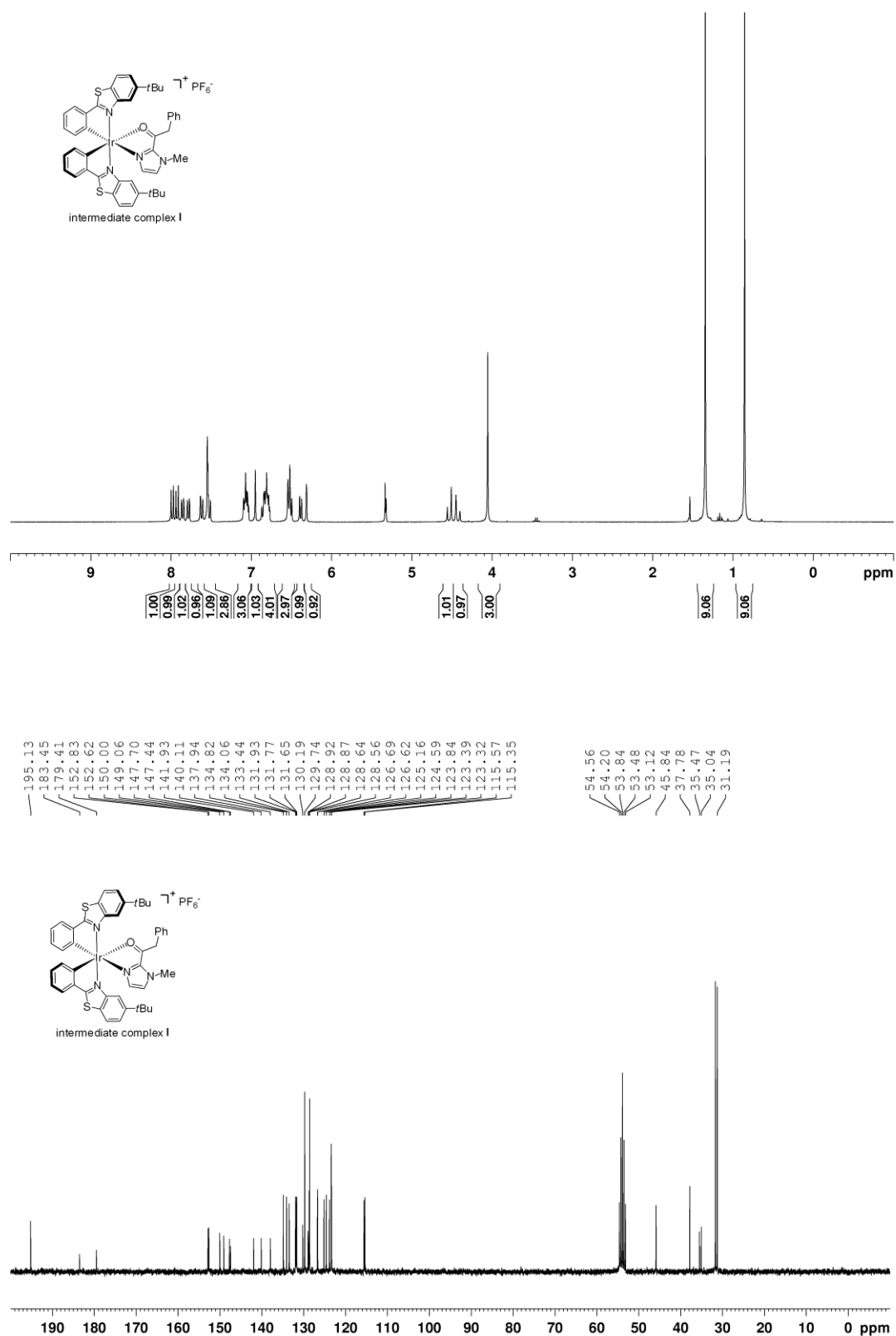


Figure 136 ¹H-NMR and ¹³C-NMR spectrum of racemic intermediate complex **I**.

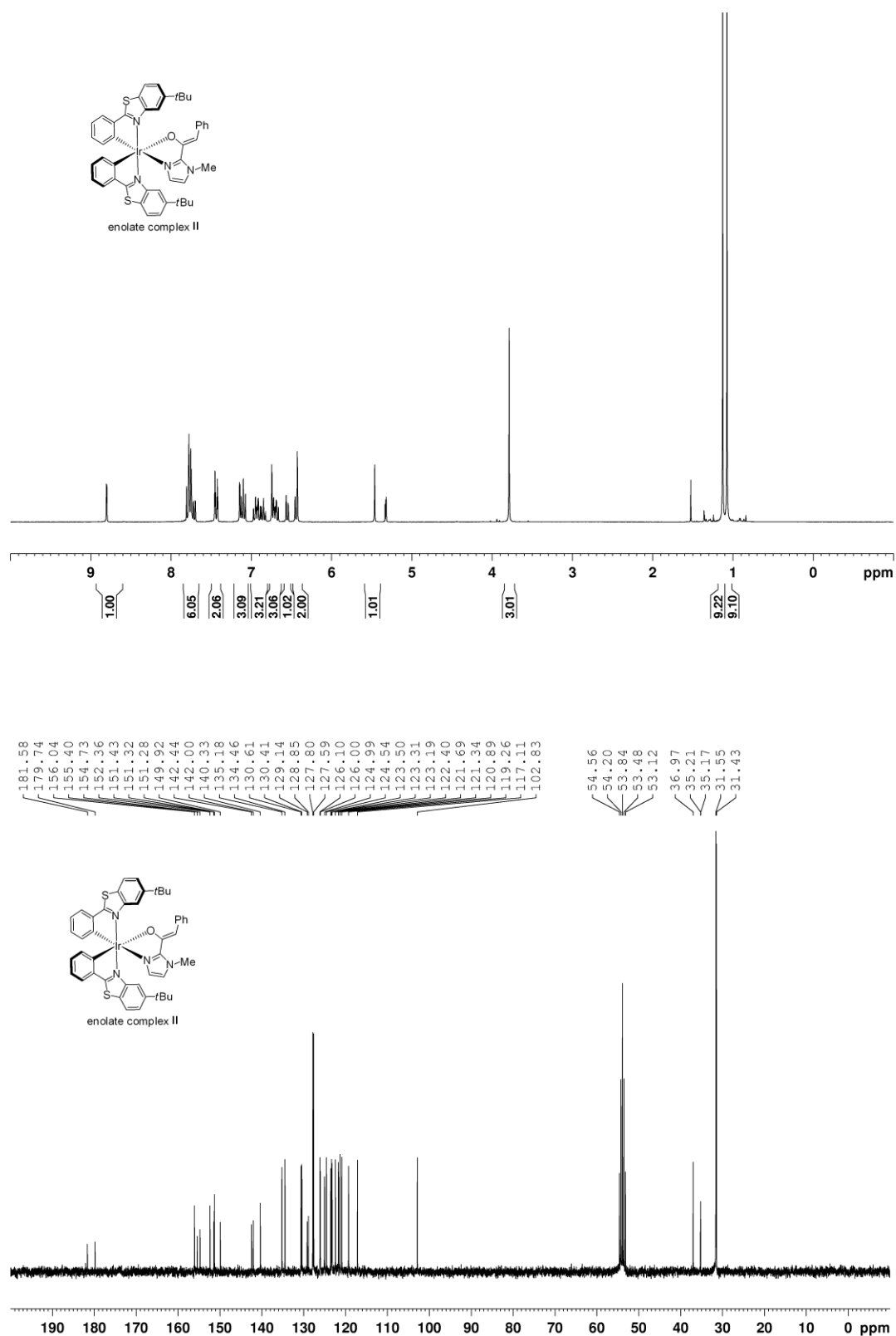


Figure 137 ^1H -NMR and ^{13}C -NMR spectrum of racemic intermediate enolate complex II.

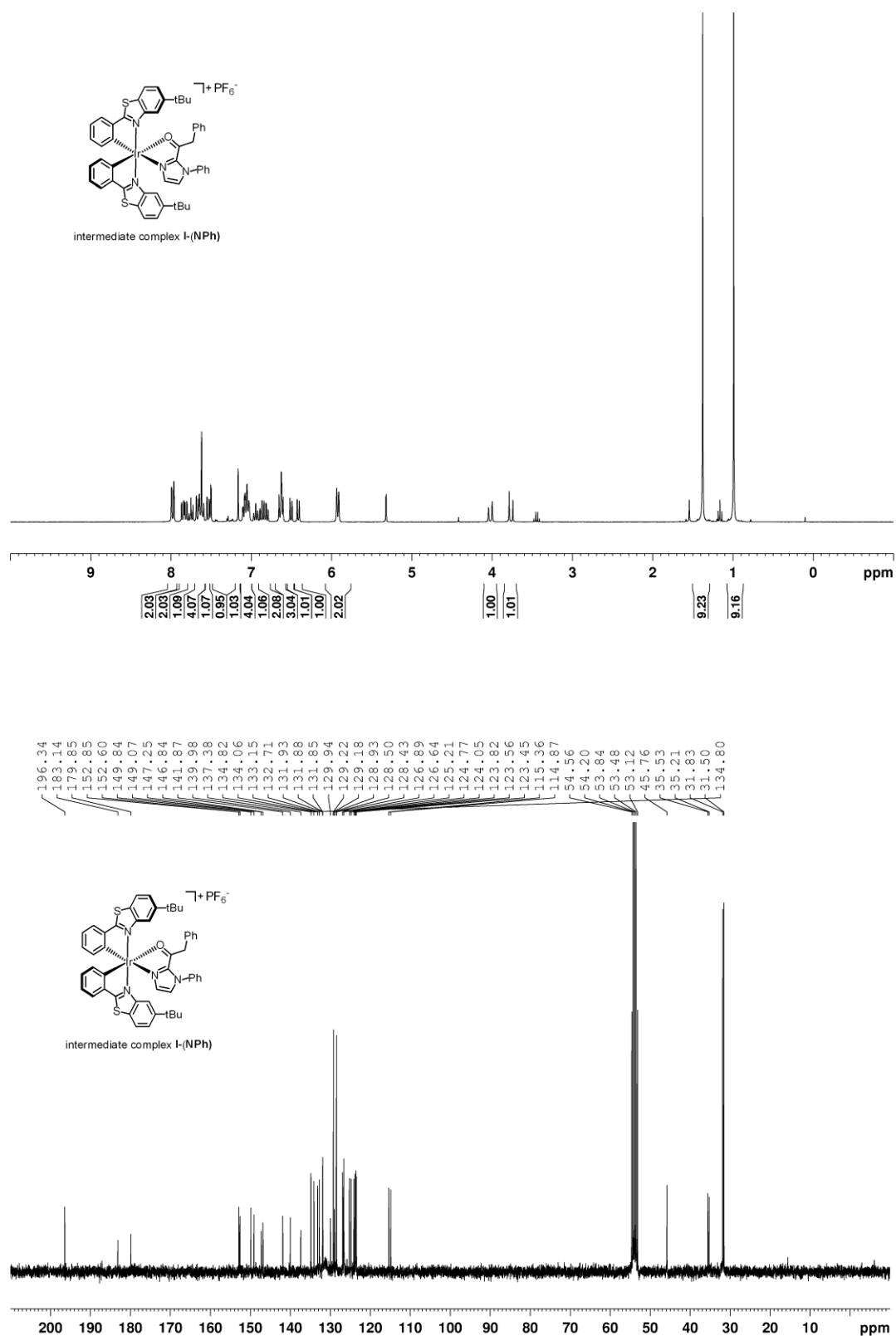


Figure 138 ^1H -NMR and ^{13}C -NMR spectrum of racemic intermediate complex **I**-(NPh).

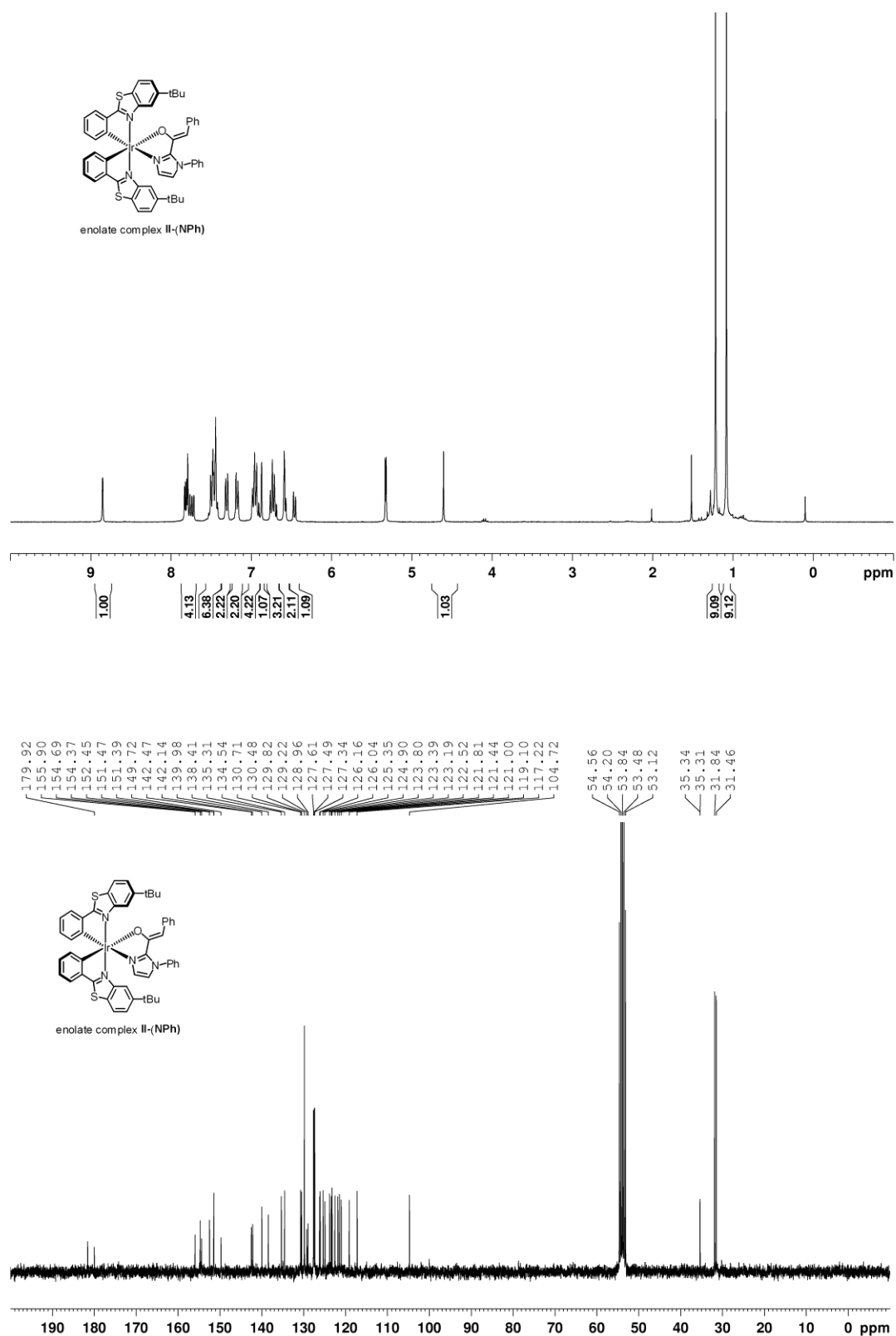


Figure 139 ^1H -NMR and ^{13}C -NMR spectrum of racemic intermediate complex II-(NPh).

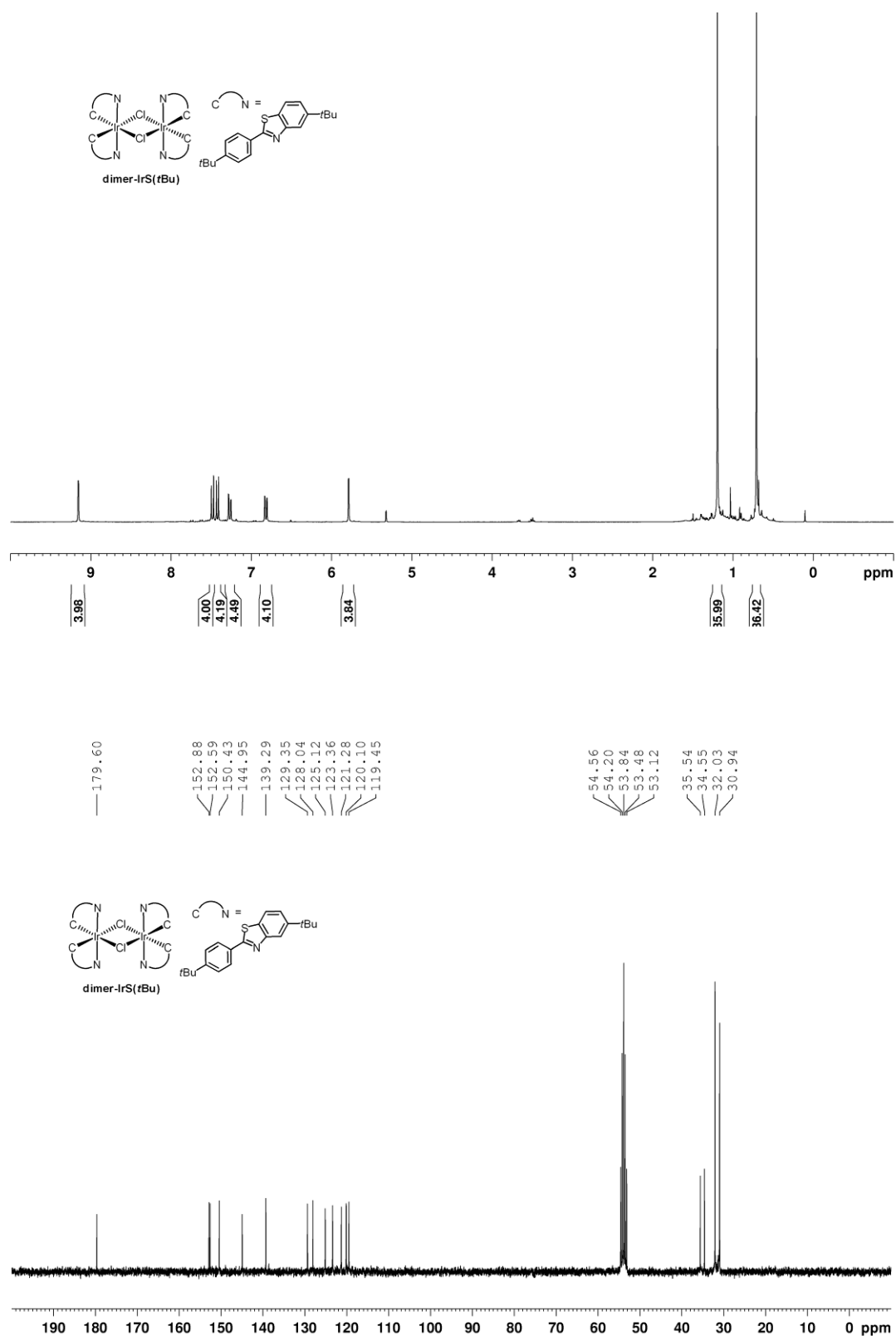
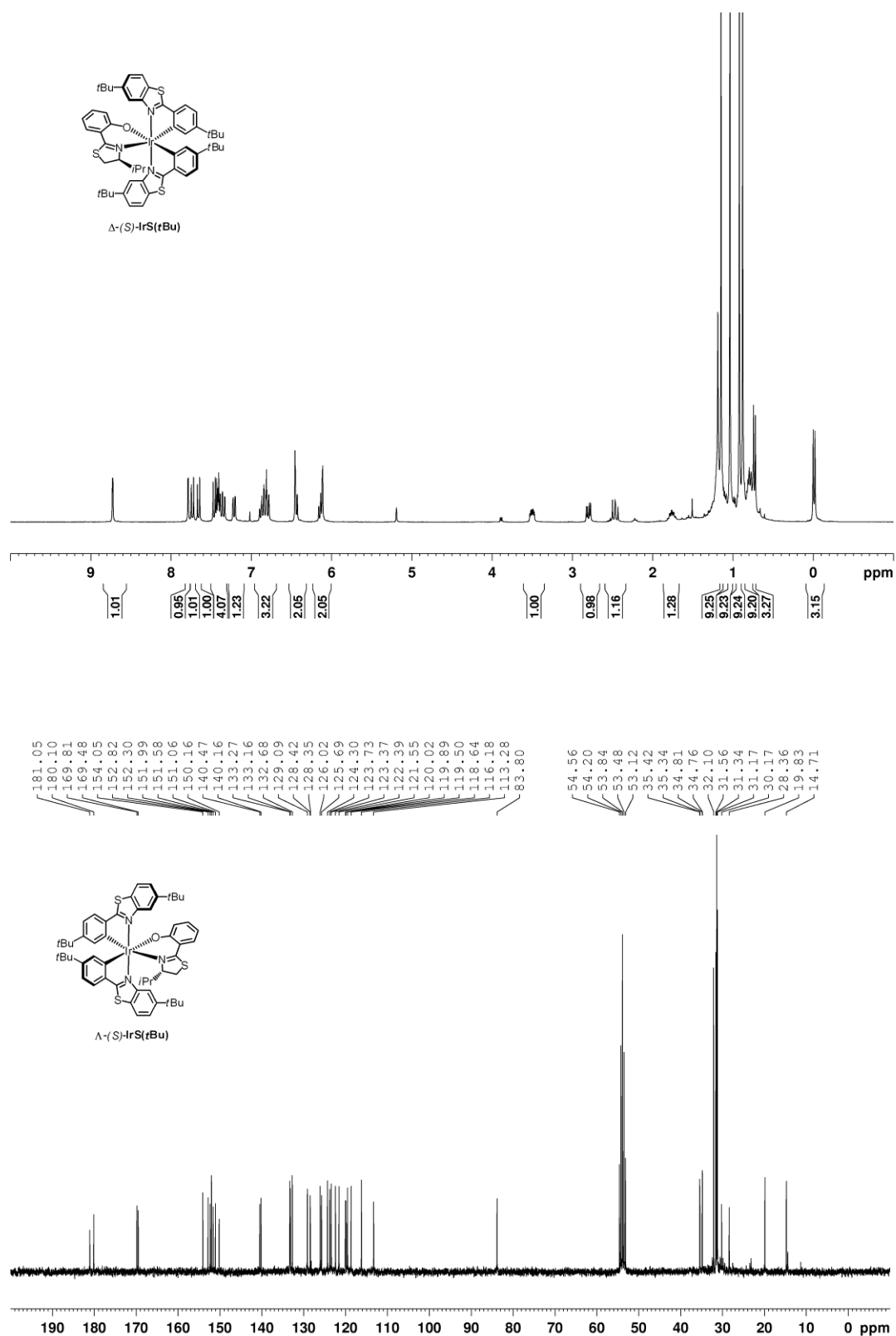


Figure 140 ^1H -NMR and ^{13}C -NMR spectrum of dimer-IrS(*t*Bu).

**Figure 141** ^1H -NMR and ^{13}C -NMR spectrum of $\Lambda^-(S)$ -IrS(*t*Bu).

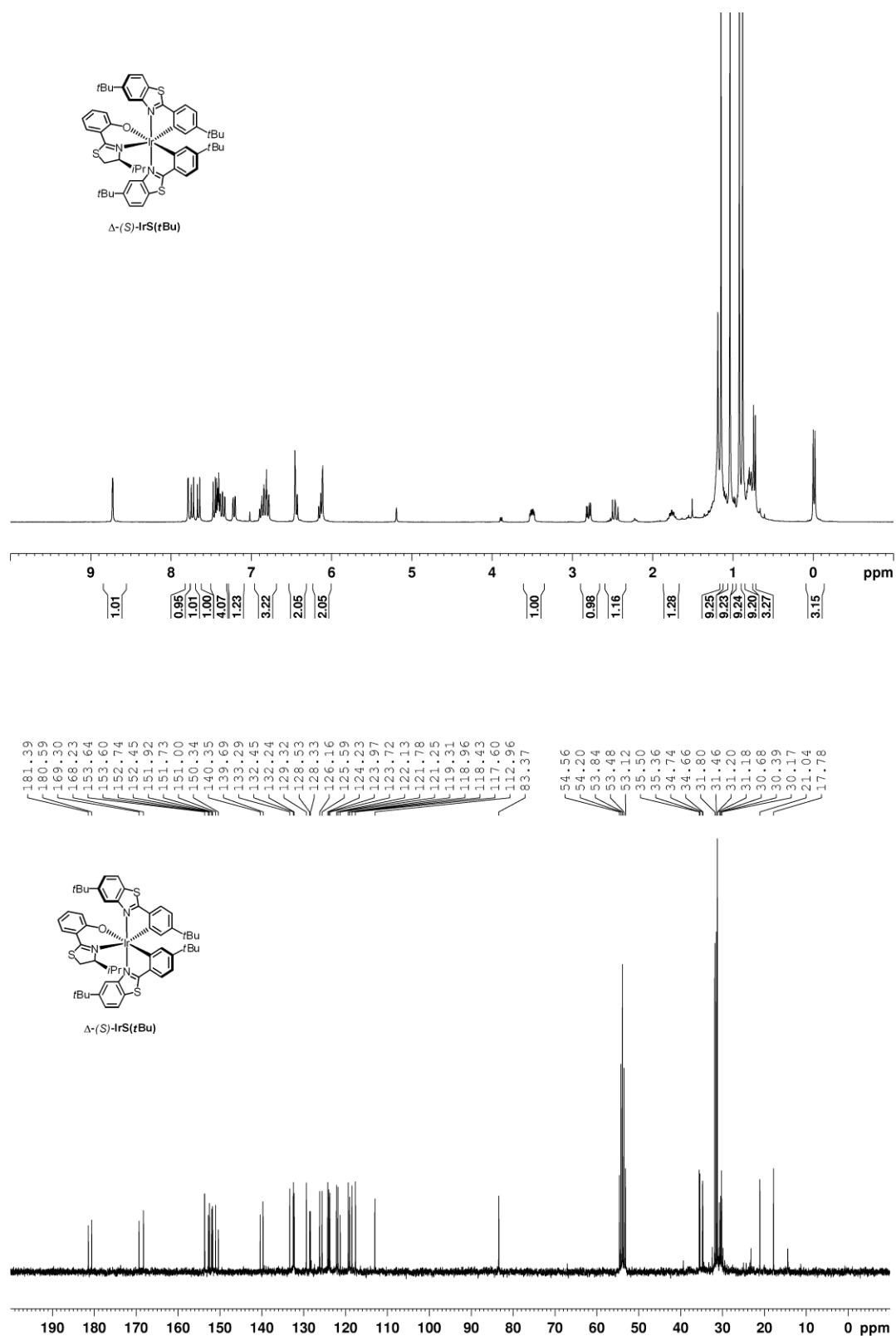
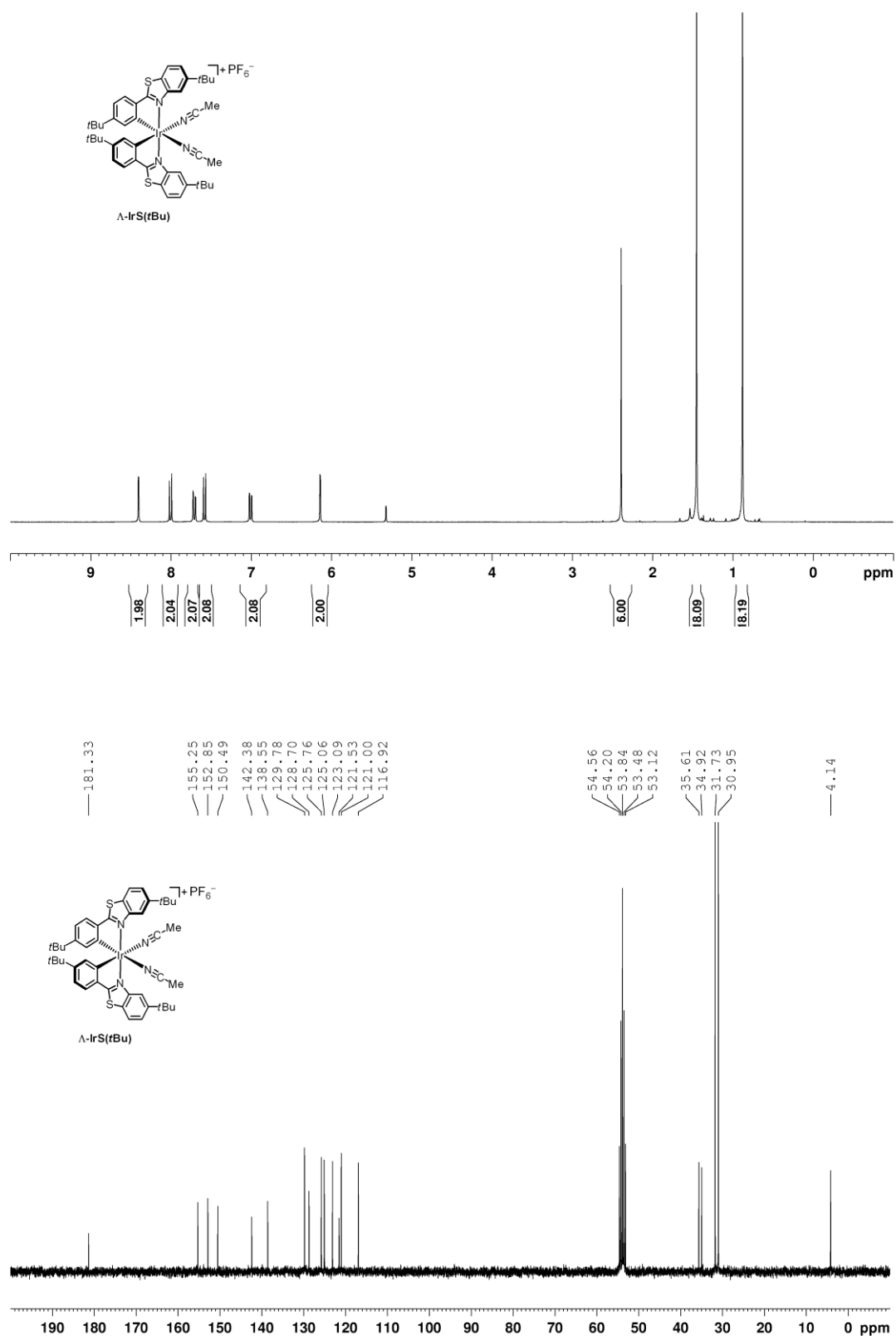


Figure 142 ^1H -NMR and ^{13}C -NMR spectrum of Δ -(S)-IrS(*t*Bu).

Figure 143 ^1H -NMR and ^{13}C -NMR spectrum of Λ -IrS(*t*Bu).

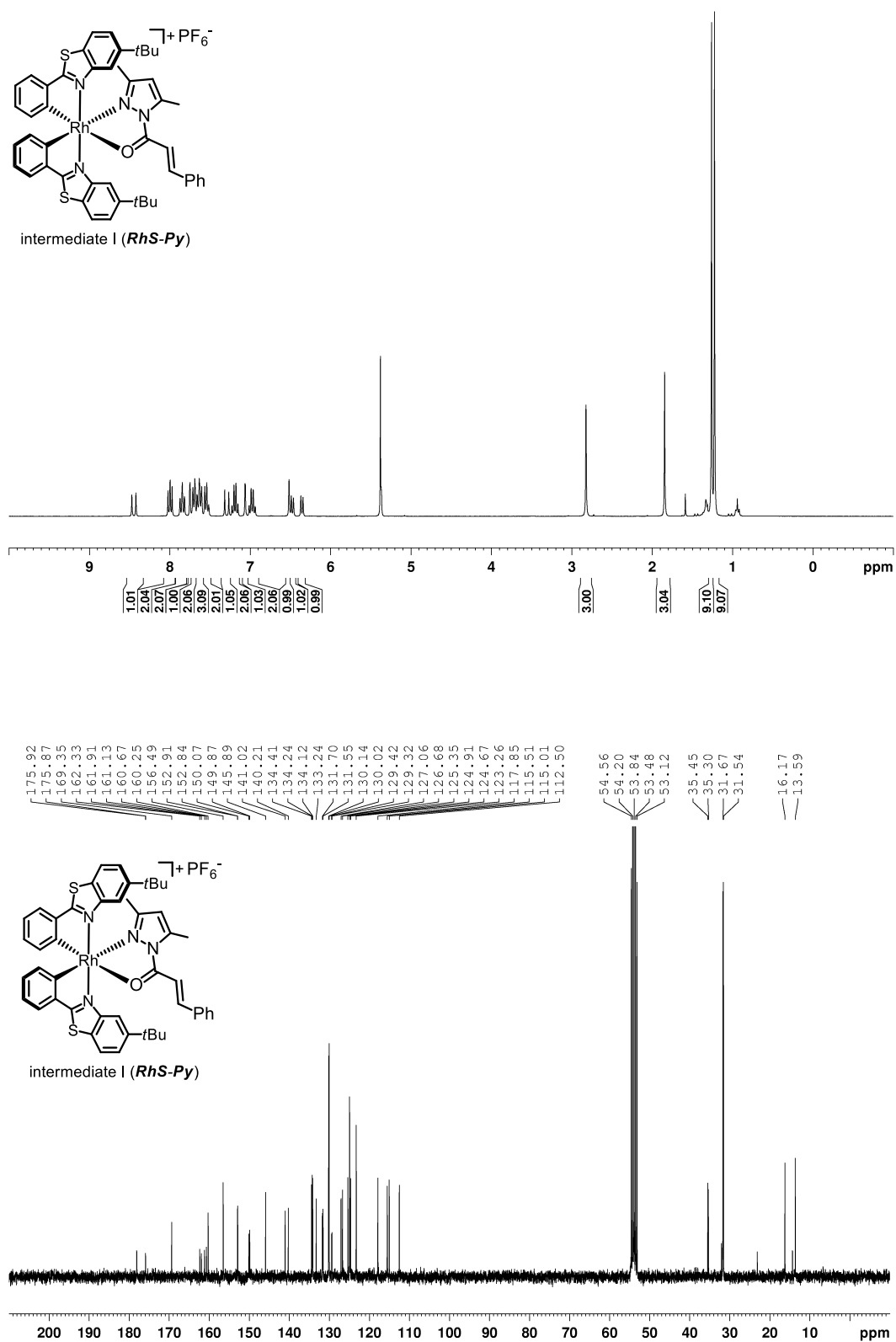


Figure 144 $^1\text{H-NMR}$ and $^{13}\text{C-NMR}$ spectrum of intermediate I (*RhS-Py*).

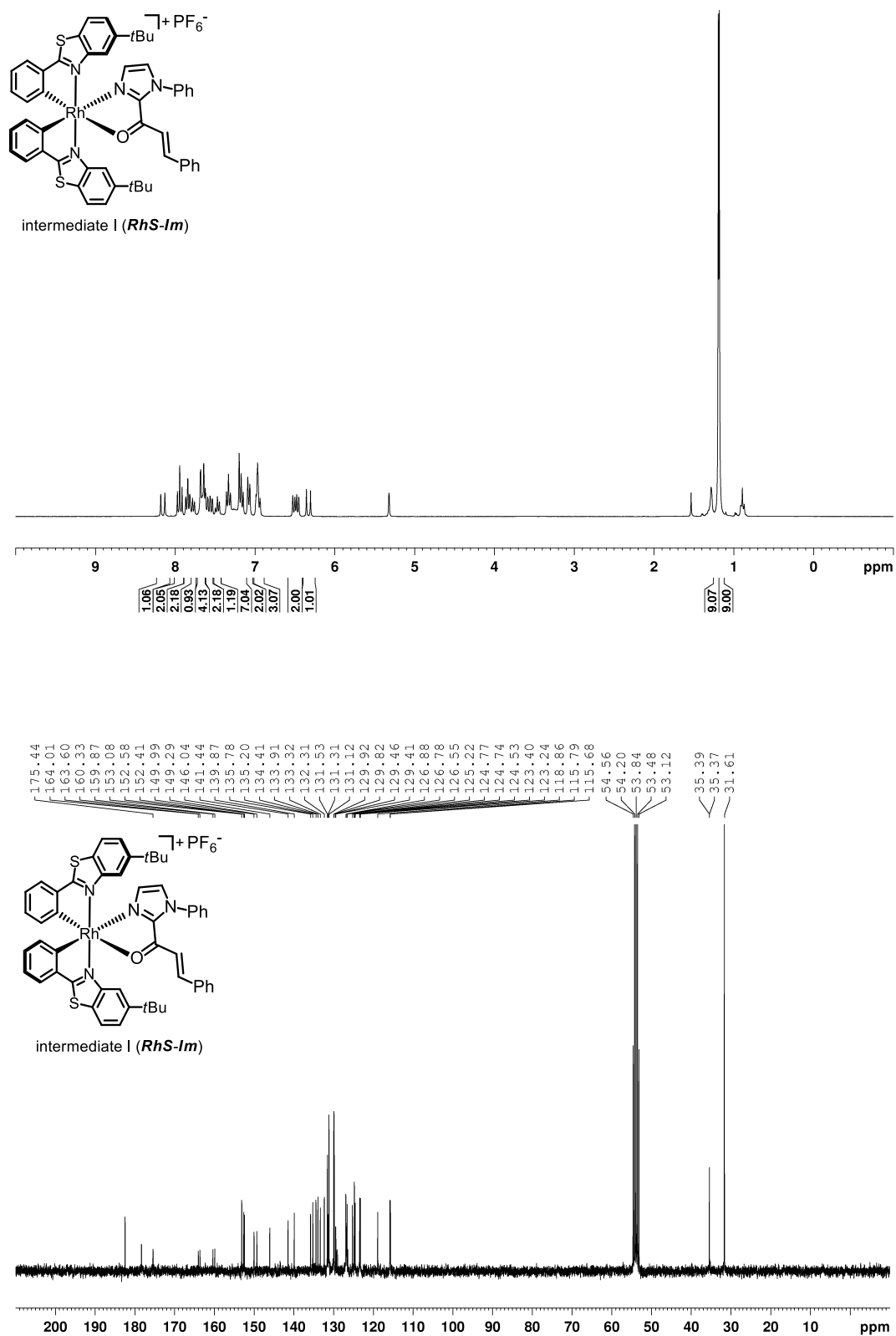


Figure 145 $^1\text{H-NMR}$ and $^{13}\text{C-NMR}$ spectrum of intermediate I (*RhS-Im*).

6.6.2 CD Spectra of Enantiopure Iridium Complexes

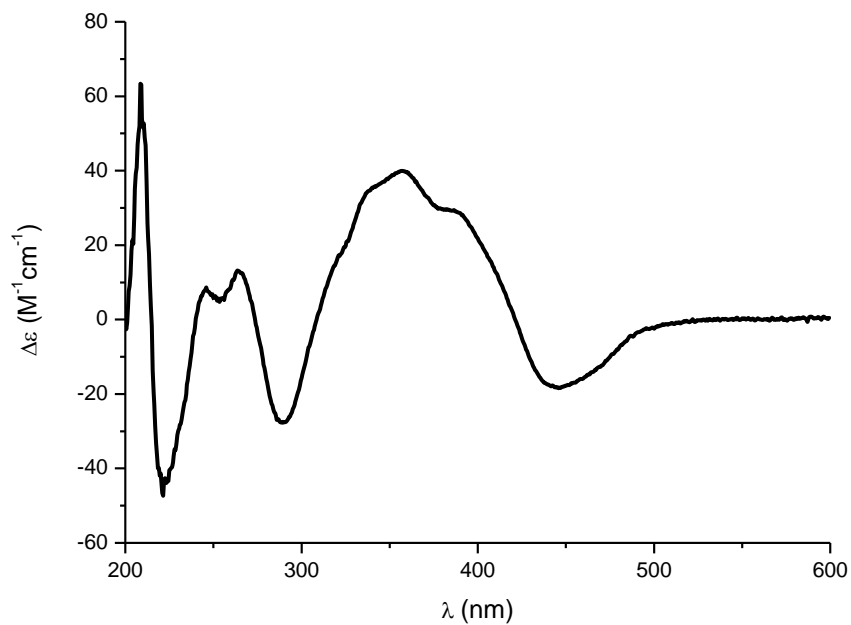


Figure 146 CD spectrum of complex Λ -(S)-9a recorded in CH_3OH (0.2 mM).

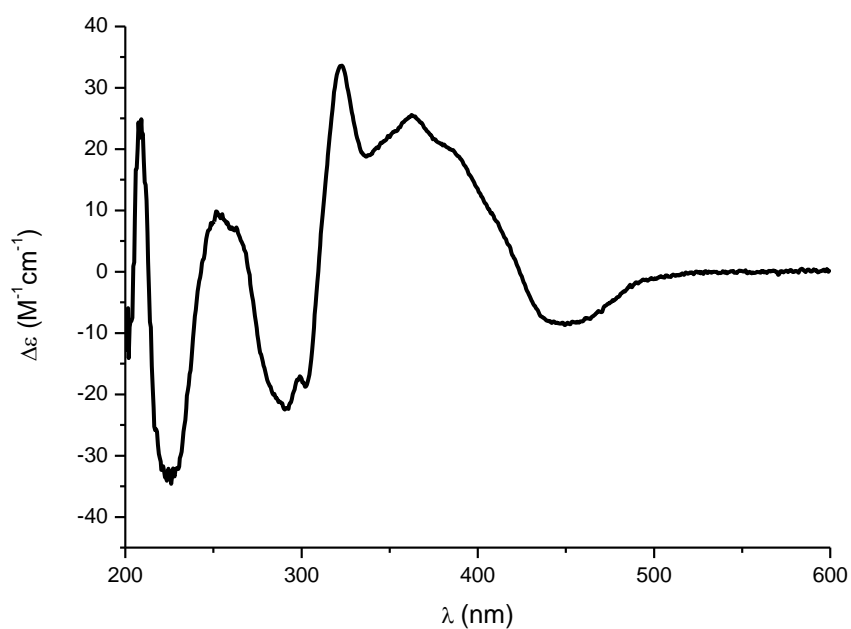


Figure 147 CD spectrum of complex Λ -(S)-9b recorded in CH_3OH (0.2 mM).

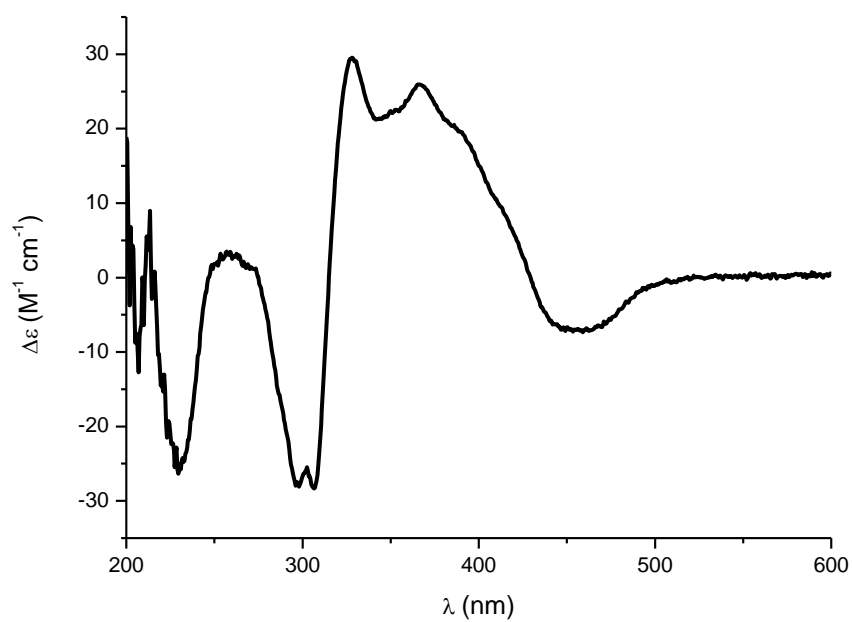


Figure 148 CD spectrum of complex Λ -(S)-9c recorded in CH_3OH (0.2 mM).

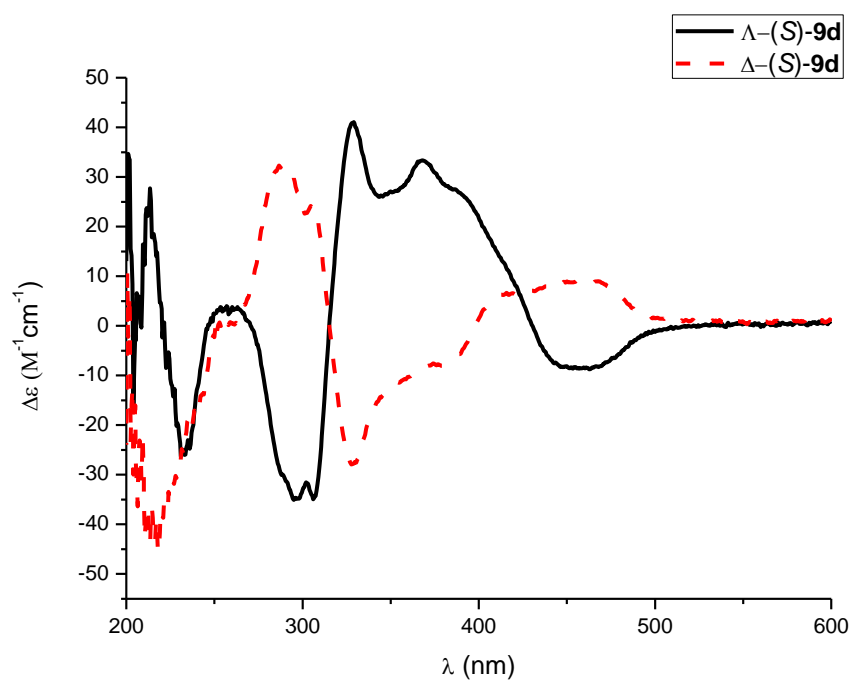


Figure 149 CD spectra of complexes Λ -(S)-9d and Δ -(S)-9d recorded in CH_3OH (0.2 mM).

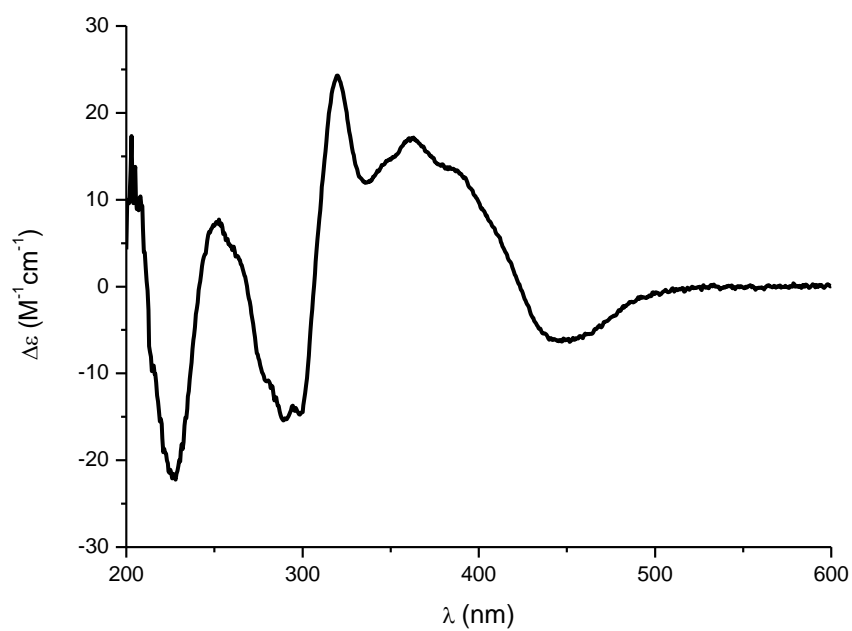


Figure 150 CD spectrum of complex Λ -(S)-**9e** recorded in CH_3OH (0.2 mM).

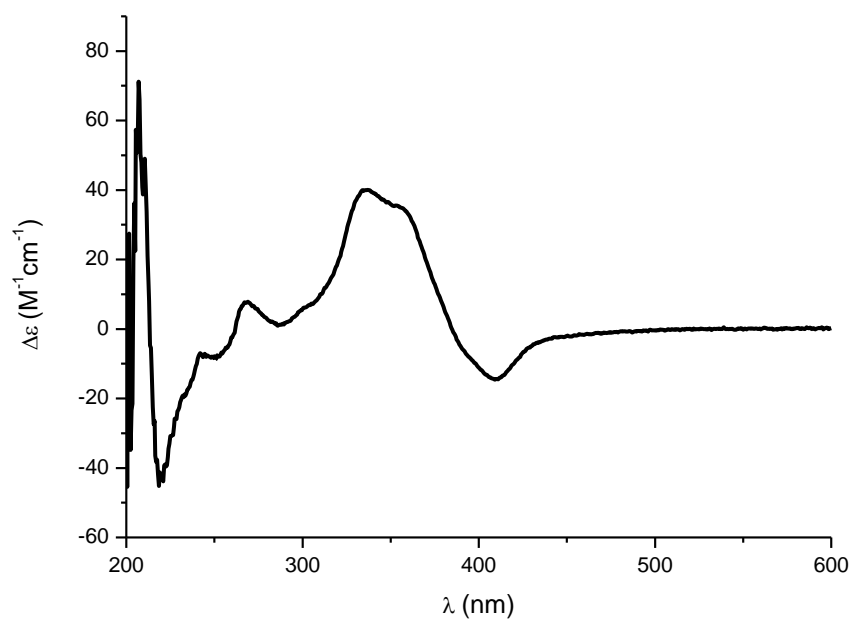


Figure 151 CD spectrum of catalyst Λ -**Ir1** recorded in CH_3OH (0.2 mM).

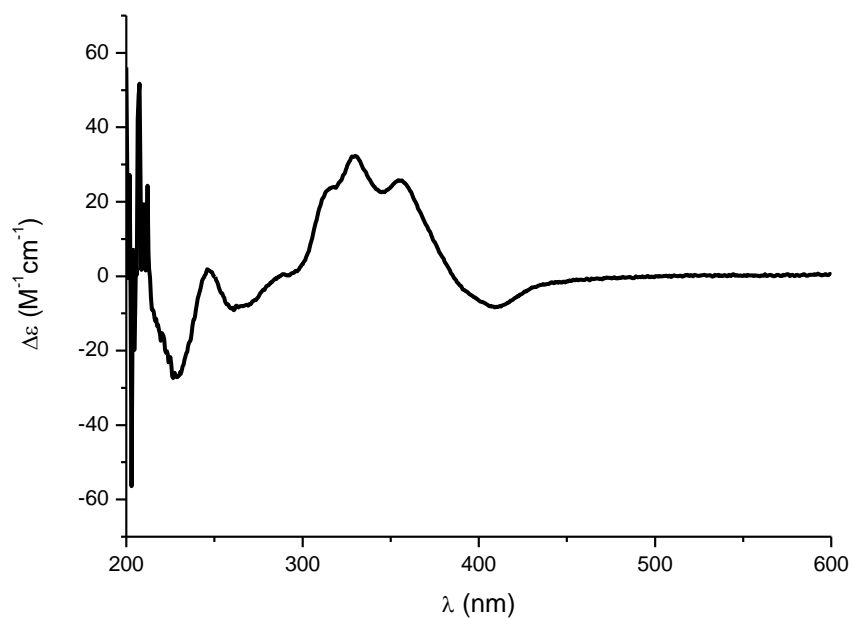


Figure 152 CD spectrum of catalyst Δ -Ir2 recorded in CH_3OH (0.2 mM).

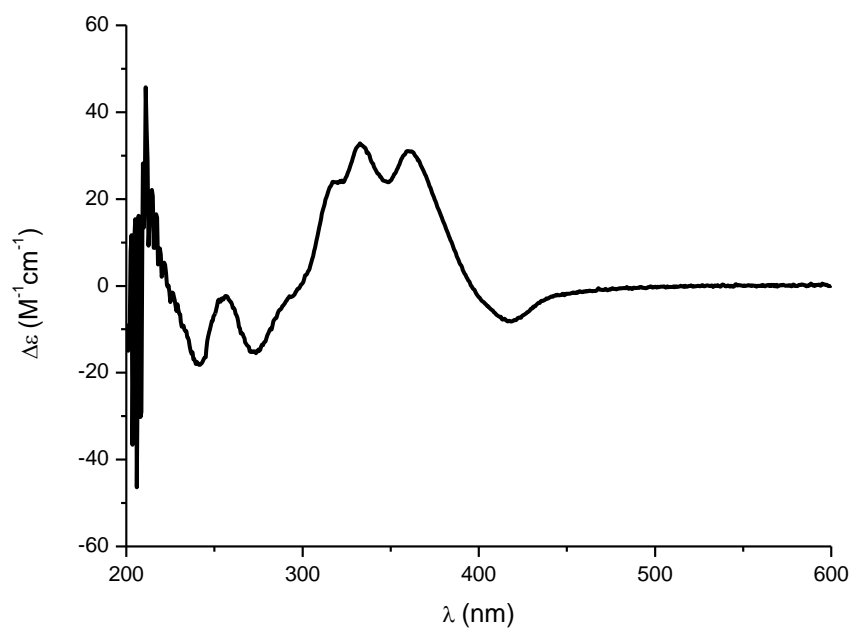


Figure 153 CD spectrum of catalyst Δ -Ir3 recorded in CH_3OH (0.2 mM).

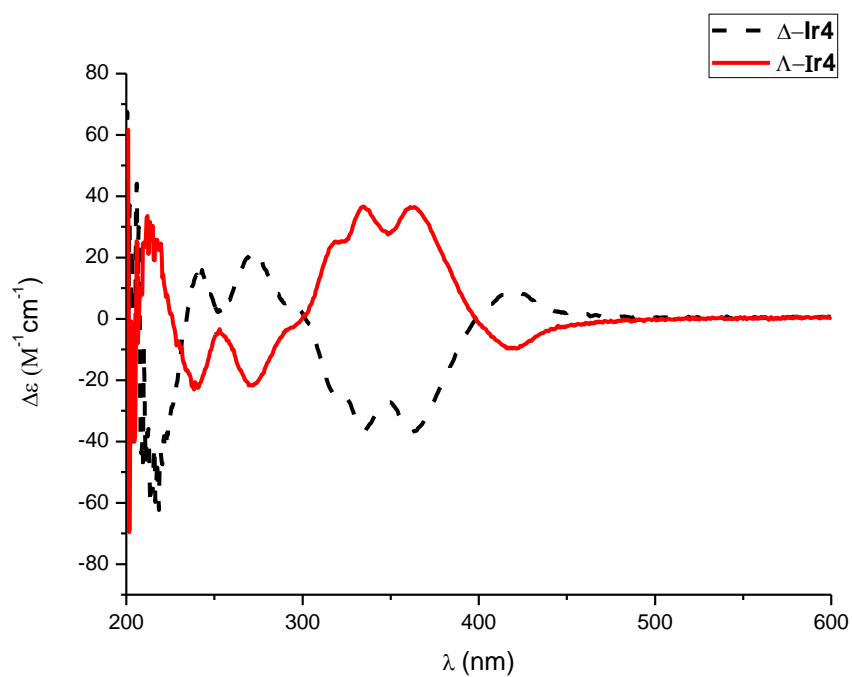


Figure 154 CD spectra of catalyst Λ -Ir4 and Δ -Ir4 recorded in CH_3OH (0.2 mM).

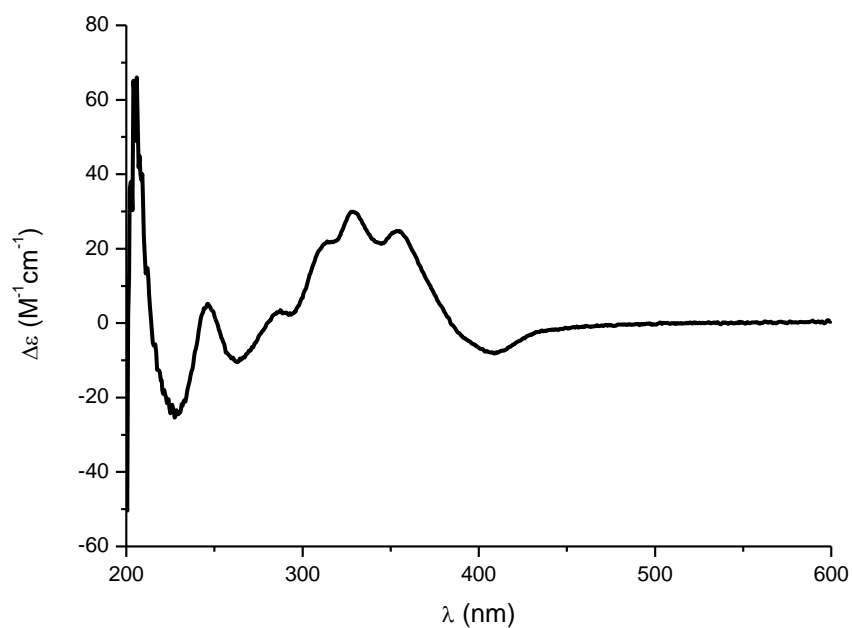


Figure 155 CD spectrum of catalyst Λ -Ir5 recorded in CH_3OH (0.2 mM).

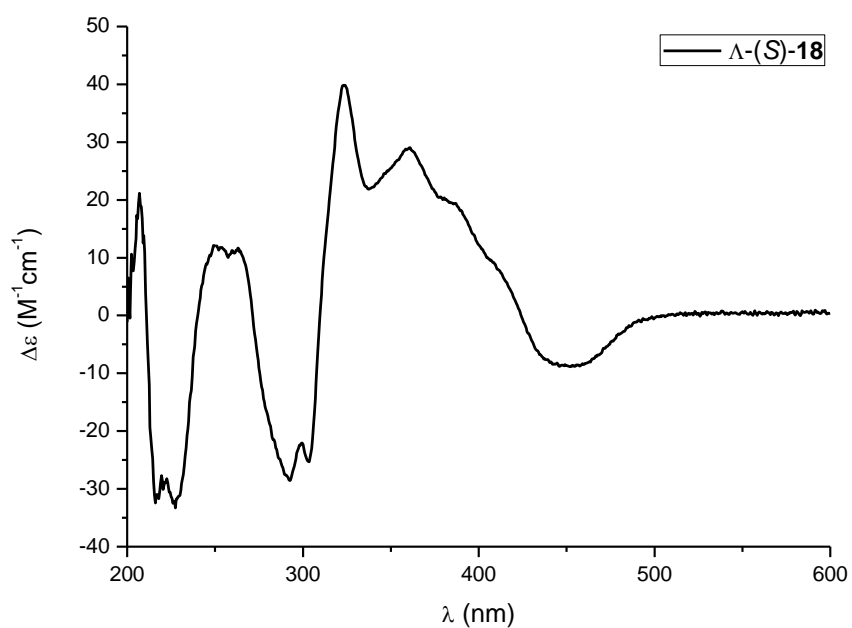


Figure 156 CD spectrum of auxiliary complex Δ -(S)-18 recorded in CH_3OH (0.2 mM).

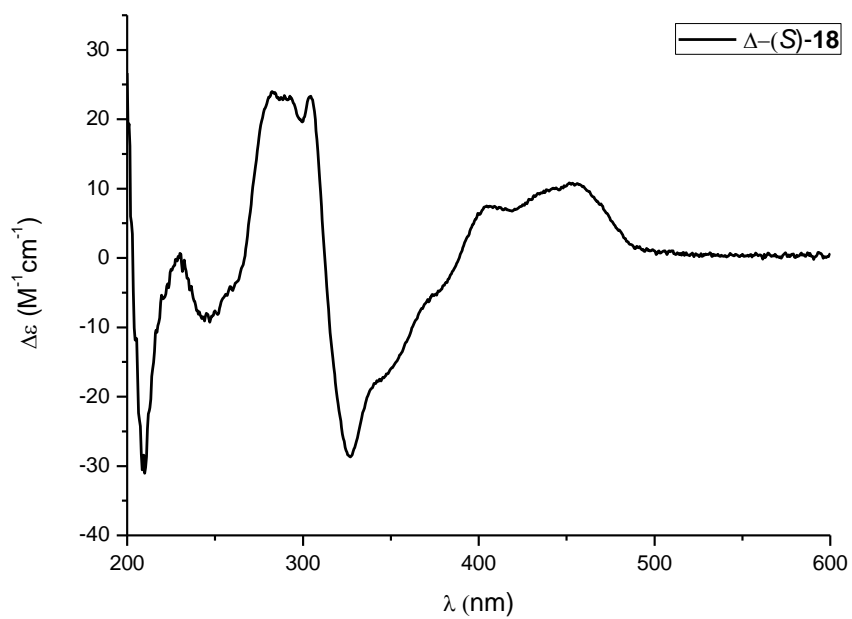


Figure 157 CD spectrum of auxiliary complex Δ -(S)-18 recorded in CH_3OH (0.2 mM).

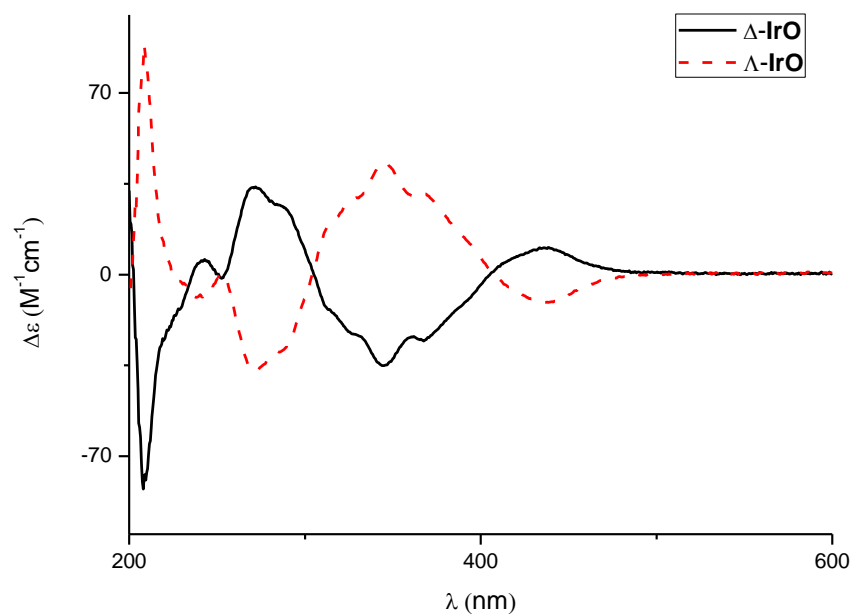


Figure 158 CD spectra of complexes $\Delta\text{-IrO}$ and $\Lambda\text{-IrO}$ recorded in CH_3OH (0.2 mM).

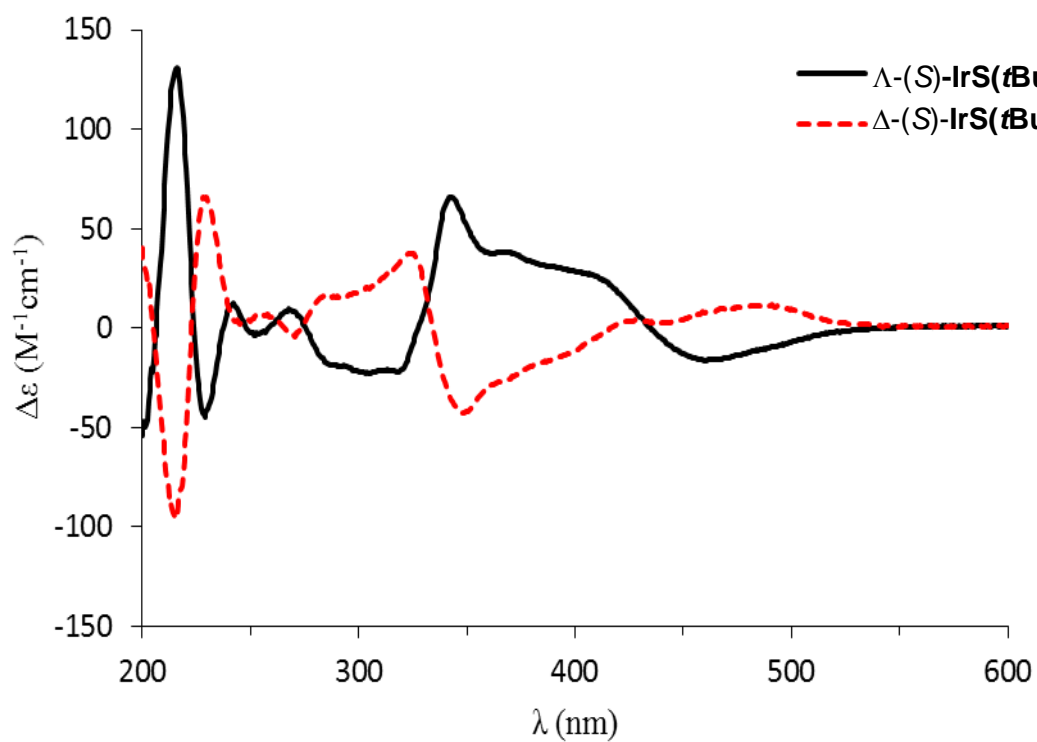


Figure 159 CD spectra of complexes $\Lambda\text{-(S)-IrS(tBu)}$ and $\Delta\text{-(S)-IrS(tBu)}$ recorded in CH_3OH (0.2 mM).

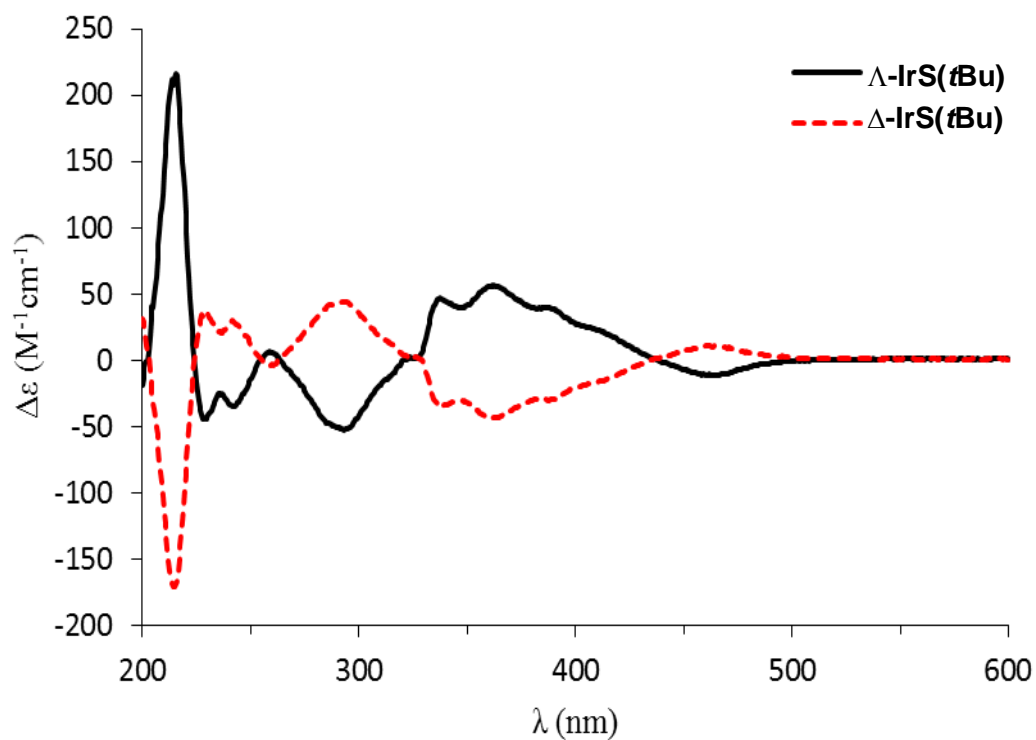


Figure 160 CD spectra of complexes $\Lambda\text{-IrS(tBu)}$ and $\Delta\text{-IrS(tBu)}$ recorded in CH_3OH (0.2 mM).

6.6.3 HPLC Spectra of Enantiopure Iridium Complexes

The analysis was performed with a Daicel Chiralpak IA (250 × 4.6 mm) HPLC column on an Agilent 1200 Series HPLC System. The column temperature was 30 °C and UV-absorption was measured at 254 nm. mobile phase: solvent A = 0.1% TFA, solvent B = MeCN, flow rate = 0.5 mL/min, column temperature = 40 °C, UV absorption = 254 nm.

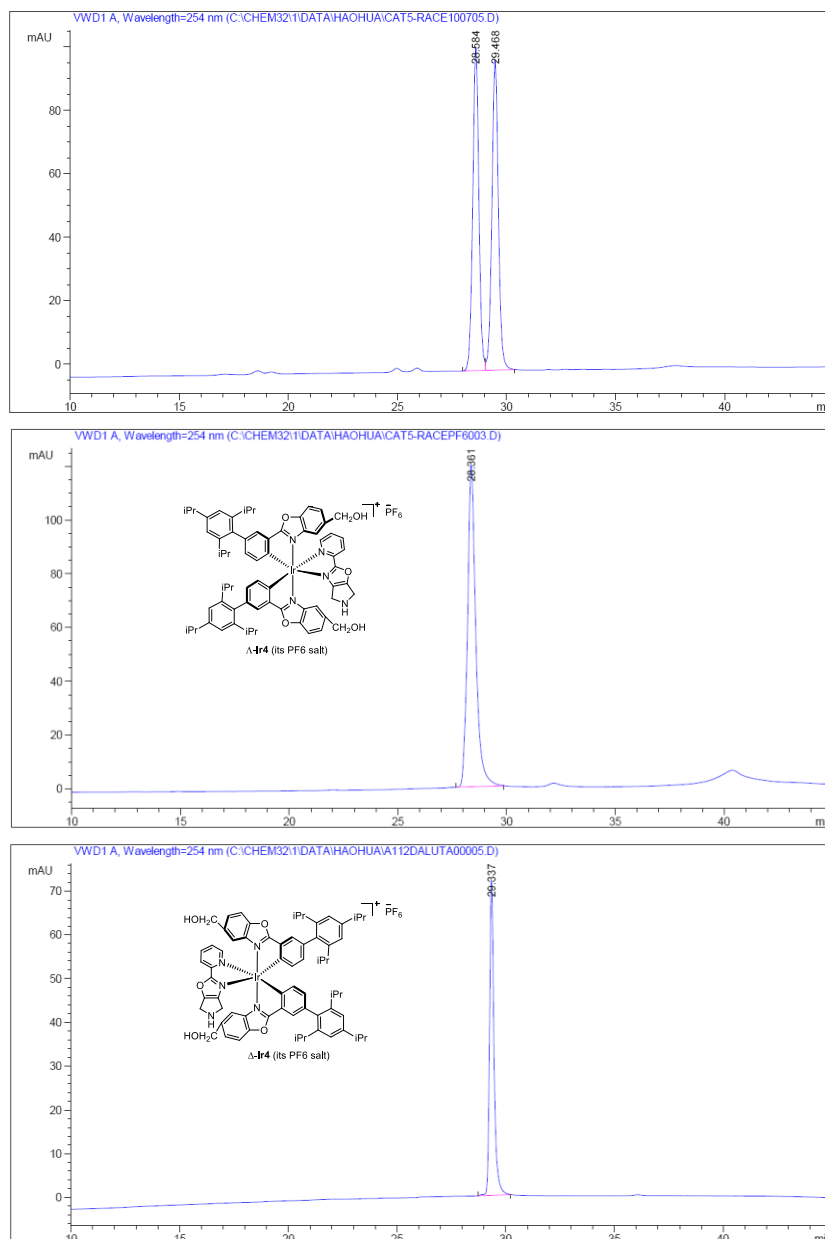


Figure 161 HPLC traces of the reference *rac*-**Ir4**, Λ -**Ir4**, and Δ -**Ir4** (all as their PF₆ salt). Integration of peak areas > 99% *ee* (Daicel Chiralpak IA, with a linear gradient of 30% to 60% B in 25 min, flow rate = 0.5 mL/min).

The analysis was performed with a Daicel Chiralpak IB (250 × 4.6 mm) HPLC column on an Agilent 1200 Series HPLC System. The column temperature was 20 °C and UV-absorption was measured at 254 nm. Solvent A = 0.1% TFA, solvent B = MeCN.

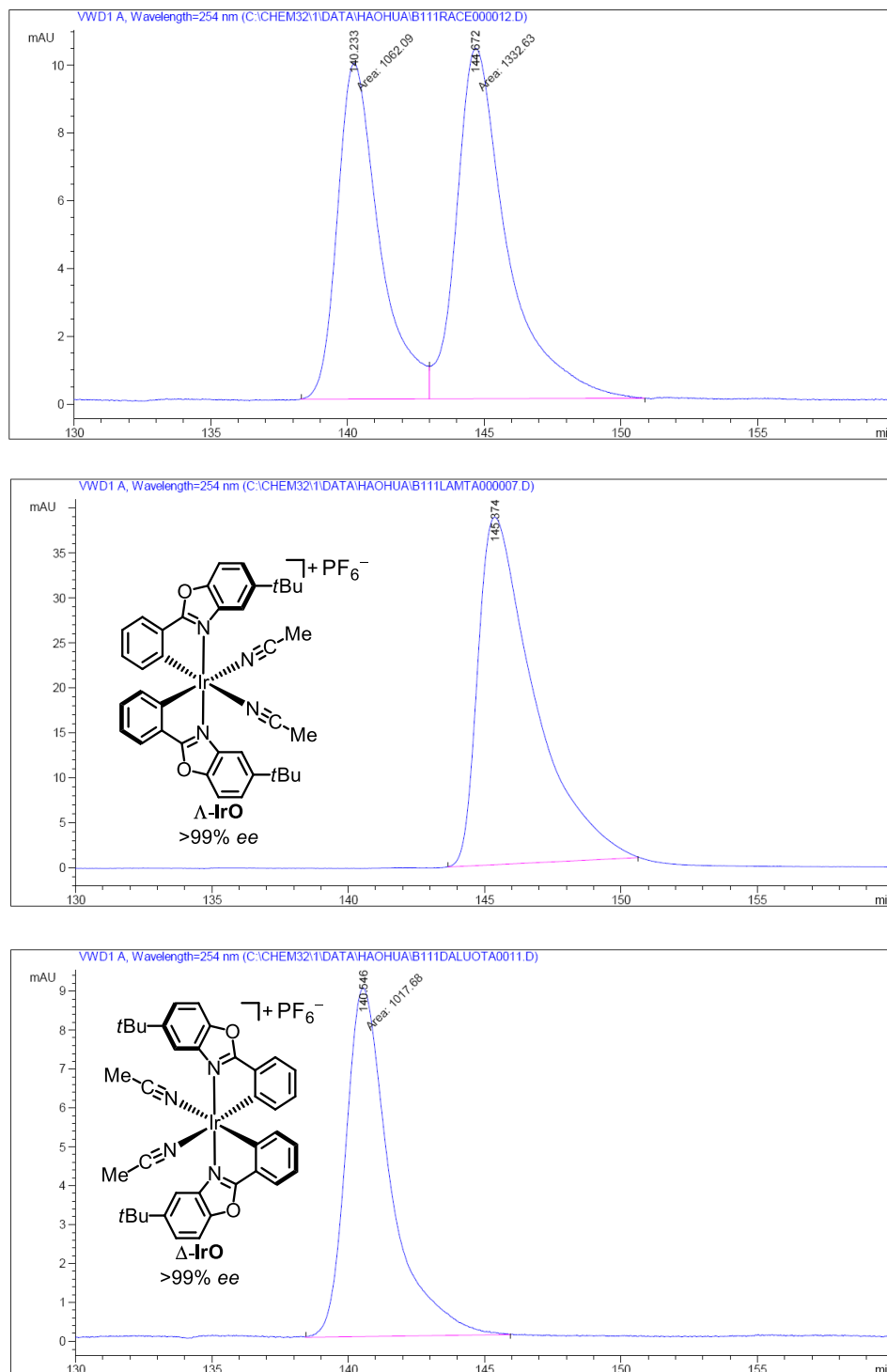


Figure 162 HPLC traces for the complex *rac*-IrO, Δ -IrO, Δ -IrO. Integration of peak areas > 100:1 e.r. (Daicel Chiralpak IB with a linear gradient of 20% to 43% B in 60 min, flow rate = 0.5 mL/min).

6.7 List of Crystal Structure Data

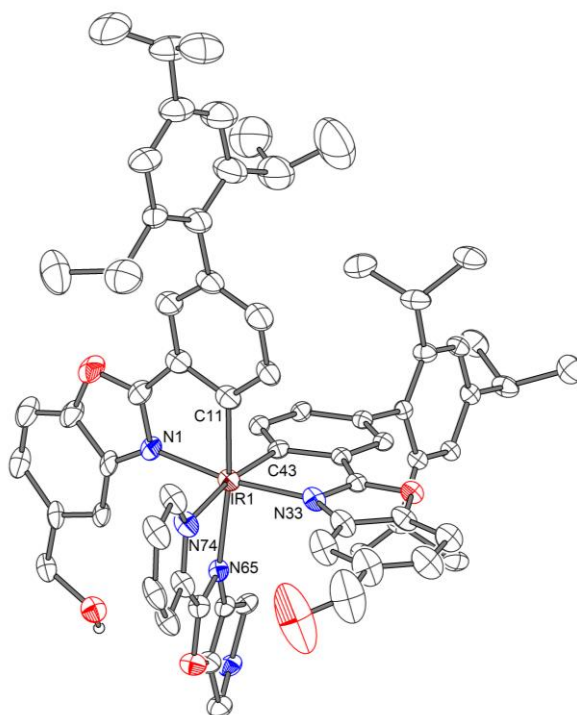


Figure 163 Crystal structure of the racemic catalyst Λ/Δ -**Ir4**. ORTEP drawing of complex 1 with 30% probability thermal ellipsoids. Iodide counterions, water molecules and CH_2Cl_2 are omitted for clarity.

Table 13. Crystal data and structure refinement for *rac*-**Ir4**.

Crystal data

Identification code	cat112_0m_sq	
Habitus, colour	plate, yellow	
Crystal size	0.609 x 0.209 x 0.044 mm ³	
Crystal system	Triclinic	
Space group	P -1	Z = 1
Unit cell dimensions	a = 14.9997(6) Å	= 105.6071(19)°.
	b = 20.6925(7) Å	= 100.893(2)°.
	c = 26.1024(10) Å	= 99.749(2)°.
Volume	7451.9(5) Å ³	
Cell determination	9717 peaks with Theta 2.5 to 27.2°.	
Empirical formula	C ₂₇₅ H ₃₀₈ Cl ₁₆ I ₁₀ Ir ₄ N ₂₀ O ₂₅	
Moiety formula	4[C ₆₈ H ₇₃ Ir N ₅ O ₅] ⁺ , 2(I ⁻), I ³⁻ , I ⁵⁻ , 3(C H ₂ Cl ₂),	
5(H ₂ O)		
Formula weight	6543.90	

Density (calculated)	1.458 Mg/m ³
Absorption coefficient	2.930 mm ⁻¹
F(000)	3238
Data collection:	
Diffractionmeter type	Bruker D8 QUEST area detector
Wavelength	0.71069 Å
Temperature	100(2) K
Theta range for data collection	2.005 to 25.371°.
Index ranges	-18<=h<=18, -24<=k<=24, -31<=l<=31
Data collection software	BRUKER APEX2 2014.1-1
Cell refinement software	SAINT V8.32B (Bruker AXS Inc., 2013)
Data reduction software	SAINT V8.32B (Bruker AXS Inc., 2013)
Solution and refinement:	
Reflections collected	173852
Independent reflections	27246 [R(int) = 0.0892]
Completeness to theta = 25.240°	99.9 %
Observed reflections	20449[I > 2sigma(I)]
Reflections used for refinement	27246
Absorption correction	Semi-empirical from equivalents
Max. and min. transmission	0.72 and 0.55
Largest diff. peak and hole	4.544 and -2.517 e.Å ⁻³
Solution	direct/ difmap
Refinement	Full-matrix least-squares on F ²
Treatment of hydrogen atoms	mixed, mixed
Programs used	SHELXS-97 (Sheldrick, 2008) SHELXL-2013 (Sheldrick, 2013) DIAMOND (Crystal Impact)
Data / restraints / parameters	27246 / 1352 / 1746
Goodness-of-fit on F ²	1.055
R index (all data)	wR2 = 0.1826
R index conventional [I>2sigma(I)]	R1 = 0.0682

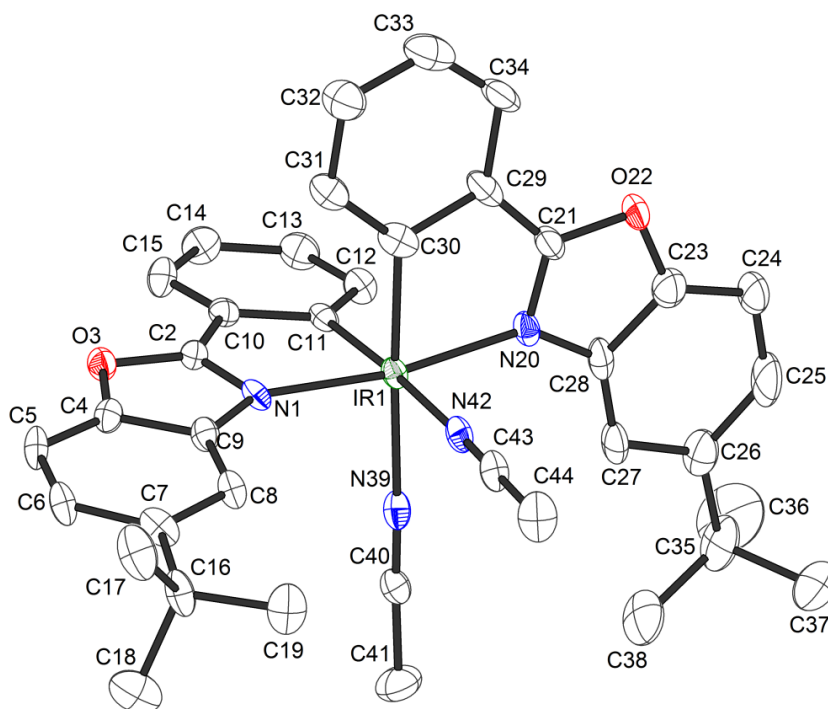


Figure 164 Crystal structure of Δ -IrO. The PF_6 counteranion is omitted for clarity. ORTEP drawing with 50% probability thermal ellipsoids.

Table 14. Crystal data and structure refinement for Δ -IrO.

Crystal data:

Identification code	Δ-IrO	
Habitus, colour	block, yellow	
Crystal size	0.32 x 0.27 x 0.15 mm ³	
Crystal system	Monoclinic	
Space group	P 2 ₁	Z = 4
Unit cell dimensions	a = 13.3232(7) Å	= 90°.
	b = 24.2827(11) Å	= 109.4451(16)°.
	c = 15.9879(8) Å	= 90°.
Volume	4877.4(4) Å ³	
Cell determination	9761 peaks with Theta 2.3 to 27.3°.	
Empirical formula	C ₃₈ H ₃₈ F ₆ Ir N ₄ O ₂ P	
Formula weight	919.89	
Density (calculated)	1.253 Mg/m ³	
Absorption coefficient	2.823 mm ⁻¹	
F(000)	1824	

Data collection:

Diffractionmeter type	Bruker D8 QUEST area detector
Wavelength	0.71073 Å
Temperature	100(2) K
Theta range for data collection	2.333 to 25.500°.
Index ranges	-16<=h<=16, -29<=k<=27, -19<=l<=19
Data collection software	BRUKER APEX II
Cell refinement software	SAINT V8.34A (Bruker AXS Inc., 2013)
Data reduction software	SAINT V8.34A (Bruker AXS Inc., 2013)

Solution and refinement:

Reflections collected	124260
Independent reflections	17607 [R(int) = 0.0589]
Completeness to theta = 25.242°	99.9 %
Observed reflections	16949[II > 2(I)]
Reflections used for refinement	17607
Absorption correction	Semi-empirical from equivalents
Max. and min. transmission	0.68 and 0.54
Flack parameter (absolute struct.)	0.002(3)
Largest diff. peak and hole	0.902 and -0.916 e.Å ⁻³
Solution	Direct methods
Refinement	Full-matrix least-squares on F ²
Treatment of hydrogen atoms	Calculated positions, constrained refinement
Programs used	SHELXS-97 (Sheldrick, 2008) SHELXL-2013 (Sheldrick, 2013) DIAMOND (Crystal Impact)
Data / restraints / parameters	17607 / 1 / 953
Goodness-of-fit on F ²	1.067
R index (all data)	wR2 = 0.0728
R index conventional [I>2sigma(I)]	R1 = 0.0305

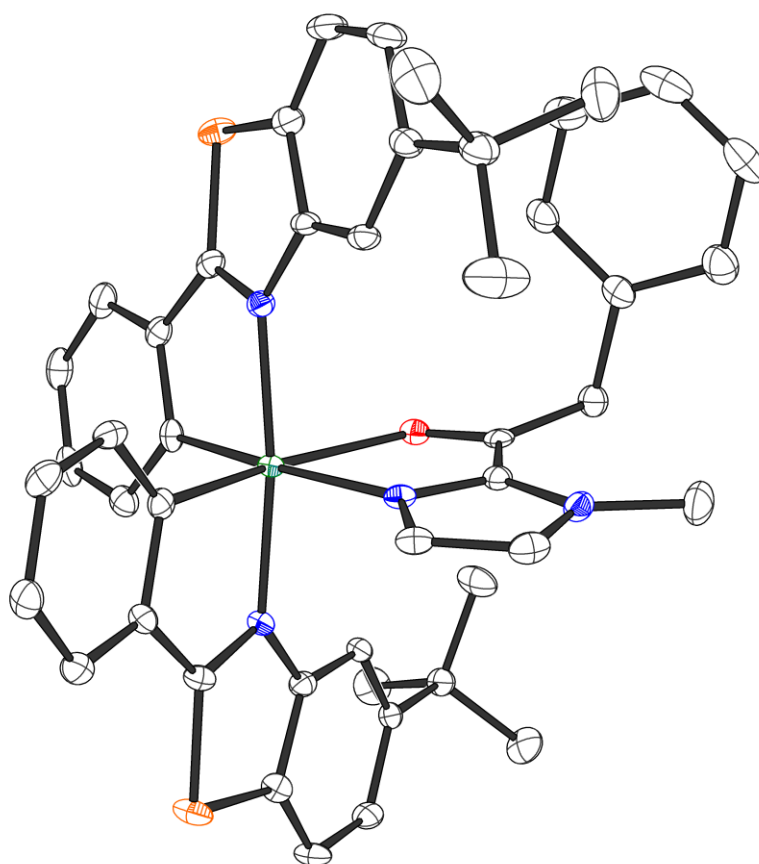


Figure 165 Crystal structure of intermediate complex **I**. The PF_6 counteranion is omitted for clarity. ORTEP drawing with 50% probability thermal ellipsoids.

Table 15. Crystal data and structure refinement for intermediate complex **I** (zll3_0m).

Crystal data

Identification code	zll3_0m	
Habitus, colour	block, red	
Crystal size	0.30 x 0.27 x 0.12 mm ³	
Crystal system	Monoclinic	
Space group	P 2 ₁ /c	Z = 4
Unit cell dimensions	a = 15.4718(5) Å	= 90°.
	b = 16.7746(6) Å	= 98.7851(12)°.
	c = 19.3571(7) Å	= 90°.
Volume	4964.9(3) Å ³	
Cell determination	9819 peaks with Theta 2.3 to 25.3°.	
Empirical formula	C ₄₈ H ₄₈ Cl ₄ F ₆ Ir N ₄ O P S ₂	
Moiety formula	C ₄₆ H ₄₄ Ir N ₄ O S ₂ , F ₆ P, 2(C H ₂ Cl ₂)	

Formula weight	1239.99
Density (calculated)	1.659 Mg/m ³
Absorption coefficient	3.085 mm ⁻¹
F(000)	2472

Data collection:

Diffractionmeter type	Bruker D8 QUEST area detector
Wavelength	0.71073 Å
Temperature	115(2) K
Theta range for data collection	2.194 to 25.326°.
Index ranges	-18<=h<=17, -20<=k<=20, -23<=l<=23
Data collection software	BRUKER APEX2 2014.1-1
Cell refinement software	SAINT V8.34A (Bruker AXS Inc., 2013)
Data reduction software	SAINT V8.34A (Bruker AXS Inc., 2013)

Solution and refinement:

Reflections collected	43808
Independent reflections	9050 [R(int) = 0.0350]
Completeness to theta = 25.242°	99.8 %
Observed reflections	8088[I > 2σ(I)]
Reflections used for refinement	9050
Absorption correction	Numerical
Max. and min. transmission	0.71 and 0.46
Largest diff. peak and hole	0.791 and -0.442 e.Å ⁻³
Solution	Direct methods
Refinement	Full-matrix least-squares on F ²
Treatment of hydrogen atoms	Calculated positions, constr. ref.
Programs used	XT V2014/1 (Bruker AXS Inc., 2014) SHELXL-2014 (Sheldrick, 2014) DIAMOND (Crystal Impact)
Data / restraints / parameters	9050 / 147 / 666
Goodness-of-fit on F ²	1.048
R index (all data)	wR2 = 0.0464
R index conventional [I > 2σ(I)]	R1 = 0.0200

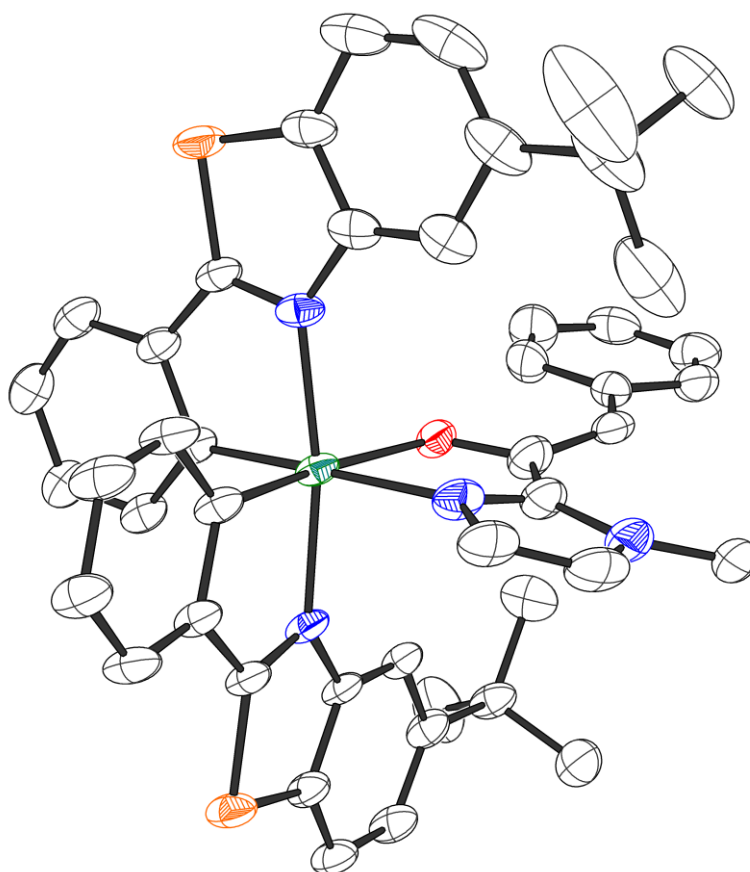


Figure 166 Crystal structure of enolate complex **II**. The PF₆ counteranion is omitted for clarity. ORTEP drawing with 50% probability thermal ellipsoids.

Table 16. Crystal data and structure refinement for enolate complex **II** (zll4_0m).

Crystal data

Identification code	zll4_0m	
Habitus, colour	block, red	
Crystal size	0.42 x 0.18 x 0.07 mm ³	
Crystal system	Monoclinic	
Space group	P 2 ₁ /c	Z = 4
Unit cell dimensions	a = 18.2905(7) Å	= 90°.
	b = 13.3765(5) Å	= 100.0007(14)°.
	c = 16.8996(7) Å	= 90°.
Volume	4071.9(3) Å ³	
Cell determination	9963 peaks with Theta 2.4 to 25.3°.	
Empirical formula	C ₄₆ H ₄₃ Ir N ₄ O S ₂	
Moiety formula	C ₄₆ H ₄₃ Ir N ₄ O S ₂	

Formula weight	924.16
Density (calculated)	1.508 Mg/m ³
Absorption coefficient	3.422 mm ⁻¹
F(000)	1856

Data collection:

Diffractometer type	Bruker D8 QUEST area detector
Wavelength	0.71073 Å
Temperature	115(2) K
Theta range for data collection	2.148 to 25.325°.
Index ranges	-20 ≤ h ≤ 21, -16 ≤ k ≤ 16, -20 ≤ l ≤ 20
Data collection software	BRUKER APEX2 2014.1-1
Cell refinement software	SAINT V8.34A (Bruker AXS Inc., 2013)
Data reduction software	SAINT V8.34A (Bruker AXS Inc., 2013)

Solution and refinement:

Reflections collected	51042
Independent reflections	7409 [R(int) = 0.0384]
Completeness to theta = 25.242°	99.9 %
Observed reflections	6331 [I > 2σ(I)]
Reflections used for refinement	7409
Absorption correction	Numerical
Max. and min. transmission	0.80 and 0.37
Largest diff. peak and hole	1.230 and -0.632 e.Å ⁻³
Solution	Direct methods
Refinement	Full-matrix least-squares on F ²
Treatment of hydrogen atoms	Calculated positions, constr. ref.
Programs used	XT V2014/1 (Bruker AXS Inc., 2014) SHELXL-2014 (Sheldrick, 2014) DIAMOND (Crystal Impact)
Data / restraints / parameters	7409 / 111 / 571
Goodness-of-fit on F ²	1.079
R index (all data)	wR2 = 0.0503
R index conventional [I > 2σ(I)]	R1 = 0.0221

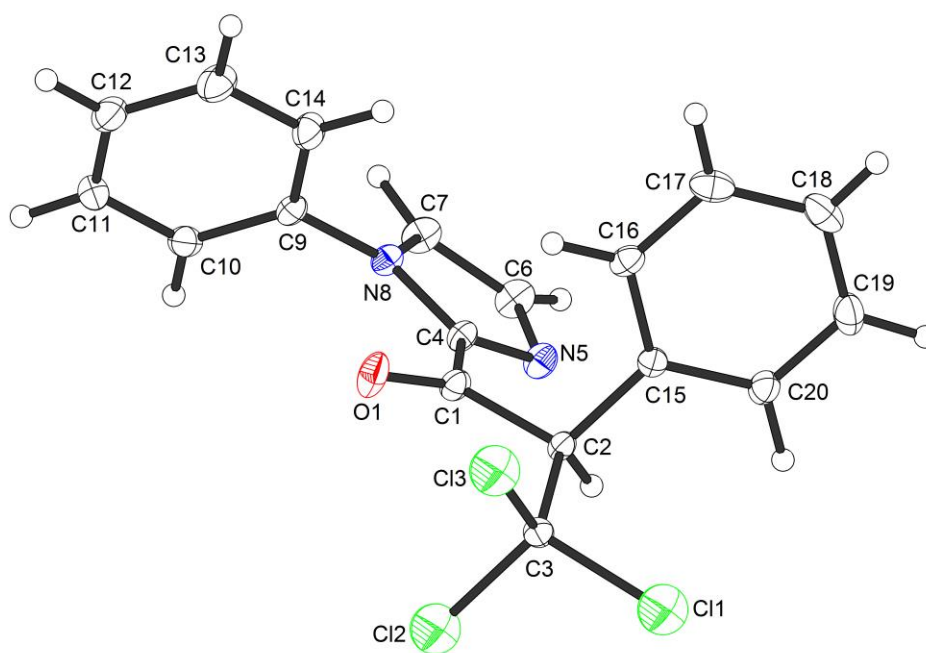


Figure 167 Crystal structure of (*R*)-**31a**. ORTEP drawing with 50% probability thermal ellipsoids.

Table 17. Crystal data and structure refinement for test_0m.

Crystal data

Identification code	test_0m (3hnb)	
Habitus, colour	plate, colourless	
Crystal size	0.35 × 0.23 × 0.05 mm ³	
Crystal system	Orthorhombic	
Space group	P2 ₁ 2 ₁ 2 ₁	Z = 4
Unit cell dimensions	a = 8.5247(3) Å	= 90°
	b = 9.7490(4) Å	= 90°
	c = 20.5673(7) Å	= 90°
Volume	1709.29(11) Å ³	
Cell determination	9868 peaks with Theta 2.3 to 29.6°.	
Empirical formula	C ₁₈ H ₁₃ Cl ₃ N ₂ O	
Moiety formula	C ₁₈ H ₁₃ Cl ₃ N ₂ O	
Formula weight	379.65	
Density (calculated)	1.475 Mg/m ³	
Absorption coefficient	0.543 mm ⁻¹	
F(000)	776	

Data collection:

Diffractometer type	Bruker D8 QUEST area detector
Wavelength	0.71073 Å
Temperature	110(2) K
Theta range for data collection	2.312 to 29.602°.
Index ranges	-11≤h≤11, -10≤k≤13, -28≤l≤28
Data collection software	BRUKER APEX2 2014.9-0
Cell refinement software	BRUKER SAINT
Data reduction software	SAINT V8.34A (Bruker AXS Inc., 2013)

Solution and refinement:

Reflections collected	16634
Independent reflections	4796 [R(int) = 0.0228]
Completeness to theta = 25.242°	99.8 %
Observed reflections	4638[I>2sigma(I)]
Reflections used for refinement	4796
Absorption correction	Numerical
Max. and min. transmission	0.97 and 0.79
Flack parameter (absolute struct.)	0.039(11)
Largest diff. peak and hole	0.281 and -0.206 e.Å ⁻³
Solution	Direct methods
Refinement	Full-matrix least-squares on F ²
Treatment of hydrogen atoms	Located, isotropic refinement
Programs used	XT V2014/1 (Bruker AXS Inc., 2014) SHELXL-2014/7 (Sheldrick, 2014) DIAMOND (Crystal Impact)
Data / restraints / parameters	4796 / 0 / 269
Goodness-of-fit on F ²	1.068
R index (all data)	wR2 = 0.0583
R index conventional [I>2sigma(I)]	R1 = 0.0233

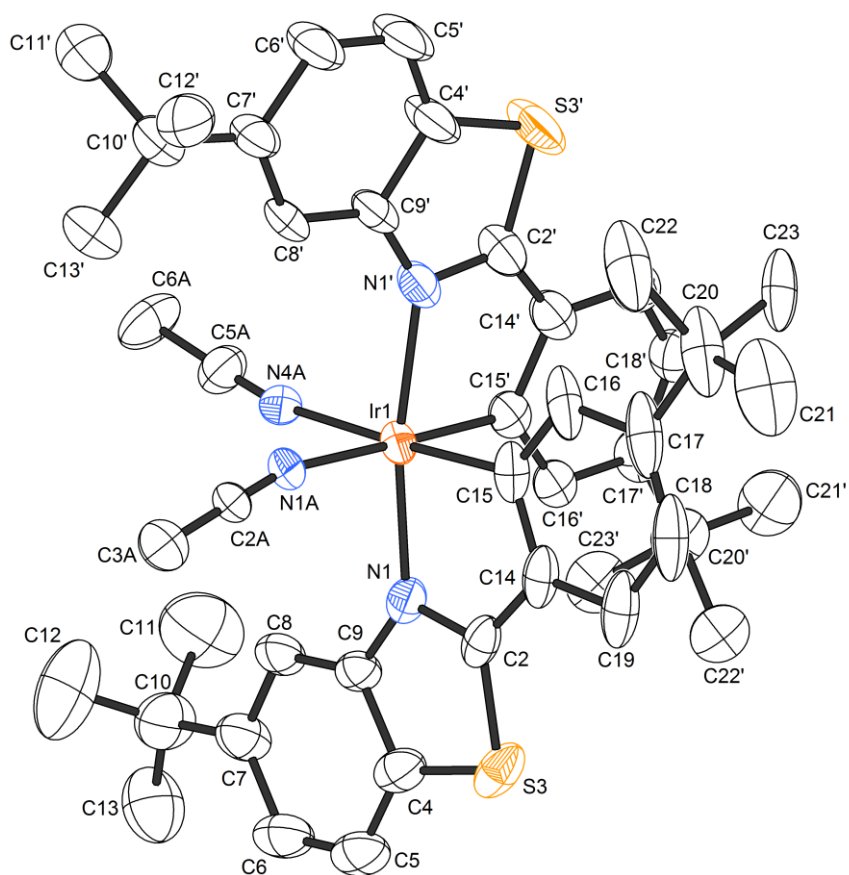


Figure 168 Crystal structure of Δ -IrS(*t*Bu). ORTEP drawing with 30% probability thermal ellipsoids.

Table 18. Crystal data and structure refinement for test_0m.

Crystal data

Identification code	hxqA74_0m
Habitus, colour	prism, yellow
Crystal size	0.18 x 0.13 x 0.08 mm ³
Crystal system	Tetragonal
Space group	P4 ₃ 2 ₁ 2
Unit cell dimensions	$a = 15.7940(7) \text{ \AA}$ $b = 15.7940(7) \text{ \AA}$ $c = 47.212(2) \text{ \AA}$
	$Z = 8$ $= 90^\circ$ $= 90^\circ$ $= 90^\circ$
Volume	11777.2(12) Å ³
Cell determination	9731 peaks with Theta 2.5 to 24.8°.
Empirical formula	C _{59.30} H _{69.20} F ₆ Ir N ₄ P S ₂
Moiety formula	C ₄₆ H ₅₄ Ir N ₄ S ₂ , F ₆ P, 1.9(C ₇ H ₈)
Formula weight	1239.27
Density (calculated)	1.398 Mg/m ³
Absorption coefficient	2.424 mm ⁻¹
F(000)	5048

Data collection:

Diffractometer type	Bruker D8 QUEST area detector
Wavelength	0.71073 Å
Temperature	100(2) K
Theta range for data collection	2.154 to 25.271°.
Index ranges	-18≤h≤18, -18≤k≤16, -42≤l≤56
Data collection software	BRUKER APEX2 2014.9-0
Cell refinement software	BRUKER SAINT
Data reduction software	SAINT V8.34A (Bruker AXS Inc., 2013)

Solution and refinement:

Reflections collected	46629
Independent reflections	10657 [R(int) = 0.0237]
Completeness to theta = 25.242°	99.9 %
Observed reflections	9518[I>2sigma(I)]
Reflections used for refinement	10657
Absorption correction	Numerical
Max. and min. transmission	0.83 and 0.62
Flack parameter (absolute struct.)	-0.012(2)
Largest diff. peak and hole	0.800 and -1.568 e.Å ⁻³
Solution	Direct methods
Refinement	Full-matrix least-squares on F ²
Treatment of hydrogen atoms	Calculated positions, constr. ref.
Programs used	XT V2014/1 (Bruker AXS Inc., 2014) SHELXL-2014/7 (Sheldrick, 2014) DIAMOND (Crystal Impact)
Data / restraints / parameters	10657 / 1907 / 948
Goodness-of-fit on F ²	1.037
R index (all data)	wR2 = 0.1240
R index conventional [I>2sigma(I)]	R1 = 0.0465

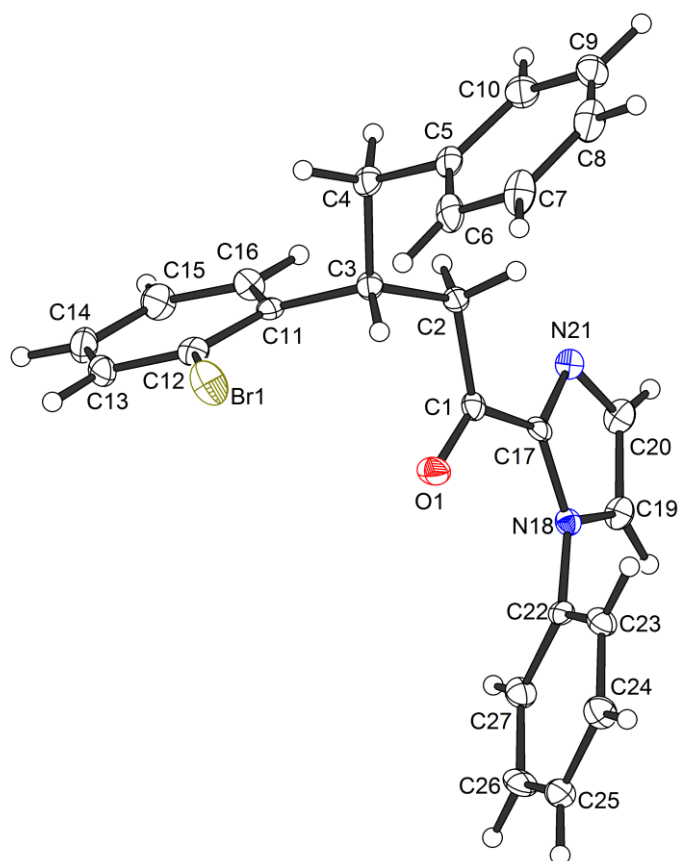


Figure 169 Crystal structure of (*R*)-**55k**. ORTEP drawing with 50% probability thermal ellipsoids.

Table 19. Crystal data and structure refinement for H53_0m.

Crystal data

Identification code	H53_0m
Habitus, colour	block, colourless
Crystal size	0.45 x 0.16 x 0.10 mm ³
Crystal system	Monoclinic
Space group	P2 ₁
Unit cell dimensions	$a = 10.7672(5) \text{ \AA}$ $b = 7.0157(3) \text{ \AA}$ $c = 14.4654(6) \text{ \AA}$
Volume	1021.83(8) Å ³
Cell determination	9845 peaks with Theta 2.9 to 25.3°.
Empirical formula	C ₂₅ H ₂₁ Br N ₂ O
Moiety formula	C ₂₅ H ₂₁ Br N ₂ O
Formula weight	445.35
Density (calculated)	1.447 Mg/m ³
Absorption coefficient	2.030 mm ⁻¹
F(000)	456

Data collection:

Diffractometer type	Bruker D8 QUEST area detector
Wavelength	0.71073 Å
Temperature	100(2) K
Theta range for data collection	2.919 to 25.295°.
Index ranges	-12<= <i>h</i> <=12, -8<= <i>k</i> <=8, -17<= <i>l</i> <=17
Data collection software	APEX3 (Bruker AXS Inc., 2015)
Cell refinement software	SAINT V8.35A (Bruker AXS Inc., 2015)
Data reduction software	SAINT V8.35A (Bruker AXS Inc., 2015)

Solution and refinement:

Reflections collected	24779
Independent reflections	3729 [R(int) = 0.0583]
Completeness to theta = 25.242°	99.8 %
Observed reflections	3551 [<i>I</i> > 2(<i>I</i>)]
Reflections used for refinement	3729
Absorption correction	Semi-empirical from equivalents
Max. and min. transmission	0.82 and 0.61
Flack parameter (absolute struct.)	-0.005(3)
Largest diff. peak and hole	0.292 and -0.346 e.Å ⁻³
Solution	direct/ difmap
Refinement	Full-matrix least-squares on F ²
Treatment of hydrogen atoms	Calculated positions, constr. ref.
Programs used	XT V2014/1 (Bruker AXS Inc., 2014) SHELXL-2014/7 (Sheldrick, 2014) DIAMOND (Crystal Impact) ShelXle (Hübschle, Sheldrick, Dittrich, 2011)
Data / restraints / parameters	3729 / 1 / 262
Goodness-of-fit on F ²	1.076
R index (all data)	wR2 = 0.0517
R index conventional [<i>I</i> > 2sigma(<i>I</i>)]	R1 = 0.0207

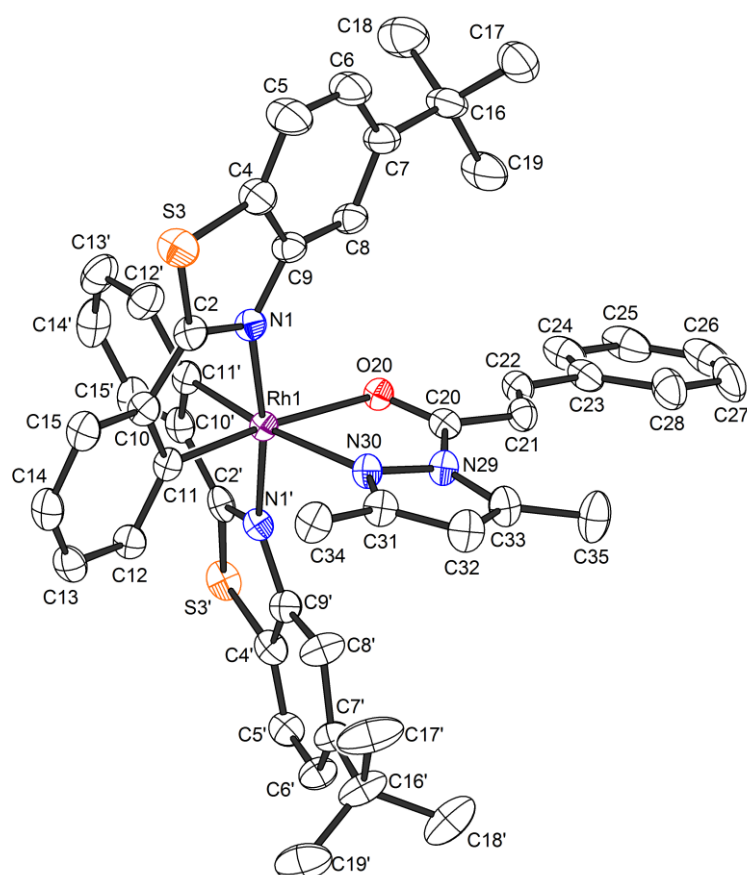


Figure 170 Crystal structure of intermediate **I** (RhS-Py). ORTEP drawing with 50% probability thermal ellipsoids.

Table 20. Crystal data and structure refinement for G160_0m.

Crystal data

Identification code	G160_0m
Habitus, colour	prism, green
Crystal size	0.39 x 0.22 x 0.17 mm ³
Crystal system	Orthorhombic
Space group	P2 ₁ 2 ₁ 2 ₁
Unit cell dimensions	$a = 15.1642(9) \text{ \AA}$ $b = 18.1335(10) \text{ \AA}$ $c = 19.1046(11) \text{ \AA}$
	$Z = 4$ $= 90^\circ$ $= 90^\circ$ $= 90^\circ$
Volume	5253.4(5) Å ³
Cell determination	9448 peaks with Theta 2.4 to 27.4°.
Empirical formula	C _{49.75} H _{49.50} Cl _{3.50} F ₆ N ₄ O P Rh S ₂
Moiety formula	C ₄₈ H ₄₆ N ₄ O Rh S ₂ , F ₆ P, 1.75(C H ₂ Cl ₂)
Formula weight	1155.51
Density (calculated)	1.461 Mg/m ³
Absorption coefficient	0.675 mm ⁻¹
F(000)	2358

Data collection:

Diffractometer type	Bruker D8 QUEST area detector
Wavelength	0.71073 Å
Temperature	120(2) K
Theta range for data collection	2.410 to 27.548°.
Index ranges	-19<=h<=18, -21<=k<=23, -24<=l<=24
Data collection software	APEX3 (Bruker AXS Inc., 2015)
Cell refinement software	SAINT V8.35A (Bruker AXS Inc., 2015)
Data reduction software	SAINT V8.35A (Bruker AXS Inc., 2015)

Solution and refinement:

Reflections collected	87903
Independent reflections	12110 [R(int) = 0.0410]
Completeness to theta = 25.242°	99.9 %
Observed reflections	11172[I > 2(I)]
Reflections used for refinement	12110
Absorption correction	Numerical Mu From Formula
Max. and min. transmission	0.89 and 0.78
Flack parameter (absolute struct.)	0.46(3)
Largest diff. peak and hole	0.888 and -0.786 e.Å ⁻³
Solution	Direct methods
Refinement	Full-matrix least-squares on F ²
Treatment of hydrogen atoms	Calculated positions, constr. ref.
Programs used	XT V2014/1 (Bruker AXS Inc., 2014) SHELXL-2014/7 (Sheldrick, 2014) DIAMOND (Crystal Impact) ShelXle (Hübschle, Sheldrick, Dittrich, 2011)
Data / restraints / parameters	12110 / 504 / 796
Goodness-of-fit on F ²	1.050
R index (all data)	wR2 = 0.0954
R index conventional [I>2sigma(I)]	R1 = 0.0354

Statement

gemäß § 10, Abs. 1 der Promotionsordnung der mathematisch-naturwissenschaftlichen Fachbereiche und des Medizinischen Fachbereichs für seine mathematisch-naturwissenschaftlichen Fächer der Philipps-Universität Marburg vom 15.07.2009

Ich erkläre, dass eine Promotion noch an keiner anderen Hochschule als der Philipps-Universität Marburg, Fachbereich Chemie, versucht wurde und versichere, dass ich meine vorgelegte Dissertation

Asymmetric Catalysis with Chiral-at-Metal Complexes: From Non-Photochemical Applications to Photoredox Catalysis

selbst und ohne fremde Hilfe verfasst, nicht andere als die in ihr angegebenen Quellen oder Hilfsmittel benutzt, alle vollständig oder sinngemäß übernommenen Zitate als solche gekennzeichnet sowie die Dissertation in der vorliegenden oder ähnlichen Form noch bei keiner anderen in- oder ausländischen Hochschule anlässlich eines Promotionsgesuchs oder zu anderen Prüfungszwecken eingereicht habe.

Haohua Huo
Marburg, den 06.06.2016

Curriculum Vitae

(Updated May 30, 2016)

Haohua Huo

Born March 6, 1987 in Guangdong, P. R. China

E-mail: haohuahuo@163.com

Education

11/2012–present	Ph.D. Organic Chemistry, University of Marburg, Germany Advisor: Prof. Eric Meggers
09/2009–09/2012	M.S. Organic Chemistry, Xiamen University, China Advisor: Prof. Peiqiang Huang
09/2005–06/2009	B.S. Chemistry, Xiamen University, China

Research Experiences

✧ **Ph.D. Study: Directing Asymmetric Catalysis with Metal-Centered Chirality**

Publications:

1. H. Huo, K. Harms, E. Meggers, *J. Am. Chem. Soc.* **2016**, *138*, 6936–6939.
2. H. Huo, E. Meggers, *Chimia*, **2016**, *70*, 186–191. (review)
3. H. Huo, X. Huang, X. Shen, K. Harms, E. Meggers, *Synlett*, **2016**, *27*, 749–753.
4. H. Huo, C. Wang, K. Harms, E. Meggers, *J. Am. Chem. Soc.* **2015**, *137*, 9551–9554.
5. H. Huo, X. Shen, C. Wang, L. Zhang, P. Röse, L.-A. Chen, K. Harms, M. Marsch, G. Hilt, E. Meggers, *Nature* **2014**, *515*, 100–103.
6. H. Huo, C. Fu, K. Harms, E. Meggers, *J. Am. Chem. Soc.* **2014**, *136*, 2990–2993.
7. H. Huo, C. Fu, C. Wang, K. Harms, E. Meggers, *Chem. Commun.* **2014**, *50*, 10409–10411.
8. X. Shen, H. Huo, C. Wang, B. Zhang, K. Harms, E. Meggers, *Chem. Eur. J.* **2015**, *21*, 9720–9726.
9. C. Wang, L.-A. Chen, H. Huo, X. Shen, K. Harms, L. Gong, E. Meggers, *Chem. Sci.* **2015**, *6*, 1094–1100.
10. C. Wang, Y. Zheng, H. Huo, P. Röse, L. Zhang, K. Harms, G. Hilt, E. Meggers, *Chem. Eur. J.* **2015**, *21*, 7355–7359.

✧ **M.S. Study: Enantioselective Total Synthesis of Natural Products**

Publications:

1. H. Huo, X. E. Xia, H. K. Zhang, P. Q. Huang, *J. Org. Chem.* **2013**, *78*, 455–465.
2. H. Huo, H. K. Zhang, X. E. Xia, P. Q. Huang, *Org. Lett.* **2012**, *14*, 4834–4837.
3. J. Chen, A. E. Wang, H. Huo, P. Q. Huang, *Sci. China-Chem.* **2012**, *55*, 1175–1212.
4. H. K. Zhang, Z. J. Lin, H. Huang, H. Huo, Y. J. Huang, J. L. Ye, P. Q. Huang, *Chin. J. Chem.* **2010**, *28*, 1717–1724.